INDIAN JOURNAL OF PHYSICS

VOL. XXIII

AND

PROCEEDINGS

OF THE

Indian Association for the Cultivation of Science, Vol. XXXII

(Published in Collaboration with the Indian Physical Society)

(With Thirtyfive Plates)

PRINTED BY SIBENDRANATH KANJILAL, SUPERINTENDENT (OFFG.), CALCUTTA UNIVERSITY PRESS, 48, HAZRA ROAD, BALLYGUNGE, CALCUTTA, AND PUBLISHED BY THE REGISTRAR, INDIAN ASSOCIATION FOR THE CULTIVATION OF SCIENCE

210, Bowbazar Street, Calcutta

1949

Price Rs. 20 *or* £2

INDIAN JOURNAL OF PHYSICS VOL. XXI (1949)

CONTENTS

PART I

PAGE

1. On the Raman Spectra of Chloro- and Bromo-Acetyl Chloride in the Solid state– By S. B. Sanyal and M. M. Majumder ... 1
2. A new Mechanical Violin player and some Experiments with it—By B. K. Sen 7
3. Instrumental Landing system for Aircrafts—By A. N. Bhattacharyya 13
4. The Relative Intensity of Doublet Spectra—By K. C. Kar and S. Sengupta 19
5. Ultra-Violet Bands of the Zinc iodide molecule. Part III—By C. Ramasastry 35

PART II

6. On the Geiger-Nuttall Relationship—By Sukumar Biswas ... 51
7. On the propagation of Supersonic waves through Liquids and Solutions –By B. B. Ghosh 79
8. Microwave Radio Blind Landing system for Aircrafts—Ay A. N. Bhattacharyya 88
9. Studies of a Schrage Three-phase Shunt Commutator Motor. I Vector diagram at Synchronous and Super-synchronous speeds — By H. P. Bhattacharyya and S. B. Deb 93

PART III

10. Fission cross-section of Uranium^{235}—By S. Biswas and A. P. Patro 97
11. On the Fluorescence of Solid di-normal propyl Ketone—By B. S. Kastha 107
12. Absorption of Heterogeneous Scattered X-rays—By H. K. Pal ... 111
13. Electron Transit time in negative Grid oscillator—By S. K. Chatterjee and B. V. Sreekantan 119
14. Magnetic studies on single crystals of Tungstenite (WS_2)—By A. K. Dutta and B. C. Roy Chowdhury 131

PART IV

15. Dielectric constant of Silica—By S. K. Kulkarni Jatkar and B. R. Yathiraja Iyengar 145
16. Feeble Paramagnetism of Chromium trioxide and Potassium chromate—By D. S. Datar and S. S. Datar 153

PAGE

17 New bands of the Asundi Band-system of Co—By Satya Narain Garg 161

18. The Spectrum of highly ionised Iodine. I—VI—By S. G. Krishnamurty and I. Fernando 172

19. Micro-wave modulation by Variable circuit elements comprising Wave guides or Cavity resonators—By A. N. Bhattacharyya ... 175

20. Band Spectrum of Thallium Iodide—By P. Tiruvenganna Rao and K. R. Rao 185

PART V

21. The near Ultra-violet Spectra of Benzene, Part I. The Emission Bands—By R. K. Asundi and M. R. Padhye 199

22. The Principal Magnetic Susceptibilities of Single Crystals of Rare earth salts at low Temperatures. Part I. Cerium Salts—By A. Mookherji 217

23. Some new features of the green and U. V. bands of Na_2 and the Blue bands of K_2 and of the Continua accompanying these bands—By S. P. Sinha 229

PART VI

24. The near Ultra-violet spectra of Benzene. Part II. A comparative study of the Absorption and Fluorescence bands—By R. K. Asundi and M. R. Padhye 237

25 The Structure of the Resonance line of Hg filtered through Hg vapour—By G. S. Kastha 247

26. On the Raman spectra of CS_2 at different temperatures—By N. C. Majumdar 253

27. Forty electron system of Molybdenum Mo III—By V. Ramkrishna Rao 258

28. Thallium Isotope effect in the band spectrum of Thallium bromide —By P. Tiruvenganna Rao 265

29. Mahajan's maximum and minimum Hygrometers—By L. D. Mahajan 269

30. Absorption and Reflexion of U. H. F. waves (300—500 Mc/s) —By S. K. Chatterjee and B. V. Sreekantan 273

PART VII

31. The near Ultra-violet spectra of Benzene. Part III. Fermi Resonance in the Emission spectrum of Benzene—By R. K. Asundi and M. R. Padhye 281

32. Theory of Doublet spectra under Magnetic perturbation—By S. Sengupta 287

33. Emission spectrum of the di-atomic Halides of Manganese. Part I. MnCl—By P. Tiruvenganna Rao 301

PAGE

34. The Principal Magnetic susceptibilities of single crystals of Rare earth salts at low Temperatures. Part II. Praseodymium salts—By A Mookherji 309
35. Emission spectrum of Lead Iodide—By P. Tiruvenganna Rao ... 321

PART VIII

36. The near Ultra-violet spectra of Toluene. Part I. The absorption bands with particular reference to the new bands observed—By M. R. Padhye 331
37. The near Ultra-violet spectra of Toluene. Part II. The emission bands—By R. K. Asundi and M. R. Padhye 339
38. Evaluation of Spectrograms of High-speed Steel for minor Elements. Plate calibration method By B. N. Bhaduri ... 347
39. A study of a Wilson's Cloud chamber with large Sensitive time and of its Application in measuring Range of α-particles emitted by Pu^{239}—By H. P. De 363
40. Indian Tropical storms and Zones of Heavy rainfall—By S. Mull and Y. P. Rao 371

PART IX

41. The Emission spectrum of Bismuth iodide By P. Tiruvenganna Rao 379
42. Fortyone electron system of Molybdenum. Mo II—By V. Ramakrishna Rao 387
43. New bands of the TlCl molecule—By P. Tiruvenganna Rao ... 393
44. Radiation Resistance of Skew wire Radio transmission lines—By S. S. Banerjee and R. R. Mehrotra 403
45. The Principal Magnetic susceptibilities of single Cryslats of Rare-earth salts at low temperatures. Part III. Neodymium salts—By A. Mookherji 410
46. A note on the Comparison between Emission and Fluorescence spectra (Ultra-violet) of Benzene —By R. K. Asundi and M. R. Padhye 421

PART X

47. New bands in the Spectrum of Thallium bromide—By P. Tiruvenganna Rao 425
48. Preliminary study of some Metallic oxide smokes with Electron Microscope—By A. K. Chaudhury and M. L. De 430
49. A Multi-stage Turbo expander Air Liquefier · By A. Bose ... 433
50. The Principal Magnetic susceptibilities of single crystals of Rare-earth salts at low temperatures. Part IV. Samarium Salts —By A. Mookherji 445
51. Band spectrum of Cadmium bromide—By C. Ramasastry ... 453

PAGE

52. Studies of a Schrage Three phase shunt Commutator Motor—By H. P. Bhattacharyya 459
53. On the Raman spectra of solid CH_3Cl and CH_2Cl_2—By N. C. Majumdar 465

PART XI

54. Plausible speed limit for Metallic Projectiles—By K. R. Dixit ... 469
55. The Spectro-Chemical determination of Carbon in Ferrous alloys —By K. C. Mazumder and M. K. Ghosh 477
56. Variation of Intensity of distant Atmospherics with Frequency Channels—By S. R. Khastgir and Asit Sen 483
57. On the Absorption of U. H. F. Radio waves in Organic liquids at different temperatures—By S. N. Sen 495
58. Estimation of Solvation of Ions in a solution from Kinetic theory —By H. Mukherjee 503
59. The Complex Spectrum of the Diatomic molecules of Chromium Chloride (CrCl)—By V. Ramakrishna Rao and K. R. Rao ... 508

PART XII

60. Emission spectrum of the Manganese Halides—By P. Tiruvenganna Rao 517
61. On the influence of Solar Activity on the Intensity of Cosmic rays —By I. L. Chakraborty and S. D. Chatterjee 525
62. The Complex band spectrum of Titanium chloride (The diatomic molecule TiCl) ... ... — ... 535
63. The Wavestatistical theory of Complex spectra—By S. Sengupta ... 547

AUTHOR INDEX

Author	Subject	Page
Asundi, R. K. and Padhye, M. R.	The near Ultra-violet Spectra of Benzene Part I. The Emission Bands ...	109
	The near Ultra-violet Spectra of Benzene Part II. A comparative study of the absorption and fluorescence Bands ...	237
	The near Ultra-violet spectra of Benzene Part III. Fermi Resonance in the Emission spectrum of benzene ...	281
	The near Ultra-violet spectra of Toluene Part II. The Emission bands ...	339
	A Note on the comparison between Emission and Fluorescence Spectra (Ultra-violet) of Benzene	421
Banerjee, S. S. and Mehratra, R. R.	Radiation Resistance of Skew wire Radio transmission lines	403
Bhaduri, B. N.	Evalution of Spectrograms of High speed steel for Minor elements	347
Bhattacharyya, A. N.	Instrumental Landing system for Aircrafts	13
	Micro-wave Radio Blind Landing system for Aircrafts	88
	Micro-wave Modulation by Variable circuit elements comprising Wave guides or Cavity Resonators	175
Bhattacharyya, H. P.	Studies of a Schrage Three-phase shunt Commutator Motor	459
Bhattacharyya, H. P. and Deb, S. B.	Studies of a Schrage Three-phase shunt Commutator Motor, I. Vector diagram at Synchronous and Supersynchronous speed	93
Biswas, Sukumar	On the Geiger-Nuttall Relationship ...	51
Biswas, S. and Patro, A. P.	Fission cross-section of Uranium ...	97
Bose, Akshayananda	A multi-stage Turbo expander Air Liquefier	430
Chakraborty I. L. and Chatterjee, S. D.	On the influence of Solar Activity on the Intensity of Cosmic rays	525

Author	Subject	Page
Chatterjee, S. K. and Sreekantan, B. V.	Electron transit time in Negative Grid Oscillator	119
	Absorption and Reflexion of U. H. F. waves (300—500 Mc/s)	273
Chaudhury, A. K. and De, M. L.	Preliminary study of some Metallic Oxide smokes with Electron Microscope ...	430
Datar, D. S. and Datar, S. S.	Feeble Paramagnetism of Chromium trioxide and Potassium chromate ...	153
De, H. P.	A study of a Wilson's Cloud chamber with large Sensitive time and of its Application in measuring Range of α-particles emitted by Pu^{239}	363
Dixit, K. R. ...	Plausible Speed limit for Metallic Projectiles	469
Dutta, A. K. and Roy Chowdhury, B. C. ...	Magnetic studies on single crystals of Tungstenite (WS_2)	131
Garg, Satya Narain ..	New bands of the Asundi band system of CO	161
Ghosh, B. B. ..	On the propagation of Supersonic waves through Liquids and Solutions ..	79
Jatkar, S. K. Kulkarni and Jyengar, B. R. Yathiraja ..	Dielectric constant of Silica ...	145
Kar, K. C. and Sengupta S.	The Relative Intensity of Doublet Spectra	19
Kastha, G. S. ...	On the Fluorescence of Solid dinormal propyl Ketone	107
	The Structure of the Resonance line of Hg filtered through Hg Vapour ...	247
Khastgir, S. R. and Sen, Asit	Variation of Intensity of distant Atmospherics with Frequency channels ...	483
Krishnamurty, S. G., and Fernando, I. ..	The Spectrum of highly ionised Iodine I-VI.	172
Mahajan, L. D. ..	Mahajan's Maximum and minimum Hygrometers	269
Majumdar, N. C. ..	On the Raman spectra of CS_2 at different temperatures	253
	On the Raman spectra of solid CH_3Cl and CH_2Cl_2	465
Mazumder, K. C. and Ghosh, M. K.	The Spectro-chemical determination of Carbon in Ferrous alloys	477

Author	Subject	Page
Mookherji, A.	The Principal Magnetic susceptibilities of single Crystals of Rare earth salts at low temperatures. Part I. Cerium Salts	217
,, ,,	The Principal Magnetic susceptibilities of single Crystals of Rare earth salts at low temperatures. Part II. Praseodymium Salts	309
Mookherji, A.	The Principal Magnetic Susceptibilities of single Crystals of Rare earth salts at low temperatures. Part III. Neodymium Salts	410
	The Principal Magnetic Susceptibilities of single Crystals of Rare earth salts at low temperatures. Part IV. Samarium Salts	445
Mukherjee, H.	Estimation of Solvation of ions in a solution from Kinetic theory	503
Mull, S. and Rao, Y. P.	Indian Tropical storms and Zones of heavy rainfall	371
Padhye, M. R.	The near Ultra-violet spectra of Toluene. Part I. The absorption bands with particular reference to the new bands observed	331
Pal, H. K.	Absorption of Heterogeneous scattered X-rays	111
Ramasastry, C.	Ultra-violet Bands of Zinc iodide molecule	35
	Band spectrum of Cadmium bromide ...	453
Rao, P. Tiruvenganna	Thallium isotope effect in the Band spectrum of Thallium bromide ...	265
	Emission spectrum of the diatomic Halides of Manganese	301
Rao, P. Tiruvenganna	Emission spectrum of Lead iodide ...	321
	Emission spectrum of Bismuth iodide ...	379
	New bands of the TlCl molecule ...	393
	New bands in the spectrum of Thallium bromide	425
	Emission spectra of Manganese halides ...	517
Rao, P. Tiruvenganna and Rao, K. R.	Band spectrum of Thallium iodide ...	185

AUTHOR	SUBJECT	PAGE
Rao, V. Ramakrishna	Forty electron system of Molybdenum. Mo III.	258
	Fortyone electron system of Molybdenum. Mo II.	387
Rao, V. Ramakrishna	The Complex band spectrum of Titanium Chloride (The diatomic molecule TiCl) ...	535
Rao, V. Ramakrishna and Rao, K. R.	The Complex spectrum of the Diatomic molecules of Chromium Chloride. (CrCl)	508
Sanyal, S. B. and Majumder, M. M	On the Raman spectra of Chloro- and Bromo-Acetyl chloride in the solid state ...	1
Sen, B. K.	A new Mechanical Violin player and some Experiments with it	7
Sen, S. N.	On the Absorption of U. H. F. Radio waves in Organic liquids at different temperatures	495
Sengupta, S.	Theory of Doublet spectra under Magnetic perturbation	287
	The Wave statistical theory of Complex spectra	425
Sinha, S. P.	Some new features of the Green and U. V. bands of Na_2 and the Blue bands of K_2 and the Continua accompanying these bands	229

SUBJEC INDEX

Subject	Author	Page
Air Liquefier, A Multi-stage Turbo Expander,	Akshayananda Bose	433
Asundi Band system of CO, New bands of,	Satya Narain Garg	161
Bands of the TlCl molecule, New	P. Tiruvenganna Rao	393
Band spectrum of Cadmium bromide	C. Ramasastry	453
Band spectrum of Thallium iodide	P. Tiruvenganna Rao and K. R. Rao	185
Complex band spectrum of Titanium Chloride (The diatomic molecule TiCl), The,	V. Ramakrishna Rao	535
Complex Spectra. The Wave Statistical Theory of	S. Sengupta	525
Complex spectrum of the Diatomic molecules of Chromium chloride. (CrCl), The	V. Ramakrishna Rao and K. R. Rao	508
Cosmic rays. On the influence of the solar Activity on the Intensity of	I. L. Chakraborty and S. D. Chatterjee	525
Dielectric Constant of Silica	S. K. Kulkarni Jatkar and B. R. Yathiraja Iyengar	145
Doublet Spectra. The Relative Intensity of	K. C. Kar and S. Sengupta	19
Doublet Spectra under Magnetic Perturbation. Theory of	S. Sengupta	287
Electron Transit time in Negative Grid Oscillator	S. K. Chatterjee and B. V. Sreekantan	119
Emission and Fluorescence Spectra of Benzene (Ultra-violet)	R. K. Asundi and M. R. Padhye	421
Emission spectrum of Bismuth iodide. The	P. Tiruvenganna Rao	379
Emission Spectrum of the diatomic Halides of Manganese. Part I. MnCl	P. Tiruvenganna Rao	301
	Do	517
Emission Spectra of Manganese Halides	P. Tiruvenganna Rao	517
Emmission Spectrum of Lead iodide		321
Fission Cross-section of Uranium^{235}	S. Biswas and A. P. Patro	97
Fluorescence of Solid di-normal propyl Ketone. On the	G. S. Kastha	107

Subject	Author	Page
Geiger-Nuttall Relationship. On the	Sukumar Biswas	51
Hygrometers. Mahajan's Maximum and Minimum	L. D. Mahajan	269
Indian Tropical Storms and Zones of heavy Rainfall	S. Mull and Y. P. Rao	371
Instrumental Landing system for Aircrafts	A. N. Bhattacharyya	13
Intensity of distant Atmospherics with Frequency channels. Variation of	S. R. Khastgir and Asit Sen	483
Magnetic studies on single Crystals of Tungstenite (WS_2)	A. K. Dutta and B. C. Roy Choudhuri	131
Magnetic Susceptibilities of Single Crystals of Rareearth salts at low Temperatures. The Principal Part I. Cerium salts	A. Mookherji	217
Magnetic susceptibilities of Single Crystals of Rare earth salts at low temperatures. The Principal Part II. Preseodymium Salts	A. Mookherji	309
Magnetic Susceptibilities of Single Crystals of Rare earth salts at low temperatures. The Principal Part III. Neodymium salts	A. Mookherji	410
Magnetic Susceptibilities of Single Crystals of Rare earth Salts at low temperatures. Th Principal Part IV. Samarium Salts	A. Mookherji	445
Metalic Projectiles. Plausible Speed limit for	K. R. Dixit	469
Metallic Oxide smokes with Electron Microscope. Preliminary Study of some	A. K. Choudhury and M. L. De	430
Microwave Modulation by Variable guides Circuit Elements Comprising wave or Cavity Resonators	A. N. Bhattacharyya	175
Microwave Radio Landing system for Aircrafts	A. N. Bhattacharyya	88
Molybdenum. Forty electron system of Mo III	V. Ramakrishna Rao	258
Molybdenum. Forty one electron system of Mo II	V. Ramakrishna Rao	387
Paramagnetism of Chromium trioxide and Potassium Chromate. Feeble	D. S. Datar and S. S. Datar	153

SUBJECT	AUTHOR	PAGE
Raman Spectra of Chloro- and Bromo-acetyl Chloride in Solid state. On the,	S. B. Sanyal and M. M. Majumder	1
Raman Spectra of CS_2 at different Temperature. On the	N. C. Majumdar	253
Raman Spectra of Solid CH_3Cl and CH_2Cl_2. On the	N. C. Majumdar	465
Range of α-Particles emitted by Pu^{239}. A study of a Wilson's Cloud Chamber with large Sensitive time and of its application in measuring	H. P. De	363
Resonance line of Hg filtered through Hg vapour. The Structure of the	G. S. Kastha	247
Schrage Three-Phase shunt Commutator Motor. Studies of a I. Vector diagram at Synchronous and Super-synchronous Speed	H. P. Bhattacharyya and S. B. Deb	93
Schrage Three-Phase Shunt Commutator Motor. Studies of a II. Behaviour of the motor running supersynchronous on no-load and subsynchronous on load for identical brush position	H. P. Bhattacharyya	459
Skew-wire Radio Transmission Lines. Radiation Resistance of	S. S. Banerjee and R. R. Mehrotra	403
Solvation of Ions in a Solution from Kinetic Theory. Estimation of	H. Mukherjee	503
Spectrograms of High speed Steel for minor Elements. Evaluation of Plate Calibration method	B. N. Bhaduri	347
Spectro-Chemical determination of Carbon in Ferrous Alloys. The	K. C. Mazumder and M. K. Ghosh	477
Spectrum of Highly ionised Iodine. I-VI, The	S. G. Krishnamurty and I. Fernando	172
Spectrum of Thallium bromide. New bands in the	P. Tiruvenganna Rao	425
Supersonicwaves through Liquids and Solutions On the Propagation of	B. B. Ghosh	79
Thallium Isotope effect in the Band Spectrum of Thallium bromide	P. Tiruvenganna Rao	265
U. H. F. Radio waves (300—500 Mc/s). Absorption and Reflexion of	S. K. Chatterjee and B. V. Sreekantan	273

Subject	Author	Page
U. H. F. waves in Organic Liquids at different Temperatures. On the Absorption of	S. N. Sen	495
Ultra-violet Bands of the Zinc iodide molecule. Part III	C. Ramasastry	35
Ultra-violet Spectra of Benzene. The near Part I. The Emission bands.	R. K. Asundi and M. R. Padhye	199
Ultra-violet spectra of Benzene. The near Part II. A Comparative study of the Emission and Fluorescence bands	R. K. Asundi and M. R. Padhye	237
Ultra-violet Spectra of Benzene. The near Part III. Fermi Resonance in the Emission spectrum of Benzene	R. K. Asundi and M. R. Padhye	281
Ultra-violet Spectra of Toluene. The near Part I. The Absorption Bands with particular reference to the new Bands observed	M. R. Padhye	331
Ultra-violet spectra of Toluene. The near Part II. The Emission Bands	R. K. Asundi and M. R. Padhye	339
U. V. Bands of Na_2 and the Blue bands of K_2 and of the Continua accompanying these bands. Some new features of	S. P. Sinha	229
Violin Player, A new Mechanical, and some Experiments with it	B. K. Sen	7
X-Rays. Absorption of Heterogeneous Scattered	H. K. Pal	111

ON THE RAMAN SPECTRA OF CHLORO AND BROMO-ACETYL CHLORIDE IN THE SOLID STATE.

By S. B. SANYAL, and M. M. MAJUMDAR.

(*Received for publication, Nov. 3, 1948.*)

Plate I

ABSTRACT. The Raman spectra of chloro-and bromo-acetyl chloride in the liquid and solid states as well as the polarisation of the Raman lines of these liquids have been studied. It is observed that in the liquid state the former compound yields a smaller number of lines than the latter, which again gives much more lines than those expected theoretically. In the latter case some of the prominent lines disappear in the solid state, while in the case of chloro-acetyl chloride no such change takes place. New lines in the low frequency region appear in the solid state in both the cases. The changes observed in the case of bromo acetyl chloride are ascribed to the formation of strongly associated molecules in which the C-Cl and C-Br valence forces in the molecule are affected in the liquid state. It is pointed out that in the case of propyl bromide also similar explanation was offered by previous workers.

INTRODUCTION

The Raman spectra of acetyl chloride and acetyl bromide have been studied in the liquid as well as in the solid state by Bishui (1948a). It has been reported that all the prominent Raman lines due to the liquid state are also present in the solid state. It has, therefore, been concluded that there is no rotational isomers in these liquids. It has been argued by him that the presence of two extra lines below 1200 cm^{-1} in the Raman spectra of each of the substances may be due to the formation of associated groups of molecules in the liquid and solid states of the substances. In order to get definite information regarding the structure of molecules in these cases two halogen substituted derivatives of acetyl chloride have been chosen in the present investigation. The Raman spectra of chloro-acetyl chloride and bromo-acetyl chloride in the liquid and solid states have thus been studied in order to find out the difference in the Raman spectra due to the two states. Incidentally, the Raman spectra of bromo-acetyl chloride was not studied by any previous worker and it was not known how the Raman spectra is affected when the chlorine atom attached to the CH_2 group in acetyl chloride is replaced by a bromine atom. The polarisation of the Raman lines due to these two liquids has also been studied in order to get information regarding the symmetry of the molecules.

EXPERIMENTAL

The liquids from Kahlbaum's original packings were obtained from old stock of this laboratory and were redistilled in vacuum. The method for studying the Raman spectra of the compounds at low temperatures was the same as that described by Bishui (1948b). A long pyrex glass tube containing the distilled liquid was held in the vapour of the liquid oxygen which was constantly being evaporated from the lower portion of the transparent Dewar vessel. The level of the liquid oxygen in the transparent Dewar vessel was maintained at a position about a centimetre below the bottom of the tube containing the distilled liquid. Evaporation of the liquid oxygen was frequently accelerated by pumping out the cold vapour above the surface of the liquid oxygen with a Cenco Hyvac pump. A pentane thermometer, which passed through a cork fitted into the mouth of the transparent Dewar vessel, was held in the vapour of the liquid oxygen to record the temperature. The solidification of the experimental liquid took place slowly and a semi-transparent solid mass of the substance was obtained. Light from two vertical mercury arcs, condensed by two six inch glass condensers, was focussed on the substance from opposite sides.

A Fuess glass spectrograph, having a dispersion of 13.5 Å per mm. in the region of 4046 Å, was used in this investigation. A blue-violet glass filter was placed in the path of the incident light in order to diminish the continuous background in the blue-green region. The polarisation of the Raman lines due to the liquids was studied in each case by photographing simultaneously the vertical and horizontal components of the scattered light with the help of a double image prism. Light from a mercury arc, focussed by means of a glass condenser, was used as the incident light in these cases.

RESULTS AND DISCUSSIONS

The spectrograms for the liquid and the solid state are reproduced in Plate I. The results are given in Tables I and II. The results reported by some previous workers have been given in the first column in the case of chloro-acetyl chloride only. The data for the solid obtained in the present investigation are given in the last column. The letters e, k, i, c represent exciting lines in Kohlrausch's notation. P means $\rho << 6/7$ and D means $\rho = 6/7$. The approximate visually estimated intensities are given in parentheses.

It can be seen from Tables I and II that the numbers of Raman lines, having frequency shifts less than 1000 cm^{-1}, observed in the case of the two liquids are quite different from each other. The results reported by Cheng (1934) in the case of chloro-acetyl chloride show that there are seven Raman lines in the region mentioned above of which the line 899 cm^{-1} is extremely weak. With the exception of this line all the other lines have been observed in the present investigation. It has further been observed that all these lines

TABLE I

Chloro-acetyl chloride

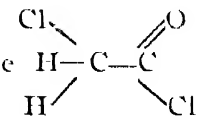

Liquid at 30°C		Solid at about −150°C
Hua-chi-cheng (1934)	Present authors	Present authors
		48 – (0) k
304 – (10) c ± , k, i, f	300 – (5) c ± , k, c, P	300 – (1) c, k
452 – (10b) c ± k, i, c	453 – (6) c ± , k, c, P	459 – (3) c, k
562 – (1) c	560 – (0 b) c, k, P	565 – (0) sl c, k
719 – (3b) c, k	712 – (1b) c, k, c, P	724 – (1) c, k
784 – (10) c ± k, i, c	780 – (6) c, k, P	780 – (5) c, k
899 – (00) c, k ?		
970 – (5) c	970 (0 b) c, k, P	X
1179 – (1) c, k		
1400 – (2) c, k	1402 – (2b) c, k, D	1400 – (0) c
1800 – (2) c	1810 – (2b) c, P	1803 – (0 s) c
2950 – (10) c, k, i	2952 – (6) c, k, P	2946 – (6) c, k
2997 – (5) c, k	2992 – (1) c, k, P	2992 – (2) c, k

TABLE II

Bromo-acetyl chloride

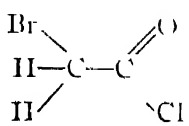

Liquid at 30°C	Solid at about −150°C
Present authors	Present authors
	40 – (0) k
150 – (1) D	
188 – (2b) c, D	170 – (0) c
250 – (3) c ± , k, P	258 – (3) c, k
297 – (0), c, P	297 – (1) c
363 – (2) c, k, D	V
449 – (5) c ± , k, P	452 – (5) c, k
490 – (6) c, P	
526 – (3) c, k, P	V
704 – (1) c, k, P	672 – (0) c
730 – (5) c, k, P	735 – (5) c, k
953 – (0) c, k, P	
1393 – (2) c, k, D	1385 – (0) c, k
1816 – (2b) c, P	1812 – (0) c
2956 – (5) c, k, P	2980 – (8) c, k
3014 – (1) c, k, P	3014 – (2) c, k

are polarised. No data for bromo-acetyl chloride are available and it seems that this liquid was not investigated before. The number of Raman lines, having frequency shifts below 1000 cm^{-1}, observed in this case is eleven. Three of these lines are observed to be totally depolarised. The Raman

lines in this region are given by the vibrations of the group $X-C-\overset{\overset{O}{\|}}{C}-Cl$

where X stands for Cl and Br in the two cases. It is thus evident that when there are two Cl atoms in this group at the two ends the number of Raman lines is reduced Ordinarily, according to the group theory this group having only a plane of symmetry would yield altogether nine Raman lines of which seven are polarised and two are totally depolarised as can be seen from Table III.

TABLE III

C_s	E	σ	n'	T & R	Raman effect.
A'	1	1	10	3	7 P
A''	1	−1	5	3	2 D
UR	5	5			
$h_1\chi_1$	15	5			
$h_2\psi_1$	9	5			

It is thus evident that in the case of chloroacetyl chloride the number of Raman lines due to the group $Cl-C-\overset{\overset{O}{\|}}{C}-Cl$ actually observed in less than that expected theoretically and that the totally depolarised lines are absent. On the other hand in the case of bromoacetyl chloride the number of such lines actually observed is much more than that expected theoretically. This peculiar difference in the behaviour of the two molecules can be explained on the assumption that in the case of chloroacetyl chloride the selection rules for the appearance of the Raman lines due to the vibration of the group Cl-C-C-Cl is not affected very much by the presence of the divalent oxygen atom attached to one of the carbon atoms. In that case this group of four atoms would have a centre of symmetry and would yield only three lines, all polarised, and due to the presence of the oxygen atom three more lines, all polarised, would be expected. In other words, out of the nine lines, mentioned in Table III, only six would be observed and besides the two depolarised lines mentioned therein another line, due to the antisymmetric valence oscillation of C-Cl group, would be absent. Taking into account the line at 1810 cm^{-1} due to the C=O oscillation, it is found that

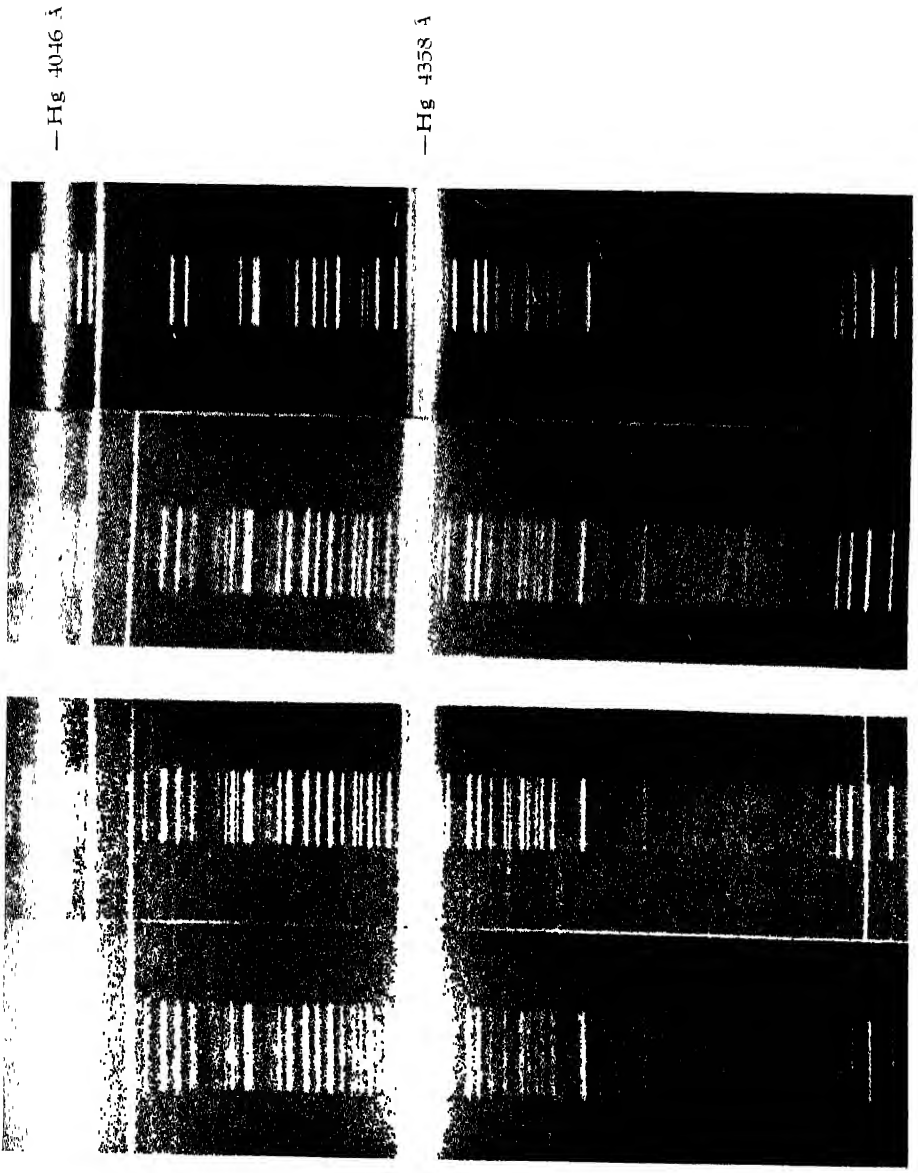

Raman Spectra

Fig. 1.—Chloroacetyl Chloride at about + 30°C.

Fig. 2.— " " " " − 160°C.

Fig. 3.—Bromoacetyl Chloride at about + 30°C.

Fig 4.— " " " " − 160°C.

besides these lines an extra line appears in the Raman spectrum of this substance in the liquid state. This line may be due to the association of the molecules.

In the solid state at the low temperature the intensity of the line 1810 cm^{-1} diminishes appreciably and its frequency also diminishes by 8 wave numbers. The line 560 cm^{-1} becomes sharper in the solid state and an extra line at 48 cm^{-1} appears in the neighbourhood of the Hg line 4046 Å. This latter line is quite sharp and considering the complicated structure of the molecule it is difficult to ascribe this line to rotational oscillation of the molecule in the lattice as suggested by Kastler and Rousset (1941) in the case of benzene and naphthalene.

In order to explain the appearance of many extra lines in the case of bromoacetyl chloride the hypothesis of co-existence of rotational isomers in the liquid state could be put forwards as was done in the case of other dihalogen derivatives of ethane by Mizushima *et al* (1936). There is, however, a serious difficulty in applying the same hypothesis in the present case, because if the rotational isomers could be present in the liquid state of bromoacetyl chloride they would also be present in the case of chloracetyl chloride, but actually it has been shown above in the latter case there is strong evidence for the existence of only one type of the molecule. Hence in the case of bromo-acetyl chloride also rotational isomers cannot be present. Probably in the latter case the molecules are strongly associated and on solidification due to uniform distribution of the molecules some of the virtual bonds become loosened and the corresponding Raman lines disappear. Such an explanation has been offered in the case of propyl bromide by Bishui (1948c). The remarkable changes observed in the Raman spectrum of bromoacetyl chloride with the solidification of the substance can thus be explained. The changes observed are rather large, because the strong lines 363 and 526 cm^{-1} disappear and the line 207 cm^{-1} becomes more intense in the solid state. Also the frequency shift of the line 2956 cm^{-}, due to C−H oscillation, increased to 2980 cm^{-1} in the solid state and the intensity of the line 1812 cm^{-1} diminishes appreciably. The changes are not observed in the case of chloroacetylchloride probably because the virtual attachment of chlorine atom to any of the two carbon atoms produces the same change in the C−Cl frequency in both the groups to the same extent. A comparison of the Raman spectra of the liquid and solid states of chloro-and bromo-acetyl chloride thus seems to support the hypothesis put forward by Bishui (1948c) regarding the changes occurring in the Raman spectra of propyl bromide with the change of state.

ACKNOWLEDGMENTS

The authors are indebted to Prof. S. C. Sirkar for his kind interest and guidance throughout the progress of the work and to the Council of the

Indian Association for the Cultivation of Science for kind permission to work in the laboratories of the Association.

Indian Association for the
Cultivation of Science,
210, Bowbazar Street,
Calcutta.

REFERENCES

Bishui, B.M., 1948a *Ind. J. Phys.* **22**, 167.

,, ,, 1948b *Ind. J. Phys.* **22**, 319.

,, ,, 1948c *Ind. J. Phys.* **22**, 333.

Cheng, Hua Chi, 1934 *Z. f. Physik. Chem. B.* **26**, 288.

Mizushima S., Morino. Y. and Noziri, Y. 1936, *Sc. Papers Inst. Phys. Chem. Research* (*Tokyo*) **29**, 63 and 188.

A NEW MECHANICAL VIOLIN-PLAYER AND SOME EXPERIMENTS WITH IT

By B. K. SEN

(*Received for publication, Sept. 10, 1948*)

ABSTRACT. The paper gives the description of the construction of a new model of the mechanical violin-player with sensitive arrangements for the measurements of pressure and velocity of the bow. Some of the experiments done by Raman with his mechanically played violin have been repeated and extended as well with the help of the new apparatus. The preliminary results obtained do not generally confirm Raman's conclusion regarding the relation between the minimum bowing pressure to excite the fundamental tone and the distance of the bowed region from the bridge but confirms that regarding the relation between pressure and velocity of the bow, when the bowed region is kept unaltered

INTRODUCTION

Raman (1920) by his experiments with the mechanically played violin constructed by him has shown that—

(1) the bowing pressure to excite the fundamental varies inversely as the square of the distance of the bow from the bridge;

(2) for very small bowing speeds, the bowing pressure necessary tends to a finite minimum value and the increase of bowing pressure with speed is at first rather slow but later becomes very rapid;

(3) the bowing pressure for different frequencies shows a series of maxima which approximately coincide in position with the resonance frequencies of the instrument.

Further, Raman studied the effect of muting on the bowing pressure and found that the mute produced profound alterations in the form of the pressure frequency curve.

In Raman's experiments the bowing was done not by moving the bow in the usual way to and fro across a fixed violin but by moving the violin itself, keeping the bow fixed. The pressure of the bow on the violin in his apparatus could not be kept constant throughout the entire run of the violin. This variation of pressure as the violin moved was, however, kept small by having a long lever. Moreover, the observations of the character of the tone were made for a particular position and direction of movement of the violin; but the method by which the speed of the bow was determined, it appears, gave only the average speed for full strokes to and fro, which, evidently, is quite different from the average speed over a small region in the neighbourhood of the particular position for which the character of the tone was observed and the pressure to excite it, measured. The present

author has devised a new and improved form of mechanical violin-player in which the violin is kept fixed and the bow is moved in the usual way across the string. The bowing pressure in the new apparatus can be kept at any constant value during the bowing. Arrangement has been made for the measurement of the pressure from the vertical displacement of the violin the magnitude of which is measured by applying the principle of mechanical magnification. Instead of measuring the average velocity of the bow over its entire run, that for a small distance near the middle of the run has been measured and observations of pressure and characteristic of tones have also been made for the same region.

The object of the present investigation has been to construct a new model of the mechanical violin-player with sensitive arrangements for the measurements of pressure and velocity and to study some characteristics of the bowed string with its help. Some of Raman's experiments have, however, been repeated with the help of the new apparatus.

DESCRIPTION OF THE APPARATUS

A shaft AB is moved to and fro smoothly through two guides G,G by means of an arrangement of crank, wheels, speed-reducing gears and motor as shown in the schematic diagram (Fig. 1). The speed is controlled by

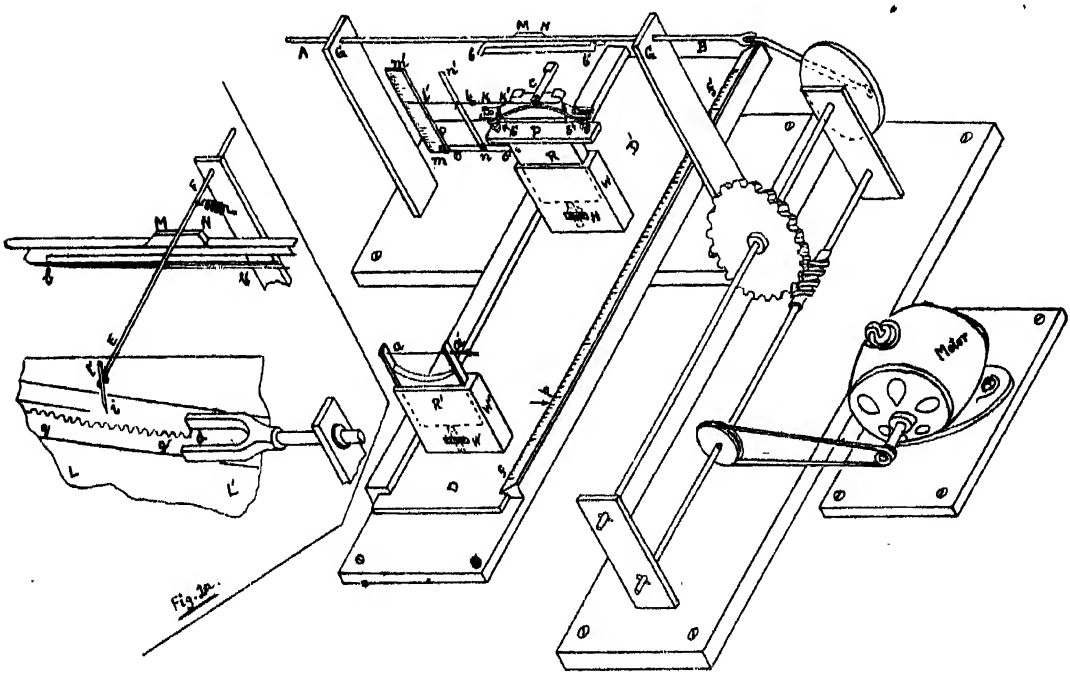

FIG. 1
Schematic diagram of mechanical violin-player.

adjusting rheostats connected with the motor. To the shaft is fixed the bow bb' which is made to move in a given horizontal plane by the shaft, the

distance over which it moves being nearly one foot. Below the bow is placed the belly of the violin in a cradle *C* which touches the violin at its three nodal points only. The cradle is supported on a spring system *s*,*s*, *s*,*s*, carried on a small horizontal platform *P* attached to a vertical piece *R* moving smoothly in grooves in a vertical stand *W*. The up and down movement is effected by means of a screw head arrangement *H*. The handle of the violin is supported on a horizontal axis *aa'* passing through a small hole made at the end of the handle. Thus the violin is supported at one end by the axis *aa'* and at the other end by the cradle *C* and lies horizontally between *aa'* and *C* with its face upwards and is free to move in a vertical plane about the axis. The axis, made of a piece of steel wire, is supported on a U-shaped vertical stand *R'* which can also be moved up and down along grooves made in a vertically fixed wooden piece *W'*. The up and down movement is effected by a screw-head arrangement *H'*. The vertical wooden pieces with grooves carrying the supports of the violin at the two ends are fixed on another large piece of wood *DD'* which is capable of horizontal movement at right angles to the direction of the length of the bow and can be fixed in any position on the wooden base of the apparatus. With the help of a scale *ff'* attached to the base and a pointer *p* fixed to the sliding wooden piece the distance of the bowed region from the bridge can be determined after applying index correction. The distance of the bow from the bridge is always measured from the centre of the bowed region.

PRESSURE RECORDER

For recording pressure a small pin *kk'* is fixed to the bottom of the cradle carrying the belly of the violin. This pin presses against the end of the smaller arm of a lever *ll'*, the end of the longer arm of which moves over a vertical scale *mm'*. The fulcrum of the lever is fixed on a vertical thin stand *nn'*. This stand and the vertical scale are supported by means of a cross-piece *oo'*, rigidly attached to the vertical support *R* of the platform carrying the spring system. For measuring any pressure the scale *mm'* is previously calibrated by means of actual weights placed at desired points.

ARRANGEMENT FOR MEASURING VELOCITY OF THE BOW.

This arrangement is shown separately in Fig. 1*a*, in which a part of the shaft and the bow and other additional adjuncts are given.

The horizontal run of the bow is nearly one foot and the average velocity of the bow is measured over a distance of 6 cms. near the middle of the run. Pressure and tone characteristics are also observed over this region. For the measurement of velocity a piece of smoked paper *qq'* is drawn along a smooth platform *LL'* parallel to the bow under a thin stylus *d* attached to a prong of a vibrating tuning fork of frequency 100, supported horizontally on a vertical stand so that a wavy curve is produced on the paper. A

pin *ii'* is attached to the end of a lever *EF* resting on a thin short piece of wood *MN* fixed on the shaft in a region corresponding to that of the middle of the travel of the bow. The end of the pin lies by the side of the stylus from the prong. The pin is adjusted in such a way that it normally touches the smoked paper and makes a straight line on it parallel to the wavy curve so long as the lever rests on the shaft only. But when during the movement of the shaft the lever comes over the thin wooden piece *MN* on the shaft the end of the pin is raised from the paper and there is a break in the line drawn by it. The pin again goes on tracing the line when the lever has just passed over the piece of wood. The length of the break is compared with the number of waves lying parallel to it by putting the smoked piece of paper under a travelling microscope. From the known frequency of the fork, the length of the piece of wood *MN*, and the number of waves corresponding to the break in the straight line drawn by the pin *ii'* the velocity of the bow is determined.

RESULTS

(1) *Pressure-distance relation :*

Experiments have been done with the G-string of the violin and the results obtained are shown graphically. Keeping the bowing speed constant the pressure was measured for different distances '*d*' of the bowed region from the bridge. The results obtained point to a rectangular hyperbolic relation between P_m and d, *i.e.*, the pressure varies inversely as the distance approximately, as shown in the P_m-d curve in Fig. 2. Raman has, however, found P_m to be proportional to $1/d^2$.

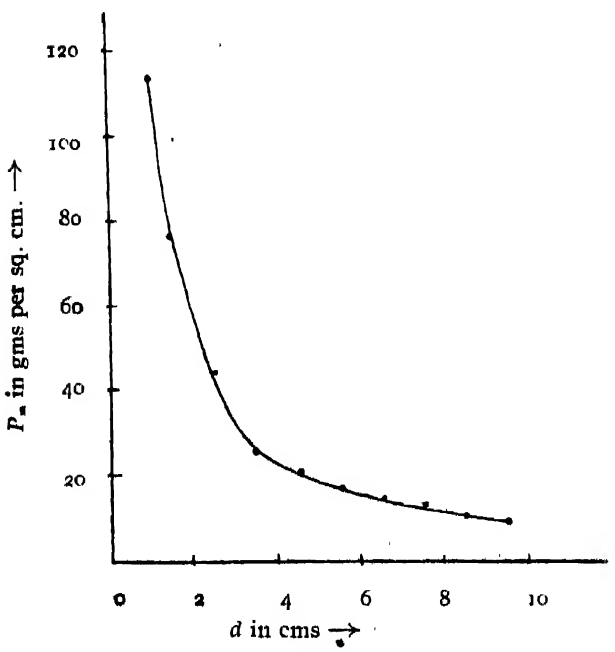

FIG. 2
P_m-d curve (velocity = constant)

(1*a*) The frequency of the string was then altered and kept at a fixed value by changing the tension only and the experiment to find out the variation of P_m with d was repeated. This was done for three different frequencies. It was found that the form of the P_m-d curve for every new frequency remained the same as before but P_m increased with the increase of the frequency of the string of the violin under investigation. This is shown by the curves

I, II, and III in Fig. 3. For every curve the relation $P_m \propto 1/d$ holds good approximately.

(2). Pressure-velocity relation :

Experiments were next performed at a particular frequency of the string keeping the bowed region constant but changing only the velocity of the bow. The pressures necessary to excite the fundamental for different bowing speeds were measured and the pressure-velocity curve obtained is shown in Fig. 4. The nature of the curve is found to be the same as that obtained by Raman. Just as in Raman's experiment, the pressure required to excite the fundamental tone increased slowly at first and later rapidly as the velocity of the bow increased. The latter part of the curve shows that the pressure necessary increases roughly in proportion to the speed. In Raman's experiment it was also found that for very small bowing speeds the bowing pressure tends to a finite minimum value. The experiment of the present author was not, however, carried down to very low velocities, but the bend of the curve near the lower end, it appears, gives a definite indication of the validity of Raman's conclusion.

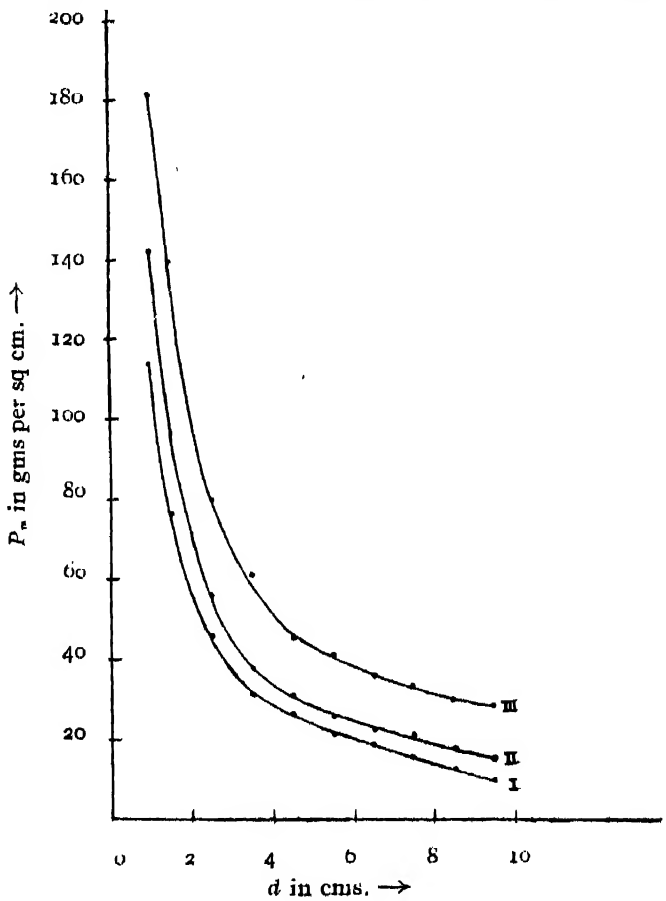

FIG. 3

I. Frequency = 288 approx.
II. ,, = 384 ,,
III. ,, = 480 ,,
} velocity same for all.

In all the above experiments the minimum pressure necessary to excite the fundamental tone has been measured. It was, however, noticed during the above investigation that the pressure can, in all cases, be increased by a small amount without altering the tone characteristics; but when increased beyond a certain limit, the string becomes loaded and the tone changes. Thus for every frequency of the string, for all distances of the bow from the

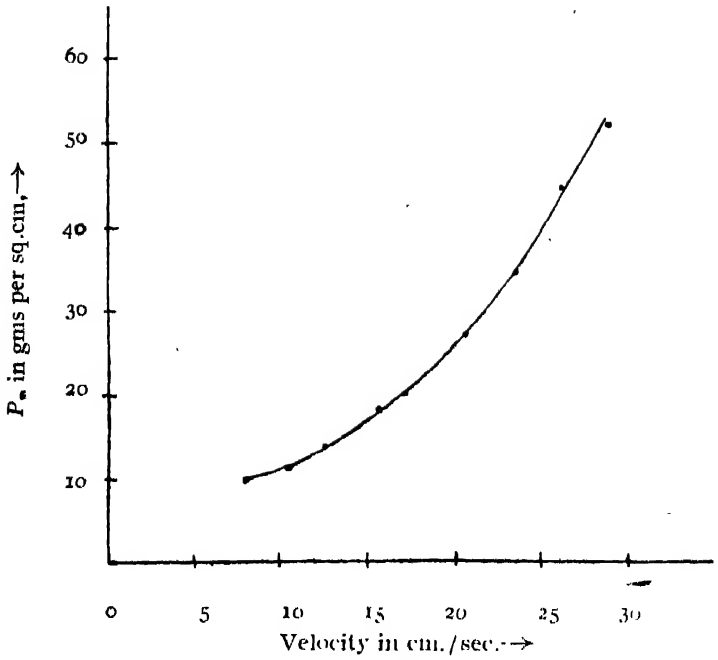

FIG. 4

Pressure-Velocity curve
Frequency = 341 approx.

bridge and for all speeds of bowing the pressure necessary for the excitation of the fundamental lies between certain definite limits.

REMARKS

The investigation was carried in the Rajshahi College Physical Laboratory. It is regretted that the wide range of studies aimed at with the new apparatus could not be completed on account of the partition of Bengal and the apparatus which could be made a very sensitive one with certain additions and alteration contemplated by the author had to be left behind at Rajshahi College. In this paper an account of some of the preliminary experiments performed has only been recorded.

ACKNOWLEDGMENTS

In conclusion the author desires to express his indebtedness to Dr. K. C. Kar, D.Sc., for suggesting the problem and for his helpful criticism during the progress of the work.

Department of Physics,
B.E. College, Sibpur,
Calcutta, Howrah.

REFERENCE

Raman, C.V., 1920, *Proc. Ind. Asso. for Cult. Sc.* Vol. VI, parts I + II, p. 19.

INSTRUMENTAL LANDING SYSTEM FOR AIRCRAFTS

By A. N. BHATTACHARYYA

(Received for publication, Aug. 6, 1948)

ABSTRACT. Following the principle of interference of electro-magnetic waves radiated from two sources, the relative phases of the two waves remaining constant, it is shown that by arranging two pairs of such sources, one pair emitting waves of frequency different from that of the other, a glide path is defined by the intersecting portion of the central fringes corresponding to two sets of fringes formed in the space.

INTRODUCTION

One of the important features of the radio aids to aviation is that with the help of radio instruments an aeroplane may land under conditions of poor or even zero visibility. Such arrangements for landing aircrafts are commonly known as "blind landing systems" and "instrumental landing systems" and provide the pilot with lateral guidance, vertical guidance and position 'fixes.' Most of the instrumental landing systems are based on the principle of partial superposition of radio beams and creation of an equisignal zone. This paper describes a system utilising the principle of interference of radio waves radiated from two aerials which are excited in the same phase with one high frequency current. The loci of the maxima and minima in space form a system of confocal hyperboloids, the two sources or aerials being the foci.

DESCRIPTION OF THE SYSTEM

The principle utilised in this system will be explained with reference to Fig. 1. One pair of aerials O, O' is situated above the ground level

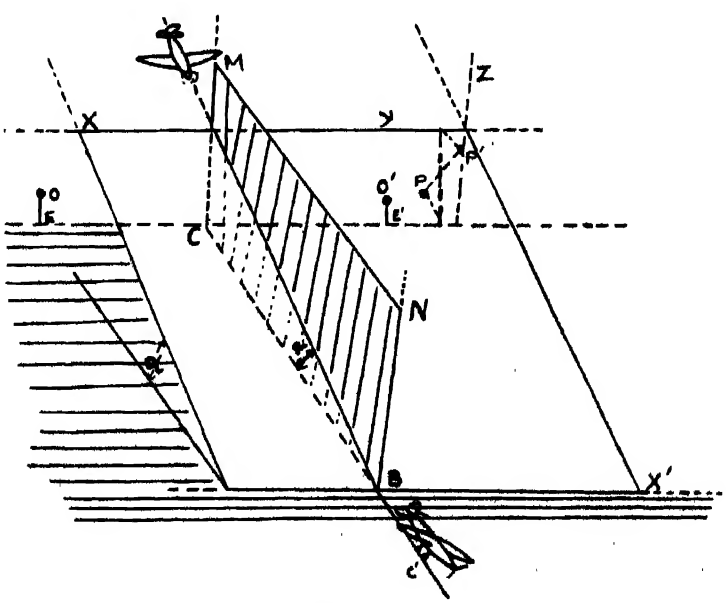

FIG. 1

at the same height, the distance between O and O' being at least 500 yds. The runway CC' passes through the middle point of EE' and is perpendicular to the line EE'. The points E and E' are the ground points just below O and O' respectively. The aerials O, O' are excited in the same phase with one ultra-high frequency (f_1) current. In this case the central fringe (*i.e.*, the bright fringe for which the phase difference between the waves from O and O' is zero) will coincide substantially with a vertical plane (which is partly shown as $CMNB$) over the runway CC'. Other fringes of the same set will be confocal hyperboloids of which O and O' are foci. Another pair of aerials P and P' is situated near O or O' at different heights from the ground and lies in a vertical plane which is parallel to the plane CMN. These two aerials P and P' are so arranged that the line $P\,P'$ makes an angle (α) with the vertical line $P'Z$ passing through the higher aerial P'. It will be seen that when P and P' are excited in the same phase with another ultra-high frequency (f_2) current the central fringe will substantially coincide with a plane partly shown as XX' which makes an angle (α) with the ground plane. The angle (α) is not greater than 3° and it is the desired angle of landing or glide angle. Other fringes of the second set will be confocal hyperboloids of which P and P' are foci. The line of intersection AB of the two central fringes will be the desired glide path.

Ultra-high frequency waves are utilised in this system because width of a fringe depends on the wave length and sharpness of the glide path depends on the narrowness of the fringes. The wave lengths may range between 5 to 10 metres. It may be shown that the width of any fringe increases as the distance of a point on the same fringe, from the sources increases. For the aerials O, O' the fringes will be narrowest at the points of intersection with the line O, O'. The glide path will be a channel of substantially rectangular cross-section. This cross-sectional area will be minimum when the airplane reaches the vertical plane containing O, O' and at the point B of landing it will be slightly greater than the minimum. The field strength along the glide path will increase to a maximum value when the vertical plane through O, O' is reached and it will decrease gradually until landing is effected, if the effects of earth's reflection are not considered. The glide path is surrounded by a dark region of considerable width depending on the wave lengths used. The aircraft following the glide path will receive signals from both pairs of aerials O, O' and P, P'. If the aircraft moves left, right, up or down from the glide path AB, the current in the output meter of one of the two receivers f_1 or f_2 will be zero at first and will increase when the next bright fringe is reached. Thus the system provides lateral as well as vertical guidance.

For providing position "fixes" the system uses two marker beacons having fan type radiation pattern, the beams being relatively very narrow in one vertical plane and relatively wide in the vertical plane at right angles to the first mentioned vertical plane. Each of these marker beacons uses

microwaves and cylindrical parabolic reflectors shown in Fig. 4. The wider portion of the beam of the outer beacon is parallel and coincident with the vertical plane containing the runway. The wider portion of the beam corresponding to the inner marker is as usual at right angles to said plane. These marker beacons are utilised for the identification of the central fringes.

LANDING OPERATION

When the aircraft approaches the airport, it moves round to find signals from the outer marker and identifies the central fringe corresponding to O, O'. Proceeding towards the runway it glides down to the point A' (Fig. 2) which is at predetermined height. The aircraft then follows the

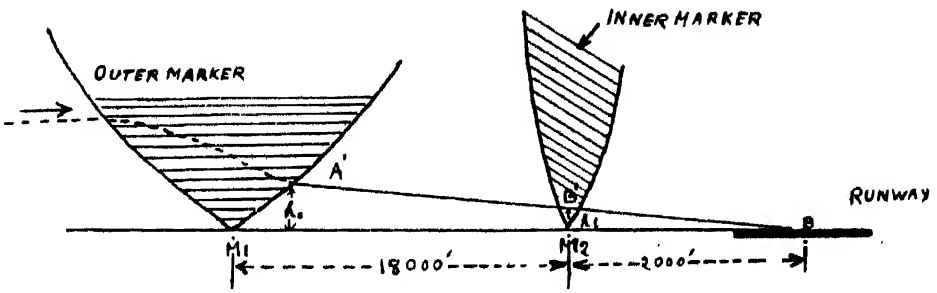

FIG. 2

straight line glide path $A'B'B$ until landing is effected. At point B' which is also at predetermined height checked by the altimeter, the aircraft crosses the inner marker. Both the points A' and B' are in the plane containing the central fringe corresponding to P P'.

ALTERNATIVE FORMS

If known type of ultra-high frequency localizer beacon is used for left right guidance, the aerials O, O' may be dispensed with. For the vertical guidance the plane containing the central fringe corresponding to P, P' will be followed by the aircraft. In this case fan-type marker beacons are arranged in the usual way, the beams being wider in planes at right angles to the plane containing the runway. The central fringe corresponding to P, P' may be identified if the aircraft glides down to predetermined heights when crossing the marker beacons.

In another modification of the system using ultra-high frequency carrier waves, the aerials O, O' transmit contemporaneously pulses of different width. A cathode ray tube receiver is used in the aircraft for identifying the central fringe corresponding to O, O'. While the aircraft is in the plane of this central fringe, the pulses from O and O' will be received at the same time and indications of the two pulses in the cathode ray tube will be superposed. When the aircraft is in any other plane the pulses will show separate indications the angular separation of the indications in the cathode ray tube

which uses circular time base circuit, depends on the angular position of the aircraft with respect to the plane of the central fringe corresponding O, O'. The aerials P, P' radiate ultra-high frequency modulated waves and the central fringe corresponding to P, P' may be identified by gliding down to pedetermined heights while crossing the marker beacons.

DISCUSSION

The ground waves consists of two components, a 'surface wave' and a 'space wave.' The surface wave moves along the surface of the earth and the space wave is the result of the direct wave and a ground reflected wave. The fringe system described so far, is formed by the space waves only. When horizontally polarised waves are used, the antenna heights may be expressed in terms of a "numerical height" q which is defined as

$$q = \frac{2\pi h}{\lambda} \left(\frac{x}{\cos b'} \right)^{\frac{1}{2}} \qquad \ldots \quad (1)$$

where h/λ = height of the antenna in wave lengths

$$x = \frac{1.8 \times 10^{12} \sigma}{f_{mc}}$$

σ = earth conductivity in e.m.u

$$b' = \tan^{-1} \frac{\epsilon - \cos^2 \psi_2}{x}$$

ψ_2 = angle of incidence of ground reflected wave with earth

f_{mc} = frequency in mega cycles

ϵ = dielectric constant of earth (taking dielectric constant of air as unity).

The space wave and surface wave will have equal intensity when the height of the receiving antenna is such that $1 < q < 2.5$. Calculation of the field strength taking into account the space wave only neglecting the surface wave will be approximately correct until the q of either the transmitting or receiving antenna is less than 1.5. For horizontally polarised waves the numerical height corresponding to a physical height is so great that, the surface wave can be neglected.

The general formula for calculating the intensity of the space wave at an elevated receiving point B produced by an elevated transmitter at A under conditions where B is above the line of sight with respect to A is

$$\text{wave}_{\text{space}} = \frac{E_0}{d} \cos^3 \psi'_1 \left[1 \pm \frac{\cos^3 \psi'_2}{\cos^3 \psi'_1} Dr \angle \rho - \theta \right]$$

$$= \frac{E_0}{d} \cos^3 \psi'_1 \left[1 + \left(\frac{\cos^3 \psi'_2}{\cos^3 \psi'_1} Dr \right)^2 \pm 2 \frac{\cos^3 \psi'_2}{\cos^3 \psi'_1} Dr \cos (\rho - \theta) \right]^{\frac{1}{2}} \qquad \ldots \quad (2)$$

where E_0 = field that would be produced at unit distance if the antenna were in the free space and the currents were the same as are actually present

$D = \dfrac{}{1+\dfrac{2h'_1h'_2}{kad\tan^3\psi'_2}}$ = a factor taking into account diverg-

ence of reflected wave produced as a result of reflection from the spherically curved surface of the earth

r= magnitude of reflection co-efficient as calculated by Eq. (3)

ρ = phase angle of reflection as calculated by Eq. (3)

$\theta = \dfrac{2\pi\, l_2 - l}{\lambda}$ = phase difference between direct and ground-reflected

waves due to differences in path

λ = wave length

$l_1 = \sqrt{d^2+(h'_1-h'_2)^2}$ = path length of direct wave

$l_2 = \sqrt{d^2+(h'_1+h'_2)^2}$ = path length of ground reflected wave

ψ'_1, ψ'_2, d, h'_1, h'_2, l_1 and l_2 are as shown in Fig. 3.

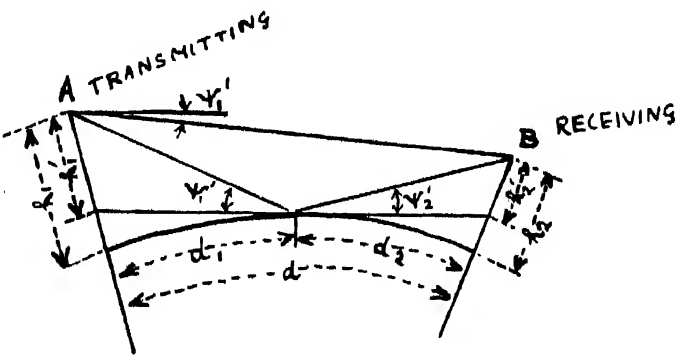

FIG. 3

For horizontally polarised waves for which ($\rho \sim 0$) the negative sign applies. The vector ratio R of reflected to incident wave is termed as reflection co-efficient and for horizontal polarisation

$$R = r\lfloor\rho = \frac{\sqrt{\epsilon'-\cos^2\psi_2}-\sin\psi_2}{\sqrt{\epsilon'-\cos^2\psi}+\sin\psi_2} \qquad (3)$$

where ψ_2 = angle of incidence

$\epsilon' = \epsilon - j\,60\,\sigma\,\lambda \times 10^{12}$

ϵ = dielectric constant of earth (air taken as unity)

σ = earth conductivity in e.m.u.

From Eq. (2) it may be shown that the ground reflected wave from any antenna, say O, will not cancel completely the corresponding direct wave, when both the transmitting and receiving antenna are several wave lengths above the ground.

While proceeding towards the runway along the glide path the resultant field strength for (O, O') and (P, P') will depend on several factors, such as

1. The distance between transmitting and receiving antenna.
2. The directivity of the transmitting antenna.
3. Interference caused by ground reflected waves.

The transmitting antenna may be Alford type (Fig. 5) which radiates

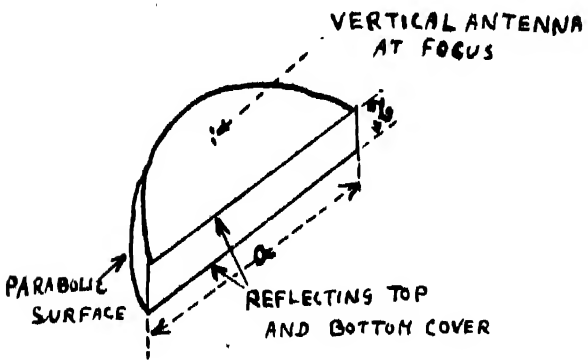

FIG. 4

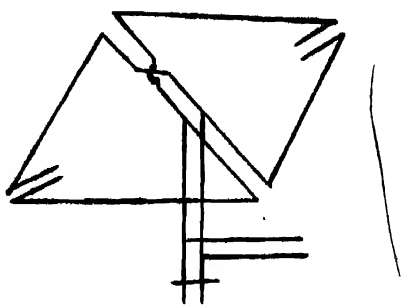

FIG. 5

only horizontally polarised waves. The aerials (O, O') are situated nearly 100 ft above the earth's surface. The aerials P and P' are situated at points which are 50′ and 200′ above the earth's surface respectively. While crossing outer marker h_o (Fg. 2) will be approximately 1000′ and for the inner marker h_i is approximately 100 ft. when the glide angle is 3°. The supporting towers for the aerials O, O', P, P' and the inner marker beacon are situated in a line perpendicular to the produced portion of the runway. Lastly, it may be mentioned that if the waves from the aerials are frequency modulated, the central fringes will be stationary while the other fringes of the two sets will oscillate in space.

ACKNOWLEDGMENTS

In conclusion, the author wishes to express his respectful thanks to Dr. H. Rakshit for his kindly interest and going through the subject matter of this paper and to Dewan Bahadur K. Rama Pai, M.A., Controller of Patents and Designs, for his encouragement and kind permission to publish this paper.

PATENT OFFICE (GOVERNMENT OF INDIA)
214, LOWER CIRCULAR ROAD,
CALCUTTA

REFERENCES

Depenning, W. F., 1942, Indian Patent Specification No. 28981.
Terman, F. E., 1942, Radio Engineer's Handbook, p. 691.

THE RELATIVE INTENSITY OF DOUBLET SPECTRA

By K. C. KAR and S. SENGUPTA

(*Received for publication, Sept. 10, 1938*)

ABSTRACT. A general wave statistical approximation method is developed for calculating the spin and relativity corrections of eigen-energy The method has also been extended to calculate the relative intensities of simple and compound doublet spectra. The intensiites thus calculated are in agreement with those obtained from the application of Burger and Dorgelo's empirical rule. Incidentally the selection rule for m_s is also obtained.

The relative intensities of simple and compound doublet lines have so far been calculated by Bechert (1930) and Saha-Banerjee (1931), using Dirac's theory. From discussions of the problem in different treatises available to us it appears that the general opinion about it is that the intensity of doublets can only be calculated from Dirac's theory which considers electron spin. It is also thought that the splitting up of Schrodinger wave-function into four eigen-functions by the non-commutative method of Dirac is necessary in these problems.

The object of the present paper is to show that the relative intensities may be very easily calculated by the wave-statistical method in which nowhere the usual commutative laws have been violated. It may be mentioned that in the wave-statistical theory we have considered the relativity and spin-orbit corrections of energy separately. It has been shown that the two corrections of eigen-energy are of the same order and are so small that the wave-functions are unchanged to a first approximation. In other words, the wave-functions are same as in the non-relativistic problem. Consequently, the question of splitting the wave function into four as in Dirac's theory, does not at all arise. The intensity has been calculated with the help of these non-relativistic wave-functions.

Before we actually go into the problem of intensity, it would be advisable to give in outline the methods of deriving Sommerfeld-Dirac's spin-relativity formula for doublet levels. Of the three methods to be given below, the second has been already discussed by one of us (Kar and Mukherjee, 1934). We shall, however, present it in the following avoiding certain approximations made previously.

It has been shown before that the frequencies of χ_1 and χ_2 waves are respectively

$$\left.\begin{aligned} \nu_1 &= \frac{2E_{kin}}{h} \\ \nu_2 &= \frac{E}{h} \end{aligned}\right\} \qquad (1)$$

It is well known in the theory of relativity that

$$E_{\text{kin}} = E_0 \left\{ \frac{1}{\sqrt{1-\beta^2}} - 1 \right\}$$

If E_{s-0} be the perturbation energy due to the spin-orbit interaction, we have

$$E - E_{s-0} - V = E_{\text{kin}}$$

where E is the total energy. On combining of the two above equations, we have after easy transformations

$$v_1 = c. \frac{\{(E - E_{s-0} + E_0 - V)^2 - E_0^2\}^{\frac{1}{2}}}{E - E_{s-0} + E_0 - V} \qquad \ldots \quad (2)$$

which is the velocity of the χ_1-wave being equal to the instantaneous velocity of the electron. Now, from (1) we have for the frequency of the χ_1-wave

$$\nu_1 = \frac{2E_{\text{kin}}}{h} = \frac{mv_1^2}{h} = \frac{1}{h} \cdot \frac{(E - E_{s-0} + E_0 - V)^2 - E_0^2}{E - E_s + E_0 - V} \qquad \ldots \quad (2.1)$$

Therefore, after eliminating time we have for the χ_1-wave equation

$$\Delta\chi_1 + \frac{1}{v_1^2} \cdot 4\pi^2 \nu_1^2 \chi_1 = 0$$

or,

$$\Delta\chi_1 + \frac{4\pi^2}{h^2 c^2}\{(E - E_{s-0} + E_0 - V)_s^2 - E_0^2\}\chi_1 = 0 \qquad \ldots \quad (2.2)$$

Again, as $p = \frac{m_0}{\sqrt{1-\beta^2}} \cdot v_1$ and the velocity of the χ_2-wave is p we have for its value (when projected in the q-space)

$$v_2 = \frac{EC}{\{(E - E_{s-0} + E_0 - V)^2 - E_0^2\}^{\frac{1}{2}}} \qquad \ldots \quad (3)$$

Hence after eliminating time we have for the χ_2-equation

$$\Delta\chi_2 + \frac{1}{v_2^2} \cdot 4\pi^2 \nu_2^2 \chi_2 = 0$$

or,

$$\Delta\chi_2 + \frac{4\pi^2}{h^2 c^2}\{(E - E_{s-0} + E_0 - V)^2 - E_0^2\}\chi_2 = 0 \qquad \ldots \quad (3.1)$$

being same as the χ_1-equation as it should be. After easy transformations, the χ-equation may be written in the form ($E_0 = m_0 c^2$)

$$\Delta\chi + \frac{8\pi^2 m_0}{h^2}\left\{E - E_{s-0} - V + \frac{1}{2m_0 c^2}(E - E_{s-0} - V)^2\right\}\chi = 0 \qquad \ldots \quad (4)$$

It is evident that if in the above equation (4) we neglect the small energy corrections E_{s-0} and $\frac{1}{2m_0 c^2}(E - E_{s-0} - V)^2$ we get the non-relativistic χ-equation. Now, in the second correction which is small because $m_0 c^2$ is

great, we may neglect E_{s-0} which is already small. Thus (4) becomes

$$\Delta\chi+\frac{8\pi^2 m_0}{h^2}\left\{E-E_{s-0}-V+\frac{1}{2m_0c^2}(E-V)^2\right\}\chi=0 \qquad (4.1)$$

in which E_{s-0} and $\frac{1}{2m_0c^2}(E-V)^2$ are obviously the spin-orbit and relativistic corrections of energy.

Frenkel (1926) and almost simultaneously Thomas (1927) have shown that in the case of spinning electron moving in an orbit one should use Lorentz transformation for a rotating axis. With this idea they find that the total relativity effect is to produce the usual relativistic change of mass and, in addition, a precession, the energy corresponding to which is

$$E_{s-0}=\frac{Ze^2}{2m_0^2c^2r^3}\ (\mathbf{LS}) \qquad (5)$$

where **L** and **S** are respectively the orbital and spin angular momenta. As E_{s-0} in (5) varies inversely as r^3 it is not possible to get a rigorous solution of (4.1). If, however, the spin is neglected Eq. (4.1) admits of a rigorous solution, as is well-known, discussed by Schrodinger for the relativistic problem.

EIGEN-ENERGY WITH SPIN AND RELATIVITY CORRECTIONS

In the following we shall adopt a perfectly general approximation-method which is admissible because the spin and relativity effects are small. The principle of the method may be stated in a nutshell as follows. At first we neglect the small spin and relativity corrections in (4.1) and obtain the approximate non-relativistic wave-function χ. With this approximate χ function we next calculate the average values of E_{s-0} and $E_r=\frac{1}{2m_0c^2}(E-V)^2$. Now, instead of their actual values we take these average values in (4.1). As the averages are constant, (4.1) can be easily solved as in the non-relativistic case and we get the eigen-energy corrected for spin and relativity.

First Mothod :—We have for the wave-statistical average of the relativistic correction of energy

$$\overline{E_r}=\frac{1}{2m_0c^2}\int\chi_1\chi_2(E-V)^2d\tau \qquad (6)$$

Because it is a correction, E within the integral in (6) should be the unperturbed eigen value of energy being equal to $-Rhc\frac{Z^2}{n^2}$ calculated non-relativistically in the usual way. After integrating with respect to θ and ϕ, we have form (6)

$$\overline{E_r}=\frac{1}{2m_0c^2}\int_0^\infty\left(E^2+\frac{2EZe^2}{r}+\frac{Z^2e^4}{r^2}\right)R^2r^2dr \qquad \ldots\ (6.1)$$

After integrating with respect to r we have

$$\bar{E}_r = \frac{E}{m_0c^2}\left(\frac{E}{2} + \frac{Z^2c^2}{an^2}\right) + \frac{Z^4e^4}{2m_0c^2a^2n^3(l+\frac{1}{2})} \quad \ldots \quad (6.2)$$

where $a = \dfrac{h^2}{4\pi^2 m_0 e^2}$. On substituting for a and E we get after easy transformations

$$\bar{E}_r = Rhc\left\{\frac{\alpha^2 Z^4}{n^3(l+\frac{1}{2})} - \frac{3}{4}\frac{\alpha^2 Z^4}{n^4}\right. \quad \ldots \quad (6.3)$$

where the fine structure constant $\alpha = \dfrac{2\pi e^2}{hc}$. In the same way we have for the average spin-orbit interacting energy (vide Eq. (5))

$$\bar{E}_{s-0} = \int \chi_1\chi_2 E_{s-0}\, d\tau = \frac{Ze^2}{2m_0^2c^2}\,(\mathbf{LS})\int \chi_1\chi_2 \frac{1}{r^3}\, d\tau \quad \ldots \quad (7$$

Because E_{s-0} is independent of θ and ϕ, integrations with respect to these co-ordinates give unity. Hence we have from (7) after θ and ϕ integrations remembering that $\dfrac{h}{(2\pi)}$ is the unit of **L** and **S**,

$$\bar{E}_{s-0} = \frac{Ze^2}{2m_0^2c^2}\left(\frac{2\pi}{h}\right)^2 (\mathbf{LS})\int \frac{R^2}{r^3}\, r^2\, dr \quad \ldots \quad (7.1)$$

The r-integral (7.1) gives the average $\overline{\dfrac{1}{r^3}}$ whose standard value is well-known. Thus we have

$$\bar{E}_{s-0} = \frac{Ze^2}{2m_0^2c^2}\left(\frac{h}{2\pi}\right)^2 (\mathbf{LS})\frac{1}{a^3}\,\frac{Z^3}{n^3(l+1)\,(l+\frac{1}{2})l} \quad \ldots \quad (7.2)$$

On substituting the value of a given before we get after transformation

$$\bar{E}_{s-0} = Rhc\;\frac{d^2Z^4}{n^3}\;\frac{(\mathbf{LS})}{l(l+1)\,(l+\frac{1}{2})} \quad \ldots \quad (7.3)$$

As the scalar product

$$(\mathbf{LS}) = \frac{(\mathbf{L}+\mathbf{S})^2 - \mathbf{L}^2 - \mathbf{S}^2}{2} = \frac{j(j+1) - l(l+1) - s(s+1)}{2}$$

$$= \frac{l}{2} \text{ for } j = l+\tfrac{1}{2}$$

$$= -\frac{l+1}{2} \text{ for } j = l-\tfrac{1}{2} \qquad \ldots \quad (7.4)$$

we have from (7.3)

$$\bar{E}_{s-0} = +Rhc.\frac{d^2Z^4}{n^3}\cdot\frac{1}{2(l+1)\,(l+\frac{1}{2})} \text{ for } j = l+\tfrac{1}{2}$$

$$= -Rhc.\frac{d^2Z^4}{n^3}\cdot\frac{1}{2l(l+\frac{1}{2})} \text{ for } j = l-\tfrac{1}{2} \qquad \ldots \quad (7.5)$$

On substituting the average values $\bar{E}_{s-0}$ and $\bar{E}_r$ in place of their actual values in (4.1) we have for the corrected discrete values of energy

$$\left.\begin{aligned} E &= -Rhc\left\{\frac{Z^2}{n^2}+\frac{\alpha^2Z^4}{n^4}\left(\frac{n}{l+1}-\frac{3}{4}\right)\right\} \text{ for } j=l+\tfrac{1}{2} \\ &= -Rhc\left\{\frac{Z^2}{n^2}+\frac{\alpha^2Z^4}{n^4}\left(\frac{n}{l}-\frac{3}{4}\right)\right\} \text{ for } j=l-\tfrac{1}{2} \end{aligned}\right\} \quad \ldots \quad (8)$$

which is the spin-relativity formula of Sommerfeld and Dirac.

Second Method.—The spin-orbit interaction energy may also be written in the form

$$E_{s-0}=\frac{V^2(\mathbf{LS})}{2m_0c^2}\cdot\frac{h^2}{4\pi^2m_0Ze^2}\cdot\frac{1}{r} \quad \ldots \quad (9)$$

remembering that $\left(\frac{h}{2\pi}\right)$ is the unit of **L** and **S** and denoting $V=\frac{Ze^2}{r}$. It has been already pointed out that as E_{s-0} involves $\frac{1}{r^3}$, the wave equation (4.1) cannot be solved by the direct method. In the previous method the difficulty was overcome by taking the wave-statistical average value. In the present method, however, we get rid of the difficulty by taking the wave-statistical instantaneous value of $\frac{1}{r}$. Thus after sub-titution of this value, E_{s-0} depends on $\frac{1}{r^2}$ and Eq. (4.1) may be rigorously solved in the usual way.

$$\chi=A_{r\theta\phi}\rho^l e^{-\frac{\rho}{2}}\,\mathbf{L}_{n+l}^{2l+1}(\rho)\,P_l^{ml}(\theta)\,e^{im_l\phi} \quad \ldots \quad (10)$$

where $\rho=\frac{2r}{r_0}$, $r_0=\frac{nh^2}{4\pi^2m_0Ze^2}$ and $A_{r\theta\Phi}$ the averaging factor for $r\rho\phi$-co-ordinates. It is evident that the phase density $\chi_1\chi_2$ generally depends on r and θ but is independent of ϕ. The instantaneous most probable value of r may be obtained from the condition

$$\frac{d}{d\rho}(\chi_1\chi_2)=0$$

$$i.e., \quad \frac{d}{d\rho}\left[\rho^{2l}e^{-\rho}\,\mathbf{L}_{n+l}^{2l+1}(\rho)\right]^2=0 \quad \ldots \quad (10.1)$$

It is not possible to get a general expression for r in a simple form, from the above condition. So we calculate its value for the special case $l=n-1$ corresponding to the classical circular orbit. It may be easily seen that for this special case

$$r=\frac{h^2}{4\pi^2m_0Ze^2}\,l(l+1)=\frac{h^2\mathbf{L}^2}{4\pi^2m_0Ze^2} \quad \ldots \quad (11)$$

on substituting the above value of r in (9) we get

$$E_{s-0}=\frac{V^2}{2E_0}\frac{(\mathbf{LS})}{\mathbf{L}^2} \qquad (12)$$

on substituting this value of E_{s-0} in the wave equation (4.1), we find

$$\Delta\chi+\frac{8\pi^2 m_0}{h^2}(E-V)\chi+\frac{4\pi^2}{h^2c^2}(E-V)\chi^2-\frac{4\pi^2}{h^2c^2}V^2\frac{(\mathbf{LS})}{\mathbf{L}}\chi=0 \quad \ldots \quad (13)$$

The solution of the above equation obtained in the usual way is

$$\chi=R(r)\,P_l^{ml}(\theta)\,e^{im\varphi} \qquad \ldots \quad (13.1)$$

where the $R-$equation is

$$\frac{d^2R}{dr^2}+\frac{2}{r}\frac{dR}{dr}+\left(A+2\frac{B}{r}+\frac{C}{r^2}\right)R=0 \qquad \ldots \quad (13.2)$$

in which

$$A=\frac{8\pi m_0}{h^2}\left(E+\frac{E^2}{2m_0c^2}\right),\quad B=\frac{4\pi^2 m_0 Ze^2}{h^2}\left(1+\frac{E}{m_0c^2}\right)$$

and

$$C=-l(l+1)+\alpha^2Z^2-\alpha^2Z^2\frac{(\mathbf{LS})}{\mathbf{L}^2}=-\gamma(\gamma+1) \qquad \ldots \quad (13.3)$$

It should be noted that $E\ll m_0c^2$; so the second terms in the values of A and B are the relativity corrections. In the value of C given in (13.3), the second term is the relativity correction while the third term is the correction for spin. On proceeding as in the ordinary Kepler problem remembering that we have to take γ in place of l we find

$$-\frac{B^2}{A}=(n_r+\gamma+1)^2=\frac{m_0c^2\alpha^2Z^2}{2E}\cdot\frac{\left(1+\dfrac{E}{m_0c^2}\right)^2}{1+\dfrac{E}{2m_0c^2}} \qquad \ldots \quad (13.4)$$

on transforming (13.1) we get

$$1+\frac{E}{m_0c^2}=\left\{1+\frac{\alpha^2Z^2}{(n_r+\gamma+1)^2}\right\}^{-\frac{1}{2}} \qquad \ldots \quad (13.5)$$

in which the value of γ may be easily calculated from (13.3) and we have

$$\gamma=\sqrt{(l+\tfrac{1}{2})^2-\alpha^2Z^2+\alpha^2Z^2\frac{(\mathbf{LS})}{\mathbf{L}^2}}-\tfrac{1}{2} \qquad \ldots \quad (13.6)$$

on substituting the above value of γ in (13.5) and after approximations, remembering that the relativity and spin corrections are small, we get

$$E=-Rhc\left\{\frac{Z^2}{n^2}+\frac{\alpha^2Z^4}{n^4}\left(\frac{n}{l+\frac{1}{2}}-\frac{3}{4}\right)-\frac{\alpha^2Z^4}{n^3}\frac{(\mathbf{LS})}{\mathbf{L}^2(l+\frac{1}{2})}\right. \qquad \ldots \quad (14)$$

on remembering that $\mathbf{L}^2=l(l+1)$ and using the value of $(\mathbf{LS})$ for $j=l-\frac{1}{2}$ and $j=l-\frac{1}{2}$ given in (7.4), we at once get the spin-relativity formula of Sommerfeld-Dirac given in (8).

Third method :—This method has been used by Condon and Shortly p. 1935). The wave equation has been taken with only the relativity correction. The mean value of the spin-orbit interaction energy has been calculated as in the first method with the non-relativistic wave-function. Thus the method may be considered as a combination of the two methods already discussed. Accordingly it is unnecessary to discuss it here in detail.

Wave-function for a spinning electron moving in Kepler-orbit.

It has been found, in deducing the relativity and spin corrections of eigen energy that the wave function for the Kepler motion is not materially affected by these energy corrections. Therefore, to a first approximation the wave-function is given as in the non-relativistic case by Eq (10).

There is, however, another effect of spin which cannot be neglected. Even if we ignore for the moment the orbital motions, the spinning motions of the electrons remain. And we have an assembly of electron rotators. The wave-function for the rotators is given by

$$\chi'_{m_s} = \Lambda_{\theta'\phi'} P^{m_s}_{s}(\theta') e^{im_s\phi'} \tag{15}$$

where $s=\frac{1}{2}$, $m_s=-\frac{1}{2}$.

It should be noted that the spin coordinates θ', ϕ' in (15) are different from the orbital coordinates θ, ϕ in (10), the origin in the former case being the centre of the electron while that for the latter the nucleus. The orbital energy is only slightly affected by the spin-orbit interaction while the spin energy E_s if practically unaltered by the orbital motion. Thus the two motions and so the corresponding wavefunctions are approximately independent of each other. Consequently, from the law of joint probability we have for the total wave-function

$$\chi_{nlm_l m_s} : \chi_{nlm_l} \chi'_{m_s} \tag{16}$$

For a spinning electron moving in a Kepler orbit. It may be mentioned that the splitting of the electronic motion into two parts as above is somewhat similar to the case of resolution of a general motion into irrotational and rotational motions.

Now, before passing on to other aspects of the problem we should note some of the special features of the wave function taken in (15) ; we have assumed $\frac{1}{2}$-integral value for m_s. Accordingly the wave-function is double valued. Even then the probability given by the product $(\chi'_1)_{m_s}(\chi'_2)_{m_s}$ is single valued as it should be from physical considerations. Thus there is no objection to our taking $m_s=\pm\frac{1}{2}$. On the other hand, the fact that the spin moment is $\frac{1}{2}$ in all directions would suggest that the wave-function

cannot be one valued but should be double valued. From this point of view it follows that the orbital wave-function (10) should be on the other hand single valued and m_l should have different whole number values for different directions given by the condition $m_l \geq l$. Again a direct consequence of our taking half-harmonic values for m_s is that the Legendre functions in (15) should assume either of the forms $P_{\frac{1}{2}}^{\frac{1}{2}}(\theta')$ and $P_{\frac{1}{2}}^{-\frac{1}{2}}(\theta')$ as taken in problems on the scattering of spinning electrons.

PRINCIPLE OF EVALUATING THE INTENSITY OF DOUBLET SPECTRA

The wave statistical value of the charge density for the nth state is given by

$$\rho_n = e\chi_1^n \chi_2^n . e^{\frac{4\pi i}{h} E_k^n i n t} e^{\frac{2\pi i}{h} E^n t}$$

Since the phase waves are stationary we may always drop the time factor in any phase integral taken over the whole phase space.

Thus, for example,

$$\int \rho_n d\tau = e \int \chi_1^n \chi_2^n d\tau = e$$

For mn-transition, the phase density and the corresponding electric moments are

$$\rho_{mn} = e\chi_1^m \chi_2^n e^{\frac{2\pi i E_m}{h} t} e^{\frac{4\pi i E_k^n}{h}}$$

$$M_{mn} = e \int q\chi_1^m \chi_2^n e^{\frac{2\pi i E_m}{h} t} e^{\frac{4\pi i E_k^n}{h}} d\tau$$

$$= e\, e^{\frac{2\pi i}{h}(E_m - E_n)t} \int q\chi_1^m \chi_2^n d\tau \qquad \ldots \quad (17)$$

on dropping the time factor for reasons given above.

Or, $$M_{mn} = e . e^{2\pi i \nu_{mn} t} \int q\chi_1^m \chi_2^n d\tau \qquad \ldots \quad (17.1)$$

which is the wave statistical value of the electric moment.

Now, it has been proved by the electro-magnetic theory that the intensity of radiation emitted is proportional to $\ddot{M}_{mn}^2$. From (17.1) it follows that,

$$\ddot{M}_{mn}^2 = \nu_{mn}^4 M_{mn}^2 \qquad \ldots \quad (18)$$

where it should be noted that ν_{mn} is practically constant for different doublets. Therefore the doublet insensity is proportional to M_{mn}^2.

It can be easily shown that $M_{mm} = 0$ and $M_{nn} = 0$ showing that the electric charge is symmetrially distributed from the wave-statistical point of view,

at the stationary states. But for an allowed transition $M_{mn} \neq 0$ showing that the charge distribution is not symmetrical. Thus both at the initial and final states the distributions are symmetrical while during the transition it is asymmetrical. Consequently there would be a violent wave-statistical oscillation of the electric charges on transition thereby causing a radiation to be emitted or absorbed as the case may be.

CALCULATION OF THE RELATIVE INTENSITIES OF DOUBLETS

From the foregoing discussion it is evident that the problem of calculating the relative intensities of doublets reduces itself to the problem of finding the corresponding transition moments. In calculating the transition moments we shall have to use of course the non-relativistic wave function $\chi_{nl m_l m_s}$ given in (16). As, however, the wave function is $(2l+1)-$ and $(2s+1)-$ fold degenerate with respect to m_l and m_s respectively, we must take the sum of all these transitions in order to get the total moment for a given doublet line. Now, in taking this sum, we should note that l and s are coupled and that because of the half harmonic value of s, $m_s = \pm \frac{1}{2}$ in all directions. Consequently $m_s = \pm \frac{1}{2}$ in the direction of m_l. Thus although the orbital co-ordinates r, θ, ϕ are different from the spin co-ordinates θ', ϕ', $m = m_l + m_s = m_l \pm \frac{1}{2}$ would represent the total moment in case of spin. Again, it is evident that because $m_s = \pm \frac{1}{2}$, for two values of m_l, namely, $m_l = m_l$ and $m_l = m_l + 1$, m will have the same value and will represent the same coupled state. Thus the wave function for this state determined by n, l, j, m may be written in the form

$$\chi_{nljm} = A\chi_{nlm_l\frac{1}{2}} + B\chi_{nlm_l+1\frac{1}{2}} \quad \ldots \quad (19)$$

$$= A\chi_{nlm_l=m-\frac{1}{2},\frac{1}{2}} + B\chi_{nlm_l=m+\frac{1}{2},-\frac{1}{2}} \quad \ldots \quad (19.1)$$

Therefore to evaluate the total moment one must use the wave functions $\chi_{n\,l\,jm}$ summed for all values of m between the limits $+j$ to $-j$. Before proceeding to find the transition moment we have to determine the weight factors A and B for a given coupled state, *i.e.*, for a given m. This may be done in the following way. From the averaging condition, *viz.*,

$$\int (\chi_1)_{n\,l\,jm}(\chi_2)_{n\,l\,jm} d\tau = 1$$

we get,

$$A^2 + B^2 = 1 \quad \ldots \quad (20)$$

Now there will arise two cases according as $j = l + \frac{1}{2}$ or $j = l - \frac{1}{2}$. We shall consider them separately.

Case I: $j = l + \frac{1}{2}$. It is evident that for $m = l + \frac{1}{2}$, m_l may have values l or $l+1$. Because the maximum value of m_l cannot exceed l, the second value $l+1$ must be rejected. So in this case the second wave-function in (19.1)

does not exist. And we have from the averaging condition (20)

$$A^2=1 \quad \text{and so} \quad B^2=0 \qquad \ldots \quad (20,1)$$

Similarly it may be shown that for $m=-(l+\frac{1}{2})$ the first function in (19.1) does not exist. Hence we have from (20)

$$B^2=1 \quad \text{and so} \quad A^2=0 \qquad \ldots \quad (20.2)$$

It also follows from the limiting conditions (20.1) and (20.2) that A^2 and B^2 are functions of m.

We tentatively take them to be the simplest linear functions. So we write,

$$\left.\begin{aligned} A^2&=a_1m+b_1\\ B^2&=a_2m+b_2 \end{aligned}\right\}$$

On adding the two equations in (21) we have at once

$$1=(a_1+a_2)m+(b_1+b_2) \qquad \ldots \quad (21.1)$$

Hence,

$$\left.\begin{aligned} a_1+a_2&=0\\ b_1+b_2&=1 \end{aligned}\right\} \qquad \ldots \quad (21.2)$$

On using the relations (21.2) and the limiting conditions (20.1) and (20.2) we find,

$$\left.\begin{aligned} A^2=1&=a_1(l+\tfrac{1}{2})+b_1\\ B^2=1&=a_1(l+\tfrac{1}{2})+1-b_1 \end{aligned}\right\} \qquad (21.3)$$

On solving the two equations in (21.3) for a_1 and b_1, we get

$$a_1=\frac{1}{2l+1}, \quad b_1=\tfrac{1}{2} \qquad (21.4)$$

Hence from (21)

$$A^2=\frac{l+m+\frac{1}{2}}{2l+1}$$

$$B^2=\frac{l-m+\frac{1}{2}}{2l+1} \qquad (22)$$

Case II : $j=l-\frac{1}{2}$. In this case the maximum possible values of m are $\pm(l-\frac{1}{2})$. Hence for $m=\pm(l+\frac{1}{2})$ the wave function χ_{nljm} should vanish. However on looking back to (19.1) we find that the wave-function $\chi_{nlm_l=m+\frac{1}{2},\frac{1}{2}}$ actually vanishes for $m=l+\frac{1}{2}$, since in this case $m_l=l+1$. So B is unknown. The wave-function $\chi_{nlm_l=m-\frac{1}{2},\frac{1}{2}}$ on the other hand does not vanish since in this case $m_l=l$ for $m=l+\frac{1}{2}$. Therefore, in order that χ_{nljm} may be zero, we must have,

$$A=0 \text{ and so from (20) } B=1 \qquad \ldots \quad (23)$$

Similarly it may be proved that for $m=-(l+\frac{1}{2})$ we have,

$$B=0 \text{ and so from (20) } A=1$$

Thus corresponding to (21.3) we have in this case

$$\left.\begin{aligned} A^2=0&=a_1(l+\tfrac{1}{2})+b_1 \\ B^2=0&=a_1(l+\tfrac{1}{2})+1-b_1 \end{aligned}\right\} \quad \ldots \quad (23.2)$$

On solving we have corresponding to (21.4)

$$a_1=-\frac{1}{2l+1}, \quad b_1=\tfrac{1}{2} \quad \ldots \quad (23)$$

With these values we have from (21)

$$\left.\begin{aligned} A^2&=\frac{l-m+\frac{1}{2}}{2l+1} \\ B^2&=\frac{l+m+\frac{1}{2}}{2l+1} \end{aligned}\right\} \quad \ldots \quad (24)$$

It should be noted that the values of A^2 and B^2 are interchanged in the two cases. Now the signs of A and B may be + or −. It is, however, immaterial whether both are taken with + or − sign. So we are to find out whether both A and B will have the same or different signs. This question may be settled from the orthogonal property

$$\int \chi_{nlj=l+\frac{1}{2},m}\chi_{nlj=l-\frac{1}{2},m}\,d\tau=0 \qquad (25)$$

which gives

$$A_{l+\frac{1}{2}}A_{l-\frac{1}{2}}+B_{l+\frac{1}{2}}B_{l-\frac{1}{2}}=0 \qquad (25.1)$$

Because from (22) and (24) we have,

$$A_{l+\frac{1}{2}}=B_{l-\frac{1}{2}}$$
$$A_{l-\frac{1}{2}}=B_{l+\frac{1}{2}}$$

we at once find from (25.1) that if for Case I, the two terms in (19.1) are taken with the same sign, then for Case II the two terms must have opposite sign or *vice versa*. Thus we have for $j=l+\frac{1}{2}$

$$\chi_{nljm}=\sqrt{\frac{l+m+1}{2l+1}}\;\chi_{nlm_1=m-\frac{1}{2},\frac{1}{2}}+\sqrt{\frac{l-m+\frac{1}{2}}{2l+1}}\;\chi_{nlm_1=m+\frac{1}{2},-\frac{1}{2}} \qquad (26)$$

and for $j=l-\frac{1}{2}$

$$\chi_{nljm}=\sqrt{\frac{l-m+\frac{1}{2}}{2l+1}}\;\chi_{nlm_1=m-\frac{1}{2}}-\sqrt{\frac{l+m+\frac{1}{2}}{2l+1}}\;\chi_{nlm_1=m+\frac{1}{2},\frac{1}{2}} \qquad (27)$$

With these wave functions for a given coupled state m for the two cases $j=l+\frac{1}{2}$ and $j=l-\frac{1}{2}$, we next proceed to calculate the relative intensities for the doublet lines resulting from a transition $nl\rightarrow n'l'$.

Now because both the initial and final levels are doublets with $j=l\pm\frac{1}{2}$ and $j'=l'\pm\frac{1}{2}$, it follows that in general there will be altogether four lines from the possible transitions. It is well known that unless the selection rule for l is satisfied, the transition moment *i. e.*, the intensity must always vanish. So we have to consider transitions for which $l'=l+1$ or $l-1$. In the following we consider the case for which $l'=l-1$.

Thus the four transitions are,

$$\begin{aligned}
&(1)\quad nlj=l+\tfrac{1}{2} \rightarrow n'l'j'=l'+\tfrac{1}{2}\\
&(2)\quad nlj=l+\tfrac{1}{2} \rightarrow n'l'j'=l'-\tfrac{1}{2}\\
&(3)\quad nlj=l-\tfrac{1}{2} \rightarrow n'l'j'=l'+\tfrac{1}{2}\\
&(4)\quad nlj=l-\tfrac{1}{2} \rightarrow n'l'j'=l'-\tfrac{1}{2}
\end{aligned}$$

Because $l'=l-1$, the changes of j, *i.e.* Δj in the four transitions are respectively $-1, -2, 0$ and -1.

(1) The wave function for the initial state for a given m value is given by {vide Eqs. (16) and (26)}

$$\chi_{nlj=l+\frac{1}{2},\,m}=\sqrt{\frac{l+m+\frac{1}{2}}{2l+1}}\;\chi_{nlm_l=m-\frac{1}{2}}.\chi'_{+\frac{1}{2}}$$

$$+\sqrt{\frac{l-m+\frac{1}{2}}{2l+1}}\;\chi_{nlm_l=m+\frac{1}{2}}.\chi'_{-\frac{1}{2}} \qquad \ldots\quad (28)$$

The wave function for the final state for a given m' value is obtained by putting simply dashed quantum numbers for the undashed in (28) and we have

$$\chi_{n'l'j'=l'-\frac{1}{2},m'}\equiv\chi_{n'l'=l,j'=l-\frac{1}{2},m'}=\sqrt{\frac{l+m'-\frac{1}{2}}{2l-1}}\chi_{n'l=l,m'_l=m'-\frac{1}{2}}.\chi'_{=\frac{1}{2}}$$

$$+\sqrt{\frac{l-m'-\frac{1}{2}}{2l-1}}\;\chi_{n'l=l,m'_l=\frac{1}{2}}.\chi'_{=\frac{1}{2}} \qquad \ldots\quad (29)$$

Now because the wave functions in (28) and (29) depend on five co-ordinates, namely, γ, θ, ϕ and θ', ϕ', we shall have to take the generalised transition moments given by

$$\left.\begin{aligned}
M_x&=e\int(x+x')\chi_{nlj=l+\frac{1}{2},m}\chi_{n'l-1,j'=l-\frac{1}{2},m'}d\tau\\
M_y&=e\int(y+y')\chi_{nlj=l+\frac{1}{2},m}\chi_{n'l-1,j'=l-\frac{1}{2},m'}d\tau\\
M_z&=e\int(z+z')\chi_{nlj=l+\frac{1}{2},m}\chi_{n'l-1,j'=l-\frac{1}{2},m'}d\tau
\end{aligned}\right\} \qquad \ldots\quad (30)$$

where x, x'...etc. are taken parallel in order to avoid unnessary complications.

It is apparent that the generalised transition moment is the sum of the orbital transition moment and the spin transition moment. The $x-$component of the latter is,

$$e\int x'\chi_{nlj=l+\frac{1}{2},m}\chi_{n'l=l,j'=l-\frac{1}{2},m'}d\tau$$

From (28) and (29) it is obvious that the above integral may be taken as the sum of products of a number of orbital and spin integrals in which the spin integrals vanish either through ϕ' or θ' integration. Thus (30) reduces only to the orbital transition moment. Now, in calculating it with the help of the wave functions given in (28) and (29) we shall have altogether four terms, of which the cross terms will vanish through the spin integral (ϕ'). For the remaining terms the spin integrals are obviously unity. It should be noted that the condition for non-vanishing of the spin-integral (ϕ') is

$$\Delta m'_s = 0 \qquad \ldots \quad (31)$$

This gives the selection rule for m_s.

Now, because $m = m_l + m_s$ and $\Delta m_s = 0$, we must have always

$$\Delta m = \Delta m_l \qquad \ldots \quad (31.1)$$

which means that the selection rules of m and m_l are identical. Thus $M_z = M_y \neq 0$ if $\Delta m = \pm 1$ and $M_z \neq 0$ if $\Delta m = 0$. Here we have for M_x and M_y after ϕ-integration for the case $\Delta m = -1$

$$M_x = M_y = \tfrac{1}{2}\frac{\sqrt{(l+m+\frac{1}{2})(l+m-\frac{3}{2})}}{4l^2-1} R_{nl;n'l-1}\int_0^\pi P_l^{m-\frac{1}{2}} P_{l-1}^{m-3/2}\sin^2\theta d\theta$$

$$+\tfrac{1}{2}\frac{\sqrt{l-m+\frac{1}{2})(l-m+\frac{1}{2})}}{4l^2-1} R_{nl;n'l-1}\int_0^\pi P_l^{m+\frac{1}{2}} P_{l-1}^{m-\frac{1}{2}}\sin^2\theta d\theta$$

in which the averaging factors for γ and θ co-ordinates are included in the respective functions. On integrating with respect to θ using the well known relation

$$\sin\theta\, P_l^{m_l} = -\sqrt{\frac{(l+m_l+1)(l+m_l+2)}{(2l+1)(2l+3)}} P_{l+1}^{m_l+1} + \sqrt{\frac{(l-m_l)(l-m_l-1)}{4l^2-1}} P_{l-1}^{m_l+1}$$

$$= \sqrt{\frac{(l-m_l+1)(l-m_l+2)}{(2l+1)(2l+3)}} P_{l+1}^{m_l-1} - \sqrt{\frac{(l+m_l)(l+m_l-1)}{4l^2-1}} P_{l-1}^{m_l-1}$$

We find after easy transformations, remembering that $j = l + \frac{1}{2}$,

$$M_x = M_y = -\frac{\sqrt{(j+m)(j+m-1)}}{2(2l+1)} R_{nl;n'l-1} \qquad \ldots \quad (32)$$

Similarly it may be shown that for $\Delta m = +1$ we have

$$M_x = M_y = \frac{\sqrt{(j-m)(j-m-1)}}{2(2l+1)} R_{nl;n'l-1} \qquad \ldots \quad (32.1)$$

Thus on squaring and adding (32) and (32.1) we have for $\Delta m = \pm 1$

$$M_x^2 = M_y^2 = \frac{j(j-1)+m^2}{2(2l+1)^2} R^2_{nl;n'l-1} \quad \ldots \quad (32.2)$$

Similarly we have for the Z−component after ϕ integration

$$M_z = \sqrt{\frac{(l+m+\frac{1}{2})(l+m-\frac{1}{2})}{4l^2-1}} R_{nl;n'l-1} \int_0^{\pi} P_l^{m-\frac{1}{2}} P_{l-1}^{m-\frac{1}{2}} \sin\theta\cos\theta\, d\theta$$

$$+ \sqrt{\frac{(l-m+\frac{1}{2})(l-m-\frac{1}{2})}{4l^2-1}} R_{nl;n'l-1} \int_0^{\pi} P_l^{m+\frac{1}{2}} P_{l-1}^{m-\frac{1}{2}} \sin\theta\cos\theta\, d\theta \quad \ldots \quad (33)$$

On integrating with respect to θ using the well known transformation formula

$$\cos\theta\, P_l^{m_l} + \sqrt{\frac{(l-m_l+1)(l+m_l+1)}{(2l+1)(2l+3)}} P_{l+1}^{m_l} + \sqrt{\frac{(l-m_l)(l+m_l)}{4l^2-1}} P_{l-1}^{m_l}$$

we get after easy transformations, remembering that $j = l + \frac{1}{2}$

$$M_z = \frac{\sqrt{j^2-m^2}}{2l+1} R_{nl;n'l-1} \quad \ldots \quad (33.1)$$

On squaring the components and adding, we get M^2_m for a particular value of m. The total moment is obtained from the relation $M^2 = \sum_{-j}^{+j} M^2_m$. Thus we have from (32.2) and (33.1)

$$M^2 = \sum_{-j}^{+j} M_m^2 = \frac{2l(l+1)(2l-1)}{4l^2-1} R^2_{nl;n'l-1} \quad \ldots \quad (34)$$

giving the intensity of the line $nlj = l + \frac{1}{2} \rightarrow n'l'j' = l' + \frac{1}{2}\ (l' = l-1)$. Here $\Delta j = -1$.

(2) In this case the wave function for the initial state for a particular m value is given by (28). The wave function for the final state for a particular m' value is, however, given by {vide Eqs. (16) and (27)}

$$\chi_{n'l'j'=l'-\frac{1}{2},m'} \equiv \chi_{n'l-1,j'=l-3/2,m'} = \sqrt{\frac{l-m'-\frac{1}{2}}{2l-1}} \chi_{n'l-1,m'_l=m'-\frac{1}{2}} \cdot \chi'_{+\frac{1}{2}}$$

$$- \sqrt{\frac{l+m'-\frac{1}{2}}{2l-1}} \chi_{n'l-1,m'_l=m'+\frac{1}{2}} \cdot \chi'_{-\frac{1}{2}} \quad \ldots \quad (35)$$

On calculating the moments as before using the wave functions given in (28) and (35), we get

$$M_x = M_y = M_z = 0$$

Thus it follows that for the transition $nlj = l + \frac{1}{2} \rightarrow n'l'j' = l' - \frac{1}{2}\ (l' = l-1)$ the resultant intensity vanishes. In other words the transition for which $\Delta j = -2$ is forbidden. It should be noted that this selection rule for j is a secondary effect, being based on the fundamental selection rules for l, m_l and m_s associated with the wave functions.

(3) In this case the wave function for the initial state for a particular m value is given by (*vide* (16) and (27))

$$\chi_{nlj=l-\frac{1}{2},\,m}=\sqrt{\frac{l-m+\frac{1}{2}}{2l+1}}\,\chi_{nlm_l=m-\frac{1}{2}}\chi'_{+\frac{1}{2}}-\sqrt{\frac{l+m+\frac{1}{2}}{2l+1}}\,\chi_{nlm_l=m+\frac{1}{2}}\cdot\chi'_{-\frac{1}{2}} \quad \ldots \quad (36)$$

The wave function for the final state for a given m' value is given by (29).

On calculating the moments as before using the above wave functions, we find

$$M_x=M_y=\sqrt{\frac{2j(j+1)-2m^2}{4l^2-1}}\,R_{nl;n'l-1} \quad \ldots \quad (37)$$

and

$$M_z=\frac{2m}{4l^2-1}\,R_{nl;n'l-1} \quad \ldots \quad (38)$$

Hence we get for the total moment after summing for m between $+j$ and $-j$

$$M^2=\frac{2l}{4l^2-1}\,R^2_{nl;n'l-1} \quad \ldots \quad (39)$$

giving the intensity of the line $nlj=l-\frac{1}{2}\rightarrow n'l'j'=l'+\frac{1}{2}$ $(l'=l-1)$.

In this case $\Delta j=0$.

The wave functions for the initial and final states are already given in (36) and (35) respectively. On calculating the moments as before using the above wave functions, we find

$$M_x{}^2=M_y{}^2=\frac{j(j-1)+m^2}{2(2l-1)^2}\,R^2_{nl;n'l-1} \quad \ldots \quad (40)$$

and

$$M_z{}^2=\frac{j^2-m^2}{(2l-1)^2}\,R^2_{nl;n'l-1} \quad \ldots \quad (41)$$

Hence we have for the total moment

$$M^2=\frac{2l(l-1)\,(2l+1)}{4l^2-1}\,R^2_{nl;n'l-1} \quad \ldots \quad (42)$$

giving the intensity of the line $nlj=l-\frac{1}{2}\rightarrow n'l'j'=l'-\frac{1}{2}$ $(l'=l-1)$.

In this case $\Delta j=-l$.

In (34), (39) and (42) we have obtained general expressions for the intensities of the three lines resulting from the transition $nl\rightarrow n'l-1$. Their relative intensities are evidently given by

$$(l+1)\,(2l-1)\,:\,1\,:\,(l-1)\,(2l+1) \quad \ldots \quad (43)$$

being independent of n and n'.

Special Cases

Before concluding we shall consider a few interesting special cases. Let us first consider the case of a simple doublet $^2P-{}^2S$. In this case $b=1$. So from (43) the relative intensities are given by

$$2\,:\,1\,:\,0 \quad \ldots \quad (43.1)$$

Showing that here we have only two lines, *viz.*, $^2S_{\frac{1}{2}} \rightarrow {}^2P_{3/2}$ and $^2S_{\frac{1}{2}} \rightarrow {}^2P_{\frac{1}{2}}$. Next we consider the case of the compound doublet $^2D - {}^2P$. In this case $l=2$. So from (43) the relative intensities are given by,

$$^2D_{5/2} \rightarrow {}^2P_{3/2} : {}^2D_{3/2} \rightarrow {}^2P_{3/2} : {}^2D_{3/2} \rightarrow {}^2P_{\frac{1}{2}} = 9 : 1 : 5 \qquad (43.2)$$

Similarly it may be shown that for the compound doublet $^2F - {}^2D$, the relative intensities of the three lines are given by ($l=3$)

$$20 : 1 : 14 \qquad (43.3)$$

The ratios thus obtained are in perfect agreement with those obtained from the application of Burger and Dorgelo's empirical rule.

ACKNOWLEDGMENT

In conclusion the junior author expresses his indebtedness to the Government of West Bengal for awarding him a scholarship and fecilities.

PHYSICAL LABORATORY
PRESIDENCY COLLEGE.

REFERENCES

Bechert 1930, *Ann.der Phys.* **6**, 700.
Condon and Shortley, 1935, Theory of Atomic Spectra, Camb. Univ.
Frenkel, 1926, *Zeit. f. Phys.* **37**, 243.
Kar, K.C. and Mukherjee, K.K. 1934, *Phil. Mag.* **17**, 993.
Saha, M.N. and Banerjee, A.C. 1931, *Zeit. f. Phys.* **68**, 704.
Thomas, L.H. 1926, *Nature.* **117**, 514.
,, 1927, *Phil Mag.* **8**. 1.

ULTRAVIOLET BANDS OF THE ZINC IODIDE MOLECULE. PART III

By C. RAMASASTRY

(*Received for publication, Aug. 23, 1948*)

Plate II

ABSTRACT. A new group of bands (designated as system D_1) of the zinc iodide molecule, lying in the region λ2990–λ2700, is recorded and analysed, isotopic component heads due to $Zn^{64}I^{127}$, $Zn^{66}I^{127}$, and $Zn^{68}I^{127}$ are well resolved and appear conspicuously. The vibrational numbering of the various bands is derived from considerations of the observed isotope shifts. The constants calculated for the D_1 system are :

$$\omega_e' = 80.0 \quad x_e'\omega_e' = 1.25$$

$$\nu_e = 39911.4 \quad \omega_e'' = 220.1 \quad x_e''\omega_e'' = 0.825$$

Predissociation is observed in the upper state at the vibrational level $v' = 2$.

Six characteristic continua, observed in the emission spectrum of ZnI, are also reported for the first time.

A discussion is presented giving a correlation of the electronic configuration and molecular states of the zinc iodide molecule with the observed band systems.

INTRODUCTION

In a recent communication, the author (Ramasastry 1948) described the vibrational structure of a band system of zinc iodide, designated as system E, lying in the region λ2450 to λ2250. Mention was also made of another system, designated as D_1, extending from λ2715 to λ2990, which appeared to have the same general characteristic features as the system E, such as the zinc isotopic heads and predissociaton. The elucidation of the vibrational analysis of this new system and a general consideration of the electronic transitions of the zinc iodide molecule form the subject of this paper.

This new system D_1 is photographed under the same experimental conditions as that employed for obtaining system E and are described fully in the earlier contribution. The general continuum, which obliterated the essential band systems themselves, was the main source of difficulty in photographing the bands. This was reduced to a minimum in order to secure the maximum contrast for the band heads, by adjusting the conditions such as the slit width, exposure time, etc., to an optimum value.

As the existence of this system was not even mentioned by any of the previous investigators, care was taken to get additional evidence from the

experimental view point before ascribing it to the zinc iodide molecule. The spectrum was excited using three different samples of zinc iodide reported to be of high degree of purity and obtained from (1) Burgoyne Burbridges & Co., (2) British Drug Houses, and (3) prepared by the author from pure *a. r.* chemicals. Identical spectra were obtained in all cases. Comparison was also made with other known band systems. The conclusion that the emitter of this system must be zinc iodide molecule was finally confirmed by the study of the vibrational structure of the system.

ANALYSIS

The more refrangible end of the band system (below λ2815) consists of a number of distinct and isolate groups, each group comprising of three bands. But considerable overlapping occurs only in the region above λ2815. The three bands in each group are of successively decreasing intensity, the more refrangible head being the weakest (Plate II). These groups give at first the impression of clear sequences but both the intensity distribution and the variation of wave-number intervals between the bands do not support this point of view ; if they are to be considered as sequences the sequence degradation will have to be in a direction opposite to that of the individual bands in the system. Nor can the three heads in each group be regarded as components of a triplet state, for the molecule of zinc iodide gives rise to electronic states of even multiplicity. The only possibility of interpretation is to ascribe the three components to the isotopic molecules $Zn^{64}I^{127}$, $Zn^{66}I^{127}$, $Zn^{68}I^{127}$.

When the most intense bands, taken one from each of these successive groups, are arranged in a row, the wave-number intervals show a regular diminution as we pass from the short to the long wavelength end of the system. They are hence considered as members of a progression of the lower state of the molecule. But the order of magnitude of the interval, equal to 193 cm^{-1}. *i. e.* of $\Delta G''(v'')$ is too small compared to the ground state frequency of 224.5 cm^{-1}. of the zinc iodide molecule, as determined from previously published analysis of the other characteristic band systems of the zinc iodide molecule (Ramasastry, 1948). In spite of this, it is considered that the lower state of this system is the ground state itself and that very large v'' values are assignable to the bands, as this would be in keeping with the large magnitude of the isotopic shifts (about 30 cm^{-1}. for $Zn^{66}I^{127}$) observed in these groups.

A second progression could be started with the band at λ2787.2 as its first member and extended towards longer wavelengths. A third progression commenced at λ2824.5 and could be similarly extended. The vibrational scheme is shown in Table I.

ZINC IODIDE BANDS (SYSTEM D_1')

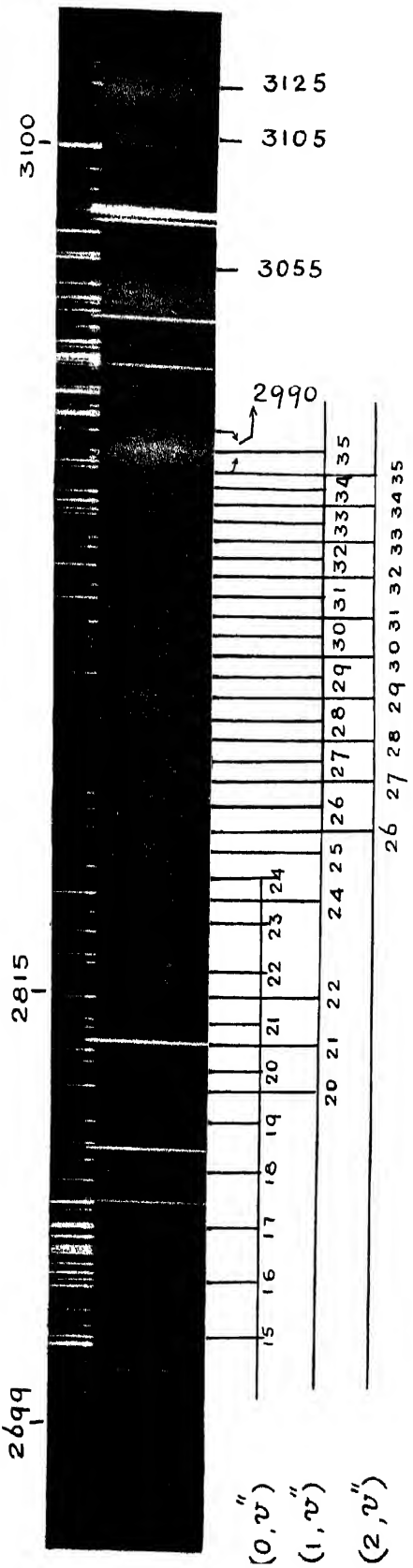

The constants of the upper state are $\omega_e' = 80.0$ and $x_e'\omega_e' = 1.25$. Predissociation is evident at $v'' = 2$, as no bands are observed with higher values of v'.

Some difficulty was experienced regarding the v'' numbering of the band heads ; the following procedure is adopted for arriving at these values. The vibrational constants for the lower state of this system are taken as $\omega_e'' = 224.5$ and $x_e''\omega_e'' = 0.875$, which represent the mean values of the constants of the common lower state of the C and E systems of ZnI. A tentative and approximate value of v'' is to be assigned to the first band at $\nu = 36736.3$ in order to give the difference of 193.1 and obtained as

$$\frac{224.5 - 193.1}{1.75} \approx 18$$

i. e. values of v'' of the order of 18 must be assigned to the bands of this system. The final v'' numbering is derived with the help of the isotopic displacements. The isotopic shifts are calculated for the bands with various (v', v'') values using the above quoted constants and the appropriate mass factors given below :

for $Zn^{66}I^{127}$ $\quad (\rho - 1) = -0.01$ and $\quad \rho^2 - 1 = -0.02$

for $Zn^{68}I^{127}$ $\quad (\rho - 1) = -0.02$ and $\quad (\rho^2 - 1) = -0.04$

It is noticed that the agreement between the observed and calculated shifts is close if the quantum number 15 is assigned for the v'' value of the band at $\nu = 36736.3$. Table I gives the vibrational numbering that is finally adopted and Table II shows the observed and calculated isotopic displacements.

CALCULATION OF ν_e

The value of ν_e calculated from the first six bands (0,15) to (0,20) of the $(0,v'')$ progression using the constants $\omega_e'' = 224.5$, $x_e''\omega_e'' = 0,875$, $\omega_e' = 80$ and $x_e'\omega_e' = 1.25$ does not give a constant ; the disagreement between the different values is not sporadic but a systematic increase of about 4.4 cm.$^{-1}$ for an increase in the v'' number by unity is found. This variation can be corrected only by reducing the ω_e'' value by 4.4 units. With this change in ω_e'' (*i.e.* from 224.5 to 220.1) and the remaining constants as given above, ν_e is obtained as 39911.4 from the six bands which alone could be claimed to have been measured accurately. It should be noted that this determination of ν_e involves a large extrapolation.

If $\omega_e'' = 220.1$ is adopted, the estimated isotope shifts would be changed but the magnitude of this change is not found to be high. It is approximately 0.6 cm.$^{-1}$ for the (0,20) band, which are well within observational errors. Hence the vibrational numbering of the bands needs no alteration.

The following formula :—

$$\nu = 39911.4 + (80.0u' - 1.25u'^2) - (220.1u'' - 0.875u''^2)$$

represents correctly only the bands between $v'' = 15$ and $v'' = 20$.

TABLE I

Vibrational Scheme of ZnI bands – System D_1

v'' \ v'	0		1		2	$\Delta G''(v'')$
15	36736.3 193.1					193.1
16	36543.2 190.8					190.8
17	36352.4 189.5					189.5
18	36162.9 188.2					188.2
19	35974.7 186.7					186.7
20	35788.0 181.2	79	35867 181			181.1
21	35606.8 180.8	79	35686 181			180.9
22	35426 181	79	35505			181,0
23	35245 172		—		35395 170	171.0
24	35073	73	35146 166	79	35225	166.0
25			34980 173		—	173.0
26			34807 163	78	34885 160	161.5
27			34644 167	81	34725 170	168.5
28			34477 162	78	34555 160	161.0
29			34315 159	80	34395 163	161.0
30			34156 153	76	34232 155	154.0
31			34003 144	74	34077 147	145.5
32			33859 147	71	33930 143	145 0
33			33712 131	75	33787 142	136.5
34			33581 135	64	33645 134	134.5
35			33446	65	33511	
$\Delta G'(v')$		77.5		75		

TABLE II

Isotope shifts for $Zn^{66}\ I^{127}$ and $Zn^{68}\ I^{127}$ *w.r.t.* $Zn^{64}\ I^{127}$

All shifts are positive

v'' \ v'	0		1		2	
	Obs.	Cal.	Obs.	Cal.	Obs.	Cal.
15	—	—				
	—	—				
16	31.8	32.0				
	72.0	64.0				
17	34.8	33.7				
	69.1	67.4				
18	35.6	35.3				
	73.1	70.6				
19	34.2	37 0				
	69.8	74 0				
20	37.0	38.5				
	78.5	77.0	32.9	37.3		
			79.3	74.6		
21	38.0	40.1				
	79.0	80.2	38.0	38.9		
			77.0	77.8		
22	—	41.8	—			
	79.0	82.6	—	40.1		
				80.2		
23	—	43.1	—			
	85.0	86.2	—	42.3	—	41.5
				84.6	88.0	83.0
24	—		50 0			
	—		—	43.7	—	42.9
				87.4	—	85.8
25			42.0			
			—	44.9	—	44 1
				89.8	—	88.2
26			47.0			
			—	46.4	—	45.6
				92.8	—	91.2
27						
			—	47.7	43.0	46.9
			—	95.4	—	93.8
28			48.0			
			—	49.1	—	48.3
				98.2	66.0	96.6
29			49.0			
			—	50.4	44.0	49.6
				100.8	—	99.2
30						
			—	51.8	51.0	51.0
			—	103.6	—	102.0
31						
			49.0	53.1	—	52.3
			—	106.2	—	104.6
32						
			42.0	54.5	46.0	53.7
			—	109.0	—	107.4
33						
			47.0	55.8	57.0	55.0
			—	111.6	114.0	110.0
34						
			—	57.2	40.0	56.4
			—	114.4	—	112.8
35						
			—	58.5	—	57.7
			—	117.0	—	115.4

A suitable formula for the remaining bands is not feasible as the discrepancies in the $\Delta G''(v'')$ values may be either inherent or arise partly from errors in micrometer settings. A single formula for the entire band system could not obviously be obtained. This is considered as a peculiarity of the system due to a variation in the ground state frequency ω_e'' giving rise to irregularities in the spacing of the vibrational levels of the ground state. Discontinuities of this kind occur between $v''=23$ and $v''=24$ and also at some point or points between $v''=24$ and $v''=35$. The first of these at least is considered definite.

A complete catalogue of the band head measurements as well as the vibrational and isotopic assignments are given in Table III. The wavelength values are the mean of three measurements made on two different medium quartz spectrograms. The bands were also photographed on the Hilger Littrow quartz instrument but no measurements were possible because of the superposition of OH band at 2811A and the overlying general continuum which became prominent due to the long exposure time of about four hours.

ELECTRON CONFIGURATION AND MOLECULAR STATES OF ZnI

In this section, the nature of the electron states involved in the emission of the band spectrum of the zinc iodide molecule is discussed. The entire emission spectrum comprises of the following discrete band systems and continua :—

1. The long wave-length end commences with a continuum at about λ 6100, which rises to a peak intensity at about λ 6000 and gradually fades off towards shorter wave-lengths.

2. The visible bands (system *B*) occur in the region λ6000 to λ3500. These are observable both in H. F. emission and fluorescence. Due to overlapping, the system is partly masked by the continuum referred to above.

3. Another continuum extends from λ 3425 to λ 3390.

4. The Wieland system (system *C*) extends from λ3392.6 to λ3257.8. The continuum mentioned in (3) lies just at the red end of this system. The (0, 0) band of this system is distinctly observed to be consisting of two component heads.

5. The brief system (system *D*) reported by P. Tiruvenganna Rao and K. R. Rao (1946) consisting of about five pairs of diffuse bands between λ3277.7 and λ3193.5.

6. A continuum between λ3055 to λ3040.

7. At the violet end of this continuum, referred to in (6) occurs the system D_1 discussed in this paper extending from λ2989 to λ2715.2. The vibrational levels above $v'=2$ are absent.

8. Somewhat narrow continua are observed with their intensity maxima at about λ3125, λ3105 and λ2990. The first two are superposed on the OH band and the third on the system D_1.

TABLE III

Bands of the Zinc Iodide molecule, System D_1

Wave-length	Int.	Wave-number	Assignment (v', v'') Zn Isotope
2715.24	1*D*	36818.3	— —
2721.30	1	36736.3	(0,15) 64
2727.24	2	36656.3	— —
2730.30	2	36615.2	68
2733.30	2	36575.0	66
2735.08	3	36543.2	(0,16) 64
2744.82	1	36421.5	68
2747 41	2	36387.2	66
2750.04	3	36352.4	(0,17) 64
2758.87	1	36236.0	68
2761.73	2	36198.5	66
2764.45	4	36162.9	(0,18) 64
2768.41	1	36111.2	— —
2773 53	1	36044.5	68
2776.27	2	36008.9	66
2778 91	3	35974.7	(0,19) 64
2781.15	1	35945.8	68
2783.96	1	35909.4	66
2787.29	2	35866.5	(1,20) 64 and (0,20) 68
2790.53	1	35825.0	66
2793.41	2	35788.0	(0,20) 64
2795.4	2	35763	68
2798.4	1	35724	66
2801.4		35686	(1,21) 64 and (0,21) 68
2804.6	2	55645	66
2807.6	3	35607	(0,21) 64
2815.7	4	35505	(1,22) 64 and (0,22) 68
2817.4	4	35483	(2,23) 68
2821.9	5	35426	(0,22) 64
2824.5	1d	35395	(2,23) 64
2826.6	2d	35368	— —
2829.6	1	35330	68
2836.5	2	35245	(0,23) 64
2838.1	1	35225	(2,24) 64
2840.4	1	35196	— —
2844.4	2	35146	(1,24) 64

TABLE III (*contd.*)

Wavelength	Int.	Wavenumber	Assignment (v', v'') Zn Isotope
2847.9	1	35103	— —
2850.3	3	35073	(0,24) 64
2854.5	1	35022	66
2857.9	3	34980	(1,25) 64
2865.7	3*D*	34885	(2,26) 64
2868.3	2	34854	66
2872.2	4	34807	(1,26) 64
2873.7	2	34788	— —
2875.4	1	34768	66
2878.9	3	34725	(2,27) 64
2885.7	2	34644	(1,27) 64
2887.6	1	34621	— —
2893.1	3	34555	(2,28) 64
2895.7	2	34525	66
2899.4	2*D*	34477	(1,28) 64
2902.9	2*D*	34439	66
2906.3	3	34395	(2,29) 64
2909.2	1	34364	66
2911.8	1	34335	— —
2913.3	2	34315	(1,29) 64
2916.1	2	34283	66
2920.4	1*D*	34232	(2,30) 64
2926.9	3	34156	(1,30) 64
2933.7	3	34077	(2,31) 64
2935.8	2	34052	66
2940.1	2	34003	(1,31) 64
2942.4	2	33976	66
2946.4	4	33930	(2,32) 64
2948.9	1	33901	(2,33) 68
2952.6	4	33859	(1,32) 64
2953.9	1	33844	(2,33) 66
2958.8	2	33787	(2,33) 64
2961.4	2	33759	66
2963.3	2	33736	—
2965.4	3	33712	(1,33) 64
2967.8	2	33685	—
2971.4	4	33645	(2,34) 64
2977.0	3	33581	(1,34) 64
2983.2	5	33511	(2,35) 64
2989.0	6	33446	(1,35) 64

9. The system E, from λ2450 to λ2250, was analysed by the author previously. There is an impression of a general continuum overlapping the less refrangible bands of this system and the bands corresponding to v' quantum numbers higher than 2 are diffuse.

If the molecule Zn I is formed from zinc and iodine atoms both taken in their normal states, the possible electronic states are $^2\Sigma^+$ and $^2\pi$ (Mulliken, 1932)

$$4s^2\,{}^1S_g(Zn) + 5s^2 5p^5\,{}^2P_u(I) \longrightarrow {}^2\Sigma^+ \text{ and } {}^2\pi(ZnI)$$

As the lowest electronic states of a molecule are usually those that dissociate into normal atoms, these $^2\Sigma^+$ and $^2\pi$ states may be considered to be the low levels of the ZnI molecule. Taking the electronic configuration of the normal zinc iodide molecule as

$$[1s^2 2s^2 2p^6 3s^2 5p^6 3d^{10} 4s^2(Zn)] + [1s^2 2s^2 2p^6 3s^2 3p^6 3d^{10} 4s^2 4p^6 4d^{10} 5s^2 5p^5(I)]$$
$$\longrightarrow KLM\ KLMN\ (z\sigma)^2(Y\sigma)^2(W\pi)^4(x\sigma)^1,\ {}^2\Sigma^+$$
$$\text{or briefly,}\quad \sigma^2\sigma^2\pi^4\sigma,\ {}^2\Sigma^+$$

we obtain $^2\Sigma^+$ as the normal state of the molecule. This may be identified with the $^2\Sigma^+$ state derived by combining a normal zinc atom with a normal iodine atom. The second state $^2\pi$ resulting from the same normal atoms may correspond to the electronic configuration

$$\sigma^2\sigma^2\pi^3\sigma^2,\ {}^2\Pi_i$$

of the molecule. This inverted $^2\pi$ will also be one of the low lying states and it may be expected to be nearer to $^2\Sigma^+$ (with the same dissociation products, *i.e.*, the normal atoms of zinc and iodine) than any other electronic state of the molecule. The first band system may be expected to be due to the transition

$$\sigma^2\sigma^2\pi^3\sigma^2,\ {}^2\pi_i \qquad \sigma^2\sigma^2\pi^4\sigma,\ {}^2\Sigma^+$$

No such system seems to have been observed as yet in this or any other similar halide molecules. It may be that the energy of the transition is low and the corresponding bands appear only in the infra-red, for, successive electron orbits of a molecule, as in the case of an atom, become closer together as the molecule gets heavier and in ZnI the two states may be very near each other. Or, our failure to detect the bands of the above transition may be due to the fact that the $^2\pi_i$ is a repulsive state. The latter is more probable as it is in agreement with the general observation that the potential energy curves of about half or more than half of the molecular states derived from two atoms in specified states are either repulsive or form shallow minima at very large internuclear distance (Mulliken, 1932). Further, if most of the binding strength is attributed to the π^4 group of electrons, the change of electron configuration from $\pi^4\sigma$ to $\pi^3\sigma^2$ may have made the molecule unstable *i.e.*, the potential energy curve repulsive. Hence the electronic state

$$\sigma^2\sigma^2\pi^3\sigma^2,\ {}^2\Pi_i$$

may be a repulsive one, lying close to and having the same dissociation products as the state $\sigma^2\sigma^2\pi^4\sigma$, $^2\Sigma^+$, the normal state of the ZnI molecule. On this view, it is expected that every transition into the lowest ground state

$^2\Sigma^+$ might be accompanied also by the transition into the repulsive $^2\Pi_i$ state, whereas the former gives rise to discrete bands, the latter (if the selection rules permit) gives a continuum at or in the proximity of the long wavelength end of the discrete bands. This continuum may be well defined having a peak intensity or may spread over a certain wavelength region depending on the type of the P. E. curve of the $^2\Pi_i$ state. Observation of the band spectra has actually shown the existence of such continua; the emission continua mentioned in (1), (3), (6) and (9) above may have this repulsive $^2\Pi_i$ level as their final states.

System *B* lies in the least refrangible end of the band spectrum of ZnI (as is the case in the other halides) and consists of red degraded bands. The analysis of these bands is far from complete, except in the case of HgCl for which Wieland (1941) has obtained the vibrational constants in which ω'_e is less than ω''_e. The appearance of these bands in the case of all the molecules indicates a similarity of transition. As the bands are not double-headed, the transition may, in all probability, be $^2\Sigma^+ - {}^2\Sigma^+$. The electron configuration, $\sigma^2\sigma\pi^4\sigma^2$, gives rise to $^2\Sigma^+$ state which will also be one of low energy. The upper state of the visible bands may hence be identified with this $^2\Sigma^+$. Change of an electron from an inner σ to an outer σ orbit is consistent, as was shown by Howell (1942) in the HgCl bands, with the expected diminution in the vibrational frequency of a red-degraded band system. This $^2\Sigma^+$ and other excited states of the molecule should be those derived from the zinc and iodine atoms with one or the other or both of them in their excited atomic states. If the iodine atom is taken in the excited condition the energy will be too high to account for the low ν_e of the known ZnI band systems in the near ultra-violet. On the other hand, the zinc atom in its first excited state and normal iodine will give rise to six doublet and six quartet molecular states thus

$$4s4p^3P_u(Zn) + 5s^25p^{5\,2}P_u(I) \rightarrow {}^2\Sigma^+(2),\ {}^2\Sigma^-,\ {}^2\pi(2) \text{ and } {}^2\Delta.$$

Not all these states can give rise to discrete band systems. The doublet levels alone may be considered as the transition probabilities from quartet states to the $^2\Sigma^+$ ground state are small. The levels $^2\Sigma^-$ and $^2\Delta$ are not expected to combine with the ground level (selection rules). Of the remaining four levels, two can perhaps be definitely identified as follows. One of the two Σ^+ levels may correspond to the upper state of the visible bands discussed in the above paragraph. The molecule in this state should therefore dissociate into $^3P(Zn)$ and $^2P(I)$. Verification is possible only after an analysis of these bands is obtained.

The upper levels of the systems *C* and *D* are interpreted as components of a $^2\Pi$ state and the systems themselves occur in the vicinity of the resonance line $^1S - {}^3P$ of zinc. This state may well be one of the expected $^2\Pi$ states referred to above and can be represented thus in terms of the electronic configuration,

$$\sigma^2\sigma^2\pi^4\sigma^0\pi,\ {}^2\Pi_r$$

the products of dissociation being $^3P(Zn)$ and $^2P(I)$. The two remaining states $^2\Sigma^+$ and $^2\Pi$ are prabably repulsive and may account for the emission continua at $\lambda 3125$ and $\lambda 3105$.

Before assigning electron configurations to the upper states of these continua, the nature of the electron orbits of the configuration, $\sigma^2\sigma^2\pi^4\sigma$ as regards their bonding, anti-bonding and non-bonding capacity will be discussed. By comparison of the ground state frequencies of beryllium oxide (12 electrons) and beryllium fluoride (13 electrons) and their electron configurations,

BeO $KK\sigma^2\sigma^2\pi^4$, $^1\Sigma$ ground state ($\omega_e'' = 1487 cm^{-1}$.)
BeF $KK\sigma^2\sigma^2\pi^4\sigma$, $^2\Sigma$ ground state ($\omega_e'' = 1266 cm^{-1}$.)

Howell (1943) pointed out that the addition of an electron to BeO to form BeF results in a reduction in ω_e value, thereby indicating that the added electron has a definite anti-bonding tendency. A similar comparison is made in the table below in the case of the halides of Cu, and GaZn in which each halide of a metal has one electron more than the corresponding halide of the preceding metal.

Ground state ω_e values

Metal	Suggested electron configuration of the halides	Fluoride	Chloride	Bromide	Iodide
Copper	$\sigma^2\sigma^2\pi^4$, $^1\Sigma$	620.59	417.02	314.10	265.13
Zinc	$\sigma^2\sigma^2\pi^4\sigma$, $^2\Sigma$	≈ 620	390.5	~ 312*	224.5
Gallium	$\sigma^2\sigma^2\pi^4\sigma^2$, $^1\Sigma$	—	365.0	263.0	216.4

The ω_e values in each column show a decrease from copper to gallium. This indicates, in the light of the suggested electron configurations, that both the outer σ electrons have got a slight anti-bonding effect, in agreement with Howell's inference from the considerations of BeO and BeF. But the smallness of the magnitude of diminution of ωe with the addition of each electron in this case shows that for the heavier diatomic molecules, the ground state frequency is mostly determined by the heaviness (resultant mass) of the molecule and relatively insensitive to changes in electron configuration, as was pointed out by Howell (1943).

Again from considerations of vibrational frequencies of normal and excited states of BeO alone,

$\sigma^2\sigma^2\pi^4$, $^1\Sigma$ $\omega_e = 1487$
$\sigma^2\sigma^2\pi^3\sigma$, $^1\pi$ $= 1128$ (difference 359)
$\sigma^2\sigma\pi^4\sigma$, $^1\Sigma$ $= 1371$
$\sigma^2\sigma\pi^3\sigma^2$, $^1\pi$ $= 1006$ (difference 365)

Howell (1943) has shown that most of the molecular binding is due to the π^4 group and the removal of an electron from this group reduces the vibrational frequency considerably. As was pointed out earlier in this paper, $\sigma^2\sigma^2\pi^3\sigma^2$, $^2\Pi_i$, of ZnI was considered as a repulsive state giving rise to emission

* from author's unpublished results.

continua on the long wave-length side of the origins of the various systems of discrete bands, *i.e.* while the presence of an incomplete π shell in the electron configuration has only resulted in a large reduction of ω_e value in the case of BeO, it has given rise to a repulsive molecular state with its P.E. curve showing only a tendency to form an unpronounced minimum in the case of the comparatively heavier molecule ZnI. It may therefore be expected that the excited states of the continua of ZnI at $\lambda 3125$, $\lambda 3105$ and $\lambda 2990$ should have an incomplete π shell (or π^3 group) in their configurations.

All the nine molecular states

$$^2\Sigma^+, ^2\Sigma^-, ^2\Delta, ^4\Sigma^+, ^2\Sigma^+, ^4\Sigma^-, ^2\Sigma^-, ^4\Delta, \text{ and } ^2\Delta$$

arising from the electron configuration, $\sigma^2\sigma^2\pi^3\sigma\pi$ may be taken as repulsive, if we attribute all the binding strength in the molecule to the π^4 group of electrons; the last π is definitely a very slightly bonding or atomic orbital as it is due to ^{3}P(Zn) atom (ω_e' slightly greater than ω_e'' for *C* system) and the σ is known to be slightly anti-bonding from a comparison of the ground state vibrational frequencies and electron configurations of the iodides of Cu, Zn and Ga. Also, from the considerations of the energies of the transitions, all these repulsive states should lie slightly to the violet side of the origin ($\lambda 3319.4$) of the *C* system. Of these only the two $^2\Sigma^+$ states are expected to give rise to continua by transition to the $^2\Sigma^+$ ground state of the molecule.

The systems D_1 and *E* may next be considered. Unlike the other systems, these two show strong predissociation. There is experimental evidence then of four moreenergy levels of the molecule which are yet to be identified—the upper states of D_1 and *E* and the predissociating levels. Normal zinc (^{1}S state) and iodine in the ^{4}P state give rise only to two molecular states

$$4s^2\ ^1s\ (\text{Zn}) + 6s\ ^4\text{P}\ (\text{I}) \longrightarrow {}^2\Sigma, {}^4\Sigma\ (\text{ZnI})$$

while excited zinc in the ^{1}P state and normal iodine (^{2}P state) yield six molecular levels, thus

$$^1\text{Pu(Zn)} + {}^2\text{Pu(I)} \rightarrow {}^2\Sigma^+(\text{Z}),\ {}^2\Sigma^-,\ {}^2\pi(\text{Z}) \text{ and } {}^2\Delta(\text{ZnI})$$

of which, as in the case of ^{3}Pu (Zn) + ^{2}Pu(I), only four levels need be taken. From the ν_e values of the band systems in this and other halides, it would seem that the levels $^2\Sigma^+$ and $^2\Pi$ of the latter combination correspond to the upper states of the D_1 and *E* systems respectively of ZnI. There would then be correspondence between these on the one hand (derived from the ^{1}P state of Zn) and the upper states of systems *B* and systems *C* and *D* on the other, derived from ^{3}P state of Zn. The proximity of the *E* system to the $^1\text{P} - {}^1\text{S}$ line of Zn and the occurrence of the D_1 system to the long wavelength side of the *E* system are consistent with this view. It must, however, be pointed out that the expected second component of system *E* has not been found and that there is not much evidence for considering the system *E* as due to a transition $^2\Pi - {}^2\Sigma$.

TABLE IV

Band system of zinc iodide molecule

System designation.	Region.	Brief description of bands.	ν_e	ω_e'	$x_e'\omega_e'$	ω_e''	$x_e''\omega_e''$	Reference
E	2252—2458	About 135 red-degraded bands with prominent isotopic component heads due to zinc isotopes 64, 65 and 68; predissociation at $v'=2$ in the upper state; (0,0) band not recorded.	44114.5	142.5	3.0	225.6	1.0	Ramasastry (1948)
D_1	2715—2990	About 80 bands with the same appearance as in system e; predissociation at $v'=2$; bands with $v''=0$ to 14 are not measurable.	39911.4	80.0	1.25	224.5	0.875	Present work.
D	3193—3278	About four pairs of diffuse bands.	30506.3	211.7	2.5	~220	...	Tiruvenganna Rao and K. R. Rao (1946).
C	3257—3393	A number of closely spaced violet degraded intense bands appearing as discrete sequences with the (0,0) band as strongest isotopic heads due to zinc 64 and 66 are observed.	30117.6	248.2	0.7	223.4	0.75	Wieland (1929).
B	3560—6000	bands appear as line-like; probably red-degraded; masked by a strong general continuum.	Not yet analysed					Wieland (1929), Oeser (1935), and present work.

The electron configurations of the upper states of the different systems may be given as below.

$\sigma^2\sigma\pi^4(x\sigma^2), {}^2\Sigma \longrightarrow$ System B

$\sigma^2\sigma^2\pi^4(x\sigma)^0\,(v\pi)^1, {}^2\pi_r \longrightarrow$ Systems C and D

$\sigma^2\sigma^2\pi^4(x\sigma)^0(v\pi)^0(u\sigma)^1, {}^2\Sigma \longrightarrow$ System D_1

$\sigma^2\sigma^2\pi^4(x\sigma)^0(v\pi)^0(u\sigma)^0(t\pi)^1, {}^2\pi_r \longrightarrow$ System E

Such an assignment is consistent with the changes in the vibrational frequencies of the upper states of the systems relative to that of the ground state as can be seen from Table IV. Unlike the $(v\pi)$ orbit, which is slightly bonding in ZnI and slightly antibonding in ZnCl and ZnF, the $(t\pi)$ orbit is highly antibonding, and $(u\sigma)$ still more anti-bonding than $(x\sigma)$.

Identification of the levels giving rise to predissociation in systems D_1 and E is difficult. They may be the two unassigned levels derived from $^1P(Zn)$ and $^2P(I)$. Such an assumption does not violate Kronig's selection rules with respect to such states.

In conclusion, a diagramatic representation of the different energy states and the suggested electron configurations is given in Fig. 1 and the constants associated with them are collected in Table IV.

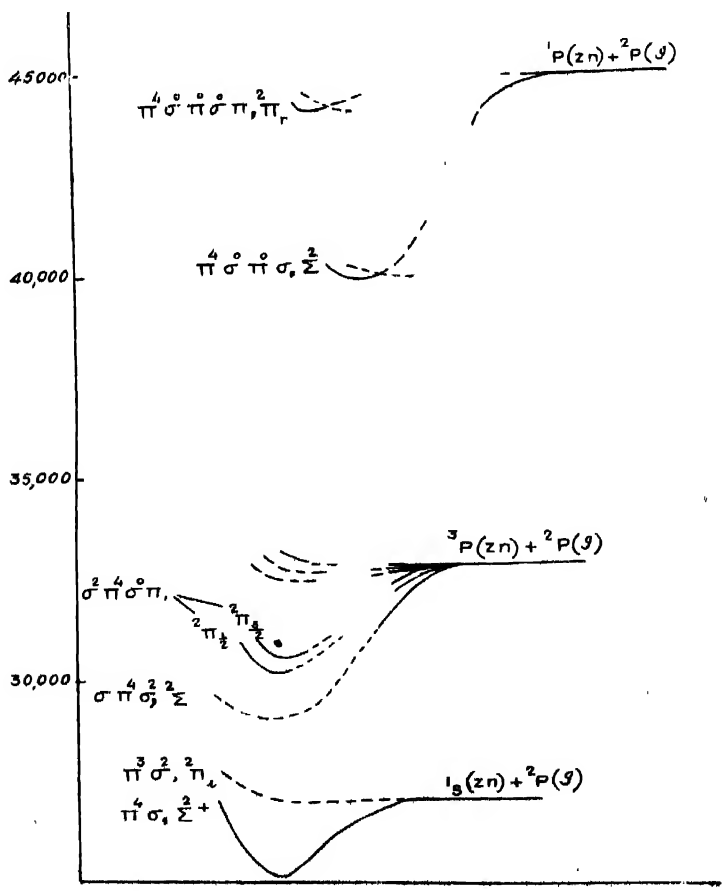

FIG. 1

ACKNOWLEDGMENT

The author considers it a great privilege to work under the inspiring guidance of Prof. K. R. Rao who also suggested the problem and it is with great pleasure that he records his sincere thanks to him.

DEPARTMENT OF PHYSICS,
ANDHRA UNIVERSITY, WALTAIR

REFERENCES

Howell (1943), *Proc. Roy. Soc.*, **182**, 95.
Oeser (1935), *Zeit. F. Phys* , **95**, 699.
Mulliken (1932), *Rev. Mod. Phys.*, **4** 90.
Ramasastry (1948), *Ind. Jour. Phys* , **22**, 119.
Tiruvenganna Rao and K. R. Rao (1946), *Ind. Jour. Phys.*, **20**, 49,
Wieland (1929), *Helv. Phys. Acta.*, **2**, 46 and 77.

7—1712P—1

ON THE GEIGER-NUTTALL RELATIONSHIP*

By SUKUMAR BISWAS

(*Received for publication, Nov. 27, 1948*)

ABSTRACT. It is shown in the present work that the Geiger-Nuttall relationship is more satisfactory and refined when the log λ, E curve is plotted for isotopes having the same atomic number Z. From the theoretical study of α-emission it has been shown that only points, referring to nuclei having the same atomic number, fall on a continuous curve. Even in this case there appears to be some deviation of the actual curve from the theoretical one on both ends (for nuclei having shortest and longest lives). The experimental data of all α-active nuclei have been systematically studied and the modified Geiger-Nuttall curves have been drawn for all elements from Bi to Pu. The α and β stability considerations are used to predict the probable α or β activities as yet unknown. Some of the nuclei suspected of weak α-activity are UX_1^{234}, $Ms'ThI^{228}$ and UY^{231}.

INTRODUCTION

The Geiger-Nuttall relation, $\log \lambda = a + bE$, which was first obtained from empirical data has played a very fundamental part in the understanding of nuclear phenomena. It was the basis of Gamow's famous work on the escape of α-particle through potential barriers.

The latest position of this famous relation is given in Gamow's "Structure of Atomic Nuclei," p. 86. As given there, the ($\log \lambda$, E) curve for three radioactive series is not a continuous one but it is shown to consist of three distinct ones corresponding to the U, AcU and Th series. Even the curve for a single series, *e.g.*, for Ac is not continuous. When these curves were compiled the half-lives and energies of some of the products particularly the extremely short-lived and extremely long-lived ones were not very accurately known. But recently much more data on these points have been obtained and the series have been prolonged and it appears advisable to re-examine the whole question. The present work has been undertaken with the point in view.

Recently Berthellot (1942) suggested that the points on the Geiger-Nuttall diagram ($\log \lambda$, E curve) fall on a continuous line if the data belong to nuclei having the same charge number Z. This has been verified by Broda and Feather (1947) in case of Po and led to the interesting discovery that RaE, well-known for its β-activity is also slightly α-active. The ratio of α-activity to β-activity is found as $\sim 10^{-7}$ to 1.

* Communicated by Prof. M. N. Saha.

THEORETICAL BACKGROUND

The object of the present work is to examine critically whether the Geiger-Nuttall curve, log λ against E, is a smooth one only when α-active isotopes of the same atomic number are plotted. Let us now interpret the above assumption of constancy of atomic number Z, in Geiger-Nuttall law from theoretical point of view.

The phenomenon of spontaneous α-radioactivity was first explained by Gamow (1929) and Condon and Gurney (1929) who calculated the transmission factor of the potential barrier by the application of wave-mechanical method. Since then a large number of investigators have attacked this problem assuming different types of potential field in the nucleus. These results differ in the method of attack and the degree of accuracy of the results, but the main term in the transmission factor is the same as given by Gamow.

The disintegration constant λ is calculated from the transparency of the potential barrier either by the semi-classical argument by Laue (1929) or by the assumption of complex eigen-values as is done by Gamow (1937). The form of the potential barrier is assumed to be an inverse square field up to a distance r_0 and a rectangular hole of potential U for distance less than r_0. The transparency factor, calculated by Saha (1944) and Laue's semi-classical arguments yield the relation :

$$\lambda = \frac{v}{r_0} e^{-2k} \qquad \ldots \quad (1)$$

where v = velocity of the α-particle

r_0 = radius of the nucleus $Z-2$.

$$2K = \frac{16\pi e^2(Z-2)}{hv}(u_0 - \sin u_0 \cos u_0)$$

$$u_0 = \cos^{-1}\left[\frac{mv^2 r_0}{4e^2(Z-2)}\right]^{\frac{1}{2}}$$

Using the complex eigen function method, the following relations are obtained between λ and E, for $l=0$ (Preston, 1947)

$$\mu = -\tan u_0 \tan(\mu k r_0) \qquad \ldots \quad (2)$$

$$\lambda = \frac{2v}{r_0}\frac{\mu^2 \tan u_0}{\mu^2 + \tan^2 u_0} e^{-2k} \qquad \ldots \quad (3)$$

where $\mu = (1 - U/E_a)^{\frac{1}{2}}$, $k = \frac{2\pi mv}{h}$

It can be easily seen that if we have $U=0$, $\mu=1$, the equation (3) reduces to

$$\lambda = \frac{v}{r_0} \sin 2u_0 . e^{-2k} \qquad \ldots \quad (4)$$

This expression has been used by Sexl (1933). Thus three expressions for λ are available.

$$\lambda = \frac{v}{r_0} e^{-2k}$$

$$\lambda = \frac{v}{r_0} \sin 2u_0 . e^{-2k}$$

$$\lambda = \frac{2v}{r_0} \cdot \frac{\mu^2 \tan u_0}{\mu^2 + \tan^2 u_0} e^{-2k}$$

The factors $\sin 2u_0$, $\frac{2\mu^2 \tan u_0}{\mu^2 + \tan^2 u_0}$ are of the order of unity. The value of λ changes so rapidly with small adjustments in the value of the constant r_0 in e^{-2k} that the multiplying factor is not of much consequence.

In these calculations the effect of relative motion of the $Z-2$ nucleus is to be taken into account. So we are to use total energy $E = E_\alpha \left(1 + \frac{m_\alpha}{m_r}\right)$, relative velocity of α-particle $v = v_\alpha \left(1 + \frac{m_\alpha}{m_r}\right)$ and reduced mass $m = \frac{m\, m_r}{m_\alpha + m_r}$ in place of E_α, v_α and m_α respectively.

Using the first formula, (1),

$$\log_{10}\lambda = \log_{10} v - \log_{10} r_0 - \cdot 4343\gamma [u_0 - \sin u_0 \cos u_0] \qquad \ldots \quad (5)$$

where $$\gamma = \frac{16\pi e^2 (Z-2)}{hv},$$

$$\log \gamma = 9\cdot 2476 + \log (Z-2) - \log v$$

$$u_0 = \cos^{-1} \left\{ \frac{mv^2/2}{2e^2(Z-2)/r_0} \right\}^{\frac{1}{2}}$$

$$2 \log \cos u_0 = 6.8549 - .4343 \frac{m_\alpha}{m_r} + \log r_0 + 2 \log v - \log (Z-2)$$

From relation (5), we see that $\log \lambda$ depends not only on the velocity of the ejected α-particle but also on the atomic number $(Z-2)$ and the nuclear radius r_0. So in general case it can not be represented in a two dimensional graph. The curve, $\log \lambda$ against E, is approximately valid if $(Z-2)$ is kept constant since the variation of r_0 is small from one isotope to other ones. The nuclear radius r_0 may be assumed to vary as the cube root of mass number of the nucleus.

The reason why Geiger-Nuttall could get a more or less smooth curve by plotting $\log \lambda$ against E, is, as pointed out by Gamow (1937, p. 104), due to the fact that variation of Z, E and r_0 in a radioactive series is practically

monotonic as we go down the series. Anomalies occur in the original Geiger-Nuttall curve where this regularity breaks down. Thus the Geiger-Nuttall curves with constant Z, will be more refined and less susceptible to anomalies.

The validity of the theoretical relation could be examined if the theoretical curve of log λ against E for constant Z, could be drawn and compared with the experimentally observed ones. But unfortunately this cannot be directly done since the above relation contains three variables λ, E and r_0, of which λ and E are known experimentally. The other terms, the nuclear radius r_0 cannot be determined as yet from any other independent observation. Hence what is done in this case for verifications is to see whether the values of r_0 calculated from the theoretical relation with the help of experimentally observed values of λ and E, are consistent for different nuclei. As it has been shown by different investigators, (Gamow 1937, Preston 1946, 1947) that the value of r_0 is more or less consistent excepting for the actinium series. For other nuclei r_0 nearly follows the relation $r_0 = RA^{\frac{1}{3}}$ obtained from liquid drop model. No satisfactory explanation is at present available for the abnormally low values of r_0 for ThC$\rightarrow$ThC″, RaC$\rightarrow$RaC″ and AcC$\rightarrow$AcC″.

As the experimental curves are plotted as log λ against E (in MeV) let us transform the equation (5) in terms of energy in MeV. For numerical calculation we use the relation

$$\log \lambda = 21.8428 + \tfrac{1}{2}\log E_v + .217\frac{m_a}{m_r} - \log r_0$$

$$- 1.104\frac{Z-2}{E_v^{\frac{1}{2}}\left(1+\frac{m_a}{m_r}\right)^{\frac{1}{2}}}\cos^{-1}\left[.5896\frac{E_v^{\frac{1}{2}}r_0^{\frac{1}{2}}}{(Z-2)^{\frac{1}{2}}}\right] + .6504\frac{(Z-2)^{\frac{1}{2}}r_0^{\frac{1}{2}}}{\left(1+\frac{m_a}{m_r}\right)^{\frac{1}{2}}}$$

$$- .1131\frac{r_0^{\frac{3}{2}}}{(Z-2)^{\frac{1}{2}}\left(1+\frac{m_a}{m_r}\right)^{\frac{1}{2}}}E_v \qquad \ldots (6)$$

where E_v = disintegration energy in MeV.

r_0 = radius in 10^{-13} cm. units.

The relation (6) exhibits explicit dependence of log λ on the disintegration energy E, charge number $Z-2$ of the product nucleus and radius r_0. Since r_0 varies as $A^{\frac{1}{3}}$, the effect of variation of r_0 from one number to other will be small; but if Z varies for different members, the variation will be much pronounced. So constancy of Z becomes a necessary condition for a two dimentional curve.

The Geiger-Nuttall law has been stated as

$$\log \lambda = a + bE \qquad (7)$$

But the actual theoretical relation is much complicated as seen from the relation (6). As it will be seen in later section that Po contains largest number of α-active isotopes, the theoretical relations deduced above can be conveniently compared with experimentally observed values. Taking an average value of $r_0 = 8.63 \times 10^{-13}$ cm. (for Po^{216}, ThA) ,the following theoretical relation for Po is obtained from the relation (6).

$$\log \lambda = a - \frac{b}{E_v^{\frac{1}{2}}} \cos^{-1}\left(cE_v^{\frac{1}{2}}\right) + d \log E_v - e E_v$$

$$= 38{\cdot}0664 - \frac{89{\cdot}71}{E_v^{\frac{1}{2}}} \cos^{-1} \left(.1923 E_v^{\frac{1}{2}}\right) + \tfrac{1}{2}\log E_v - .3225E \qquad (8)$$

With relation (8) the theoretical curve given in Fig. (1 *a*) is drawn. The curve passing through experimental points is given in Fig.1 (*c*). The agreement with the experimental curve (*c*) is seen to be satisfactory, in the middle part from (214) to (218) but on both sides the theoretical curve diverges from the experimental one. However instead of taking r_0 constant for all isotopes we can take the variation of r_0 from one isotope to other into account according to the relation, $r_0 = R.A^{\frac{1}{3}}$ Thus another theoretical curve (*b*) (Fig. 1)

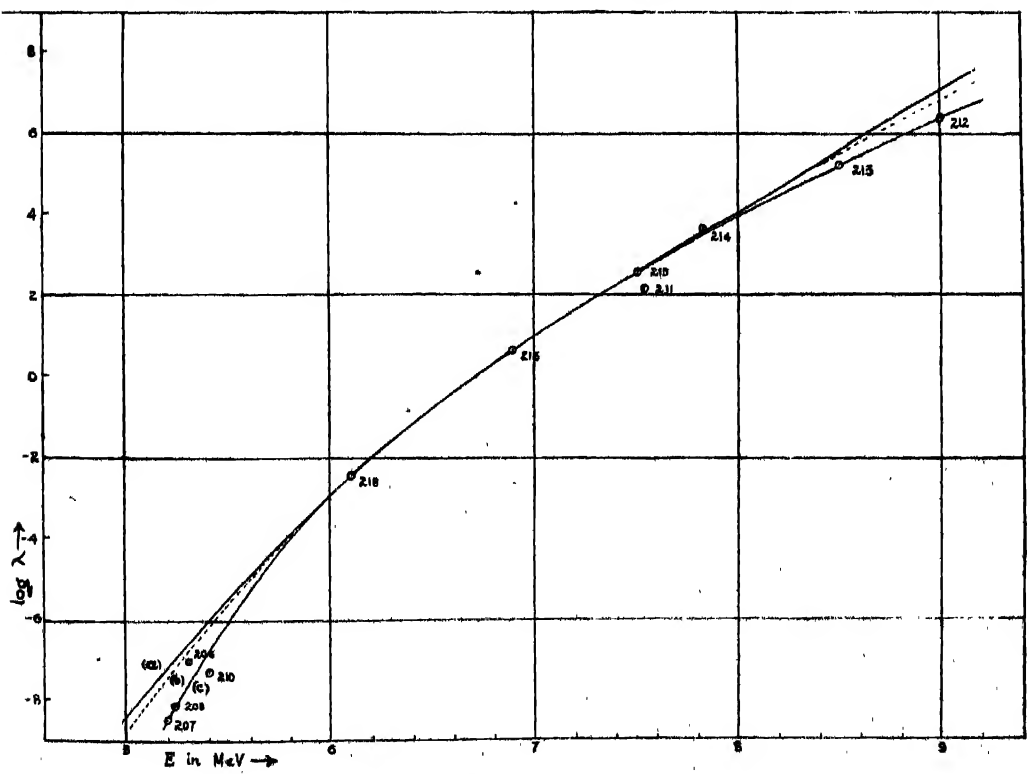

FIG. 1

is drawn from relation (6). The curve (*b*), approaches the experimental curve (*c*) at the end; but discrepancy still remains at the two ends, which shows that the theory of α-particle emission fails to account for very short lived products as well as very long-lived ones.

EXPLANATION OF THE METHOD.

Now the modified Geiger-Nuttall curves are to be drawn for each element starting from Bi. For dealing with the large amount of data we have made use of the nuclear chart originally given by Saha, Sirkar and Mukherjee (1940). The usefulness of this chart has been extended by the work of Saha and Saha (1946) and others on "Nuclear Energetics and β-activity". The part of the diagram dealing with our work is reproduced in Fig. 2.

As the chart shows all α-radio-activity appears to cease with Pb (82). This means, that the activity is too small to be measured. But from 83 onwards, α-activity has been found in many nuclei. Some of these nuclei are also simultaneously β-active and it is possible that, many of which have been found so long only γ- or only β-active may be found, as has been found by Feather in the case of RaE, to show the other type of activity on a very much feebler scale. We have therefore made use of our criterion for β-activity as given by Biswas and Mukherjee (1948) for dealing with each individual cases.

The correct determination of the data namely λ and E is the most important task. For E we have taken, not the energy with which the α-particle comes out, but the total energy of the reaction. As is well-known, this is given by the formula

$$E = E_0 \frac{A}{A-4}$$

In the case of a nucleus which decays both ways by α-disintegration, β-decay or K-capture, experiments give us only the composite life T. As is well-known

$$\frac{1}{T} = \frac{1}{T_\alpha} + \frac{1}{T_\beta}.$$

When we are considering λ, E relation for α-rays, we require T_α. To obtain this we must know the second relation, the ratio of $\frac{T_\alpha}{T_\beta} = \frac{\lambda_\beta}{\lambda_\alpha}$, which gives the ratio of the particles disintegrating by β-decay to that by α-decay. In many cases this ratio is known but in many cases we need have recourse to surmise. These points will be discussed in the proper places.

EXCITED STATES IN α-EMISSION:

It is well-known that many α-active nuclei do not emit α-particles of one energy, but α-particles of several energy groups are found. This is due to the formation of excited states of the initial or the product nucleus in α-emis-

The nuclei emitting complex α-spectra can be divided into two classes.

TABLE I

Bismuth (8_3)

Isotopes	Observed half life	$\frac{\alpha}{\beta}$ ratio	α-half life	λ_α (sec^{-1})	α-Energy, E_α (Mev)	Decay energy, E (Mev)	Produced by	Remarks
Bi^{204}	12h (*K*-cap) (H_4)	...	...	...	...	...	Pb^{204} (d, 2n) Tl^{203} (α, 3n) (H_4, T1)	...
Bi^{205}	?	...	...	...	...	...	Pb^{206}(d, 3n) ? (T1)	*K*-capture expected
Bi^{206}	6·4d (*K*-cap) (H_4, T1)	...	...	...	...	...	P_0^{206} *K*-cap. Tl^{205} (α, 3n) Pb^{206} (d,2n) Pb^{207} (d,3n) (T1)	...
Bi^{207}	?	...	...	...	...	...	Pb^{207} (d,2n) ? P_0^{207} K-cap (T1)	*K*-capture and α-activity expected.
Bi^{208}	?	...	...	...	...	...	Bi^{209}(n,2n) ? (H_4)	*K*-capture and β^--activity expected
Bi^{209}	Stable (100%)	...	...	...	...	...	...	
Bi^{210} (RaE)	5d (C6)	$\frac{10^{-7}}{1}$ (B_4)	1.37×10^6y	$1{\cdot}60 \times 10^{-13}$	4·87 (B_4)	4·975	RaD β^- decay	...
Bi^{211} (AcC)	2·16m (C6)	$\frac{99{\cdot}68}{32}$ (C6)	2·166m	$5{\cdot}33 \times 10^{-3}$ $\lambda_{a0} = 4{\cdot}78 \times 10^{-3}$	6·619 (H_3)	6·747	AcB β^- decay	...
Bi^{212} (ThC)	60·5m (C6)	$\frac{35}{65}$ (K_3)	2·99h	$6{\cdot}44 \times 10^{-5}$ $\lambda_{a0} = 1{\cdot}75 \times 10^{-5}$	6·054 (B_3, H_3)	6·170	ThB β^- decay	...
Bi^{213}	46m (E_1, H1)	$\frac{98}{2}$ (E_1)	46h	$4{\cdot}18 \times 10^{-6}$	5·86 (E_3)	5·97	At^{217} α-decay	Observations rather preliminary
Bi^{214} (RaC)	19.7m (C6)	$\frac{\cdot 04}{96{\cdot}96}$ (C6)	34·2d	$2{\cdot}35 \times 10^{-7}$ $\lambda_{a0} = 1{\cdot}06 \times 10^{-7}$	5·502 (L_4)	6·608	RaB β^- decay	...

(1) Class I: In this class, the α-particles of maximum energy have highest intensity (group O) and the intensity of other groups are smaller but of the same order as the group O. This is due to the formation of the excited states of the product nucleus. The examples are ThC $\rightarrow$ ThC″, RaAc $\rightarrow$ AcX, etc.

In the present discussion, the α-emission between the ground states of two nuclei (group O) are considered. Hence the observed disintegration constant λ_α is to be corrected so as to give partical disintegration constant for the zero group λ_{α_0}. Taking the case of ThC″ $\rightarrow$ ThC″ we find that intensity of group O α-particles is 27.2% of the total intensity. So λ_{α_0} will be 27.2% of the total λ_α (6.44×10^{-5}). Thus the corrected λ_{α_0} is $1.75 \times 10.^{-5}$

Similar correction is applied for all α-emitters of Class I as will be referred to later on.

(2) Class II: This class includes a few α-active nuclei where the α-particles of lowest energy have the highest frequency and α-particles of higher energy are very infrequent, relative intensity being of the order of 1 in 10^6. This is due to the existence of excited states in the initial nucleus. Only the normal α-particles (group O) are included in this discussion. Since the intensities of other groups of α-particles are very small compared to group O, we can put $\lambda_{\alpha_0} \simeq \lambda_\alpha$ and no correction for the complex spectrum is required.

The examples of this type are ThC′ $\rightarrow$ ThD, RaC′ $\rightarrow$ RaD.

(83) *Bismuth*

The isotopes of Bi range from mass number 204 to 214. All the relevant data are given in Table I.

Bi^{204}: This recently obtained isotope of Bi shows a 12 hr K-capturing activity. This is an agreement with the findings of Biswas and Mukherjee (1948) on β-energetics consideration.

Bi^{205}: No distinct activity assignable to Bi^{205} could be found in the reaction expected. It is expected, from the studies of Biswas and Mukherjee (1948) to be a K-capturing nucleus.

Bi^{206}: The 6.4 d K-capturing activity of this nucleus is in agreement with findings of Biswas and Mukherjee (1948).

Bi^{207}: No activity could be assigned to Bi^{207} which is expected in the reaction studied. According to Biswas and Mukherjee (1948) this ought to be a K-capturing nucleus with long life.

Corson *et al* (1940) reports the production of 85^{211} by the reaction Bi^{209} $(\alpha, 2n)$ and showed that it is dually active, 60% being α-active 40% K-active. The product of the α-active branch would be Bi^{207}, but he was unable to trace any activity of Bi^{207}.

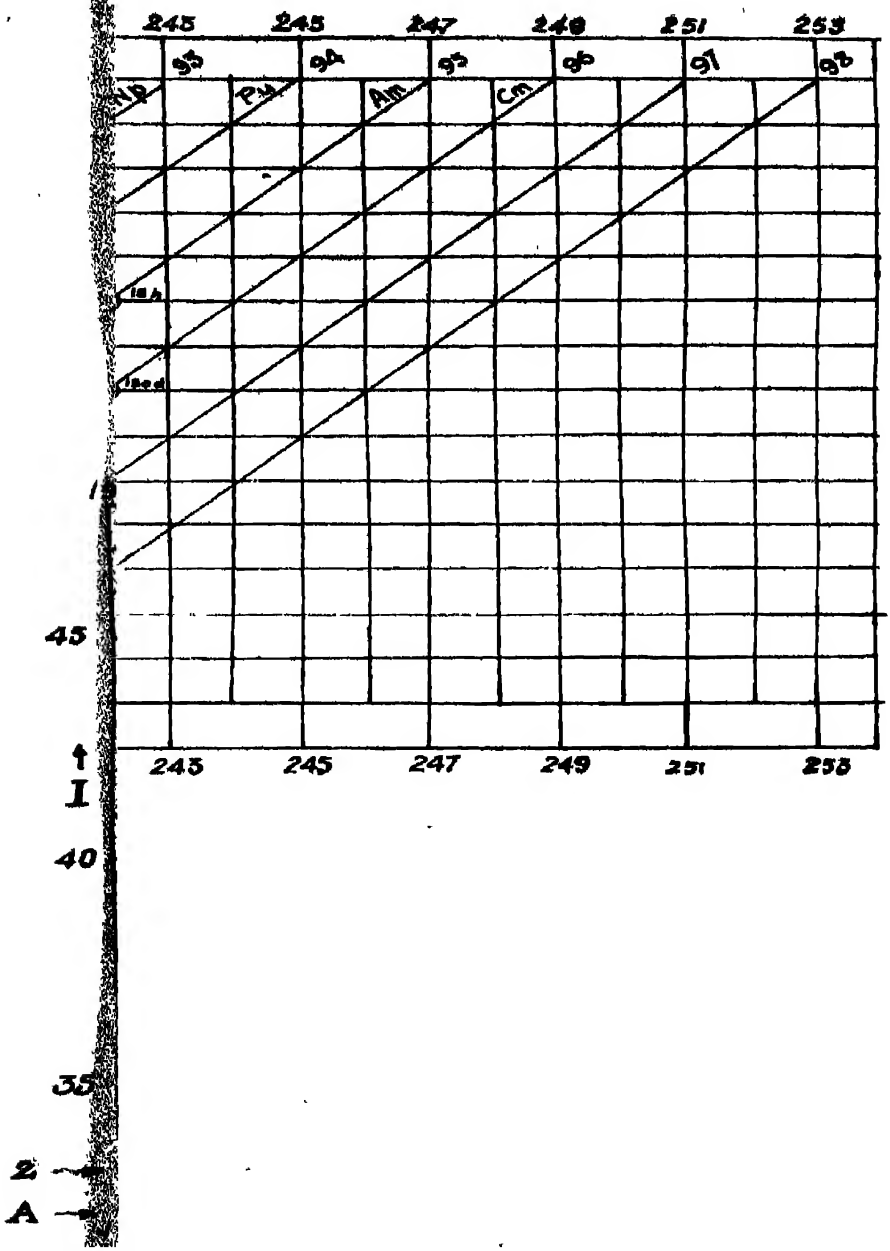

[Facing page 56

Bi^{208} : The production and mode of decay of this isotope are as yet uncertain. According to Biswas and Mukherjee (1948) it ought to show both K-capture and β^-activity.

Bi^{209} : This is the only stable isotope of Bi.

Bi^{210} : (RaE) : Broda and Feather (1947) have recently shown that in addition to 5 d β-activity, a small fraction of RaE decays by α-activity to Th^{206}. The branching ratio of α and β is estimated as $\sim 1 \times 10^{-7} : 1$. The energy of α-particles has been obtained from the equivalence of energy-release in the two branches as shown in Fig. 3. The value of E_α is to be confirmed by direct experiment. A little alteration in the value of branching ratio and E_α will shift the point on the curve to a small extent.

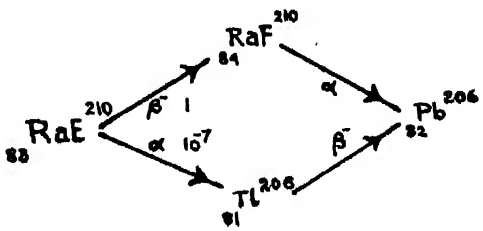

Fig. 3.

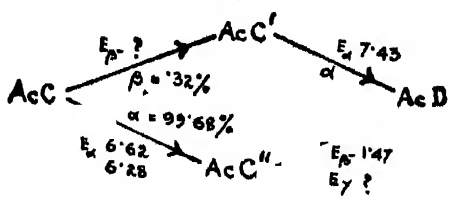

Fig. 4.

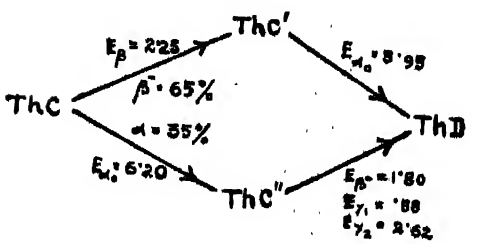

Fig. 5.

Bi^{211} : (AcC) : The dual disintegration scheme of AcC is given in FIG. 4. The main disintegration of AcC is by α-emission (99.68%) to AcC''. Two groups of α-particles are emitted. The complex α-spectra fall in Class I. The intensity of group O α-particles is 84%. Thus $\lambda_\alpha = 5.33 \times 10^{-3}$ sec^{-1} is corrected to give $\lambda_{\alpha 0}$ which becomes 4.478×10^{-3} sec^{-1}. This isotope falls close to the log $\lambda_{\alpha 0}$ curve for Bi.

The energy of the β-emission in AcC$\rightarrow$AcC′ is not yet determined. From the equivalence of energy-release in two branches, $E\beta^-$ comes out as .66 MeV. The study of the disintegration of AcC is not yet complete.

Bi^{212} (ThC) : The dual disintegration scheme of ThC is well studied by Ellis and this is given in Fig. 5. In the α-disintegration branch ThC$\rightarrow$ThC″, the observed composite half-life is resolved to give α-half-life and λ_α. The α-spectra is complex consisting of five components (Class I). The intensity of Group O α-particles in 27.2%, and $\lambda_{\alpha 0}$ is calculated as 1.749×10^{-5} from the value of λ_α (6.439×10^{-5}). This isotope falls on the smooth log $\lambda - E$ curve for Bi.

Bi^{213} : This isotope is the corresponding C-product in the newly discovered $(4n+1)$ radio-active series. The data for branching ratio, composite half-life and α-energy release are taken after the determination of English *et al* (1947). The study of this new series is rather preliminary and further investigation is required.

Bi^{214} (RaC) : The complete disintegration scheme of RaC to RaD has not yet been established. In the disintegration RaC to RaC″ two groups of α-particles having energies of 5.612 and 5.549 MeV have intensities of 45.4% and 54.6%. The α-disintegration constant is calculated from composite halflife; this λ_α is corrected to give partial disintegration constant $\lambda_{\alpha 0}$ which becomes 1.056×10^{-7} sec^{-1}.

The Refined Geiger-Nuttall Curve For Bi

With the data given in Table I, the Geiger Nuttall plot, log λ against E, is made for the isotopes of Bi (Fig. 6). The points lie close to a smooth curve excepting Bi^{214} (RaC). This curve is somewhat different than that given by Broda and Feather (1947) in the study of α-activity of RaE. The curve given by them is drawn through the points corresponding to α-particles other than the zero group, whereas the present curve is drawn for Group O α-particles of the isotopes of Bi. The α-active isotopes of Bi includes C-products and it has been shown by Gamow (1937) that none of these C$\rightarrow$C″ bodies show normal behaviour.

(84) *Polonium*

Polonium contains largest number of α-active nuclei. Its isotopes range from mass number 206 to 218 with exception of 209 and 217. The relevant data are given in Table II.

Po^{206} : This recently obtained Polonium isotope exhibits simultaneous α-emission and K-capture processes. The K-capture activity of this even-even nucleus is due to its position in the extreme right flank of the I-group. As pointed out by Biswas and Mukherjee, this nucleus is a good confirmation of the Saha-Saha theory (1946).

No daughter of Po^{206} by α-emission has been reported. The product Pb^{202} should be α-active.

TABLE II

Polonium (84)

Isotopes	Observed half-life	$\frac{\alpha}{\beta}$ ratio	α-half-life	λ_α (sec^{-1})	α-energy, $E\alpha$ (Mev)	Decay energy, E (Mev)	Produced by	Remarks
Po^{206}	9d (T2)	$\frac{\alpha}{K} = \frac{10}{90}$ T(2)	90d	$8{\cdot}92 \times 10^{-8}$	5·2 (T2)	5·3	Pb^{204} (α, 2n) (H4)	...
Po^{207}	5·7h (T2)	$\frac{\alpha}{K} = \frac{\cdot 01}{99{\cdot}99}$ (T2)	6·5y	$3{\cdot}38 \times 10^{-9}$	5·1 (T2)	5·2	Pb^{206} (d, 3n) (H4)	...
Po^{208}	~3y (T2)	...	—3y	$7{\cdot}33 \times 10^{-9}$	5·14 (T2)	5·24	Pb^{207} (α, 3n) (H4)	...
Po^{209}	?	...	...	...	...	...	Bi^{209}(d, 2n) ? (T2)	K-capture and α-activity expected.
Po^{210}	140d (C6)	...	140d	$5{\cdot}89 \times 10^{-8}$ (C2)	5·303(C2) 5·298 (H3)	5·405	RaF β^-decay Bi^{209} (d, n) (C_3, H_5)	...
Po^{211} (AcC')	5×10^{-3} s (C6)	...	5×10^{-3} s	$1{\cdot}39 \times 10^{2}$	7·434 (L_4)	7·543	AcC β^-decay 85^{211} K-cap	...
Po^{212} (ThC')	3×10^{-7} s (D1)	...	3×10^{-7} s	$2{\cdot}31 \times 10^{6}$	8·776 (B_3, H_3)	8·944	ThC β^-decay	...
Po^{213}	$4{\cdot}4 \times 10^{-6}$s (E1, H1)	...	$4{\cdot}4 \times 10^{-6}$s	$1{\cdot}58 \times 10^{5}$	8·336 (F1)	8·496	Bi^{313} β^-decay (E1, H1)	...
Po^{214} (RaC')	$1{\cdot}5 \times 10^{-4}$s (D1, R4, W1)	...	$1{\cdot}5 \times 10^{-4}$s	$4{\cdot}62 \times 10^{3}$	7·680 (B_3, H_3)	7·827	RaC β^-decay	...
Po^{215} (AcA)	$1{\cdot}83 \times 10^{-3}$s (W1)	...	$1{\cdot}83 \times 10^{-3}$s	$3{\cdot}79 \times 10^{2}$	7·365 (L_4)	7·504	An^{219} α-decay	...
Po^{216} ThA)	·158 s (W1)	$\frac{99{\cdot}086}{\cdot 014}$ (K1)	·158s	4·39	6·774 (B_3, H_3)	6·902	Tn^{220} α-decay	...
Po^{217}	?	...	...	...	...	...	...	Not yet known. This will be β^--active.
Po^{218} (RaA)	3·05m (C6)	$\frac{99{\cdot}96}{\cdot 04}$ (K2)	$3{\cdot}06_2$m	$3{\cdot}77 \times 10^{-3}$	5·998 (B_3, H_3)	6·110	Rn^{222} α-decay	...

Po^{207} : This also is a simultaneous α and K-active nucleus. The high K-capture process (99.99%) is in agreement with Biswas and Mukherjee's findings. No daughter of Po^{207} is found. Po^{207} will decay to Bi^{207} by K-capture. As given before Bi^{207} should decay by K-capture.

Po^{208} : The 3 year α-activity of Po^{208} is in agreement with the stability rule. According to Biswas and Mukherjee, this even even nucleus should have no β^- or K-capture activity.

Po^{209} : No activity could be assigned to Po^{209} which is expected in the reaction studied, Bi^{209} (d, 2n) Po^{209}. This isotope will decay by K-capture (Biswas and Mukherjee, 1948) as well as by α-activity.

Po^{210} : The investigation of Chang (1946) revealed that Po^{210} (RaF) does not emit homogeneous α-rays, but seven groups of particles are present. The intensity ratios of the higher order groups to the main group are at variance with the present theory of α-emission of excited states. The α-energy of Group O is highest and the relative intensity is 10^6, compared to other groups whose energies are smaller than the main group. Thus the α-spectra do not fall in either of Class I or Class II as stated before. Taking the experimental observation as correct, Po^{210} presents a problem, hitherto unknown and unexplained, in α-emission.

Po^{211} : (AcC′) : The normal α-particles of 7.434 MeV from AcC′ is surely attended by long range α-particles of very low intensity as in the case of ThC′ and RaC′. These have not yet been studied. Accurate determination of the extremely short half-life of AcC′ is required as no recent data are available for this. The α-spectra of AcC⟶AcD should fall in Class II as in other C-products, and hence no correction for λ_a is required.

The absence of β-activity of this nucleus follows from the studies of Biswas and Mukherjee (1948).

Po^{212} (ThC′) : The spectra of ThC′⟶ThD has been completely investigated and with the main group of 8.776 MeV two long range α-particles of very small intensity are present. The complex α-spectra fall in Class II and no correction of λ_a is required. The short half-life (3×10^{-7} sec) has been accurately determined by Dunworth (1939).

No β-activity is possible for this even-even nucleus.

Po^{213} : In the same line with ThC′ and AcC′, this isotope is the corresponding C′ body of the newly discovered $(4n+1)$ radio-active series. The half-life is reported as 4.4×10^{-6} sec. Further investigation is sure to show long range α-particles of very small relative intensity.

No β-activity of this nucleus is possible as shown by Biswas and Mukherjee.

Po^{214} (RaC′) : It has been observed by Lewis & Bowden that twelve long range α-groups of very small relative intensity are present with the main group of α-particles. The number of γ-rays, due to transitions

between these levels, as pointed out by Ellis, should be many more than at present observed. The half-life has been accurately determined by Dunworth (1939), Rotblat (1941) and Ward (1942).

This α-spectra of Class II require no correction for λ_a. The β-stability of this nucleus is accounted for by its even-even property.

Po^{215} (AcA) : The α-spectrum is simple as observed by Lewis and Bowden (1934). The short half-life, 1.83×10^{-3} sec., has been accurately measured by Ward (1942). According to Biswas and Mukherjee *loc. cit.*, low energy β-emission is probable for Po^{215} (AcA). The isotopes, ThA and RaA of two other radioactive series have been observed to emit low intensity β-rays in addition to strong α-activity (Karlik and Bernert, 1943). Thus the predicted β-activity of very weak intensity will be in agreement with the A-products of two other series. This will be worthy of further investigation.

Po^{216} (ThA) : Karlik and Bernert (1943*a*) showed that low intensity β-ray branching (.014%) exists for this strong α-active nucleus. The β-ray energy has not yet been measured. Very low energy β-emission from this even-even nucleus is explained by its position in the flank of the group I=48. This is in confirmation of Saha-Saha theory (1946).

The short half-life (.158 sec) has been accurately measured by Ward (1942).

Po^{217} : This isotope of Po is yet unknown. This should belong to $(4n+1)$ radioactive series ; but 85^{217} is the only known isotope of this mass number in $(4n+1)$ radioactive series. If ever obtained, this will be β^- active of very short half-life.

Po^{218} (RaA) : The investigations of Karlik and Bernert (1943*b*) revealed a low intensity β-ray branching (.04%) for this predominantly α-active nucleus. The β-ray energy has not yet been measured. The β-activity of this even-even nucleus is due to its position in the extreme flank of Group I=50, and is in good agreement with Saha-Saha theory (1946). As indicated by Biswas and Mukherjee, β-ray energy-release is expected to be $\sim .2$ MeV.

The Geiger-Nuttall Curve for Po.

Since Po contains largest number of α-active isotopes, the validity of the refined Geiger-Nuttall relationship can be tested with the data provided by it. The curve, log λ against E, (Fig. 6) is plotted with the data given in Table II. It is observed that almost all the isotopes fall on a smooth curve. Small deviations occur for Po^{211} (AcC'), Po^{210} and Po^{206}. In case of Po^{211} (AcC') it has already been pointed out

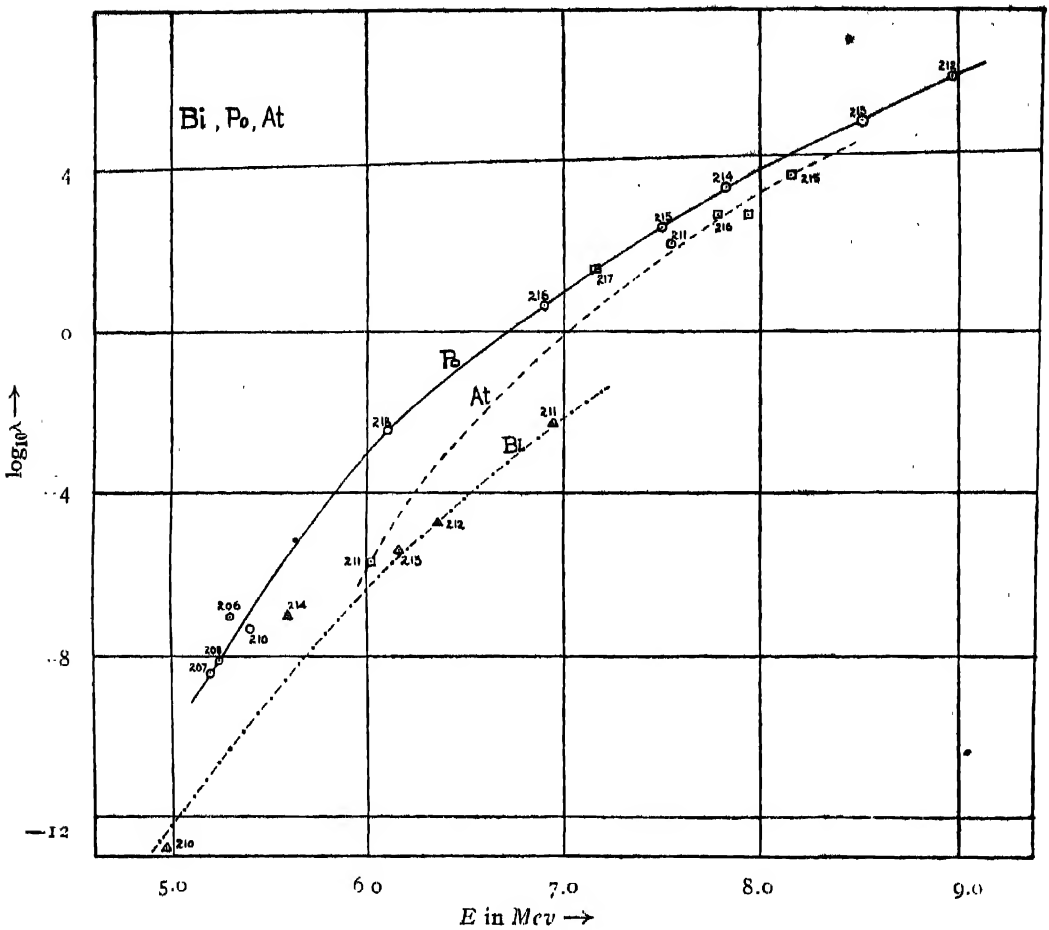

FIG. 6

that the short half-life (5×10^{-3} sec) has not been measured with accuracy in recent years. Po^{210} exhibits a new type of α-activity as indicated before. The data for the other isotope, Po^{206} are rather preliminary. Thus the proposed refinement of the Geiger-Nuttall relation is seen to hold good.

(85) *Astatine*

At present five isotopes of element 85 are known, all of which show α-activity. The data for one isotope is insufficient. The relevant data are given in Table III.

$85At^{211}$: This isotope was obtained in artificial transmutation by 40 MeV α-particles on Bi^{209} by Corson *et al* (1940). The observed K-capture activity of this, in addition to α-activity is well explained by the β-energetics for I=41 (Biswas and Mukherjee, 1948).

At^{215} : This isotope is α-active and β-stable. The β-stability of this is in agreement with β-energetics considerations.

TABLE III

Astatine (85)

Isotopes	Observed half-life	$\frac{\alpha}{\beta}$ ratio	α-half-life	λ_α (sec^{-1})	α-energy (MeV)	Decay energy E_t (MeV)	Produced by	Remarks
At^{211}	7.5 h (c 5)	$\frac{\alpha}{K} = \frac{60}{40}$	12.5h	1.54×10^{-5}	5.94 (c5)	6.03	$Bi^{209}(\alpha, 2n)$ (c5)	α-decay product not yet observed.
At^{215}	10^{-4}s (G 2a)		$\sim 10^{-4}$s	6.93×10^{3}	8.00 (G2a)	8.15	Fr^{219} α-decay	
At^{216}	$\sim 10^{-3}$s (G 2a)		$\sim 10^{-3}$s	6.93×10^{2}	7.64 (G2a) 7.79 (K1)	7.79 7.93	Fr^{220} α-decay ThA^{216} β-decay	Also β^--activity expected.
At^{217}	2.1×10^{-2}s (E1, H1)		2.1×10^{-2}s	33.0	7.02 (E1, H1)	7.16	Fr^{221} α-decay	
At^{218}	Few Sec ? (K2)				6.63 (K2)	6.75	$RaA^{218}\beta$-decay	Data incomplete.

$85At^{216}$: This isotope is formed in weak β^--branching of ThA (Karlik and Bernert, 1943*a*) and by α-decay of Fr^{220}. The half-life is stated as $\sim 10^{-3}$s. The α-energy is given as 7.64 MeV according to earlier determination and 7.97 MeV according to later determination. This is also expected to show β^--activity, but probably this is overshadowed by the more intense α-activity.

$85At^{217}$: This isotope is a member of the newly discovered $(4n+1)$ radio-active series. Its α-activity has been observed, but it may be also β^--active with small energy-release.

$85At^{218}$: This isotope is produced in the β-branching of RaA which is only 0.04%. The value of half-life is uncertain and is given as several seconds. The α-energy is reported as 6.63 MeV by Karlik and Bernert (1943). Further investigation of this isotope is required. Taking the value of E_α as correct, the half-life of At^{218} may be estimated from the Geiger-Nuttall curve for At. This comes out as $\sim$'5 sec.

The Geiger-Nuttall Curve for At,

Of five α-active isotopes of At, the available data permit to plot four of them. As seen in Fig. 6 these lie on smooth log λ, E curve within the limits of experimental error. This curve is similar to that of Po and lies below the latter. This Geiger-Nuttall curve for At is useful to determine half-life from a knowledge of E_α and *vice versa* for any other isotope with incomplete data. Using this curve half-life of At^{218} comes out as $\sim$'5 sec.

(86) *Radon*

All three nown isotopes of Rn are α-active. The relevant data are given in Table IV.

Rn^{218} : This isotope is obtained in the co-lateral chain of Ra-series. The α-energy is not directly obtained from Rn^{218} but is assigned to it in order of half-life.

Rn^{219}(An) : The α-spectra of Rn^{219} is complex consisting of 4 groups. The intensity of the zero group α-particles is 70%. Accordingly the value of $\lambda\alpha_0$ is .124 sec^{-1}.

TABLE IV

Radon (86)

Isotopes	Observed half-life	$\frac{\alpha}{\beta}$ ratio	α-half-life	λ_α (sec^{-1})	α-energy (MeV)	Decay energy E (MeV)	Produced by	Remarks
Rn^{218}	.019 s (s 12)		.019 s	36.5	7.1 (S12)	7.23	Ra^{222} α-decay	
Rn^{219} (An)	3.92 s (c6)		3.92 s	.17 $\lambda_{\alpha 0}$=.12	6.82 (H_3)	6.95	AcX^{223}α-decay	
Rn^{220} (Tn)	54.5 s (c6)		54.5 s	1.27×10^{-2}	6.28 (B_3, H_3)	6.40	ThX^{224}α-decay	
Rn^{221}	?							β^--activity expected.
Rn^{222}	3.825 d (c6)		3.825 d	2.10×10^{-6}	5.486 (B_3, H_3)	5.587	Ra^{226}α-decay	

Rn^{220}(Tn) : The α-particles from Tn^{220} are homogeneous as observed by Briggs (1936) and Lewis and Bowden (1934).

Rn^{221} : This isotope of Rn is not yet known. This may be formed if a small α-branching exists in Ra^{225} which is not unlikely. Rn^{221} will be predominantly β^--active.

Rn^{222} : The α-particles of Rn^{222} are homogeneous according to the observation of Lewis and Bowden (1934) and Briggs (1936).

The β-stability of all three known isotopes of Rn follows from the studies of Biswas and Mukherjee (1948).

Geiger-Nuttal Curve for Rn.

With the data given a Table IV, the log λ, E curve is drawn from the isotopes of Rn (Fig. 7). It is seen that the three points lie on a smooth curve

while the one of Rn^{219} falls outside, A redetermination of λ and R_a of Rn^{219} is required.

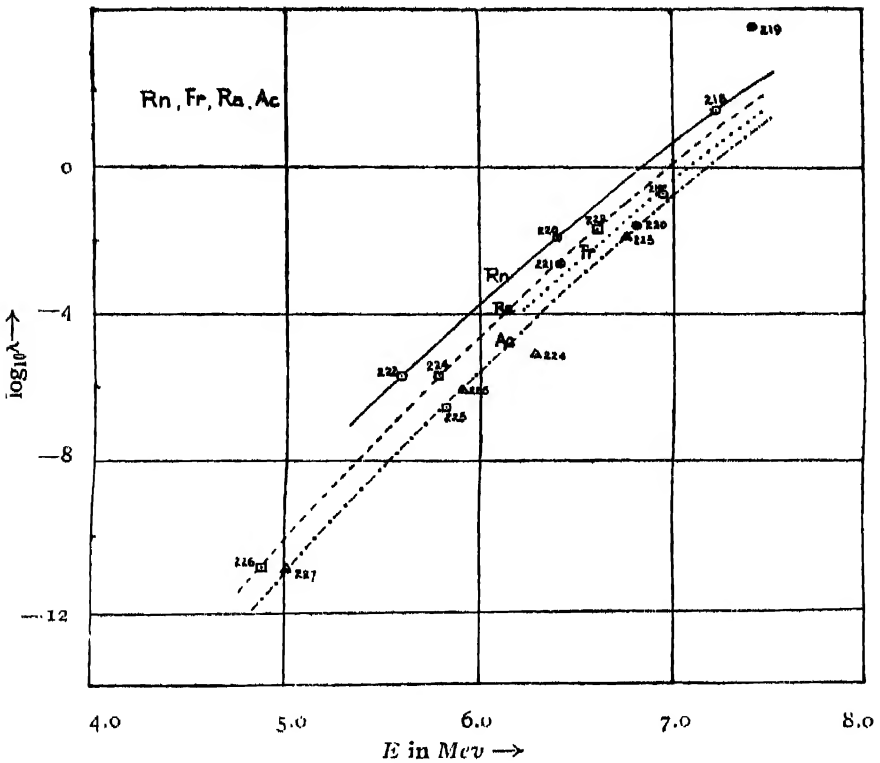

FIG. 7

(87) *Francium*

At present four isotopes of element 87 are known of which one is β^--active. The relevant data are given in Table V.

Fr^{219} : This is obtained in a colateral chain of Ac series recently synthesised. As expected this is β-stable.

Fr^{220} : This isotope is observed as α-active. This is expected to be also β^--active.

Fr^{221} : This isotope is a member of the recently discovered $(4n+1)$ radioactive series. The β-energetics curves for $I=47$ shows that this will be β-stable.

Fr^{222} : This isotope is not yet known. This isotope will be β^--active.

Fr^{223} : (AcK) Perey and Lecoin (1939) discovered a small α-activity of Ac^{227}, $\alpha:\beta$ branching ratio being 1 : 99. The α-decay product is $_{87}Fr^{223}$ which is called AcK. This decays by β^--activity to AcX^{223}.

The β^--activity of Fr^{223} is in agreement with the studies of Biswas and Mukherjee (1948). The β^--ray energy of 1.2 MeV is supported by theoretical considerations, but no γ-ray of so high energy, >3 MeV, as reported by them, should exist with this isotope.

TABLE V

Francium (87)

Isotopes	Observed half-life	$\frac{\alpha}{\beta}$ ratio	α-half life	λ_α (Sec^{-1})	α-energy (MeV)	Decay energy, E (MeV)	Produced by	Remarks
Fr^{219}	$\sim 10^{-4}$ s (G2α)		$\sim 10^{-4}$ s	6.9×10^{3}	7.30 (G2α)	7.43	Ac^{223} α-decay	Precise value of λ is required.
Fr^{220}	$\sim$30 s (G2α)		$\sim$30 s	2.3×10^{-2}	6.63 (G2α)	6.81	Ac^{224} α-decay	β^--activity also expected.
Fr^{221}	5 m (F1, H1)		5 m	2.3×10^{-3}	6.31 (E1)	6.42	Ac^{225} α-decay	
Fr^{222}	?							This will be β^--active.
Fr^{223} (AcK)	21m (β^-) (P1, P2)						Ac^{227} α-decay	

Geiger-Nuttall curve for Fr.

As the experimental data are approximate, the point of Fr^{220} and Fr^{221} lie close to the G-N-Curve for Fr, while Fr^{219} lies much above the curve (Fig. 7). Precise experimental values are required for these.

(88) *Radium*

The known isotopes of Ra range from Ra^{222} to Ra^{228} (MsThI) with the exception of Ra^{227}. The useful data are given in Table VI.

Ra^{222}: This is β-stable as expected from β-energetics, and is only α-active. The α-energy has not been obtained from separated isotope but is assigned in order of half-life.

Ra^{223} (AcX): As reviewed by Bethe (1937), the α-spectra of AcX is complex consisting of four groups. The intensity of group zero α-particles is 4%. The observed disintegration constant is used to give λ_{α_0} equal to 2.86×10^{-7} sec.$^{-1}$.

The β-stability of Ra^{223} is explained by β-energetics considerations.

Ra^{224}(ThX): The α-particles of Th^{224} are homogeneous according to the investigation of Briggs (1936).

Ra^{225}: This isotope is a member of the $(4n+1)$ radio-active series. The β^--activity of Ra^{225} is in agreement with the studies of β-energetics. It is a

descendant of 7×10^3 yr α-active Th^{229}. Hence it is plausible that feeble α-activity of Ra^{225} may exist which is masked by a more intense β-activity. The suspected α-activity of $R\alpha^{225}$ requires further investigation.

Ra^{226} : The α-particles from Ra^{226} are not homogeneous, but belong two groups (Lewis and Bowden, 1934). The intensity of Group O particles is 97.8% from which λ_{α_0} is estimated as 1.35×10^{-11} sec.$^{-1}$

Ra^{227} : This Ra isotope is not yet known. It may be formed if weak α-activity of Th^{231} is detected which is not unlikely. This will show β^--activity according to β-energetics studies.

TABLE VI

Radium (88)

Isotopes	observed half-life	$\frac{\alpha}{\beta}$ ratio	α-half life	$\lambda\alpha$ (Sec^{-1})	α-energy (MeV)	Decay Energy, E (MeV)	Produced by	Remarks
Ra^{222}	38s (S12)	..	38s	...	6.5 (S12)	6.61	Th^{226}α-decay	...
Ra^{223} (AcX)	11.2d (c6)	...	11.2d	7.14×10^{-7}	5.72 (L4)	5.82	$RdAc^{227}$α-decay	Data require redetermination
Ra^{224} (ThX)	3.61d (L3)	...	3.64d	2.2×10^{-6}	5.68 (B3)	5.78	$RdTh^{228}$α-decay	...
Ra^{225}	14d (β) (H1, H11)	...	...	...	...	...	Th^{229}α-decay	α activity probable
Ra^{226}	1590y (c6)	...	1590y	1.38×10^{-11} $\lambda_{\alpha_0}=1.35 \times 10^{-11}$	4.79 (L4)	4.88	I_0^{230}α-decay	...
Ra^{227}	?	...	...	...	...	...	...	β^--activity expected
Ra^{228} (MsTh1)	6.7y (β) (c6)	...	...	..	...	...	Th^{232}α-decay	weak α-activity probable

Ra^{228} (MsTh1) : The low energy β^--activity of the even-even nucleus, $_{88}MsTh1^{228}$ is in good agreement with Saha-Saha theory as indicated in the β-energetics study of the Group I = 52. Since it is the decendant of 1.39×10^{10} yr α-active Th^{232}, it is likely that α-activity also occurs for MsTh1 with a half-life of the order of a million years which is probably overshadowed by the more intense β^--activity. The probable α-activity of MsTh1 is to be searched for.

The refined Geiger-Nuttall Curve for Ra.

The plot of the experimental data in Table VI is given in Fig. 7. It is observed that out of four α-active isotopes of Ra, one point Ra^{228} do not fall on the smooth curve. Some anomaly in the experimental data is seen to exist in case of AcX^{223} and ThX^{224}. The α-energy values of these are 5.719

and 5.681 MeV respectively according to spectroscopic determination of Lewis and Bowden (1934) and Briggs (1936). But the disintegration constant λ_α of ThX^{224} having lower α-energy is given as greater than λ_α for AcX^{223}. These data are incompatible with the theory of α-activity. The data for Ra^{223} (AcX) should be re-investigated and revised.

(89) *Actinium*

The isotopes of Ac range from Ac^{223} to Ac^{228} with the exception of Ac^{226}. The relevant data are given in Table VII.

Ac^{223} This should exhibit *K*-capture in addition to observed α-activity.

TABLE VII

Actinium (89)

Isotopes	Observed half-life	$\frac{\alpha}{\beta}$ ratio	α-half-life	$\lambda\alpha$ (Sec^{-1})	α-energy (MeV)	Decay energy *E* (MeV)	Produced by	Remarks
Ac^{223}	~2m (G2*a*)	...	~2m	1.16×10^{-2}	6.64 (G2*a*)	6.76	Pa^{227} α-decay	*K*-capture activity probable.
Ac^{224}	~2.5h (G2*a*)	$\frac{K}{\alpha} \sim \frac{1}{10}$	27.5h	7.7×10^{-6}	6.17 (G2*a*)	6.28	Pa^{228} α-decay	Precise data required
Ac^{225}	10d (E_1,H_{11})	...	10d	8.02×10 ?	5.801 (E_1)	5.906	Ra^{225} β⁻-decay	...
Ac^{226}	...	...	...	⋮	...	...	...	This will be β⁻-active.
Ac^{227}	13.5y (C6)	$\frac{1}{99}$ (P_1,P_2)	1350y	1.63×10^{-11}	5.0 (P_1', P_2)	5.09	Pa^{231} α-decay	
Ac^{228} (MsThII)	6.13h (C6)	$\frac{\alpha}{\beta}$? (G5,G6)	...	...	4.5 (G5,G6)	4.58	$MsThI^{228}$ β-decay	

Ac^{224} : The observed *K*-capture activity along with α-emission is in agreement with β-energetics considerations.

Ac^{225} : This is a member of the recently discovered (4n + 1) radioactive series. The β-stability of this isotope is in agreement with the β-energetics studies.

Ac^{226}: This isotopes is not yet known. If ever obtained, it will be predominantly β⁻-active.

Ac^{227} : Perey and Lecoin (1939) discovered that along with strong β⁻-activity of Ac^{227}, a weak α-activity exists to the extent of 1:99. The β-activity of Ac^{227} is in agreement with β⁻-energetics studies. The α-branching of Ac^{227} produces AcK, which is an isotope of element 87.

Ac^{228} (MsThII): This predominatly β⁻-active isotope has been reported to be very weakly α-active by Gueben (1933). The branching ratio, as well

as the α-decay product, Fr^{224} has not yet been observed. The α-energy is reported as 4.5 MeV from range measurement. This nucleus requires further studies.

Taking the α-energy to be correct, the modified Geiger-Nuttall Curve can be used to find out λ_a for Ac^{228}. The α-half-life comes out as 1.5×10^6 years, from which $\alpha : \beta$ branching ratio becomes $5 \times 10^{-8} : 1$.

Modified Geiger-Nuttall Curve for Ac.

Of four isotopes of Ac, three points lie on the smooth G-N Curve for Ac (Fig. 7) only Ac^{224} falls outside. Precise determinations of λ, E_a and $K : \alpha$ ratio are required for Ac^{224}. The unknown data for $MsThII^{228}$ can be roughly estimated from this curve. Taking the α-energy data of MsThII to be correct, the α-half-life and the ratio of $\alpha : \beta$ emissions are calculated as given above.

(90) *Thorium*

The isotopes of Th range from Th^{226} to Th^{234}. Five of them are α-active. The relevant data are tabulated in Table VIII.

Th^{226} : No other activity is expected from β-energetics studies. Th^{227} (Rd Ac) : As observed by Lewis and Bowden (1934) the α-spectra of RdAc is found to be highly complex consisting of eleven α-groups. The spectra is of Class I and the intensity of Group O α-particles is 24%. From this the value of λ_{a0} comes out as 1.018×10^{-7} sec^{-1}.

Th^{228} (RdTh) : The studies of Lewis and Bowden (1934) revealed the α-spectra from $RdTh^{228}$ to be complex consisting of two groups. The intensity of Group O α-particles is 85%. The partial disintegration constant λ_{a0} comes out as 9.33×10^{-9} sec^{-1}. Energetically no other activity is probable for this.

Th^{229} : This one is a member of the $(4n+1)$ radioactive series. The experimental data are rather preliminary. Very weak β^--activity is not unlikely from β-energetics consideration.

Th^{230} (Io) : The α-particles are homogeneous. The α-energy value given by Winand (1937) appear satisfactory from the Geiger-Nuttall Curve for Th.

Th^{231} (UY) : The observed β^--activity of Th^{231} is in agreement with energetics consideration. As it is the α-decay product of U^{235} this isotope is strongly suspected to show α-activity with long life like Ac^{227}. This possibly remains masked by strong β^--activity. This requires further studies.

Th^{232} : The energy of α-particles from natural thorium is different investigators. Ionisation chamber measurements by Schintlmeister (1937) give α-energy as 4.2 MeV. Latest determination is due to Faraggi (1936) who

TABLE VIII

Thorium (90)

Isotope	Observed half-life	$\frac{\alpha}{\beta}$ ratio	α-half-life	λ_α (Sec^{-1})	α-energy (MeV)	Decay energy E(MeV)	Produced by	Remarks
Th^{226}	30.9m (S12)	...	30.9m	3.74×10^{-4}	6.3 (S12)	6.41	$U^{230}\alpha$-decay	...
Th^{227} (RdAc)	18.9d (c6)	...	18.9d	4.24×10^{-7} $\lambda_{\alpha\alpha}=1.02\times10^{-7}$	6.049 (L4)	6.156	$Ac^{227}\beta$-decay	...
Th^{228} (RdTh)	1.90y (c6)	...	1.90y (c6)	1.10×10^{-8} $\lambda_{\alpha\alpha}=9.33\times10^{-9}$	5.418 (L4)	5.514	MsThI^{228} β-decay	...
Th^{229}	$\sim5\times10^3$y (E1, H1)	...	$\sim5\times10^3$y	4.4×10^{-12}	$\sim$.5 (E1H1)	$\sim$5.09	$U^{233}\alpha$-decay	Data very approximate.
Th^{230} (Io)	8.3×10^4y (c6)	...	8.3×10^4y	2.65×10^{-13}	4.81 (W3)	4.865	UII$^{234}\alpha$-decay	...
Th^{231} (UY)	24.6h (β) (c6)	...	...	...	...	...	$U^{235}\alpha$-decay Th^{232}(n,2n) (N_3)	weak α-activity probable.
Th^{232}	1.39×10^{10}y (K_3)	...	1.39×10^{10}y	1.58×10^{-18}	4.2 (S6) 3.90 (F_1)	4.27 3.97	Natural Source	...
Th^{233}	23m (β) (G_4)	...	...	...	...	...	Th^{232}(n,γ) (M2)	...
Th^{234} (UX_1)	24.5m (β) (c6, s4)	...	...	...	...	...	$U^{238}\alpha$-decay	weak α-activity probable.

determined the range of α-particles by photographic method. With the range-energy curve by Holloway and Livingstone (1938), E_α becomes 3.90 MeV. This value appears too low.

Th^{234} : This, being the decay product of long-lived U^{238}, is expected to show weak α-activity which probably remains masked by strong β^--activity.

Geiger-Nuttall Curve for Th.

With the data given in Table VIII a continuous curve can be drawn through the five plotted points (Fig. 8) and only Th^{227} falls outside. In case of Th^{232} isotope the α-energy is not consistent for different works. The modified Geiger-Nuttall curve gives us the clue regarding the correctness of the values of E_α. As observed from this curve, in case of Th^{232}, the value of Schintlmeister (1937) appear more satisfactory than the other.

(91) *Protoactinium*

Of six known isotopes of Pa, three are α-active. The data are given in Table IX.

Pa^{227} : This is the starting member of the co-lateral chain of Ac series. The K-capture activity is in agreement with β-energetic studies.

Pa^{228} : This is the starting member of the colateral chain of Th series. This shows high-K-capture activity as expected from β-energetics.

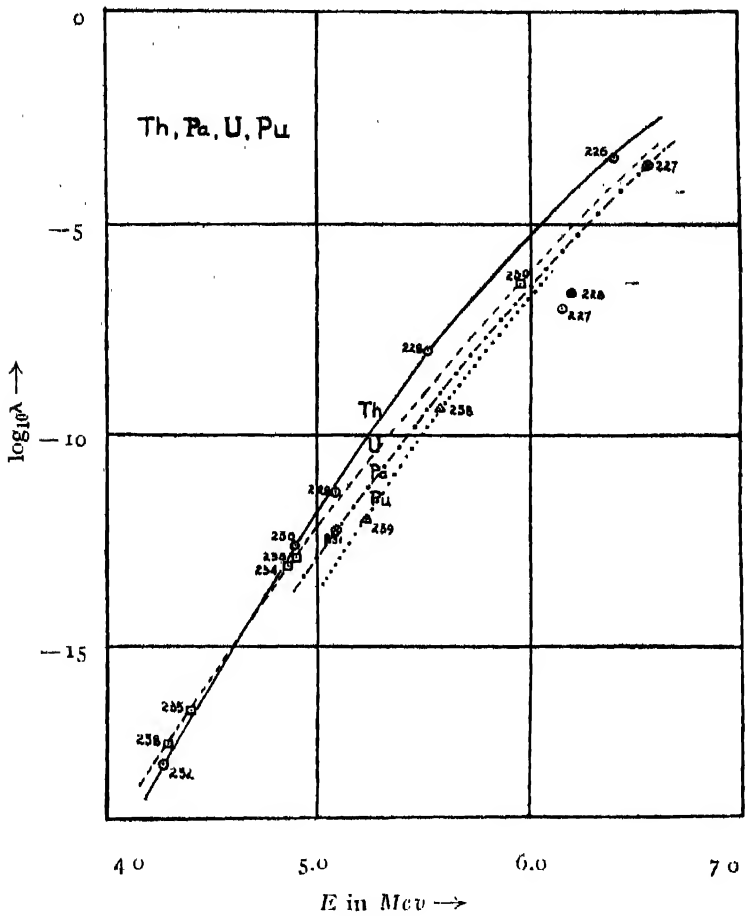

FIG. 8

Pa^{229} : Not yet known. According to β-energetics, this will decay by K-capture.

Pa^{230} : The β-activity of this follows from β^--energetics studies.

Pa^{231} : The α-particles from this isotope, so long known to be homogeneous have recently been shown to have fine structure by San-Tsiang et al (1946). Three groups of α-particles of energies 5.00, 4.72 and 4.69 MeV are found ; the intensity of group o α-particles is about 81%. Thus $\lambda_{\alpha 0}$ becomes 5.59×10^{-13} sec^{-1}.

Pa^{232} : Not yet known. May be obtained from Pa^{231} (n,γ), reaction. This isotope will show predominant β^--activity.

Pa^{233} : The observed β^--activity is in good agreement with β-energetics studies.

Pa^{234} (UX_2, UZ) : Two isomeric nuclei exists for Pa^{234}. $_{90}UX_1^{234}$ goes over to UX_2^{234} by β^--decay. UX_2^{234} has an isomeric transition to UZ^{234} and both UX_2 and UZ, decay to UII^{234} by β^--emission.

TABLE IX

Protoactinium (91)

Isotopes	Observed half-life	$\frac{\alpha}{\beta}$ ratio	α-half-life	λ_α (Sec^{-1})	β-energy (MeV)	Decay energy E (MeV)	Produced by	Remarks
Pa^{227}	38m (G2a)	$\frac{\alpha}{K} \sim \frac{5}{1}$	45.6m	2.53×10^{-4}	6.46 (G2a)	6.57	Th^{232}(d 7n)	
Pa^{228}	22h (G2a)	$\frac{\alpha}{K} \sim \frac{1}{50}$	46 8d	1.68×10^{-7}	6.09 (G2a)	6.20	Th^{232}(d,6n)	
Pa^{229}	?	...	...	...	...	...	Th^{232}(d,4n)	This will show K-capture
Pa^{230}	17d(β^-) (S12)	..	...	...	...	...	Th^{232}(α,p5n)	
Pa^{231}	3.2×10^4y (G3)	..	3.2×10^4y	6.9×10^{-13} $\lambda_{av}=5.6\times10^{-13}$	5.0 (S3)	5.09	$UY^{231}\beta^-$-decay	
Pa^{232}	?	...	...	...	...	...	...	This will decay by β^--activity.
Pa^{233}	27.4d(β^-) (G4)	..	..	...	...	...	$Th^{233}\beta^-$decay	
Pa^{234}	6.7h (β^-)	..	...	..	...	...	UX_2I.T.	
(UZ, UX_2)	1.14m(β^-) I.T.	...	.	...	...	...	$UX_1\beta^-$-decay	

Geiger-Nuttall Curve for Pa.

Of three isotopes, Pa^{228} lies a little below the G-N curve for Pa (Fig. 8). This is probably due to the approximate value of $\alpha : K$ ratio.

(92) *Uranium*

At present seven isotopes of U are known. Four of these are α-active. The relevant data are given in Table X.

U^{238} : This is β-stable as expected.

U^{232} : Not yet known. Expected to show α-activity.

U^{233} : This recently discovered isotope of U is highly fissionable and this is the starting isotopes in the $(4n+1)$ radioactive series.

U^{234} : The experimental data for α-energy vary for different investigators by different methods. Latest determination of α-energy by range measurement in ionisation chamber by Wytzes and Van de Maas (1947) yield α-energy as 4.78 MeV.

TABLE X

Uranium (92)

Isotopes	Observed half life	$\frac{\alpha}{\beta}$ ratio	α-half life	λ_α (Sec^{-1})	α energy (MeV)	Decay energy E_r (MeV)	Produced by	Remarks
U^{230}	20.8d (S12)	...	20.8d	3.86×10^{-7}	5.86 (S12)	5.96	$Pa^{230}\beta^-$-decay $Th^{232}(\alpha, 6n)$	...
U^{232}	...	...	...	...	...	...	...	α-activity expected
U^{233}	1.63×10^5y (E1,H1)	...	1.63×10^5y	1.35×10^{-13}	4.825 (E1,H1)	4.898	$Th^{233}\beta^-Pa^{233}\beta^-$	
U^{234} (UII)	2.69×10^5y (N1)	...	2.70×10^5y	8.14×10^{-14}	4.71(R1) 4.78(S10) 4.76(S_5) 4.78(W_4)	4.86	$Pa^{234}\beta^-$-decay	
U^{235}	7.13×10^8y (N1)	...	7.13×10^8y	3.08×10^{-17}	4.33(V1)	4.40	Natural Source	
U^{236}	?	...	...	...	...	...	$U^{235}(n, \gamma)$?	Instantly fissioned
U^{237}	7d(β^-) (M1, N2)	...	...	...	...	...	$U^{238}(n, 2n)$ (M1, N2)	...
U^{238}	4.56×10^9y	...	4.56×10^9y	4.82×10^{-18}	4.15(R1) 4.23(S10) 4.21(S_5) 4.21(W_4)	4.29	Natural Source	...
U^{239}	23m(β^-) (I1 S9)	...	...	...	...	...	$U^{238}(n, \gamma)$ (H14)	...

U^{235} : The α-energy is obtained from the range of α-particles and the range-energy relation of Holloway and Livingstone (1938).

U^{236} : The isotope U^{236} is not yet known. U^{235} by neutron capture becomes U^{236} which instantly undergoes fission.

U^{237} : The observed β^--activity of U^{237} is in agreement with the β-energetics studies.

U^{238} : The results of various investigations regarding α-energy of U^{238} varies to certain extent. Latest range determination by Wytzes and Van de Maas (1947) yield α-energy as 4.21 MeV. The α-particles are of homogenous energy.

U^{239} : The observed β^--activity of U^{239} is in accordance with the energetics studies. The β^- energy has not yet been measured.

The Geiger-Nuttall Curve for U.

With the data given in Table X, the log λ, E curve for the isotopes of U is drawn (Fig. 7). It is seen that all of five U isotopes lie on a smooth G-N curve for U.

(93) *Neptunium*

Np^{237} is the only α-active isotope of Np known so far, The value of α-energy is not yet known.

(94) *Plutonium*

Three isotope of plutonium are known two of which Pu^{238} and Pu^{239} are α-active. The data are given in Table XI.

TABLE XI

Plutonium (94)

Isotopes	Observed half life	$\frac{\alpha}{\beta}$ ratio	α half-life	λ_α (Sec^{-1})	α-energy, (MeV)	Decay energy E, (MeV)	Produced by	Remark
Pu^{236}	...	...	...	..	...	...	$Np^{236}\beta^-$-decay $Cm^{240}\alpha$-decay	...
Pu^{238}	50y (S8)	...	50y	1.39×10^{-10}	5.49 (C1)	5.58	$Np^{238}\beta^-$-decay $Cm^{242}\alpha$-decay	...
Pu^{239}	24,000y (S8)	...	24,000y	9.16×10^{-13}	5.15	5.23	$U^{239}\beta$-decay	...
Pu^{241}	long(β)	..	...	...	..	...	$U^{238}(\alpha,n)$ (S8)	...

Pu^{236} : Nothing is reported about this isotope which must have been produced in β^--decay of Np^{236} and α-decay of Cm^{240}.

This will be γ-active, decaying to U^{232}.

Pu^{238} : The recent report of the range of α-particles from Pu^{238} by Chamberlain et al (1947) yield α-energy of 5.49 MeV from the range-energy curve (Holloway and Livingstone, 1938).

Pu^{239} : The range measurements by Chamberlain et al (1947) yield α-energy as 5.15 MeV.

Pu^{241} : The observed longlife β^--activity of Pu^{241} is in agreement with β-energetices studies.

The Geiger-Nuttall Curve for Pu.

With two points corresponding to two α-active isotopes of Pu, the long λ, E curve is an approximate one. The curve is of the same nature as with other elements (Fig.8).

CONCLUSION

Thus it is seen that experimental data of all α-active nuclei can be plotted quite satisfactorily on seperate Geiger-Nuttall curves for each element. Deviation occuring in some cases are mostly due to the uncertainties in the experimental data as pointed out. These curves will be of much help in ascertaining for any new α-active isotope the half life or α-energy when any one of them is known.

ACKNOWLEDGMENT

The author expresses his gratitude to Prof. M. N. Saha, F.R.S. for his continued interest and guidance during the progress of the work. The author is also thankful to C.S.I.R. for the award of a scholarship which enabled him to carry out to work.

INSTITUTE OF NUCLEAR PHYSICS,
UNIVERSITY OF CALCUTTA,

REFERENCES

B1. Berthellot, 1942, *J. Phys. Radium.*, **3**, 52.
B2. Biswas and Mukherjee, 1948, *Ind. Jour. Phys.*, **22**, 80.
B3. Briggs, 1936, *Proc. Roy. Soc. Lond A.*, **157**, 183
B4 Broda and Feather, 1947, *Proc Roy., Soc. A.*, **190**, 20.
C1. Chamberlain, Gofman, Segre & Wohl, 1947, *Phys. Rev.*, **71**, 528.
C2. Chang, 1946, *Phys. Rev.*, **69**, 60.
C2a. Condon and Gurney, 1929, *Phys. Rev*, **33**, 127.
C3. Cork, Halparn and Tatel, 1940, *Phys. Rev.*, **57**, 371.
C4. Corson, Mackenzie and Segre, 1940, *Phys Rev*, **57**, 459 & 1087.
C5. Corson, Mackenzie and Segre, 1940, *Phys. Rev.*, **58**, 672
C6. Curie, Debierne, Eve, Geiger, Hahn, Lind, St. Meyer, Rutherford, and Schweidler, 1931, *Rev. Mod Phys.*, **3**, 427.
D1. Dunworth, 1939, *Nature.*, **144**, 152.
E1. English, Cranshaw, Denners, Hervey, Hincks, Jelley and May, 1947, *Phys Rev.*, **72**, 253.
F1. Faraggi, 1946, *J. Phys. Radium*, **7**, 353.
G1. Gamow, 1929, *Zeits. f. Physik.*, **52**, 510.
G2. Gamow, 1937, Structure of Atomic Nuclei and Nuclear Transformations (Oxfd. Clarendon Press).
G2a. Ghiorso, Meinke and Seaborg, 1948, *Phys. Rev.*, **74**, 695.
G3. Gratias and Collie, 1932, *Proc. Roy. Soc. Lond. A.*, **135**, 299.
G4. Grosse, Booth and Dunning, 1941, *Phys. Rev*, **59**, 322.
G5 Gueben 1932, *Ann. Soc. Sci Bruxelles. B.*, **52**, 60.
G6. Gueben, 1933, *Ann Soc. Sci. Broxelles B.*, **53**, 115.
H1. Hagemann, Katzin, Studier, Ghiorso and Seaborg, 1947, *Phys. Rev.*, **72**,252.
H1a. Hahn and Strassmann, 1939, *Naturwiss.*, **27**, 11.
H2. Henderson and Lawrence, 1937, *Phys. Rev.*, **52**, 46.
H3. Holloway and Livingstone, 1938, *Phys. Rev.*, **54**, 18.
H4 Howland, Templeton and Perlman, 1947, *Phys. Rev.*, **71**, 552.
H5. Hurst, Latham and Lewis, 1940, *Proc. Roy. Soc. Lond. A.*, **174**, 126.
I1. Irvin (jr.) 1939, *Phys. Rev.*, **55**, 1105.
K1 Karlik and Bernert, 1943*a*, *Naturwiss.*, **31**, 492.
K2. Karlik and Bernert, 1943*b*, *Naturwiss*, **31**, 298.
K3. Kavorik and Adams, 1938, *Phys. Rev*, **54**, 413.
K4. Kovarik and Adams, 1941, *J. Appl. Phys.*, **12**, 296.
L1. Laue, 1929, *Zeit. f. Physik.*, **52**, 726.
L2. Livingstone and Bethe, 1937, *Rev. Mod., Phys.* **9**, 266.
L3. Lecoin, 1938, *J. Phys. Radium.*, **9**, 81.
L4. Lewis and Bowden, 1934, *Proc. Roy. Soc. Lond. A.*, **145**, 235

M1. McMillan, 1940, *Phys. Rev.*, **58**, 178.
N1. Nier, 1939, *Phys. Rev.*, **55**, 150.
N2. Nishina, Yasaki, Ezoe, Kimura and Ikawa, 1940, *Phys. Rev.*, **57**, 1182.
N3. Nishina, Yasaki, Kimura and Ikawa, 1938, *Nature*, **142**, 874.
P1. Perey, 1939, *Compt. Rend*, **208**, 97
P2. Perey and Lecoin, 1939, *J. Phys. Radium.*, **10**, 435.
P3. Preston, 1946, *Phys. Rev.*, **69**, 535.
P4. Preston, 1947, *Phys. Rev.*, **71**, 865.
R1. Rayton and Wilkins, 1937, *Phys. Rev.*, **51**, 818.
R2. Ringo, 1940, *Phys. Rev.*, **58**, 942
R3. Ringo, 1941, *Phys. Rev.*, **59**, 107.
R4. Rotblat, 1941, *Proc. Roy. Soc. Lond. A.*, **177**, 260.
S1. Saha A. K. 1944, *Proc. Nat. Int. Sci. Ind.*, **10**, 373.
S2. Saha M. N., and Saha A. K., 1946, *Trans. Nat. Inst. Sci. Ind.*, II, 193.
S2a. Saha M. N., Sirkar and Mukherjee, 1940, *Proc. Nat. Inst. Sci. Ind.*, **6**, 45.
S3. San-Tsiang, Bachelet and Bouissiers, 1946, *Phys. Rev.*, **69**, 39.
S4. Sargent, 1939, *Can. J. Research A.*, **17**, 103.
S5. Schintlmeister and Lintner, 1939, *Sitz. Akad. Wiss-Wien. Abt. IIa.*, **148**, 27
S6. Schintlmeister, 1937, *Sitz. Akad. Wiss. Wien. Abt. IIa.*, **146**, 371.
S7. Seaborg, 1944, *Rev. Mod. Phys.*, **16**, 1.
S8. Seaberg, 1946, *Science.*, **104**, 379.
S9. Segre, 1939, *Phys. Rev.*, **55**, 1104.
S9a. Sexl, 1933, *Zeits. f. Physik*, **81**, 163.
S10. Sizoo and Wytzes, 1937, *Physica.*, **4**, 791.
S11. Starke, 1942, *Naturwiss*, **30**, 577.
S12. Studier and Hyde, 1948, *Phys. Rev.*, **74**, 591.
T1. Templeton, Howland and Perlman, 1947, *Phys. Rev.*, **72**, 768.
T2. Templeton, Howland and Perlman, 1947, *Phys. Rev.*, **72**, 758.
V1. Van Der Maas and Yntema, 1947, *Physica.*, **13**, 453.
W1. Ward, 1942, *Proc. Roy. Soc. Lond. A*, **181**, 183.
W2. Wilkins and Crowford, 1938, *Phys. Rev.*, **54**, 316.
W3. Winand, 1937, J. *Phys. Radium.*, **8**, 429.
W4. Wytzes and Van der Maas, 1947, *Physica.*, **13**, 49.

ON THE PROPAGATION OF SUPERSONIC WAVES THROUGH LIQUIDS AND SOLUTIONS

By B. B. GHOSH

(*Received for publication, Aug. 26, 1948*)

ABSTRACT. A survey of the position of absorption and dispersion of supersonic waves in liquids, both theoretical and experimental, has been made. Different theories including those of the author have been critically discussed and the theoretical expression deduced by the author has been further extended to calculate the dispersion in electrolytic solutions. It has been suggested that the experimental observations on the dispersion in water and $MgSO_4$ solution might be explained on the basis of water structure and the mutual interaction of electronic atmospheres of molecules.

EXPERIMENTAL AND DISCUSSION

The experimental observations on the absorption and dispersion of supersonic waves in liquids are not explained by the existing theories. The exact position can be indicated in the following lines.

When sound waves or elastic waves travel in any medium, liquid or gas, the co-efficient of absorption, due to the viscosity and the heat conductivity of the material, is given by the classical formula of Stokes (1840) and Kirchoff (1868). This can be expressed in the form,

$$\alpha_{(\text{classical})} = \alpha_s + \alpha_k = \frac{2\pi^2}{\lambda^2 V\rho}\left[\frac{4}{3}\eta + \frac{c_p - c_v}{c_p c_v}k\right]$$

where, λ = Wavelength of the sound wave.

V = Velocity

ρ = Density of the medium.

η = Co-efficient of viscosity of the medium.

k = Co-efficient of conductivity.

and c_p, c_v – the specific heats at constant pressure and volume.

The contribution of the second term is generally much too small compared with the first term, so that the absorption is determined by the viscosity of the material. It has been found that the calculated absorption on this classical line, is much lower than the observed absorption in the case of gases, whereas, in case of liquids the observed absorption is, as a rule, much higher than the calculated values. It was further found that in case of those gases, where high absorption has been observed, there is observed a

dispersion as well. Liquids, however, have not shown any well-established and noteworthy dispersion in the supersonic region.

Kneser (1931) Herzfeld and Rice (1928) and others, later developed a theory, based on what is known as the relaxation principle. The essential idea of this mechanism is that the impressed energy, which is in the form of translatory energy, is not generally immediately converted into the form of molecular energy. A definite time is required before the translatory energy can be converted into oscillatory energy. If the time period of the impressed energy is comparable to this time, a part of this impressed energy will not be assimilated into internal energy. When the impressed energy is not assimilated, the specific heat decreases and the velocity increases. This gives rise to a dispersion. Further for a harmonic distubance, any variation with time involves an imaginary quantity. It is then automatically associated with absorption.

The theoretical expressions derived from this relaxation principle explained the absorption and dispersion phenomenon in gases in general. In the case of liquids, however, the theoretical position in explaining the experimental observations was found to be very disappointing. Attempts by many, such as, Lucas and Biquard (1937) Clays, Errera and Sack (1937) to find out suitable theoretical explanations were all unsuccessful.

Dutt (1938), following this relaxation mechanism suggested by Kneser (1938) and using certain thermodynamic relations, developed a theoretical expression for the dispersion of supersonic waves in liquids. The expression

$$\frac{V_\infty^2}{V_0^2} = \begin{vmatrix} c_a + \dfrac{\psi^2 v_m T}{\chi} & c \\ c_a & c + \dfrac{\psi^2 v_m T}{\chi} \end{vmatrix} \Bigg/ \begin{vmatrix} c & c \\ c_a & c + \dfrac{\psi^2 v_m T}{\chi} \end{vmatrix}$$

is given by, where V_∞ and V_0 are velocities at very high and very low frequencies, ψ is the co-efficient of expansion, χ is the co-efficient of compressibility, v_m is the molar volume and c_a is related in the following way :—

$$c = c_a + c_i \quad \text{and} \quad c'_i dT = c_i F(\omega) dT$$

where $c'_i dT$ denotes the change in energy due to the assimilation in the internal degrees of freedom and should be considered as a function of frequency. $c_a dT$. denotes the change in energy in other possible ways, like translatory motion etc.

Calculations based on this formula showed that the value of V_∞^2/V_0^2 for toluol, xylol, aniline, carbon-bisulphide, etc., varies from 1.01 to 1.057 and that in the case of water no dispersion is expected. Experimentally, however, it has been reported by a number of workers (Spakovskij (1935 and 1937); Hiedemann, Seifen and Schenrer (1936); Parthasarathy (1935 and 1936); Dutt (1938); Richardson (1940)); that in the case of liquids in general

although a very high order absorption is generally obtained no well-defined dispersion has ever been reported. In the case of water, some very conflicting results have been obtained by various workers. Dutt (1938); Dutt and Ghosh (1941); Bar (1938); Matossi (1939); Krishnan (1939).

Thus while in the case of absorption, we have practically no theoretical explanation for the experimental observations, which are rather definite; in the case of dispersion both theoretical and experimental observations are not only inadequate but vague.

A theoretical expression for absorption of supersonic waves in liquids was derived by Dutt and Ghosh (1939) on the basis of relaxation principle. The expression so obtained, was found to contain the expression for dispersion and the frequency for maximum absorption which corresponds to the frequency of inflexion ω_i in the curve for dispersion *vs.* frequency. The expressions so derived are given below ;—

$$(a)\quad \mu_m = \pi \frac{V_\infty^2 - V_0^2}{V_0^2}. \qquad (b)\quad \mu = 2\mu_m \frac{\nu/\nu_m}{1+(\nu/\nu_m)^2}$$

$$(c)\quad (V^2 - V_0^2) = (V_\infty^2 - V_0^2)\frac{(\nu/\nu_m)^2}{1+(\nu/\nu_m)^2}. \qquad (d)\quad \alpha/\nu^2 = \frac{2\mu_m}{V\nu_m}.$$

Where μ – is the co-efficient of absorption per unit wave length.

μ_m – is the co-efficient of maximum absorption.

α – is the co-efficient of absorption per unit length.

ν_m – is the frequency for maximum absorption. $= 2\pi\omega_m$.

ν – is the frequency at which the absorption is measured.

V – is the velocity at this frequency.

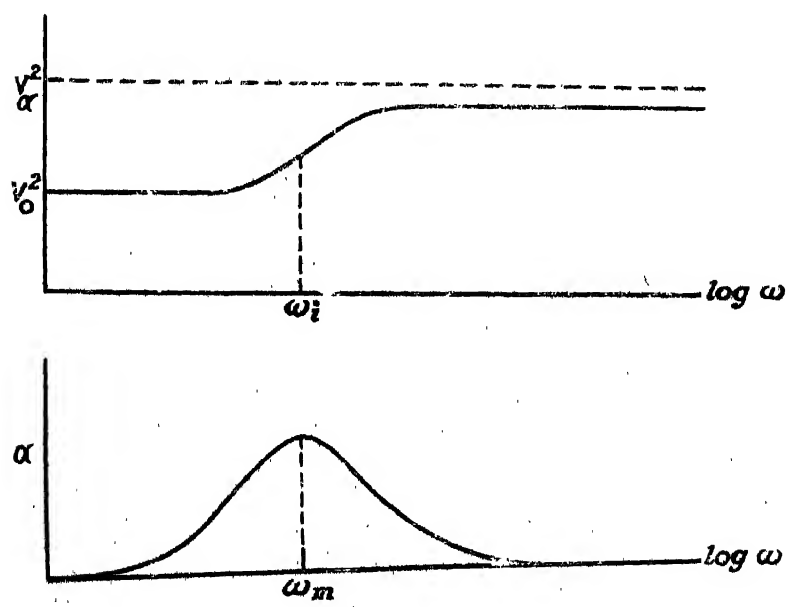

FIG. 1.

Kneser had worked out a general dispersion formula and had derived some similar expressions as given above. The present derivations, although based on relaxation principle of Kneser and others, involve some thermodynamical relations for liquids and contain known constants. It has thus been possible to calculate theoretically the amounts of dispersion and the frequency of dispersive region for liquids. The conclusions that directly followed from these theoretical calculations are :—

(1) The frequency for dispersion in the case of liquids is of the order of 10^8c/s, the attainment of which is not possible with the present day experimental arrangement (Bhagabantham and Rao, 1946). This explains why dispersions in liquids in general have not been, so far, experimentally established.

(2) There is a group of liquids such as CH_3 COOH, CH_3COOCH_3, $CH_3COOC_2H_5$, CS_2 etc., which show what may be called anomallous absorption and dispersion.

(3) In general, the experimental observations in liquids can be accounted for.

(4) No absorption is expected in the case of water according to this theory and it should not have any dispersion and its frequency of dispersive region comes out to be an ambiguous one. Experimentally, however, water shows quite an appreciable amount of absorption and many contradictory results are reported for dispersion.

The amount of dispersion in water was, however, measured by Dutt and Ghosh (1941) employing a method which eliminated all possible sources of errors that might have occurred in the experiments of all other workers in the line (Bar 1938; Motossi 1939; Krishnan 1939; Sorensen 1936). It was established that at about 33°C temperature, there is dispersion of 1.5 ± 0.2 parts in 1000, in the frequency range 3 to 30 Mc/s. The dispersion in water reported previously by Dutt (1938) among others was 1.7 ± 0.2 in 1000 at a temperature of about 27°C. It was also found by Dutt and Ghosh (1941) that the amount of dispersion decreases with increasing temperatures as also with increasing concentrations of $MgSO_4$ in water.

In view of this observations on $MgSO_4$ the case of electrolytic solutions can be considered in the following way. The equation may be written in the form

$$\alpha/\nu^2 = \frac{2\mu_m}{V\nu_m} = \frac{2\mu_m}{(\lambda\nu)\nu_m}.$$

also the sound velocity, V is given in the form,

$$V = \frac{1}{\sqrt{\rho\beta_{ad}}}.$$

where ρ is density and β_{ad} adiabatic compressibility. For electrolytes β_{ad} is linearly dependent on concentration in the following way,

$$\beta_{ad}=\beta_1+Ac+Bc^{\frac{3}{2}}$$

where A and B – are constants, c – concentration and β_1 – compressibility of the pure solvent.

Therefore we have

$$\alpha/\nu^2=\frac{2\mu_m}{\nu_m}(\rho)^{\frac{1}{2}}(\beta_1+Ac+Bc^{\frac{3}{2}})^{\frac{1}{2}}$$

which shows that (assuming variation of the ratio μ_m/ν_m with c is small) α/ν^2 is directly proportional to a certain power of concentration and when concentration is constant, it decreases when the frequency is increased. This has been experimentally verified by Buss (1938) for $MgSO_4$, Na_2SO_4, NaCl and NH_4Cl.

Now since α is given by

$$I_x=I_0.e^{-\alpha x}$$

and μ the co-efficient of absorption per unit wave length is given by, $I_x=I_0.e^{-\mu x/\lambda}$ We get, by substitution in

$$\alpha/\nu^2=\frac{2\mu_m}{V.\nu_m}. \quad , \quad \mu=\frac{2\mu_m}{\nu_m}.\ \nu.$$

also since $\mu=2\pi\tan\phi$

$$\text{and } \tan\phi=\frac{(V_\infty^2-V_0^2)\omega_i.\omega.}{V_0^2\omega_i^2+V_\infty^2\omega^2}.$$

on simplification we get,

$$a\omega_i^2+\omega_i-\omega_i x^2+bx^2=0. \quad \text{Where } a=\mu/4\pi^2\nu.$$

$$b=\mu\nu.$$

$$\text{and} \quad V_\infty^2/V_0^2=x^2.$$

by giving any two values to μ and ν, this becomes,

$$\omega_i^2=\frac{b_2-b_1}{a_1-a_2}x^2=\frac{(\mu_2\nu_2-\mu_1\nu_1)}{\left(\frac{\mu_1}{4\pi^2\nu_1}-\frac{\mu_2}{4\pi^2\nu_2}\right)}\cdot\left(\frac{V_\infty^2}{V_0^2}\right).$$

The experimental values for μ_1 and μ_2 at ν_1 and ν_2 for $MgSO_4$ are available from the works of Bazuline (1938) so that the values of ω_i and $x=V_\infty/V_0$ can be obtained from the above expression.

Thus in this case also, the dispersive region lies in the neighbourhood of 10^8 c/s. Even in this region the effect is rather small at comparatively lower concentrations. At higher concentrations the effect is more marked and

becomes a measurable quantity. But it shows an increase with concentrations while our experiments show a decrease with concentrations.

TABLE I

Dispersion in $MgSO_4$ solution—(Theoretical.)

"c"—concentration Mol/litre.	Frequency range		Frequency corresponding to the frequency of inflexion ω_i	Dispersion over this frequency range $x = V_\infty / V_6$
	$\nu_1 = 3{,}162{,}000$ cps (Exptl.) $\mu_1 \times 10^3$	$\nu_2 = 31{,}620{,}000$ cps (Exptl.) $\mu_2 \times 10^3$		
0.01	0.437	1.8125	$1.648 \; 10^9 . x$	1.0002936
0.30	0 625	3·500	1.516 ,, x	1.0003864
0.47	1.812	6.3125	1.433 ,, x	1.00106

TABLE II

Dispersion in $MgSO_4$ solution—(Experimental)

To be added to 31°C		Liquids	Concentration Mol/litre	Low frequency		High frequency		Ratio	Dispersion (after deducting) 1.5 ± 0.2 o/oo for water
Temperature read by Beckmann thermometer				Order of the spec. tra	Mean distance	Order of the spectra	Mean distance		
L.F.	H.F.								
3 04	3.05	Water	..	3	6.016	1	19.708	9.827	
3,05	3.05	$MgSO_4$	0.229	2	3.902	1	19.212	9.842	-0.0 ± 0.2 o/oo
2.41	2 41	Water	...	2	1.011	1	19.705	9.825	
2 41	2.42	$MgSO_4$	0.475	3	5.901	1	19 400	9 845	-0.7 ± 0.2 o/oo
1.75	1.75	Water	...	3	6.030	1	19.820	9.861	
1.76	1.75	$MgSO_4$	0.700	3	5.936	1	19.633	9.886	-1.0 ± 0.2 o/oo

The same method that was employed to measure the dispersion effect in the case of water (Dutt and Ghosh, 1941) was followed in this case as well. The experiments, however, could not be continued as the H. F. crystal got damaged in the course of experiments.

We may now proceed to explain these observations in the case of water and of solutions with water as solvent.

In general, in the case of relaxation theory the equilibrium between vibrational and translational energy is sought through temperature and change in specific heats, etc., and the variation in compressibility always comes into considerations for velocity changes of supersonic waves through liquids. It is possible that in addition to this, some other factor due to the interaction of molecules while in the process of vibrations, is involved giving rise to two types of absorptions, one on the basis of relaxation principle and the other on the basis of molecular interaction. This we consider in the following way :—

It is generally seen that absorption in different liquids, measured experimentally, is usually greater than the calculated ones. So it is quite possible that the differences between the two values is due to the contribution from a source other than from the relaxation mechanism.

In gases, the molecules are far apart and consequently there is little or no interaction except when collisions take place between molecules. In liquids the molecules are nearer and the molecular interaction is immense. The molecular interaction assumes the form of mutual influence of electronic atmosphere.

When a sound beam is propagating through liquids, during compressions, the molecules may come so close to each other that they affect each other's electronic atmospheres. As a consequence, vibrations in the molecules will be started. The energy for these vibrations will be derived from the energy of the propagating sound waves. Since these vibrations will not be in equilibrium with temperature, they will tend to be lost quickly by collisions or otherwise. Now it is very uncommon that vibration will be transferred to other molecules as vibrations. That is to say that resonance for vibrational energy is an exception rather than a rule, and as such the vibrating molecule will give out its energy not in one degree of freedom but many, not in one form, but will be divided up in vibrational, rotational and translatory forms of energy.

In relaxation principle we consider that the extra energy, imparted to the liquid is at first in the form of energy of translation. Due to this higher translatory energy, the system is heated and other forms of internal energy are excited. Further a definite time is required for this transference of energy from translatory to other forms of energy. It is this time factor that is the controlling unit, so to say, to determine whether the transference is complete or incomplete. If the transference is not complete the unassimilated energy heats up the system causing changes in specific heat etc. In the type of molecular interaction as considered here the transference is a direct one and as such is capable of exciting very high vibrations in the molecules that do not ordinarily come into the relaxation theory and is therefore left out of consideration. In this new mode of absorption, the

compressibility variations do not come in, except as a second order effect which might set in at high frequencies. In other words, generally in case of liquids, absorption should be unaccompanied by dispersion except at very high frequencies. This accounts for the absence of any dispersion in liquids at ordinary frequencies.

Dispersion in water.—Dispersion in water also can be explained on the basis of this new mode of vibrational theory.

The water forms what may be called a structure or association of a number of water molecules. Now when the H_2O molecules vibrate in the sound waves propagating through the liquids, the molecules may, on coming near each other, so transform their electronic atmosphere, that a new mode of vibration level as stated above, may be operative for the nuclii. The vibrational energy may, on account of this, rise so high that the water molecules may have to separate themselves from the existing structure in conformation to the new mode of vibration. As a result the compressibility will be affected and so the velocity.

Now it may be shown why the velocity in water will be higher at higher frequencies.

During each vibration, some free molecules of water are set up. They tend to recombine again. Hence there will be an equilibrium between the two opposite tendencies. The higher the frequency of the sound waves the greater will be the equilibrium shift towards the greater number of free water molecules, and compressibility will be less than at lower frequencies. Velocity is higher at higher frequency and hence the dispersion.

Temperature effect on dispersion.—As we have seen before, dispersion decreases with increasing temperatures. This is due to the fact that at higher temperature we have greater number of broken up water structures due to temperature alone. So that at higher frequencies, at this temperature, the available number of water structure is less, with the result that the equilibrium shift towards the greater number of free water molecules is less than at lower temperatures. Consequently, lowering of compressibility by increasing the frequency at higher temperatures is less than that at lower temperatures. Thus dispersion decreases with increasing temperatures.

This also accounts for the experimental observation why dispersion in $MgSO_4$ solution in water decreases with increasing concentrations. The introduction of $MgSO_4$ molecules into water results in the breaking up of water structures in the same way as the increase of temperature.

In a previous paper Dutt and Ghosh, (1943) have reported the variation of supersonic velocity with concentration for various electrolytic solutions and have shown that the curves for the velocity of supersonic waves *vs.* concentration of electrolytic solutions can only be partly explained from the stand point of ionic theory of Debye and Falkenhagen. On comparing

these curves with the curves for viscosity *vs.* concentration, some interesting points were revealed and it was suggested there that the velocity of supersonic waves in electrolytic solutions has got to be considered from an angle from which viscosity of the solution might as well be viewed.

The theory outlined above for the dispersion of supersonic waves in water on the basis of molecular interaction and breaking up of the water structure, can also be further extended to explain the above curves in general.

The details will be reported in another paper.

ACKNOWLEDGMENT

My thanks are due to Dr. A. K. Dutta for many helpful discussions on the preparation of this paper. I am also indebted to Prof. D. M. Bose, Director, Bose Research Institute for various sorts of helps received from him, in carrying out this work. I also take this opportunity to express my sincere thanks to the Chief Engineer, All-India Radio, for granting me necessary official permission for its publication.

BOSE RESEARCH INSTITUTE,
CALCUTTA.

REFERENCES

Bar, R., 1938, *Proc. Ind. Acad. Sci.*, **8A**, 289.
Bazulin, P., 1938, *Compt. Rendu. U. S. S. R.*, **19**, 153.
Bhagabantham and Rao, 1946, *Nature*, **158**, 484.
Buss, W., 1938, *Ann. der. Phys.*, **33**, 143.
Clays, Errera and Sack, 1937, *Trans. Farad. Soc.*, **33**, 137.
Dutt, A. K., , 1938, *Phys. Zeits.*, **39**, 186.
Dutt, A. K. and Ghosh, B. B., 1939, *Trans. Bose. Res. Inst.*, **13**, 31.
,, ,, , 1941, *Trans. Bose. Res. Inst.*, **14**, 127.
,, ,, , 1943, *Ind. Jour. Phys.*, **18**, 19.
Herzfeld and Rice, 1928, *Phys. Rev.*, **31**, 691.
Hiedemann, Seifen and Schenrer, 1936, *Naturwiss*, **24**, 681.
Kirchhoff, 1868, *Pogg. Ann.*, **134**, 177.
Kneser, 1931, *Ann. der Phys.*, **11**, 761.
,, , 1938, *Ann. der. Phys.*, **32**, 281.
Krishnan, K. G., 1939, *Proc. Ind. Acad. Sci.*, **9A**, 382.
Lucas and Biquard, 1937, *Trans. Farad. Soc.*, **33**, 130.
Matossi, F., 1939, *Phys. Zeits.*, **40**, 294.
Parthasarathy, S., 1935, *Proc. Ind. Acad. Sci.*, **4**, 17.
,, , 1936, *Proc. Ind. Acad. Sci.*, **4A**, 222.
Richardson, E. G., 1940, *Proc. Phys. Soc.*, **52**, 480
Spakovskij, B., 1934, *C.R., U. S. S. R.*, **3**, 588.
,, , 1938, *C. R., U. S. S. R.*, **1** , 169.
Sorensen, C., 1936, *Ann der Physik*, **26**, 121.
Stokes, 1840, *Cambr. Trans. Phil. Soc.*, **8**, 287.

MICRO-WAVE RADIO BLIND LANDING SYSTEMS FOR AIRCRAFTS

By A. N. BHATTACHARYYA

(*Received for publication, Sept. 24, 1948*)

ABSTRACT. The system uses two rotating sharply defined radio beams radiated from two rotating aerials using paraboloidal reflectors and excited with micro-waves. The two aerials rotate in opposite directions in a plane which is inclined at an angle α to the earth's surface. The rotating movement of the aerials is so synchronised that the radio beams simultaneously cross the vertical plane which is perpendicular to the line joining two aerials It will be seen that the moving beams trace a line or path in the said vertical plane, which is inclined at an angle α to the earth's surface. The angle α is the desired glide angle.

INTRODUCTION

A known micro-wave radio blind landing system (MIT—CAA Micro-wave system) operating at frequencies of the order of 750 Mc uses two sectoral horns for the localizer transmitter, the glide path being established by means of a second pair of horns. Equisignal localizer path and equisignal glide path are obtained in this system. The system described in this paper operate at frequencies of the order of 20,000 Mc and there is no necessity of separate localizer and glide path beacons. Vertical guidance is obtained due to the fact that the beams are very narrow, say 2° in the vertical plane (referred henceforth as *P*) normal to and passing through the middle point of the line joining the two aerials. Lateral guidance is obtained because the two beams simultaneously meet only at the said vertical plane. The glide path is defined by the line of intersection of the said vertical plane and the plane inclined at an angle α to the earth's surface in which two aerials rotate. It may be mentioned that during the last five or six years radar principles have been applied to ground based landing aids exclusively for the military use.

DESCRIPTION OF THE SYSTEM

The aerials 1 and 2 (Fig. 1) are similar and of the type using paraboloidal reflector (Fig. 2) and excited in the same phase with very high frequency current. They are spaced nearly 400 yards apart and the runway is equidistant from each of the said aerials. 1 and 2 are situated at equal and suitable heights above the ground. They are also arranged to rotate in opposite directions in a

plane inclined at an angle α to the earth's surface which is the desired glide angle. The rotational movements of the aerials 1 and 2 are so

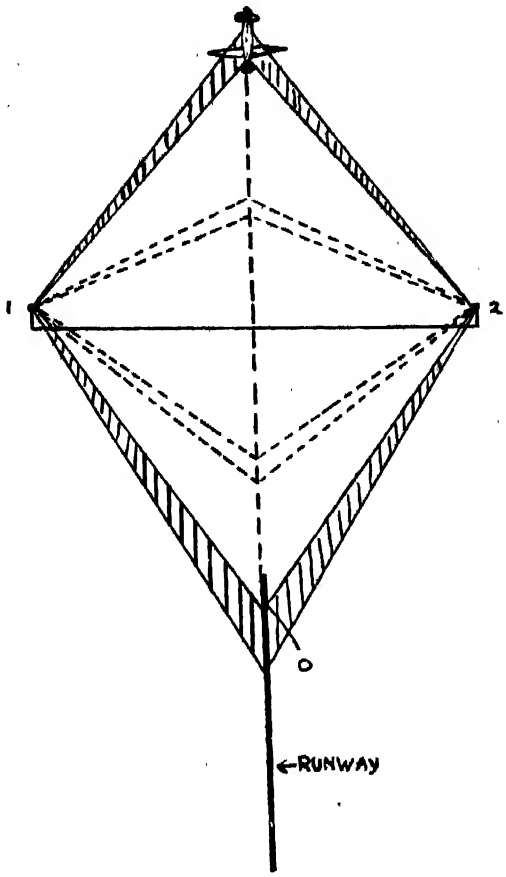

FIG. 1

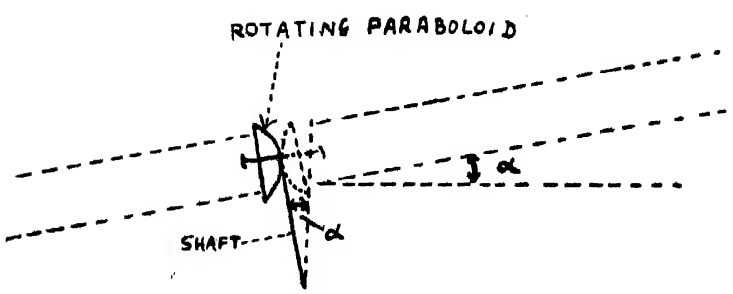

FIG. 2

synchronised that the beams radiated therefrom simultaneously meet at the vertical plane P containing the runway. Such synchronism is obtained by using "Selsyn transmitter and receiver" which is widely used in radar systems and illustrated in Fig. 5. The transmitter and receiver are electrically identical, each comprising of three stator windings wound in slots in the stator core and displaced 120^0 from one another and a rotary winding. When connections are made as shown in Fig. 5 and the rotor windings are

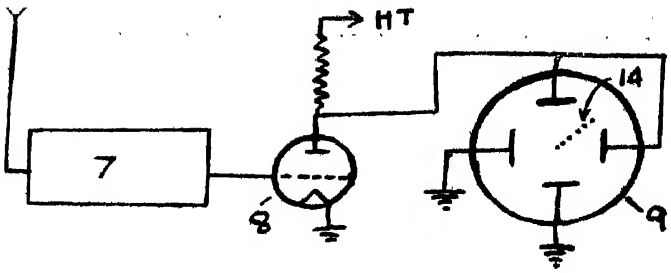

FIG. 3

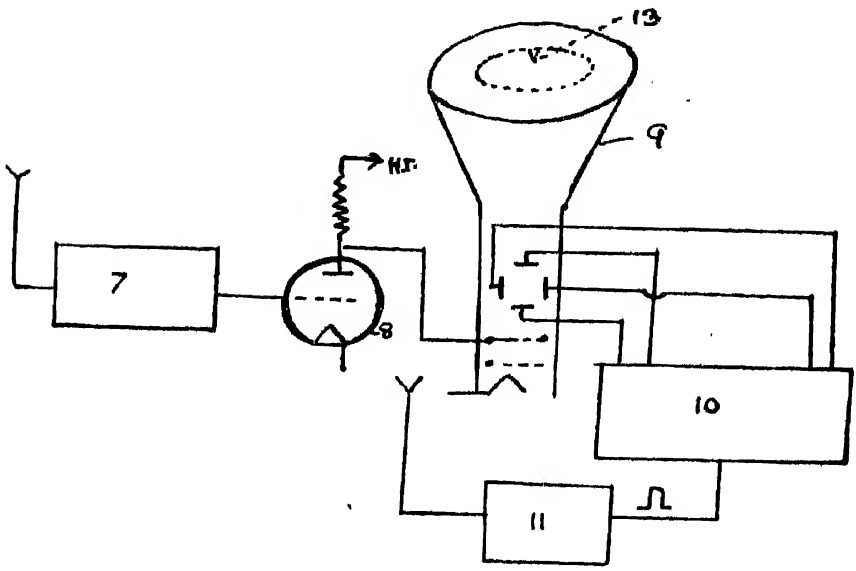

FIG. 4

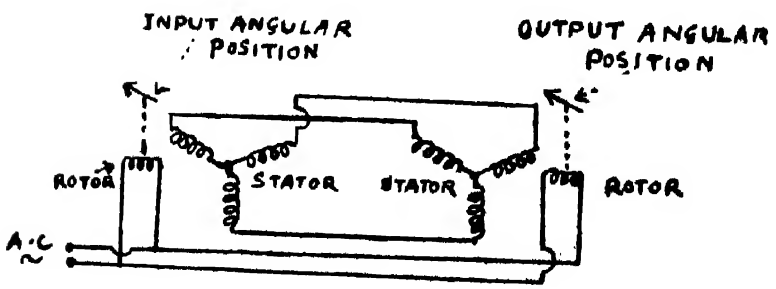

FIG. 5

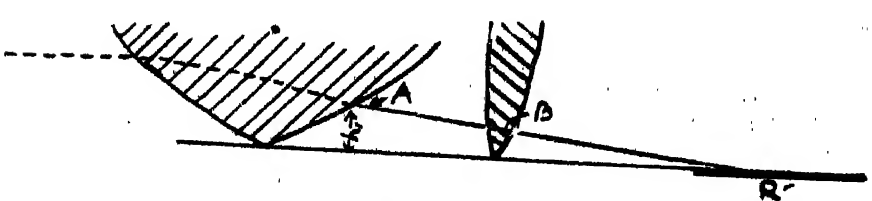

FIG. 6

energised by alternating current from the same source the rotor winding of the receiver takes up an angular position that corresponds to the position of the rotor in the transmitter. By using suitable gearing at the receiver which drives the shaft of one of the aerials say 1 through an intermediate mechanism, 1 may be arranged to rotate in opposite direction to that of 2.(Fig. 1) If "Selsyn transmitter and receiver system" which is also widely known as "Synchro" is not able to supply sufficient torque a servo-mechanism may be used.

The beam width Θ between nulls, in degrees assuming that the radiation from the exciting antenna is omnidirectional is approximately given by the equation

$$\Theta = \frac{137.5}{\left(\frac{D}{\lambda}\right)}$$

where D/λ is the mouth diameter in wave lengths. If Θ is 2° and $D = 1$ metre it will be seen that λ is of the order of 1.46 c.m. Magnetrons using cavity resonators are capable of producing continuous wave power at levels as high as several kilowatts even when such high frequency waves are to be generated.

When continuous waves are radiated from the aerials 1 and 2 the receiver in the aircraft includes a cathode ray tube 9 (Fig.4). The centimetre wave receiver 7 (Fig. 3) comprising silicon crystal mixer, klystron local oscillator and I.F. amplifier and detector stages applies a voltage pulse to the grid of the tube 8 (Fig 3 and 4) whenever the rotating radio beams are intercepted by the aircraft. The output voltage of tube 8 is applied to the X and Y plates of the cathode ray tube 9 so that a line 14 is indicated in the cathode ray tube. The length of the line 14 (Fig. 3) depends on the output voltage of tube 8 and its length will be maximum when the aircraft follows the glide path or when two beams are intercepted simultaneously.

When the magnetron oscillator is pulsed like radar transmitters, the receiver of the aircraft is of the type shown in Fig. 4, the cathode ray tube 9 uses circular time base 10 (Fig. 4) synchronised by rectangular pulses sent by an auxiliary transmitter in the ground. For generating these synchronising pulses, the triggering pulses of the modulator of the magnetron before amplification are applied to Eccles-Jordan "Flip-Flop" multivibrator which generates rectangular pulses. These pulses modulate the carrier of an auxiliary transmitter. In this case a stationary pulse 13 will be indicated in the cathode ray tube when the output of tube 8 is used to modulate the potential of the anode 12 of 9. When the glide path is followed the amplitude of the pulse 13 is maximum.

Two micro-wave marker beacons are used in this system for finding the position fixes. Both the beacons use cylindrical parabolic reflector with closed top and bottom. The outer marker fan beam is very narrow in the

transverse direction of the runway and much wider in the longitudinal direction of the same. The converse is the case with the inner marker fan. The outer marker beacon is so adjusted that the wider portion of its beam coincides with the vertical plane P containing the glide path. Finding out the outer marker fan the plane proceeds through the wider portion of the same and glides down to a predetermined height h, at the point A. At the point A the aircraft will intercept the two rotating radio beams simultaneously and proceed along the straight line glide path. The point B is also at a predetermined height. In some cases the inner marker may be dispensed with.

DISCUSSION

It will be seen that in this system there are no complications arising out of reflection of waves from the surface of the earth. In several known types of blind landing systems beam switching methods are utilised whereas in this system beam sweeping action takes place. If the markers of the known type are arranged in the usual manner the aircraft will glide down to a predetermined height while crossing the outer marker and the cathode ray tube will indicate whether the glide path is approached.

If this system is modified to a "Lock follow Radar System" wherein the scanner can be automatically locked on to the target, the aircraft will in course of landing continuously receive energy from the rotating aerials.

ACKNOWLEDGMENTS

The author wishes to express his thanks to Dr. H. Rakshit, for his kind interest and for going through the subject matter of this paper and to Dewan Bahadur K. Rama Pai, M.A., Controller of Patents and Designs for his encouragement and kind permission to publish this paper.

Patent Office (Government of India)
214, Lower Circular Road, Calcutta.

REFERENCES

Fink, Donald G., Radar Engineering, p.564. M.I.T. Radiation Laboratory Series, Radar System Engineering, p. 498.

Terman, F. E., Radio Engineer's Hand book, p. 838.

STUDIES OF A SCHRAGE THREE-PHASE SHUNT COMMUTATOR MOTOR

1. Vector Diagrams at Synchronous and Super-Synchronous Speeds

By H. P. BHATTACHARYYA and S. B. DEB

(*Received for publication, Feb. 14, 1949*)

ABSTRACT. The paper gives the vector diagrams representing all the currents and voltages both on the primary and secondary sides of the Schrage three-phase shunt commutator motor at its synchronous and super-synchronous speeds with a view to obtaining a better understanding of the working of the motor.

INTRODUCTION

The Schrage three-phase shunt commutator motor is a remarkable discovery in electrical engineering practice. It is almost like an ordinary induction motor, having as usual, primary and secondary windings and being rotor-fed the stator winding is the secondary. But unlike the induction motor it has an extra winding called the 'Lap winding' which is electrically insulated from the primary but housed in the same slots as those of the latter. It is, therefore, assumed that there is no leakage of flux between the primary and the lap windings. The lap winding is connected to a commutator on which brushes are placed. For a bi-polar three-phase machine, there are six half-brushes, each pair of which being connected to two ends of each stator secondary phase. This motor can have sub-synchronous, synchronous and super-synchronous speeds, the power factor increasing inherently as it moves faster and faster. Even at sub-synchronous speeds power factor improvement can be brought about by suitably displacing the brush axis from the common stator-rotor axis. Owing to these properties the Schrage motor is widely used in industrial practice now-a-days. One such motor alone, when properly designed, has a wide speed range and thus it is very valuable as a drive where large variation in speeds is required. In point of fact, this variation of speed may be over such a wide range that it will be necessary to use a number of induction and synchronous motors if a Schrage machine is not used.

It is well known that the study of vector diagrams of any A.C. machine is essential for the proper understanding of its operations. Each machine of the ordinary induction or synchronous type has one and only one vector diagram which provides a scientific explanation for its behaviour. But in the case of a Schrage motor, it is felt that its entire operation cannot be fully explained with the help of a single such diagram. For each of the sub-synchronous, synchronous and super-synchronous speed ranges separate vector diagrams are necessary in order to explain the then conditions of the motor. The vector diagram at sub-synchronous speeds of this motor has

been worked out by Arnold (1926) but no attempt has yet been made to work out the vector diagrams at the synchronous and super-synchronous speeds. The present paper deals with such vector diagrams.

VECTOR DIAGRAMS

Before describing the vector diagrams it is worthwhile mentioning that voltages are induced in the lap winding due to the primary at the supply frequency, but the voltages collected across any pair of half-brushes are of slip frequency, that is, frequency of the air-gap flux. Below and above synchronism, the slips are positive and negative respectively but at exactly the synchronous speed of the motor the slip is zero. The air-gap flux induces voltages in the stator winding at slip frequencies. These combine with the voltages from the lap winding *via* the brushes. Now since the number of commutator segments between any pair of half-brushes can be varied by rotating the brush-gear thereby varying the voltage injected to the stator, different speeds of the motor are obtained for different injected voltages. It may be noted that the stator induced voltage and the injected voltage from the lap winding are always in opposition. The brush-spread between any pair of half-brushes is generally maximum while the motor is at standstill, and it diminishes as the motor speeds up to a value very close to the synchronous speed when the brushes are short-circuited. Beyond this speed the brushes are crossed over and the voltages are again in opposition, but the current through the stator flows in the same direction as before, thus accounting for the unidirectional rotation of the motor. At sub-synchronous speeds the stator induced voltage dominates over the voltage injected from the lap winding whereas at super-synchronous speeds the case is reverse. At synchronous speed, however, the stator voltage is theoretically equal to zero, although the voltage collected across each pair of half-brushes has a finite value and is unidirectional in nature. At this speed, therefore, there is only a direct current flowing in the lap-secondary combination circuit, which has, however, no influence on the primary side. The diagrams given here are all schematic and refer to symmetrical brush positions of the motor, thus ensuring its inherent tendency for the improvement of the power factor with increasing speed.

The following notations have been used. These refer to per-phase values and it is assumed that the ratio of turns of the rotor primary and the stator secondary is unity.

V = Primary applied voltage

E_1 = Primary induced voltage from the stator

S = Fractional Slip

n = Ratio of effective lap turns for 180 electrical degrees brush displacement to effective stator turns.

α = Ratio of effective lap turns for brush displacement of β electrical degrees to the effective lap turns for brush displacement of 180 electrical degrees, where,

$$\alpha = \text{Sin } \beta/2$$

SE_1 = Stator induced voltage at the slip 'S'.

E_L = Voltage induced in the lap winding between the half-brushes when they are separated by 180 electrical degrees.

E_L/n = Lap induced voltage on the primary.

αE_L = Voltage injected from lap to secondary.

I_1 = Primary current.

I_2 = Secondary stator – lap combination current.

R_1 = Primary Resistance.

X_1 = Primary leakage reactance at supply frequency.

R_2 = Effective stator – lap combination resistance.

X_2 = Effective stator leakage reactance at supply frequency.

Fig. 1 gives the vector diagram at the synchronous speed. According to usual convention the portions above and below the reference axis (the horizontal line to the plane of the paper here) represent respectively the primary and the secondary components of the machine. The stator induced voltage being actually zero in the present case has not been shown. αE_L the lap induced voltage is the only voltage here in the secondary side for producing secondary current I_2. It may be noted that αE_L is just out of phase from E_L/n which is equal to $V - I_1R_1$, where I_1R_1 is the primary resistance drop. Both αE_L and I_2 are unidirectional here. The motor is synchronous in action at this stage and the only difference from an ordinary synchronous motor lies in the fact that it has no salient poles, its rotor is taking the A.C. input power and the stator is taking the D.C. field excitation from the lap winding *via* the brushes. The primary alternating current I_1 shall be considerably larger in magnitude than the secondary direct current I_2 just as in an ordinary synchronous motor.

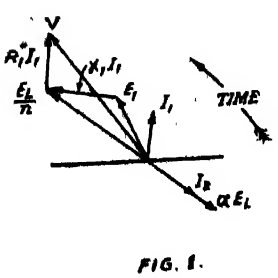

FIG. 1.

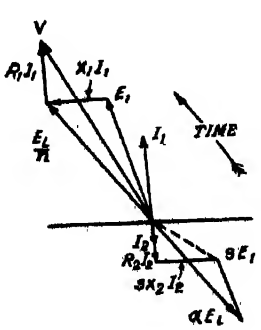

FIG. 2.

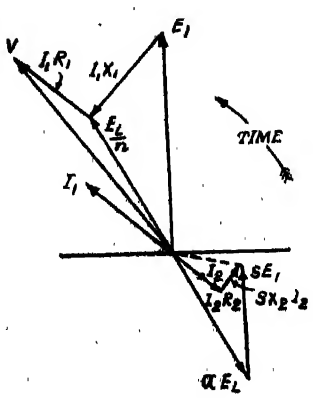

FIG. 3.

Fig. 2 and Fig. 3 represent vector diagrams at super-synchronous speed—power factor lagging and at super-synchronous speed—power factor leading respectively. It may be noted here that though the primary currents are lagging and leading respectively from the supply voltage, the secondary currents in both the cases lag from the respective resultant voltages on this side. In each of the above cases there are two voltages on the secondary side, namely, the lap voltage αE_L and the stator induced voltage SE_1. These two voltages after combining with each other produce a resultant voltage which directs the current I_2 through the secondary circuit. The primary current I_1 is lagging from V in the former case and leading from it in the latter. Accordingly, the primary resistance drop has been subtracted from the supply voltage V in each case to obtain E^L/n the lap voltage induced on the primary. As in Fig. 1, αE_L has been drawn in opposition to E_L/n. The voltage SE_1 though strictly out of phase from E_1, has been taken here in a direction parallel to E_1 in order that it can oppose the voltage αE^L. At any position if the secondary current be I_2 then the primary reflected current I_1 should be given by $I_1 = I_2 (1 + p)$, where $p = \alpha n$.

DISCUSSION

It is worthwhile mentioning here that the principle of drawing of the above vector diagrams is equally applicable when the motor is loaded. The only difference that may arise from the no-load condition is in the degree of the lag of the primary current from the applied voltage, which is definitely less for a loaded motor. A motor at no-load does not ordinarily attain a leading power factor at a super-synchronous speed. Also the possibility of not taking a leading current from the supply is not far from truth even for a motor running at full load and at highest super-synchronous speed. Leading power factor is encountered only in special cases. The primary magnetising current which is small has not been shown separately in the diagrams.

The evaluation of the various performance characteristics of this motor which is likely to throw new light on its performance will be reported in a subsequent communication.

ACKNOWLEDGMENT

Our thanks are due to Prof. P. C. Mahanti, Head of the Department and to Dr. A. K. Sen Gupta, Lecturer-in-Charge of the Electrical Machines Laboratory for their valuable suggestions and encouragement during this work.

Electrical Machines Laboratory,
Department of Applied Physics,
University College of Science & Technology,
Calcutta

REFERENCE

Arnold, A. H. M. (1926), *J.I.E.E.*, **64**, 359.

FISSION CROSS-SECTION OF URANIUM^{235} FOR THERMAL NEUTRONS

By SUKUMAR BISWAS and A. P. PATRO

(*Received for publication, March, 15, 1949*)

ABSTRACT. The cross-section of fission of U^{235} for thermal neutrons has been determined in the present work. The copper cathode of a proportional counter was coated with electrolytically deposited U-compound which was converted to U_3O_8 by heating. The exact amount of U was determined by accurate weighing. The fission counter and a Ra-Be neutron source were placed inside a large paraffin block. Operating the counter in the proportional region large fission pulses were detected against a background of natural α-ray pulses, with usual amplifier, discriminator, scaling and recording circuits. In order to separate the effects of thermal neutrons, the observations were taken with and without a $\frac{1}{2}$mm Cd-shield round the counter and the difference gives the rate of thermal neutron fissions, which are ascribed to U^{235} isotope. To measure the neutron flux a BF_3 counter of identical dimensions was placed in the same position in the paraffin block as the fission counter and the number of thermal neutrons were counted with the Cd-difference method. Using the well-known value of $\sigma_a\nu$ for boron, the value of $\sigma_f\nu$ was obtained. Hence σ_f (U^{235}) for thermal neutrons was determined as $(526 \pm 10) \times 10^{-24}$ cm^2.

INTRODUCTION

Since the discovery of fission of uranium nucleus under neutron bombardment by Hahn and Strassmann in 1939, various aspects of this new phenomenon engaged active attention of a large number of investigators. As in other types of nuclear reactions, one of the most important aspects of fission phenomenon is the probability of the process. The absolute probability of any nuclear reaction is expressed by the cross-section of the process. The cross-section of fission σ_f is defined for thin target as

$$\sigma_f = \frac{n_f}{I.n} \qquad (1)$$

where n_f = number of fissions per unit time

I = number of incident bombarding neutrons per unit area per unit time.

n = number of uranium nuclei.

The advantage of expressing the probability in terms of cross-section lies in the fact that this definition is independent of any particular experimental condition and expresses the absolute probability of the process involved.

According to early observations thermal neutrons were found more effective in producing fission. Anderson *et al* (1939) obtained the value of σ_f for average

uranium isotopes as about 2×10^{-24} cm^2 for thermal neutrons and the value of σ_f for fast neutrons as about 1×10^{-24} cm^2. These early observations on fission cross-section were rather preliminary and uncertain due to the fact that the mechanism of fission and its dependence on the neutron energy and isotopic property of uranium were not clearly known. Bohr and Wheeler (1939) first showed from theoretical study of fission process from the liquid drop model of the nucleus that U^{238} is fissionable with only fast neutrons having a threshold energy of about .75 Mev and the rarer isotope U^{235} is fissionable with thermal neutrons and this has a large value of fission cross-section. These theoretical predictions were first verified by direct experiment by Nier (1940) with the help of separated U-isotopes. Nier (1940), however, could not obtain the precise value of fission cross-section because the amount of isotope that was separated by mass spectrograph was not definitely known. He estimated the value of σ_f for U^{235} for thermal neutrons as 400×10^{-24} cm^2 to 500×10^{-24} cm^2. Since then no value of σ_f for U^{235} has been reported in literature. Hence the present work is undertaken with a view to determining the fission cross-section of U^{235} for thermal neutrons which is of fundamental importance in atomic energy work, although it is certain that this important value is known to a few selected investigators in this field.

THEORY OF THE EXPERIMENT

In this experiment a 'uranium counter' was employed to observe the fission phenomenon. A thin optimum layer of U_3O_8 was deposited electrolytically on the inner surface of the Cu-cathode of a proportional counter. The amount of U_3O_8 deposited was determined by accurate weighing of the counter before and after deposition. This was filled with argon and organic ether vapour in the conventional way. This counter was placed inside a large paraffin cylinder at a suitable distance from a Ra-Be neutron source placed inside paraffin, and thus U was exposed to a flux of neutrons, a large percentage of which is of thermal energy. The counter was operated in the proportional region so that the output pulses were proportional to initial ionisation. The natural α-particles in U produce corresponding pulses. Any fission of U nucleus produces very high energy fission fragments whose specific ionisation is many times that of α-particles. Hence proportionally large pulses were obtained in fission when the counter was worked in the proportional region. The discriminating bias of the recording circuit was put at a suitable high value so that only fission pulses and no α-pulse were counted. Since each fission process is accompanied by two fragments flying in opposite directions, only one pulse was produced per fission and consequently whatever be the direction of fission fragments, one ionisation was produced. Since both slow and fast neutrons were producing fissions and since cross-sections of fission is a function of neutron energy, neutrons of definite energy or energy group are to be selected out in order to ascribe definite meaning to the cross-

section value obtained. This was most conveniently done by the cadmium difference method. The observations on fissions were taken with and without a Cd shield of $\frac{1}{8}$ mm. in thickness placed round the counter. Since Cd absorbs all thermal neutrons of the energy of the order of .025 eV, the difference between these two readings gives the number of fissions caused by thermal or C-group neutrons. Since it has been conclusively shown by Nier (1940) that only U^{235} nuclei are fissionable by thermal neutrons, the thermal neutron fissions are ascribed to U^{235} atoms present in uranium. The ratio of U^{235}/U^{238} present in natural uranium is taken as 1/139 according to Nier's determination (1939). Thus n_f and n of relation (1) are determined.

To determine the neutron flux I, a neutron counter filled with BF_3 is employed. This counter is of identical geometrical dimensions as the uranium counter and is held in exactly the same position as the uranium counter. The BF_3 counter is operated in the proportional region so that big pulses are produced corresponding to B^{10} (n, α) Li^7 disintegration in the background of small secondary electron pulses due to Ra γ-rays. The discriminating bias is adjusted so as to record only big pulses. The number of neutrons counted in a BF_3 counter is given by the relation as given by Korff (1942, 1946)

$$N = VLp\int I(v)\sigma(v)dv\ ;\ I(v) = \rho v,\ \sigma(v) = \frac{\sigma}{v}$$

$$\therefore \quad N = VLp\rho\sigma_B v_B \qquad \ldots \quad (2)$$

where V = sensitive volume of the counter

L = Loschmidt number

p = pressure of the counter in atmospheres

ρ = density of slow neutrons

σ_B = capture cross-section of B^{10} for neutrons of known velocity v_B

Hence the neutron flux of velocity v_B through the counter is

$$I = N / VLp\sigma_B \qquad (3)$$

With these relations efficiency of the counter for neutrons of velocity v_B can be calculated as given by

$$E = Lp\sigma_B d \qquad \ldots \quad (4)$$

where d is the average path of the neutrons through the counter. This may be taken as the diameter of the counter to a sufficient degree of approximation.

Since we are concerned with only the thermal neutrons, the neutron counting is made with and without a thin Cd-shield. The difference gives the number of thermal or C-group neutrons. With the help of known boron absorption cross-section for thermal neutrons, the actual neutron flux of velocity v_h per second is calculated from the number of thermal neutrons counted.

The absorption cross-sections of boron have been determined accurately by a number of investigators by neutron velocity spectrometers and boron is found to obey $1/v$ law of absorption very accurately. Recent values of boron absorption are

$\sigma_a v = 1.61 \pm .02 \times 10^{-24}$ cm^2.metre/μsec. (Sutton *et al*, 1947)

$\sigma_a v = 1.63 \times 10^{-24}$ cm^2. metre/μsec. (Rainwater & Havens, 1946)

$\sigma_a v = 1.55 \times 10^{-24}$ cm^2. metre/μsec. (Bacher, Backer & McDaniel, 1946)

Using Sutton's value of $\sigma_a v$ and $v_{th} = 2200$ metres/sec. for thermal neutrons ($E = .026$eV), σ_a for boron is 732×10^{-24} cm^2.

Since experimental observations by Anderson *et al* (1939) indicate that thermal neutron fissions most probably obey $1/v$ law, $\sigma_f v$ will be a constant quantity. Hence using the value of $\sigma_a v$ of boron, $\sigma_f v$ for U^{235} is obtained. For thermal neutrons of energy $(\pi/4)\ kT = .026$ eV, velocity v_{th} is 2200 metres/sec. ; hence σ_f (U^{235}) is calculated for thermal neutrons.

EXPERIMENTAL METHOD

A. Fission Counter

In the fission counter a uniform film of U_3O_8 was produced by electrolysis of a solution of ammonium diuranate in ammonium carbonate. A copper cylinder 15.2 cm in length and 2.9 cm. in diameter was made from 5 mil. Cu-sheet and a thick tungsten lead was sealed at one end. The cylinder was throughly cleaned with NaOH and chromic acid solution, dried and carefully weighed in a semi-microbalance. 5 gms of pure uranyl nitrate was dissolved in water and uranium was precipitated by ammonia. The precipitate was thoroughly washed till free from nitrate and then dissolved in 100 c.c. of 2 N NH_4OH solution containing 10 gms of $(NH_4)_2\ CO_3$. The solution was filtered and kept as a stock solution.

A number of test experiments were performed to find out the best condition for a coherent deposit. The copper cylinder was placed in a glass cylinder of slightly wider diameter and a platinum foil which served as an anode wrapped round a narrow glass tube ran along the axis of the copper cylinder. It was found that a solution concentration equivalent to .005 gms of U_3O_8 per c.c., a current density of about .03 amp/cm^2 and a short time (6 minutes) gave the

most satisfactory deposit. An electrolysis for a longer period precipitates a greenish substance probably due to cathodic reduction. This is, however, a nuisance for coherent deposit.

In the final experiment a solution of concentration equivalent to .0056 gms of U_3O_8 per c.c. was taken in the glass cylinder and the copper cylinder which served as cathode was placed inside it and the platinum foil which served as anode was fitted as described above. 2.8 amp. of current was passed for 5 minutes from 220 V mains through an adjustable resistance. After electrolysis the copper cylinder was carefully washed and a coherent deposit of hydrated oxide somewhat brown in colour was thus obtained. The cylinder was dried in air and was heated in an electric furnace at 400°C for two hours which turns it to U_3O_8 that formed a jet black coating. The cylinder was again weighed and the increase in weight gave the weight of U_3O_8 deposited. To guard against errors due to deposit of some oxides of copper, a copper cylinder of identical size was weighed and heated along with the counter cylinder. The increases in weight was deducted. (The increase was only .00112 gms., *i.e.*, about 1.5% of uranium deposit). The values are given in Table I. The amount of U_3O_8 was .47 mg/cm^2. This being much less than the range of fission fragments in U_3O_8 (about 10 mg/cm^2), all fission fragments could emerge from the deposit and hence were counted.

With this coated copper cylinder a pyrex glass G-M counter was made with a 4 mil. tungsten wire as the central wire. This was filled with argon and petroleum ether vapour to a pressure of 14 cm. of Hg. of which 3 cm. was due to organic vapour. The starting voltage was about 850 volts.

B. Neutron Source and Counter Arrangements in Paraffin Medium

The neutron source was a 40 mC Ra-Be source. This was contained in four brass capsules, 10 mgs. in each. In order to slow down the neutrons to thermal velocities, a paraffin cylinder 25 cm. in diameter and 22 cm. in height was used. The counter was introduced inside paraffin through a hole 3.8 cm. in diameter along the axis of the cylinder. The source was introduced

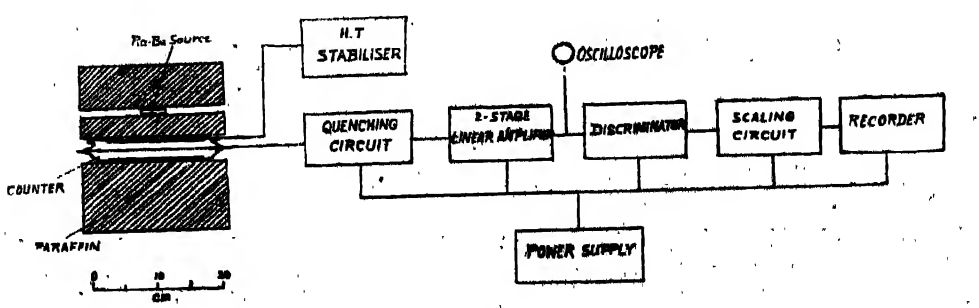

FIG. 1

Schematic diagram of the arrangement.

in a small hole parallel to the axis of the cylinder at a distance of 5.2 cm. from the axis. At this distance the slow neutron intensity per unit area was found to be near about the maximum as observed by Fink (1936). The arrangement is diagrammatically shown in Fig. 1. As given in Sec. 3*D*, 93% of neutrons counted with this arrangement were slowed down to below .2 eV as determined by ½ mm Cd filter.

C. Neutron Counter

The neutron counter was made with a pyrex glass envelope having similar geometrical dimensions as the uranium counter (Cu-cathode 15.2 cm. long, 2.9 cm. in diameter). The copper cathode was oxidised similar to conventional G-M counters. This is filled with BF_3 at a pressure of 21.6 cm. Since BF_3 attacks rubber, the filling system was made totally of glass, as advised by Korff (1942). A small rubber tube was employed only at one place but this was discarded immediately after use. Commercial BF_3 was purified to some extent by passing over concentrated H_2SO_4 saturated with B_2O_3 which absorbs moisture and HF if present. The starting voltage of the counter was 1860 volts. The counting rate-voltage curve of the counter with a 10 mC Ra-Be source near it is shown in Fig. 2.

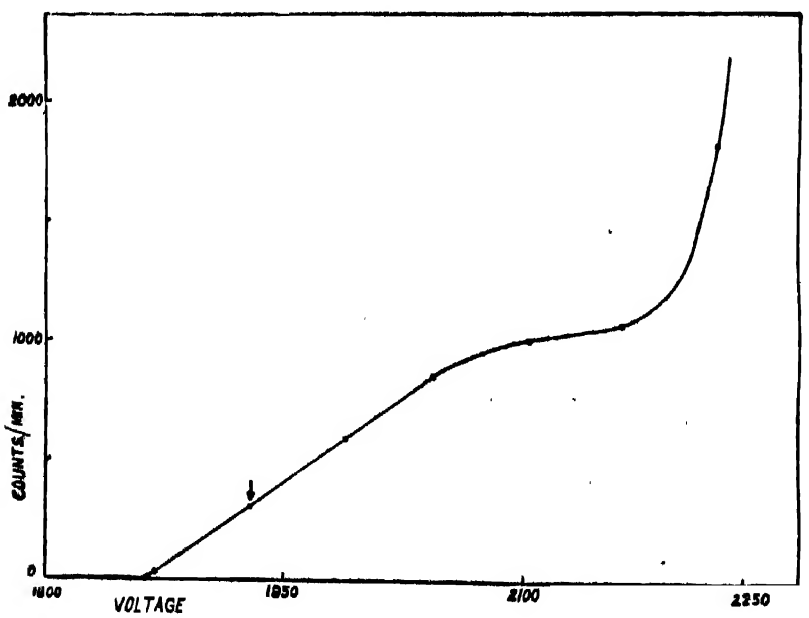

FIG. 2

Counting rate of the BF_3 counter with a 10 mg. Ra-Be source.

The proportional region extends up to 2160 volts beyond which there is the Geiger-region. The background of the counter was 1 count per min. The efficiency of the neutron counter as calculated from Boron absorption cross-section was 1.58% for thermal neutrons.

D. Detecting Circuits and Measurements

The schematic diagram of the detecting circuit is shown in Fig. 1.

The high voltage stabilizer used to supply the cathode voltage of the counters was a modification by Banerjee (1942) of the Neher-Pickering's circuit (1939). Stabilized voltages up to 2600 volts could be given from this stabilizer.

The quenching circuit employed was of Neher-Pickering type (1938), output pulses being taken from the cathode. This was fed to a two-stage linear amplifier having variable amplification. The output pulses from the amplifier were observed in the oscilloscope and passed into the discriminator, scaling and recording circuits. The discriminator and the scale of 8 circuit were of Don DeVault (1943) type with some altered values of circuit constants. For slow counting as in uranium fissions scale of 2 was employed, while for fast counting scale of 8 was used. The recorder was a Cenco impulse counter driven by a current through a 6V6 tube which is normally biased to cut off. Positive pulses from the scaling circuit trips the recorder. Two power supplies were employed, one for the amplifier and the other for the scaling unit.

Since the 40 mC Ra-Be source produced about 5 fission counts per min. the counting was taken for a long time, about 12 hours, in order to bring down the statistical error in counting to about 1 per cent. The fission counter was operated at 930 volts, very near the starting. The amplifier was used with minimum amplification and discriminating bias was kept at 115 volts. Fission counts were taken without and with a Cd-shield .5 mm thick round the counter for 12 hours each time

Next the neutron counter was placed in the same position as the uranium counter. The neutron counter was operated at 1920 volts. With the amplifier gain set at a certain intermediate value discriminating bias of 20 volts was employed. The counts were taken with and without the Cd-shield. From these countings it was observed that 93 per cent of the neutrons counted were due to thermal neutrons.

TABLE I

Weight of U_3O_8 deposited	= .06480 gms.
Weight of Cu-oxides	= .00112 gms.
Exact weight of U_3O_8	= .06368 gms.
Amount of U	= .05400 gms.
Amount of U^{235}	= .000383 gms.
No. of U^{235} atoms	$= 9.7 \times 10^{19}$.

The results are given in Table II.

TABLE II

	Time	Total counts	Counts/min
Fission counts without Cd-shield	12 hrs.	3990 ± 42	5.52 ± .05
Fission counts with ½ mm. Cd-shield	12 hrs.	1462 ± 26	2.03 ± .03
Fission counts with Thermal neutrons	12 hrs.	2528 ± 49	3.50 ± .07
Neutron counts without Cd-shield	5 min.	20016 ± 94	4003 ± 19
Neutron counts with ½ mm Cd-shield	5 min.	1356 ± 36	271 ± 7
∴ No. of Thermal neutrons	5 min.	18660 ± 100	3732 ± 20

Taking the value of $\sigma_a v$ for boron $= 1.61 \times 10^{-24}$ cm^2 .metre/μsec. (*i.e.*, with absorption cross-section $\sigma_a(B) = 732 \pm 9 \times 10^{-24}$ cm^2 for .026 eV neutrons) for fission of U^{235}, $\sigma_f (U^{235}) \times v = 1.16 \pm .02 \times 10^{-24}$ cm^2. metres/μsec. Assuming $v_{th} = 2200$ metres/sec. for .026 eV thermal neutrons, fission cross-section $\sigma_f (U^{235}) = 526 \pm 10 \times 10^{-24}$ cm^2 for thermal neutrons of .026 eV energy.

DISCUSSION

Since boron absorption cross-section obeys $1/v$ law accurately up to 10,000 eV, $\sigma_a v$ is a constant quantity according to the measurements of Sutton *et al* (1947), Rainwater and Havens (1946) with slow neutron velocity spectrometer. Using this value of $\sigma_a v$ for boron, $\sigma_f v$ for U^{235} is calculated assuming that same $1/v$ law of absorption holds also for fission. This is justifiable from the experimental observations of Anderson *et al* (1939). They observed by comparison of the thermal neutron fission process with boron absorption that within the limits of experimental error fission process may be assumed to obey $1/v$ law similar to boron. Hence the measured value of $\sigma_f v$ is a constant quantity, and σ_f can be calculated for any velocity within the range of applicability of $1/v$ law. Since the present observation is mainly confined to thermal neutrons, σ_f is calculated for thermal neutrons of energy $\frac{\pi}{4} kT$ (= .026 eV) equivalent to 2200 metres/sec.

Fermi and Marshall (1947) obtained the value of boron absorption cross-section as 703×10^{-24} cm^2 for neutrons of velocity 2200 metres/sec. by mechanical velocity selector. This value is somewhat lower than that obtained from the value of $\sigma_a v$ according to measurements of Sutton *et al* (1947) ($\sigma_a = 732 \pm 9 \times 10^{-24}$ cm^2 for 2200 m/sec. neutrons). In view of the close of agreement of the values of $\sigma_a v$ given by Sutton *et al* and Rainwater and Havens (1946) ($\sigma_a v = 1.63 \times 10^{-24}$), the value of $\sigma_a v$ for boron is taken according to Sutton *et al* (1947).

The number of fissions observed is due to the mixed effect of both slow neutrons and fast neutrons ($\geqq 1$ Mev). Since Ra-Be neutron source emits neutrons of considerable energy (~ 5 Mev) and ~ 3 cm paraffin thickness is used, there will be considerable number of fast neutrons above 1 Mev which produces fission in U^{238}. Slow neutrons above .2 eV produced fission in U^{235} whose cross-section is assumed to vary as $1/v$. The actual number of slow neutrons ($>.2$ eV) is much greater than 7% because the efficiency of boron counter decreases as $1/v$. The estimate of the contribution of these two groups of neutrons is, however, not possible as their effects are not separated in the present observation.

Another point in counting fission processes is that a few fissions will be occurring so that the two fragments will fly tangentially to the surface. They will produce no ionisation and will not be recorded. However, taking isotropic distribution of fission fragments, the proportional number of such tangential fissions will be less than 1 *p.c.* and hence can be neglected. Thus the experimentally determined value gives a fairly accurate estimate of fission cross-section.

The value of fission cross section obtained in this experiment may be employed to ascertain the approximate order of other characteristics of nuclear level structure, *e.g.*, resonance energy, level width and level spacing. The dispersion formula of Breit and Wigner (1936) as applied to the fission phenomena induced by thermal neutrons, by Bohr and Wheeler (1939), is used for this purpose. If the levels of the compound nucleus are assumed to be well separated so that any particular level is mainly effective, we have :

$$\sigma_f = \pi(\lambda/2\pi)^2 \frac{(2J+1)}{(2s+1)(2i+1)} \cdot \frac{\Gamma_n'.\Gamma_f}{(E-E_0)^2+\Gamma^2/4}$$

where Γ_n', Γ_f and Γ are neutron width, fission width and total width respectively ; s, i and J are spins of incident particle, initial nucleus and compound nucleus respectively. Now $s=\frac{1}{2}$, $i=\frac{5}{2}$, (Anderson and White, 1947), hence $J=3$ or 2. For thermal neutrons $\pi(\lambda/2\pi)^2 = 23\times10^{-18}$, $\Gamma_n' = 10^{-4}$ eV, so that

$$\frac{\Gamma_f}{E_0^2+\Gamma^2/4} = \frac{5.26\times10^{-22}}{23\times10^{-18}\times10^{-4}} \times \begin{cases} 1.7 \text{ if } J=3 \\ 2.4 \text{ if } J=2 \end{cases}$$

$$= .4 \text{ or } .55 \ (\text{eV}^{-1}) = R$$

Since $$\Gamma_f < \Gamma, \quad E_0^2 < \frac{\Gamma}{4}\left(\frac{4}{R} - \Gamma\right)$$

$$\Gamma \leqq 10 \text{ or } 7 \text{ eV. and } |E_0| \leqq 5 \text{ eV.}$$

$$\Gamma_f \leqq 10 \text{ or } 7 \text{ eV.}$$

If, however, level widths are of the same order as level spacing, the fission process will be due to many overlapping levels. In such a case the dispersion

formula becomes, as given by Bohr and Wheeler (*loc. cit.*),

$$\sigma_f = \pi(\lambda/2\pi)^2 . \Gamma_n/(\Gamma_f/\Gamma) . \frac{2\pi}{d} \times \tfrac{1}{2}, \text{ where } d = \text{level spacing}$$

$$\text{Assuing } \Gamma_f/\Gamma \simeq 1,\ d = \frac{23 \times 10^{-18} \times 10^{-4}}{5.26 \times 10^{-22}} \cdot \frac{2\pi}{2} \simeq 14 \text{ eV}.$$

Thus if considerable overlapping of levels is assumed, fission width Γ_f will be at least 7 eV. Since $1/v$ law is obeyed in thermal region first resonance level cannot be less than a few eV. Hence E_0 is expected as $\simeq 4$ eV.

ACKNOWLEDGMENTS

The authors express their gratitude to Prof. M. N. Saha, F. R. S., for his kind interest and encouragement in the work, and to Dr. B. D. Nag for helpful discussions. The authors are also thankful to Mr. B. M. Banerjee for his valuable suggestions regarding electronic circuits, and to Mr. B. C. Purkayastha for his valuable assistance in the chemical portion of the work.

INSTITUTE OF NUCLEAR PHYSICS,
UNIVERSITY OF CALCUTTA,
CALCUTTA.

REFERENCES

Anderson, Booth, Dunning, Fermi, Glasoe and Slack (1939), *Phys Rev*, **55**, 511
Anderson and White (1947), *Phys. Rev*, **71**, 911.
Bacher, Backer and McDaniel (1946), *Phys. Rev.*, **69**, 443.
Banerjee, B. M. (1942), *Ind. Jour. Phys.*, **16**, 87.
Bohr and Wheeler (1939), *Phys. Rev.*, **56**, 426.
Don DeVult, (1943), *Rev. Sci. Inst.*, **14**, 23.
Breit and Wigner (1936), *Phys. Rev.*, **49**, 519
Fermi, Marshall and Marshall (1947), *Phys. Rev.*, **72**, 193.
Fink, (1936), *Phys. Rev.*, **50**, 738.
Hahn and Strassmann (1939), *Naturwiss.*, **27**, 11.
Korff (1942), *Rev. Mod. Phys.*, **14**, 1.
Korff (1946), Electron and Nuclear Counters, p. 50 (Van Nostrand Co).
Neher and Pickering, (1938), *Phys. Rev.*, **53**, 316.
,, ,, (1939), *Rev. Sci. Inst.*, **10**, 53.
Nier (1939), *Phys. Rev.*, **55**, 150.
Nier, Booth, Dunning and Grosse (1940), *Phys. Rev.*, **57**, 546.
Phys. Rev., **57**, 748.
Rainwater and Havens (1946), *Phys. Rev.*, **70**, 136.
Sutton, McDaniel, Anderson and Lavatelli (1947), *Phys. Rev.*, **71**, 272.

ON THE FLUORESCENCE OF SOLID DINORMAL PROPYL KETONE*

By G. S. KASTHA

(*Received for publication, Dec. 27, 1948*)

Plate III

ABSTRACT. The fluorescence of dinormal propyl ketone in the solid state at about −170°C has been studied using different exciting frequencies. It is observed that four strong fluorescence bands at 4937, 5251, 5397 and 5683 Å appear when the substance is solidified and cooled down to about −170°C. The bands do not appear at higher temperatures below or above the melting point of the substance. These bands are observed to be excited by Hg lines 4046 Å group and other lines of shorter wave length in the near ultraviolet. When the solid at −170°C is illuminated by the Hg lines of still shorter wavelength in the ultraviolet region, a continuous fluorescence band extending from 4000 Å up to about 4600 Å is observed besides the four bands mentioned above. The significance of these results is discussed.

INTRODUCTION

It was first observed by Sirkar and Bishui (1946) that dinormal propyl-ketone in the solid state at about −170°C, when illuminated with light from a mercury arc, exhibits strong fluorescence bands in the region between the Hg lines 4916 Å and 5461 Å. It was also pointed out by them that the bands did not appear as soon as the liquid was solidified at a temperature a few degrees below its freezing point, but they made their appearance only when the solid was cooled down to the temperature of liquid oxygen. As the fluorescence of lower ketones have been investigated recently (Kaskan and Duncan, 1948) at low temperatures and in different regions of the spectrum it was thought worthwhile to study in detail the fluorescence of dinormal propyl ketone for different exciting frequencies and at different temperatures, so that the results might be compared with those for lower ketones. An improved arrangement for keeping the substance at different low temperatures has therefore been used in the present investigation to investigate the fluorescence of solid dinormal propyl ketone at different temperatures and with different exciting frequencies.

EXPERIMENTAL

Merck's dinormal propyl ketone distilled repeatedly in vacuum was used in the present investigation. The purity of the liquid was tested by

* Communicated by Prof. S. C. Sirkar.

photographing its Raman spectrum which showed the characteristic Raman frequencies without any trace of the fluorescence bands in the region from 4916 Å up to the yellow doublet of mercury. The liquid was introduced in a vertical container of Pyrex glass which was suspended inside a Pyrex Dewar vessel through a cork fitting in the mouth of this vessel. One end of a Pyrex tube bent twice at right angles entered in the Dewar vessel through the cork and the other end was dipped in liquid oxygen in a metallic double walled container. A third glass tube passing through the cork entered into the Pyrex Dewar vessel, its other end being connected to a Cenco Hyvac pump through a Pyrex stop cock. In this arrangement a few strokes of the pump brought liquid oxygen from the metallic container into the Pyrex Dewar vessel. The upper level of the liquid oxygen in this vessel could be maintained at any height from the bottom and the temperature of the experimental liquid in the Pyrex container depended on the distance of this surface of liquid oxygen from the bottom of the container. Thus by gradually raising the surface of the liquid oxygen till it surrounded the experimental liquid in the Pyrex container it was possible to keep the liquid at any temperature below the room temperature up to about −180°C. A pentane thermometer was used to measure the temperature in the neighbourhood of the container in the Pyrex Dewar vessel.

For the study of the fluorescence bands in the visible region a Fuess glass spectrograph having a dispersion of about 13.5 Å in the 4046 Å region was used. Light from two Hg arcs placed on opposite sides of the Pyrex container was focussed on the substance and the light scattered in the transverse direction was focussed on the slit of the spectrograph with a lens. Visual examination showed that the bands did not appear even when the substance was solidified and cooled down to about −100°C. A photograph of the spectrum of the scattered light under this condition was taken. The level of the liquid oxygen was next allowed to rise till the liquid oxygen surrounded the frozen mass of the substance. Bright bands in the green region were visible at this stage. The level of the liquid oxygen was then allowed to descend a little in order to avoid complications which might arise from the surrounding liquid. It was observed that the temperature of the frozen mass of the substance did not rise appreciably even when only the bottom portion of the container was kept immersed in the liquid oxygen after once surrounding the whole substance with the refrigerant. The spectrum of the light scattered by this solid mass at about −170°C was photographed in the usual manner.

In order to find out which of the Hg lines were responsible for the excitation of the bands two more spectrograms were recorded one with a filter of strong aqueous solution of sodium nitrite and another with a solution of sulphur monochloride in benzene placed in the path of the incident light.

An attempt was next made to investigate whether the frozen mass of

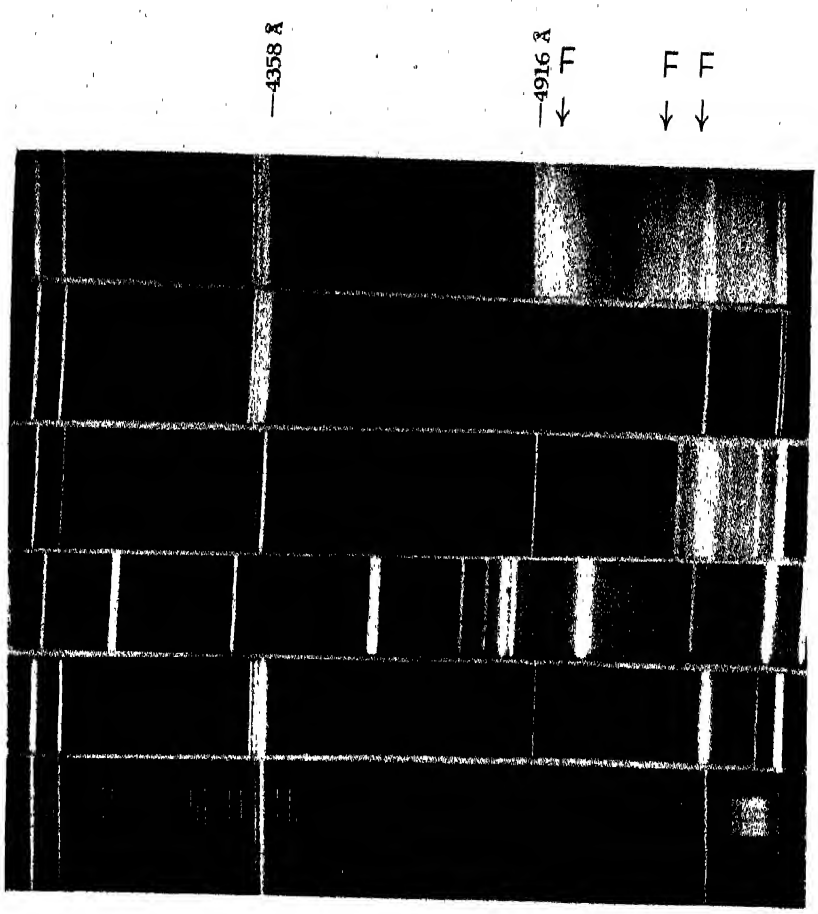

Fluorescence of dinormal propyl ketone.

Fig. 1. Bands in the green region.

Fig. 2. Exciting 4046 Å line reduced in intensity.

Fig. 3. Both the exciting 4046 Å and 4358 Å lines almost cut off.

Fig. 4. Fluorescence with ultra-violet exciting lines.

Fig. 5. Hg. arc spectrum.

Fig. 6. Raman spectrum of the liquid

the substance exhibited any fluorescence in the ultraviolet region. For this purpose a Pyrex Dewar vessel was replaced by a double walled vessel of fused quartz. Dinormal propyl ketone redistilled in vacuum was introduced in a quartz test tube closed with a ground glass stopper and the substance was frozen by immersing the bottom of the test tube in the liquid oxygen as before. Light from two vertical quartz mercury arcs was focussed with quartz lenses on the frozen substance and the spectrum of the scattered light was photographed with an Adam Hilger medium quartz spectrograph.

RESULTS AND DISCUSSION

The fluorescence bands of dinormal propyl ketone at about $-170°C$ excited by the Hg lines in the visible region of the spectrum are reproduced in Fig. 1, Plate III, Figs. 2 and 3 show these bands photographed with a strong solution of sodium nitrite and a solution of sulphur monochloride in benzen respectively in the path of the incident light. It will be seen that instead of two bands reported by Sirkar and Bishui there are actually four prominent broad bands in the fluorescence spectrum, the wave lengths of the peaks of these bands being 4937, 5251, 5397 and 5683 Å respectively. It can also be seen from figures 2 and 3 that the bands are excited mainly by the 4046 Å line and the other lines of Hg of shorter wave lengths, because the intensity of the bands diminish greatly as the 4046 Å line of Hg is weakened by the filter without weakening the 4358 Å line. The intensities of the bands are not altered appreciably when further the 4358 Å line is also cut off by the filter. The 4046 Å line is weaker in Fig. 3 than in Fig. 2 and the bands are also absent in the former figure.

Fig. 4 shows the fluorescence spectrum of dinormal propyl ketone at $-170°C$ excited by all the Hg lines transmitted by the solid. It can be seen that besides the bands in the green region, there is a continuous fluorescence extending from about 4000 Å up to 4600 Å. The Hg arc spectrum reproduced in Fig. 5 does not show any intense continuous background in this region. Also in Fig. 1 this continuous fluorescence is almost absent. Hence this portion of the fluorescence spectrum is excited by the group of Hg lines 3650 Å and 3131 Å which are transmitted with almost undiminished intensity by the solid. As can be seen from Fig. 4 the Hg lines of wavelengths shorter than 3131 Å are absorbed by solid dinormal propyl ketone. The absorption bands in this region may be responsible for the continuous fluorescence mentioned above, while there may be a second narrow absorption band between 4046 Å and 4358 Å which may be responsible for the discrete bands observed in the green region.

The fluorescence in solid dinormal propyl ketone is different from that observed in the case of acetone (Kaskan and Duncan, 1948). In the case of acetone even the vapour illuminated by wave length 3130 Å shows a blue fluorescence. Dinormal propyl ketone in the liquid state, however, does not show any fluorescence even when illuminated by ultraviolet light. The

Raman spectrum of the liquid reproduced in Fig. 6 does not show any trace of fluorescence. Visual observation showed that even when the liquid is contained in a quartz tube and irradiated by ultraviolet light from a Hg arc no trace of fluorescence appears in the visible region. The fluorescence also does not appear just after the solidification of the substance even at about $-100°C$ although collision is diminished in the solid state. Hence it appears that at about $-170°C$ due to strong intermolecular field produced by contraction new electronic levels are formed some of which are metastable and give rise to the fluorescence bands mentioned above.

ACKNOWLEDGMENT

The author is indebted to Prof. S. C. Sirkar for his kind interest and guidance throughout the course of the work and to the authorities of the Indian Association for the Cultvation of Science for the award of a research scholarship.

INDIAN ASSOICATION FOR THE CULTIVATION OF SCIENCE
210, BOWBAZAR, STREET, CALCUTTA 12.

REFERENCES

Kaskan, W. E and Duncan, A. B. F., 1948, *J. Chem. Phys.*, **16**, 223.

Sirkar, S. C. and Bishui, B. M., 1946, *Nature*, **156**, 333;

" " 1946, *Ind. J. Phys.* **20**, 35.

ABSORBABILITY OF HETEROGENEOUS SCATTERED X-RAYS*

By HIRENDRA KUMAR PAL

(*Received for publication, Nov. 20, 1948*)

ABSTRACT. The absorbability $X\phi$ of a heterogeneous beam of scattered X-rays in direction ϕ has been compared to X_{90} for different scatterers and for different primary radiations. In the region of backward scattering, $X\phi > X_{90}$ invariably, as required by the Compton theory of scattering for homogeneous radiation. The agreement is of the right order of magnitude.

In the forward direction, the experimental results may be the classified under the following 3 distinct types, depending on the average wavelength of the primary beam and the nature of the scattering material. (*a*) $X_\phi < X_{90}$, (*b*) $X_\phi = X_{90}$, and (*c*) superficially appearing to contradict the Compton theory. An interpretation on the basis of the Compton theory of this anomaly has been attempted

In a previous paper by the author, (Pal, 1948), an account of the investigation on the intensity distribution of scattered X-radiation was published. In that work heterogeneous beams of X-rays of different degrees of hardness were scattered from different radiators—paraffin, carbon, filter paper, aluminium and sulphur ; and in each case, the scattered intensity $I\phi$ was compared to I_{90}, where ϕ means the angle subtended by the direction of scattering with the forward direction of the primary beam.

For the arrangement of apparatus reference should be made to the previous paper. The scattered beams were intercepted, before entering the ionisation chamber, by equal thickness t of aluminium and the ionisation Z_ϕ and Z_{90}, corresponding to a certain definite deflection in the primary electroscope, were noted from the deflection of the secondary electroscope turned (with the ionisation chamber) alternately into these directions. This process was repeated by gradually increasing the thickness of the intercepting aluminium till a 50% reduction in intensity was in general, obtained. Two graphs showing (*i*) ionisation Z_ϕ against thickness t, (*ii*) ionisation Z_{90} against thickness t, could be drawn and from them the value of the relative absorbability $X_{90}/X\phi$ computed as follows:

Since over the range of wavelengths used in these experiments, the absorptions in SO_2 and aluminium were proportional, we may replace $X_{90}/X\phi$ for SO_2 by the corresponding quantity for a very thin layer of aluminium of thickness Δt. Hence

$$X\phi = \Delta Z\phi / Z\phi \quad \text{and} \quad X_{90} = \Delta Z_{90} / Z_{90}$$

$$\therefore \quad X_{90}/X\phi = \frac{1}{Z_{90}} \cdot \frac{\Delta Z_{90}}{\Delta t} \Big/ \frac{1}{Z\phi} \frac{\Delta Z\phi}{\Delta t} \qquad \ldots \quad (1)$$

Part of a Thesis approved for the Ph.D. degree of the Edinburgh University in 1937.

The quantities $\frac{1}{Z_{90}} \cdot \frac{\Delta Z_{90}}{\Delta t}$ and $\frac{1}{Z_{\phi}} \cdot \frac{\Delta Z_{\phi}}{\Delta t}$ at the origin, $t = 0$, could be easily found from the abovementioned two graphs and hence X_{90}/X_{ϕ} determined.

In practice, either the numerator or the denominator in the R.H.S. of equation (1) was determined as already indicated and the other from the difference between the two, which could be obtained from a curve showing the relation between $Z\phi/Z_{90}$ ($= Y$ say) and the thickness of the intercepting aluminium. For,

$$\frac{1}{Y} \frac{\Delta Y}{\Delta t} = \frac{1}{Z\phi} \frac{\Delta Z\phi}{\Delta t} - \frac{1}{Z_{90}} \cdot \frac{\Delta Z_{90}}{\Delta t}$$

and since $\frac{1}{Y} \frac{\Delta Y}{\Delta t}$ could be determined from a graph Y against t.

The results of observation are recorded in Table I. They are also illustrated by 3 typical graphs in which

(*i*) Y decreases with t, (Fig. 1)
(*ii*) Y is independent of t, (Fig. 2)
(*iii*) Y increases with t, (Fig. 3)

A survey of the results recorded above will show that

(1).. In the backward direction $\phi = 150°$, the scattered radiation is softer than in the direction $\phi = 90°$, as predicted by Compton, in every case without exception. This is shown by $X_{90}/X\phi$ which is greater than and also by the course of the curve Y plotted against t sloping down from left to right (Fig. 1). Increase of hardness of the primary beam in the case of paraffin wax and filter paper increases, in general, the ratio of the absorbabilities. This is also in accord with the Compton theory.

(2). In the forward direction, the experimental results may be classified under 3 distinct types, *viz.* (*a*) that in which $X_{90}/X > 1$, *i.e.* the scattered radiation is observed to possess a smaller absorbability than that in the direction $\phi = 90°$ as required by the Compton theory, as applied to a homogeneous radiation, (*b*) that in which $X_{90}/X\phi = 1$, *i.e.* the scattered radiation is observed to possess an absorbability equal to that of the radiation scattered at right angles to the primary (within experimental error). (*c*), that in which $X_{90}/X\phi < 1$, *i.e.* the scattered radiation is observed to possess a greater absorbability than the radiation scattered in the direction $\phi = 90°$.

The observations (*b*) and (*c*) superficially appear to contradict the Compton theory.

Under type (*a*) come paraffin and carbon radiators. The $Y - t$ curves have generally an ascending course from left to right as in Fig. 3.

Filter paper (70 sheets) is an outstanding instance of type (*b*), especially in the case of softer incident radiations. Here the $Y - t$ curves may be seen to be horizontal as in Fig. This result was also noticed by Barkla

TABLE I

Scatterer	Incident equivalent* wavelength in A. U.	X_{90}/X_{φ} $\varphi=150°$	X_{90}/X_{φ} $\varphi=30°$	X_{90}/X_{φ} $\varphi=20°$	I_{30}/I_{90} corrected	I_{20}/I_{90} corrected	X_{90}/X_{φ} $\varphi=40°$	X_{90}/X_{φ} $\varphi=60°$
(1)	.77	.96	1.025	1.00	2.16	3.04		
Paraffin	.635	...	1.03	1.01	2.04	2.64		
1.8 cm	.49	.91	1.03	1 035	1.97	2.40		
thick	.44	.90	1.02	...	1.90	...		
	.38	...	...	1.07	...	2.28		
	.34	.84	1.03	...	1.85	...		
	.33	...	.	1.08	...	2.23		
	.275	.83	1.04	...	1.82	...		
	.25	.82	1.04	...	1.79	...		
	.225	.805	...	...	?	...		
(2)	.635	...	1.02	...	2.26	...		
Carbon	49	...	1.04	...	2.13	...		
0.6 cm. thick	.33	.895	1.06	...	1.98	...		
(3)	.77	.97	1.00	1.00	2.94	4.65		
Filter	.635	...	1.00	1.00	2.46	3.80		
paper	.49	.90	1.00	1.00	2.21	3.13	1.00	1.02
70	.41	.88	1.00	...	2.16	...	(I_{φ}/I_{90} =1.78)	(I_{ϕ}/I_{90} =1.30)
sheets	.38	...	...	1.04	...	2.83		
	.34	.845	1.00	...	1.98	...		
	.33	...	...	1.05	...	2.61		
	.275	.85	1.02	...	1.89	...		
	.25	.87	1.01	...	1.81	...		
	.225	...	1.05	...	1.72	...		
(4)	.635	...	1.00	...	4.74	...		
Aluminium	.49	.945	.93	...	3.61	...		
0.87 mm. thick	.38	...	.97	...	3.08	...		
(5)								
Sulphur 1 mm. thick	.49	.96	.96	...	4.74	...		

* The meaning of equivalent wavelength was explained in the previous paper Pal (1948).

and Khastgir (1926) which they interpreted in terms of the J-phenomenon and subsequently also by Khubchandani.

The (c) type of results yielded by aluminium (0.87 m.m. thick) and sulphur (1 m.m. thick) radiators, as illustrated by the $Y-t$ curve descending from left to right, similar to that in Fig. 1. This was, at first, quite unexpected and perplexing, as it seemed to violate established theory.

Barkla and Mackenzie (1926), working with an aluminium scatterer found that the scattered radiation in the directions $\phi=60°$ and $\phi=120°$-directions equally inclined to that for which $\phi=90°$, were to start with, equally absorbable with respect to each other ; but when a difference occurred, it occurred by an abrupt jump or discontinuity which she called the 'J discontinuity'. A similar behaviour was frequently observed by her in the case of paraffin scatterer also. Miss Mackenzie's experiment has been repeated separately with incident wavelengths .49 Å. U. and .51 Å. U., using an aluminium scatterer,

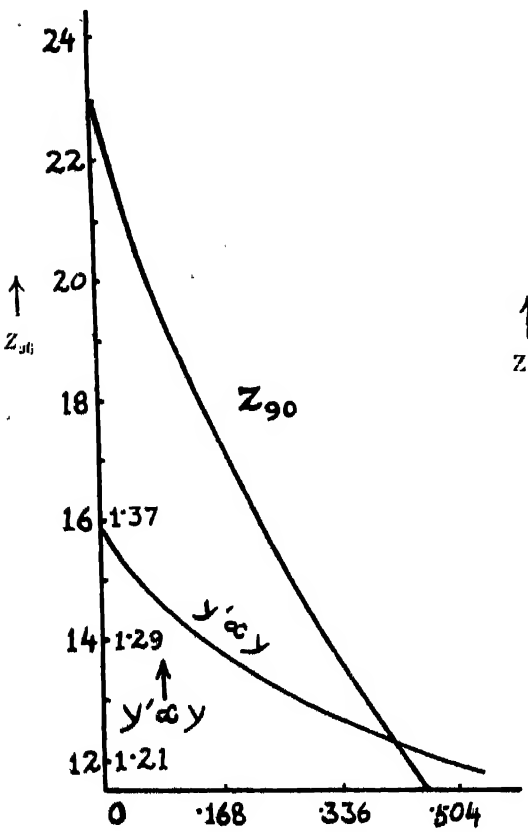

FIG. 1

Paraffin wax
$\phi=150°$
$\lambda_{equiv}=.25$ Å

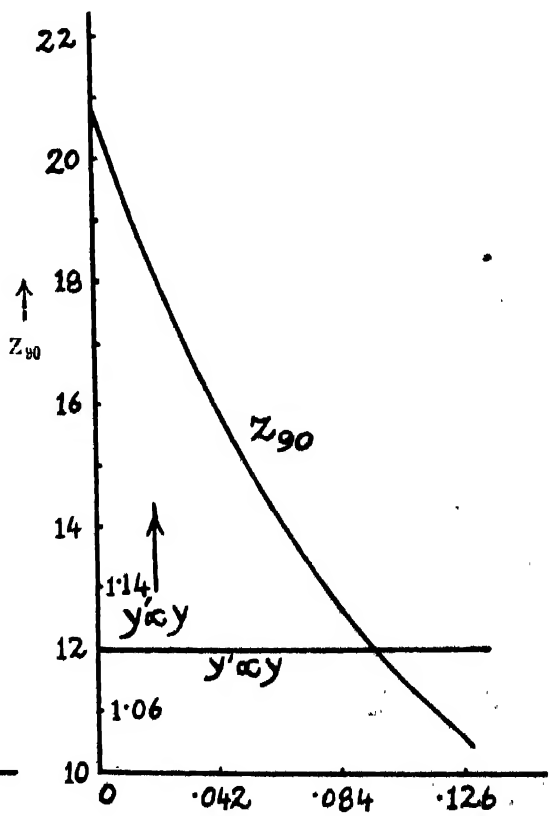

FIG. 2

Filter paper
$\phi=30°$
$\lambda_{equiv}=.49$ Å

by the author who confirmed her results as to the equality of absorption, but failed to reproduce the discontinuity at least up to a 50% absorption of the beam.

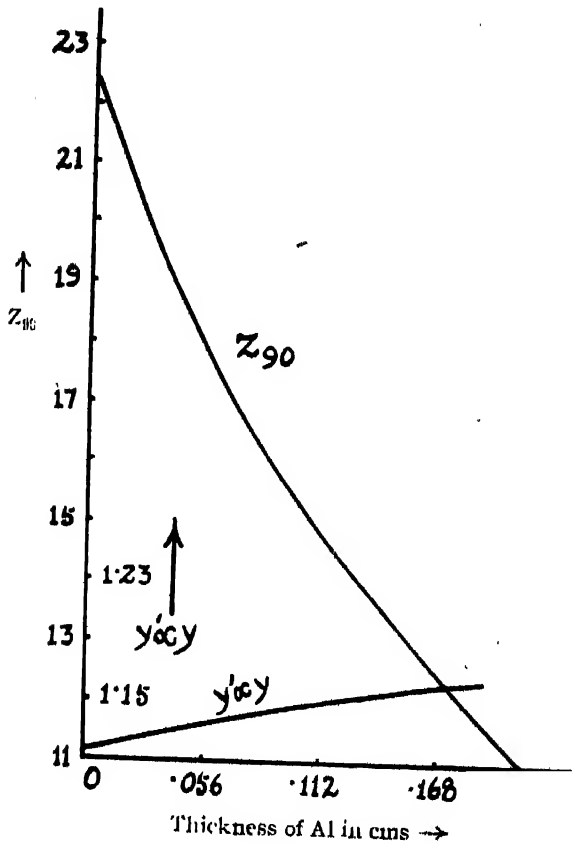

FIG. 3

Paraffin wax
$\phi = 20°$
λ equiv = .38 Å

A natural suggestion may be that the absorption (which hardens a heterogeneous radiation, the more so, the softer the radiation) within the material of the scatterer, even though adjusted in the manner suggested by Barkla and Ayres (1911), was responsible for the observations of the type (*b*) and (*c*). Absorption, however, could not be the only cause, which was proved by repeating experiments (*b*) and (*c*) for an incident wavelength .49 Å.U. – experiment (*b*) with a much thinner radiator of filter paper (24 sheets instead of 70) and experiment (*c*) with a much thicker radiator of sulphur (4 m.m. thick, instead of 1 m.m.). The two results in each experiment were indistinguishable from each other, although absorptions in the two cases differed widely for each material. Further, absorption alone cannot explain the large disparity between the degrees of modifications suffered by any one radiation in the directions $\phi = 150°$ and $\phi = 30°$.

Neither does the apparently capricious nature of the behaviour of the scattered radiation signify an actual departure from the accepted theory of scattering—the Compton effect. This will become evident from the following considerations. These peculiarities are seen to be associated with the forward direction only. The phenomenon, which was pointed out in the earlier paper by the author (Pal, 1948) called "excess scattering" also has been explained to be connected with the forward direction only, (see the previous paper). Hence the anomalous absorbability and 'excess scattering' seem to be intimately related to each other; indeed one follows directly from the other. What happens is that, 'excess scattering' superposes on the Compton effect, assumed present—another effect of opposite sense.

The 'excess scattering' in the forward direction with all its characteristics is accounted for—as is well known—on the basis of the interference between rays coherently scattered by different sources, such as electrons within the same atom or the neighbouring atoms themselves. A larger incident wavelength, a smaller angle of scattering and a greater atomic number (and hence a closer packing of electrons, inside the atom) of the scatterer, are all conditions favourable for a greater coherence and they will, consequently, contribute to a greater excess scattering. Hence, out of the vast multitudes of wavelengths present in the heterogeneous incident beam, the longer ones will, on account of interference, preponderate with greater intensity, in the scattered radiation, thus producing a general softening * of the same as a whole. It follows therefore, that the greater the 'excess scattering,' the greater is this softening. The effect of interference, considered alone, would be thus to make the heterogeneous scattered radiation, in the forward direction, more absorbable than that in the direction $\phi = 90°$. Such an effect is opposite in sense to the Compton effect. These two effects, superposed one upon the other and combined with the occurrence of somewhat unequal hardening due to absorption within the scatterer, along the two directions concerned, suffice to interpret all the observed results.

Thus, (*i*). in the case of paraffin and carbon, 'excess scattering' being small (the ratio I/I_{90} is recorded for convenience of reference in columns 6 and 7 of the table), the superposed effect is small too, and so, the Compton change predominates. A considerable increase in the correction factor towards the hardest incident radiation, in the case of $\phi = 20°$, may be, in part, ascribed to a relatively higher homogeneity of the beam (due to its progressive filtration at a lower voltage 80 K.V. instead of at 100 K.V. used for paraffin and filter paper, $\phi = 30°$). (*ii*) In the case of filter paper, the 'excess scattering' in the region of longer wavelengths, is much greater than for paraffin and carbon, and the effect superimposed is larger and may actually

* It may be remarked that the softening produced by interference and hardening produced by absorption are based on similar reasonings).

balance the Compton effect making $X=X_{90}$, as may be noted in connection with the smaller angles $\phi=40°$, 30°, and 20°. (*iii*) In the case of aluminium and sulphur, on the other hand, the 'excess scattering' is vastly greater than for paper; so that the Compton effect is relatively weaker compared to the superposed effect, which explains the behaviour of type (*c*). (*iv*) As the wavelength is made smaller, the Compton change of absorbability becomes more and more prominent whereas the 'excess scattering' diminishes; consequently, the Compton effect is outstanding.

In conclusion, it may be stressed that, during absorption experiments with heterogeneous scattered X-rays, such as described above, the nature of the results to be expected will, to a large extent, be controlled by the following factors:

(*i*) Direction of scattering.
(*ii*) Incident wavelength.
and (*iii*) Scattering material.

and may be interpreted on the basis of the Compton effect, the interference phenomenon and internal absorption inside the scatterer; no other special hypothesis such as J-postulate is necessary for this purpose.

ACKNOWLEDGMENTS

The author wishes to take this opportunity of expressing his deep sense of gratitude to late Professor C. G. Barkla, F.R.S., N.L. of the University of Edinburgh, for his kind and constant supervision. His thanks are also due to the members of the staff of the Physics Department of the said University who helped him in many ways during this work, and to Prof. K. Banerjee, D.Sc., F.N.I. for helpful discussions.

A. M. College,
Mymensingh.

REFERENCES

Allen, S. I. M., 1926, *Phys. Rev.*, **28**, 907.
Barkla, C. G., 1925, *Phil. Mag.*, May, **49**, 1033.
,, and Ayres, 1911, *Phil. Mag.*, **21**, 270.
,, and Khastgir, S. R., 1926, *Phil. Mag.*, **2**, 642.
,, ,, 1927, *Phil. Mag.*, **4**, 735.
,, and Mackenzie, G. I., 1926, *Phil. Mag.*, **1**, 542.

Barkla and Mackenzie, G. I., 1926, *Phil. Mag.*, **2**, 1116.

Bragg and Pierce, 1914, *Phil. Mag.*, **28**, 626.

Jonsson, 1928, Diss. Uppsala ,p. 12.

Kirchner, 1930, Handbuch. d. Exp. Physik, **24**, 230.

Pal, H. K., 1939, Proceedings of the Indian Science Congress.

,, 1948, *Ind. Jour. Phys.*, **22**, 291.

ELECTRON TRANSIT TIME IN NEGATIVE GRID OSCILLATOR

By S. K. CHATTERJEE and B. V. SREEKANTAN

(*Received for publication, July 23, 1948*)

ABSTRACT. Expressions for the time of flight of electrons between cathode to grid and grid to anode of a triode working as class C oscillator have been derived taking into account the effect of a.c. voltages on the plate and grid and also the grid bias. The expressions have been employed to calculate transit time in the case of some tubes and certain interesting conclusions have been arrived at.

INTRODUCTION

The effect of electron transit time on the performance of a vacuum tube oscillator becomes significant at ultra-high frequencies. One of the effects of finite transit time in an oscillator is the fall of efficiency. It is usual to study plate or overall efficiencies as function of transit angle. Negative grid triodes constitute the most widely used class of vacuum tube oscillators. It is, therefore, worthwhile to calculate the transit time between cathode and grid, and grid anode space, to understand properly the behaviour of negative grid oscillator at ultra-high frequencies. Derivation of an expression for transit time in a tube under class 'C' oscillatory condition should involve the consideration of the following factors:

(1) Inital velocity of emission of electrons.

(2) Space-charge effect between cathode-grid space.

(3) D.C. and a.c. potentials on grid and plate.

(4) Amplitudes of alternating voltages on grid and plate.

(5) Trajectory of electrons.

(6) Magnetic fields, if any.

(7) Electromagnetic fields—particularly important at u.h.f.

(8) Shape of electrodes.

It has not so far been feasible to arrive at a practically useful expression for the transit time, without making any simplifying assumption. Amongst the various methods adopted for the solution of this problem, one or the other of the following assumptions is inevitably present:

(1) Velocities of emission of electrons are either neglected or considered uniform.

(2) Density of current is regarded as small and hence the space charge effect in the grid anode space is neglected.

(3) When space charge is taken into consideration, it is assumed that a steady state space charge distribution has been established and the effect of a.c. fields is regarded as a perturbation small in comparison with the steady state components. It is also assumed that the time taken by electromagnetic waves to travel the inter electrode distance is negligible compared to transit time and period of oscillation. Or in Maxwell's notation

$$\nabla^2 V = -4\pi\rho + \frac{1}{c^2}\cdot\frac{\partial^2 V}{\partial t^2} = -4\pi\rho$$

(4) The effect of magnetic and electromagnetic fields is negligible.

(5) Electrodes are plane or cylindrical and of infinite extent.

(6) Electrons travel in straight line between electrodes.

(7) Voltage at the grid plane is assumed to be the same as the effective value of the voltage on the grid.

(8) Effects of negative grid bias and a.c. voltages on the grid and plate are neglected.

In the following analysis it is assumed that the electrodes are plane, parallel and of infinite extent.

Effect of negative grid bias and a.c. voltages on the grid and plate has been taken into consideration. The analysis makes no restriction of small signal input. The initial velocities of emission of electrons are neglected.

CATHODE GRID TRANSIT TIME

Assuming the electrodes to be plane and of infinite extent, the electron transit time τ_{kg} in the space charge limited region between cathode and grid can be shown (McPetrie, 1933) to be three times the time of flight that would be taken by electrons moving throughout with uniform velocity equal to the velocity of arrival at the grid. Or

$$\tau_{kg} = \frac{3d_{kg}}{\sqrt{\frac{2e}{m}\cdot E}} = \frac{3d_{kg}}{5.97\times 10^7\sqrt{E}} \qquad \ldots \quad (1)$$

where e/m represents the ratio of electronic charge to mass and d_{kg} is the distance between cathode and grid. The effective potential E expressed in volts at the grid plane can be considered to be equal to $\frac{E_b}{\mu}$, E_b being the potential at the anode and μ the amplification factor except for very low values of μ provided the oscillation is very weak and the alternating potentials on the grid and the anode are very small. Under this limiting condi-

tion of weak oscillation the grid voltage obtained by grid leak bias may be taken to be zero. But under actual class C working condition, the effective potential at the grid will involve terms due to grid bias, alternating potentials on the grid and anode and term due to transit angle. This may be shown as follows :

Let the time be reckoned from the instant (Fig. 1) when a.c. voltage on the plate is zero. Grid voltage attains a maximum value E_g at $t = \frac{T}{4}$. The

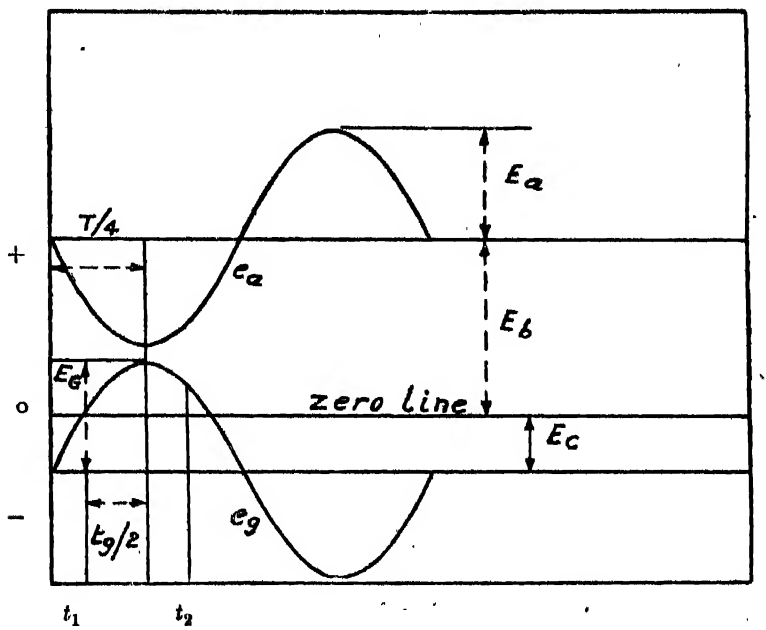

FIG. 1

instantaneous anode voltage e_a and grid voltage e_g may be written as follows :

$$e_a = E_b - E_a \sin \omega t$$

$$e_g = -E_c + E_g \sin \omega t$$

The above expressions for the instantaneous plate and grid voltages are not strictly accurate at ultra high frequencies, because due to transit time effects the phase relation between plate current and grid voltage that exists at low frequencies will not hold good. This phase lag in plate current will make the plate voltage differ in phase from grid voltage by an amount different from 180°. Neglecting this difference for convenience of analysis, the following procedure may be adopted.

Let an electron starting from the cathode at the instant t_1 when the grid starts on its positive cycle, arrive at the grid plane at an instant t_2. Then the instantaneous anode voltage at t_2 can be written as follows :

$$(e_a)_{t_2} = E_b - E_a \sin \omega t_2$$

$$= E_b - E_a \sin \omega \left[\frac{T}{4} - \frac{t_g}{2} + (t_2 - t_1) \right]$$

$$= E_b - E_a \sin \omega \left[\frac{T}{4} - \frac{t_g}{2} + \tau_{kg} \right]$$

Similarly, the instantaneous grid voltage at t_2 is given by

$$(e_g)_{t_2} = -E_c + E_g \sin \omega \left[\frac{T}{4} - \frac{t_g}{2} + \tau_{kg} \right]$$

The effective voltage on the grid plane at the instant is given by the following expression

$$(e_g + \frac{e_a}{\mu})_{t_2} = -E_c + E_g \sin \omega \left[\frac{T}{4} - \frac{t_g}{2} + \tau_{kg} \right]$$

$$+ \frac{E_b}{\mu} - \frac{E_a}{\mu} \sin \omega \left[\frac{T}{4} - \frac{t_g}{2} + \tau_{kg} \right]$$

$$= \left(-E_c + \frac{E_b}{\mu} \right) + \left(E_g - \frac{E_a}{\mu} \right) \cdot \cos \left(\theta_{kg} - \frac{\theta_g}{2} \right) \quad \ldots \quad (2)$$

where $\theta_k = \frac{2\pi}{T} \cdot \tau_{kg}$ and $\theta_g = \frac{2\pi}{T} \cdot t_g$

From eqns. (1) and (2), the expression for τ_{kg} is obtained as given below

$$\tau_{kg} = \frac{3 d_{kg}}{5.93 \times 10^7} \cdot \frac{1}{\sqrt{\left[\left(-E_c + \frac{E_b}{\mu} \right) + \left(E_g - \frac{E_a}{\mu} \right) \cdot \cos \left(\theta_{kg} - \frac{\theta_g}{2} \right) \right]}} \quad \ldots (3)$$

Though this expression in the present form is not useful in evaluating τ_{kg} as the denominator under the root sign contains θ_{kg}, certain interesting conclusions as mentioned below can be drawn.

(1) When the amplitude of grid voltage E_g is $1/\mu$ times the amplitude of anode voltage, E_a the transit time τ_{ga} becomes independent of the amplitudes of alternating voltages on the grid and the anode.

(2) When $\theta_{kg} = \frac{\theta_g}{2}$ *i.e.*, when there is no lag between electron motion and voltage on the grid $\cos \left(\theta_{kg} - \frac{\theta_g}{2} \right)$ becomes unity and τ_{kg} reduces to

$$\tau_{kg}=\frac{t_g}{2}=\frac{3d_{kg}}{5.93\times10^7}\cdot\frac{1}{\sqrt{\left(E_g-E_c\right)+\left(\frac{E_b-E_a}{\mu}\right)}}$$

$$=\frac{3d_{kg}\sqrt{\mu}}{5.93\times\sqrt{E_b}}\cdot\frac{1}{\left\{\mu\left(\frac{E_g-E_c}{E_b}\right)+\left(\frac{E_b-E_a}{E_b}\right)\right\}^{1/2}}$$

$$=\frac{\tau'_{kg}}{\left\{\mu\left(\frac{E_g-E_c}{E_b}\right)+\left(\frac{E_b-E_a}{E_b}\right)\right\}^{1/2}} \quad \ldots \quad (4)$$

In class 'C' operation E_g-E_c, the maximum positive grid voltage may be considered to be equal to the minimum anode voltage E_b-E_a. Denoting this by E_o, τ_{kg} may be written as follows

$$\tau_{kg}=\frac{\tau'_{kg}}{\left\{\frac{E_o}{E_b}\left(\mu+1\right)\right\}^{1/2}} \quad \ldots \quad (5)$$

In eqn. (4), τ'_{kg} indicates the transit time as given by Gavin (1939). The correction factor $K=\left\{\frac{E_o}{E_b}\left(\mu+1\right)\right\}^{1/2}$ to be applied to Gavin's expression for the transit time, when the effects of grid bias and a. c. voltages on the grid and anode are taken into account, in the case of several valves for particular values of E_0/E_b is shown in Fig. 2. The values for E_o in the case of different

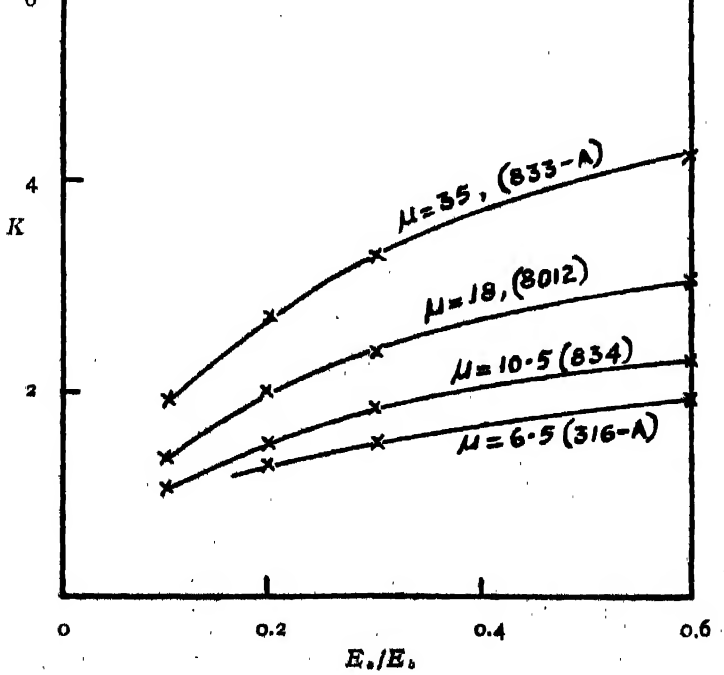

FIG. 2

valves have been found by class 'C' analysis. It will be observed that for values of E_c/E_b lower than 0.1 and for valves having low μ the correction factor tends to be less than unity and so τ_{kg} becomes greater than τ'_{kg}. But for values of E_c/E_b greater than 0.2 and for valves having higher μ the value for τ_{kg} becomes less than τ'_{kg}.

GRID ANODE TRANSIT TIME

The grid anode space may be regarded as free of space charge. If v is the velocity of an electron at a distance x from the grid at an instant t then the time of flight τ_{ga} of electron between grid and plate is given by the following expression.

$$\tau_{ga} = \int_0^{d_{ga}} \frac{dx}{v}$$

where d_{ga} is the distance between grid and anode.

In the above expression for τ_{ga} the velocity v is a function both of x and t. Let us consider the case of the electron which arrives at the grid when the grid voltage is at its positive maximum value. Let the time be reckoned from this instant. So the instantaneous values of anode and grid voltages given by

$$e_a = E_b - E_a \cos \omega t \quad \text{and} \quad e_g = -E_c + E_g \cos \omega t$$

reduces to

$$(e_a)_{t=0} = E_b - E_a \quad \text{and} \quad (e_g)_{t=0} = -E_c + E_g$$

at time

$$t = 0$$

The potential at a point distant x from the grid at the instant t is given by the following expression

$$V(x, t) = \left(e_g + \frac{e_a}{\mu}\right) + \left\{e_a - \left(e_g + \frac{e_a}{\mu}\right)\right\} \frac{x}{d_{ga}}$$

$$= \left(\frac{E_b}{\mu} - E_c\right) + \left\{E_b - \left(\frac{E_b}{\mu} - E_c\right)\right\} \cdot \frac{x}{d_{ga}}$$

$$+ \left[\left(E_g - \frac{E_a}{\mu}\right) + \left\{-E_a - \left(E_g - \frac{E_a}{\mu}\right)\right\} \cdot \frac{x}{d_{ga}}\right] \cdot \cos \omega t \qquad \ldots \quad (6)$$

The potential at a point at various instants between grid and anode can be evaluated from eqn. 6 as follows.

(1) At $t = 0$ and $x = d_{ga}$ the potential at the anode is given by

$$V(x, t) = \left(\frac{E_b}{\mu} - E_c\right) + \left(E_b - \frac{E_b}{\mu} + E_c\right) + \left(E_g - \frac{E_a}{\mu}\right) - \left(E_a + E_g - \frac{E_a}{\mu}\right)$$

Or the potential at the anode is $V(d_{ga}, o) = E_b - E_a$ when the electron is in the grid plane

$$(ii)\ \text{At } t = \frac{T}{4},\ x = d_{ga},\ \cos \omega t = o$$

The potential at the anode is given by

$$V\left(d_{ga}, \frac{T}{4}\right) = \left(\frac{E_b}{\mu} - E_c\right) + \left(E_b - \frac{E_b}{\mu} + E_c\right) = E_b$$

(*iii*) At $t = o$, $x = o$, the potential at the grid is given by

$$V(o, o) = \frac{E_b}{\mu} - E_c + E_g - \frac{E_a}{\mu} = (E_g - E_c) + \left(\frac{E_b - E_a}{\mu}\right)$$

In a class 'C' oscillator if the maximum positive grid voltage is assumed to be equal to minimum anode voltage, *i. e.*,

$$(E_b - E_a) = (E_g - E_c)$$

then the potential at the grid plane at $t = o$ is greater than the anode potential by an amount $\frac{E_b - E_a}{\mu}$.

At the instant the electron leaves the grid $\cos \omega t = 1$ and so the expression for $V(x, t)$ in eqn. (6) reduces to

$$V(x, t) = \left(\frac{E_b}{\mu} - E_c\right) + \left(E_g - \frac{E_a}{\mu}\right) + x\left[\frac{1}{d_{ga}} \cdot \left\{E_b - \left(\frac{E_b}{\mu} - E_c\right)\right\} - \frac{1}{d_{ga}}\left\{E_a + \left(E_g - \frac{E_a}{\mu}\right)\right\}\right]$$

$$= A + B.x$$

Where $$A = \left(\frac{E_b}{\mu} - E_c\right) + \left(E_g - \frac{E_a}{\mu}\right)$$

$$B = \frac{1}{d_{ga}} \cdot \left[\left\{E_b - \left(\frac{E_b}{\mu} - E_c\right)\right\} - \left\{E_a + \left(E_g - \frac{E_a}{\mu}\right)\right\}\right]$$

The velocity of the electron at x at time t is given by

$$v(x, t) = \sqrt{\frac{2e}{m}} \cdot \sqrt{V(x, t)}$$

So, $$\tau_{ga} = \int_0^{d_{ga}} \frac{dx}{\sqrt{\frac{2e}{m}} \cdot \sqrt{A + Bx}} = \frac{2}{5.93 \times 10^7} \cdot \left\{\frac{\sqrt{A + B.d_{ga}} - \sqrt{A}}{B}\right\} \quad (7)$$

If a. c. voltages on the grid and anode and grid bias are neglected, then

$$A = \frac{E_b}{\mu} \text{ and } B = \frac{E_b}{d_{ga}}\left(1 - \frac{1}{\mu}\right)$$

$\therefore$ τ_{ga} (eqn. 7) reduces to

$$\tau_{ga} = \frac{2d_{ga}}{5.93 \times 10^7} \cdot \frac{1}{\sqrt{E_b}} \cdot \frac{\sqrt{\mu}}{\sqrt{\mu}+1}$$

TOTAL TRANSIT TIME

The total time τ of flight between cathode to anode is found from eqns. (4) and (7).

$$\tau = \tau_{kg} + \tau_{ga} = \frac{3d_{kg}}{5.93 \times 10^7 \sqrt{\left(\frac{E_b - E_a}{\mu}\right) + \left(E_g - E_c\right)}} + \frac{2}{B \times 5.93 \times 10^7} \cdot \left\{ \sqrt{A + Bd_{ga}} - \sqrt{A} \right\}$$

$$= \frac{1}{5.93 \times 10^7} \left\{ \frac{3d_{kg}}{\sqrt{A}} + \frac{2}{B} \cdot \left(\sqrt{A + B.d_{ga}} - \sqrt{A} \right) \right\}$$

The above expression for τ reduces to Gavin's (1939) expression

$$\tau = \frac{1}{5.93 \times 10^7} \cdot \sqrt{\frac{\mu}{E_b}} \cdot \left\{ 3d_{kg} + \frac{2d_{ga}}{\sqrt{\mu}+1} \right\}$$

when a. c. voltages and grid bias are neglected.

In the general case when $t \neq 0$

$$V(x, t) = \left(\frac{E_b}{\mu} - E_c \right) + \left\{ E_b - \left(\frac{E_b}{\mu} - E_c \right) \right\} \cdot \frac{x}{d_{ga}} + \left[\left(E_g - \frac{E_a}{\mu} \right) + \left\{ -E_a - \left(E_g - \frac{E_a}{\mu} \right) \right\} \frac{x}{d_{ga}} \right] \cdot \cos \omega t$$

$$= A' + B'x + C \cos \omega t + Dx \cos \omega t$$

$$= (A' + C \cos \omega t) + (B' + D \cos \omega t).x$$

At ultra-high requency t being very small of the order of 10^{-8} to 10^{-10} secs., terms inside brackets may be regarded as constants. So $V(x, t)$ may be written as

$$V(x, t) = A_0 + B_0 x$$

So, $$v = \sqrt{\frac{2e}{m}} \cdot V(x, t) = 5.93 \times 10^7 \sqrt{A_0 + B_0 x}$$

Therefore, $$\tau_{ga} = \int_0^{d_{ga}} \frac{1}{5.93 \times 10^7} \cdot \frac{dx}{\sqrt{A_0 + B_0 x}}$$

$$= \frac{2}{5.93 \times 10^7 . B_0} \left\{ \sqrt{A_0 + B_0 . d_{ga}} - \sqrt{A_0} \right\} \quad \ldots \quad (8)$$

From eqn. (8), the following conclusions may be drawn

i) At $t=0$ if $(E_b-E_a)=E_g-E_c+\frac{E_b-E_a}{\mu}$

then $B_0=0$ and τ_{ga} becomes infinite

ii) At $t=0$ if $E_b-E_a=E_g-E_c$ then $B_0=-\frac{E_b-E_a}{\mu}$

and τ_{ga} becomes negative.

iii) In either of the above cases, τ_{ga} has no definite meaning.

Therefore, in order that an electron, which leaves the grid when the voltage on it is a maximum, may reach the plate the following necessary condition should be satisfied :

$$(E_b-E_a)>\left\{E_g-E_c+\frac{E_b-E_a}{\mu}\right\}$$

or

$$(E_b-E_a)\left(1-\frac{1}{\mu}\right)>(E_g-E_c)$$

Calculation of τ_{ga} for some valves :

To find τ_{ga} for any tube from eqn. (8), it is necessary to evaluate A_0 and B_0. Table 1, where

$$\phi=\frac{\sqrt{A_0+B_0d_{ga}}-\sqrt{A_0}}{B_0}$$

shows the result of calculation in case of some valves. Transit times

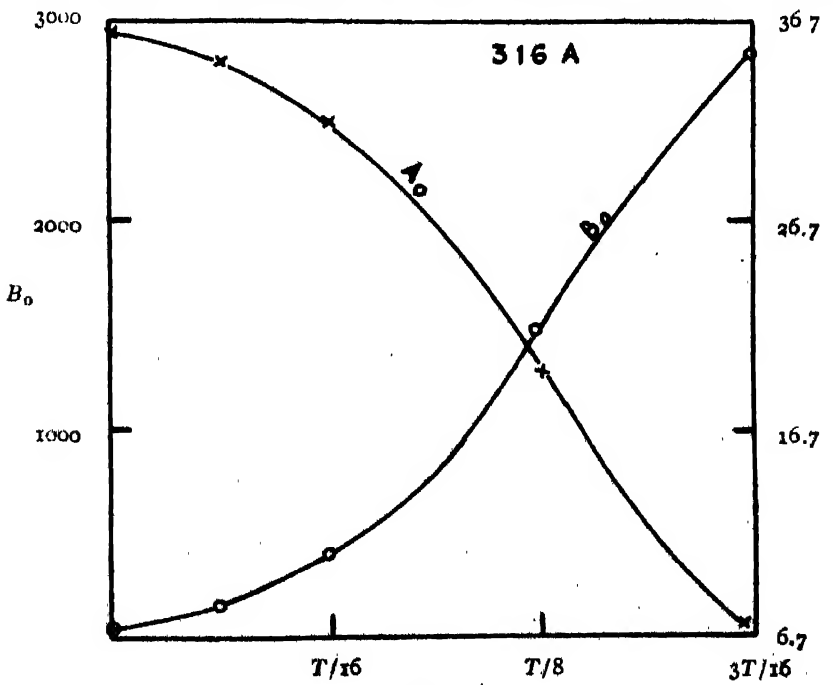

FIG. 3

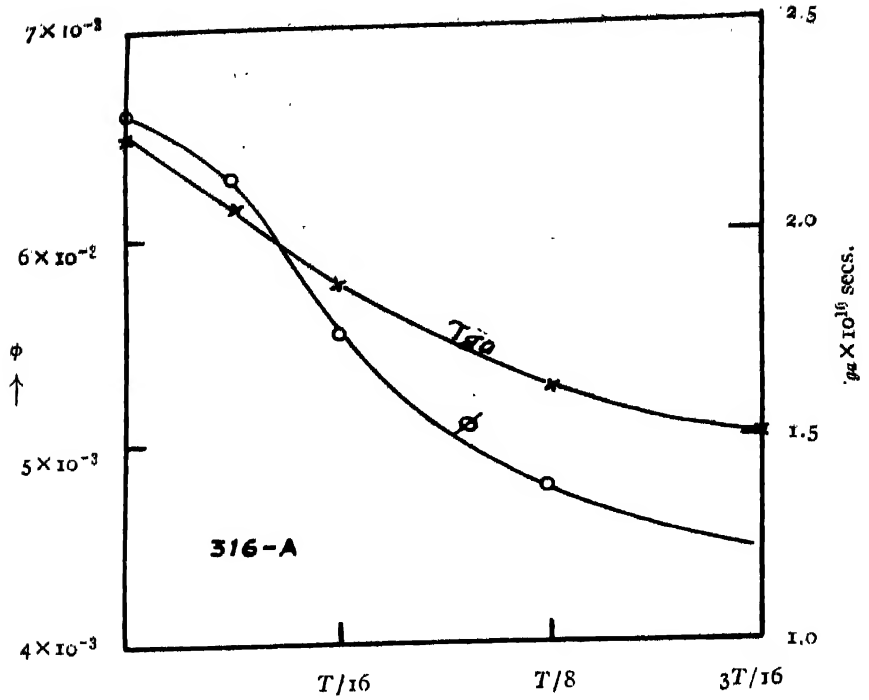

FIG. 4

for different electrons leaving the grid at different instants ($t=0$, $t=\frac{T}{32}$, $t=\frac{T}{16}$, $t=\frac{T}{8}$ etc., where T is the period of oscillation) are given in Table I. The last column gives the transit time between the grid and anode as calculated from Gavin's expression. Values of A_0, B_0, ϕ and τ_{ga} for electrons leaving the grid at different instants for the tube 316-A can be studied from Figs. 3 and 4.

GRAPHICAL REPRESENTATION OF THE METHOD

If we assume a steady positive potential $(E_b)_+$ on the plate and a steady positive potential $(E_g)_+$ on the grid, then the potential at any point distant x from the grid is

$$V(x)=\left\{\frac{(E_b)_+}{\mu}+(E_g)_+\right\}+\left[(E_b)_+-\left\{\frac{(E_b)_+}{\mu}+(E_g)_+\right\}\right]\frac{x}{d_{ga}}$$

denoting $\frac{(E_b)_+}{\mu}+(E_g)_+$ by A'

and $\frac{1}{d_{ga}}\left[(E_b)_+-\left\{\frac{(E_b)_+}{\mu}+(E_g)_+\right\}\right]$ by B'

$$V(x)=A'+B'x. \qquad \ldots \quad (9)$$

Therefore the transit time between the grid and the anode under those conditions will be given by :

TABLE I

Tube	t	A_0	B_0	$\Phi \times 10^2$	$\tau_{ga} \times 10^{10}$ secs.	τ_{ga} (Gavin)
838-A						
$E_b = 1000$ v	0	154.56	6	3.333	11.24	
$E_a = 840$ v	$T/32$	149.86	30	3.300	11.13	
$\mu = 35$	$T/16$	136.16	102	3.235	10.90	7.843×10^{-10} seconds
$E_c = -115$ v	$T/8$	83.96	374.2	2.932	9.88	
$E_g = 265$ v	$3T/16$	24.86	682.7	2.883	9.72	
$d_{ga} = 0.86$ cm						
834						
$E_b = 1000$ v	0	127.8	7	2.0	6.744	
$E_a = 870$ v	$T/32$	118.79	74	1.527	5.148	
$\mu = 10.5$	$T/16$	101.33	270	1.452	4.897	1.139×10^{-10} seconds
$E_c = -310$ v	$T/8$	27.13	1071	1.385	4 671	
$E_g = 425$ v	$3T/16$	−58.67	1871	—	—	
$d_{ga} = 0.35$ cm						
8012						
$E_b = 1000$ v	0	37.20	28	8.106	2.733	
$E_a = 960$ v	$T/32$	35.83	225	7.341	2.131	
$\mu = 18$	$T/16$	31.74	813	6.145	1.881	8.632×10^{-11} seconds
$E_c = -90$ v	$T/8$	16.08	3048	4.566	1.631	
$E_g = 125$ v	$3T/16$	−0 39	5581	—	—	
$d_{ga} = 0.10$ cm						
316-A						
$E_b = 400$ v	0	36.1	48.8	6.661	2.229	
$E_a = 360$ v	$T/32$	35.05	150.0	6.320	2.131	
$\mu = 6.5$ v	$T/16$	31.94	443.7	5.578	1.881	7.226×10^{-11} seconds
$E_c = -80$ v	$T/8$	20.11	1566	4.838	1.631	
$E_g = 110$ v	$3T/16$	6.72	2838	4.454	1.502	
$d_{ga} = 0.08$ cm						

$$\tau_{ga} = \frac{2}{5.93 \times 10^7 B'} \left\{ \sqrt{A' + B' d_{ga}} - \sqrt{A'} \right\} \quad \ldots \quad (10)$$

Under oscillatory conditions the instantaneous plate and grid voltages are given by

$$e_a = E_b - E_a \cos \omega t \quad \ldots \quad (11)$$

$$e_g = -E_c + E_g \cos \omega t \quad \ldots \quad (12)$$

If we confine our attention to that portion of the cycle during which the grid is positive, then using (11) and (12) we can draw the curves e_a *vs.* t and e_g *vs.* t for values of $t = 0$, $T/8$, $T/4$ etc. From these curves we get the values of $(E_b)_+$, $(E_g)_+$ for the various instants $t = 0$, $T/8$, $T/4$ etc. Hence we get the transit time corresponding to the various instants of the electrons leaving the grid plane. Hence the transit time against plate voltage curves for various values of grid voltage can be drawn (Fig. 5). From the figure we see for example that corresponding to $l = T/16$ the grid voltage is 130 volts and the plate voltage is 280 v and the transit time between the grid and the

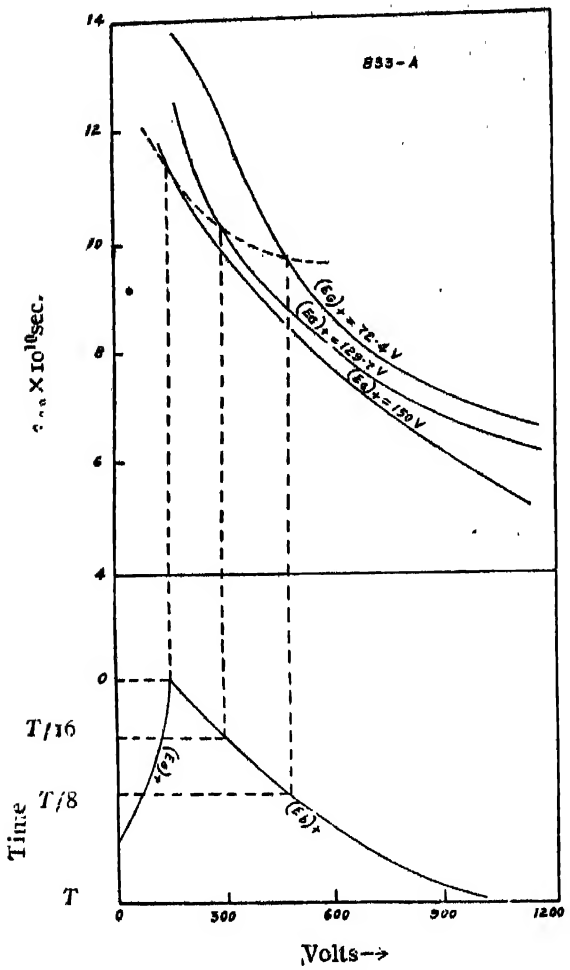

FIG. 5

anode is 10.3×10^{-10} sec. The fall of transit time as the plate voltage increases from its lowest positive value and the grid voltage decreases from its maximum positive value can also be seen.

ACKNOWLEDGMENT

The authors wish to express their grateful thanks to the Head of the Department for the encouragement given during the course of the investigation.

DEPARTMENT OF ELECTRICAL COMMUNICATION ENGINEERING,
INDIAN INSTITUTE OF SCIENCE, BANGALORE

REFERENCES

Gavin, M. R , 1939, *Wireless Engineer*, **16**, 287.
McPetrie, J. S., 1933, *Phil. Mag.*, **16**, 284.

MAGNETIC STUDIES ON SINGLE CRYSTALS OF TUNGSTENITE (WS_2)

By AJIT KUMAR DUTTA and BENOY CHANDRA ROY CHOWDHURY

Received for publication, November 16, 1948)

ABSTRACT. Tungstenite (WS_2) crystal possesses a structure similar to that of molybdenite (MoS_2). Recent magnetic measurements on single crystals of molybdenite by Dutta revealed some very interesting facts regarding its electronic energy structure. Magnetic measurements on single crystals of tungstenite have therefore been undertaken in this laboratory with a similar objective in view. But unlike molybdenite it was found to be paramagnetic. The paramagnetic susceptibility along the hexagonal axis, $\chi_{\parallel}$, is about 4917×10^{-6} c.g.s. e.m units per gm. mol. at 30°C while $\chi_{\perp}$, that at right angles to the axis is about 6314×10^{-6} c.g.s. e.m. units per gm. mol at the same temperature, which corresponds to an anisotropy of about 24 per cent. These measurements have been extended to various temperatures ranging from 700°K down to about 80°K. The effective magnetic moment along both the directions have been found to have maxima values near about the room temperature and have been found to decrease continuously with either increase or decrease of temperature within the present range. W^{+4} ion is in a ground state $5d^2\ {}^3F_2$ and the available X-ray data indicate that the crystalline electric field acting on the ion is presumably of a trigonal symmetry. The Stark pattern of the ground state under such a field is shown to be one degenerate doublet lying lowest and one singlet separated from it by several hundred cm^{-1}. On this basis an explanation of the anisotropy and the variation of magnetic moments with temperature has been attempted.

INTRODUCTION

In recent years the study of the properties of semi-conductors have engaged the attention of the theoretical as well as of the experimental physicists. All theoretical investigations on this subject are based on the ideas sponsored by Wilson (1931, 1932, 1939), while a fairly large amount of experimental work on it has been done mainly by the Russian (Gudden, 1934) and the German (Gudden *l. c.*) schools of physicists. But the experimental data are so varied and most often so conflicting and unsystematic that these are not always amenable to any theoretical treatment. Moreover, a study of the behaviour of this class of solids in the state of single crystals, which is expected to furnish the most interesting and essential informations regarding their structure and the structure sensitive physical properties, has been much neglected. It was to elucidate this aspect of the problem that Ganguly and Krishnan (1936, 1941) initiated the studies on single crystals of graphite Instead of, however, investigating directly the electrical conductivity of the substance in the manner of the previous workers in this line, they started with the magnetic properties and arrived at some highly

interesting conclusions. They were able to show from their investigations that the abnormal diamagnetism of graphite is entirely a "free" electronic phenomenon. For a detailed account of the nature of this free electron diamagnetism in graphite, it would be best to refer to their original papers. Continuing in the same line of investigations, Dutta (1944, 1945) showed that the highly unidirectional and large diamagnetism in single crystals of molybdenite (MoS_2), which is known to be a semi-conductor and which possesses a hexagonal structure, has the same origin as that in graphite and the results have been reported in some recent papers.

Tungstenite (WS_2) which possesses a structure similar to that of molybdenite would naturally be expected to be a semi-conductor also. But no data electrical or magnetic are available for this substance so as to be able to verify such an expectation. Consequently it was thought desirable to start an investigation on single crystals of tungstenite. A complication, however, arises due to the fact that unlike the crystals of graphite and molybdenite, tungstenite is found to be strongly paramagnetic. The present paper gives an account of the measurements of the magnetic properties of single crystals of tungstenite at temperatures ranging from 700°K down to about 80°K.

EXPERIMENTAL

Since tungstenite (WS_2) is a hexagonal crystal having a layer lattice, a determination in two directions of the magnetic susceptibility namely, $\chi_\parallel$, in a direction parallel to the hexagonal axis and $\chi_\perp$, that at right angles to the axis are enough. To obtain these values the procedure of Krishnan and his collaborator (1935) is adopted. It essentially consists of :

(*i*) The determination of the principal anisotropy, *i. e.*, the difference $\chi_\parallel - \chi_\perp$ between the principal susceptibilities.

(*ii*) The determination of the absolute value of one of these magnetic susceptibilities.

A short account of the methods of these measurements at room temperatures as well as of the adaptations necessary for extending the measurements to various other temperatures are given below.

MEASUREMENT OF ANISOTROPY

(*a*) *Room temperatures.*—In the particular case of tungstenite, the crystal is suspended vertically along its basal plane in a uniform horizontal magnetic field from one end of a fine calibrated quartz fiber, the other end of which is attached to a graduated torsion head. The crystal tends to bring its basal plane to parallelism with the field, showing that the susceptibility of the crystal along directions in the basal plane, *i.e.*, $\chi_\perp$, is greater than that along the symmetry axis, $\chi_\parallel$. The torsion head is suitably rotated so that when the crystal sets in the magnetic field, there is

no torsion on quartz fibre.' If the torsion head be now rotated the crystal will also rotate but through a smaller angle, until there will come a stage, corresponding to a rotation of the torsion head through an angle α_c and of the crystal through an angle of $\frac{\pi}{4}+\sigma_c$, when the equilibrium of the crystal in the field will become unstable and the crystal will turn round suddenly towards the next position of stable equilibrium. It can then be shown that the difference in the maximum and minimum susceptibilities in the horizontal plane of suspension is given by

$$\frac{1}{2}\frac{m}{Mc}H^2(\chi_\perp-\chi_\parallel)=\lambda(\text{say})=\frac{\alpha_c-\pi/4-\sigma_c}{\cos 2\sigma_c} \quad \ldots \quad (1)$$

$$\text{where } \sin 2\sigma_c=\frac{1}{2\lambda} \quad \ldots \quad (2)$$

This equation enables us to determine the value of $\chi_\perp-\chi_\parallel$, the value of m and M, the mass and the molecular weight of the crystal respectively, c, the torsional constant of the fibre and H, the magnetic field strength being previously known. In actual practice the value of the field strength and the dimensions of the fibre are so adjusted that α_c is always sufficiently large so that the factor σ_c may be neglected and the anisotropy $\chi_\perp-\chi_\parallel$ can be expressed by the simpler relation

$$\frac{1}{2}\frac{m}{Mc}H^2(\chi_\perp-\chi_\parallel)=(\alpha_c-\pi/4) \quad (3)$$

(*b*) *Low temperatures.*—For measurements at low temperatures, the crystal is suspended with its basal plane vertical from one end of a long glass rod the other end of which is attached to one end of a fine, calibrated quartz fibre, the other end being attached to a graduated torsion head and the crystal with the major portion of the glass rod is kept hanging inside a gas-flow cryostat designed by Bose (1947) for magnetic measurements with which temperatures down to about 80°K can be attained. The measurement of anisotropy at different low temperatures is then made in the usual manner (Bose, *loc. cit*). By this process measurements can be made at temperatures down to about 80°K.

(*c*) *High temperatures.*—The measurements of anisotropy at higher temperatures are performed in a manner similar to that utilised by Dutta (1945). The suspension of the crystal in this case consists of two parts, the upper one is a fine quartz fibre which has been kept at the room temperature by means of water circulation ; the lower one is a thin pyrex glass rod to the lower end of which the crystal is attached with its basal plane vertical by means of a dental cement which has been previously tested and

found to be very feebly diamagnetic and isotropic. The measurement of anisotropy is then made in the same manner as of Dutta (1945).

MEASUREMENT OF $\perp$. THE MAGNETIC SUSCEPTIBILITY PERPENDICULAR TO THE SYMMETRY AXIS

At room temperatures.—The absolute magnetic susceptibility of tungstenite crystals along directions perpendicular to that of the symmetry axis, $\chi_\perp$, is measured by the method of Dutta (1944) as well as by that of Bose (1947). The method of Dutta (*loc. cit.*) is essentially the method of balancing the horizontal force exerted on the crystal when it is placed in a non-homogeneous magnetic field (the horizontal gradient being only effective) by applying torsion to a horizontally stretched fibre (usually of silver) from the centre of which the crystal is rigidly suspended with its basal plane vertical and kept in the setting position by means of a fine glass rod. The torsional balancing is done by keeping the crystal immersed successively in two liquid media of known volume susceptibilities K_1 and K_2 so that the volume susceptibility of the crystal is given by

$$\frac{K_c - K_1}{K_c - K_2} = \frac{\theta_1}{\theta_2} \qquad \ldots \quad (4)$$

where K_c is the volume susceptibility of the crystal and θ_1 and θ_2 respectively are the angles of torsion needed to balance the magnetic force on the crystal when immersed in the two liquids. The method of Bose (1947) is the method of balancing the vertical force exerted on a crystal suspended in the usual manner from one arm of a torsional micro-balance specially designed by him for magnetic measurements. It is so arranged in his method that the vertical component of the magnetic force is only effective. The torsional balancing is done in this case also in two different liquid media of known volume susceptibilities. The calculation of the volume susceptibility is the same as that in the method of Dutta.

A determination of the density of the crystal will enable us to calculate the value of $\chi_\perp$.

At low temperatures.—The procedure for measuring the absolute susceptibility $\chi_\perp$ of the crystal is the same as that adopted by Bose (1947) for the study of paramagnetic crystals of the iron group of elements at low temperatures.

At higher temperatures.—The measurement of $\chi_\perp$ at higher temperatures was done as in the case of low temperatures by the quartz microbalance the low temperature cryostat being replaced by the heater and using dental cement instead of shellac as the attaching material.

TABLE I

Diamagnetic Correction :

$W^{+4} = -35.19 \times 10^{-6}$
$S^{-2} = -31 \times 10^{-6}$
} 66.19×10^{-6} per gm mol.

At 30°C

Crystal	Anisotropy $(\chi_\perp - \chi_\parallel) \times 10^6$ per gram mol.	Volume susceptibility $K \times 10^6$ per c c	Density	Corresponding gram molecular susceptibility at right angles to the symmetry axis, $\chi_\perp \times 10^6$	Mean anisotropy $(\chi_\perp - \chi_\parallel) \times 10^6$ per gram mol	Mean $\chi_\perp \times 10^6$ (after diamagnetic correction)	Mean gram molecular susceptibility along the symmetry axis, $\chi_\parallel \times 10^6$	Percentage of anisotropy
1	1381	195.1	7.63	6342				
2	1387	182 2	7.00	6457				
3	1501	182.36	7.52	6018	1397.40	6314.19	4916.79	23.89 %
4	1255	205.1	8.2	6203				
5	1463	193.93	7.73	6220				

TABLE II

Temperature °K	$(\chi_\perp - \chi_\parallel) \times 10^6$	$\chi_\perp \times 10^6$	$\chi_\parallel \times 10^6$	$\mu_\perp^2$	$\mu_\parallel^2$	$\bar{\mu}^2$
84	10630	19500	8870	13.33	6.01	10.89
88	10220	19050	8830	13.45	6.27	11.06
100	9080	17300	8220	13.95	6.63	11.51
120	7350	14900	7550	14.41	7.31	12.04
140	5750	12850	7100	14.51	8.02	12.35
160	4500	11250	6750	14.52	8.71	12.58
180	3670	10100	6430	14.66	9.33	12.88
200	3025	9175	6150	14.80	9.92	13.17
250	2000	7450	5450	15.03	10.99	13.68
300	1410	6230	4820	15.07	11.66	13.93
350	1100	5270	4170	14.87	11.77	13 84
400	875	4450	3575	14.35	11.53	13.41
450	720	3800	3080	13.79	11.19	12.92
500	600	3230	2630	13.03	10.61	12.22
550	510	2740	2230	12.15	9.89	11.39
600	410	2300	1890	11.13	9.14	10.47
630	350	2075	1725	10.54	8.77	9.95
650	340	1940	1600	10.12	8.38	9.54
660	310	1860	1550	9.90	8.25	9.35
670	300	1800	1500	9.73	8.11	9.19
680	300	1750	1450	9.59	7.95	9.04

RESULTS

Since the naturally occuring crystal of tungstenite contain varying amounts of impurities depending on the source from which it is obtained, the measurements had to be repeated with a number of specially chosen single crystals so that errors possibly arising out of the presence of impurities was a minimum and consistent. The room temperature measurements on five different single crystals of tungstenite are shown in Table I The values of the susceptibilities are expressed in electromagnetic C. G. S. units. In Table II are given the measurements at temperatures from about 700°K down to about 80°K. The values of $\mu_{\parallel}$ and $\mu_{\perp}$ effective magnetic moments expressed in Bohr magnetons for fields along and at right angles to the axis of symmetry, respectively are calculated according to the relation

$$\chi_i = \frac{N\mu_i^2 \beta^2}{3kT} \quad i = \parallel \text{ or } \perp \qquad \ldots \quad (5)$$

where N is the Avogadro number, β, the Bohr Magneton number and k is the Boltzman constant. The variation of $\mu_{\parallel}$, $\mu_{\perp}$ and $\mu = \sqrt{\frac{2\mu_{\perp}^2 + \mu_{\parallel}^2}{3}}$ with temperature are also given in Table II. The variation of susceptibilities and effective magnetic moments with temperature are represented graphically in figures 1 and 2 respectively.

CRYSTAL STRUCTURE OF TUNGSTENITE (WS_2) AND THE CHOICE OF CRYSTALLINE FIELD

Like molybdenite, tungstenite is a hexagonal crystal having a layer lattice. The cleavage between the different layers are fairly easy, but not as much as in the case of molybdenite. The structure of tungstenite was determined by van Arkel (1926). The unit cell contains two molecules of tungstenite (WS_2), *i.e.* two atoms of W and four atoms of S. The unit cell has the following dimensions

$$a = 3.18\text{Å}, \; c = 12.5\text{Å}$$

$$\text{and} \quad \frac{c}{a} = 3.93$$

and the various interatomic distances are

$$W - W = 3.18 \text{ Å} ; \quad S - S = 3.18 \text{ Å} ; \quad W - S = 2.48 \text{ Å}$$

It is evident that the W-atoms in the crystal are arranged in layers parallel to the basal plane and each such layer is sandwiched between two similar and parallel layers of sulphur atoms. The three layers form a *composite layer*, by the repetition of which the whole structure is built up. The sulphur atoms in the two alternate layers lie directly above one another

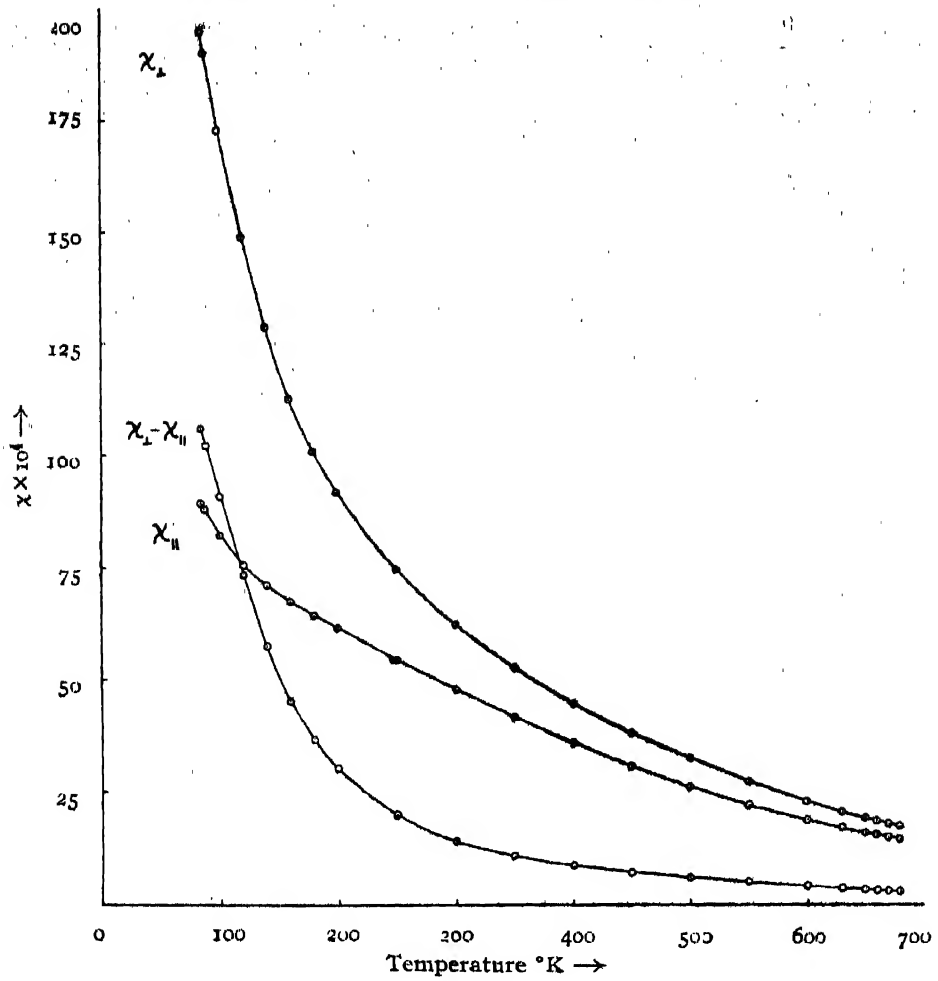

FIG. 1

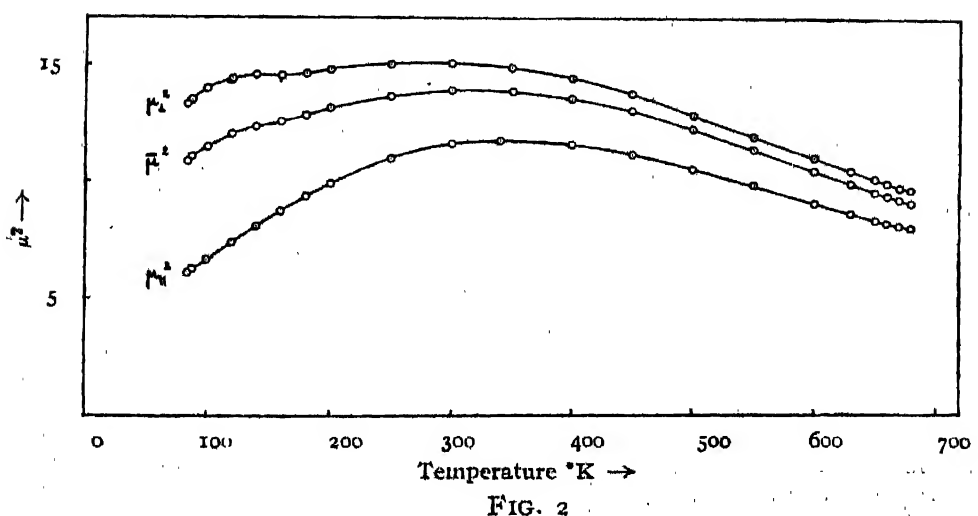

FIG. 2

and each is directly above or below the centre of the triangle formed by the W-atoms in the intermediate layers, and similarly for the W-atoms. The

W-atoms in one composite layer are again directly above or below the sulphur atoms in the next composite layer. Each atom of tungsten is surrounded by six equidistant sulphur atoms which lie at the corners of a right equilateral triangular prism. On the other hand each sulphur atom is equidistant from three tungsten atoms at the corners of an equilateral triangle.

The distance between similar atoms in the same layer W-W or S-S are seen to be much larger than that between dissimilar atoms, W-S. The distance between two adjacent composite layers is also large namely 3.13 Å. This explains the good basal cleavage of the crystal.

Thus in tungstenite (WS_2) crystal the group of six sulphur atoms surrounding each tungsten ion evidently has a trigonal symmetry and hence the crystalline electric field surrounding the central positive ion may be taken to be predominantly cubic one on which a small trigonal component has been super-imposed. Further the two sets of field axes for the two positive ions in the unit cell will be evidently parallel to each other leading to great simplification of the correlation between ionic and crystalline magnetic behaviours.

SPECTROSCOPIC STATE OF THE ION AND CONSIDERATIONS ARISING THEREFROM

Tungsten belongs to the platinum group of metals in which the $5d$ shell, which was left with only one electron until the element lutecium is reached, is in the course of being filled up. In tungsten the $5d$ shell contains 4 electrons and the $6s$ shell 2 electrons. In tungsten sulphide (WS_2) the two $6s$ and two $5d$ electrons take part in bond formation so that the tungsten ion is quadruply charged W^{+4}, and is left with 2 electrons in the incomplete $5d$ shell. According to Hund's theory the assignments of the lowest lying spectral states for the different ions in the $3d$ and $5d$ transition groups of elements are as is shown in Table III for comparison, and it will be seen that W^{+4} ion has a ground state $5d^2\ {}^3F_2$, the same as in the case Ti^{++} and V^{+++} belonging to the iron group of elements. Such identity of spectroscopic

TABLE III

Number of d electrons	0	1	2	3	4	5	6	7	8	9	10
Ground state	$^1S_0$	$^2D_{3/2}$	$^3F_2$	$^4F_{3/2}$	$^5D_0$	$^6S_{5/2}$	$^5D_4$	$^4F_{9/2}$	$^3F_4$	$^2D_{5/2}$	$^1S_0$
Ions of iron group	K^+ V^{+5}	Sc^{++} Ti^{+++} V^{+4}	Ti^{+2} V^{+3}	V^{+2} Cr^{+++} Mn^{+4}	Cr^{++} Mn^{+3}	Mn^{++} Fe^{++}	Fe^{++}	Co^{++}	Ni^{++}	Cu^{++}	Ca^+ Cu^+
Ions of platinum group	Ta^{5+} Hf^{+4}	Ta^{+4} Hf^{+3} Lu^{+2}	W^{+4} Ta^{+3}	W^{+3} Re^{+4}	Re^{+3} W^{+2}	Os^{+3} Re^{+2} Ir^{+4}	Os^{+2} Ir^{+3} Pt^{+4}	Ir^{+2} Pt^{+3}	Pt^{+2} Ir^+ Au^{+3}	Pt^+ Au^{+2}	Au^+

ground state with iron group, in fact, occurs throughout the platinum group. We can, in consequence, directly take over many of the considerations in regard to iron group, as being applicable to the platinum group also. For example, from the spectroscopic state we can at once calculate the effective magnetic moment for the "free" W^{+4} ion which comes out as 1·63 Bohr magnetons while the "spin only" value is 2·83. On the other hand it is known that in the heavier atoms such as of the rare-earth elements or the platinum group elements the multiplet width is very large (Laporte, O , 1928). So that the coupling between L and S is not easy to break under the action of external electric fields. In the rare-earth ions this is more so because the $4f$ electrons are protected from the effect of external electric fields by outer complete shells of electrons. In consequence, the ions in both these groups should be expected to behave as if they are more or less free. Even though they may not exactly correspond with the Hund's value for the "free ion" calculated on the assumption that the overall multiplet width is infinitely large, the very small action of the crystalline field will not lead to a quenching of the orbital moment as apart from the spin moment ; but will at best lead to a restriction of the orientation of the J moment as a whole (Penney and Schlapp, 1932). Experimental investigations on rare-earth salts agree very well with such contentions (Selwood, 1943; Mookerjee).* But accurate data on platinum and other heavy group salts is very meagre. Some of the data available (Bose, D.M., 1927 ; Van Vleck, 1932 ; and Selwood, 1943) on a few compounds of Mo^{+++} and Ru^{+4} of the molybdenum group, of W^{+3} and W^{+4} of the platinum group and of U^{+4} of the uranium group seem indeed to show the validity of such a conclusion in these salts also. But we should be very cautious in accepting such an interpretation of the experimental data, in view of a number of complicating factors which will be introduced in the next section.

NATURE OF CHEMICAL BINDING AND THE CRYSTALLINE ELECTRIC FIELD

We should remember that in the platinum group the $5d$ electrons are not at all screened from the action of the external fields. Further, though the spin-orbit coupling is generally high in the platinum group of elements it is not relatively so high in the earlier elements in the group as in the latter. Lastly, it is well known that the elements of the platinum group have a strong tendency for the formation of covalent bonds in which the bond energy is very much higher than in ordinary ionic bonds. In tungsten sulphide, for example, the two sulphur atoms are known to be bound to the tungsten by a pair of double covalent bonds, the W-S distance being 2.48 Å. In such cases of complex formations the crystalline field will be exceedingly high and may break down totally the Russel-Saunders coupling not only of L's and S's but even between individual l's and s's. The electrons in the

* A. Mookerjee, unpublished work, part of a thesis for D.Sc. degree, kindly communicated to the senior author.

incomplete shell will then have to be assigned to different $5d$ orbitals, which are left over after suitable assignment has been made of the electrons taking part in the covalent bonds. In this process those electrons which are not paired in the orbitals will contribute to the spin moment of the ion, orbital moment having been completely quenched except for small "high frequency" contributions. It will be seen that in such cases when spins pair off completely the substance will become diamagnetic altogether. Evidence for such covalent complex formations is obtained in large numbers in not only iron group elements but to an even larger extent in palladium and platinum groups. A study of the magnetic behaviour of these groups of salts shows a very large number of cases in which the effective magnetic moment is abnormally low and quite often zero. This is, in fact, observed even in such ions as Ru^{+3} Os^{+3} Ir^{+4} (Selwood, 1943) which are in the S-state and hence on which the crystalline field should ordinarily have little direct influence. Thus, a low value of effective moment in the first half of the transition group should rather be ascribed to such covalent bond formation rather than to free ion behaviour as might appear at first sight. Intermediate cases must also be sometimes met with, *i.e.*, compounds in which the covalent bond field may not be so high as to split altogether the l's and s's but still high enough leading only to a splitting of L and S, since L-S coupling is strong comparatively to the iron group. Such a case is exactly analogous to the ordinary ionic salts of the iron group. It is *presumably* this state of affairs which we come across in tungsten sulphide. The experimental investigations undertaken by us over a wide range of temperatures indeed points to such a conclusion. From the table of data (Table II) for the effective magnetic moment of the W^{+4} ion we see that the mean magnetic moment of the crystal varies only moderately and at room temperature the value is 3.732 Bohr magnetons, which is widely different from the "free" ion value of 1·63, and even greater than the "spin only" value of 2·83. This evidently signifies that the spin orbit coupling is not so high as to remain unaffected by the crystalline field nor is the latter so high as to produce a complete breakdown of the L-S coupling. On the other hand, moderately large orbital contributions acting in the same direction as the spin contribution comes, giving a value in excess of the "spin only" value. The deviation from Curie law of temperature variation of the effective magnetic moment is also moderately large and complicated as will be seen from the Table II. Finally, the crystal is found to have a large anisotropy of the order of about 24%. These two latter facts also rule out not only a "free ion" hypothesis but also a complete breakdown of Russel-Saunders coupling for W^{+4} ion in tungstenite. The explanation of the afore-mentioned behaviour hence, must be that in spite of the generally wide multiplet separation in the group the covalent co-ordination of the W^{+4} ion with the sulphur atoms are such as to break down partially the L-S coupling of the $5d$ electrons and lead to a crystalline Stark splitting of the same nature as in the case of the ionic salts of the iron group.

THE STARK PATTERN OF THE GROUND STATE OF THE W^{++} ION AND THE EFFECTIVE MAGNETIC MOMENT

From what we have said before regarding the different spectroscopic states of the ions it will be seen that W^{++} ion, in common with Ti^{++} and V^{+++} belonging to the iron group of elements, has a ground state $^3F_2$.

In our earlier discussion about the nature of the crystalline field in WS_2 crystal we noted that the central tungsten ion is at the centre of an equilateral triangular prism the six corners of which are occupied by six sulphur atoms. This as is evident would give us a trigonal electric field with its axis of symmetry coinciding with the hexagonal axis of the crystal. Van Vleck (1939) and Siegert (1936) have shown that in titanium and vanadium alums, in both of which the paramagnetic ions are *trivalent*, the crystal field which has to be chosen from X-ray data on the crystals is of a trigonal character superposed on a predominant cubic field. Under such a trigonal field the Stark splitting of the degenerate cubic components in Ti^{+++} is given as in Fig. 3*a*, *i.e.*, a doublet of which

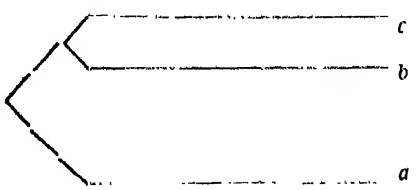

Fig. 3a

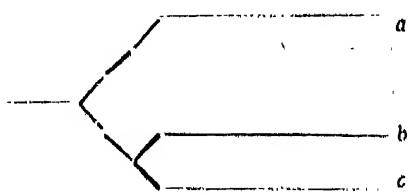

Fig. 3b

the lower component is orbitally nondegenerate but the upper level retains its orbital degeneracy in spite of the trigonal field. It is further shown by Van Vleck (1939) that except under certain special circumstances the pattern suffers an inversion as we pass from one electron Ti^{+++} to two electron V^{+++} *i.e.*, the degenerate state comes lowest for V^{+++} (see Fig. 3*b*). It is evident that in the case of W^{++} also, in WS_2 crystal, since it has the same electron configuration as V^{+++} we can take a similar Stark-splitting of the ground state under the existing trigonal field, with an inversion of the pattern as in V^{+++}. The trigonal separation postulated by Van Vleck (1939) is of the order of a few hundred cm^{-1} and we can in our case assume a separation of the same order from our previous arguments. Magnetic moment in this case will not only depend on the degenerate level *bc* but also upon the level *a*, since the separation between $bc \rightarrow a$ is ordinarily comparable to kT. The orbital contribution should therefore, be fairly large as has been actually found by us experimentally. The distribution of population amongst the various split levels will evidently depend upon temperature and in consequence we should expect complicated variation of the magnetic moment with temperature.

Actually, from the Table II, we see that along the hexagonal axis of the crystal the value of the effective magnetic moment at 84°K is 2.45 Bohr magnetons and gradually increases to a maximum of about 3.431 near about

330°K and decreases again and there is a tendency of its attaining an approximately constant value of 2.82 near about the highest observed temperature of about 700°K. A very similar temperature variation is observed also along directions in the hexagonal plane of the crystal, the value rising from 3.651 at 84°K to a maximum of 3.880 at about 300°K decreasing after this and tending to attain nearly a constant value of 3.100 at about 700°K. The temperature variation of the moment will, to a first approximation, be due to two parts, one obeying a Curie law due to the lowest degenerate doublet level in the Stark pattern, the other due to a change in the relative population of the two levels of the trigonal Stark pattern separated by a few hundred cm^{-1} and will thus give an effective moment first increasing with temperature then decreasing and finally having a tendency of becoming constant.* A simple calculation will show that the assumed order of separation of the trigonal components will actually lead to a maximum in the effective magnetic moment curve in the region of room temperature but afterwards when the contribution from the lower level diminishes more rapidly with temperature the value of the effective moment will decrease and then become constant again as the separation becomes small compared to kT at sufficiently high temperatures. It is also obvious that since the orbital contribution comes chiefly from the lower degenerate component, as this level becomes depopulated at high temperatures the constant value which the effective moments tend to attain should be more or less the 'spin only' value 2·83. This is also verified.

LARGE ANISOTROPY OF THE WS_2 CRYSTAL

As the main orbital contribution to the effective magnetic moment in a particular direction in the crystal depends inversely on the frequency corresponding to the separations between the levels $bc \rightarrow a$, the contribution to the effective moment will be confined mainly to one direction namely the hexagonal axis of the crystal which coincides with the trigonal axis of the field. Further, the absolute value of the effective spin moment being small the ratio of the orbital to spin contribution is large. Thus the anisotropy of the crystal will be very high. It will be interesting to note that actually the value of $\mu_\parallel$ is smaller than $\mu_\perp$ which is readily understood when we remember that W^{+4} belongs to the first half of the group in which the orbital contribution acts against the spin. Again it is in this very direction that the temperature variation of the moment is the larger. Lastly the high frequency contributions are not at all negligible as will be evident from the deviation from spin only value even at high temperatures in the direction of $\mu_\perp$, where low frequency orbital contribution is not of much importance.

It may be mentioned finally that since the W^{+4} ion is surrounded by six sulphur ions and W—W distance fairly large namely 3.18 Å, the exchange

* It should be remembered that the contribution to the moments from "high frequency" terms is directly proportional to the temperature and will somewhat modify the above variations according to its magnitude.

interaction between the W^{+4} ions may not be of very great importance at least within the temperature range employed by us. A preliminary investigation on the WS_2 crystal at varying field strength failed to show any field dependence of the effective moment at ordinary temperatures and hence the exchange or magnetic dipole interactions may be for the present purpose excluded.

ACKNOWLEDGMENTS

In conclusion the authors wish to express their best thanks to Prof. K. Banerjee, D.Sc., F.N.I. for kind interest in the work, to Dr. A. Bose, D.Sc. for helpful discussions and to Mr. B. Basak, M.Sc. for verifying the structure of the crystal.

INDIAN ASSOCIATION FOR THE
CULTIVATION OF SCIENCE,
CALCUTTA

REFERENCES

Bose, A., 1947, *Ind. Jour. Phys.*, **21**, 275.
Bose, A., 1948, *Ind. Jour. Phys.*, **22**, 195, 276 and 483.
Bose, D. M., 1927, *Zeits. f. Phys.*, **43**, 864.
Dutta, A K., 1944, *Ind. Jour. Phys.*, **18**, 249.
1945, ,, ,, ,, **19**, 225.
Ganguli, N., 1936, *Phil. Mag.* **21**, 355.
,, ,, and Krishnan, K.S., 1941, *Proc. Roy. Soc.* **177**, 168.
Gudden, B., 1934, Ergeb. d. Exakt. Naturwiss., 223.
Krishnan, K. S. and Banerjee, S., 1935, *Phil. Trans.*, A, **234**, 265.
Laporte, O., 1928, *Zeits. f. Physik.*, **47**, 761.
Penny, W. G., and Schlapp, R., 1932, *Phys. Rev.* **41**, 194.
—— —— **42**, 666.
Selwood, P. W., 1943, "Magneto Chemistry", New York (Interscience Publication)
Siegert, A., 1936, Physica, **3**, 85.
Van Arkel, A. E., 1926, *Rec. d. trav. d. Pays-Bas.*, **45**, 437-444,
(Quoted in Struktur Bericht, 1943—1926, page 215).
Van Vleck, J. H., 1932, "The Theory of Electric & Magnetic Susceptibilities", Oxford.
Van Vleck, J. H., 1932, *Phys. Rev.*, **41**, 208.
Van Vleck, J. H. and Siegert, 1939, *Jour. Chem. Phys.* **7**, 61.
Wilson, A. H., 1931, *Proc. Roy. Soc.*, **A., 133**, 458.
,, ,, 1932, ,, ,, ,, **A., 134**, 277.
,, ,, 1939, Semi Conductors and Metals (Cambridge University Press).

'BOROSIL'

NEUTRAL LABORATORY GLASSWARE

Borosil Reagent Bottles 8. ozs, and 16. ozs. with dust proof stoppers, now available.

(Narrow mouth and wide mouth)

All sizes of Neutral bottles manufactured to client's requirements.

INDUSTRIAL & ENGINEERING APPARATUS COMPANY., LIMITED.

CHOTANI ESTATES, PROCTOR ROAD, GRANT ROAD,

B O M B A Y-7.

Branch Offices :

MADRAS.—23-24, Second Line Beach.

NEW DELHI.—Pahar Ganj Road, Krishna Market.
Near Delhi Cloth Mills Depot.

MASULIPATAM.—Kojjillipet.

DIELECTRIC CONSTANT OF SILICA

By S. K. KULKARNI JATKAR AND B. R. YATHIRAJA IYENGAR

(*Received for publication, Nov. 24, 1948*)

ABSTRACT. The dielectric constant of crystal quartz and fused silica plates are 4.54 and 3.2 respectively as determined by the plate method. The mixture method gives the dielectric constant of powdered quartz as 4.55.

The dipole moment of silica calculated by the new equation $(\epsilon - n^2)M/d = 4\pi N\mu^2/k(T-\theta)$ where θ, the critical temperature is 575°C. ($\alpha\beta$ quartz inversion temperature) is 1.0 D. Considering SiO_2 moment as a vector of two mutually tetrahedrally inclined Si–O bonds the moment (observed) of Si–O bond is 0.86 D. The true moment of a free Si–O bond is 0.86 × 2 (co-ordination number) = 1.72 D agreeing with the calculated value, $\rho \times d \times \frac{Z_{Si}}{Z_{Si}+Z_0} \times n$ where Z's are atomic numbers and $n = 1/3$. At low temperatures ($\theta = 0$) the observed Si–O moment is 0.43 D so that the true moment of the free Si–O bond is again 1.72 D (0.43 × 4, the co-ordination number).

INTRODUCTION

Considerable amount of work has been done on the dielectric constant of quartz. Still the data are not quite satisfactory. Various observers have reported values which differ considerably from one another. The results of the previous investigators are summarised as follows in Table I.

TABLE I

Method	ϵ		Authors
	Field ∥ (optically active)	Field ⊥ (piezo-electric)	
	4.49	4.55	Curie (1889)
Plate condenser	4.60	...	Richardson (1915)
	...	4.65	Rubens (1915)
	...	4.58	Jaeger (1917)
Liquid replacement ...	4.46	4.38	Ferry (1897)
	4.73	4.73	Starke (1897)
	4.34	4.60	Schmidt (1904)
Measurement of forces on a fragment.	5.06	4.70	Fellinger (1902)
	4.55	4.60	Thornton (1909)

TABLE I (*contd.*)

VITREOUS SILICA

Method	ϵ	Author
Plate condenser	3.72	Jaeger (1917)
Liquid replacement	3.20	Schulze (1914)
Measurement of forces on a fragment ...	3.78	Thornton (1909)

The present work has been undertaken not only with a view to confirming the rather old and inconsistent data on the dielectric constant of quartz but also with the idea of investigating the dipole moment of the Si-O bond in silica. Three types of plates (1) optically active (2) piezo-electric and (3) vitreous silica were used. Obviously the applied field was parallel and perpendicular to the optical axis for (1) and (2) respectively.

The fact that the dielectric constants of ionic solids like silica are higher than the squares of their refractive indices implies that in addition to an electronic polarisation, an orientative effect also comes into play. The new relationship between dielectric constant and dipole moment : $(\epsilon - n^2)\frac{M}{d} = \frac{4\pi N\mu^2}{kT}$ (Jatkar *et al* (1946) which has been successfully applied to the case of a large number of liquids (normal and associated) and plastics can be used to interpret quantitatively the dielectric constants of solids in terms of the dipole moment of the constituent molecules. The equation is based on the concept of hindered orientation (along and opposite field direction) in quasi-crystalline liquids and solids. In the latter case the mechanism of orientation may involve either a complete turn over of the molecule as in the case of molecules of spherical contour (*e.g.*, hydrogen halides) or a mere "rattling of ions" in the crystalline structure (*cf.* symposium on "Dielectrics" Trans. Farad. Soc. 1946). Both cases conform to idea of orientations being confined to the direction of the field and opposite. In the case of ionic solids this may happen by a tunnel effect.

In the case of the ferro-electric class of solids, which show an electric Curie point, the new equation becomes $(\epsilon - n^2)M/d = 4\pi N\mu^2/k(T-\theta)$. It has been found that θ = m.p. for associated liquids and transition point (λ) for crystalline solids. It will be shown elsewhere that this equation has successfully accounted for the high dielectric constants and the temperature coefficient of TiO_2, titanates, rochelle salt, etc., in terms of the dipole moments of the molecules indicating thereby that there exists some form of dipole orientation in solids. The co-ordination number diminishes the moment below transition point. In the present paper the dielectric constant of silica has been interpreted on the above basis.

EXPERIMENTAL

Dielectric Constant of Silica by the Plate Condenser method

The apparatus used and the experimental technique is similar to that described by Jatkar and Nagamani, (1942). Measurements were conducted on a number of quartz plates, piezo electric, optically active as well as vitreous silica. Some of the specimens used were silvered on the surface so as to ensure good contact with the applied electrodes while even in the rest of the cases good contact was ensured in as much as the quartz surface as well as the surface of the electrode were optically plane. Special care was taken to see in the later case that the entire area of the electrode rested on the surface of the quartz. In all the measurements a correction was applied to account for the stray capacity of the leads connecting the electrode to the circuit and also for the capacity of the switch establishing the connection with the H. T. It was possible to obtain a value for these corrections by the following method. After measuring the capacity of the silica condenser, the specimen as well as the electrode were removed. Then two readings of capacity were taken, one with the switch on and also with a wire similar and equivalent in dimensions to the lead wire connected on to the switch and the second reading with the switch off. The difference between the readings gives the correction for the switch plus the leads.

If c is the observed capacity of the specimen condenser in $\mu.\mu$.f then the dielectric constant is given by $\epsilon = \frac{4\pi d(C-a)}{A \times 1.1}$ where a is the stray capacity, d = thickness of plate, and A = its area.

The thickness of the plates was accurately measured by a sensitive spherometer while a screw guage was employed for measuring the other larger dimensions.

The results are tabulated in Table II.

The mean value for optically active quartz plate (field $\parallel$) is 4.58 while that for piezo electric quartz plate (field $\perp$) is 4.50. This compares very well with the most probable values of 4.6 and 4.5 for the respective specimens as given by Sosman (1927) in a survey of dielectric properties of silica.

The dielectric constants of the two specimens of vitreous silica studied are found to be 3.21 and 3.32 respectively. This is in accordance with the value of 3-2 given by Schulze while Thornton (1909) and Jaeger (1917) give higher values of 3.78 and 3.72.

RESULTS

TABLE II

Piezo-electric quartz

(Field $\perp$)

$f^{*}_{k.c.s.}$	25	45 200	50	125 560	300	500	800
ϵ	4.44	(4.27)	4.56	4.52	4.53	4.61	4.42 ϵ_{lit} : 4.5

Optically active quartz

(Field $\parallel$)

Specimen No.	1	2	3	4
ϵ	4.70	4.45	4.53	4.62 ϵ_{lit} : 4.6

Fused quartz.

Specimen No.	1	2	
ϵ	3.24	3.31	ϵ_{lit} : 3.2, 3.8

* natural frequency of vibration

ϵ_{lit} (Sosman (1927))

DIELECTRIC CONSTANT OF POWDERED SILICA USING THE MIXTURE METHOD

The method consists in finding by graphical methods the dielectric constant of that liquid mixture whose dielectric constant remains unchanged when powdered silica is introduced into it.

The powdered silica used in these experiments was purified by repeated washings with warm dilute hydrochloric acid, followed by washing with water and dried in an oven and finally stored dry before being used in experiments. Thoroughly purified nitrobenzene and xylene were used as the components for the liquid mixture in the experiments.

After preliminary trials a series of mixtures was prepared of such compositions as to possess dielectric constants whose range was in the neighbourhood of the approximately known value of the dielectric constant of silica.

The dielectric constant of each of these mixtures was at first determined as such and then again after the addition of the powdered silica.

Special care was taken to see that the condenser was filled up to a particular level each time and further it was seen that the excess of liquid above this mark which would come up when the powdered solid was put in was removed and the level adjusted to the original mark.
The results are given in Table III.

TABLE III

Composition of liquid mixture.	Dielectric constant of liquid mixture	Dielectric constant of liquid mixture with powdered silica.
8.3% nitrobenzene 91.7% xylene	3.50	4.16
10.1% nitrobenzene 89.9% xylene	3.75	4.25
12.3% nitrobenzene 87.7% xylene	4.05	4.36
16.6% nitrobenzene 83.4% xylene	4.65	4.59
20.5% nitrobenzene 79.5% xylene	5.18	4.79

The differences between the dielectric constant with and without the powdered silica were plotted against dielectric constant of liquid mixtures. The value corresponding to zero difference gives the dielectric constant of the suspended silica. This was found to be 4.55.

DIELECTRIC CONSTANT OF SILICA AT A HIGHER TEMPERATURE

A mixture of xylene and nitrobenzene of a slightly higher dielectric constant than that of silica was prepared. The temperature coefficient of the dielectric constant of this liquid mixture with and without the solid was determined and the two corresponding curves were plotted. The curves meet at 65°C corresponding to a value of 4.60 for the dielectric constant of the mixture. Hence 4.60 is the value of the dielectric constant of the powdered quartz at 65°C.

Liquid mixture used 18.74% nitrobenzene; 81.26% xylene.

TABLE IV

Temperature °C	ϵ of liquid mixture.	ϵ of liquid mixture with powdered quartz.
20	5·18	4·79
30	5·04	4·74
40	4·90	4·69
60	4·62	4·59
70	4·48	4·48 (80°)

Results of the mixture method :—

TABLE V

t°C	ϵ
20	4·55
65	4·57

Thus the dielectric constant is practically the same over a range of 45°. It is interesting in this connection to recall the experiments of Gagnebin on the effect of temperature on the dielectric constant of optically active as well as piezo-electric quartz pieces. He reports a nearly constant value for the former from 0 to 200° and for the latter from 0 to 500°.

ELECTRIC MOMENT OF SILICA AT ORDINARY TEMPERATURES

Using the values of dielectric constants 4·55 and 3·25 for crystal quartz and vitreous quartz plates respectively the electric moments were determined by using a new relationship

$$(\epsilon-1)\frac{M}{d}-(n^2-1)\frac{M}{d}=4\pi N\mu^2/kT$$ [Jatkar, Iyengar and Sathe (1946)],

with the usual notations. The moments for vitreous silica and crystal quartz so calculated come out as 0.48D and 0.58 D respectively.

ELECTRIC MOMENT OF SILICA AT HIGHER TEMPERATURES

It is well known that quartz has an inversion point at 573°C when the α to β transition occurs. The inversion point is marked by abrupt changes in the temperature dependence of the various physical properties of quartz, *e.g.*, heat capacity, specific volume, axial ratio, Young's modulus, refractive

index, rotatory power, etc. In interpreting the dielectric constant of quartz this transition temperature has to be taken into account. Accordingly moments have been calculated by the modified new equation

$$(\epsilon - n^2)\frac{M}{d} = \frac{4\pi N\mu^2}{k(T-\theta)} \qquad (1)$$

where θ = transition temperature = 575°C ($\alpha \rightarrow \beta$ quartz inversion temperature). The results are tabulated (Table VI).

TABLE VI

Piezo-electric quartz (Field ⊥)		$P_E = 32.2$ $\theta = 575°C.$		Optically active quartz (Field ‖)			
t°C	ϵ*	P_0	μ	t°C	ϵ*	P_0	μ
623	8.50	145.6	0.35	591	12.00	228.8	0.26
676	9.65	172.6	0.56	639	12.11	231.2	0.52
804	11.75	222.2	0.96	748	12.15	231.8	0.85

* Gagnebin (1924)

The moments which initially increase with temperature show a definite trend towards attaining a constant value at a higher temperature. The initially lower values are due to the fact that at lower temperatures the dielectric constant has not yet reached the static value but is still in the dispersion region. At higher temperatures the dielectric constants at the measured frequencies approach the static values. It can be seen by extrapolation that at higher temperature the moment tends to attain the constant value of 1.00D In the low temperature region (25°C) the moment is 0.48 (calculated by equation (1) putting $\theta = 0$).

The three main forms of silica, namely, quartz, tridimite and crystabolite are all built up of SiO_4 tetrahedra (*i.e.*, O\Si/O angle = 109°28′). The Si−O distance in some silicates has been observed as 1.60Å [Wells (1945)] The ionic character of the Si−O bond has been given as 50 per cent by Pauling (1944) and 37 per cent by Hannay and Smyth (1946). Recently Jatkar and

TABLE VII

—	C.N	n	$i = \frac{Z_A}{(Z_A + Z_B)^n}$	$\mu_{(Si-O)}$ Calc $\left(= \frac{e \times d \times i}{C\,N}\right)$	$\mu_{(Si-O)}$ obs $\left(= \frac{\mu_{SiO_2}}{1.16}\right)$
$T > \theta (= 573°C)$ ...	2	1/3	0.21	0.81	0.86
$T = 25°C (\theta = 0°K)$...	4	1/3	0.21	0.41	0.43

Gopalaswamy (1948) have found that the ionic character "i" of a bond is related to the atomic numbers Z_A and Z_B of the constituents of the bond by the relation $i = \frac{Z_A}{Z_A + Z_B} n$ where n is a fraction or an integer. Table VII gives the calculated and observed moments of Si—O bond.

The first column gives the co-ordination number. It appears that above the transition ($T > \theta$) the co-ordination number is only two while below ($T < \theta$) it is four. Thus the $\alpha \rightarrow \beta$ inversion has the effect of apparently halving the co-ordination. In fact it has been found that the structure of the α and β form of silica differ from each other only in detail and might involve a mere relative rotation of SiO_4 tetrahedra (Wells (1945). The latter fact could be the cause of a change in the co-ordination number of the Si—O bond at the $\alpha \rightarrow \beta$ inversion. The last column in the tables gives the moment of Si—O bond which is $\frac{\mu_{SiO_2}(obs)}{1.16}$ since $^{\mu}SiO_2$(obs), the vector of two Si—O bond moments mutually inclined at a tetrahedral angle is 1.16 times the moment of each Si - O bond. In the absence of co-ordination it is seen that the true moment of the Si—O bond $= 0.4 \times 4 = 1.6$.D. It can be predicted that the observed Si—O moment will reach this value at higher temperatures where a Curie point of dielectric constant ought to be realized.

Department of Pure and Applied Chemistry,
Indian Institute of Science, Bangalore.

REFERENCES

Curie, J. (1889) *Ann. Chem. et. Phys.*, (6) **17**, 385.
Fellinger, R. (1902), *Ann. d. Phys.*, (4), **7**, 333.
Ferry, R. S. (1897), *Phil. Mag.*, (5) **44**, 404.
Gagnebin, S. (1924), *Arch. Sci. Phys. Nat.*, (5) **6**, 161.
Hanny, N. B. and Smyth C. P. (1946), *J. Amer. Chem. Soc*, **68**, 171.
Jaeger, (1917), *Diss. Berlin.*
Jatkar, S. K. K. and Gopalaswamy S. N. (1948), *Proc. 35th Ind. Sci. Cong.*
Jatkar, S. K. K., Iyengar B. R. Y, and Sathe N. V. (1946) J. *Ind. Inst. Sci*, **28A**, 1.
Jatkar, S. K. K. and Nagamani S. R. (1942), *J. Ind. Inst. Sci.* **24A**, 65.
Pauling, L. (1944) "The Nature of the Chemical bond" II Edn., p. 71.
Richardson, S. W. (1915), *Proc. Roy. Soc. Lond.*, **92A**, 41.
Rubens H. (1915) *Ber. Berl. Acad.*, **2**, 4.
Schmidt. W. (1902), *Ann. d. Phys.*, (4) **9**, 919.
Schulze, F. A. (1904), *Ann. d. Phys.*, (4), **14**, 384.
Sosman, R. B. (1927), *A. C. S. Mon.*, **37**, 515.
Starke, H. (1897), *Ann. d. Phys, U. Chem.*, **60**, 629.
Thornton, W. M. (1909), *Proc. Roy. Soc. Lond.*, **82A**, 422.
Wells, A. F. (1945), "Structural Inorganic Chemistry," p. 464.

FEEBLE PARAMAGNETISM OF CHROMIUM TRIOXIDE AND POTASSIUM CHROMATE

By D. S. DATAR and S. S. DATAR

(*Received for publication, Nov. 3, 1948*)

ABSTRACT. It has been shown that the partial freedom of the electronic spin due to imperfect pairing accounts for the paramagnetism exhibited by hexavalent chromium ions in ^1S state. The imperfect pairing is due to the partially covalent bonding of electrons between chromium and oxygen in chromium trioxide and chromate radical. The factor for the unpaired spin was calculated using diagrams constructed on the basis of the known X-ray data and ionic radii assuming spherical charge distribution for electron. The factor in both the cases works out to be about 6%. The values for the paramagnetic susceptibility of CrO_3, K_2CrO_4 and Na_2CrO_4 calculated using this factor show remarkable agreement with the values obtained from the experimentally observed specific susceptibility for the above compounds.

INTRODUCTION

Feeble paramagnetism [Weiss & Collet (1924), Collet and Janet (1925), Weiss (1926), Ladenburg (1927), Freed and Kasper (1930) and Grey and Drakers (1931)] is exhibited by certain ions in ^1S state for example Sc^{+3}, Ti^{+4}, Ce^{+4}, V^{+5}, Cr^{+6}, and W^{+6}. As the spin quantum number in this case is zero, Van Vleck (1932) suggested that the paramagnetism is due to the contribution of the high frequency elements of the orbital moment, the material being diamagnetic or paramagnetic depending on whether the first term or the second term in the following equation is the greater :

$$\chi_{mol} = \frac{Ne^2}{6mc^2} \sum r^2 + \frac{2}{3} N \sum_{n' \neq n} \frac{|M^0(n'; n)^2|}{h\nu(n'; n)}$$

The calculation (Frank and Van Vleck, 1929) of the two parts of the above equation has been, however, attempted only for the hydrogen molecule, where the second term is only a little over 10% of the first. This result indicates that the orbital paramagnetism in general has a very low value and may not form a basis for satisfactorily explaining feeble paramagnetic effect. An attempt (Datar & Datar, 1946) has, therefore, been made in this paper to suggest the source for the paramagnetism shown by the ions in ^1S state. Hexavalent chromium compounds have been selected for this study as accurate X-ray diagrams [Brükken (1931), Zachariasen and Ziegler (1931)] and magnetic data (Grey and Drakers, 1931) for these compounds are available.

Feeble paramagnetism of chromium trioxide

In chromium trioxide, Cr^{+6} structure is attained when all the six electrons in the $3d$ and $4s$ shells of chromium are removed. The very simple electronic arrangement for chromium trioxide is obtained by transferring the electrons two each to three oxygen atoms as in structure I, the direction

of the arrows indicating the position of the six electrons

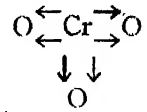

... I

In the crystalline state (Bräkken, 1931), the elementary cell of chromium trioxide consists of four molecules and the metal atoms are surrounded by six oxygen atoms. These considerations led Datar and Jatkar (1939) to suggest a structure for chromium trioxide, which can be graphically shown as below :

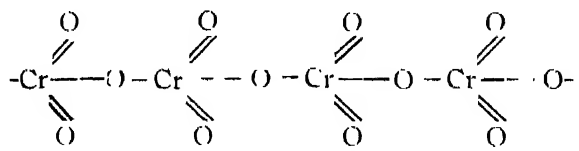

The electronic arrangement for such a structure of chromium trioxide will be as shown in structure II.

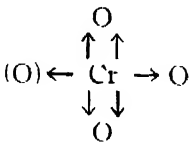

... II

It is further possible that in the crystalline CrO_3 there exists a resonance between the structure II and the stable structure I. During this change the electronic configuration similar to the structure III shown below may occur at the intermediate stage

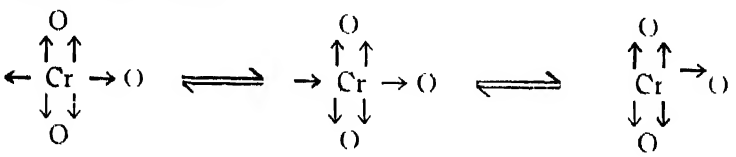

II III I

In the electronic structures I and II all the electrons in chromium are paired and consequently the contribution of chromium towards paramagnetism is zero. In the structure II, however, the electron in chromium is unpaired and it will show paramagnetism. The electrons in oxygen are paired.

Evidently the unpaired state of the electron can be calculated with the help of a diagram obtained by tracing the path of the electron thus resonating between the two oxygen atoms through chromium and finding out the ratio of the orbital path of the electron in chromium to the total path. The structure diagrams have been constructed on the basis of the X-ray data and ionic radii assuming that the electronic charge distribution is spherical. The values for ionic radii (Rice, 1940) are taken for drawing this diagram as $Cr^{+6}=0.81$Å and $O^{-2}=1.76$Å and the distance (Bräkken, 1931) between chromium and oxygen atoms is 2.07Å, the oxygen atoms being octahedrally arranged. The time factor for which the electron is associating with chromium atom gives the unpaired state. The determination of this factor is shown in Fig. 1

Determination of the unpaired spin in chromium trioxide

Let (o_1, r_1) be chromium sphere and (o_2, r_2), (o_3, r_3) oxygen spheres. $r_1 = 0.81$; $r_2 = r_3 = 1.76$, $o_1o_2 = o_1o_3 = 2.07$; o_1, o_2 and o_3 lie in a st. line.

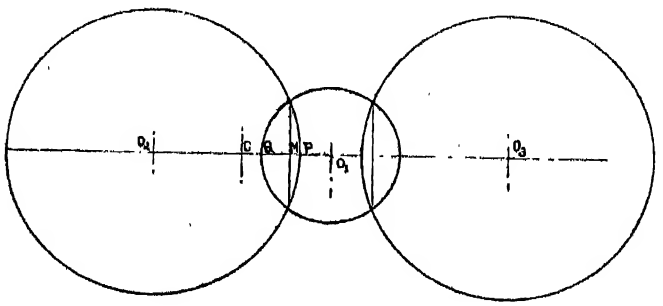

FIG. 1

The area of the spheres is calculated from the formula $4\pi r^2$. The area of the oxygen sphere is 38.92 and the area of the chromium sphere is 8.245.

When the spheres chromium (o_1, r_1) and oxygen (o_2, r_2) intersect, let the plane of common section meet o_1o_2 in M, C the mid-point of o_1o_2 and o_1o_2 meet oxygen in P and chromium in Q. Then $CM = \frac{}{2o_1o_2} = 0.5896$

$\therefore$ $MP = 0.135$ and $MQ = 0.365$.

The area of the spherical cap on the oxygen path due to the intersection of chromium is $2\pi r_2$. $MP = 1.51$.

The area of the spherical cap on the chromium path due to the intersection of oxygen is $2\pi r_1$. $MQ = 1.858$.

The area available on chromium path $= 8.245 - 2\,(1.858) = 4.529$.

The area available on each of the oxygen path $= 38.92 - 1.51 = 37.41$.

Total area available $= 4.529 + 2(37.41) = 79.349$.

$$\frac{\text{Area available on chromium path}}{\text{Total area available}} = \frac{4.529}{79.349}$$

Unpaired spin $= 0.0571$

Using the equation (Van Vleck, 1932) $\chi = \frac{NB^2}{3kT}(4S(S+1))$

for calculating paramagnetism from the number of spin electrons, where N (Avogadros' number) $= 6.064 \times 10^{23}$ per mol ; B (Bohr magneton) $= 0.9174 \times 10^{-20}$ erg per gauss : k (Boltzmann constant) $= 1.371 \times 10^{-16}$ erg/degree ; T (Absolute temperature corresponding to 25°C) $= 298$ and S (Spin quantum number) $= \frac{1}{2}$ for one electron, we get $\chi = 1249.8 \times 10^{-6}$ for one unpaired electron. But as paramgnetism in case of chromium trioxide is contributed by 0.0571 and the remaining fraction does not exhibit any paramagnetic properties, the total paramagnetism per gm. mol of CrO_3 should be 5.71% of the paramagnetic value for one electron *i.e.*, 71.32×10^{-6}.

It will be seen that this value agrees with the value for the paramagnetic susceptibility calculated from the experimentally observed specific susceptibility for chromium trioxide using the formula

$$\text{Sp. susceptibility} = \frac{\text{Paramagnetic susceptibility} + \text{Ionic dimagnetism of constituent ions}}{\text{Mol. wt.}}$$

The values given by Augus (1932) have been employed in this paper for the correction of ionic diamagnetism *viz* : $Cr^{+6} = -5.15 \times 10^{-6}$, $Na^{+1} = -3.74 \times 10^{-6}$, $K^{+1} = -13.06 \times 10^{-6}$ and $O^{-2} = -11.25 \times 10^{-6}$. Grey and Drakers (1931) have experimentally obtained 0.41×10^{-6} for the sp. magnetic susceptibility for chromium trioxide. From the above formula

$0.41 \times 10^{-6} \times$ mol. wt. = molecular paramgnetic susceptibility + ionic diamagnetism ;

therefore molecular paramgnetic susceptibility

$$= 0.41 \times 10^{-6} \times 104 + 10^{-6}(5.15 + 3 \times 11.25) = 10^{-6}(42.84 + 38.90) = 81.74 \times 10^{-6}$$

It is surprising that in spite of the smallness of the magnetic effect and uncertain estimate of diamagnetism and other factors the results show a concordance.

It will be of interest to note here that in the structures given to CrO_3, the bond formation is due to the transfer of electrons from chromium to oxygen *i.e.*, ionic and partly due to sharing of electrons *i.e.*, covalent. It is obvious that the bonding in CrO_3 is mainly ionic and contains covalent bond formation (*cf* Brökken, 1931) to the extent of 5.71%

Feeble paramagnetism of potassium chromate

The partial freedom of the spin due to imperfect pairing accounts for the fractional paramagnetic effect exhibited by Cr^{+6} in chromium trioxide. It will be presently shown that the above considerations are applicable in case of potassium chromate, which also shows feeble paramagnetism [Grey and Drakers (1931)].

The structural formula of K_2CrO_4 is

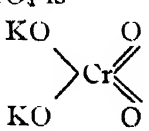

As in case of chromium trioxide, the possible resonating structures are :

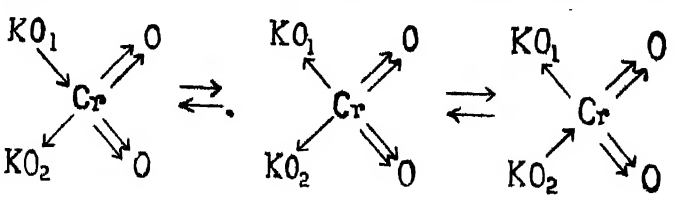

II I III

It will be seen that the electronic spin in structure I is paired. In structure II the spin of the electron returning from O_1 to Cr is unpaired so long as it

remains in the orbit of Cr. So also in case of the structure III, the spin of the electron returning from O_2 to Cr is unpaired. The return of the electron from oxygen to chromium leaves another electron in oxygen in the

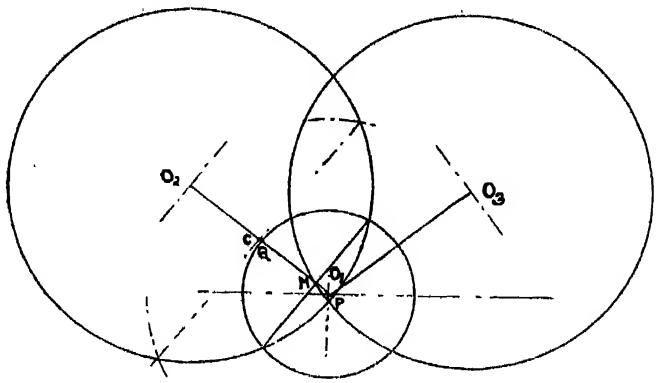

FIG. 2

unpaired spin state. The total unpaired spin will be equal to the unpaired state in chromium. The spin effects in O_1 and O_2 are equal and neutralise each other. The unpaired state is determined as shown in Fig. 2.

Determination of the unpaired spin in potassium chromate

The structure of K_2CrO_4 has been studied by Zachariason and Zeigler (1931) by X-ray measurements. According to them, 4 oxygen atoms surrounding each chromium atom from a nearly regular tetrahedron with chromium in the centre. The Cr-O distance is 1.60.

Let (o_1, r_1) be chromium sphere, (o_2, r_2), (o_3, r_3) oxygen spheres.

$r_1=0.81$; $r_2=r_3=1.76$; $o_1o_2=o_1o_3=1.6$ o_1 is at the centre of the regular tetrahedon whose one edge is o_2o_3.

So $\widehat{o_2o_1o_3}$ will be $\cos^{-1}(-1/3)$ or $109°28'$. From this $o_2o_3=2.612$.

The area of the oxygen spheres is 38.92 and the area of the chromium sphere is 8.245.

To find the area of the uncut portion of any of the spheres the sum of the areas of the two spherical caps is subtracted from the area of the sphere to which area common to the spherical caps is added.

When chromium (o_1, r_1) and oxygen (o_2, r_2) spheres intersect one another, let the plane of common section meet o_1o_2 in M, C be the mid point of o_1o_2 and o_1o_2 meet oxygen path in P and chromium path in Q. Then

$CM=\dfrac{r_2^2-r_1^2}{2\,o_1o_2}=0.763$. From this $MP=0.20$ and $MQ=0.77$.

The area of the spherical cap on the oxygen path due to the intersection of chromium path is $2\pi r_2.MP=2.212$.

The area of the spherical cap on the chromium path due to the intersection of oxygen path is $2\pi r_1.MQ=3.917$.

If o_2o_3 intersects the two oxygen spheres in R_1 and R_2, D be the mid point of o_2o_3 (the plane of common section of two oxygen spheres pass through D), then $R_1D=.454$ and the area of the spherical cap on the oxygen path due to intersection of oxygen sphere is $2\pi r_2$. $R_1D=4.975$.

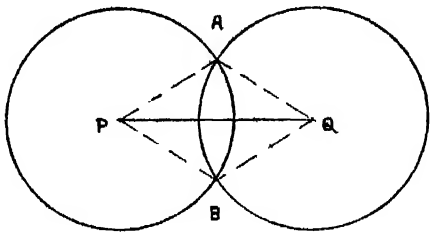

FIG. 3

Next we find the area on the chromium sphere common to both the spherical caps due to oxygen spheres. Let A, B be the points where three spheres intersect, and o_1o_2, o_1o_3 meet chromium sphere in P and Q. (Fig. 3)

PA, PB, QA, QB are arcs of great circles. The area of the portion common to both the spherical caps = Area APB + Area AQB − Area $APBQ$

$$\cos APQ = \frac{\cos AQ - \cos AP \cos PQ}{\sin AP \sin PQ}$$

But $PQ = \overset{\frown}{Po_1Q} = \overset{\frown}{o_2o_1o_3} = \cos^{-1}(-1/3) = 1.91$ radians. To find PA, through P, A, draw the great circle and let perpendicular from A upon diameter through P meet it in M (Fig. 4)

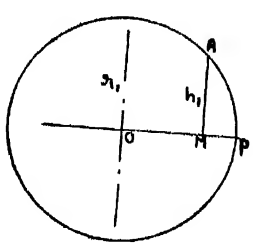

FIG. 4

$$\text{Arc } PA = \int_{r_1-h_1}^{r_1} \sqrt{1+\left(\frac{dy}{dx}\right)^2}\, dx$$

$$\text{but } \frac{dy}{dx} = \frac{-x}{y}$$

$$\text{Arc } PA = \int_{r_1-h_1}^{r_1} \sqrt{1+\frac{x^2}{y^2}}\, dx = \int_{r_1-h_1}^{r_1} \sqrt{\frac{r_1^2}{r_1^2-x^2}}\, dx = r_1 \left[\sin^{-1}\frac{x}{r_1} \right]_{r_1-h_1}^{r_1}$$

$$= r_1 \left[\pi/2 - \sin^{-1}\frac{r_1-h_1}{r_1} \right] = 1.52 \text{ radians}$$

$\cos APQ = 0.0716$ $\therefore$ $APQ = 1.499$ radians
by symmetry $AQP = 1.499$,,
Similarly arc $PAQ = 1.914$ radians

$$\text{Area } APQ = (\overset{\frown}{APQ} + \overset{\frown}{PQA} + \overset{\frown}{QAP} - \pi) r_1^2 = 1.162$$

$$\text{Area } APBQ = \text{Area } APB + \text{Area } AQB = 2.324$$

$$\text{Area } APB + \text{Area } AQB = 2 \times \frac{2.998}{2\pi} \times 3.917 = 3.740$$

The area of the portion common to both the caps = 1.416. The area of the uncut portion on chromium sphere = $8.245 - 2 \times 3.917 + 1.416 = 1.823$

On any one of the oxygen spheres area common to the spherical caps due to intersection of oxygen and chromium spheres is found to be 1.314.

Area of the uncut portion = $38.92 - 2.212 - 4.975 + 1.314 = 33.047$

Total portion available for the electron = $1.823 + 33.047 + 33.047 = 67.917$

$$\frac{\text{Area available on chromium path}}{\text{Total area available}} = \frac{1.823}{67.917} = .02682$$

The total unpaired state in potassium chromate molecule = 0.0536

Using this factor the paramagnetic susceptibility is calculated per gram molecule of potassium chromate which comes to 67.01×10^{-6}. Grey and Drakers (1931) have experimentally observed that the specific magnetic susceptibility of potassium chromate is zero. The paramagnetic susceptibility calculated from this value after correcting for diamagnetism comes out to be 76.27×10^{-6}. Thus the value for paramagnetism calculated from the observed specific magnetic susceptibility value is in agreement with that obtained using the unpaired spin factor.

It has been shown by Grey and Drakers (1931) that sodium chromate also shows feeble paramagnetism. The X-ray diagram of this compound is not known. If we assume that the structure of sodium chromate is similar to that of potassium chromate then the spin factor will also be the same. The molecular paramagnetic susceptibility calculated from the observed specific susceptibility for Na_2CrO_4 as given by Grey and Drakers (1931) viz., 0.120×10^{-6} is 77.55×10^{-6} which agrees with the paramagnetism shown by K_2CrO_4 and also with that calculated from the unpaired spin factor for chromate radical. The results heretofore obtained are summarised in the following Table :

	Sp susceptibility $\times 10^{-6}$	Unpaired spin.	Paramagnetic susceptibility calculated from	
			sp. susceptibility	unpaired spin
CrO_3	0.41	0.0571	81.74	71.32
K_2CrO_4	0	0.0536	76.27	67.01
Na_2CrO_4	0.120	0.0536	77.55	67.01

The unpaired spin for chromium trioxide is about 6%. The factor for the unpaired spin of the chromate radical is also nearly the same.

ACKNOWLEDGMENT

Thanks of the authors are due to Dr. S. K. K. Jatkar for suggesting the problem and for his keen interest and helpful suggestions during this research.

Central Laboratories For Scientific & Industrial Research, Hyderabad, Deccan
and
Department of Mathematics, Pratap College, Amalner

REFERENCES

Augus (1932), *Proc. Roy. Soc.*, **136**, 569.
Bräkken (1931), *Zeit. Krist.*, **78**, 484.
Collet and Janet (1925), *Comptes. Rendus.*, **181**, 1057.
Datar and Datar (1946), *Nature*, **158**, 518.
Datar and Jatkar (1939), *J. Ind. Inst. Sc*, **22A**, 287.
Frank (Miss) and Van Vleck (1929), *Proc. Nat. Acad*, **15**, 539
Freed and Kasper (1930), *J. Amer. Chem Soc.*, **52**, 4671.
Grey and Drakers (1931), *Phil Mag.* **7.X**, 297.
Ladenburg (1927), *Zeit. Phys. Chem*, **126**, 133.
Rice (1940), Electric Structure & Chem. binding, 220.
Van Vleck (1932), Electric & Magnetic susceptibilities, **275**, 286
Weiss (1926), *Comptes Rendus*, **182**, 105
Weiss and Collet (1924), *Comptes Rendus*, **178**, 2146.
Zachariasen and Ziegler (1931), *Zeit Krist.*, **80**, 164.

NEW BANDS OF THE ASUNDI BAND-SYSTEM OF CO

By SATYA NARAIN GARG

(*Received for publication, Aug. 4, 1948*)

ABSTRACT. A large number of bands has been recorded in an uncondensed discharge through a tube containing $SnBr_4$ at very low pressure and carbon as the usual impurity. Most of them are found to belong to the Asundi system ($a'^3\Sigma \rightarrow a^3\pi$) of CO. The following is the equation found to represent satisfactorily these bands as well as the already known ones of this system:

$$\nu = 6953.6 + (1208.6\ v' - 9.5\ v'^2) - (1726.5\ v'' - 14.4\ v''^2)$$

$$\text{or,}\quad \nu_r = 7213.8 + (1218.1\ u' - 9.5\ u'^2) - (1740.9\ u'' - 14.4\ u''^2)$$

where, $u = v + \frac{1}{2}$ and the v' numbering is that proposed by Gerö and Lorinczi. A few bands which cannot find suitable places in the system appear to be fragments of an unknown system.

INTRODUCTION

The spectrum of CO has been the subject of much investigation due, among other causes, to its occurrence in almost all discharge tubes where CO or CO_2 occurs as impurity. Presence of other substances has often introduced many peculiarities in the spectrum of CO. An interesting example of the effect of foreign gases is provided by Merton and Johnson's method of production and isolation of the triplet bands of CO. Thus, if in a tube, having carbon electrodes and helium under high pressure, and, showing the comet-tail bands of CO, a trace of hydrogen is introduced, the comet-tail system disappears and the triplet system takes its place. Again if in a tube, having argon under high pressure and carbon electrodes, and showing the Swan bands, a trace of hydrogen is introduced, the Swan bands disappear and the triplet bands take their place. Before the discovery and classification of the triplet bands by Merton and Johnson, some bands were known to be associated with Angstrom bands in the red and yellow regions. These bands and those discovered by Merton and Johnson were collectively called as triplet system, though no satisfactory classification was forthcoming. Later on, Asundi (1929) photographed the bands associated with Angstrom bands in the red and yellow regions, which were tentatively included previously in the triplet system. He had no helium or hydrogen in his tube, yet he obtained a few bands of Merton and Johnson, although very weak. He measured those bands in the visible and the photographic infra-red and came to the conclusion that a large majority of them could not go with the Triplet system. For such bands he gave an analysis and showed that their

upper state is the then newly discovered level at 58927 cm^{-1} (Hopfield and Birge, 1927) of CO, and the lower state coincides with the lower state of the third positive bands of CO. He represented these bands by the following equation :—

$$\nu = 10491 + (1154.4\ v' - 9.5\ v'^2) - (1721.5\ v'' - 13.7\ v''^2) \quad \ldots \quad (1)$$

These bands which were also previously observed by McLennan, Smith and Peters (1925) are known as Asundi bands.

Later work done so far on the Asundi bands is summarised below :—

(1) Estey (1930), on the basis of a private communication from Birge that the upper level ($a'^3\Sigma$) is at 57763 cm^{-1}, proposed an increment of one unit in the v' numbering given by Asundi.

(2) Schmid and Gerö (1937) estimated the ν-values for bands from $v'=8$ onwards (with a few exceptions) from perturbations of $a'^3\Sigma$ level by $b^3\Sigma$ level and by an extrapolation obtained the energy of dissociation of CO as 11.06 volts. They also reported some new bands which they interpreted as members of the Asundi system with high v' values.

(3) Gerö (1938) performed the rotational analysis of two of these bands—(30,1) and (34,0)—and found the structure to be analogous to that of the bands recorded by Asundi.

(4) Gerö and Lorinczi (1939) proposed an increase of three units in the v' numbering given by Asundi.

Observation of bands with high quantum numbers by Gerö and others suggested an attempt at extending the known bands with low quantum numbers. A tube with a bulb containing $MgCO_3$ (to serve as a source of CO_2) gave only further evidence of some bands between successive Angstrom bands. The faint traces obtained on the plates were unsuitable for measurements. Next, while preparing a tube for studying the emission from $SnBr_4$ vapour, however, it was observed that in the initial stages, when pressure of CO was sufficient and that of $SnBr_4$ vapour low, bands similar to the known Asundi bands were well developed. The present paper deals with these additional bands. Measurements and analysis indicate that a large number of these bands can be included in the Asundi system.

EXPERIMENTAL

The discharge tube employed was a Π type one, 30 cm. long and 1.2 cm. in diameter. It had aluminium electrodes, 20 cm. apart, and drying tubes containing KOH, NaOH and anhydrous $CaCl_2$ on both sides : one side leading to the pump and the other to a bulb containing $SnBr_4$. The solid $SnBr_4$ (since room temperature was below 31°C) was allowed to evaporate of its own accord under reduced pressure. The usual carbon impurity in the tube itself was sufficient to produce intense Angstrom bands. As the pressure of $SnBr_4$

vapour in the tube increased gradually (though still very low), the Angstrom bands slightly weakened and the new bands belonging to the Asundi system developed distinctly.

The tube was excited by an uncondensed discharge from a transformer giving about 7000 volts, fed by A.C. obtained from a 1/4 kilowatt rotary convertor working off the D.C. 220 volts mains.

For the resolving instrument a two-prism glass spectrograph, constructed in this laboratory by the author, having dispersion of 80Å/mm. at 6500Å, 31Å/mm. at 5070Å, 17Å/mm. at 4500Å, and 8Å/mm. at 3800Å was used. Exposures of about one to two hours were necessary for photographing the bands on Ilford HP3 plates.

Wavenumbers in vacuo of band-heads were obtained from Kayser's Schoringungs zahlen from the mean wavelengths in air from measurements of three independent plates. The ν values are expected to be correct to about ± 4 cm^{-1}.

ANALYSIS

The analysis of these bands presents the usual difficulties which are encountered in all such extended systems. A small change in vibrational functions used may not apparently make any appreciable difference in the representation of bands with low quantum numbers but it may produce large deviations for high quantum numbers. Hence the vibrational function of initial or final (or both) state given from an analysis of a few bands is liable to modifications if it is to represent a greater amount of data to a good degree of approximation.

From his analysis of the Asundi Bands observed by him, Asundi derived the following equation :—

$$\nu_h = 10491 + (1154.4\ v' - 9.5v'^2) - (1721.5\ v'' - 13.7\ v''^2) \qquad (1)$$

He observed : "Assuming a transition to exist between the new level at 58927 ν as the initial level and the final level at 48438 ν of the third positive carbon bands as the final level, it will give rise to bands whose heads can be represented by

$$\nu_h = 10489 + (1155\ v' - 9\ v'^2) - (1726.5\ v'' - 14.4\ v''^2) \quad \ldots \quad (2)$$

The equation representing the new bands is very close to this. There is a possibility of considerable error in the measurements of the bands of higher wave-lengths because the dispersion of the instrument falls rapidly in that region. Therefore the discrepancy between the two equations may be taken to be within the limits of experimental error."

The function $(1726.5\ v'' - 14.4\ v''^2)$ is well-established and reliable, being common also to third positive carbon bands, 5B bands, 3A bands, and the Cameron bands. Thus there are two ways open for us : (*a*) to use equation (2) as such ; (*b*) to use equation (2) with the first function $(1155\ v' - 9v'^2)$ modified to a desirable extent.

(*a*) Using equation (2) as such the observed-calculated values of wave numbers of bands observed by Asundi are given in Table I and of bands observed by the present author are given in Table II.

TABLE I

ν_{vac}	v'	v''	O-C cm^{-1}	ν_{vac}	v'	v''	O-C cm^{-1}
11636.0	1	0	+ 1.0	14693.2	7	2	−44.4
12158.5	3	1	− 2.4	14953.2	4	0	−11.3
12761.8	2	0	− 1.2	15348.5	6	1	−34.4
13237.0	4	1	−15.9	15702.0	8	2	−55.6
13668.4	6	2	−31.2	16011.0	5	0	−28.0
13861.5	3	0	− 8.5	16375.0	7	1	−45.9
14048.0	8	3	−55.1	17057.2	6	0	−37.8
14301.8	5	1	−25.1	17389.2	8	1	−51.7

TABLE II

No.	ν_{vac}	v'	v''	O-C cm^{-1}	No.	ν_{vac}	v'	v''	O-C cm^{-1}
1	15439.0 15467.2	11	4	37.8	9	17627.4 17666.7 17700.5 17726.5	10	2	−17.1
2	15510.9 15608.5	20	9	− 8.4	10	17780.1	19	7	−25.0
3	15975.6 16009.2	5	0	−29.8	11	18222.2	14	4	2.8
4	16230.6 16295.1 16315.4 16338.0	12	4	−39.4	12	18352.3 18400.6 18428.7 18446.8	9	1	3.9
5	16977.0 17013.1 17032.8 17072.4	6	0	−22.6	13	18460.1 18531.2	18	5	8.8
6	17128.8 16198.7	22	9	27.8	14	18553.6 18573.2 18594.6 18617.2	20	7	8.1
7	17297.4 17315.7 17327.1	13	4	19.7	15	19019.9 19086.7	15	4	−26.7
8	17398.6 17504.9	15	5	−11.6	16	19170.9	8	0	17.9
					17	19618.9 19663.7	12	2	6.1

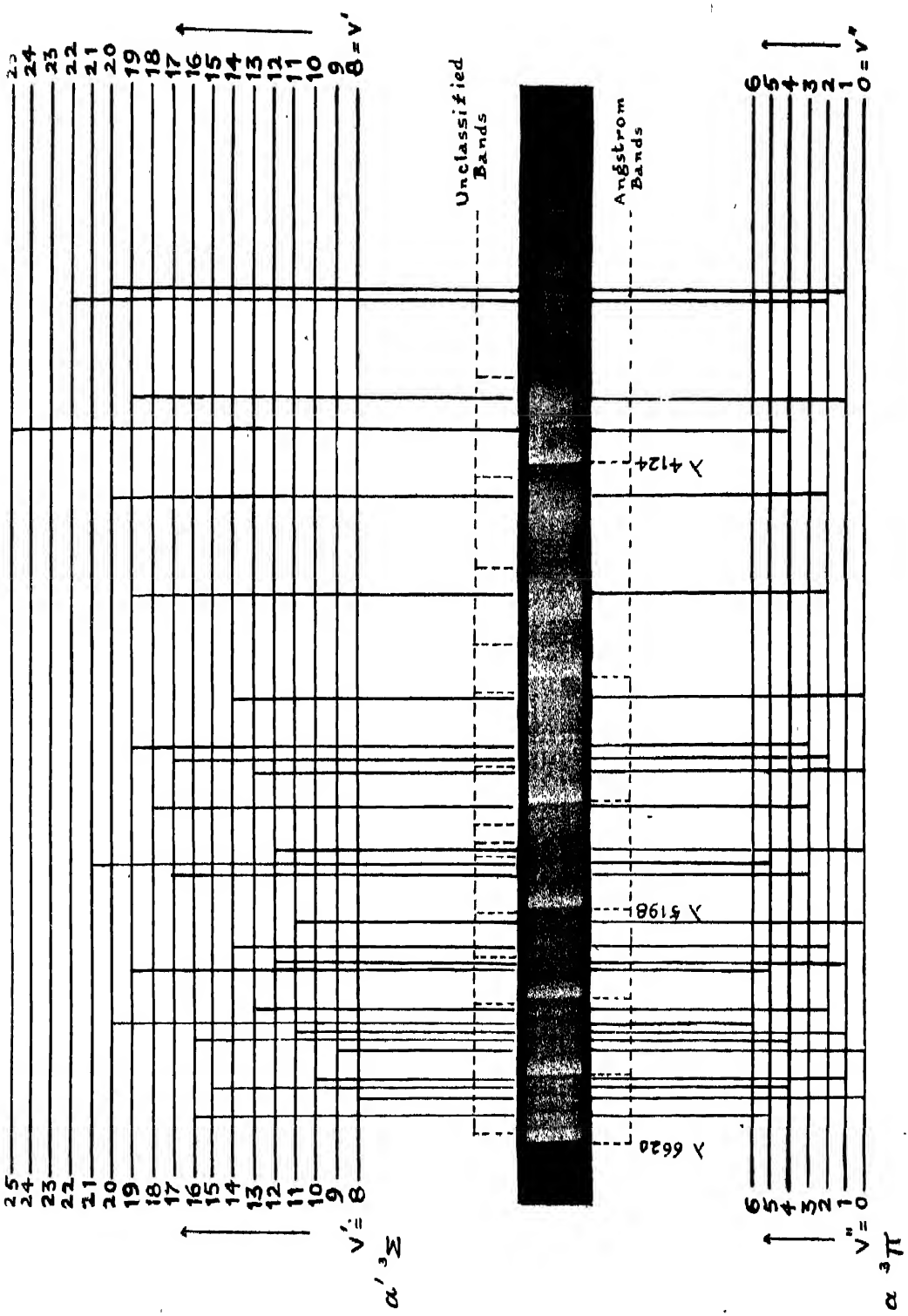
Unclassified Bands
Angstrom Bands
λ 4124
λ 5198
λ 6620
8 = v'
0 = v''
v' = 8
v'' = 0
α' ³Σ
α ³Π

TABLE II (*contd.*)

No	ν_{vac}	v'	v''	O-C cm^{-1}	No.	ν_{vac}	v'	v''	O-C cm^{-1}
18	19767.5 19815.3 19839.7 19860.2	14	3	15.1	28	22478.2 ? 22511.1 ? 22559.4	19	4	50.0
19	19908.0 19924.3 20006.4	16	4	17.0	29	23024.4 23083.9	12	0	30.9
20	20021.8 20032.9 20049.0 20078.8	18	5	−11.7	30	23186.2	14	1	3.3
21	20161.4 ?	9	0	6.4	31	23270.4	16	2	0.8
22	20382.1 ?	11	1	−19.8	32	23317.1	18	3	7.0
23	20516.4 20578.9 20597.5	13	2	9.9	33	23962.6	13	0	−20.4
24	21057.4 21141.1	10	0	2.1	34	24010.4 24031.7 24053.1 24082.1	15	1	5.2
25	21267.0 21300.1 21344.7	12	1	3.8	35	24115.8	17	2	−11.8
26	21402.7 21420.6	14	2	Masked by a Herzberg band.	36	24566.1	26	6	−29.3
					37	24722.2 24752.2 24776.8	24	5	24.3
					38	24839.0 24861.8	14	0	−33.2
27	22014.5 22036.8	11	0	Masked by an Angström band.	39	24924.4 24943.1 24956.8	16	1	3.9
					40	25466.0 25486.1	25	5	19.6
					41	25529.7 25614.7	23	1	− 2.7

A survey of the Tables I and II shows that whereas the O-C values in Table II are both positive as well as negative the O-C values in Table I are all, except one, negative and increase rapidly with the quantum numbers. It is incomprehensible that the equation should behave in a divergent manner up to some quantum numbers and in an irregular manner afterwards. When an attempt was made to introduce a third degree term in the vibration function of the initial state, keeping equation (2) as a first approximation, it was found that again the equation remained divergent up to certain quantum numbers and then deviated irregularly. Also it was noted that the situation became rather worse ; the absolute magnitude of error became one and a half times that of the original. Hence it was decided to use equation (2) with a modification in the initial vibration function.

(b) Accepting for the vibration function of the final state that known from other systems mentioned above, it was found that the most suitable equation representing the bands recorded by Asundi would be:

$$\nu_h = 10493.9 + (1151.6v' - 9.5v'^2) - (1726.5v'' - 14.4v''^2) \quad \ldots \quad (3)$$

Table III shows the comparison between the values calculated from equation (3) and those observed by Asundi.

TABLE III

No.	ν_{vac}	v'	v''	O-C cm^{-1}	No.	ν_{vac}	v'	v''	O-C cm^{-1}
1	11636.0	1	0	0	9	14693.2	7	2	−1.0
2	12158.5	3	1	7.4	10	14953.2	4	0	4.9
3	12761.8	2	0	2.7	11	15348.5	6	1	0.9
4	13237.0	4	1	0.8	12	15702.0	8	2	−1.3
5	13668.4	6	2	2.3	13	16011.0	5	0	3.4
6	13864.5	3	0	1.3	14	16375.0	7	1	−2.5
7	14048.0	8	3	−0.8	15	17057.2	6	0	−4.3
8	14301.8	5	1	−0.5	16	17389.2	8	1	2.6

Though both equations (1) and (3) represent Asundi's data to the same extent of accuracy, equation (3) is preferred since it contains the better known term $(1726.5\ v'' - 14.4\ v''^2)$ for the lower state. Equation (3) may now be extrapolated to correspond to the increase of three units in v' numbering proposed by Gerö and Lorenzei. It becomes:

$$\nu_h = 6953.6 + (1208.6\ v' - 9.5\ v'^2) - (1726.5\ v'' - 14.4\ v''^2) \quad \ldots \quad (4)$$

This equation for the band-heads may be written in the less convenient, but theoretically more significant, form as:

$$\nu_e = 7213.8 + (1218.1\ u' - 9.5u'^2) - (1740.9\ u'' - 14.4\ u''^2) \quad \ldots \quad (4a)$$

where $u = v + 1/2$.

Table IV gives the bands observed by Asundi as well as those observed by the present author. ν-values calculated from equation (4) are also indicated.

TABLE IV

No.	ν_{vac} Asundi	ν_{vac} Garg	I	ν_{cal}	v′	v″	O-C cm^{-1}
1	— — — — 11636.0			11636.0	4	0	0 A
2	12072.5 — — — 12158.5			12151.1	6	1	7.4 A
3	12674.0 — — — 12761.8			12759.1	5	0	2.7 A
4	13157.7 — — — 13237.0			13236.2	7	1	0.8 A
5	13585.1 — — — 13668.4			13666.1	9	2	2.3 A
6	13776.0 — — — 13864.5			13863.2	6	0	1.3 A
7	— — — — 14048.0			14048.8	11	3	−0.8 A
8	— — — — 14301 8			14302.3	8	1	−0.5 A
9	14612.7 — — — 14693.2			14694.2	10	2	−1.0 A

Some of the bands listed in Table II cannot be accommodated in the analysis given in Table IV. Such bands are given in Table V. A similar case is obtained in the wellknown triplet carbon bands where a few weak bands still remain unaccounted for. It may be that the bands put in Table V here and those unaccounted for in the triplet carbon system form together a new system that remains to be investigated further.

TABLE V

ν_{vac}	I	Remarks	ν_{vac}	I	Remarks
15439.0 15467.2	5	Probably Triplet carbon (0, 0)	22036.8	4	Probably Triplet carbon (8,1)
17700.5 17726.5 17780.1	5	Probably Triplet carbon (2, 0)	22478.2 22511.1 22559.4	6	Probably a Triplet carbon (unassigned)
18400.6 18428.7 18446.8 18460.1	6	Probably a Triplet carbon (unassigned)	23186.2 23270.4 23317.1	7	
19170.9	8	Probably Triplet carbon (5, 1)	24010.4 24031.7 24053.1 24082.1 24115.8	6	
19908.0 19924.3	6		24839.0 24861.8 24924.4 24943.1 24956.8	6	
20161.4	9	Probably Triplet carbon (6,1)			
20382.1	6				
21141.1	7	Probably Triplet carbon (7, 1)			

An inspection of Table IV shows that bands with v' equal to 15 or lower have O-C values well within errors of observation. From $v'=16$ onwards the O-C values have a tendency to increase. It is difficult to say whether such irregular deviations are due to any perturbations. For example there are four bands with $v'=19$ with residuals $+7.2, -17.0, -8.2, +1.4$, and three bands with $v'=20$ with residuals $+19.0, +32.4, +1.2$. In some cases such irregular deviations might be due to a possibility of wrong identification of the particular subhead used to calculate the O-C values.

Schmid and Gerö's (1937) estimated term values of the vibrational levels of the $a'\,{}^1\Sigma$ level cannot be represented by a usual function with any reasonable error however large. It may, therefore, be said that the perturbations observed by them are due to some level other than $a'^1\Sigma$. The two bands at 33548 and 37447 cm^{-1} reported by Schmid and Gerö as having quantum numbers (32, 1) and (36, 0) in the Asundi system do not fit in the proposed equation (4) except as bands (32, 1) and (38, 1) respectively. Even then the residuals will be -30 and -3 cm^{-1} respectively. The changes in the v' values may be likely because the extrapolation of rotational constants used by Schmid and Gerö is rather long. But the same cannot be said of v'' values. Hence with due reservation it seems that these two bands may belong to a new system along with the other bands given in Table V and the unassigned bands of the triplet system.

ACKNOWLEDGMENTS

The author takes the opportunity to express his heartfelt gratitude to Dr. R. K. Asundi for having suggested this problem and for his valuable remarks and discussions from time to time.

DEPARTMENT OF PHYSICS
BENARES HINDU UNIVERSITY

REFERENCES

Asundi (1929), *Proc. Roy. Soc.*, **124**, 277.
Estey (1930), *Phy. Rev.*, **36**, 309.
Gerö (1938), *Z.f.P.*, **109**, 216.
Gerö and Lorinczi (1939), *Z.f.P.*, **113**, 449
Hopfield and Birge (1927), *Phy. Rev.*, **29**, 922.
McLennan, Smith and Peters (1925), *Trans. Roy. Soc. Canada* , **19**, 39.
Schmid and Gerö (1937), *Z.f.P.*, **105**, 36.
Schmis and Gerö (1937), *Naturwissensch.*, **25**, 90.
Schmid and Gerö (1937), *Nature*, **140**, 508.

THE SPECTRUM OF HIGHLY IONISED IODINE—I VI

By S. G. KRISHNAMURTY and I. FERNANDO

(Received for publication, Nov. 8, 1948)

ABSTRACT. Using the regular and irregular doublet laws, appropriate lines possibly belonging to the spectrum of iodine VI have been picked up from the far ultraviolet data of highly ionised iodine due to Blochs and Felici, and a scheme set up The important intervals $5p$ $(^3P_0 - ^3P_1)$ and $5p$ $(^3P_1 - ^3P_2)$ have been found to be 3593 cm^{-1} and 10,124 cm^{-1} respectively.

Our knowledge of the spectrum of highly ionised iodine is as yet very meagre. In a previous publication, one of the authors (Krishnamurty, 1936) reported a regularity in the spectrum of trebly ionised iodine and set up a scheme consisting of the $6s$, $6p$, and $5d$ terms. Since then Blochs and collaborator (1937) published a long list of lines of highly excited iodine from $\lambda 200$ to $\lambda 1{,}000$. They showed that the excitation obtained in their experiments was very high, by picking up from the list, two lines belonging to I VIII.

However, they did not classify their data into the lines belonging to I VII, VI, V, etc., but only into seven groups denominated 2−, 2, 2+, 3−, 3, 3+, and 4 in increasing order of excitation. They point out that all lines attributed to I II are contained in their group 2. Group 3, they think, contains "about all" the lines due to I III but as no reliable analysis of I III lines is as yet made, they do not feel sure of this conclusion. Group 4 contains, according to them, lines due to iodine IV, V, VI, VII and VIII.

Starting from the clue afforded in the last sentence, we made an attempt in the present paper, to pick out from the data given by the Blochs, lines of I VI, which are expected to result from the allowed combinations of the terms listed in Table I.

TABLE I

Terms of I VI

Term prefix	Terms
$5s^2$	^1S
$5p$	^3P ^1P
$5d$	^3D ^1D
$5p^2$	^3P ^1P ^1P
$6s$	^3S ^1S

The main procedure adopted is the application of the law of variation of the frequencies of corresponding lines in iso-electronic spectra as shown in Table II.

TABLE II

Corresponding lines in Cd I—like spectra

Spectrum.	$5p^3P_2-5d^3D_3$	$5p^3P_1-5d^3D_2$	$5p^3P_0-5d^3D_1$
In II	56479 26128	58825 27503	59812 17957
Sn III	82607 24652	86328 26234	87769 36708
Sb IV	107259 23853	112562 25552	114477 29626
Te V	131112 22943	138114 25162	144103 22049
I VI	154055	163276	166152
Spectrum	$5p^3P_2-5p^2\,{}^3P_2$	$5p^3P_1-5p^2\,{}^3P_1$	$5p^3P_2-5s^2\,{}^1S_0$
In II	59735 15599	59898 15023	63036 16872
Sn III	75334 15623	74921 14761	79908 16044
Sb IV	90957 15638	89682 14714	95952 15755
Te V	106595 15702	104396 14819	111707 15468
I VI	122297	119215	127175

TABLE III

Screening Constants.

Z	Spectrum	$5p(^3P_1-^3P_2)$	S	ΔS	$\Delta^2 S$
48	Cd I	1171	33.03		
				2.09	
49	In II	2478	30.94		·75
				1.34	
50	Sn III	4034	29.6		·34
				1.0	
51	Sb IV	5860	28.6		.21
				·79	
52	Te V	7974	27.81		.12
				.67	
53	I VI	10423	27.14		

As far as possible, only group 4 lines of the Blochs were selected in this process, which yielded the scheme presented in Table IV. Further

confirmation for the selection was obtained from the law of variation of screeing constants shown in Table III.

The numbers printed above the frequencies in Table IV represent the group to which the selected lines are assigned in the list of the Blochs. It will be seen that some group 3 lines are also selected for the scheme. It is hoped that, in view of the want of absolute certainty in the assignment of the lines to the various known stages of excitation, these lines will fit ultimately into the I VI scheme, when further work on I III, I IV etc., which is in progress, is completed. The behaviour of intervals and intensities is throughout normal. One line, ν 154055 (20) looks quite of an abnormal intensity, but in addition to representing the present combination, which should be about the brightest line (compare intensities of the $5d^3D$—$5p^3P$ multiplet with other multiplet lines) it (alone) is found to represent another combination in I VII too.

TABLE IV

Multiplet Scheme of I VI

	$5p^3P_0$	(3595)	$^3P_1$	(10424)	$^3P_2$
$5s^2\,{}^1S_0$			3 127175 (8)		
$5p^2\,{}^3P_0$			3 110945(0)		
$^3P_1$	4 122805 (3)		3 119215(2)		4 108781(7)
$^3P_2$			3+ 132723(2)		4 122297(3)
$^1D_2$			4 120172(3)		4 109749(3)
$5d^3D_1$	4 166152(5)		4 162557(4)		
$^3D_2$			4 163276(6)		4 152854 (4)
$^3D_3$					4 154055(20)
$^1D_2$			4 166653(1)		3 156223(2)
$6s^3S_1$			4 207005(3)		

DEPARTMENT OF PHYSICS,
PRESIDENCY COLLEGE, MADRAS

REFERENCES

Bloch and Felici, 1937 *Jour. de Phy. et Rad.*, **8**, 9.
Krishnamurty, S. G., 1936, *Proc. Lond. Phy. Soc.*, **48**, 277.

MICRO-WAVE MODULATION BY VARIABLE CIRCUIT ELEMENTS COMPRISING WAVE GUIDES OR CAVITY RESONATORS

By A. N. BHATTACHARYYA

(*Received for publication, Sept. 24, 1948*)

ABSTRACT. A driving mechanism similar to that of an electro-dynamic loudspeaker is utilised for varying the dimensions of a wave guide or cavity resonator according to the voice frequency signals so that micro-waves passing through the guide may either be amplitude or phase modulated and the micro-wave output of the cavity resonator may be amplitude modulated. The same mechanism is also applied for varying the length of a probe inside a guide resulting in load impedance modulation.

INTRODUCTION

Amplitude modulation system wherein an impedance is varied in accordance with the signals to be transmitted is perhaps the first modulation system ever used in radio communication. In one of such system, the resistance of the antenna circuit is varied in accordance with the resistance of a carbon microphone. Another system uses the modulating voltage for varying the energy absorbed from the high frequency oscillations, a losser thermionic valve to the grid of which signal voltages are applied being connected across the tank circuit of a class C power amplifier. These modulating systems are rarely used at present. The micro-wave radio communication has been vastly developed during the last war and this paper describes methods of modulating micro-waves utilising principles stated above which were used in earliest days of radio. Micro-wave transmission circuits widely use wave guides and cavity resonators as transmission line and tuned circuits respectively. For any wave guide when the frequency is above cut-off, the phase velocity in the guide is greater than that in the free space ($v_p > c$) and the phase constant which is phase shift per unit length of the guide is equal to $\left(\frac{2\pi}{\lambda_g}\right)$ where λ_g is the wave length inside the guide (Terman, 1943). Thus it is seen that by varying the length of a guide in accordance with a signal current it is possible to phase modulate the micro-waves propagating through a guide. The resonant frequency of a cavity resonator may be varied by changing its dimensions and if any dimension is varied in accordance with the signals to be transmitted the output of the resonator will correspondingly vary resulting in amplitude-modulated micro-waves when for maximum or minimum signal

current, the resonator is tuned to the exciting micro-wave input. For a re-entrant coaxial resonator (Fig. 4) which we shall specially consider, the resonant wave length (Fink, 1947)

$$\lambda_0 = 2\pi\sqrt{\frac{2ha^2}{d}\left(\log_e \frac{b}{a}\right)}$$

and this paper describes means for varying d in accordance with the signals. When load impedance modulation is desired the length of a probe inside the wave guide or a cavity resonator may be varied in accordance with the signal. This will also result in amplitude modulation. Variation of the radiation resistance of the exciting antenna inside of the wave guide will also result in amplitude modulation of the micro-waves.

MODULATION INSIDE WAVE GUIDE

The cylindrical guides illustrated in figures 1 and 2 consist of two parts: A and B. The part A is fixed while the part B is arranged to slide over A. The wall thickness of B is very small in comparison with the diameter of the guide. In Fig. 1 the guide is excited in TE_{11} mode while in Fig. 2

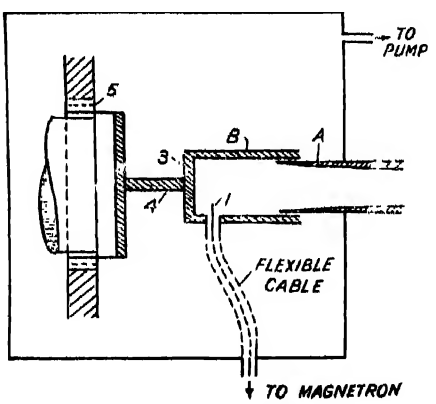

FIG. 1

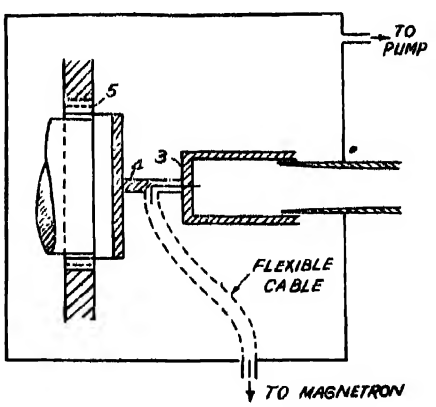

FIG. 2

the guide is excited in TM_0, mode. The metallic end piece 3 which is rigidly connected with B, is coupled through a rod 4 to a driving mechanism similar to that of a electrodynamic speaker. The centering arrangement of the voice coil 5 is not illustrated in the figure. The signal frequency amplifier feeds the moving coil wound over 2. Vibration of 2 causes linear movement of B over A resulting in variation in the length of the wave guide. Variation in length of the guide results in phase modulation of micro-waves emitted from the open end 6 of the guide. In Fig. 2 the coupling rod is partly hollow so that the central conductor of the coaxial cable exciting the antenna 1 may pass through it. The guide should be so mounted that lateral vibration of the same is prevented. The aerial 1 also should be prevented from vibrating.

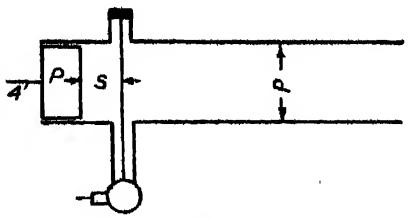

FIG. 3

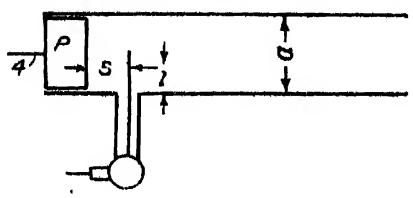

FIG. 4

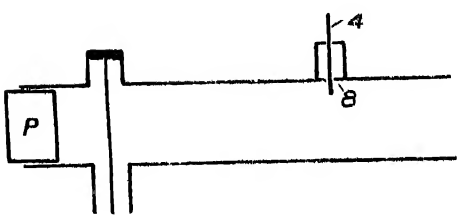

FIG. 5

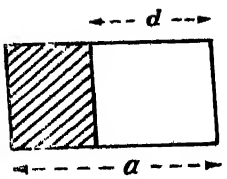

FIG. 5a

A method depending on the variation of radiation resistance of the exciting antenna 1 inside a rectangular wave guide 7 is illustrated in figures 3 and 4. The wave guide is excited in $TE_{0,1}$ mode. The radiation resistances of the antenna 1 of Figs. 3 and 4 are given by the expressions (M.I.T. Radar School, 1946)

$$R_r = 2Z_w K \sin^2\left(\frac{2\pi S}{\lambda_g}\right) \text{ for } K < 0.5 \quad \ldots (1)$$

$$\text{and } R_r = 2Z_w \frac{l^2}{ab} \sin^2\left(\frac{2\pi S}{\lambda_g}\right) \quad \ldots (2)$$

respectively, where

K = ratio of the smaller to the larger dimension of the guide $= \left(\frac{a}{b}\right)$

wave impedance $Z_w = 120\,\pi \frac{\lambda_g}{\lambda_a}$ is the wave guide anologue of the characteristic impedance of conventional transmission lines,

λ_g = wave length in the guide.

λ_a = free space wave length of the source.

S = distance of the plunger P from the antenna 1.

l = length of the antenna 1 (Fig. 4).

The net reactance of the antenna is a function of S and l. The optimum condition of transmission (*i.e.*, when there is no reflection from the junction between the coaxial line and wave guide) both l and S are about $\lambda_g/6$. The plunger P is coupled to a driving mechanism similar to that of figures 1 and 2, so that the distance S is varied in accordance with the signal to be transmitted. When the arrangement is such that for maximum signal current, the optimum condition of transmission is reached, variation of S will cause amplitude-modulation of the waves passing through the guide. The coupling arrangements, illustrated in figures 3 and 4, when properly adjusted for feeding power into the guide, are also well adjusted for taking power out. In the transmitting system shown in Fig. 7 which uses a biconical horn excited in TEM mode, one portion Q of the central conductor of the coaxial cable receives energy from the magnetron while another portion acts as the radiator. In this case, if the plunger P is coupled to a driving mechanism described before and S is varied according to the signal current, radiated waves will be amplitude modulated if for maximum or minimum signal current the optimum value of S is reached. This system may be used for broadcasting purposes.

In Fig. 5, the length of a probe 8 coupled to the wave guide 7 at a suitable place, is varied according to the signals to be transmitted. The probe 8 must be in good electrical contact with the guide.

In each case the magnet M and a part of the wave-guide should be enclosed inside a low pressure metal chamber which is continually evacuated. (This is not illustrated in figures 3-5.)

MODULATION INSIDE CAVITY RESONATORS

The modes of cavity resonator may be designated by symbols TE_{lmn} or TM_{lmn} where l is the number of half-period variations of the electric field along the length of the resonator or X-axis. In a cylindrical guide of length x_0 and radius a in which m represents the number of full period variations of the radial electric field along the direction and n represents the number of half period variations of the angular component of the electric field in the radial r direction for TE_{lmn}, the resonant frequencies which exist are obtained by (Sarbacher and Edson, 1946)

$$f_{lmn}=\sqrt{\left(\frac{cl}{2x_0}\right)^2+\left[\left(\frac{c}{2\pi}\right)\left(\frac{r'_{nm}}{a}\right)\right]^2}, \qquad l=1, 2, 3,\ldots$$

and for TM_{lmn}

$$f_{lmn}=\sqrt{\left(\frac{cl}{2x_0}\right)^2+\left[\left(\frac{c}{2\pi}\right)\left(\frac{r_{nm}}{a}\right)\right]^2}, \qquad l=0, 1, 2, 3,\ldots$$

where r_{nm} and r'_{nm} are the roots of the equations

$$J_n(r_{nm})=0$$

$$J'_n(r'_{nm})=0$$

Thus variation of x_0 causes change in resonant frequency for all modes other than TM_{010}
for which $l=0$ is permissible and

$$f_{010}=\frac{c}{2\pi}\left(\frac{2.405}{a}\right)$$

$$\lambda_{010}=2.61a$$

For TM_{010} mode the resonant frequency depends only on the value of a, and the electric field is wholly parallel to the axis of the resonator and

$$E_z=AJ_0\left(r\frac{r_{01}}{a}\right)e^{j\omega t}$$

$$H_\phi=jA\frac{\omega\epsilon_1}{r_{01}}aJ_1\left(r\frac{r_{01}}{a}\right)e^{j\omega t}$$

The maximum energy W_m stored in the magnetic field in this case is given by

$$W_m=\frac{\mu_1}{2}\int_{\phi=0}^{2\pi}\int_{\gamma=0}^{a}\int_{x=0}^{x_0}\left|H_\phi\right|^2 rd\phi drdx$$

$$=\frac{1}{2}\left(\frac{a}{r_{01}}\right)^2 lA^2\epsilon_1\left(\frac{\omega}{c}\right)^2 J_1^2(r_{01})$$

$$=\frac{1}{2}VA^2\epsilon_1 J_1^2(r_{01})$$

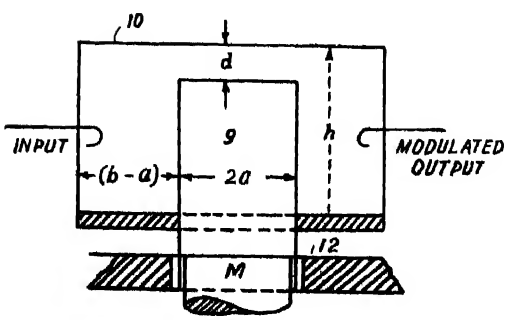

FIG. 6

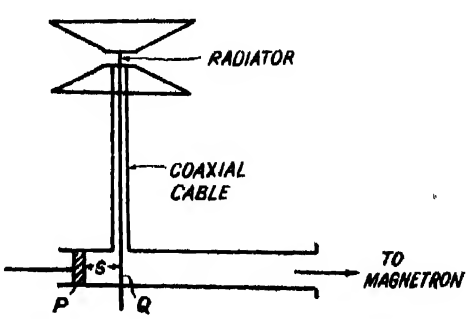

FIG. 7

From the equation of W_m it is apparent that variation of ϵ_1 by changing air pressure inside the resonator will cause variation of (W_m/V) or the magnetic energy density.

The value of x_0 or ϵ_1 may be varied by coupling the plunger P (Fig. 8) to a driving mechanism similar to that previously described. If for maximum value of signal current $x_0=x_{res.}$, *i.e.*, resonating conditions are reached, the output from the resonator will be amplitude-modulated For TM_{010} mode due to the variation of magnetic energy-density (W_m/V) the output will be amplitude modulated but the percentage of modulation will be small.

In another transmitting system illustrated in Fig. 9 the resonator is coupled to a horn antenna through a slit N and excited by a probe E.

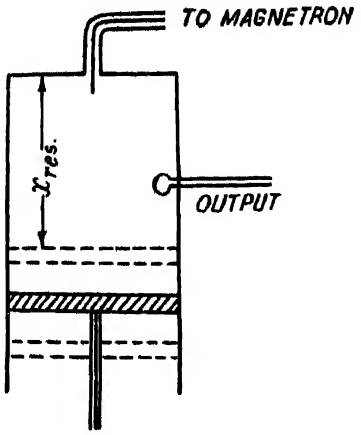

FIG. 8

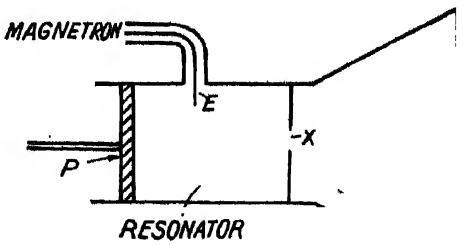

FIG. 9

Vibration of P according to signal current will result in amplitude-modulation of the waves radiated by the horn if the resonator is tuned to the exciting waves either when the axial length of the resonator is maximum or when it is minimum in course of vibration.

In a further transmitting system, illustrated in Fig. 10, the resonator is coupled to a parabolic antenna and the plunger P may be driven in a manner similar to that described before.

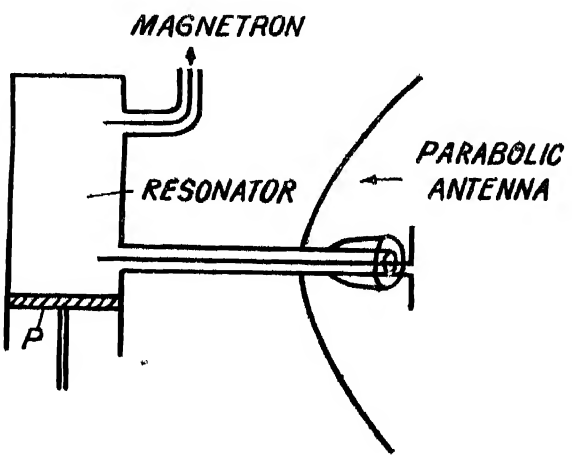

FIG. 10

In the re-entrant cavity resonator, illustrated in Fig. 6, the central post 9 slides inside the outer cylinder 10 so that d may be varied. The bottom portion 11 of the outer cylinder is comparatively thicker so that the oscillation of 9 changes only the dimension d of the resonator. The wall thickness of 9 is small and the moving coil 12 is wound over it. When signal power amplifier 5 feeds 12 the central post 9 will oscillate and the distance d will vary according

to the signals to be transmitted. Variation of d causes change in the resonant wage length

$$\lambda_0 = 2\pi \sqrt{\frac{2ha^2}{d}\left(\log_e \frac{b}{a}\right)}$$

If in normal position of 9 (*i.e.* when no signals are applied to 12) the cavity resonator is not exactly tuned to the input micro-waves, variation of d according to the signal current in 12 will cause variation in the output current taken through the loop and the radiated waves will be amplitude modulated, if resonating condition is approached when d is maximum or minimum.

If the length of a losser probe inside the resonator is varied according to the signals to be transmitted, the load current will vary correspondingly and amplitude modulation results. In this case the resonator may be of any type like rectangular, cylindrical, spherical or the re-entrant type.

In each case the cavity resonator wholly or in part and the magnet M should be enclosed in a low pressure metal chamber.

DISCUSSIONS

In the amplitude modulating systems described above it is necessary to consider whether linear operation is obtained. Let us consider the system described with reference to Fig. 3. The magnetron feeds power to the wave

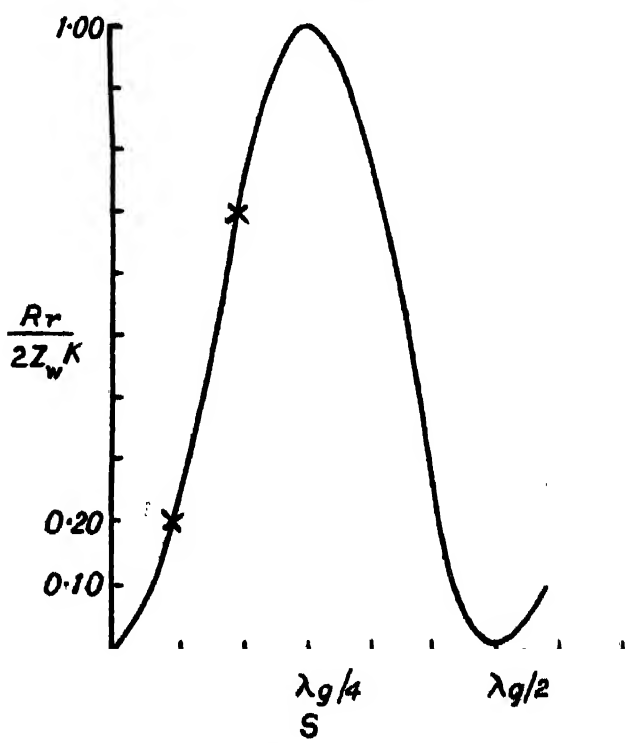

FIG. 11

guide through the coaxial line and for maximum possible transfer of power it is essential that the coaxial line is terminated in its characteristic impedance. The input impedance of the antenna is $(R_r + X_a)$ but by adjusting the reactance X_s of the short circuited stub, the antenna reactance may be cancelled. Then the impedance looking into the wave guide will be merely the radiation resistance R_r. The variation or R_r with respect to S is shown in Fig. 11. The optimum value of S is $\lambda_g/6$ and the variation in R_r is substantially linear within the limits $S=\lambda_g/12$ and $S=\lambda_g/6$. If for no signal condition $S=\lambda_g/8$ and a limiter amplifier (as used in broadcast transmitters) is utilized so that the variation in S never exceeds $\lambda_g/12$, the load impedance connected across the coaxial line will vary linearly and the modulation will be substantially linear. This system may be considered in principle similar to a load impedance modulation system. The performance of the system, described with reference to Fig. 4, appears to be similar to that of the system just considered so far as the linearity of modulation is concerned. The system described with reference to Fig. 5 which uses variation in the length of a probe is also a load impedance modulation system. The probe introduces a capacitive susceptance when it extends less than a free-space quarter wave-length into the guide but the variation in susceptance is not perfectly linear with the variation in the length of penetration of the probe. The arrangement should be such that maximum power flows through the guide when the probe length is zero and with no signal condition the probe length should be $(\lambda_a/8)$ where λ_a is the free space wave length. In this case also a limiter amplifier is necessary in the signal input circuit because the variation in the length of the probe should not exceed $(\lambda_a/8)$. The modulation in this case is not satisfactory from the view point of linearity of modulation. If instead of using a probe inside the guide an asymmetrical inductive diaphragm of the type, shown in Fig. 5*b*, is used it is possible to vary the width d of the open space which will result in the variation of the shunt susceptance B which is given by the expression (M.I.T. Radiation Lab. Series, 1948)

$$B = -\frac{\lambda_g}{a} \cot^2 \frac{\pi d}{2a}\left(1+\operatorname{cosec}^2 \frac{\pi d}{2a}\right).$$

If (a/λ) is equal to (0.5) and (d/a) does not exceed (0.7) the variation of B with respect to change in d will be substantially linear and faithful amplitude modulation is expected.

The modulation systems, described with reference to figures 6, 8, 9 and 10, which use cavity resonators are also cases of load impedance modulation. It is presumed that only one mode of oscillation exists in the resonator. The input impedance of the loaded cavity resonator is maximum when resonance occurs and when d (Fig. 6) or x_0 (Fig. 8) is varied from its resonant value the input impedance rapidly drops to small fraction of the coupling loop or probe impedance. Near resonant frequency the input impedance of the

cavity resonator varies in much the same manner as the impedance of a parallel resonant circuit and it appears that for small change in dimension of the cavity, substantially linear amplitude modulation will take place.

The methods of modulation described in this paper may be applicable to systems utilising several kilowatts of radio frequency power and the carrier wave length may be less than one centimetre.

In all the modulating arrangements comprising wave guides, the structure should be light as far as practicable. As for instance the portion B including 3 (figures 1, 2) and the coupling arrangement of antenna 1 should be such that it is possible to make B oscillate in the manner described. The low pressure chamber is used for reducing air vibration which is one of the potent damping factors.

When the wave length is less than 10 centimetres it is not feasible to produce amplitude modulated continuous waves by using valve modulating circuits. Signals may be transmitted at such high frequencies if time-modulated electric pulses are radiated.

From the expression of phase velocity v_p inside a rectangular guide,

$$v_p = \frac{c}{\sqrt{1-(a/2b)^2}}$$

it appears that variation of b (wider dimension of the guide) will cause variation in the phase velocity of the waves passing through the guide, resulting in phase modulation of the said waves. In this case due to the simultaneous variation of Z_w which is equal to

$$\frac{120\pi}{\sqrt{1-(a/2b)^2}}$$

for any T. E. mode, amplitude modulation also takes place.

ACKNOWLEDGMENT

In conclusion the author wishes to express his thanks to Dewan Bahadur K. Rama Pai, M.A., Controller of Patents and Designs for his encouragement and kind pesmission to publish this paper.

PATENT OFFICE (GOVT. OF INDIA)
214, LOWER CIRCULAR ROAD,
CALCUTTA.

REFERENCE

Fink, Donald G., 1947, Radar Engineering, p. 216.

M. I. T. Radar School, 1946, Principles of Radar, p. 10

M. I. T. Radiation Laboratory Series, 1948, Micro-wave Transmission Circuits, p 212.

Sarbacher, Robert I. and Edson, William A., 1946, Hyper and Ultra High Frequency Engineering, pp. 250, 381, 386.

Terman, F. E., 1943, Radio Engineer's Hand Book, 253, 254 and 261.

ERRATUM

In pages 10, 11 and 12 (No. I, Vol. 23), please read " P_m in gms " in the place of " P_m in gms per sq. cm " along the ordinates of the Figs. 2, 3 and 4.

ACKNOWLEDGMENT

We thankfully acknowledge the receipt of a grant of Rupees seven hundred only from the Government of India through the National Institute of Sciences of India, for the financial year 1948-49.

BAND SPECTRUM OF THALLIUM IODIDE

By P. TIRUVENGANNA RAO and K. R. RAO

(*Received for publication, Nov. 4, 1948*)

Plates VA and VB

ABSTRACT. An extensive band system attributed to the diatomic molecule thallium iodide, has been obtained for the first time in emission between λ5300–λ3800 in a high frequency discharge with external electrodes. The bands at the violet end are red-degraded; those in the central portion are headless; at the red end they are diffuse and broad. A number of them occur in well-separated groups, each consisting of four or five equi-spaced components with an interval of about 28 units; the intensity among these rises gradually to a maximum and then falls off. The system has been interpreted as due to the transition $^3\pi_1 - {}^1\Sigma^+$ with the origin near the extreme violet end. A vibrational analysis which includes most of the band heads, has led to the following formula:–

$$\nu = 25794.2 + (91.2\ u' - 0.09\ u'^2) - (121.0\ u'' - 0.09\ u''^2)$$

A second brief system of about 25 slightly violet degraded bands is also obtained between λ3680–λ3600. Four diffuse groups of bands, overlaid by a continuum, are measured. The system has been interpreted as the component $^3\pi_0{}^+ - {}^1\Sigma^+$ having the same lower state as that of the main system. Electron transitions are compared for the observed band systems of the four halide molecules of thallium.

INTRODUCTION

As part of a detailed investigation into the molecular spectra of a series of heavy diatomic fluorides, Howell (1937) studied the thallium fluoride spectrum and reported several points of unusual interest. Extending this investigation to the other halides of the same element, thallium chloride and thallium bromide, Howell and Coulson (1938, 1941) were enabled to make a comparison of the electronic levels and transitions for these three molecules. The band spectrum of the remaining halide, thallium iodide, does not appear to have been analysed.

In 1929, Butkow recorded a few bands in absorption by a column of thallium iodide vapour, but no vibrational scheme was reported; nor was any work published on the emission spectrum of the molecule, as far as the authors are aware. In the course of a systematic investigation in our laboratory of the band spectra of diatomic molecules and particularly, the iodides, the spectrum of thallium iodide has been photographed and it is the purpose of the present paper to describe this spectrum and to report the analysis of it as interpreted by the authors.

EXPERIMENTAL

The discharge tube employed is a simple straight one of pyrex glass about 30 cm. long and 1 cm. in diameter, drawn out at one end into an adapter,

the other end being closed by a quartz window. The substance, a pure sample of thallium iodide obtained from B.D.H. is spread inside the tube over a length of about 8 to 10 cms. The tube is continuously evacuated by a Cenco Hyvac pump through a row of absorbing and condensing towers. The discharge is excited by a low power H.F. oscillator constructed for the purpose and described elsewhere (Ramasastry, 1947) in detail, working at a frequency of 5 to 10 megacycles and using external copper electrodes about 5 cm. apart. The substance was heated at regular intervals for a steady maintenance of the discharge ; such intermittent heating was found necessary also for suppressing the iodine bands which would otherwise obscure the thallium iodide system. The discharge is intense green, due to the thallium radiation λ5350.

The bands were obtained also in a discharge from a 1/4 Kw. transformer in an ordinary H type tube containing the vapour. The H.F. discharge was found more favourable for the production of the system.

A number of spectrographs were used to photograph the spectrum—a Fuess glass instrument, Hilger large glass and quartz Littrow instruments and a 10-foot concave grating in the first order. On account of the peculiar nature of the spectrum, measurements had to be made on the small as well as the large dispersion spectrograms on a number of plates for different regions. The usual international iron arc standards were adopted to reduce the plates.

DESCRIPTION OF THE SPECTRUM

The spectrum cannot be adequately described without reference to the photographs, some of which are reproduced in Plates VA and VB. Figures *a*, *b* and *c* of Plate VA are glass Fuess spectrograms from λ4900 to λ3800, giving a general view of the entire system of bands. The development of the system below λ3900, which is poor in the glass instrument, is shown in the quartz Littrow picture, Fig. *d*, Plate VA. The heads give the appearance of a complex system, with one marked regularity. Over a wide range towards the violet end, they occur in well-separated groups each consisting of about four or five equi-spaced components with an interval of approximately 28 wave-number units. The fluctuations of intensity show a kind of wave appearance such as is observed in the band systems of sulphur or of selenium. There are altogether about 200 band heads within the region λ5300 to λ3800, being very crowded in the central portion. The bands near the red-end show greater diffuseness and many of them appear double. In each of the groups at the violet end, the intensity rises and falls suggesting the formation of short sequences. At the violet end, the heads are sharper and clearly red-degraded ; diffuseness sets in and increases as one goes towards the red. The peculiarities of appearance noticed by Howell in the thallium chloride and thallium fluoride bands are not observed in the iodide system—namely the

doubling at the head and the occurrence of the so called "absorption lines" in the emission spectrum, nor does the iodide system resemble closely that of the bromide, which consists of long progressions with very intense, sharp and line-like heads near the shortwave side.

The kind of evidence of the existence of isotope effect that is found in thallium chloride and thallium bromide bands is absent in this system as iodine has no isotopes, leading to a special difficulty in the interpretation of its structure. The effect due to the thallium isotopes, however, is seen in the doubling or broadening of the heads in the region of longer wave lengths. An evidence of this is seen in Plate VB Figs. *e* and *f*, which are enlargements of the spectra in this region taken by the Fuess and the concave grating respectively. Fig. *g*, in Plate VB shows another system between λ3680-3600 which is also ascribed to the thallium iodide molecule. It consists of three or perhaps four continuous patches superposed by distinct sequences of bands having nearly the same wave number interval of about 28 units as in the first system.

RESULTS

Table I is a catalogue of the band heads assigned to the first system and Table II gives the data for the second system. The tables are self-explanatory.

TABLE I

Wave length	Int.	Wave number	Classification v', v''	Wave length	Int.	Wave number	Classification v', v''
3812 96	2	26218 9	5,0	23.93	4	25477.5	2 4
17.52	2	26187.6	6 1	28.33	4	25448.9	3,5
21.64	2	26159.4	7,2	32.95	3	25419.0	4,6
				37.76	2	25388 0	5,7
25.60	2	26132.3	4,0				
29.96	2	26102.6	5,1	3940.90	3	25367.8	
34.60	2	26071.0	6,2	45.30	1	25339.5	
				49.80	1	25310.6	
38.60	2	26043.8	3,0	51.92	1	25297.0	
12.90	2	26014.7	4,1				
47 40	2	25984.2	5,2	56.51	3	25267.7	5,8
				60.86	4	25239.9	6,9
51.90	2	25953.9	2 0	65.73	3	25208.9	7,10
56.66	2	25921.9	3,1	69.74	4	25183.5	8,11
61.41	2	25890.0	4,2	81.91	1	25106.5	
				84.26	2	25091.7	
65.31	2	25863.8	1,0				
69.43	2	25836.3	2,1	88.99	3	25061.9	8,12
73.75	3	25807.5	3,2	93.37	4	25034.5	9,13
				96.89	4	25012.4	10,14
77.88	5	25780 0	0,0	4005.96	1	24955.8	
88.28	3	2575 .8	1,1	10.04	1	24930.4	
				13.82	1	24906.9	
96.80	2	25654 8	0,1				
3900 78	5	25628 7	1,2	17.00	4	24887.2	10,15
04.92	4	25601.5	2,3	21.81	4	24857.4	11,16
09.19	3	25573.5	3,4	26.53	3	24828.3	12,17
17.84	1	25517.1		31.49	2	24797.7	13,18
20.10	1	25502 4		42.52	1	24730.1	

TABLE I (*contd.*)

Wave length	Int.	Wave number	Classification v', v''	Wave length	Int.	Wave number	Classification v', v''
46.30	1	24707.0	12,18	4306.18	3	23215.9	28,43
50.33	3	24682.4	13,19	11.23	3	23188.7	29,44
55.09	3	24653.4	14,20	15.92	5	23163 5	30,45
57.88	4	24636 5	15,21	21.32	4	23134.6	31,46
60.43	1	24621.0					
62.57	1	246.8.0					
64.91	1	24593.9	16,22	4326.14	3	23108 8	32,47
				31.62	3	23079 6	33,48
79.48	2	24506.0	15,22	37.43	2	23048.7	34,49
84.31	4	24477.1	16,23				
88.80	5	24450.2	17,24	42.58	5	23021.3	31,47
93.88	2	24419.8	18,25	47.69	3	22994.8	32,48
				52.88	3	22966.9	33,49
4113.18	5	24305.3	18,26	57.87	3	22940.6	34,50
18.23	4	24275.5	19,27	62 61	2	22915.6	35,51
23.38	3	24245.1	20.28	67 24	1	22891.4	36,52
27.99	1	24218.1					
28.13	1	24217.2	21,29	69.33	4	22880.4	32,49
				74.91	3	22851.2	33,50
39.76	2	24149.2	19.28	80.09	2	22924 2	34,51
42.75	3	24131 8	20,29				
45.21	1	24117.5		85.04	3	22798.4	31,49
47.59	3	24103.6	21,30	89.84	4	22773.5	32,50
				95 61	2	22743.6	33,51
4152.24	3	24076.6	22,31	4400.93	2	22716.1	34,52
57.14	2	24048.2	23,32				
62.37	1	24018 0	24,33	06.75	2	22686.1	31,50
				11.98	3	22659.2	32,51
67.02	0	23991.2	21,31	17.47	4	22631.1	33,52
71.35	1	23966.3	22,32	22.57	5	22605.0	34,53
77.64	1	23930.2	23,33	28 89	2	22572.7	35,54
82.50	3	23902.4	24,34	33.53	2	22549.1	36,55
87.27	4	23875.2	25,35	39.63	1	22518.1	37, 6
92.36	2	23846 2	26,36				
96.36	1	23823.5		44.56	1	22493.1	34,54
				50.28	4	22464.2	35,55
4207.73	2	23759.1	25,36	55.70	3	22436.9	36,56
10.09	1	23745.8		60 82	2	22411.0	37,57
13.28	5	23727.8	26,38	66.40	1	22383.8	38,58
17.36	4	23704.9	27,38	67.52	1	22377.5	
				72.64	1	22351.9	39,59
23.26	1	23671.8	24,36	75.01	1	22340.1	
27.60	1	23647.9	25,37				
32.69	2	23619.0	26,38	77.88	5	22325.8	36,57
36.15	1	23599.7		84.19	3	22294 3	37,58
38.27	4	23587.9	27,39	88 87	3	22271.0	38,59
40.78	2	23574.0		94.57	3	22242.9	39,60
43.61	3	23558.2	28,40				
48.45	3	23531.4	29,41				
53.41	3	23504.0	30,42	4500.35	1	22214 3	36,58
				06.62	3	22183 4	37,59
58.31	3	23476.9	27,40	11.64	5	22158 7	38,60
63.47	3	23448.5	28,41	17 43	4	22130 3	39,61
69.66	5	23414.5	29,42	22.88	3	22103.6	40,62
74.76	2	23386.6	30,43	28.54	2	22076.0	41,63
77.41	1	23372.1		34.16	2	22048.6	42,64
79.75	1	23359.3	31,44				
81.95	1	23347.3		39.76	2	22021.4	39,62
84.33	3	23334.4	32,45	45.57	3	21993.3	40,63
				47.86	1	21982.2	
89.26	4	23307.5	29,43	51.71	3	21963.6	41,64
94.34	4	23279.9	30,44	57.14	5	21937.5	42,65
99.80	3	23250.4	31,45	62.79	4	21910.3	43,66

Fig. a. Fig. b. Fig. c Fig. d.

Thallium iodide band spectrum (Fe arc comparison).

Fig

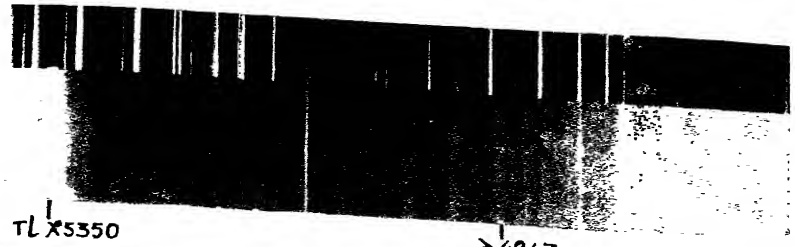

Fig. *f*.

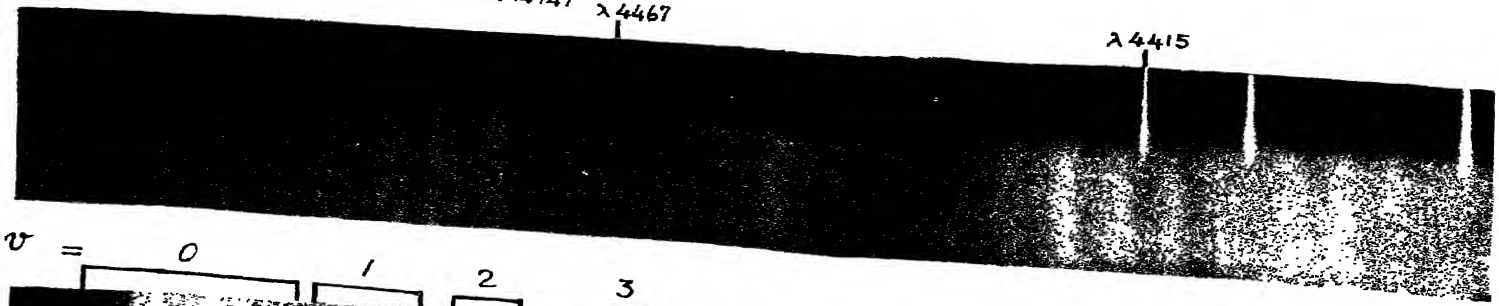

Fig. *g*.

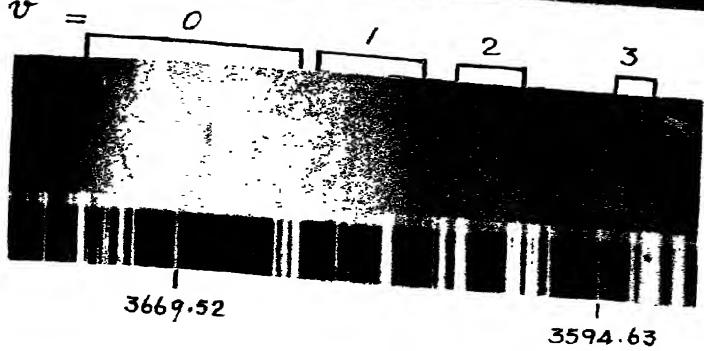

Thallium iodide d spectrum (Fe arc comparison)

TABLE I (*contd.*)

Wave length	Int.	Wave number	Classification v', v''	Wave length	Int.	Wave number	Classification v', v''
73.54	3	21858.0	41.65	4728	2	21143	51,79
76.98	1	21842.4		4737	4	21103	48,77
80.18	3	21827.1	42,66	4749	2	21052	
86.07	4	21799.1	43,67	4785	2	20894	
91.27	5	21774.4	44,68	4795	3	20849	49,80
93.30	3	21764 8		4822	3	20733	49,81
4615.15	2	21661 7	44,69	4832	1	20692	
20.85	5	21635.2	45.70	4843	1	20642	48,81
27.99	2	21601.6	46,71	4853	1	20601	
32.30	2	21581.5	43,69	4898	2	20411	48,63
38.73	2	21551.6	44,70	4932	1	20269	
43 85	2	21527.9	45,71	4947	3	20211	47,84
50 66	2	21496 3	46,72	4968	2	20122	46,84
56.21	3	21470 7	47,73	4981	3	20070	
62.19	2	21443 2	48,74	5038	2	19844	48,88
67.78	2	21417.5	49,75	5060	1	19760	47,88
75.40	4	21382.6	46,73	5069	1	19723	48,89
85.89	3	21334.7	48,75	5077	2	19690	49,90
91.94	2	21307.2	49,76	5091	1	19636	47,89
97.05	1	21284 0	50,77	5113	0	19554	
4703.05	4	21256.9	47,75	5118	1	19532	
10.02	4	21225.4	48,76	5150	2	19412	47,91
22.10	4	21171.1	50,78	5134	2	19396	
				5186	2	19277	48,93
				5235	0	19098	
				5255	1	19025	49,96

TABLE II

Wave length	Int.	Wave number	Classification
3688.87	0	27100.9	(0,0)
84.98	1	27129.5	(1,1)
81.24	1	27157.1	(2,2)
77.86	1	27182 0	(3,3)
74 12	1	27209.7	(4,4)
70.79	2	27234 4	(5,5)
67.07	1	27262.0	(6,6)
63.80	1	27286.3	(7,7)
60.59	1	27310.3	(8,8)
57 40	1	27334.1	(9,9)
53.94	1	27360.0	(10,10)
50.31	1	27387.2	(11,11)
44.61	1	27430.0	(8,7)
41.04	2	27456.9	(9,8)
37.45	1	27484.0	(10,9)
34.51	1	27506.2	(11,10)
30 12	1	27539 5	(12,11)
26.38	1	27567.9	(13,12)
19.65	1	27619.1	(11,9)
16.30	1	27644.7	(12,10)
12.68	1	27672.4	(13,11)
08.91	1	27701.3	(14,12)
05 61	0	27726 7	(15,13)
3588.03	1	27862.5	(16,13)
85.13	1	27885.1	(17,14)

VIBRATIONAL ANALYSIS

The well marked regularity in the band system mentioned earlier served as a starting point in the anaiysis. The clearly separated groups, each consisting of a few almost equi-spaced bands with gradual rise and fall off in intensity, are considered as different sequences. Two chief difficulties, however, presented themselves in working out the analysis further ; (1) The location of the origin of the system. At this stage a comparison is made with the known systems of the other thallium halides whose structures are well-established. The main system in each of these molecules occurs in the near ultraviolet with the system origin located at the most refrangible end ; if a similar feature is expected in the main system of thallium iodide and if intensity considerations and variations of the interval between the successive groups are also taken into account, it seemed that the strongest band at $\nu = 25780.0$ cm.$^{-1}$ may be the (0,0) band of the system. (2) The second difficulty is in respect of the magnitude of the values of ω' and ω'' ; several alternatives of choice are available ; the interval of 28 cm.$^{-1}$ between the nearly equi-spaced bands in each sequence suggested the approximate value of the difference between ω' and ω''. The individual values may be one of the following sets :—

90	120
120	150
150	180
180	210

Petrikaln and Hochberg (1933) have quoted (p. 229, table 14.) a value 150 for ω''. It is a common observation in band spectra that the vibrational constants are not much altered in the case of a row of heavy diatomic molecules, formed by a successive addition of an electron. The following table illustrates this feature in the halides of Au, Hg, Tl etc.

TABLE III

Ground State Constants

	Au	Hg	Tl	Pb	Bi
F	—	490.8	475.0	506 9	512.0
Cl	383	293.4	287 5	304.2	308.4
Br	—	186.3	192.1	207.5	209.5
I	—	125.7	121.0	—	163.9

TABLE IV

Vibrational Constants of Thallium Halides *

	ν_e	ω_e'	$x_e'\omega_e'$	ω_e''	$x_e''\omega_e''$
TlF	35180.7	439.8	8 60	475.0	1.89
TlCl	31054.2	216 9	6.80	287.5	1 24
TlBr	29191.5	108.3	5.15	192.1	0.39
TlI	25685.9	91.0	0.20	121.0	0 18

Table III suggests that for thallium iodide, the value of ω'' may be approximately either 150 cm.$^{-1}$ or 120 cm^{-1}. A further comparison of the ground and excited state constants of the thallium halides as shown in Table IV indicates that of these two probable values the latter *i.e.* 120 cm.$^{-1}$ is probably to be preferred, as it would simultaneously lead to an ω' value which is quite consistent with the corresponding values of the other halides. If 150 cm.$^{-1}$ be adopted for ω'', the value of ω'† will be 120 which is entirely out of step. Hence, of the different possible alternative schemes of the vibrational analysis of the bands, the authors have adopted the one which gives $\omega' \sim 90$ cm. and $\omega'' \sim 120$ units.

The classification of the bands arrived on the above basis is shown in the last column of Table I. It has been possible to include all the bands right up to λ 5300 into a single vibrational scheme, although, as will be seen later, a doubt exists regarding the classification of the bands in the extreme red.

VIBRATIONAL CONSTANTS AND ISOTOPE EFFECT

Confirmation of the vibrational analysis from a study of the isotope effect is desirable in dealing with systems of this type. But the difficulty has been that iodine has no isotopes. Thallium has two isotopes of mass 205 and 203 in the abundance ratio 2.4 : 1 and it should be possible to detect the weaker 203 isotopic head for the $Tl^{203}I^{127}$ molecule; particularly when band heads with very large vibrational quantum numbers are identified. For this purpose the vibrational constants for the system are derived as accurately as possible. The source of error, here arises from the absence of long progressions or sequences and the very low value of the anharmonic constant, apart from the uncertainty in the measurement of wavelengths due to diffuseness. A graphical method is made use of, trying to average out the discrepancies in the $\Delta G(v)$ values for both upper and lower states. Curves

* Values for TlI, contained in this table, are those obtained in the present work.

† A value of 30 may also be possible, but is equally out of step.

in Fig. 1 show the manner in which $\Delta G(v')$ and $\Delta G(v'')$ vary. If linear curves are drawn through the points, the estimated constants are

$$\omega_e' = 91.2 \qquad \omega_e'' = 121.2$$
$$x_e'\omega_e' = 0.10 \qquad x_e''\omega_e'' = 0.09$$
$$\nu_e = 25794.7.$$

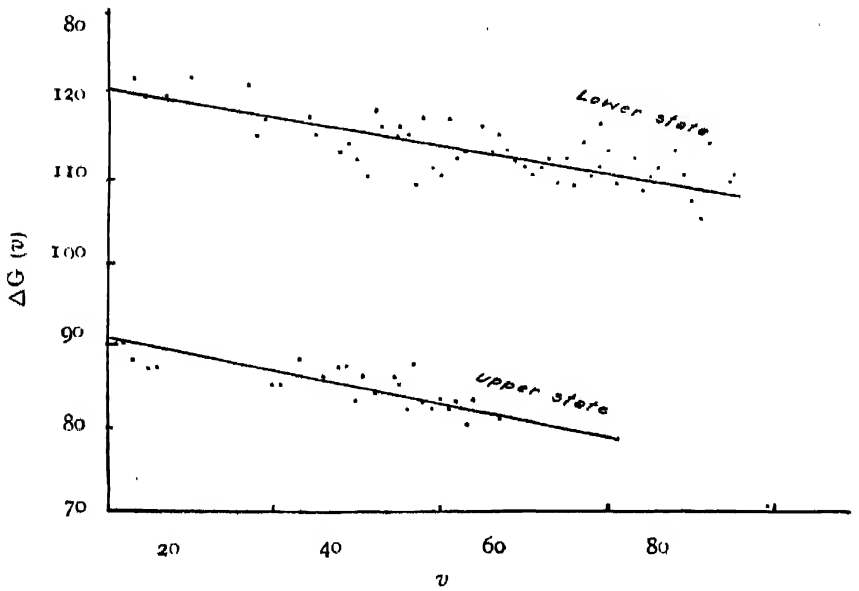

FIG. 1

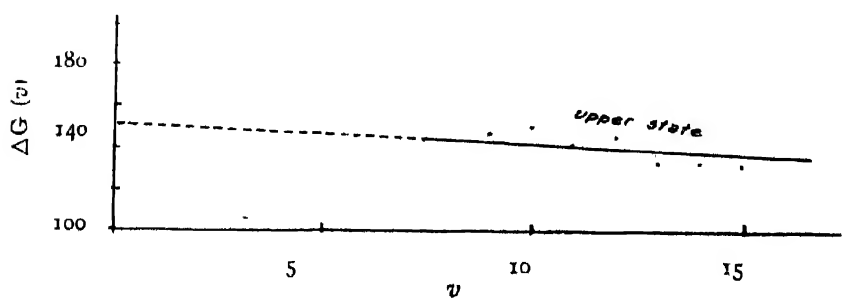

FIG. 2

The ν_e values calculated from bands spread-over the entire region of the spectrum seldom differ by more than 5 wave number units. Hence the usual quantum formula with the above vibrational constants represents the entire system.

Using the above approximate values of the vibrational constants and the factor $(\rho - 1) = 0.0019$ for the thallium iodide molecule, the isotopic separations given by the usual formula (Jevons' Report, p.213)

$$\nu' - \nu = (\rho - 1)\ (\omega_e' u' - \omega_e'' u'') - (\rho^2 - 1)\ (x_e'\omega_e' u'^2 - x_e''\omega_e'' u''^2) +$$

is calculated for a number of bands. The order of separation for bands at the extreme red is about six wave number units; *e.g.*, for the (39,58) and (49,73) bands it is 5·7 and 6·8 wave number units respectively. Plate VB, Fig. *f* is a concave grating spectrogram of the bands in the red region taken in order to identify the $Tl^{203}I^{127}$ isotopic heads. It is easily seen that the bands are extremely diffuse and unsuitable for measurement. But evidence is found in these bands either of a broadening or in several cases of the splitting of the head into two components with an estimated interval of the same order as the expected isotopic displacement. No further detailed study of the isotope effect has been possible in this system.

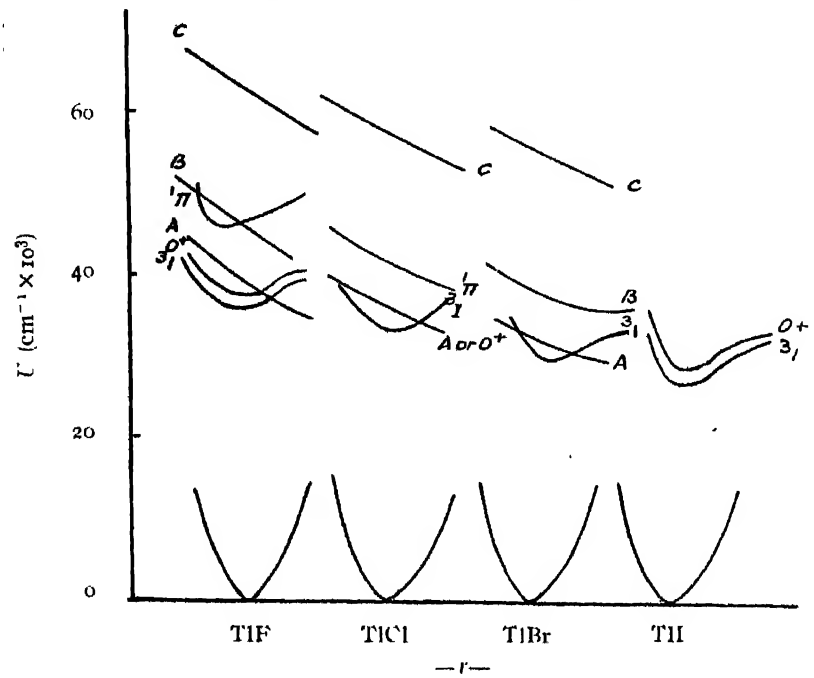

FIG. 3
Energy levels of TlF, TlCl, TlBr and TlI.

INTENSITY DISTRIBUTION

The intensity distribution among the bands, if the proposed analysis is correct, is an exceptional feature of the system. The distribution is represented in a vibrational matrix in Table V in which the visual estimates of intensity are shown in place of the wave numbers. A prominent difference between this and the other halide systems of thallium is noticeable in respect of this intensity distribution. Predissociation is detected in thallium fluoride, chloride and bromide bands; the upper state being cut off at a specific vibrational level which is different for the different molecules. This predissociation is considered as probably responsible for an indentical intensity distribution among the bands both in emission and absorption. In thallium bromide in particular, there are just six progressions which are observed up to

a very high value of v''. No evidence of predissociation exists in the thallium iodide system. Table V shows that bands occur involving high values of both v' and v'' This peculiar distribution may in part, arise from the absence of predissociation and may also be due to the low values of x_e for the ground and excited states and the relative magnitude of ω' and ω''. These latter constants are neither nearly equal which would lead to a narrow Condon parabola nor is their ratio too large or too small which would give a very wide and open parabola. The ratio is such that just a few bands alone may appear in a sequence or a progression.

If a curve is drawn through the more intense bands, we obtain, instead of the usual parabola, one in which one arm is exceptionally long. At the end of the system, the intensity distribution is erratic. It must be stated that due to this and the possible large errors in measurement, the classification of the bands in this region may be uncertain.

One view which prevailed from the outset owing to the exceptional intensity distribution was (Rao and Rao, 1948) to regard the system as made up of two different overlapping systems. The crowding of the bands and the rise in general intensity in the central portion of the system at about λ4300 (Refer Plate VA Fig. *a*) are suggestive of such a division. Just at this region, the origin of the second system may be situated with the system extending towards the red. But a more detailed examination revealed that at the red end of the system, the order of the intervals between the groups is about 110 cm.$^{-1}$. If these bands form part of a second system with the origin near λ4300, the value of 110 is too low, since the anharmonic constant is expected to be small, while, if they form part of an extensive system with the origin at λ3878, the value of 110 is of the right order of magnitude. It is because of this consideration and also of the difficulty, as discussed later, in interpreting the electronic transition of a brief system of bands observed on the violet end, that the view of the division of the main system into two components had to be abandoned. All the bands from λ3800 to λ5300 are regarded by the authors as a single system. (Rao and Rao, 1948).

ELECTRONIC STATES

Miescher and Wehrli (1934 and 1935), Howell and others (1937) discussed the electronic states of the halides of group III elements Al, Ga, etc., in relation to the observed band spectra. Holst (1934) and Jennergren (1948) have established the ground states of the molecules AlCl and AlBr as $^1\Sigma^+$. For the other molecules as well the ground state may be in all probability a similar $^1\Sigma^+$. Two systems are known in most of these molecules one of which is a singlet lying in the far-ultraviolet and the other a doublet system occurring in the near ultraviolet. Both have a common lower state $^1\Sigma^+$ arising from the electron configuration $\sigma^2\pi^4$. The excitation of one the π electrons produces the configuration $\sigma^2\pi^3\sigma$ giving rise to the molecular states $^1\pi$, $^3\pi_0^+$, $^3\pi_0'$, $^3\pi_1$ and $^3\pi_2$ (inverted). As shown by Howell for thallium flouride chloride and

TABLE V

Intensity distribution in the thallium iodide main system

v' \ v''	0	1	2	3	4	5	6	7	8	9	10	11	12	13	14	15	16	17	18	19	20	21	22
0	5	2																					
1	2	3	4																				
2	2	2	1	4	4																		
3	2	2	3	1	3	4																	
4	2	2	2				3																
5	2	2	2					2	3														
6		2	2							4													
7			2								3												
8												3	3										
9														4									
10															4	4							
11																	4						
12																		3	1				
13																			2	3			
14																				1	3		
15																						4	2
16																							1

v' \ v''	23	24	25	26	27	28	29	30	31	32	33	34	35	36	37	38	39	40	41	42	43	44	45
16	4																						
17		5																					
18			2	5																			
19					4	2																	
20						3	3																
21							1	3	0														
22									3	1													
24											1	3		1									
25												4	2	1									
26													2	5	2								
27														4	3								
28															3	3		3					
29																3	5		3				
30																	3	2		5			

v' \ v''	44	45	46	47	48	49	50	51	52	53	54	55	56	57	58	59	60	61	62	63	64	65	66
31	1	3	4	5		3	2																
32			4	3	3	4	4	3															
33				4	3	3	3	2	4														
34					3	2	3	2	2	5	4												
35								2			2	4											
36									1			2	3	5	1								
37													1	2	3	3							
38															1	3	5						
39																1	3	4	2				
40																			3	3			
41																				2	3	3	
42																					2	5	3
43																							4

v' \ v''	67	68	69	70	71	72	73	74	75
43	4		2						
44		5	2	2					
45			1	5	2				
46					2	2			
47							3		
48								2	

Table VI

Vibrational analysis of $^3\pi_{0^+} - {}^1\Sigma^+$ system of thallium iodide

v' \ v''	0	1	2	3	4	5	6	7	8	9	10	11	12	13	14	$\Delta G'(v')$
0	27100.9															
1		27129.5														
2			27157 1													
3				27182 0												
4					27209.7											
5						27234.4										
6							27262.0									
7								27286.3								
8								27430.0	27310.3							143.7
9									27456.9							146.6
10										27334.						149 9
11										27484 0	27360.0					140.7
12										27619 1	27506.2	27387.2				145.4
13											27644.7	27539 5				132.9
14												27672.4	27567.9			133.4
15													27701.3			132.4
16													27833 7	27725.7		135 8
17														27862.5	27885.1	
$\Delta G''(v'')$									119 7	122 8	118 5	112 1	104 5	107.0		

bromide, the singlet system may be identified as $\sigma^2\pi^3\sigma$, $^1\pi - \sigma^2\pi^4$, $^1\Sigma^+$ and the doublet system as a forbidden transition $^3\pi_0{}^+ - {}^1\Sigma^+$ and $^3\pi_1 - {}^1\Sigma^+$. The singlet system is predominant in the alluminium, gallium and indium halides and the doublet system is either absent or poorly developed, while for TlF, the two systems are of equal intensity. Such a relative intensity behaviour is consistent with the above assignment of transitions and indicates, as Howell remarked, that the binding from Ga→In→Tl approaches more and more to Hund's case (*c*) as the molecule gets heavier.* In the heaviest molecules of this type, namely TlI, one has therefore to anticipate the predominance of the forbidden transitions $^3\pi_0 - {}^1\Sigma^+$ and $^3\pi_1 - {}^1\Sigma^+$. On this account, it was at first considered probable that the extensive system observed for TlI in the appropriate wave length region might consist of two overlapping components.

Further scrutiny of the plates has revealed a second short region between λ3680 − λ3600 in which distinct band heads, overlaid by a continuum, are observed. These consist of four groups of nearly equi-spaced components with an interval of about 28 units. The four groups appear to be different sequences, the strongest of them at λ 3670 perhaps being the $\Delta v = 0$ sequence. The interval of 120 cm.$^{-1}$ also exists between certain heads in these groups which is of the same order as that of the lower state of the main system. There is an impression of a degradation of the bands in the direction of shorter wave lengths. With the aid of these regularities, the vibrational scheme in Table VI has been set up which includes all the band heads. Wave length and other data of these bands are given in Table II. The following approximate constants have been determined from the analysis, and curve in Fig 2.

$$\nu_{(0,0)} = 27101\ ;\ \omega_e' \sim 151\ ;\qquad 120.$$

If the main system is treated as itself comprising of the two components $^3\pi_0{}' - {}^1\Sigma^+$ and $^3\pi_1 - {}^1\Sigma^+$, the interpretation of the brief system becomes difficult. On the other hand when the main system, in spite of its unusual intensity characteristics, is regarded as a single component due to the transition $^3\pi_1 - {}^1\Sigma^+$, the brief system may be the other component $^3\pi_0{}^+ - {}^1\Sigma^+$. Such an interpretation would give the $^3\pi$ interval as 1321 cm.$^{-1}$, which is quite in keeping with the corresponding intervals in the other halides as shown in Table VII.

Further, the characteristic features of this brief system are intrinsically such as to support this view. While for example in TlF both the components are observed consisting of band heads, in TlCl and TlBr this second component may presumably be a repulsive predissociating state. The diffuseness of the bands overlaid by a continuum and the fragmentary development of the

* When the coupling is of this type, the states $^3\pi_0{}^+$ and $^3\pi_1$ should be denoted as $^3{}_0{}^+$ and $^3{}_1$.

system may hence be consistent with the assignment of the system as $^3\pi_0^+ - {}^1\Sigma^+$.

TABLE VII

	Al	Ga	In	Tl
F	—	—	—	1682
Cl	—	332	796	(1107)*
Br	—	370	786	(872)*
I	199	330	649	1321

* Approximate estimates from the continua.

A schematic diagram of the electronic transitions for the halides of thallium is given in Fig. 3 which is an extension of those presented by Howell.

Bands due to the transition $^1\pi - {}^1\Sigma$, if they are present in TlI, are yet to be discovered. They are not found in emission under the conditions in which they are photographed in this work. Absorption experiments too, which are in progress, may not be expected to reveal this system.

ANDHRA UNIVERSITY,
WALTAIR.

REFERENCES

Butkow, 1929, *Zeit. f. Physik.*, **58**, 232.
Holst, 1934, ,, ,, **93**, 65.
Howell, 1937, *Proc. Roy. Soc.*, **160**, 242.
Howell and Coulson, 1938, *Proc. Roy. Soc.*, **166**, 238.
,, ,, 1941, *Proc. of. Phy. Soc.*, **53**, 706.
Jennergren Carl Gustav, 1948, *Nature*, **161**, 315
Miescher and Wehrli, 1934 *Helv. Phy. Acta.*, **73**, 298.
,, ,, , 1935, ,, ,, **8**, 279.
Petrikalu & Hochberg, 1933, *Zeit. f. Physik* , **86**, 214.
Ramasastry, 1947, *Ind. Jour. Phys.*, **21**, 272.
Rao Tiruvengauna & Rao, K. R , 1948, *Curr. Sci.*, **17**, 121.
,, ,, **17**, 182.

THE NEAR ULTRA-VIOLET SPECTRA OF BENZENE PART I. THE EMISSION BANDS

By R. K. ASUNDI AND M. R. PADHYE

Plate VI

ABSTRACT. An emission spectrum of benzene in the near ultraviolet is excited by a transformer discharge through flowing benzene vapour. The spectrum which was previously recorded by Austin and Black, and Asundi and Padhye, has been considerably extended and a large number of bands, 200 or more, have been photographed and measured on suitable instruments. A full analysis of the bands is proposed which is on the basis of that of the absorption spectrum of benzene by Sponer *et al.* The results afford further proof of the correctness of the theoretical deductions regarding this molecule and its excited levels put forward by Hückel Sklar, Pauling and others. The main results of the present investigation are the following :

(1) The emission spectrum obtained is the counterpart of the corresponding absorption spectrum, the transition involved being $B_{2u} \rightarrow A_{1g}$.

(2) As is to be expected, the spectrum yields much more information about the ground state of the molecule than either absorption or fluorescence spectrum.

(3) It also exhibits a pronounced development of doublets due to Fermi resonance between the two vibrations 1596 cm^{-1} (e_g^+) and 606 cm^{-1}+ 992 cm^{-1} $^+a_{1g}$) which are traced up to four quanta of 992 cm^{-1}. These are further associated with five quanta of 160 cm^{-1} difference frequency.

INTRODUCTION

The structure of benzene a hydrocarbon discovered by Faraday in 1825 has been a difficult problem from the very beginning and it was not until 1865 that Kekule first arrived at the conception of the benzene hexagonal ring or a closed chain of six carbon atoms with six hydrogen atoms all similarly situated. From time to time many other structural formulae have been suggested to explain the characteristic properties of benzene but with the advance of the concept of structural resonance it is now clear, *e.g.*, Pauling (1948) that all of them can be represented by eigenfunctions which are linear combinations of some or all of the following five cannonical structures which, in fact, contribute to the normal benzene molecule :

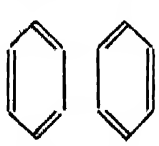

Kekule 2

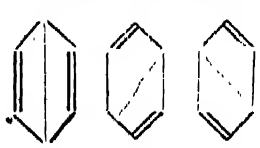

Dewar 3

The molecule acquires greater stability as a result of resonance among these five independent structures but it is interesting to find that approximately 80% of the resonance energy comes from the two Kekule structures alone.

The conception of resonance is a development which is of importance for aromatic ring molecules and for molecules with conjugated double bonds. In the case of benzene, Hückel (1931) and more directly Pauling and Wheland (1933), and Sklar (1937; 1942) have attempted to develop the theory quantitatively. Assuming that the benzene molecule has symmetry D_{6h}, these authors show that the two Kekule and the three Dewar formulae represent cannonical structures from a linear combination of whose wave functions, five electronic energy levels result for the molecule. Thus on account of structure resonance the different energy states split up and are recognised and obtained in terms of the exchange integral which can be calculated from thermochemical data.

Similar calculations have been done by Goeppert-Mayer and Sklar (1938), Mulliken (1939) and others based on the molecular orbital approximation. They treat it essentially as a six electron problem and examine the excitation of one of the electrons to the next orbital. The values obtained for the energy of the different electronic states agree in both cases after slight modifications are made to suit this particular problem. Sklar also classified the symmetries of the resulting electronic states from group theoretical considerations.

These theoretical developments were well explained on the experimental basis in a paper on the near ultraviolet absorption band system of benzene by Sponer, Nordheim, Sklar and Teller (1939). This work was followed by Sponer and many other investigators who have interpreted the absorption spectra of hexadeuterobenzene and various derivatives of benzene on similar lines. Attempts to interpret the absorption and fluorescence spectra of benzene have been made quite early by Henri and others. But obviously the results are of little interest from the present standpoint.

In recent years apart from the fluorescence and resonance emission (Ingold and Wilson, 1936) the only data on the emission spectrum of benzene have been those of McVicker, Marsh and Stewart (1923) and, Austin and Black (1930). These authors produced the spectrum by Tesla discharge through flowing benzene vapour with external and internal electrodes respectively. The wavelength data of the former workers are few and accurate to one angstrom unit. The data of the latter are more in number comprising nearly 100 band heads; the accuracy claimed is about $\pm$ 3 cm^{-1}. The number of multiatomic molecules which yield emission spectra is rather very limited. The recent advances in the theory of the benzene near ultraviolet absorption spectrum prompted us to reinvestigate the emission spectrum. A preliminary account of the results obtained in earlier experiments using a Hilger medium quartz spectrograph has already appeared (Asundi and Padhye, 1945). Later, it has been possible to extend the band system considerably towards longer waves and photograph the much more enriched spectrum consisting of 200 or more band heads with a Hilger E_1 quartz spectrograph. An account of these investigations forms the subject matter of the present paper.

EXPERIMENTAL PROCEDURE

It was found that in addition to high frequency (h.f.) discharges either from a Tesla coil or a suitable oscillatory circuit, also an ordinary transformer discharge excites the emission spectrum of benzene, so long as the vapour is continuously renewed. A discharge of any of these sources in the stagnant vapour of benzene gives only the usual spectra of CO, C_2 and CH associated with carbon compounds. It is, therefore, essential to have the discharge run through a properly regulated flow of benzene vapour. In the present experiments the high frequency oscillations (190—400 metres) generated in a modified Hartley circuit with external electrodes as also a transformer discharge with internal electrodes have been used to excite the spectrum.

The discharge tube was hence constructed to suit the two types of excitations. It consists of a simple π type tube about 35 cm. in length and 1.5 cm. in diameter. The electrodes were cylinders of aluminium attached to platinum seals, the distance between the electrodes being about 20 cm. or even more in some cases. A quartz window was attached at one end while the other end was sealed off., Since it was desired to maintain a continuous regulated flow of benzene vapour through the tube, two side tubes with high-vacuum stop-cocks were attached to the two ends of the tube, one of them being as near the window as possible so that the possibility of reabsorption by unexcited vapour is minimised. A bulb containing liquid benzene was attached to the discharge tube which was exhausted by means of a high vacuum pump through, or in some cases without, proper absorbing agents. The apparatus was firmly mounted on a wooden stand and was portable.

To start with, the discharge obtained in the case of stagnant vapour with h.f. oscillations was line-like with a greenish blue colour in the region between the two external electrodes which were about 1.5 to 3 cms apart. After some time the discharge took the form of a rotating spindle devoloping bluish tails on both sides extending beyond the external electrodes. The tails then gradually disappeared and the discharge grew brighter. In this condition the discharge gave prominently the well-known Angstrom bands which were originally scarcely visible. Accordingly, the spectrum was photographed by renewing the benzene vapour in the tube occasionally before the discharge turned bright, in which case the benzene bands with only a few Angstrom bands in the visible region were registered on the plates which were free particularly from the third and fourth positive carbon bands in the ultra-violet. Some plates were also taken when the discharge was passing through continuously flowing vapour. In this case the flow was regulated so that the discharge always remained in the first or second stage of its development mentioned above. The plates registered only the benzene bands in the ultra-violet with no trace of any of the carbon bands, even the Angstrom bands in the visible being completely absent. The discharge brings about a plastic deposit of a dark reddish brown colour on the walls of the tube. The inten-

sity of the discharge is low and the usual time of exposure needed to get a good plate on a medium quartz spectrograph was of the order of 15 hours.

The transformer discharge could be used only with the continuously flowing vapour. In stagnant vapour the discharge very quickly gets to the bright type giving only the carbon bands. The flow of vapour was adjusted so that the discharge always remained of a particular colour and brightness. The plastic deposit on the walls of the tube due to the discharge made it rather difficult to be sure of this adjustment. The rate of deposit was greater than in the h.f. discharge. After every two or three exposures, each of about four or three hours duration, the deposit had to be scraped off the tube and the window and tube cleaned with benzene. The intensity of the discharge was very much greater than in the h.f. discharge, the usual time of exposure on the same medium quartz spectro-graph being of the order of 2½ hours. The spectra could, therefore, be photographed on a bigger E_1 instrument where the time of exposure was of the order of 4 hours.

Since the bands attributed to benzene emission lie in the ultraviolet region, the work was confined to this region only. Several plates were taken with a Hilger medium quartz spectrograph. The dispersion of the instrument round about 2600 Å is nearly 10 Å per mm. Some plates were also taken with the same instrument with the transformer discharge. The other instrument used was a Hilger E_1 quartz spectrograph (Littrow mounting). Plate VII gives the reproductions of two typical plates taken with this instrument for the transformer discharge through flowing benzene vapour, the exposure time being about three hours. The dispersion of this instrument in the 2600Å region is about 3Å per mm. These plates show an extension of the emission band system by three more groups on the longer wave-length side. Kodak B 20 and Ilford special Rapid plates were used throughout the present investigations. The liquid benzene (b. p. 80°C) supplied by the Fine Chemicals Section of this University was used without further purification.

All the spectra taken were centrally superposed by the spectrum of either a copper or an iron arc taking about two amperes on 220 D.C. This served as a source of standard lines for measuring the plates. Plates were measured on a Hilger comparator whose least count is 0.0001 cm. As the whole range of the spectrum could not be measured in one stretch, the spectra were measured in two shifts. A low power adjustable objective was used and the readings refer to the sharp head of each band. Three plates were measured and the mean of the three wavelengths was taken and converted to wave-numbers in vacuo using Kayser's Tabellen. The average error between calculated and observed readings is about 3.5 wave-numbers in the case of strong bands and about 6 wave-numbers in the case of the weaker bands. The results are recorded in Table I, in which column 2 gives the band heads in terms of wave-numbers in vacuo observed in the present investigations, column 1 gives the wave-numbers as reported by Austin and Black. On the average, our readings show an excess of 5 wave-numbers over their readings.

TABLE I

Emission band heads of benzene

ν_{vac} cm^{-1} by Austin and Black	ν_{vac} cm^{-1} in present expts.	Int.	Assignments	ν_{vac} cm^{-1} of absorption bands Radle & Beck
39335	39335	4	$B^0_{2,0}+520+2\times364$	39330.6
39245	39248	2	D^0_2, E^2_0	39248
39179	39177	2.5	B^1_2	39173
	39156 (?)	3		39159
	39095 (?)	4	G^0_0, D^1_2	39092
	38571	2	$0+2\times240$	38580
	38529	0	C^0_0	38523
38411	38413	8 5	B^0_1	38407
	38353	2	a^0_2, C^1_0	38359.7
38321	38323	5	D^0_1	38316.6
	38295	2	$C^1_{1\ 1}$, A^2_0	38292.3
38250	38245	2.5	B^1_1	38245.4
	38233	1	$C^1_{2\ -2}$	
38159	38160	2.5	D^1_1	38154
	38145	2.5	$C^2_{1\ -1}$, $1^0_{\ -1}$	38141.3
38086	38088	3	$\underline{(0,0)}$, B^2_1	38089.4
	38061	.5	$C^2_{2\ 2}$	38064
38014 / 37996	38003	1.5	D^2_1, $0+520-606$	38000
	37975	1.5	$1^1_{\ -1}$	37976
	37963	2	$B^0_0+2\times240$	37962 6
	37933	1	H^0_0, $0-1178+2\times513$	37926
	37886	1	$D^0_0+2\times240$	
37843	37852	1	D^3_1	
	37818	1.5	$0-849+586$	37814
	37788	1	$0+1045-2\times671$	37795
37756	37754	2.5		
	37683	0	D^4_1	37678
	37652	1		37651 2
37618	37624	3	$A^0_{\ -1}$	37616.8

TABLE I (*contd.*)

ν_{vac} cm^{-1} by Austin and Black	ν_{vac} cm^{-1} in present expts.	Int.	Assignments	ν_{vac} cm^{-1} of absorption bands Radle & Beck
	37558	2	$0+1476-2\times1010$	
37532	37533	2	$C^0{}_{-1}$	37532.6
37478	37489	10	$B^0{}_0$	37481.9
37455	37443	0	$A^1{}_{-1}$	37452.5
	37428	0	$\alpha^0{}_1$	
37393	37399	6	$D^0{}_0$	37392.9
	37365 (?)	0	$C^1{}_{-1}$	37366
37321	37327	6.5	$B^1{}_0$	37326.8
	37285	2	$A^2{}_{-1}$, $0-2\times404$	37289 9
37238	37240	4	$D^1{}_0$	37234.1
37224	37224	4	$0-1596+2\times361$ $0-606+584-849$	37230.2
	37204	0	$C^2{}_{-1}$, $0+520-2\times703$	
37161	37167	5	$B^2{}_0$	37160.4
	37136	0	$A^3{}_{-1}$	
37078	37087	3	$D^2{}_0$	37081
	37052	1	$C^3{}_{-1}$, $0-606+265-160$	37056 8
	37024	1.5	$\beta^2{}_{2-1}$, $0+520-606-992$	37016.1
37002	37008	2	$B^3{}_0$	37000.9
36995	36995	2	$0-606-2\times703+923$	36990.7
	36979	2	$\alpha^0{}_0+2\times240$	
36956	36961	2	$\beta^0{}_0+2\times240$	
36921	36917	0	$D^3{}_0$	36925
	36891	1	$0-606-265-2\times160$	36886
	36867	.5	$\beta^3{}_{2-1}$	36866
	36847 (?)	1	$D^3{}_{1-1}$	
36835	36840	0	$B^4{}_0$	36841
36773	36777	1	$II^1{}_{-1}$	36772
	36758	1	$D_0{}^4$	36750
	36723	.7		
	36689	0	$B^5{}_0$	
	36665	1	$0+520-2\times976$	36668
36624	36634	2.5	$A^0{}_{-2}$	36624.7

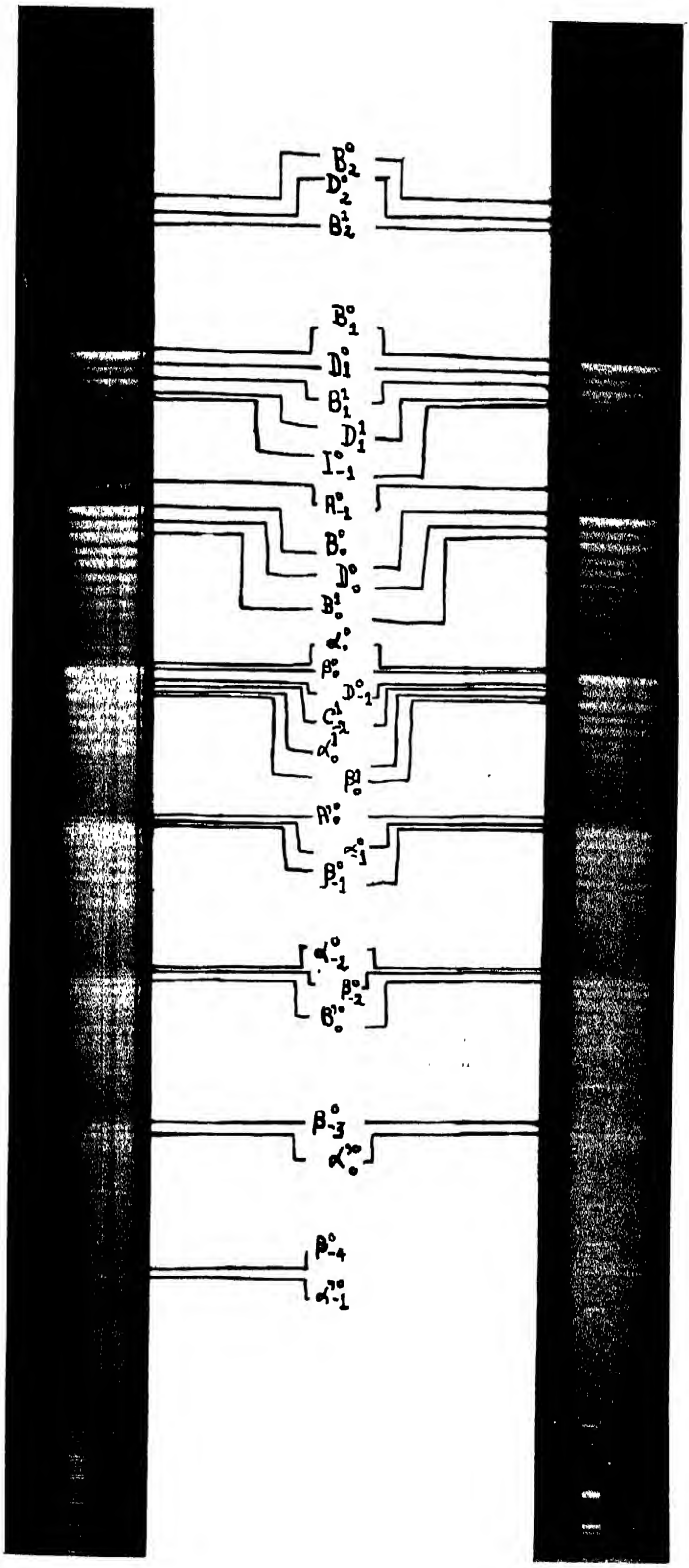
B^0_2
D^0_2
B^2_2
B^0_1
D^0_1
B^2_1
D^2_1
I^0_{-1}
A^0_{-1}
B^0_0
D^0_0
B^2_0
α^0_0
β^0_0
D^0_{-1}
C^1_{-2}
α^1_0
β^1_0
A^0_0
α^0_{-1}
β^0_{-1}
α^0_{-2}
β^0_{-2}
G^0_0
β^0_{-3}
α^{00}_0
β^0_{-4}
α^{00}_{-1}

TABLE I (*contd.*)

ν_{vac} cm^{-1} by Austin and Black	ν_{vac} cm^{-1} in present expts.	Int.	Assignment	ν_{vac} cm^{-1} of absorption bands Radle & Beck
	36590	1	$0+520-2\times1010$	
36557	36568	3	C^0_{-2}	
36532	36544	3·5	$0-703-849$	36538
36497	36504	8	α^0_0	36496.2
36478	36486	8	β^0_0	36478
36436	36442	2	α^0_{1-1}	
36413	36421	3·5	β^0_{1-1}	36413 7
36388	36398	5	D^0_{-1}	36387.8
	36371 (?)	3	C^1_{-2}, α^0_{2-2}	
36337	36343	4·5	α^1_0	36342
36317	36325	5	β^1_0	
	36301	0	A^2_{-2}	
36275	36276	1	α^1_{1-1}	
	36263 (?)	4(?)	$0+1476-2\times1648$	
36251	36254	2	B^1_{1-1}	36254
36239	36238	3	D^1_{-1}	36233
	36206	2	C^2_{-2}, $0-606-265-992$	
36176	36182	2 5	α^2_0	36174
36157	36166	3·5	β^2_0	36158
	36142	0	A^3_{-2}, $0-606-2\times671$	
	36096	2	β^2_{1-1}	
36068	36073	2	$0-606-2\times703$, D^2_{-1}	
	36052	0	C^3_{-2}, α^2_{2-2}	
36020	36033	1	α^3_0	
	36006	1.5	β^3_0	
	35983	1.5	$0-606-2\times671-160$	
	35959	0	$0+520-2\times1326, K^0_1$	
	35924	0	D^3_{-1}, β^3_{1-1}	
	35871	1	α^4_0	
	35848	1	β^4_0	
35839	85838	0		

TABLE I (*contd.*)

ν_{vac} cm^{-1} by Austin and Black	ν_{vac} cm^{-1} in present expts.	Int.	Assignments	ν_{vac} cm^{-1} of absorption Radle & Beck
	35801	1	$K^1{}_1$, 0−606−2×849	
	35759	·5	0−3047+2×364	
35701	35711	1.5	$a^5{}_0$	
	35672	0	$\beta^5{}_0$	
	35645	1		
	35601 (?)	0		
35569	35580	1.5		
35548	35556	3.5	$C^0{}_{-3}$, $A'^0{}_0$	
35511	35517	5	$a^0{}_{-1}$	
35485	35492	7	$\beta^0{}_{-1}$	
35450	35455	4	$a^0{}_{1-2}$	
	35425	4	$\beta^0{}_{1-2}$	
35417	35415	4	$D^0{}_{-2}$	
35391	35391	3	$C^1{}_{-3}$, $A'^1{}_0$	
35349	35356	3	$a^1{}_{-1}$	
	35330	4.5	$\beta^1{}_1$	
35322	35316		0+520−2×1648	
35289	35293	1	$a^1{}_{1-2}$, $a'^0{}_2$	
35269	35264	2.5	$\beta^1{}_{1-2}$, 0−606−2×1110	
35227	35231	2	$C^2{}_{-3}$, $A'^2{}_0$	
35188	35193	2	$a^2{}_{-1}$	
	35169	4.5	$\beta^2{}_{-1}$	
35094	35085	2	$A'^3{}_0$, 0−1596−2×703	
35041	35038	2	$K^0{}_0$	
	35007	1	$\beta^3{}_{-1}$	
34985	34972 (?)	1	$a'^2{}_2$	
	34925	·5	$A'^4{}_0$	
34875	34877	·5	$K^1{}_0$	
	34831	0	0−606−2×1326	
	34812 (?)	0	$a'^3{}_2$	
	34797	0	0−1596−2×849	

TABLE I (*contd.*)

ν_{vac} cm^{-1} by Austin and Black	ν_{vac} cm^{-1} in present expts.	Int	Assignments	ν_{vac} cm^{-1} of absorption Radle & Beck
	34754	1		
	34714	1.5	$K^2{}_0$	
	34592 (?)	0		
	34565	2	$C^0{}_4$	
	34546	1	$A^{10}{}_1$, $0-1596-2\times970$	
34526	34530	3	$\alpha^0{}_{-2}$	
34496	34501	4-5	$\beta^0{}_{-2}$	
34465	34473	4	$0-1596-2\times1010$	
34428	34432	5 5	$B'^0{}_0$, $D^0{}_{-3}$	
	34394	3 (?)	$C^1{}_1$, $A'^1{}_1$	
34364	34371	3	$\alpha'^0{}_1$, $\alpha^1{}_{-2}$	
34331	34338	3	$\beta^1{}_{-2}$, $D'^0{}_0$	
34301	34309	1	$\alpha'^0_2{}_{-1}$	
34264	34271	2	$B'^1{}_0$, $D^1{}_{-3}$	
34230	34238	1	$A'^2{}_{-1}$, $C^2{}_{-4}$	
34203	34208	1	$\alpha^2{}_{-2}$, $\alpha'^1{}_1$	
	34176	3	$\beta^2{}_{-2}$, $D'^1{}_0$, $0-606-2\times1326$	
	34139 (?)	1	$\alpha'^1_2{}_{-1}$	
	34122 (?)	0	$\beta^2{}_{1-3}$	
	34106	1	$B'^2{}_0$, $D^2{}_{-3}$	
	34094	0	$A'^3{}_{-1}$	
	34046	1.5	$\alpha'^2{}_1$, $K^0{}_{-1}$	
	34018	0	$\beta^3{}_{-2}$	
	34011	.5		
	33983	1	$\alpha'^2_2{}_{-1}$	
	33930	0		
33876	33885	1.5	$K^1{}_{-1}$	
	33832	0	$\alpha'^3_2{}_{-1}$	
	33726	0	$K^2{}_{-1}$	
	33575 (?)	0	$A'^0{}_{-2}$	
33540	33549	1.3	$\alpha^0{}_{-3}$ (?)	

TABLE I (*contd.*)

ν_{vac} cm^{-1} by Austin and Black	ν_{vac} cm^{-1} in present expts.	Int.	Assignments	ν_{vac} cm^{-1} of absorption Radle & Beck
33507	33512	3	$\beta^0{}_{-3}$	
33481	33490	3		
33440	33450	4	$\alpha'^0{}_0$	
	33434	4	$\beta^0{}_0$	
	33425	2	$D^0{}_{-4}$	
33378	33384	2.5	$\alpha'^0{}_{-1}$, $\alpha_-{}^1{}_3$	
33340	33347	0	$\beta_-{}^1{}_3$	
33280	33287	2	$\alpha'^1{}_0$	
33182	33189	0	$\beta^2{}_{-3}$	
	33136	0	$\alpha'^2{}_0$	
33118	33112	0	$\beta'^2{}_0$	
	33060 (?)	0	$K^0{}_{-2}$	
	32995	0		
	32978	0	$\alpha'^3{}_0$	
	32933 (?)	0		
	32890	0	$K^1{}_{-2}$	
	32819	0	$0-3047-2\times1110$	
32748	32740 (?)	0	$K^2{}_{-2}$	
32664	32675 (?)	0		
32582	32591	0		
32519	32524	1.5	$\beta_-{}^0{}_4$	
32457	32468	1.5	$\alpha'_-{}^0{}_1$	
32399	32406	2		
	32351	1	$\beta^1{}_{-4}$	
	32331	0		
32300	32295	.5	$\alpha'_-{}^1{}_1$	
	32263	0		
	32237	0		
	32210	0	$\beta_-{}^2{}_4$	
	32152	0	$\alpha'_-{}^2{}_1$	
	32099 (?)	0		
	32008	1		
	31935	0	$0-2\times3080$	
	31834	0		
	31812	0		
	31762	0		
	31671	0		
31654	31647	0		
	31599	0		
	31540	0		
	31483	1		
	31474	0	$\alpha'_-{}^0{}_2$	
	31428	0		

This discrepancy can be accounted for if due account is taken of the difference in the methods of measurement. They have taken the mean of the readings taken once when the microscope was moving forward and once when moving backward and they have pointed out that the difference in two readings was about 0.25 Å and never exceeding 0.5 Å. We have, however, measured the sharp band head which lies to the shorter wavelength side of the estimated centre of the band, the position to which their reading in fact corresponds. Column 3 Table I gives the visually estimated intensities of the bands relative to the strongest band as having an intensity 10. In the last column of the table the probable assignment is given in terms of the notation

first used by Sponer, Nordheim, Sklar and Teller in their analysis of the absorption spectrum. In the next column are recorded the wave-numbers of the corresponding absorption bands as given by Radle and Beck. The analysis is discussed in the next Section.

ANALYSIS

The ultimate analysis of the bands assigning them to various series is indicated in column 4 of Table I. The notation adopted is the one that has been used by Sponer *et al* in the analysis of the absorption system. The absorption system has been measured by a number of investigators and more recently by Radle and Beck (1940). Their values have been used by Sponer *et al* to show the general course of the analysis of the bands. In the course of the present work on emission bands where some of the bands are common to both the spectra it was found necessary to effect a detailed analysis of the absorption bands. This was done using Radle and Beck's data. In the meantime a similar analysis of the same data was published by Garforth and Ingold (1948.)* The general considerations which govern the analyses may be described as follows :—

Although the energies of the different electronic levels of benzene due to structural resonance splitting were obtained by various authors, the exact symmetry characters of the excited states were first calculated by Sklar on the assumption of the D_{6h} symmetry for benzene molecule. The ground state of the benzene molecule is one of total symmetry A_{1g} (Mulliken-Placzek notation). From the group theoretical considerations the symmetries of the electronic excited states of the molecule have been shown to be B_{1u}, B_{2u}, E_u, the last one being doubly degenerate. The ultraviolet band system in 2600Å region has been attributed to $A_{1g} \rightleftharpoons B_{2u}$ transition, the calculated energy of which is about 5 e.v. The emission bands under investigation appear to be the counterpart of the absorption bands.

This transition, however, is normally a forbidden one on the following considerations. Transition between two states (*e.g.* an excited and a ground state) with emission or absorption of light occurs only if the integral of at least one component of the electric moment P multiplied by the eigenfunctions of the ground and the excited states does not vanish, *i.e.*, $\int \psi'_{el} P \psi''_{el} d\tau_{el}$ is different from zero. Since the transformation properties of the electric moment P transform in the same way as translation, this rule may also be stated as that the direct product should contain a term which transforms like one of the translations, the direction of which determines the transition moment. Thus in the case of benzene, the component of electric moment z perpendicular to the plane of the ring transforms like B_{1g}; (A_{1g} A_{2u} $B_{2u} = B_{1g}$); while the in-plane components (x and y) transform like E_g^+; (A_{1g} E_u $B_{2u} = E_g^+$). Accordingly the transition between the two elec-

* This paper came to hand after the work was forwarded for publication.

tronic vibrationless levels A_{1g} and B_{2u} is forbidden. It can, however, be made allowed by the superposition of b_{1g} or c_g^+ vibration* on any one of the electronic levels for then the transformation condition will be satisfied Since in benzene the vibration of the symmetry type b_{1g} does not exist, the main part of the spectrum has to be explained as 0-1 or 1-0 transitions of the four c_g^+ vibrations upon which the progressions of totally symmetrical frequencies a_{1g} are superposed to any number of quanta limited only by the Boltzmann distribution and the Franck-Condon principle.

Benzene has four c_g^+ vibrations whose frequencies are 606, 1178, 1596 and 3047 †. The near ultraviolet absorption spectrum of benzene has been shown by Sponer *et al* and in more detail by Garforth and Ingold (1948) to correspond to the deductions given in the above discussion.

One main difference between the absorption spectrum and the emission spectrum may, however, be noted at the outset. The absorption spectrum shows predominantly the excitation of the excited state frequencies, while in the emission spectrum it is the ground state frequencies which are mainly excited. This means, in the notation employed, that in absorption, bands with the positive subscript as A_1, A_2, B_1 etc., and in emission the bands with negative subscript as A_{-1}, A_{-2}, B_{-1} etc., will be predominant, the subscripts themselves denoting the changes in the quantum number of the totally symmetrical C vibration 992 in the ground state and of 923 in the excited state. This is in fact what is observed, (see Table III). The superscripts refer to the difference frequency of 160 cm^{-1} superposed on the main transition.

The emission spectrum of benzene obtained in the present experiments extends from 2535Å to 3170Å. A reproduction of the spectrum is given in Plate I. The spectrum shows eight distinct groups of bands which are very well separated from one another and occur like the well separated sequences of bands in a typical diatomic molecule. They, however, lose their distinct sequence character on the longer wavelength side and the groups run into one another. The bands show sharp heads and are degraded towards the longer waves. Some of the weaker bands on the longer wavelength side do not show any pronounced heads. The groups have successive bands 160 cm^{-1} apart. Within the group there is also a parallel group with weaker intensity, the bands belonging to which lie in between the strong bands. In the second group at 2602Å, such a group is formed by the alternate bands belonging to B and D series. In the third group starting from 2666Å the alternate bands are B_0^0 and D_0^0 and are followed by 160 cm^{-1} progression. The bands in the fourth group show two heads which are in fact doublet bands due to the phenomenon of Fermi resonance between

* Following Sponer, capital letters are used to denote the symmetry properties of the electronic states and small letters to denote those of the vibrations.

† Throughout the paper the figures for frequency represent wavenumbers in cm^{-1} unit.

the vibrations 1596 $e''_{\parallel}$ and 992 $a_{1\parallel}$ 606 $e''_{\perp}$ = 1598 $e''_{\perp}$. The first bands of the following groups are due to superposition of 992 $a_{1\parallel}$ frequency on these Fermi—split levels.

The A''_0 band at 38609 is the strongest band in absorption but in emission its presence is doubtful. A''_{-1} and even perhaps A''_{-2} appear in the emission spectrum with moderate intensity, the first one at 37624* and the second at 36634. Both are loaded with one to four quanta† of the 160 difference frequency between 400 and 240 (Table IV). The band at 37489 which is the strongest in the emission spectrum is the B''_0 band (marked in Plate VI). It is further loaded with one to five quanta of 160 the difference frequency. There are two more positive members B''_1 and B''_2 at 38413 and 39335 respectively corresponding to one or two quanta of 923 ($a_{1\parallel}$) totally symmetric C vibration in the excited state. The C''_0 band at 38523 is present in plates taken with the smaller dispersion instrument and also in some plates taken with the bigger dispersion instrument but the intensity is very low. The negative members C''_{-1}, C''_{-2}, C''_{-3} and perhaps C''_{-4} are present as assigned in the table at 37533, 36514, 35556 and 34565. The C''_{-1} band lies very near B''_0 band and hence the intensity estimation may not perhaps be correct. The C''_{-3} band blends with another band. Generally the intensity of these negative members is greater than that of the C''_0 band. There are some combination bands $\Delta v = 0$ of totally symmetric frequency $a_{1\parallel}$ occurring in the spectrum *e.g.*, C''_{1-1} at 38295 and C''_{2-2} at 38223 with 160 quanta loaded on them. The band D''_0 at 37399 is strong in intensity and is further loaded with one to four quanta of 160. The band at 38323 can be interpreted as D''_1 and that at 39248 as D''_2. There are also bands corresponding to the excitation of four quanta of the 992 $a_{1\parallel}$ totally symmetric C vibration in the ground state and also some $\Delta v = 0$ transitions of the same vibration. The *E* system corresponding to 1480 frequency, which is the value of 1596 $e''_{\parallel}$ frequency in the excited state does not seem to be present.

The excitation of the 1596 $e''_{\parallel}$ frequency is rather peculiar in the spectrum. In the Raman spectrum the line corresponding to 1596 does not occur but instead two lines at 1584 and 1606 appear. This splitting into a doublet is attributed to the perturbation brought about by Fermi resonance between 1596, a pure $e''_{\parallel}$ frequency, and 606+992 (*i.e.*, B''_{-1}) = 1598, the combination of the $e''_{\perp}$ and $a_{1\parallel}$ frequencies whose total eigenfunction has the $e''_{\parallel}$ symmetry. The condition is, hence, favourable for resonance due to accidental degeneracy. In absorption there are two bands at 36496, 36478 at a distance of 1592 and 1610 respectively from the O-O band at 38088; but the bands are very weak and no further members are observed. In the case of emission, however, many series of bands involving the Fermi doublet

* In this paper the position of the bands if not given in A explicitly, is to be taken as given in cm^{-1}.

† Though 160 cannot be exactly called a quantum since it is a difference frequency due to 1-1 transition of $e''_{\perp}$ vibration, for brevity we shall continue to use that word.

TABLE II

F series (calculated)	α series (observed)	Int.	β series (observed)	Int.	B^0_{-1} series (calculated)
F^0_0 36493	α^0_0 36493	8	β^0_0 36486	8	B^0_{-1} 36491
	α^1_0 36343	4 5	β^1_0 36325	5	
	α^2_0 36182	2.5	β^2_0 36166	3	
	α^3_0 36023	1	β^3_0 36006	1 5	
	α^4_0 35871	1	β^4_0 35848	0	
F^0_{-1} 35501	α_{-1}^0 35517	5	β_{-1}^0 35492	7	B^0_{-2} 35499
	α_{-1}^1 35356	3	β_{-1}^1 35330	4.5	
	α_{-1}^2 35193	1	β_{-1}^2 35169	4.5	
	α_{-1}^3 35038	2	β_{-1}^3 35007	1	
	α_{-1}^4 34877	.5			
F^0_{-2} 34509	α_{-2}^0 34530	3	β_{-2}^0 34501	4 5	B^0_{-3} 34507
	α_{-2}^1 34371	3	β_{-2}^1 34338	3	
	α_{-2}^2 34208	1	β_{-2}^2 34176	3	
	α_{-2}^3 34046	1.5	β_{-2}^3 34018	0	
F^0_{-3} 33517	α_{-3}^0 33549	1.5	β_{-3}^0 33512	3	B^0_{-4} 33515
	α_{-3}^1 33384	2.5	β_{-3}^1 33347	0	
			β_{-3}^2 33189	0	
F^0_{-4} 32523			β_{-4}^0 32524	1.5	B^0_{-5} 32525
			β_{-4}^1 32351	1	
			β_{-4}^2 32210	0	
	α^0_1-136442	2	$\beta_1{}^0_1$36421	3.5	
	α^1_1-136276	1	$\beta_1{}^1_1$36257	2	
			$\beta_1{}^2_1$36097	2	
	α^0_1-235455	3.5	$\beta_1{}^0_2$35425	4	
	α^1_1-235393	1	$\beta_1{}^1_2$35264	2	
F^0_1 37416	α^0_1 37427	0			
	$\alpha^0_2$38353	2			

occur. The two bands at 36504 and 36486 which are the strongest bands next in intensity to the B^0_0 band are assigned to the Fermi doublet of the vibrational level. The frequency differences from the O-O band are 1584 and 1602. They have been named in the present case as α (36504) and β (36486) respectively. Among the α system of bands those at 35517 and

34530 are assigned as α^0_1 and α^0_2 bands and there are series corresponding to the 160 frequency. There are also 1-1, 1-2 and 2-2 transitions corresponding to the totally symmetric vibration. The bands at 37428 and 38353 have been classified as due to the superposition on α^0_0 of one and two quanta respectively of 923 a_{1g} frequency in the excited state. Similar bands are present in the β system. The bands in the β system extend up to the loading of one to four quanta of 992, together with the 160 series. The bands involving the excited frequency of 923 are also present. These results are shown in Table II which also gives the calculated values of frequencies for B^0_1 and F series together with the observed α and β series.

There is a weak band at 35038 which is due to the transition between the zero level of the excited electronic and the ground electronic state superposed by 3047 e^+_u H frequency. This progression which is termed K can be put down as

$$\nu = 38089 - 3047 + (v'_1 \times 923) - (v''_1 \times 992) - (v_3 \times 160).$$

k^0_{-1}, k^0_{-2} and k^0_1 have also been observed. The fourth e^+_u frequency of 1178 does not seem to be excited either in the ground or in the excited state in the emission spectrum.

The second part of the analysis, as it may be called, consists of the excitation of the frequencies other than e^+_u and a_{1g} combinations. The values of these frequencies and their assignments as given by Herzfeld, Ingold and Poole (1946) as a result of their extensive work on the various deuterated benzenes differ from those given by Herzberg (1945) especially in the case of nine inactive frequencies of benzene. In Table III all the frequencies are tabulated as given in both data.

There are three types of bands that are analysed in this Section. The first type consists of doubly excited non-totally symmetrical vibrations superposed on e^+_u vibration in either electronic state. A large number of bands are classified in this way in absorption as well as in emission. For example the band at 39614 in absorption can be classified as due to double excitation of 513 a_{2u} vibration in the excited state associated with 520 e^+_u vibration, similarly, the band at 40159 as the superposition of this vibration on 1045 e^+_u vibration which is followed by the members due to a_{1g} frequency. In emission the same vibration is doubly excited in the ground state associated with 606 in the ground state. Also the band at 39487 is classified in absorption as $-606 + 2 \times 1001$ and this latter double excitation also comes in with the ground state frequencies 1178 and 1596, both e^+_u. In emission, similar excitation involves the frequencies 1596 and 3047 in the ground state. Thus bands at 34473 and 36589 can be classified as such. The vibrations 985 and 703 b_{2g} in the ground state and the corresponding vibrations 774 and 364 in the excited state are also represented in the emission spectrum as will be seen in Table I. The b_{2u} frequencies

1648, 1110 and 1326 are also doubly excited and the bands corresponding to these have been assigned in the emission spectrum. The excited state values of these frequencies cannot be definitely determined from the absorption data. Most of these doubly excited non-totally symmetrical frequencies (non-degenerate) occur with the e_g^+ 520 and 606 vibrations.

The double excitation of non-totally symmetrical degenerate frequencies with or without the presence of e_g^+ frequency can make the transition allowed. In absorption the band at 39260 is classified as due to the double excitation of 586 e_u^- frequency in the excited state and is superposed by both the 160 and 923 progressions. The corresponding ground state frequency does not occur in emission. The band at 37285 is classified as due to excitation of 2×404 e_u^+ frequency. In addition the bands spaced 2×240 e_u^+ from the strong B^0_0, D^0_0 and α^0_0 are present and are classified as such which is analogous to the G series in absorption where this non-totally symmetrical degenerate frequency appears with the e_g^+ frequency in either state.

TABLE III

Symmetry type of vibration	ω'' according to Herzberg (19) in cm^{-1}	ω'' according to Herzfeld *et al* in cm^{-1}	ω' in cm^{-1}*
a_{1u}	992 3062	991 6 3062	923 (I) (S) 3130 (I) 2565 (S)
a_{2g}	1190	1326	
b_{1u}	1010 3063	1020 3060	1001 (I) 3138 (I)
b_{2u}	1854 1145	1648 1110	
a_{2u}	671	671	513 (I)
b_{2g}	1520 538	985 703	774 (I) 364 (I)
e_g^+	606 3046.7 1178 1596	605.6 3046.8 1178.0 1596	520 (I) (S) 3082 (I) 1045 (I) 1476 (I) (S)
e_u^-	1485 1037 3099	1485 1037 3080	
e_g^-	848.9	84.9	586 (I)
e_u^+	1160 404	970 405	708 (I) 240 (I) (S)

* The values marked (I) are those given by Ingold and Lecke (1946) and those marked (S) are used by Sponer *et al* in their analysis of the absorption spectrum.

The frequency of the other totally symmetric a_{1g} H vibration is found to be 3062 from Raman spectrum of liquid benzene, whereas the analysis of the emission spectrum gives 3054. The bands at 35556 and 33434 are due to the superposition of this frequency on A^0_0 and B^0_0 bands. Although these can be classified as C^0_3, D^0_3 the strong intensity with which they appear indicates that there is a blending of bands. The band at 33450 is classified as α^0_0—3054. These are denoted as A'^0_0, B'^0_0 etc., in Table I. These bands are followed by progressions due to frequencies 923, 992 and 160. The value of this a_{2g} H frequency in the excited state has been taken to be 2565 by Sponer *et al* (1939). But Ingold and Garfforth (1948) are of the opinion that this, as well as, other in-plane CH vibrations should increase in frequency on excitation because of the increase in the CH bond strength consequent on the weakening of the ring forming forces due to increase in size of the ring on excitation. This view appears to be substantiated by the failure of the Teller—Redlich product theorem if the proposed decreased frequencies are used and its validity if the proposed increased frequencies are employed. Theoretical calculations by Griffing (1947) indeed indicate that such frequencies should increase in the excited state.

This analysis is also completely included in Table I. Most of the bands measured are thus satisfactorily analysed. The table shows that many bands are regarded as blends which are probably not separated for want of dispersion and resolution of the spectrograph. Intensity considerations have been the main guide in ascertaining such blends. There are also cases where a weak band is masked by the presence of a strong band. This circumstance is clearly indicated when the higher members of the series stand out in comparison with the accompanying higher members of the stronger series which have lost in intensity. The proposed analysis is further corroborated by the ultraviolet fluorescence bands of benzene investigated by Ingold and Wilson (1936). The identity of bands in absorption and in emission in the region in which the two spectra are common is sufficient to prove that the emitter of both the spectra is a common molecule. The satisfactory analysis which is possible in common to absorption, emission and fluorescence is a further proof for the essential correctness of our view regarding the emitter as well as the origin of the spectra.

ACKNOWLEDGMENTS

We take this opportunity of recording our gratitude to Prof. Sir K. S. Krishnan and Prof. Dr. N. R. Dhar of the University of Allahabad for permission to use the Hilger comparator and the quartz littrow spectrograph used in these experiments.

BENARES HINDU UNIVERSITY.

REFERENCES

Asundi and Padhye, 1945, *Nature*, **156**, 368
Austin and Black, 1930, *Phys. Rev.*, **35**, 452.
Garforth and Ingold, 1948, *J. C. S.*, p. 417.
Goeppart Meyer and Sklar, 1938, *J. Ch. Phys.*, **6**, 645.
Griffing, 1947, *J. Ch. Phys* , **15**, 421.
Herzberg, 1945, Infrared and Raman Spectra of Polyatomic molecules, p. 364 (first edition).
Herzfeld, Ingold and Poole, 1946, *J. C S.*, p 316.
Hückel, 1931, *Zeit. f. Phys.*, **70**, 204.
Ingold and Leeke, 1946, *Nature*, **157**, 46.
Ingold and Wilson, (1936), *J. C. S.*, pp. 941 and 1210.
McVicker, Marsh and Stewart, 1923, *J. C. S.*, p. 642.
Mullikan, 1939, *J. Ch. Phys* , **7**, 353.
Pauling, 1948, The nature of chemical bonds, 2nd edition.
Pauling and Wheland, 1933, *J. Ch. Phys.*, **1**, 365.
Radle and Beck, 1940, *J. Ch. Phys.*, **8**, 507.
Sklar, 1937, *J. Ch. Phys.*, **5**, 669.
,, 1942, *Rev. Mod. Phys.*, **14**, 232.
Sponer, Nardheim, Sklar and Teller, 1939, *J. Ch. Phys*, **7**, 207.

THE PRINCIPAL MAGNETIC SUSCEPTIBILITIES OF SINGLE CRYSTALS OF RARE EARTH SALTS AT LOW TEMPERATURES. PART I—CERIUM SALTS

By A. MOOKHERJI

(*Received for publication, May 17, 1949*).

ABSTRACT. The principal susceptibilities of cerium salts have been measured from room temperature down to liquid air temperature The results are discussed in terms of the theory of crystalline field. It has been found that (1) the deviation of the effective mean square moment of the Ce^{+++} ion, from the Hund value for the free ion can be explained on the assumption of a single suitable cubic field, which is the same at all temperatures in the range studied (2) The mean square moment is determined almost wholly by the cubic part of the field, the rhombic part has very little effect on it. (3) The variation in the magnitude of the cubic field as we pass from hydrated salts to anhydrous halides is found to be in the proper direction. (4) The χ_1-axis of $CeNH_4(SO_4)_2 4H_2O$ crystal rotates by about 15 degrees as the temperature is lowered from 300° K to 85°K.

INTRODUCTION

Rare earth salts are eminently suitable for systematic magnetic studies from various points of view, and have therefore engaged the attention of a large number of investigators. As is well-known in the rare earth ions M^{+++}, the $4f$ shell is getting filled up progressively. All the inner levels are full as are also $5s$ and $5p$ among the outer levels. Hence in these ions the electrons in the incomplete $4f$ shell, which are responsible for the observed paramagnetic moments of the ions are partly shielded by the surrounding $5s$ and $5p$ electron shells from the strong electric fields in the crystals. This shielding action of the outer shell of electrons greatly reduces the influence of the crystalline fields on the paramagnetism. The quantum number J representing the total angular momentum, will be a good quantum number. Unlike the salts of the iron-group, where the above-mentioned shielding is absent, and hence the effect of the crystalline field on their paramagnetism is much more pronounced, rare earth ions will to a large extent retain the properties characteristic of their free states. The effect of the electric field will be to remove slightly a part of the $(2J+1)$-fold degeneracy pertaining to the given state. Following Bethe (1929), Van Vleck (1932), Penney and Schlapp (1932), we shall regard the crystalline electric field in the neighbourhood of the paramagnetic ion to conform to a potential of the type,

$$V = D(x^4 + y^4 + z_4) + [Ax'^2 By^2 - (A+B)z'^2] \quad \ldots \quad (1)$$

The square terms represents the rhombic part of the field and the fourth degree terms the cubic part. The paramagnetic ion is regarded as being at the origin of the co-ordinate system $x=y=z=0$ and $x'=y'=z'=0$. We have neglected the sixth degree terms and also a spherically symmetrical term; the influence of the sixth degree term is small compared with that of the fourth degree terms.

The cubic part of the field predominates over the rhombic part and determines to a first approximation the deviation of the mean of the three principal susceptibilities of the crystal from the ideal free ion value. The rhombic part determines the anisotropy of the crystal and its influence on the mean susceptibilities is quite small.

The principal axes of the rhombic part of the field, namely, x', y' and z' will not in general coincide with the axes of the cubic part namely x, y and z and by suitable choice of the directions of these axes and the coefficients D, A and B, one can build up a crystalline field of any required symmetry and magnitude in the neighbourhood of the paramagnetic ion. In general, the unit cell of the crystal will contain more than one paramagnetic ion. Associated with each such paramagnetic ion say i ($i=1$ to z, where z is the number of paramagnetic ions in the unit cell), there will be a crystalline field with its own set of $(x\ y\ z,\ x'\ y'\ z')_i$ axes, and its own field constants $(D, A \text{ and } B)_i$. Though A, B, and D may be the same for all the z ions and further the inclinations between the cubic and the rhombic axes, *i.e.*, between x, y, z and x', y', z' may also be the same for all the ions: in other words, though the dispositions of the negatively charged atoms about the paramagnetic ions will be the same about all the ions, still the field axes $(x\ y\ z,\ x'\ y'\ z')$ associated with different ions will not all be oriented the same way, *i.e.*, the x-axes of all the z-groups, each associated with one ion, will not be paralled to one another nor all the y's nor all the z' axes, etc. Actually the principal axes associated with different ions in the unit cell will be oriented relatively to one another in such a manner as to build up the symmetry of the unit cell from that of the individual units. Hence the observed anisotropy of the crystal as a whole will not represent the anisotropy of the individual ions in the unit cell, but will be an average effect of the different ions of the unit cell, oriented relatively to one another. Thus even in a cubic crystal when the number of paramagnetic ions in the unit cell is more than one the symmetry of the crystalline field need not be cubic at all, but may deviate considerably from cubic symmetry.

Thus the problem of explaining the observed magnetic properties of the crystals in terms of the magnitude and the asymmetry of the field associated with each ions, and the orientation of the field axes of these ions relative to one another will become extremely complicated. It is, however, fortunate that the mean of the three principal susceptibilities as we mentioned, is determined to a first approximation by the cubic part

of the field alone, so that one may obtain from the observed mean susceptibilities of the crystal a general estimate of the cubic part of the field and from the anisotropy of the crystal the rhombic part.

In this communication the results of magnetic measurements on some single crystals of Ce^{+++} ion from room temperature down to liquid air temperature are discussed in the light of crystalline field theory as discussed above.

EXPERIMENTAL

Specimens of cerium salts in the investigation were of high purity and were made available through the kindness of Professor Trombe of Paris University. Crystals were grown out of aqueous solutions.

Magnetic measurements were carried out in two parts :—(1) Room temperature measurements and (2) Low temperature measurements.

Room temperature measurements which involve : (1) the determination of the direction of the principal magnetic axes, (2) the measurement of the difference between the principal susceptibilities and (3) the determination of the absolute susceptibility along any one convenient direction in the crystal, were carried by the method of Krishnan and Banerji (1935).

Low temperature determinations on magnetic anisotropies and the principal susceptibilities were carried by a cryostatic device and a quartz micro-balance designed and used by Bose (1947). With the help of the cryostat the temperature inside the experimental tube could be maintained steady at any desired value between room temperature and the temperature of the liquid air ; the same procedure as adopted by Krishnan, Mookherji and Bose (1938) was used to determine magnetic anisotropy at low temperatures. Microbalance gave the vertical force on the crystal at any desired temperature, which is a measure of absolute susceptibility in the direction of the field. Room temperature value being known, the following expression gives the susceptibility at any temperature t.

$$F_t = \chi_t \left[1 + \frac{k_a}{\chi}(1-\gamma\Theta)(1-f)\right] \qquad (2)$$

where, χ_t and F_t are the susceptibility and the vertical force at any χ and F are the susceptibility and the vertical temperature Θ force at room temperature Θ, γ is the coefficient of cubic expansion $f=\Theta/T$; k_a = volume susceptibility of air at room, temperature Θ. k = volume susceptibility of the crystal at room temperature Θ.

For details the reader is referred to Bose's paper (1948).

RESULTS

The results of measurements are collected in Tables I to IV. The nature of the variation of the magnetic anisotropy and of the square of the principal moments with temperature are shown in figures 1 to 4.

$\chi_{\parallel}$ represents the grammolecular susceptibility along the axis of symmetry of tetragonal crystals and $\chi_{\perp}$ that along directions normal to it. For monoclinic crystals χ_3 represents the grammolecular susceptibility along 'b' axis while greater of the two in the (010) plane by χ_1 and the smaller by χ_2; ψ is the angle which the crystallographic 'c' axis makes with χ_1-axis.

Effective magnetic moments of the crystal, are calculated by the expressions $\mu_i = 2.84\sqrt{\chi'_i T}$, where χ'_i are the susceptibilities corrected for diamagnetism for both cation and anion and $i = 1, 2, 3$ or $\perp$ and $\parallel$. The diamagnetism for the Ce^{+++}ion was taken to be -28×10^{-6} (Van Vleck, 1932). Diamagnetic corrections for the different groups as given below were taken from Stoner's book, Magnetism and Matter (1934).

$SO_4^{--} = -33.6$ $\quad H_2O = -13,$ $\quad NH_4 = -22.1$

$NO_3^{-} = -14.2$ $\quad Mg^{++} = -10.$

The unit adopted for the χ_i is 10^{-6} of a c.g.s electromagnetic unit.

TABLE I

Magnetic Anisotropies at 30°C.

Crystal	Crystallographic data	Mode of suspension	Orientation in the magnetic field.	$\Delta\chi$	Magnetic anisotropy
$Ce(NH_4)(SO_4)4H_2O$	Monoclinic prism $a:b:c =$ 0.360 : 1 : 2.004 $\beta = 97°15'$	'b' axis vertical	$\psi = +77°.3$	190	$\chi_1 - \chi_2 = 190$
		'c' axis vertical	'b' axis normal to field	107	$\chi_1 - \chi_3 = 155$
		(100) plane horizontal	'c' axis normal to field	67	Cal $\psi = +78.2$
$Ce_2Mg_3(NO_3)_{12}24H_2O$	Trigonal	Trig. axis horizontal	Trig. axis normal to field	640	$\chi_\perp - \chi_\parallel = 640$

TABLE II

Absolute susceptibilities at 30°C

Crystal	Direction along which susceptibility was measured	Density of the crystal	Volume susceptibility	Corresponding gm. mol. susceptibility
$Ce(NH_4)(SO_4)4H_2O$	Along χ_1-axis	2.525	12.0	2,020
$Ce_2Mg_3(NO_3)_{12}24H_2O$	Normal to Trig. axis	2.010	5.110	3,880

TABLE III

Temperature variation of magnetic anisotropy.

Crystal	Temp. °K	Suspension used for measurement		$\chi_1-\chi_3$	ϕ
		'*b*' axis vertical	'*c*' axis vertical		
		$\chi_1-\chi_2$	$\chi_1\sin^2\phi+\chi_2\cos^2\phi-\chi_3$		
$Ce(NH_4)(SO_4)_24H_2O$	300	193	108	117	+77.3
	280	209	112	122	,, 76.6
	260	232	113	127	,, 76.0
	240	264	119	136	,, 75.4
	220	313	134	153	,, 74.8
	200	369	153	183	,, 73.4
	180	434	177	225	,, 70.6
	166	509	203	227	,, 67.6
	140	890	232	349	,, 63.8
	120	699	265	415	,, 62.4
	100	807	301	474	,, 62 4
	85	882	344	533	,, 62.4

Trigonal axis horizontal

		$\chi_\perp-\chi_\parallel$
$Ce_2Mg_3(NO_3)_{12}24H_2O$	300	658
	280	764
	260	887
	240	1,040
	220	1,220
	200	1,460
	180	1,760
	160	2,160
	140	2,780
	120	3,560
	100	4,940
	85	5,810

TABLE IV

Temperature Variation of Principal Susceptibilities and Effective Moments.

Crystal and direction along which measurement was taken.	Temp. °K	χ'_1	χ'_2	χ'_3	χ'	μ^2_1	μ^2_2	μ^2_3	μ^2
	300	2,200	2,010	2,080	2,100	5,320	4,857	5,037	5.070
	280	2,270	2,060	2,150	2,160	5,130	4,657	4,853	4,880
	260	2,390	2,160	2,260	2,270	5,006	4,519	4,740	4,789
	240	2,520	2,260	2,390	2,390	4,849	4,369	4,616	4,611
	220	2,460	2,330	2,490	2,490	4,687	4,132	4,417	4,412
$Ce(NH_4)(SO_4)_34H_2O$	200	2,790	2,430	2,610	2,610	4 506	3,911	4,211	4,209
Along 'a' axis	180	2,980	2,550	2,750	2,760	4,326	3,695	3,998	4,006
	160	3,210	2,710	2,930	2,950	4,142	3,485	3,784	3,803
	140	3,480	2,880	3,130	3,160	3,926	3,251	3.534	3,570
	120	3,740	3,040	3,320	3,370	3,616	2,939	3,214	3,256
	100	4,020	3,220	3,550	3,660	3,244	2,593	2,863	2,900
	85	4,270	3,380	3,730	3,790	2,924	2,319	2,559	2,601
		$\chi'_\perp$	$\chi'_\parallel$	$\bar{\chi}'$	$\mu^2_\perp$	$\mu^2_\parallel$	$\bar{\mu}^2$		
	300	4,519	3,850	4,290	5,454	4,657	5,168		
	280	4,720	3,960	4,800	5,328	4,468	5,041		
	260	4,940	3.060	4,650	5,184	4,253	4,873		
	240	5,240	4,200	4,890	5,069	3,925	4,688		
	220	5,520	4,300	5,110	4,897	3,816	4,537		
$Ce_2Mg_3(NO_3)_{12}24H_2O$	200	5,820	4,360	5,340	4,693	3,512	4,245		
Along $\chi_\perp$-axis	180	6,210	4,450	5,620	4,508	3,230	4,082		
	160	6,610	4,450	5,890	4,266	2,872	3,801		
	140	7,150	4,370	6,220	4,027	2,467	3,507		
	100	8,710	3,770	7,100	3,514	1,522	2,850		
	85	9,330	3,520	7,390	3,200	1,212	2,537		

DISCUSSIONS

The ground state of Ce^{+++} ion is a doublet F-state, $^2F_{5/2}$. The immediately higher level namely, $^2F_{7/2}$, is separated from the ground level by about 2510 cm^{-1} and hence at all ordinary temperatures its influence on the

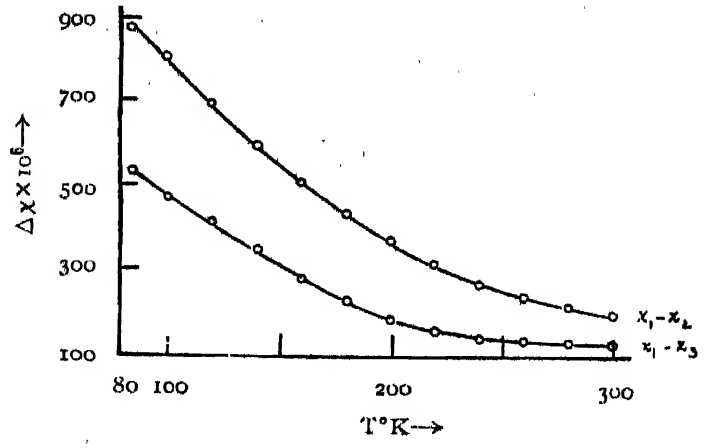

FIG. 1

$CeNH_4(LO_4)_2\,4H_2O$

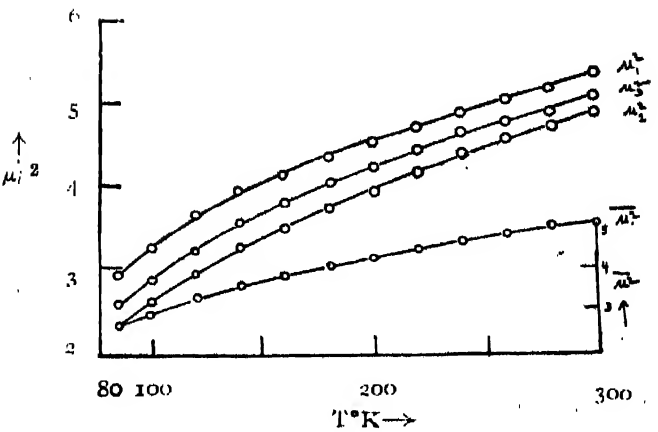

FIG. 2

$CeNH_4(SO_4)_2\,4H_2O$

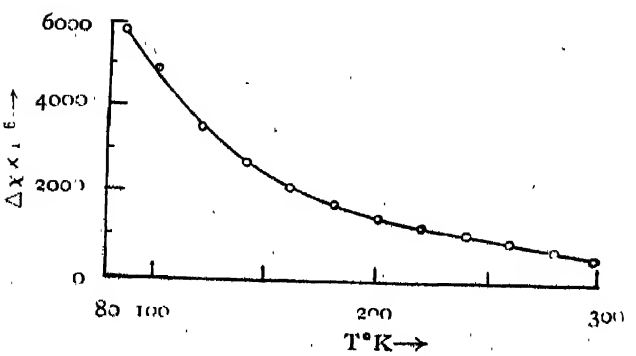

FIG. 3

$CeMg_3(NO_3)_{12}\,24H_2O$

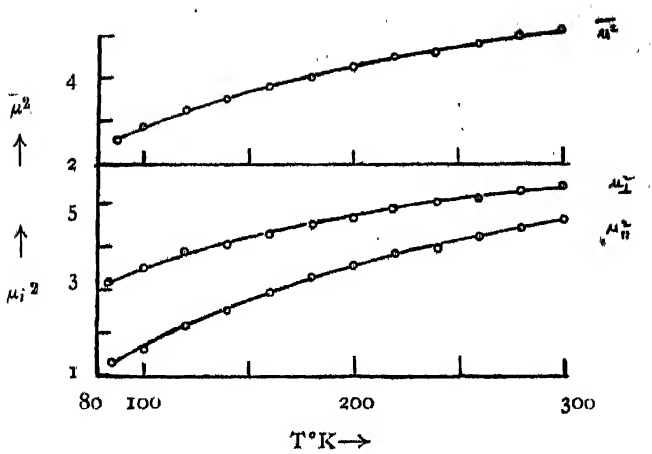

FIG. 4

$Ce_2Mg_3(NC_3)_{12}\ 24H_2O$

magnetic behaviour will be negligible. In a cubic field, the $^2F_{5/2}$ level will split up into a quartet level below and a doublet level above. With the superimposition of a rhombic field the lower quartet will separate out into the doublets, the splitting being as given below (Fig. 5) ; the two-fold degeneracy retained by each of the three levels is of the spin Kramers type, since Ce^{+++} ion has an odd number of electrons namely $4f^1$ and even in strong and highly asymmetric fields the separation of the components of each of these doublets will be very small.

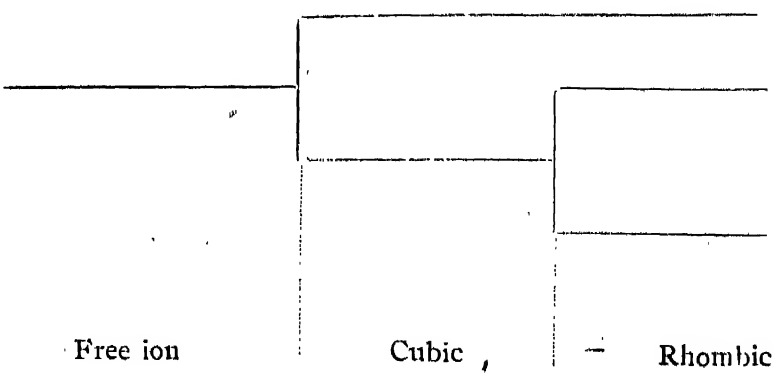

FIG. 5

The general case where the principal axes of the rhombic part of the field may have any orientation with respect to the cubic axes will be complicated. But taking the axes as coincident, and further assuming the field as a whole has trigonal symmetry, Kramers (1932) has calculated both the splitting of the levels and the principal susceptibilities. The mean gram molecular susceptibility according to Kramers (1932) is given by

$$\bar{\chi}=\frac{\frac{1}{3}Ng^2\beta^2}{e^{\nu f}+e^{-\nu f}+e^{-\nu b}}\left[\left\{\left(\frac{13f+3a}{6f(f+b)}+\frac{9(f^2-a^2)}{8f^3}\right)+\nu\left(\frac{3(f+a)^2}{8f^2}+\frac{(2f-3a)^2}{12f^2}\right)\right\}e^{\nu f}+\left\{\left(-\frac{13f-a}{6f(f-b)}-\frac{9(f^2-a^2)}{8f^3}\right)+\nu\left(\frac{3(f-a)^2}{8f^2}+\frac{(2f+3a)^2}{12f^2}\right)\right\}\times e^{-\nu f}+\left\{\frac{13b-3a}{3(f^2-b^2)^2}+\frac{3}{4}\nu\right\}e^{-\nu b}\right] \quad \ldots \quad (3)$$

where $\nu=1/kt$ and a, b and f are constants determined by the constants of the electric field. In terms of these constants the three split energy levels (each with Kramers two-fold degeneracy) taking the lowest as zero will be given by

$$0, -\frac{f^2}{b}, \frac{f^3}{ab} \qquad (4)$$

Using (3), the three constants a, b, and f can be evaluated from the known susceptibility at any three temperatures. It is found that in both $Ce(SO_4)_2NH_44H_2O$ and $Ce_2Mg_3(NO_3)_{12}\ 24H_2O$ a satisfactory fit is obtained with the following values for the constants :—

$$f=76.3\ cm^{-1},\ b=-38 \text{ and } a=-16.8.$$

as will be seen from the following table which gives the values calculated from these constants and the observed values for comparison with them :—

TABLE V

Temperature °K	$\bar{\mu}^2$ calculated	$\bar{\mu}^2$ observed	
		$CeNH_4(SO_4)_24H_2O$	$Ce_2Mg_3(NO_3)_{12}\ 24H_2O$
300	5.04	5.07	5.19
200	4.45	4.21	4.25
100	3.00	2.90	2.54
85	2.72	2 60	2.54

The corresponding values of the energy levels will be 0, 153, 696 cm^{-1} respectively; 696 cm^{-1} being the overall separation. No data are available for the absorption spectra or for the specific heats of either of these two salts by which to verify the separations of the levels predicted above from magnetic data, but it will be seen from the following considerations that they are of proper magnitude.

Both cerium fluoride (Gorter and de Hass 1930) and cerium chloride (Gorter and de Hass 1931) have been studied for their mean susceptibilities

at very low temperature and the mean square of the effective moments in these salts are given in the following Tables VI and VII :—

TABLE VI

Cerium chloride

T°K	286.5	249 5	169.5	77.52	20.42	14.35
μ^2	5.96	5.82	5.70	5.16	4.35	4.26

TABLE VII

Cerium fluoride

T°K	293	135.2	77.5	20.4	14.48
$\bar{\mu}^2$ From magnetic measurements	5.17	4.33	3.60	2.46	2.32
$\bar{\mu}^2$ From Faraday rotation	5.20	—	3.58	2.40	..

On comparing these values with the values of the two cerium salts, $Ce(NH_4)_2(SO_4)_2\,4H_2O$ and $Ce_2Mg_3(NO_3)_{12}\,24H_2O$ studied by us it will be seen that the temperature variation in CeF_3 and $CeCl_3$ is not quite so rapid as our salts pointing to a feebler crystalline field in these halides. The values of a, b and f for these two halides calculated from their magnetic susceptibilities using (3) and the separations of the levels predicted from them according to (4) are entered in Table VIII.

TABLE VIII

Salt	From magnetic data			Energy levels in cm^{-1}	
	a	b	f	From magnetic data	From absorption spectra
CeF_3	−27.2	−40.75	81.5	0, 163, 489	—
$CeCl_3$	−48	−18		0, 151, 264	0, 155, 275

The absorption spectra of cerium chloride has been studied by Freed, (1931). The energy levels deduced from these absorption measurements are also included in Table VIII.

Since the calculated and observed energy levels agree for the chloride, there is little doubt that with the much sharper fall of the mean susceptibiliti-

es with the fall of temperature and the corresponding larger fields predicted for $CeNH_4(SO_4)_2\,4H_2O$ and $Ce_2Mg_3(NO_3)_{12}24H_2O$), the separation of the energy levels in the latter salts must be larger.

There is one other salt of cerium, namely, cerium ethyl sulphate for which measurements at very low temperatures are available (Faraday and and Weirsma, 1935) see Table IX. The crystal is hexagonal; $\mu_\parallel^2$ and $\mu_\perp^2$ in the table refer to directions along the hexagonal axis and perpendicular to this axis respectively.

TABLE IX

Cerium Ethyl Sulphate

Temp. °K	$\mu_\parallel^2$	$\mu_\perp^2$	$\overline{\mu^2}=1/3(\mu_\parallel^2+2\mu_\perp^2)$
20.45	6.8	2.31	3.82
14.18	7.3	2.27	3.61

The mean square moment remains high, and that along the hexagonal axis actually rises with the fall of temperature, being even higher than the value for the free ion. This behaviour of cerium ethyl sulphate contrasts sharply with the behaviour of $CeNH_4(SO_4)_24H_2O$ and $Ce_2Mg_3(NO_3)_{12}24H_2O$ studied by us, in which not only the mean square of the moment, but the individual principal moments also, fall rapidly with fall of temperature.

From these observations one may conclude what follows.

(1) That the cubic part of the field in $Ce(SO_4)_2NH_4\,4H_2O$ and in $Ce_2Mg_3(NO_3)_{12}\,24H_2O$ salts is much stronger than in $Ce_2(C_2H_5SO_4)_6\,18H_2O$.

(2) Either (*a*) the rhombic part of the field in $CeNH_4(SO_4)_2\,4H_2O$ and in $Ce_2Mg_3(NO_3)_{12}\,24H_2O$ is much feebler than in $Ce_2(C_2H_5SO_4)_6\,18H_2O$; or (*b*) the relative orientation of atomic groups associated with the different cerium ions in the unit cell of $CeNH_4(SO_4)_2\,4H_2O$ and $Ce_2Mg_3(NO_3)_{12}\,24H_2O$ are such as to average out the anisotropies of the groups and make the resultant anisotropy much smaller, whereas in cerium ethyl sulphate the averaging is not so much marked.

The latter alternative, *i.e.*, (*b*) receives support from X-ray studies by Ketelaar (1937) on the structure of cerium ethyl sulphate, which show that there are two cerium ions in the unit cell, and considering the atomic groups associated respectively with the two cerium ions, the two groups are oriented nearly parallel to one another, *i.e.*, the x, y, z axes of one of them coincide respectively with the x, y, z axes of the other. Since magnetic data for cerium ethyl sulphate are available at two temperatures only it is not possible to calculate all the three constants a, b and f. But a rough estimate of the overall splitting from the magnetic data gives 315 cm^{-1} which is not very different from the value 365 cm^{-1} as deduced from the absorption data (Freed, 1931).

It is significant that in the cerium salts that we have studied, which are both highly hydrated and in which the cerium ions are presumably surrounded by an octahedron of water molecules with their negatively charged oxygen atoms pointing towards the central Ce^{+++} ion, the crystal field so produced is not only predominantly cubic but is much stronger than in $CeCl_3$ or CeF_3 where the neighbours of the paramagnetic ion are negatively charged halogen atoms.

In general, where the environments in the neighbourhood of the paramagnetic ion are similar, the cubic fields estimated from the magnetic data are of the same magnitude as has been found in the salts, $CeNH_4(SO_4)_2\ 4H_2O$ and $Ce_2Mg_3(NO_3)_{12}\ 24H_2O$.

It is observed that the χ_1-axis of $CeNH_4(SO_4)_2\ 4H_2O$ (see Table III) crystal rotates by about 15 degrees as the temperatures is lowered from 300°K to 85°K.

A C K N O W L E D G M E N T S

The work was carried out at the laboratories of the Indian Association for the cultivation of Science, Calcutta. The author wishes to express his thanks to its committee of management for affording all facilities, and to Sir K. S. Krishnan, Kt., D.Sc., F.R.S., F.N.I., for his keen interest in the work and his valuable advice and help. Thanks are also due to Dr. A. Bose, D.Sc. for his valuable discussions.

R E F E R E N C E S

Bethe, H. (1929), *Ann. Physik*, **3**, 133.
„ (1930), *Z. Physik*, **60**, 218.
Bose, A. (1947), *Ind. Jour. Phys.*, **21**, 275.
„ (1948), *Ind. Jour. Phys.*, **22**, 195.
Faraday, R. A. and Weirsma, E. C. (1935), *Physica*, **11**, 576.
Freed, S. (1931), *Phys. Rev*, **38**, 2268.
Gorter, C. J. and de Hass W. J. (1930), *Proc. Roy. Acad. Ams.*, **33**, 494.
(1931), „ „ „ **24**, 1249.
Ketelaar, J. A. A. (1937), *physica*, **4**, 619.
Kramers, H. A (1932), *Proc. Acad. Soc*, **35**, 1272.
Krishnan, K. S. and Banerji, S. (1935), *Phil. Trans. Roy. Soc.*, **A234**, 265.
Krishnan, K. S. and Mookherji, A. (1938) „ „ „ **A237**, 135.
Penney, W. G. and Schlap, R. (1932), *Phys. Rev.*, **41**, 194.
„ „ „ „ **42**, 666.
Stoner, E. C. (1934), Magnetism and Matter, Methuen, p. 470.
Van Vleck J. H. (1932)—The Theory of Electric and Magnetic Susceptibility Oxford, Clarendon Press, Chapter XI and p. 252.

SOME NEW FEATURES OF THE GREEN AND U. V. BANDS OF Na_2 AND THE BLUE BANDS OF K_2 AND OF THE CONTINUA ACCOMPANYING THESE BANDS*

By S. P. SINHA

Plates VIIA, B, C and D

(Received for publication, January 8, 1949)

ABSTRACT. Description of the behaviour of the green, the λ3600–λ3200 Å bands and the λ3050–λ2860 Å bands of Na_2 and the λ4550–λ4150 Å bands of K_2 and also of the continuous absorption spectra accompanying these bands, under varying conditions of temperature and pressure, is given. An attempt has been made to explain the features observed according to Franck-Condon principle, on the assumption that increase of temperature or pressure favours the formation of quasi-molecules, whose potential energy curves are the same as those of the stable Na_2 or K_2 molecules in their normal state.

INTRODUCTION

Loomis and Nile (1928) have reported the occurrence of an infra-red edge at λ8150Å and an orange edge at λ5500Å to the red band system of Na_2. The region at wavelengths just shorter than λ5500Å is comparatively transparent. At still shorter wavelengths, the green system shows up strongly so that there is a narrow transparent region which sometimes looks like an emission band. Taking account of the potential energy curves of the ground $^1\Sigma_g^+$ state and the excited $^1\Sigma_u^+$ state, they have explained these features almost quantitatively in terms of Franck-Condon principle. The potential energy curve drawn by them for the ground state was, however, not quite accurate, as the value of heat of dissociation used by them was 1.08 volts, the correct value due to Loomis and Nusbaum (1932) being 0.76 volt only. But even using the latter value of D in drawing the ground state potential energy curve nearly the same values of limiting edges are obtained and hence their explanation remains valid.

Features similar to those for the red bands described above have also been observed for the green and the ultra-violet bands of Na_2 and for the blue bands of K_2, by studying the absorption spectra of the vapours of sodium and potassium at comparatively high temperatures and pressures. The purpose of the present paper is to describe the features of these bands and

* This work forms part of the thesis approved for Ph.D. degree of the London University.

the continua associated with them and to attempt a possible explanation for the same.

EXPERIMENTAL

The experimental arrangement used is the same as has been described before (Sinha, 1948). The alkali-metals, *i.e.*, sodium or potassium, were kept at the centre of a steel tube provided with water cooled quartz windows. The tube could be heated electrically and after pumping out all air from the tube, nitrogen gas could be introduced to maintain desired pressures inside it. Using light from a hydrogen continuum the absorption spectra of sodium and potassium were photographed on a Hilger intermediate quartz spectrograph at temperatures lying between about 600 and 1100 °C and total pressures (of the metal vapour and nitrogen as indicated by a manometer connected to the system) varying from a few mm. to 760 mm. of mercury.

DESCRIPTION OF THE SPECTRA

We shall describe the features of (*a*) the green bands (*b*) the λ3600-λ3200Å bands and (*c*) the λ3050 λ2850Å bands, of Na_2, and (*d*) the λ4150-λ4550Å bands of K_2. The spectra for sodium and potassium are given in Plates VIIA, B, C and VII D respectively.

(*a*) The Green Na_2 Bands

Over the range of temperature and pressure employed in the present investigation the structure of the green bands can hardly be seen. What appears is a patch of continuous absorption broadening on both sides with increase in temperature and pressure and ultimately merging into the absorption continuum associated with the red bands on the long wavelength side and having almost a very definite edge at about λ4450 Å on the short wavelength side. The details are given in Table I.

(*b*) The λ3600-λ3200Å Na_2 Bands

At about 500°C, when the total pressure in the tube is low, the absorption line at λ3303Å is fairly sharp and no bands are seen about it. Increase of pressure by introducing more of nitrogen merely broadens the line. When the temperature is raised to about 600°C, bands begin to develop on both sides of the line, though more markedly on the longer wavelength side, and become more and more prominent, when the temperature or the total pressure is increased up to a certain value. Effect of increase of total pressure at constant temperature appears more marked than the effect of increase of temperature at a constant value of the total pressure. With further increase of temperature or pressure, however, the structure of the bands begins to disappear and instead the region seems to be continuously absorbed. The continuous absorption begins from about the same position as that of

TABLE I

Green bands of Na_2

Temp. in °C	Pressure in cm. of mercury	Region of absorption (λ in Å)
600	4	4650 – 5100
	12	4600 – 5150
	40	4600 – 5450
700	6	4600 – 5300
	12	4600 – 5300
	40	4500 – 5450
	76	4550 – merges into the red bands.
850	8	4600 – 5350

At higher pressure or temperature the long wavelength edge merges with the red bands and the short wavelength edge remains at about λ4500 Å.

TABLE II

λ3600-λ3200Å Na_2 bands

Temp. in °C	Pressure in cm. of mercury	Region of total absorption	Region over which the band heads are seen (λ in Å)
600	4	...	.....
	12	...	3300 – 3380 (faint)
	40	...	3300 – 3450 (faint)
700	6	...	3260 – 3485
	12	...	3240 – 3520
	40	3250 – 3370	3220 – 3250, and
		...	3370 – 3525
	76	3240 – 3435	3200 – 3240, and
		...	3435 – 3560
850	8	...	3250 – 3500
	26	3280 – 3325	3240 – 3280, and
			3325 – 3350
	40	3250 – 3420	3200 – 3250, and
			3420 – 3560
1000	8	3160 – 3560	.....
	16	3160 – 3560	.....
	40	3160 – 3580	.....
	76	3150 – 3620	.....
1100	The entire region at pressures greater than about 10 cm is completely absorbed.		

TABLE III

$\lambda 3050$-$\lambda 2860$Å Na_2 bands

Temp. in °C	Pressure in cm. of mercury	% of General absorption (visual estimate)
700	76	very small
850	8	very small
	26	very small
	40	30
1000	8	60
	16	70
	40	80
	76	100
1100	8	90

At higher pressures the entire region is completely absorbed.

TABLE IV

$\lambda 4550$-$\lambda 4150$Å K_2 bands

Temp. in °C	Pressure in cm. of mercury	Extent of the Spectrum	% absorbed (visual estimated)
600	10	4225—4350	50
	40	4225—4425	70
	76	4225—4425	80
700	4	4200—4500	100
	10	4175—4600	100
	40	4175—4600	100
	76	4160—4600	100
850	10	4175—4600	100
	30	4175—4625	100
	50	* —4625	100
1000	4	4200—4500	100
	10	4175—4600	100
	40	* —4620	100

* (Asterisk) denotes that the bands and the continuum merge into the broadened principal series line at $\lambda 4045$Å on the short wavelength side.

Fig. *a*.

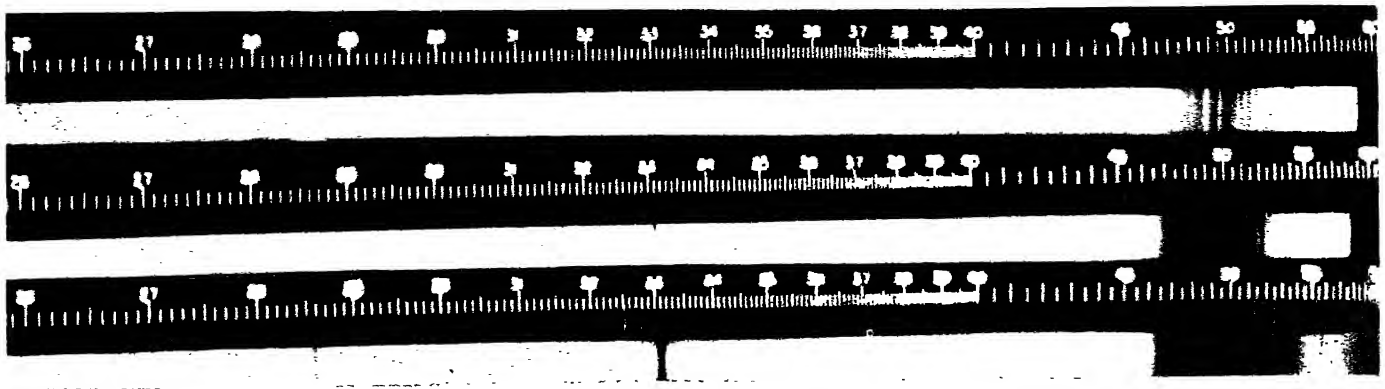

Temp.	Press.
600°C	4cm
	12cm
	40cm

Fig. *b*.

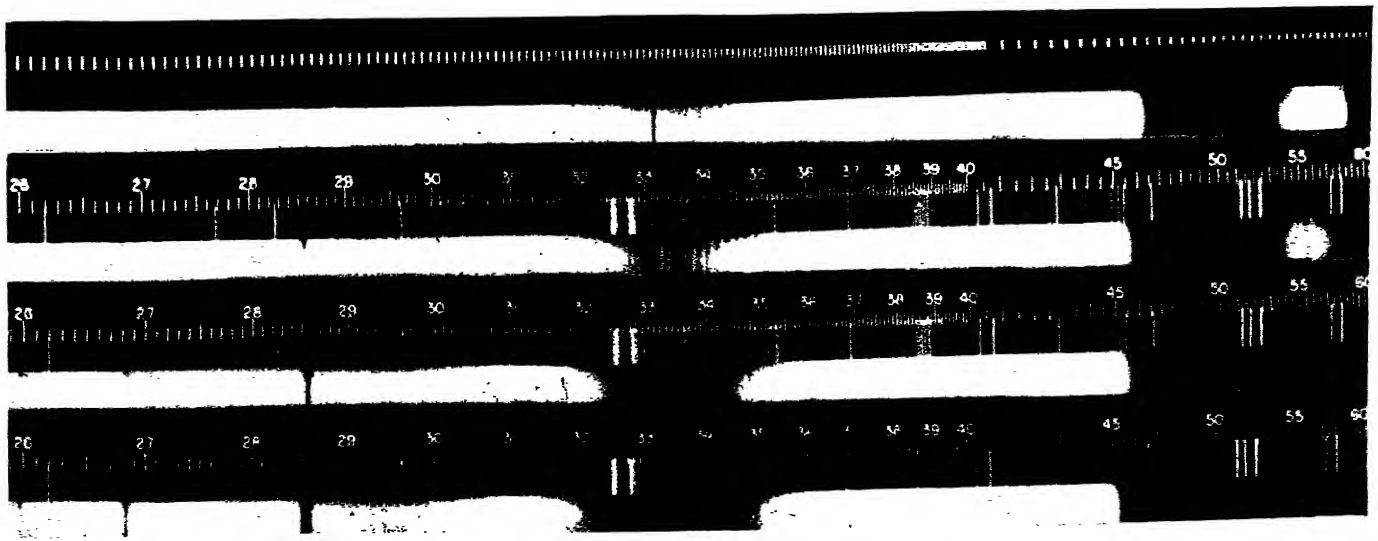

Temp.	Press.
700°C	6cm
	12cm
	40cm
	76cm

Fig. *c*.

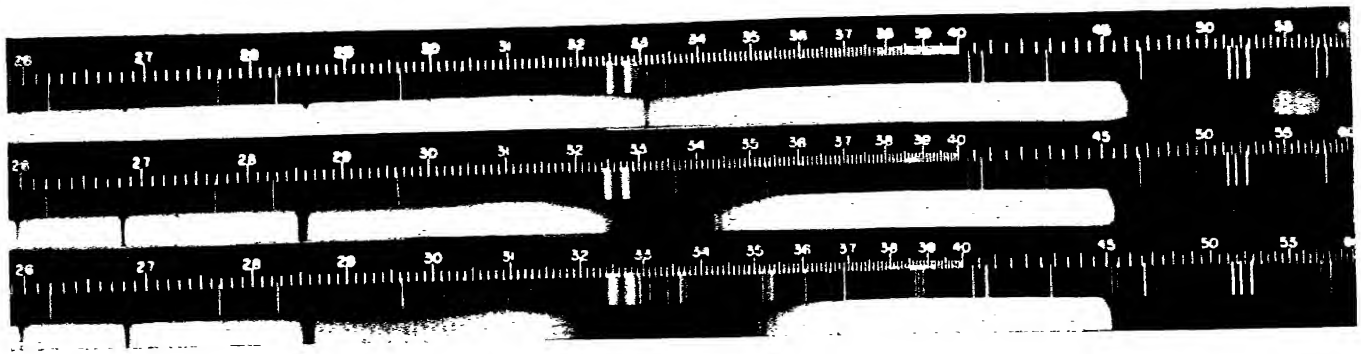

Temp.	Press.
850°C	8cm
	26cm
	40cm

Fig *d*

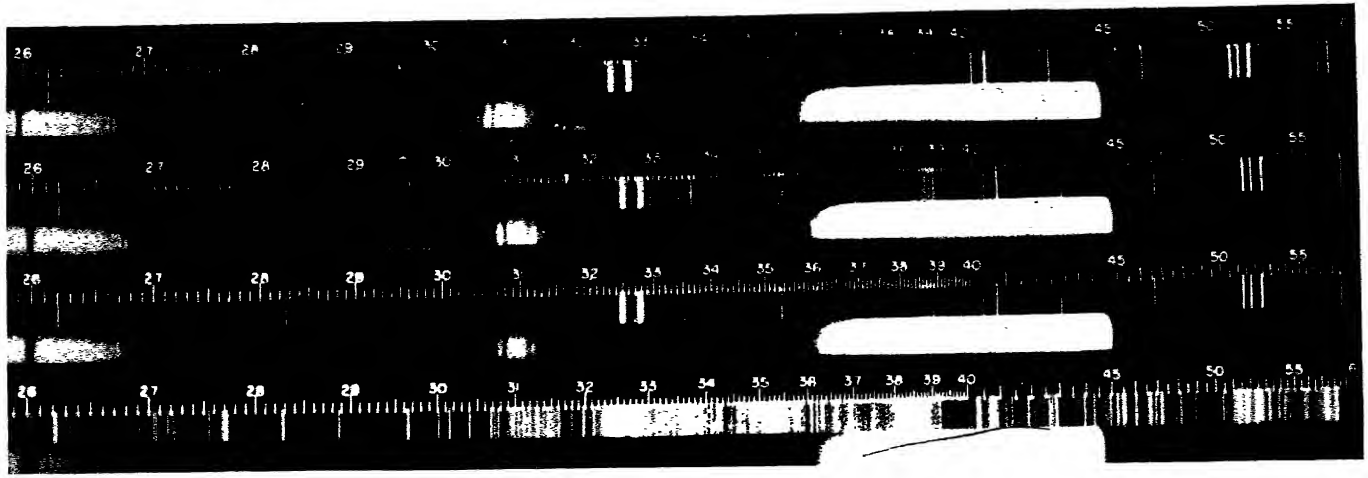

Temp.	Press.
1000°C	8cm
	16cm
	40cm
	76cm

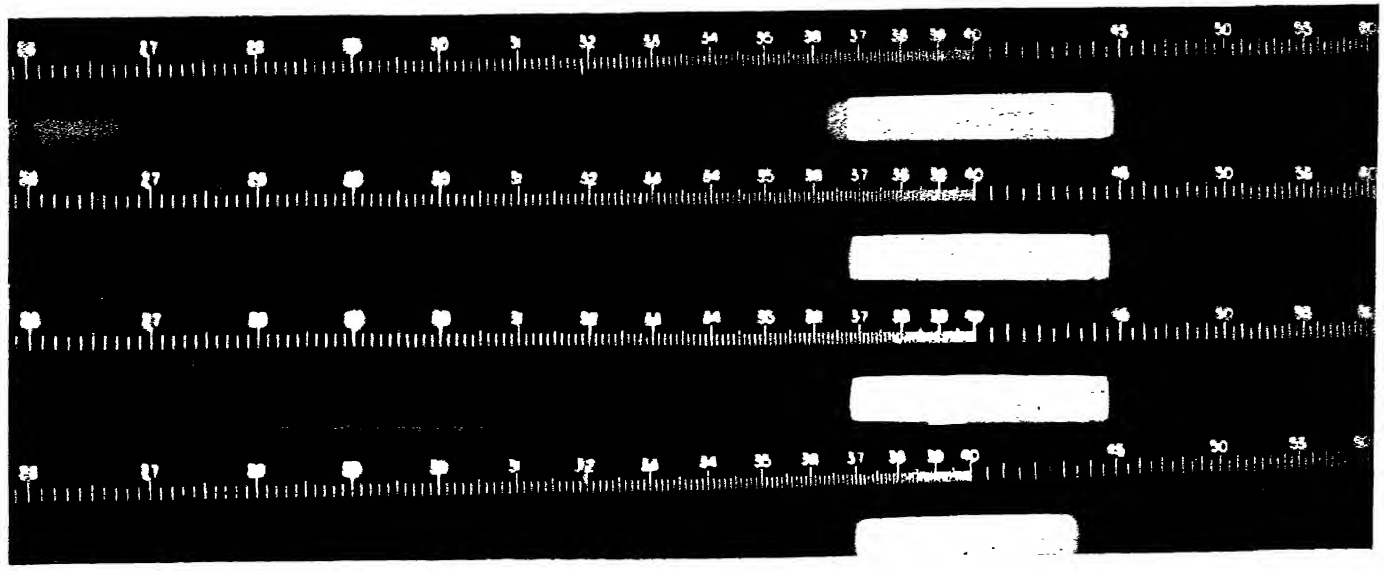

Temp.	Press.
1100°C	10cm
	20cm
	40cm
	60cm

Fig. *e*.

Temp. Press.

Fig. *f*.

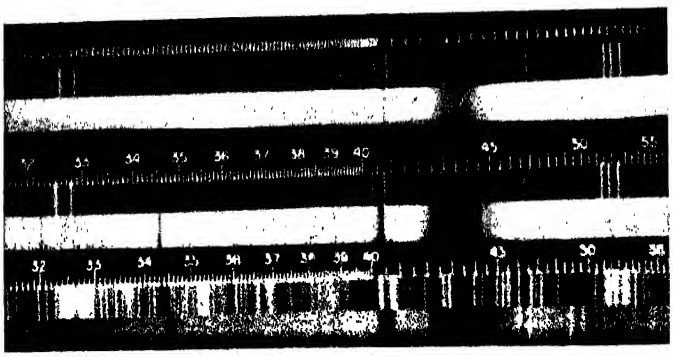

600°C 10cm

40cm

76cm

Fig. *g*.

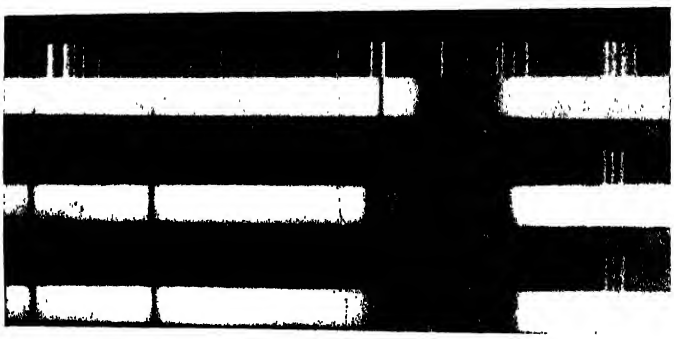

700°C 10cm

40cm

76cm

Fig. *h*.

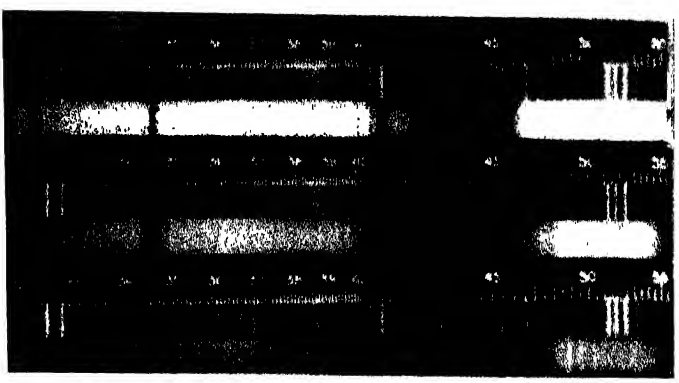

800°C 10cm

30cm

50cm

Fig. *i*.

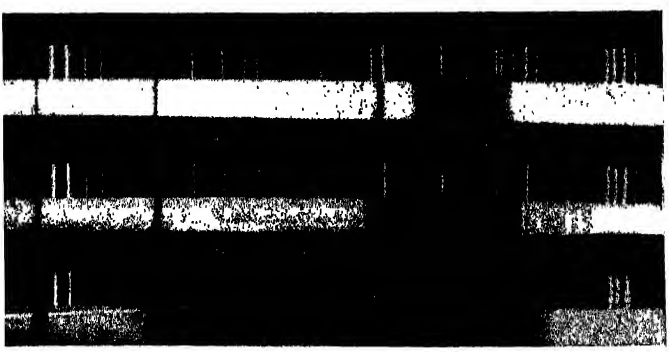

1000°C 4cm

10cm

40cm

the λ3303Å line and broadens with increase in temperature and pressure and ultimately terminates in what look like definite edges at about λ3650Å on the long wavelength side and about λ3150Å on the short wavelength side. The details are given in Table II.

(*c*) λ3050-2850Å Na_2 Bands

Bands in this region appear only at temperatures of about 700°C or above. The continuous absorption appears superposed over the bands, unlike case (*b*) where the continuous absorption began with a narrow patch and gradually broadened on both the sides. At 700°C, as the pressure is increased the band heads over the region λ3000Å to λ2860Å become more and more prominent but along with them the continuous absorption in the above region also becomes stronger. As the temperature or pressure is increased the percentage of continuous absorption goes on increasing and ultimately the entire region from about λ2830Å to about λ3030Å is completely absorbed, leaving only a narrow transparent gap between λ3050Å and λ3150Å which is similar to the one mentioned by Loomis and Nile for the green region. At about 1100 °C, when the pressure is raised higher than 10 cm. even this transparent region near λ3100Å disappears. The details are given in Table III.

(*d*) λ4550-λ4150Å bands of K_2

At the dispersion employed to photograph the spectra (Plate VIID) the bands are too close to be seen separately and the spectrum in the blue region looks like one due to continuous absorption. At low temperature and pressure, the extent of the spectrum and also the amount of light absorbed are small. On increasing these more light is absorbed and extent of the spectrum also increases till finally the entire region between about λ4550Å and λ4150Å is completely absorbed. The details are given in Table IV.

DISCUSSION

Two facts emerge from the description of the spectra in different regions of sodium and potassium given above. Firstly the bands are limited by sharp edges on both the long and short wavelength sides, and secondly superposed over the bands are continuous absorptions which also have sharp limiting edges on both the sides. Studies of some of these bands with a high dispersion instrument confirms that the continuous absorption is genuine and distinct from the bands with structure (Sinha, 1948 and 1948*a*, 1948*b*). The first fact can be explained on the Franck-Condon principle, by drawing vertical transitions between the two states responsible for the bands. If the lengths of the vertical transitions drawn between points lying over the stable regions of the potential energy curves of the two states pass through a maximum and a minimum the bands will possess sharp edges on both the sides.

To explain the presence of a continuum superposed over the bands, let us consider the various causes that can give rise to such a continuum. A molecular

continuum can arise in one of the following ways: (*a*) Ionisation continuum corresponding to transitions of electrons from Bohr's hyperbolic orbits, (*b*) Dissociation continuum joining on to a series of converging bands, (*c*) A continuum which is due to transitions between two states one, at least, of which is repulsive and (*d*) A continuum due to transitions between two states which are themselves stable but the molecules in these states are in the quasi-molecular states. The continua observed in the present case are obviously not of the type (*a*) or (*b*). They may possibly be of the type (*c*) involving transitions between the lower $^3\Sigma_u^+$ and the higher $^3\Sigma_g^+$ or $^3\pi_g$ states, all of which are repulsive. General considerations, (Kuhn, 1932) however, indicate that transitions of the type (*c*) would merely result in the broadening of the lines and would not give such extensive continua as have been observed (work in this connection is in progress). Further the fact that they are found exactly in the same region as the bands with structure suggests that they may be ascribed to type (*d*) rather than to type (*c*). We shall, therefore, discuss type (*d*) and calculate, in such cases where the potential energy curves can be drawn from experimental data, the edges of the spectra.

Let us consider the condition of sodium vapour in the chamber. It is mostly in the atomic state. When the temperature is increased the number of sodium atoms in the chamber also increases. In the absence of any foreign gas, *i.e.* when the pressure in the cooler parts of the tube is low, the metal vapour diffuses to cooler regions and condenses. Increase of total pressure by introducing more of nitrogen gas serves to check rapid diffusion of the metal vapour and thus the concentration of sodium vapour in the chamber is maintained at a fairly high level. Under this condition we have, in the chamber free sodium atoms, a certain percentage of sodium in molecular state in different vibrational levels according to Boltzmann's distribution law and an appreciable fraction of the metal vapour in the form of sodium atoms which are not free, but whose energy is modified due to collisions with similar atoms. Such atoms in the state of collisions form what are usually termed as quasi-molecules. The number of quasi-molecules increases quadratically with pressure since the number of atoms in the state of collision increases quadratically with pressure.

Suppose two unexcited sodium atoms gradually approach each other. Their energy will lie along the curve *EKOBC* (Fig. 1) which represents the potential energy curve for the ground state of Na_2. Let us first consider the case of central collisions. The slowly moving atoms, for such collisions, can cross the point *O* and reach as far as *B*. From this point they may either retrace their path and each may ultimately pass out of the sphere of influence of the other or they may lose some of their energy by collision with a third body and settle down to one of the vibrational levels inside the depth of the potential energy curve giving rise to the formation of a stable molecule or they may absorb a quantum of radiation and pass to an upper potential energy curve obeying Franck-Condon principle. Although, for central collisions, these processes have the chance of maximum occurence at the turning point, they

may occur anywhere on the curve. The last possibility, *i.e.* the quasi-molecules may absorb radiation at any point along the curve and pass over to an

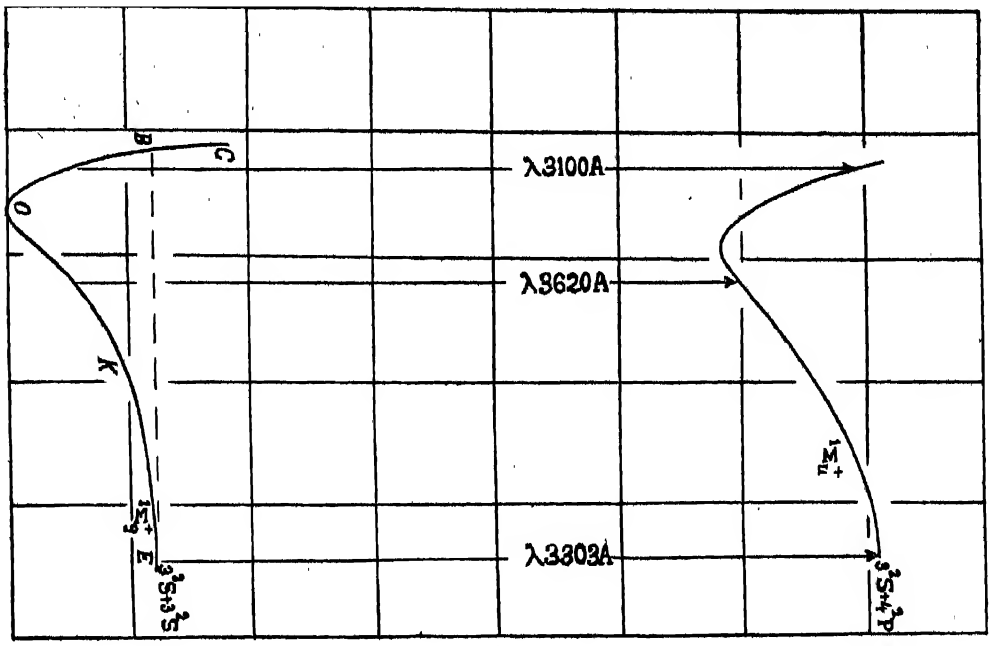

FIG. 1

excited state, will result in a continuous absorption spectrum. The maximum of the continuum on this account will correspond to the length of the vertical transition from *B* and its range will correspond to the region covered by the lengths of the vertical transitions from all points lying on the lower curve. As the temperature is raised, the turning point will shift towards *C* and the range and the maximum of the continuum will be adjusted accordingly.

However, more important than the central collisions are the non-central ones for quasi-molecular considerations. During these collisions the atoms never approach each other as close as *O* and at no point in their path is the kinetic energy zero. The turning point is no longer favoured as in the previous case and a vertical transition from each point on the portion of the curve to the right of *O* is equally probable. This will give a continuous spectrum in absorption whose maximum and minimum of wavelengths will be given by the longest and the shortest lengths of the vertical lines drawn between the two curves.

The range of the continuous spectrum and its behaviour with change in temperature and pressure can thus be worked out if the potential energy curves for both the states involved are completely known. Unfortunately, however, our knowledge of these curves is somewhat complete only in two cases, *i.e.* the green bands and the λ3600-λ3200Å bands of Na_2. The curves given in Fig. 1 refer to the ground and the excited state of the latter system. The data employed in drawing the excited state curve have been taken from the works described earlier (Sinha, 1948*a*, 1948*b*). It can be seen by drawing vertical

transitions between the two curves that, for the non-central collisions, with increase in temperature or pressure, the atomic line will broaden towards longer wavelength and ultimately will cover the whole region between $\lambda 3620$Å and $\lambda 3300$Å. Considerations of central collisions indicate that the continuum will extend to further short wavelength, roughly to about $\lambda 3100$Å. The entire continuum will thus lie between $\lambda 3620$Å and $\lambda 3100$Å. A reference to the spectrogram or to the description given in the previous section shows that the agreement between the calculated and the observed features is as good as can be expected of such a computation.

The other continua discussed above could be quantitatively explained in the same way as the one in the preceding paragraphs, if enough was known about the potential energy curves involved with them. There is, however, some difficulty in giving a satisfactory explanation for the green continuum of sodium in the above manner. If the non-central collisions are more effective in giving continuous absorption, as we expect them to be, the comparatively transparent region about $\lambda 5500$Å should not exist so prominently even in the early stages of temperature and pressure and the continuous absorption should really join on to the atomic line at $\lambda 5893$Å. This, however, happens when the temperature and pressure are sufficiently raised, *i.e.* when the conditions for quasi-molecular formation are more suitable. The short wavelength edge of the green continuum can, however, be easily explained in the same way as the edges of the ultra-violet continuum.

ACKNOWLEDGMENT

The author wishes to acknowledge his indebtedness to Dr. R. W. B. Pearse, London, for his kind help and valuable suggestions and to the authorities of the Patna University for the award of their Birla Scholarship.

SCIENCE COLLEGE,
PATNA.

REFERENCES

Kuhn, H., 1932, *Z. Phys.*, **76**, 782.
Loomis, F. W. and Nile, S. W., 1928, *Phys. Rev.*, **32**, 873.
Loomis, F. W. and Nusbaum, R. E., 1932, *Phys. Rev.*, **40**, 380.
Sinha S. P., 1948, *Proc. Phys. Soc.*, **60**, 436.
Sinha, S. P., 1948*a*, *Ind. Jour. Phys.*, **31**, 401.
Sinha, S. P., 1948*b*, *Proc., Phys. Soc.*, in the press.

THE NEAR ULTRAVIOLET SPECTRA OF BENZENE, PART II A COMPARATIVE STUDY OF THE ABSORPTION, EMISSION AND FLUORESCENCE BANDS

By R. K. ASUNDI AND M. R. PADHYE

(*Received for publication, Nov. 5, 1948*)

ABSTRACT. A comparative study is made of the ultraviolet benzene bands recorded in absorption, emission and fluorescence, as regards the distribution of intensity and the development of vibrational levels. It is found that the intensity distribution in the emission spectrum is substantially different from that in the absorption spectrum at room temperature and appears to be governed by the Boltzmann factor in the excited state and the Franck-Condon principle. The intensity distribution also differs from that of fluorescence bands in which the distribution is generally governed by the conditions of excitation. The emission spectrum gives data for a more complete picture of the state of the molecule and the selection rules governing the transition to which all the three spectra are due.

The region of the near ultraviolet absorption spectrum of benzene is between 2765Å and 2218Å and the corresponding emission spectrum lies in the region 2536Å to 3180Å. Hence there is a considerable stretch of region which is common to both the spectra.* The first bands of the E series lie outside this region whereas the first bands of the series A, B, C, D, G, H, α and β lie in this region. Among them B^0_0, B^0_1 and B^0_2 with their associated 160 quanta and A^0_{-1}, A^0_{-2}, C^0_0 and G^0_0 are common to both spectra. In D system D^0_0, D^0_1, D^1_2 are common with the associated 160 progressions as also α^0_0 and β^0_0 (*cf.* Table I).

The most prominent bands involving c^+_g vibration which are absent in the emission spectrum are A^n_0 ($n = 0, 1, 2 \ldots$). These bands are very strong in absorption, A^0_0 being the strongest. Similarly in C^n_0 series, C^0_0 is present and is very weak in emission but the higher members are absent. In the B^n_2 series the members higher than B^1_2 and in G^n_0 series members other than G^1_0 and also the members of the E series lying in this region are absent in emission although they are present in absorption. The band corresponding to the excitation of 1178 c^+_g vibration is found in absorption but not in emission. The bands corresponding to $1-1$ transition of 849 vibration which are prominent in absorption in this region are not present in emission. The bands which are present in emission but are not observed in absorption are

* The analysis of emission bands is given in Part I. The results of analysis of absorption bands proposed by Sponer *et al* and Radle and Beck, extended by Garforth and Ingold with which our own analysis agrees are utilised in this part.

TABLE I

Development of Different Band Systems in Various Near Ultraviolet Electronic Spectra of Benzene (Comparative Study)

Absorption (Radle and Beck)	Emission (present investigations)	Fluorescence (Ingold Wilson)	Emission (Austin and Black)
$A^0_0-A^4_0$		$A^0_0-A^7_0$	
$A^0_1-A^5_1$ $A^0_{-1}-A^3_{-1}$	$A^0_{-1}-A^3_{-1}$	$A^0_{-1}-A^6_{-1}$	
$A^0_2-A^5_2$	$A^0_{-2}-A^2_{-2}$	$A^0_{-2}-A^5_{-2}$	
$A^0_3-A^5_3$		$A^0_{-3}-A^3_{-3}$	
$A^0_4-A^3_4$		$A^0_{-4}-A^3_{-4}$	
$A^0_5-A^2_5$		$A^0_{-5}-A^3_{-4}$	
A^0_6			
$A^0_{1-1}-A^3_{1-1}$			
$A^0_{2-1}-A^4_{2-1}$			
$A^0_{3-1}-A^3_{3-1}$			
$A^0_{4-1}-A^2_{4-1}$			
$A^0_{1-2}-A^1_{1-2}$			
$A^0_{2-2}-$			
$A^0_{3-2}-A^3_{3-}$			
$B^0_0-B^4_0$	$B^0_0-B^5_0$	$B^0_0-B^6_0$	$B^0_0-B^4_0$
$B^0_1-B^3_1$	$B^0_1-B^4_1$	$B^0_1-B^7_1$	$B^0_1-B^2_1$
$B^0_2-B^4_2$	$B^0_2-B^1_2$		$B^0_2-B^1_2$
$B^0_3-B^2_3$			
$B^0_4-B^2_4$			
$B^0_{2-1}-B^2_{2-1}$		$B^0_{2-1}-B^3_{2-1}$	
		$B^0_{2-2}-B^3_{2-2}$	
		$B^0_{2-3}-B^2_{2-3}$	
$C^0_0-C^4_0$	C^0_0	$C^0_0-C^5_0$	
$C^0_1-C^4_1$ $C^0_{-1}-C^3_{-1}$	$C^0_{-1}-C^2_{-1}$	$C^0_{-1}-C^6_{-1}$	C^0_{-1}
$C^0_2-C^3_2$ C^0_{-2}	$C^0_{-2}-C^3_{-2}$	$C^0_{-2}-C^5_{-2}$	C^0_{-2}
$C^0_3-C^3_3$	$C^0_{-3}-C^2_{-3}$	$C^0_{-3}-C^1_{-3}$	$C^0_{-3}-C^2_{-3}$
	$C^0_{-4}-C^2_{-4}$	$C^0_{-4}-C^4_{-4}$	
$C^0_{1-1}-C^4_{1-1}$	$C^1_{1-1}-C^5_{1-1}$		
$C^0_{1-2}-C^1_{1-2}$			
$C^0_{2-1}-C^2_{2-1}$			

TABLE I (*contd.*)

Absorption (Radle and Beck)	Emission (present investigations)	Fluorescence (Ingold Wilson)	Emission (Austin and Black)
$C^0_{3-1}-C^4_{3-1}$			
$D^0_0-D^2_0$	$D^0_0-D^4_0$	$D^0_0-D^4_0$	$D^0_0-D^3_0$
$D^0_1-D^3_1$ D^0_{-1}	$D^0_1-D^4_1$ $D^0_{-1}-D^3_{-1}$	$D^0_{-1}-D^5_{-1}$	$D^0_1-D^4_1$ $D^0_{-1}-D^1_{-1}$
$D^0_2-D^3_2$	D^0_2 $D^0_{-2}-D^2_{-2}$	D^0_{-2}	D^0_2 $D^0_{-2}-D^1_{-2}$
$D^0_3-D^2_3$	$D^0_{-3}-D^2_{-3}$		$D^0_{-3}-D^1_{-3}$
D^0_4	$D^0_{-4}-D^2_{-4}$		
$D^0_{1-1}-D^1_{1-1}$	$D^0_{1-1}-D^3_{1-1}$		
$D^0_{2-1}-D^1_{2-1}$			
D^0_{3-1}			
$D^0_{4-1}-D^3_{4-1}$			
$E^0_0-E^3_0$			
$E^0_1-E^1_1$ E^0_{-1}			
E^0_3			
$E^0_{2-1}-E^1_{2-1}$			
$\alpha^0_0-\alpha^1_0$	$\alpha^0_0-\alpha^5_0$	$\alpha^0_0-\alpha^5_0$	$\alpha^0_0-\alpha^3_0$
	α^0_2 $\alpha^0_{-1}-\alpha^4_{-1}$	$\alpha^0_{-1}-\alpha^5_{-1}$	$\alpha^0_{-1}-\alpha^2_{-1}$
	α^0_2 $\alpha^0_{-2}-\alpha^2_{-2}$	$\alpha^0_{-2}-\alpha^2_{-2}$	$\alpha^0_{-2}-\alpha^2_{-2}$
	$\alpha^0_{1-1}-\alpha^1_{1-1}$		$\alpha^0_{1-1}-\alpha^1_{1-1}$
	$\alpha^0_{1-2}-\alpha^1_{1-2}$		$\alpha^0_{1-2}-\alpha^1_{1-2}$
α^0_{2-1}			
α^0_{2-2}			
β^0_0	$\beta^0_0-\beta^5_0$	$\beta^0_0-\beta^5_0$	$\beta^0_0-\beta^4_0$
$\beta^0_1-\beta^3_1$	$\beta^0_{-1}-\beta^3_{-1}$	$\beta^0_{-1}-\beta^5_{-1}$	$\beta^0_{-1}-\beta^3_{-1}$
	$\beta^0_{-2}-\beta^3_{-2}$	$\beta^0_{-2}-\beta^4_{-2}$	$\beta^0_{-2}-\beta^2_{-2}$
	$\beta^0_{-3}-\beta^2_{-3}$		$\beta^0_{-3}-\beta^2_{-3}$
	$\beta^0_{-4}-\beta^2_{-4}$		$\beta^0_{-4}-\beta^1_{-1}$
	$\beta^0_{1-1}-\beta^2_{1-1}$		$\beta^0_{1-1}-\beta^1_{1-1}$
	$\beta^0_{1-2}-\beta^1_{1-2}$		$\beta^0_{1-2}-\beta^1_{1-2}$
	$\beta^0_{1-3}-\beta^2_{1-3}$		

TABLE I (*contd.*)

Absorption (Radle and Beck)	Emission (present investigation)	Fluorescence (Ingold Wilson)	Emission (Austin and Black)
	$\beta^0{}_{2-1}-\beta^3{}_{2-1}$		
$G^0{}_0-G^2{}_0$	$G^0{}_0$		
$G^0{}_1-G^2{}_1$			
$G^0{}_2-G^2{}_2$			
$G^0{}_3-G^1{}_3$			
$G^0{}_{1-2}$			
$H^0{}_0-H^3{}_0$	$H^0{}_0$	$H^0{}_0-H^2{}_0$	
$H^0{}_1-H^1{}_1$		$H^0{}_{-1}-H^2{}_1$	
$H^0{}_2-H^1{}_2$			
$H^0{}_3-H^1{}_3$			
$A'{}_0{}^0-A'{}_0{}^1$	$A'{}_0{}^0-A'{}_0{}^4$		
$A'{}_1{}^0-A'{}_1{}^1$	$A'{}_{-1}{}^0-A'{}_{-1}{}^2$		
$A'{}_2{}^0$			
$B'{}_0{}^0$	$B'{}_0{}^0-B'{}_0{}^2$		
$B'{}_1{}^0$ $B'{}_{-1}{}^0$	$B'{}_1{}^0-B'{}_1{}^1$		
$B'{}_2{}^0$			
$C'{}_0{}^0$			
$C'{}_1{}^0$			
$D'{}_0{}^0$	$D'{}_0{}^0-D'{}_0{}^2$		
$D'{}_1{}^0$			
	$\alpha'{}_0{}^0-\alpha'{}_0{}^3$		
	$\alpha'{}_1{}^0-\alpha'{}_1{}^2$ $\alpha'{}_{-1}{}^0-\alpha'{}_{-1}{}^2$		
	$\alpha'{}_2{}^0-\alpha'{}_2{}^3$		
	$\alpha'{}^0{}_{1-1}$		
	$\alpha'{}^0{}_{2-1}-\alpha'{}^2{}_{2-1}$		
	$\beta'{}_0{}^0-\beta'{}_0{}^2$		
$I^0{}_0-I^2{}_0$			
$I^0{}_1-I^3{}_1$ $I^0{}_{-1}-I^3{}_{-1}$			
$I^0{}_2-I^2{}_2$ $I^0{}_{-2}-I^3{}_{-2}$			
$I^0{}_{1-1}-I^2{}_{1-1}$			
	$K^0{}_0-K^2{}_0$		$K^0{}_0-K^2{}_0$
	$K^0{}_1-K^1{}_1$ $K^0{}_{-1}-K^0{}_{-1}$		$K^0{}_{-1}-K^2{}_{-1}$
	$K^0{}_{-2}-K^1{}_{-2}$		

TABLE I (*contd.*)

Absorption (Radle and Beck)[1]	Emission (present investigations)	Fluorescence (Ingold Wilson)	Emission (Austin and Black)
	(530−671 a_2'')		
520+2×513	−606−2×671		
,, ,, +923			
1045+2×513 (2)*	−1178+2×513,		
3047+2×513	1045−2×671		
	(1001−1010 b_{1u})		
	+520−2×1010		
−606+2×1001			
−1596+2×1001 (2)*	−1596−2×1010		
−1178+2×1001			
	−3047−2×1010		
	(774−983 b_{2g})		
	520−2×985		
520+2× 774 (2)*			
,, ,, 923			
1476+2× 774	−1596+2×774		
,, ,, 923			
−1596+2× 774			
,, ,, 923			
1045+2× 774 (2)*			
,, ,, 923			
	−3047+2×774		
	(364−703 b_{2g})		
−606+2× 364	−606−2×703		
	+520+2×364,		
−1596+2× 364	+520−2×703		
1476+2× 364	1596−2×703		
−1178+2× 364			
+1045−703+364 (2)*			
	+3047+2×364		

* These denoted the number of bands in the 160 progression.

TABLE I (*contd*).

Absorption (Radle and Beck)	Emission (present investigation)	Fluorescence (Ingold Wilson)	Emission (Austin and Black)
	(?−1648 b_{2u})		
	+520−2×1648		
	−606−2×1648		
	1045−2×1648		
	(?−1110 b_{2u})		
	−606−2×1110		
	−1596−2×1110		
	−3047−2×1110		
	(?−1326 a_{2g})		
	+520−2×1326		
	−606−2×1326		
	(non-totally symm degenerate vibrations)		
−849+586 (2)*	−849+586	−2×849 (5)*	
		−2×849−992	
−2×586 (3)*		−849+586	
−2×586+923 (3)*		−606−264	
−2×586+2×923		,, −992	
−606+2×586			
+520+2×586			
,, ,, +923			
,, ,, +2×923			
	0+2×240 0−2×404	0+2×240	
	0−2×3080		

0—2×404 corresponding to $\Delta V = 2$ of the e_u^+ frequency, the $\alpha^0_0 + 2 \times 240$ and $\beta^0_0 + 2 \times 240$ bands and the 160 progression of the α^0_0 and β^0_0 series (*cf.* Table I).

This shows that the intensity distribution in the two spectra is not the same. This can be clearly seen from the study of the relative intensities of the prominent bands of different series which are common to both the spectra. The relevant data are given in Table II. The intensities marked are only

* These denote the number of bands in the 160 progression.

useful for the study of the relative intensities of different band groups and of the relative intensity distribution amongst the bands in the group. The intensities in the present experiments have been visually estimated and the values given are, therefore, very rough. The intensities marked by Radle and Beck seem to be more reliable since their method of estimation is more accurate.

TABLE II

Series	I absorption	I emission	Series	I absorption	I emission	Series	I absorption	I emission	Series	I absorption	I emission	Series	I absorption	I emission	Series	I absorption	I emission
A^0_0	7500	abs	B^0_0	420	10	C^0_0	620	0	D^0_0	55	6	α^0_0	4	8	β^0_0	3	8
			B^0_1	550	8.5	C^0_1	675		D^0_1	130	5	α^0_1	abs.	0	β^0_1	7	abs.
			B^0_2	350	4				D^0_2	40	2						
A^0_1	85	3				C^0_{-1}	4	2	D^0_{-1}	0	5						
A^0_2	3	2.5				C^0_2	1	3.5									

The intensities (I) given for bands in absorption spectrum are from Radle and Beck. (1940). They have given intensity 7500 to the strongest band A_0^0.

The intensities (I) given for bands in emission spectrum are those observed in the present experiments (Asundi and Padhye, 1949) the intensities being relative to the B^0_0 the strongest band being 10.

Making due allowance for these facts certain conclusions can be drawn from this Table. Thus,

(1) In absorption A^0_0 and C^0_0 bands are stronger than B^0_0 and D^0_0 whereas in emission B^0_0 and D^0_0 are definitely more intense than A^0_0 and C^0_0.

(2) A^0_{-1} and C^0_{-1} decrease in intensity in absorption whereas they increase in intensity in emission. The positive members of these series do not lie in the spectral region of the emission spectrum.

(3) Taking either α^0_0 or β^0_0 as B^0_{-1} (since it is due to Fermi degeneracy between 1596 and $606+992=1598$, B^0_{-1}), it is seen that D^0_{-1} and B^0_{-1} decrease in intensity more rapidly in absorption than in emission.

(4) B^0_1 and D^0_1 have greater intensity than B^0_0 and D^0_0 in absorption but are slightly weaker than B^0_0 and D^0_0 in emission.

(5) For B^0_2 and D^0_2 the intensity falls both in absorption and emission compared to B^0_1 and D^0_1.

(6) The band involving 1596 (either α^0_0 or β^0_0) is relatively stronger in emission than in absorption.

The bands B^0_0, D^0_0, α^0_0 and β^0_0 lie to the long wave-length limit of the absorption spectrum and bands A^0_0 and C^0_0. to the short

wavelength limit of the emission spectrum. This cannot be a sufficient argument for the weakness of the bands in the corresponding spectra more so in the emission spectrum because the bands B^0_2, D^0_2 and B^1_2 which are still to the shorter weavelength side than A^0_0 and C^0_0 bands come out with appreciable density.

In the A series the 520 frequency in the upper state is excited and transition takes place between this and the zero level of the ground state. In C series the fundamental transition is 606 (ground)—2×520 (excited), ni B, 606—0 and in D, 2×606—520. It is found that transition involving high frequencies of excited state and of low ground state are stronger in absorption than in emission (*vide* Table II). This is to be expected on the basis of the Boltzmann factor. Similarly transitions involving frequencies of low excited states and high ground state are stronger in emission than absorption. This fact seems to agree well with Sponer's (1939) hypothesis that in flourescence (hence also in emission) the 1-0 and 0-1 transitions of the $e_u{}^+$ vibration should occur with inverted intensities corresponding to the Boltzmann distribution in the upper state. The relative intensities of the groups on this basis should decrease in the following order B, α, β, D, A, C. This is also generally borne out by the data. An interesting observation is that D which involves two quanta of 606 in the ground state is stronger than A which involves no ground state frequency, although both contain one quantum of 520 in the excited state. This illustrates the operation of the Franck-Condon principle in addition to the Boltzmann equilibrium in the excited state. This inversion of intensity may be even perhaps due partly to self-absorption although in the present experiments such a possibility is rather remote.

With the superposition of the 992 frequency in the ground state, the intensity of all the four A, B, C, and D series decreases in absorption. But in emission the intensity increases in A and C series for the first quantum of 992 and decreases for the second quantum; while it decreases uniformly for B and D the decrease is not so rapid as in absorption. The superposition of the 923 quantum in the upper state raises the intensity of the D^0_0, B^0_0 and $C_0{}^0$ bands in absorption for the first quantum after which it falls. In emision it falls uniformly, This seems to agree with another observation by Sponer *et. al.* (1939) that in absorption the second member of the 923 progression is the strongest while in emission it should be the second member of the 992 progression which should be by far the most outstanding in intensity. The agreement is not strictly complete since the intensities of B^0_1 and D^0_1 are slightly less than of $B_0{}^0$ and $D_0{}^0$ in emission. In absorption, however, the agreement is uniformly satisfactory.

Turning to fluorescence spectrum in relation to emission spectrum, we find that the region of both the spectra is the same.* The flourscence

* The data of Ingold *et al* are used to analyse these bands along the lines adopted for absorption and emission. The general trend of analysis is indicated by Sponer *et al*, a detailed analysis agrees with that of Garforth and Ingold.

spectrum gives a large number of bands belonging to A series while the emission spectrum does not. On the other hand, the D series is more prominent in emission than in fluorscence. The emission spectrum also shows two intense parallel systems of bands due to Fermi resonance extending to high quanta of vibrations in the ground state whereas in fluorescence they are limited to two quanta. Similarly the 3062 a_{1g} (the value of which has been found to be 3054 in present experiments) which is expected to be present in fluorescence is not unambiguously found. In the case of emission all the bands belonging to (') series are due to the excitation of this frequency in the ground state. In emission a number of non-totally symmetrical degenerate and nondegenerate frequencies are excited. Such is not the case in fluorescence.*

The intensity distribution in the fluorescence spectrum is rather irregular. This has been already pointed out by Sponer *et al* and they say "The explanation of the relative intensities of the different band groups in the fluorescence spectrum is somewhat complicated. This is due to the fact that the bands are a result of mechanism of excitation, subsequent collision, and reabsorption. As we should expect B^0_0 series is the strongest in the spectrum." Furthermore, the scale of intensity adopted by Ingold and Wilson (1936) seems to be different from that of Wilson (1936) and since for a comparison of intensities in the emission and fluorescence spectra it will be necessary to consider all the fluorescence bands, it is not possible or profitable to discuss the relative intensity distribution in the two spectra. However, it appears that the course of intensity-decrease in fluorescence follows the order B, α β, C, A, and D while in emission bands the order is B, α β, D, A and C, α β being Fermi doublets practical of equally intensity and represent vibration mixtures.

Thus experimentally it is found that the emission spectrum obtained and discussed in Part I of this series (Asundi and Padhye, 1949) shows a great advantage over the high pressure fluorescence in the matter of excitation of the numerous ground level frequencies. It also gives a picture of intensity distribution since it is neither influenced by selection rules nor by self-absorption to a very great extent. The latter can be eliminated by the proper adjustment of the experimental conditions. The electrical method of excitation develops also the weaker bands which are not found in fluorescence and thus it gives a more complete picture of the state of the molecule and the selection rules governing such a transition.

* It may be noted that even though the same dispersion and resolution was used in both the cases, the bands in fluorescence naturally show a very open structure while in the present case they are far from being resolved.

REFERENCES

Asund and Padhye (1945), *Nature*, **156**, 368.
,, ,, (1949), *Ind. Jour. Phys.*, **23**, 199.
Garforth and Ingold (1948), *J. C. S.*, April.
Ingold and Wilson (1936), *J. Chem. Soc.*, 955.
Radle and Beck (1940), *J Chem. Phy.*, **8**, 507.
Sponer, Nordheim, Sklar and Teller (1939), *J. Chem. Phy.*, **7**, 207.
Wilson (1936), *J. Chem. Soc. P.*, 1210.

ON THE STRUCTURE OF THE RESONANCE LINE OF Hg FILTERED THROUGH Hg VAPOUR*

By G. S. KASTHA

(*Received for publication, May 12, 1949*)

Plate VIII

ABSTRACT. The structure of the resonance line 2536.6 Å of mercury filtered through a cell containing mercury vapour at different temperatures and pressures has been studied with an Adam Hilger large (E_1) quartz spectrograph. It has been observed that the mercury vapour in the absorption cell absorbs only the central portion of the resonance line, there being a feeble line transmitted on each side of the centre. The distance between these two lines increases to about 18 cm^{-1} when the temperature of the mercury in the absorbing cell is raised to 100°C. The intensity of these two lines is much less than that of the line 2534.8A° and is of the same order of magnitude as that of the Brillouin components observed by Krishnan in the case of diamond. It is pointed out that as the separation and the intensity of those Brillouin components are the same as those of the doublet in the resonance line filtered through mercury vapour it is doubtful whether the lines observed by Krishnan are genuine Brillouin components in the light scattered by diamond.

INTRODUCTION

It has been pointed out recently by Krishnan (1947) that the line 2536.6 Å of mercury scattered by diamond and afterwards filtered through mercury vapour shows, when examined with either a medium or a high dispersion quartz spectrograph, a structure which consists of a doublet, the two components being separated from each other by about 12 cm^{-1}. Each of these components on more careful examination has been found to be composed of one intense inner component and another fainter outer component. This splitting of the scattered line has been explained by Krishnan on the hypothesis that Brillouin components are produced by sound waves of thermal origin moving in the crystal, the transverse and longitudinal waves giving rise to the inner and outer pair of the components respectively. He has calculated the relative intensities of the inner and outer components from the theory put forward by Leontowitsch and Mandelstam (1932) and has found that the observed values do not agree at all with those calculated from the theory. The theory predicts that the component due to the longitudinal waves should be more intense than that due to the transverse waves, but actually the reverse is fouud to be true.

* Communicated by Prof. S. C. Sirkar

There is another discrepancy also, which has not been explicitly pointed out by Krishnan. According to the theory mentioned above, the ratio of intensity of the component scattered by the transverse sound waves to that of the undisplaced component should be about 0.31×10^{-5}. The value of this ratio actually observed has not been calculated by him, but he has mentioned that the aggregate intensity of all the Doppler components is less than one fourth the intensity of the Raman line. From this the ratio of intensity of the component due to transverse waves to that of the Raman line can be taken as 1 : 6. The Rayleigh line, however, is not more than 1000 times as intense as the Raman line, because the 1332 cm^{-1} line excited by the Hg line 4046 Å is more intense than the Hg line 4140 Å and the 4046 Å line is not more than 10^3 times as intense as the line 4140 Å. Hence the ratio of the intensity of the Brillouin component due to transverse waves in diamond at room temperature to that of the undisplaced component is of the order of 10^{-4} while theoretically it should be of the order 10^{-6}. From these facts it appeared that the problem deserved more careful reinvestigation and the present investigation was undertaken with that object in view.

EXPERIMENTAL

In the preliminary investigation a small diamond transparent to Hg line 2536 6 Å was used for photographing its Raman spectrum excited by the resonance line with an Adam Hilger medium quartz spectrograph. A cell containing a few drops of mercury and provided with quartz windows was placed in the path of the scattered light to absorb the resonance line of mercury. A quartz lens was used to focus this light on the slit of the spectrograph. There was also an arrangement for raising the temperature of the cell at will with an electric heater. The Hg line 2536.6 Å scattered by the diamond and transmitted through mercury vapour was found to consist of a doublet, the two components being placed symmetrically on the two sides of the central core which was completely absorbed by the mercury vapour in the cell. Since the proportion of stray light was very great in the light focussed on the slit of the spectrograph and yet the central core of the line 2536.6 Å was absorbed by the vapour it was suspected that even the incident resonance line of mercury when filtered through mercury vapour might be split up into two components. In order to investigate this question the direct light from a quartz mercury arc with its cathode end immersed in running water was passed through the cell containing mercury vapour and the spectrum of the transmitted light was photographed with the quartz spectrograph mentioned above and also with a large Adam Hilger E_1 quartz spectrograph.

Several photographs of the spectrum were taken keeping the mercury vapour in the cell at different temperatures. The heating coil of the cell was wound so as to produce no magnetic lines of force and in order to ensure that the results obtained were not being affected by the residual magnetic

Fig 1 Unfiltered.

Fig 2 Absorbing vapour at 25°C

Fig 3 " " 55°C

Fig 4 " " 75°C

Fig. 5 " " 100°C

Fig. 6 " " 110°C

Resonance line of Hg filtered through Hg vapour.

field produced by the heating coil, another identical cell heated with a Bunsen burner was used and the resonance line transmitted by this cell was photographed. It was observed that the results obtained with the cell heated either electrically or with a burner were identical.

RESULTS AND DISCUSSION

The spectrograms obtained with absorbing mercury vapour at different temperatures are reproduced in Plate VIII. Fig. 1 shows the spectrum of the light from the mercury arc not filtered through any mercury vapour. Figs. 2, 3, 4 and 5 show the spectrograms with the absorbing vapour at 25°C, 55°C, 75°C and 100°C respectively. Fig. 4 also shows the spectrogram with the absorbing vapour heated by a Bunsen burner to 75°C. In the case of the spectrogram reproduced in Fig. 6 the temperature of the absorbing vapour was about 110°C.

It can be seen from these spectrograms that only the core of the 2536 6Å line is absorbed by the vapour in the cell while regions on both sides of the core are transmitted. When the vapour is at about 30°C the width of the absorbed central core is only 5 cm^{-1} and the intensity of each of the two bands appearing on the two sides of the central core is almost the same as that of the line 2534.8Å. As the temperature of the vapour is raised the intensity of the doublet goes on diminishing rapidly and at 100°C the intensity becomes only about one third that of the line 2534.8A°. It is also quite clear from the spectrograms in Plate I that the separation of the two components increases rapidly at higher temperatures. The values of the separation for different temperatures are given in Table I. The width of each component of the doublet remains almost constant with the rise of temperature of the absorbing vapour.

TABLE I

Temperature in degrees Kelvin.	Separation of the doublet in cm^{-1}	Width of each component in cm^{-1}
298	5·2	4·4
328	6.33	4·5
348	11.18	4·5
373	18 6	4·5
383	24 3	4·8

A careful examination of the spectrograms reveals that in the spectrogram due to the unfiltered light from the mercury arc the intensity at a distance of 8 cm^{-1} from the centre of the 2536.6 A° line is much too feeble to account for the appearance of the two components of the doublet at these positions

in the spectrogram due to the light filtered through mercury vapour at about 100°C. This can be clearly seen from figs. 1 and 5 in both of which the Hg line 2534.8 Å is almost of the same intensity, and although there is no blackening in Fig. 1 at 8 cm^{-1} from the centre of the line 2536.6 Å, a doublet appears at this position in Fig. 5.

A small percentage of light of changed wavelengths is thus created while in the line 2536.6 Å traverses the heated mercury vapour in the cell. It is also evident from Table I that the change in frequency increases very rapidly with the rise in temperature. This fact suggests that the observed change in the frequency of the light is not due to Döppler effect on Rayleigh scattering, because the velocity of the Hg atoms increases only in the ratio $\sqrt{\frac{373}{300}}$ when the vapour at 27°C is heated to 100°C, while the change in frequency increases four times. Further, the shift due to Döppler effect would be only about 0.1 cm^{-1}, while the shift actually observed is 9 cm^{-1}. Hence this effect is to be ascribed to some other property of the vapour.

In this connection it has to be pointed out that Lennuier (1947) observed an effect which might be considered to be a reverse phenomenon of what is observed in the present investigation. He studied the scattering of light of wavelength just in the neighbourhood of that of the resonance line of mercury by mercury vapour at a pressure of 1.84×10^{-4}mm. It was observed by him that although the 2536.6 Å line itself was not present in the incident light but light of slightly different wavelength was used as the incident light, the light scattered in the transverse direction contained a large proportion of light of wavelength 2536.6 Å. He explained this phenomenon on a theory of scattering of light by the mercury atoms in the neighbourhood of resonance frequency. Later, Lennuier (1948) reported that the phenomenon is observed with the incident light of frequency ν_1, when ν_1 is either greater than or less than ν_0, where ν_0 is the resonance frequency. In his experiment ν_1 differed from ν_0, by about 1 cm^{-1} only and the incident light of these frequencies was obtained by splitting the resonance line of mercury by applying a longitudinal magnetic field to the vapour emitting the line. In the present investigation in the process of scattering in the forward direction the value of ν_0 is observed to be changed by about 9 cm^{-1}. Hence although this process may be considered to be the reverse of that observed by Lennuier the magnitude of the change is much larger than that observed by him.

This broadening of the resonance line of mercury during absorption by mercury vapour in presence of foreign gases was observed indirectly from results of measurement of absorption by mercury vapour of the resonance line long ago by previous workers. Wood (1922) showed that when the resonance radiation from mercury vapour is filtered through a cell containing cold mercury vapour and the filtered light is allowed to illuminate mercury vapour in a second cell the intensity of the resonance radiation excited in

the latter cell is very small. If, however, helium is introduced as a foreign gas in the second cell the intensity of resonance mercury radiation increases enormously. This shows that ordinarily only the core of the resonance line can excite the resonance radiation in a second cell, but when foreign gas is introduced the excitation takes place even when the core has been absorbed in the incident light. Evidently, the presence of molecules or atoms of foreign gas broadens the resonance level of the mercury atom. Orthmann (1925) calculated theoretically the broadening of the absorption of the resonance line by mercury atoms in presence of hydrogen atoms and came to the conclusion that at a pressure of 253 mm. hydrogen atoms can increase the half width of the resonance line in absorption from its original value 1.01×10^{-3} Å to about 8.0×10^{-3} Å. The broadening of the resonance line observed in the present investigation is many times larger and cannot be explained by Orthmann's theory of collisional broadening. Although atmospheric nitrogen may have been present in the cell containing the mercury vapour which was used to absorb the resonance line in the present investigation and part of the broadening of the absorption line may be due to collisional effect the magnitude of the broadening actually observed is much larger than that predicted by Orthmann's theory. On the other hand, Oldenberg (1928) observed by spectroscopic examination that when helium at a pressure of one atmosphere is mixed with mercury vapour at low pressure in a resonance lamp a band extending from 2519 Å up to 2570 Å accompanies the 2536.6 Å line. Nitrogen at low pressure may therefore similarly widen the resonance line in the resonance tube to a smaller extent.

It appears from the results of the present investigation that not only the width of the resonance line in absorption increases with the rise of the temperature and consequently with the increase in the number of collisions, but fluorescence radiations of wavelengths differing only slightly from those of the edges of the absorption band are also emitted by the mercury atoms. The difference between the wavelengths of these radiations and that of the centre of the resonance radiation also increases with the temperatue of the vapour. In this connection it may not be irrelevant to point out that in the spectrograms published by Wood (1925) in figs. 5(*b*) and 5(*c*), Plate XXV, the resonance line 2536.6 Å seems to be unusually broad. He has mentioned that water vapour and nitrogen were present in the resonance tube in the former case and helium was present in the latter case and these foreign gases gave rise to some extra bands. The widening of the resonance line was not mentioned by him explicitly although the broadening extends up to a few Angstrom units. It is clear, however, from a comparison of the spectrograms reproduced by Wood and those obtained in the present investigation that the width of the resonance line in emission is always greater than that of the line in absorption. The feeble resonance radiation

of changed wavelength is therefore not absorbed by the mercury vapour through which it has to come out.

The intensity of the two components of the filtered resonance line observed in the present investigation is of the same order of magnitude as that of the Brillouin components observed by Krishnan (1947), as can be seen from a comparison of the intensity of these components with that of the line 2534.8 Å. The intensity of the two components is of the order of 1/1000th of the intensity of the line 2536.6 Å itself, because it is a little less than that of the Raman line 1332 cm^{-1} excited by the line 2536-6 Å. The separation of the two components is also of the same order of magnitude as that observed by Krishnan (1947). These facts and also the fact that the width of the absorption line is always less than that of the emission line lead to the conclusion that the doublet observed by Krishnan may not be Brillouin components, but they may due the broadening of the resonance line in the absorbing mercury vapour as discussed in this paper.

ACKNOWLEDGMENT

The author is indebted to Prof. S. C. Sirkar for his kind interest and guidance during the progress of this work.

INDIAN ASSOCIATION FOR THE
CULTIVATION OF SCIENCE,
CALCUTTA

REFERENCES

Krishnan, R. S., 1947, *Proc. Ind. Acad. Sci.*, **26A**, 399.
Leontowitsch, M. and Mandelstam, S., 1932, *Phys. Z. Sowjet*, **1**, 317.
Oldenbarg, O., 1928, *Z. f. Phys.*, **47**, 184.
Orthmann, W., 1925, *Ann der Phys.*, **78**, 601.
Wood, R. W., 1922, *Phil. Mag.*, **44**, 1107.
,, ,, 1925, *Phil. Mag.*, **50**, 774.

ON THE RAMAN SPECTRA OF CS_2 AT DIFFERENT TEMPERATURES*

By N. C. MAJUMDAR

(*Received for publication April 20, 1949*)

Plates IXA and IXB

ABSTRACT. The Raman spectra of CS_2 at different temperatures in the liquid and solid states have been investigated. It has been observed that the prominent Raman lines shift a little with the lowering of temperature of the substance. Further, the wing which is observed to accompany the Rayleigh line at room temperature is much weakened at lower temperatures and develops into a weak broad band at 45 cm^{-1} at $-100°C$. In the case of the solid state this band is split up into two strong lines at 59 and 70 cm^{-1} at $-125°C$, which sh ft to 69 and 80 cm^{-3} respectively at $-183°C$. It is concluded that these results indicate the possibility of formation of dimers in the solid state, because the intensities of these lines do not diminish appreciably when the temperature of the solid is lowered.

INTRODUCTION

The Raman spectrum of carbon disulphide in the solid state at low temperature was first studied by Sirkar (1936) and it was observed that two new Raman lines appear in the solid state in the neighbourhood of the Rayleigh line. It is not known, however, whether the frequencies of these lines change with the temperature of the solid and whether the lines appear only after the liquid is solidified. Such information would be helpful in understanding not only the origin of these new lines but also the nature of the intermolecular field in the liquid and solid states. In the present investigation, therefore, the Raman spectra of carbon disulphide in the liquid state at a temperature just above its melting point and in the solid state at different temperatures have been studied.

EXPERIMENTAL

The arrangement for photographing the Raman spectrum of the substance at different temperatures is the same as that used in an earlier investigation by the author (Majumdar, 1949). The liquid distilled in vacuum was put in a pyrex container which was kept inside a transparent Dewar vessel and the level of liquid oxygen, introduced into the Dewar vessel by partial evacuation of the space inside it, was so adjusted that the temperature of the liquid, as measured with a pentane thermometer in contact with the outer surface of

* Communicated by Prof. S. C. Sirkar.

the pyrex container, came down to about −100°C, the melting point of the substance being −111°.6C. The Raman spectrum of the liquid at this temperature was photographed with a Fuess glass spectrograph. The level of liquid oxygen in the transparent Dewar vessel was next raised so that the temperature of CS_2 in the container came down to about −125°C and the substance was solidified. Keeping the solid at this temperature, its Raman spectrum was photographed as before. The container was finally kept immersed in liquid oxygen and the Raman spectrum of the solid at about −183°C was photographed. The Raman spectrum of the substance in the liquid state at room temperature was also photographed for comparison.

RESULTS AND DISCUSSION

The spectrograms obtained for the substance at different temperatures are reproduced in Plate IXA. Fig. 1 and Fig. 2 show respectively the Raman spectra of the liquid at about 20°C and −100°C. The spectrograms due to the solid at −125°C and −183°C are reproduced in Figs. 3 and 4 respectively. The spectra reproduced in Figs. 1 and 2 show a remarkable change in the nature of the wing accompanying the Rayleigh line with the lowering of the temperature of the liquid. At the room temperature the wing is very intense near the edge of the Rayleigh line and the intensity falls off rapidly in regions further and further away from the centre of the Rayleigh line. At −100°C, on the other hand, the intensity near the edge of the Rayleigh line seems to be much smaller than that in the case of the liquid at 20°C and there seems to be a broad band with its centre at about 45 cm^{-1} on both sides of the Rayleigh line. This is further evident from the microphotometric record reproduced in Plate IXB. The prominent Rayleigh lines at the room temperature are found to be broader than those at −100°C although their actual intensity, without the wing, is smaller at room temperature, as is evident from an examination of the relative intensities of the line 4108 Å in the two spectrograms. The intensity of the line 4077 Å seems to be larger at 20°C, because the wing is superposed on it. This widening of the line is due to the presence of the wing with its maximum starting from a point near the centre of the Rayleigh line and not due to any widening of the slit-width, as can be seen from a comparison of the width of the line 4108 Å in the two spectrograms. This line is too weak to excite the wing and its width is observed to be the same at the two temperatures. The microphotometric trace of the line 4046 Å scattered by the liquid at −100°C, however, extends up to about 110 cm^{-1} from the centre of the line, showing that there is a feeble wing at the outer regions.

It is thus evident from these two spectrograms that the total intensity of the wing diminishes with the lowering of the temperature of the liquid and the portion of the wing which persists at the low temperature tends to appear as a broad band detached from the Rayleigh line. The major portion of the wing observed at the room temperature is due to the rotation of the

molecules and not due to lattice oscillations in crystalline groups which may persist in the liquid, as shown previously by Sirkar and Mookerjee (1936) and also by Sirkar and Gupta (1938) and other workers. Since the intensity of the wing diminishes considerably at the low temperature in the present case, the rotation of single molecule ceases even in the liquid state at about $-100°C$. The remaining portion of the wing at the low temperature may be due to the rotation of a small percentage of the molecules or it may be due to the rotational oscillation of the molecule which has been postulated by Kastler and Rousset (1941) to explain the origin of the new lines in the neighbourhood of the Rayleigh line observed in the case of benzene and other aromatic compounds.

If this latter theory be correct, it is expected that the amplitude of oscillation will diminish at still lower temperature and the intensity of this portion of the wing will consequently diminish. It is seen, however, from Figs. 2, 3 and 4 that the broad band at 45 cm^{-1} observed in the case of the liquid at - 100°C is changed into two sharp lines at 59 and 70 cm^{-1} in the case of the solid at $-125°C$, and these shift to 69 and 80 cm^{-1} respectively when the solid is further cooled down to $-183°C$, there being no diminution in the intensity. On the contrary, the intensity of these two lines compared to that of the line 655 cm^{-1} seems to be larger at $-183°C$ than that at $-125°C$. Also, the lines become sharper at the lower temperature.

According to the theory put forward by Kastler and Rousset (1941) in the case of CS_2 molecule only one line would be expected to be produced by the rotational oscillation about an axis perpendicular to the axis of the molecule. Actually, however, there are two lines in the low frequency region, one being about five times more intense than the other. This does not suggest the splitting up of any degeneracy by the non-homogeneity of the intermolecular field in the lattice. Thus the facts observed in the case of CS_2 in the solid state do not support the view that the new lines observed in the case of the solid are due to rotational oscillations of the single molecule in the lattice. An alternative explanation is to be found, and in doing so the fact that these two lines become sharper at the lower temperature is to be taken into consideration.

The absolute intensity of the line 80 cm^{-1} at about $-183°C$ is about double that of the line 655 cm^{-1} due to the symmetric oscillation of the single molecule. This shows that whatever be the nature of the oscillation which produces the former line, the change in polarisability taking place during the oscillation is larger than that occurring during the symmetric valence C-S oscillation of the molecule. In free rotation of the molecule, of course, such large changes in the polarisability are possible, because the wing observed in the liquid state is many times stronger than the line 655 cm^{-1}. As mentioned already, however, the increase in the intensity of the line 69 cm^{-1} with the lowering of the temperature of the substance does not suggest that the line is due to any rotational oscillation.

The sharpness of the line further suggests that it is due to a vibration in which a definite bond is involved. In that case it has to be postulated, as pointed out earlier by Sirkar (1936), that probably at the low temperature in the solid state a virtual bond is formed between two neighbouring molecules of CS_2. When there is the tendency of such dimer-formation even in the liquid state, the rotation of the single molecule ceases, and this explains the diminution of intensity of the portion of the wing very close to the Rayleigh line in the case of the liquid at $-100°C$. Further, the appearance of the broad band in this region probably corroborates the view that the group which is formed with strong binding in the solid state is also formed loosely in the liquid state at a temperature a few degrees above its freezing point. As the new lines shift away from the Rayleigh line and become sharper with the lowering of the temperature of the substance, it is evident that the strength of the virtual bond between the two molecules goes on increasing as the temperature is gradually lowered. Probably the width of these lines is due to angular motions of small amplitude of the constituent molecules in the dimeric group and as this component of the motion ceases with the lowering of the temperature the lines become sharper. If this hypothesis be correct it is expected that with the lowering of the temperature the frequencies of the lines due to the vibration of the single molecule would also be altered slightly. The frequency-shifts of the Raman lines observed under different conditions are given in Table I.

TABLE I

Carbon disulphide

Liquid at 20°C $\Delta\nu$ in cm^{-1}	Liquid at $-100°C$ $\Delta\nu$ in cm^{-1}	Solid at $-125°C$ $\Delta\nu$ in cm^{-1}	Solid at $-183°C$ $\Delta\nu$ in cm^{-1}
	45(2b) ± k	59(10) e, ± i, ± k	69(10) e, ± i, ± k
		70(2), e, ± k	80(3) e, ± k
648(2) e, i, k	650(1), e, k		
655(6) e, i, k	657 (6) e, i, k	657 (6) e, i, k	657(6) e, i, k
796(2) e, k	800(2b) e, k	806 (2) e, k	808(2) e, k
809 (1) e, k	...	...	...

It can be seen from Table I that the frequency-shifts of both the lines 655 cm^{-1} and 796 cm^{-1} increase with the lowering of the temperature of the substance. Further, while the frequency of the 648 cm^{-1} increases with the lowering of the temperature that of the other satelite 809 cm^{-1} diminishes, so that probably both these lines tend to merge into their strong neighbours at the lower temperature. These facts show that slight changes occur in the strength of the C-S bonds at lower temperatures and lend support to

Fig 1 Unfiltered.

Fig 2 Absorbing vapour at 25°C

Fig. 3 " " 55°C

Fig 4 " " 75°C

Fig. 5 " " 100°C

Fig. 6 " " 110°C

Resonance line of Hg filtered through Hg vapour.

the view expressed above that even in the case of such simple non-polar molecule as CS_2 dimers are probably formed in the solid state at low temperatures. The satelite 648 cm^{-1} is observed to diminish in intensity when the liquid is cooled down to $-100°C$ and this fact confirms the explanation offered by Sirkar regarding the origin of this line.

ACKNOWLEDGMENT

The author is indebted to Prof. S. C. Sirkar for his keen interest in the work and to the Council of Scientific and Industrial Research for financing the scheme under which this work was carried out. Thanks are also due to Prof. M. N. Saha, F.R.S., for kindly providing facilities in the Palit Laboratory of the Physics Department, Calcutta University and to the Council of the Indian Association for the Cultivation of Science for certain other facilities.

UNIVERSITY COLLEGE OF SCIENCE,
PHYSICS DEPARTMENT,
92, UPPER CIRCULAR ROAD,
CALCUTTA

REFERENCES

Kastler, A. and Rousset, A., 1941. *Compt. Rend.*, **212**, 645.
,, ,, 1940, *J. de Physique*, **2**, 49.
Majumdar, N. C., 1949, *Jour Sc and Indust Research*, **8B**, 25.
Sirkar, S. C., 1936, *Ind. J. Phys*, **10**, 189.
Sirkar, S. C. and Gupta, J., 1938, *Ind J. Phys*, **12**, 35.
Sirkar, S. C. and Mookerjee, B. K., 1936, *Ind. J. Phys.*, **10**, 43.

FORTY ELECTRON SYSTEM OF MOLYBDENUM—Mo III

By V. RAMAKRISHNA RAO

(*Received for publication, December 3, 1948*)

Plates XA and XB

ABSTRACT. The lines spectrum of molybdenum was photographed under different conditions of excitation from λ6800 to λ1950. Multiplets of Mo III due to the combination of $4d^5\ 5s\ {}^3F$ with $4d^3\ 5p\ {}^5(DFG)$ were identified from a scrutiny of the plates.

INTRODUCTION

Structural analysis of the spectra of molybdenum was started several years ago. A number of terms in the arc spectrum of the element were identified by Catalan as early as 1923 and by Meggers and Kiess in 1926, although the division into multiplets was uncertain and the character of the terms was difficult to determine. The first spark spectrum of this element was also investigated to a certain extent by Meggers and Kiess (1926) who detected five sextet and quartet groups involving transitions between states of low electron configurations. No intercombinations were reported. Schauls and Sawyer (1940) extended the classification of Mo I to include 36 more lines and established seven new levels and the resonance triplet ${}^6S-{}^6P$ in Mo II. The identifications in Mo II were verified by Zeeman effect data due to Wilhelmy (1926). The ordinary arc and spark between molybdenum electrodes were the source used in the above investigations ; Schauls and Sawyer photographed, in addition, the hollow cathode spectrum of the element.

Of the higher spark spectra a few of the ground terms were identified in Mo IV by Eliason (1933), in Mo V by Trawick (1935 and 1934) by the application of X-ray doublet laws to the respective iso-electronic spectra.

The analysis of Mo III, the forty electron system of the element, in particular, remains completely unknown. There is no published account of even the wave-lengths of the lines attributable to this system. Molybdenum is known to emit even when excited by simple sources a complicated spectrum very rich in lines, whose origin electron transition is yet to be investigated. The purpose of this work is to study the spectrum and to determine the energy states of the atom chiefly corresponding to the first and second stages of ionisation. This paper reports the identification of a few of the fundamental multiplets in Mo III.

For the excitation of the spectrum an ordinary condensed discharge between electrodes of the metal in air proved satisfactory. Spectral lines up to Mo III were all obtained but no line of Mo IV could be traced in it.

A twenty thousand volt transformer fed by 220 A.C., condensers of 4 m. f. d. capacity and an auxiliary gap of 3 mm. in the secondary were used. The molybdenum metal was in the form of a rod, 3 mm. thick, of the H. S. brand spec-pure variety supplied by Adam Hilger and reported to be 99.95% pure. Other sources of excitation were the usual and heavy current arc and an uncondensed spark. The under-water spark was photographed for the purpose of eliminating lines of Mo I and of Mo II. The globule arc using pure molybdenum oxide in graphite rods served just for the identification of lines of Mo I. The distinction and assignment of the lines of Mo III including the fainter lines could be easily carried out by a scrutiny of the spectra of the above-mentioned sources. It should be remarked that in the ordinary arc no lines of Mo III were observed, while they were strongly excited in the condensed spark. The reproductions of the spectra shown in plates XA, B show this feature clearly.

A large number of spectrographs were employed in the investigation which are of small as well as large dispersions. They were (1) Hilger constant deviation, and large glass Littrow of high light gathering power ; (2) three typer of Hilger quartz instruments (E_1, Medium and small) and a 10 foot concave grating spectrograph. The measurements were carried out on the Littrow plates from $\lambda 3400$ to $\lambda 2160$ and the medium quartz plate from $\lambda 2600$—$\lambda 1950$. For the longer weve-lengths the grating spectra were measured. In photographing the region below $\lambda 2100$ Ilford Q as well as Ilford special rapid plates sensitised by Cenco Hyvac pump oil were used ; it has been our experience that the oil sensitised plates generally gave better results.

As a first step towards the elucidation of the structure, a close scrutiny of each line is made and its intensity variation is observed under arc, condensed spark and under-water spark conditions. In the last mentioned source many of the molybdenum I lines appeared as absorption lines, a few of Mo II are self-reversed while lines attributable to Mo III are absent. This spectrum proved useful in the region above $\lambda 2600$. The arc and condensed spark spectra extended down to the limit of observation, the condensed spark alone containing lines of Mo III. A list is drawn from $\lambda 6800$ to $\lambda 1950$. The complete list would be presented in a later communication, as it is hoped to extend the data further down to the vacuum grating region. As far as the author is aware no temperature classification of the spectrum is available in the case of molybdenum, which would have helped in confirming the assignments made.

ANALYSIS

The complete configuration of electrons for atomic molybdenum is :

$$1s^2\ 2s^2\ 2p^6\ 3s^2\ 3p^6\ 3d^{10}\ 4s^2\ 4p^6\ 4d^5\ 5s$$

giving the deepest ^7S term ; molybdenum II corresponds to a forty-one electron system, the deepest term being $4d^5\ ^6S$. The doubly-ionised atom

has forty lectrons of which four form the outermost valence electrons. The deeper configurations and the more important of the predicted terms in Mo III are shown in Table. I.

TABLE I

$4d^4$	^5D	$^3(PF)$
$4d^3\,5s$	$^5F\ ^3F$	$^5P\ ^3P$
$4d^3\,5p$	$^5(DFG)^\circ$	$^3(DFG)^\circ$
	$^5(SPD)^\circ$	$^3(SPD)^\circ$

TABLE II

Multiplets of Mo III

$4d^3(4F)5s$		$^5F_7$ 439.5 0	$^5F_2$ 609 6 439 5	$^5F_3$ 774.2 1049.1	$^5F_4$ 1043 5 1823.3	$^5F_5$ 2866.8
$^5G_2^\circ$	41588.4 733.1	415877 (10)	41147 5(5)bl	40539 4(1)		
G_3	42321.5 1090.1		41881 5(10)	41271.5(8)	40498.2(0)	
G_4	43411.6 1300.4			42362.1(15)	41587.7(10)	
G_5	44712.0 1714.1				42888.1(15)	41845.6(4)
G_6	46426 1					43559.7(20)
$^5F_7^\circ$	44291.1 89 2	44291.1(10)				
F_2	44380.3 1092 2	44380.3(8)	43941.4(15)			
F_3	45472 5 282.9		45033 6(4)	4442219(10)		
F_4	45755.4 1046.4				43927.7(15)	
F_5	45801.8				44974.1(3)	43930 6 15)
$^5D_0^\circ$	44445.8 279.6	44445.8(6)			—	
D_1	44725.5 1027.5	44725.4(2)	44286.8(10)			
D_2	45753 0 1136.2		45314.3(8)	44705.8(6)		
D_3	46889.2 342.1			45842.0(2)	45067.1(8)	
D_4	47231.3				45409.2(2)	44364.8(12)

Fig *a*

Fig. *b*

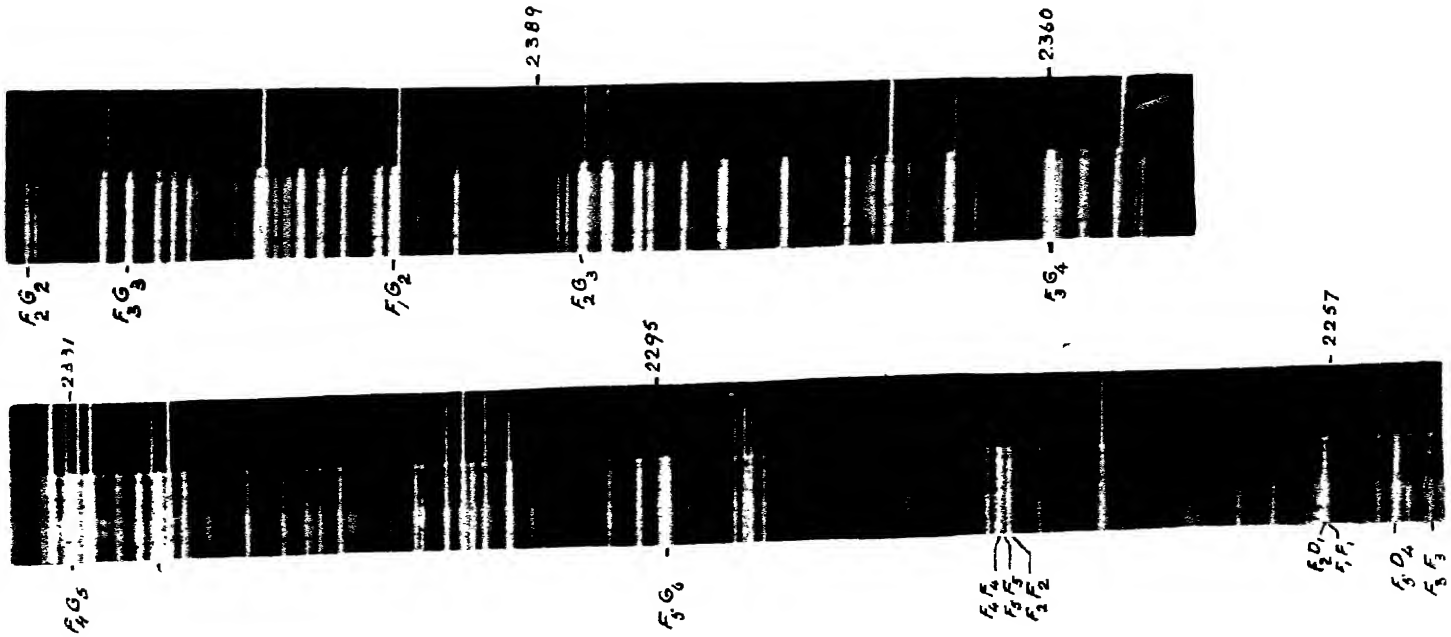

Line spectrum of molybdənum.

Fig. *a* — Littrow.
Fig. *b* — do

Upper spectrum — Arc. Lower spectrum—Condensed spark

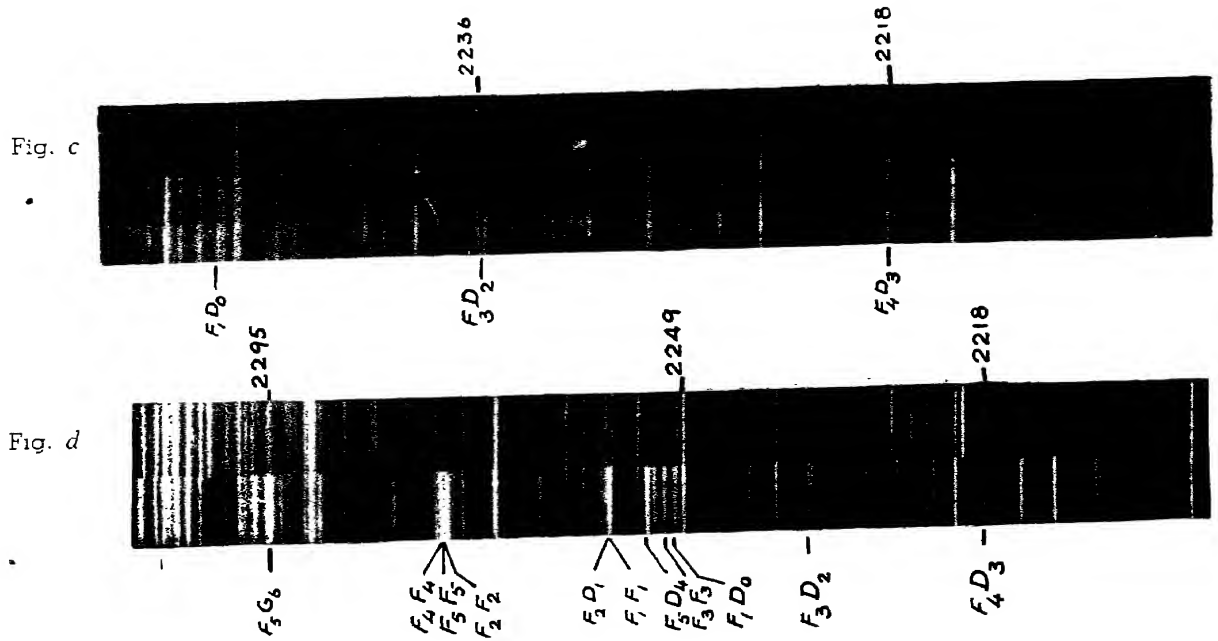

Line spectrum of molybdenum.

Fig. *c* — Littrow.
Fig. *d* — Medium quartz
Upper spectrum — Arc. Lower spectrum—Condensed spark.

The chief multiplets may be expected to be due to the transition from $4d^3\ 5p$ to $4d^4$ and $4d^3\ 5s$, of which the latter having lesser energy difference are likely to occur in the quartz region. Table II gives the multiplets identified in the present work. They are the combinations $4d^3\ 5s\ {}^5F$ with $4d^3\ 5p^5\ (DFG)^\circ$.

In the absence of Zeeman effect and hyperfine structure data the identification was facilitated only by considerations such as the intrinsic nature, behaviour and the relative intensities of the lines themselves and by comparison with other similar spectra. In zirconium I and columbium II which are identical in structure with Mo III, the most characteristic and unmistakable line in the entire spectrum which might well have been taken to be the starting point of the analysis corresponds to the combination $4d^3(^4F)\ 5s^5F_5 - 4d^3(^4F)\ 5p^5G^\circ_6$. Such a line in the spectrum of Mo III is found at λ 2294; it could be no other than this combination. The irregular doublet law, predicting a linear progression of the frequency with the atomic number in an iso-electronic sequence supports this assignment. Table III shows such progressions in Zr I, Cb II and Mo III and also in Ti I, V II and Cr III which are of similar configurations.

TABLE III

The irregular doublet-law

Spectrum	${}^5F_5 - {}^5G_6^\circ$	${}^5F_5 - {}^5F_5^\circ$	${}^5F_5 - {}^5D_4^\circ$
Ti I	20068 (12253)	22053 (12136)	23217 (11151)
V II	32321 (12574)	34189.6 (13019)	34368.3 (12320)
Cr III	44895.4	47208 3	46688.9
Zr I	21326.9 (10983.1)	23646.5 (10231.2)	24495.6 (9649.0)
Cb II	32309.1 (11250.6)	33877.7 (10052.9)	34144.6 (10220.2)
Mo III	43559.7	43930.6	44364 8

This extrapolation located the positions of ${}^5F_2 - {}^5F_5^\circ$ and ${}^5F_1 - {}^5D_4$ lines as well and led to their detection.

An estimate of the intervals in the term $4d^3\ 5s\ {}^5F$ was obtained from the law of regular doublets. The variations of the screening constants in Ti I like and Zr I line spectra are given in Table IV for the interval ${}^5F_5 - {}^5F_4$.

TABLE IV

The Regular doublet-law

$3d^3(^4F)4s$	Tl I	$^5F_5-^5F_4$ V II	Cr III	$4d^3(^4F)5s$ Zr I	Cb II	Mo III
$\Delta\nu$	100.2	194.6	319 0	348.4	603 5	1043.5
$(\Delta\nu)^{\frac{1}{4}}$	3.16	3.74	4.23	4.32	4.96	5.67
S	15.2	14 9	14.9	28.9	28.3	27.5
ΔS	.3	.0		.6	.8	

Another method yielding fairly good estimates of these intervals is provided by a study of the interval-factors as suggested by Goudsmit and Humphreys (1928) and discussed by the author (1948), and tested in relation to a few complex spectra like those of Cb I and Cb II. It was observed to be of use particularly with regard to the ground state terms in the spectra of ionised atoms. The method consists in predicting the separation of levels arising from a $d^3\,s$ configuration out of the data for terms of the d^4 configuration. In our case, Mo IV gives a $4d^3\,{}^4F$ term having the following separations :

$$F_{2\frac{1}{2}}-F_{1\frac{1}{2}}=780$$
$$F_{3\frac{1}{2}}-F_{2\frac{1}{2}}=979$$
$$F_{1\frac{1}{2}}-F_{3\frac{1}{2}}=1099.6$$

Hence, the separation factor A is equal to 277, which is the mean value derived from the individual differences and from the total separation. This separation factor A, is related to the factor A' for the Mo III ^5F levels by the equation :

$$A=4/3\,A'$$

from which A' is aproximately 208.

This predicts the following separations for the ^5F term of Mo III, 1040, 832, 624, and 416. They are shown in Table V along with the observed values taken from the multiplet Table II. A corresponding calculation for Cr III intervals derived from those of Cr IV is also indicated for comparison.

Considered in the light of the relations discussed above, the multiplets shown in Table II seemed to be the best among a number of alternatives. The choice of the first interval 1043 for $5s\ ^5F_5-{}^5F_4$ was made after a large number of trials, the criterion being that this difference ought to recur in four pairs representing combinations with $5p\ ^5G_5{}^\circ\ {}^5F_3{}^\circ\ {}^5F_4{}^\circ$ and $^5D_4{}^\circ$ levels and involving fairly prominent lines in the spectrum in the appropriate regions. One combination line with $5p\ {}^5F_4{}^\circ$ is not found, still this level is chosen from a consideration of the diagonal lines of the $5s\ {}^5F-5p\ {}^5F^\circ$

TABLE V

	Cr III		Mo III	
	Predicted	observed	Predicted	observed
F_5-F_4	301	319	1040	1043
F_4-F_3	273	263	832	774
F_3-F_2	204	200	624	610
F_2-F_1	136	136	416	441

multiplet ; these stand out clearly and are believed to be very similar to the corresponding lines in the spectrum of Cr III.

The second interval $5s\ ^5F_4-{}^5F_3=774$ is not quite in keeping with the predicted value 832, if the Lande interval rule holds exactly ; here too the selection was made from a consideration of the possible diagonal lines in the $5s\ ^5F-5p\ ^5G^0$ group. The line 44705.8 which gives abnormally large interval is possibly a blend, the high intensity of the line justifies the assumption. The last intervals $5s\ ^5F_2-{}^5F_1$ equal to 441 also does not agree exactly with the calculated value 412. Two other alternative lines 41434.0 and 41009.3 with 436.2 and 524.2 differences are rejected as less satisfactory since they did not give consistent combinations with the other levels $5p\ ^5D^0$ and $^5F^0$. The lines 44291.1 and 4444 8 are isolated combinations involving no intervals of the $5s\ ^5F$ term ; they are suggested from the probable order of the terms $5p\ ^5F^0$ and ^5D ; their identification is to be checked from other combinations.

Regarding the terms of the $4d^3\ 5p$ configuration it is seen that the $5G^0$ is the deepest, although there is considerable overlapping of the components of $^5G^0\ ^5F^0\ ^5D^0$ terms. Such an overlap is to be expected on account of the atomic number of molybdenum. A considerable deviation from the Lande interval rule is observed in the case of $5p$ terms with the probable exception of the deepest $^5G^0$ term.

The separation factors for the $^5(GFD)^0$ terms out of $4d^3\ (^4F)\ 5p$ configuration are related to the separation factor for $4d^3\ (^4F)$ of Mo IV by the expression (Rao, 1948)

$$\text{All quintets } \Sigma A = 9/4\ A'$$

The separation factor for $^5G^0=266$

$$^5F^0=179$$

$$^5D^0=279$$

$$\text{Total } \Sigma A=724$$

which gives the value of A' as 320. Further investigation of the spectrum is in progress.

ACKNOWLEDGMENT

It is a great pleasure to thank Dr. K. R. Rao for his constant interest and guidance.

PHYSICS DEPARTMENT
ANDHRA UNIVERSITY
WALTAIR

REFERENCES

Catalan, 1923, *An. Soc. Espan. Fis. y Quim.*, **21**, 213
Eliason, 1933, *Phys. Rev.*, **43**, 745.
Goudsmit and Humphreys, 1928, *Phy. Rev.*, **31**, 960.
Meggers and Kiess, 1926, *Jour. Opt. Soc. Am.* **12**, 417 and 435.
Rao, V. R. and Rao, K. R., 1918, *Ind. J. Phy.*, **22**, 189.
Schauls and Sawyer, 1940, *Phy. Rev.*, **58**, 781.
Trawick, 1934, *Ibid.*, **46**, 63.
,, , 1935, *Ibid.*, **48**, 223.
Wilhelmy 1926, *Ann, der. Phy*, 80.

THALLIUM ISOTOPE EFFECT IN THE BAND SPECTRUM OF THALLIUM BROMIDE

By P. TIRUVENGANNA RAO

(*Received for publication, Nov. 4, 1948*)

Plate XI

ABSTRACT. Bands of thallium bromide, excited by a H. F. discharge through the vapour, are photographed in the first order of a 10 ft. concave grating. The isotope effect due to the thallium isotope 203 is established for the first time from measurements on the splitting observed in many of the band heads between $\lambda 4300 - \lambda 4100$.

The absorption spectrum of thallium bromide was first studied by Butkow (1929) and by Butkow and Boizowa (1934). They obtained a band system in the region $\lambda 3400$ extending to $\lambda 3600$ and reported the analysis of 14 red-degraded bands fitted into the following quantum formula

$$\nu = 29149.6 + (103.8n' - 6.05n'^2) - (192.2n - 0.72n^2)$$

The analysis was supported by measurements on the bromine isotope effect. Later, Howell and Coulsson (1941) investigated the spectrum using a quartz Littrow spectrograph, (Hilger, E_1) in emission and absorption and published a more complete analysis of a large number of bands between $\lambda 3500$ and $\lambda 4500$. The following equation was derived for the band heads

$$\nu = 29191.5 + (108.32u' - 5.15u'^2 - 0.22u'^3) - (192.10u'' - 0.39u''^2)$$

Comparing the bromide with the other halides of thallium Howell and Coulsson interpreted the system as due to the transition $3_1 - {}^1\Sigma^+$. A second band system was also reported by them at λ 3950. It was observed only in emission. A fragmentary analysis, suggested for this system, indicated that the lower state of this is the same as the upper state of the main system.

The vibrational analysis of the main system was extensively confirmed also by Howell and Coulsson from observations of the bromine isotope effect. Each band, apart from those situated near the origin, showed the doubling to be expected for the molecules $TlBr^{79}$ and $TlBr^{81}$. The largest splitting measured was 59 $cm.^{-1}$ for the (6.41)* band.

Thallium also has two isotopes of mass 203 and 205. Miescher (1939) reported a doubling in some TlCl bands, (but no data are given) and

* This was mentioned as the (5,41) band by Howell and Coulsson.

attributed it to the isotopes of thallium. For thallium bromide, Howell and Coulsson estimated assuming the splitting factor $(\rho-1)=.0007$ the biggest isotope shift as of the order of 4 5 cm.$^{-1}$, which, in view of the diffuseness of the heads, represents about the order of uncertainty in measurement. Any possible resolution of the thallium isotopes was therefore ruled out by them.

In the course of a systematic investigation of the band spectra of the thallium halides, the author photographed the thallium bromide emission between λ3800 and λ4300 in the first order of a 10 ft. concave grating (dispersion 5.7 A per mm.). A new set of bands about 45 in number have been obtained between λ3980 and λ3800. It has also been found that bands of the main system lying in the region around λ4200 showed a definite doubling of the order of about 6 to 8 wavenumber units. This doubling appeared to be due to the thallium 203 isotope which was found unmeasurable previously by Howell and Coulsson. But the observed interval is distinctly larger than the biggest Tl isotope splitting as estimated by Howell and Coulson A recalculation of the mass factor and the expected isotope shift revealed a small error in Howell and Coulsson's estimate. The object of this paper is to establish the existence of Tl^{203} isotope done for the first time from a study and measurement of the bands. The analysis and interpretation of the new set of bands observed in addition to those found by Butkow and by Howell and Coulsson will be presented in a subsequent communication. Incidentally the author noticed that the values of v' given in Table I column (5) of Howell and Coulsson's paper for all the bands from the (3,20) band upwards are in error, due, perhaps, to oversight; the v' values must be increased by one; thus (4,20), (4,21) etc. instead of (3,20) (3,21) etc. respectively.

EXPERIMENTAL

The experimental set up is the same as that employed for the thallium iodide bands and described elsewhere. The excitation is by a H. F. oscillator with external electrodes. Intermittent heating was found necessary for maintaining the discharge steadily. Exposures from 2 to 4 hours on Ilford special rapid plates were found sufficient to photograph the spectrum in the first order of a 10 ft. concave grating. The usual iron arc standards were employed for reducing the plates.

Plate XI shows enlargements of the Tl Br band spectra. Fig.*a* is an overall picture of the spectrum from λ4350—λ4000. Fig.*b* and Fig.*c* are portions of it to show the thallium isotope doubling in some of the bands chiefly in the less refrangible end of the system.

From examination of the spectra, it has been noticed that above λ4300 the bands are faintly recorded and although doubling is observed, no

TABLE I

Wave-length (H & C)	Wave-length (Author)	Wave number	Tl isotopic separation		Mole-cule Tl Br	Classification	
			obs.	calc		(Author)	(H&C)
	4101 34	24375 4			205,81		
4102.4	02 66	24368.2	7.2	6 4	203,81	(4,28)	(3,28)
	07.04	24341.6			205,79		
4109.7	08.07	24335 5	6.1	6.4	203,79		
	31.17	24199.4			205,81		
4132.8	32 49	24191.7	7.7	6.6	203,81	(4,29)	(3,29)
	40.96	24142 2			205,79		
4141.9	42 58	24132 8	9 4	6.6	203,79		
	53.56	24369.0			205,81		
4154.8	54 83	24061.6	7.4	6 8	203,81	(5,30)	(4,30)
	60.29	24030 0			205,79		
4162.3	61.70	24021.9	8.1	6.8	203,79		
	61 70	24021.9			205,81		
4162.3	63 05	24014 1	7 8	6.8	203,8	(4,30)	(3,30)
	70 43	23971,6			205,79		
4171.4	71.91	23962.1	8 5	6.8	203,79		
	82 67	23901.5			205,81		
4185.0	83.89	23894.5	7 0	7.0	203,81	(5,31)	(4,31)
	89.34	23863 4			205,79		
4192.0	90.71	33855 6	7.8	7.0	203,79		
	92.83	23843.5			205,81		
4192.0	91.27	23835.4	8.1	7.0	203,81	(4,31)	(3,31)
	99 96	23803.1			205,79		
4201.4	420.34	23795 3	7 8	7.0	203,79		
	12.17	23734.1			205,81		
4214.4	13.36	23727.4	6.7	7.2	203,81	(5,32)	(4,32)
	22.31	23677.1			205,79		
4223.2	24.02	23067 5	9.6	7.2	203,79		
	28.54	23642.2			205,81		
4231.6	29.97	23634.2	8 0	7.4	203,81	(6,33)	(5,33)
	38 88	23584.5			205,79		
4238.8	40.34	23576.4	8.1	7 4	203,79		
	45.05	23550.2			205,81		
4245.7	46 34	23543.1	7.1	7.4	203,81	(5,33)	(4,33)
	52.50	23509.0			205,79		
4254.6	53.87	23501 4	7.6	7 4	203,79		
	64.01	23445.5			205,81		
4264.6	65.25	23438.7	6.8	7.6	203,81	(6,34)	(5,34)
	73.96	23390 9			205,79		
4274.7	75.27	23383.8	7.1	7.6	203,79		
	73.96	23390.9			205,81		
4274.7	75.27	23383.8	7.1	7.6	203,81	(5,34)	(4,34)
	82.82	23342.6			205.79		
4283.6	84.21	23335.0	7.6	7.6	203,79		

measurements have been possible. Table I contains the details of measurements on band heads lying between λ 4300 – λ 4100, in which region the

isotope effect has been established. The first column gives the H and C's wave-length data, where the Br isotope doubling alone was recorded. Each of these heads is observed here to be split into two components, the wave-lengths of these are given in the second column. The molecule and the vibrational assignments are shown in the last column. For convenience, H and C's assignments are also shown. The isotope shifts calculated with respect to the molecule Tl^{205} Br^{81} and given in the fourth column are obtained as below

$$2(\rho-1)=\frac{M'(M-M')}{M'(M+M')}\ ;\ [M=205\ ;\ M'=203\ ;\ M'=81.]$$

Substituting,

$$(\rho-1)=.0014$$

For the (5,34) band,

$$\nu_i-\nu=(\rho-1)\ (\omega'_e u'-\omega_e''u'')-(\rho^2-1)\ (x_e'\omega_e'u'^2-\ \ ''\omega\ ''u''^2)+\ldots=7.6 \text{ units}$$

(adopting the H and C's values for the vibrational constants).

The agreement between the calculated and observed values is as close as may be expected on account of the nature of the bands.

ACKNOWLEDGMENT

The author expresses his thanks to Prof. K. R. Rao, D. Sc., for his kind interest and guidance.

ANDHRA UNIVERSITY
WALTAIR

REFERENCES

Butkow, 1929, *Zeit. f. Physik*, **58**, 232.
Butkow and Boizowa, 1934, *Phy, Zeit. O. Swjet.*, **5**, 765.
Howell and Coulsson, 1941, *Proc. of. Phy. Soc (Lond.)*, **53**, 706.
Micscher, 1939, *Helv. Phy. Acta*, **12**, 296.

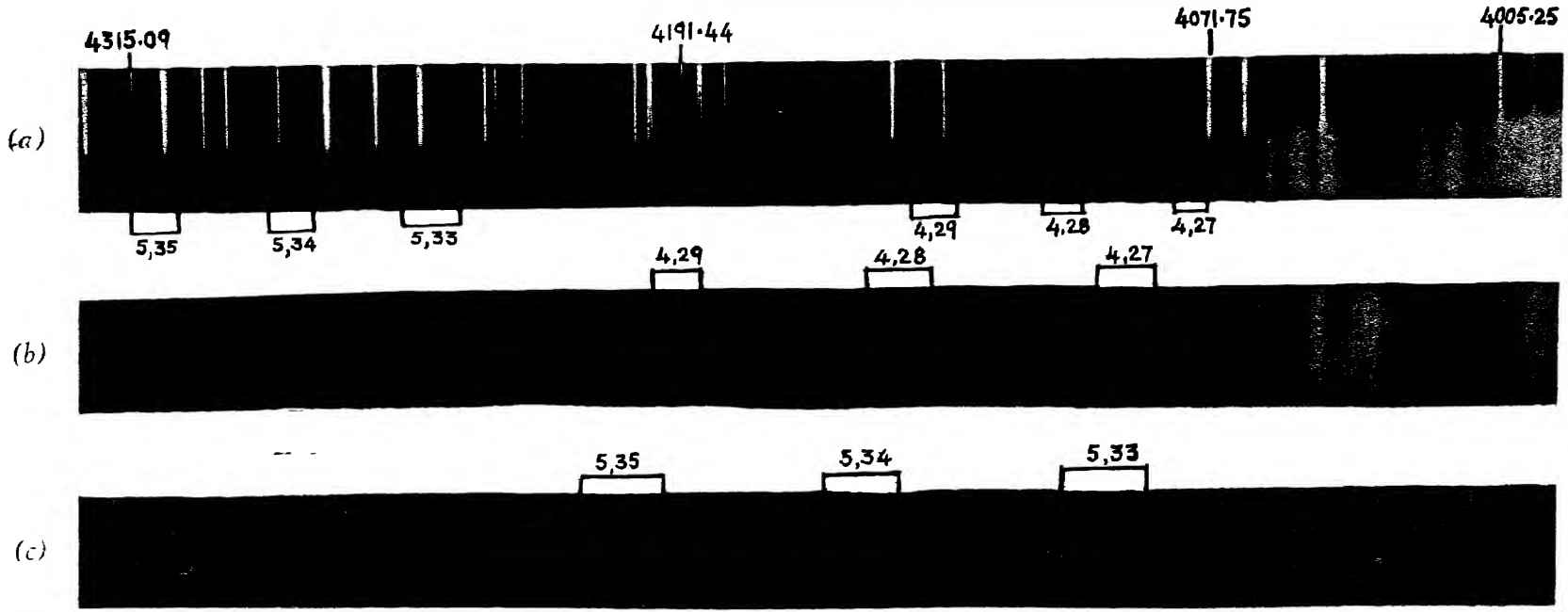

Concave grating spectra of thallium bromide

MAHAJAN'S MAXIMUM AND MINIMUM HYGROMETERS

By L. D. MAHAJAN

(*Received for publication, March 16, 1949*)

ABSTRACT. Two new types of hygrometers for recording maximum and minimum humidity is described in the present paper. They both work on the principle of Mahajan's Optical hygrometer.

INTRODUCTION

The problem of recording the maximum and minimum readings is not new. In all types of measurements it is necessary to know the maximum as well as the minimum readings. The common procedure has been to take readings at regular intervals of time and then to pick out the maximum and minimum values from the observations.

Some instruments such as maximum and minimum thermometers, are provided with an automatic arrangement for recording the maximum and minimum readings, thus avoiding the trouble of taking readings at regular intervals.

But in the case of maximum and minimum relative humidity measurements, at present, the observations are to be taken at regular intervals which is a lengthy process.

Therefore introduction of a similar automatic device in any type of humidity meter is needed to eliminate the difficulties of taking frequent observations.

Now it is found that the Mahajan's Humimeter (Mahajan, 1946) recently devised by the author is very suitable for this purpose. Two devices have been designed, and are given below :—

CONSTRUCTION OF DEVICE I

It consists of four vertical rectangular supports *A*, *B*, *C* and *D*, each 10 cms high, 5 mm. thick and 5 mm. broad (figure 1). They are fixed in a

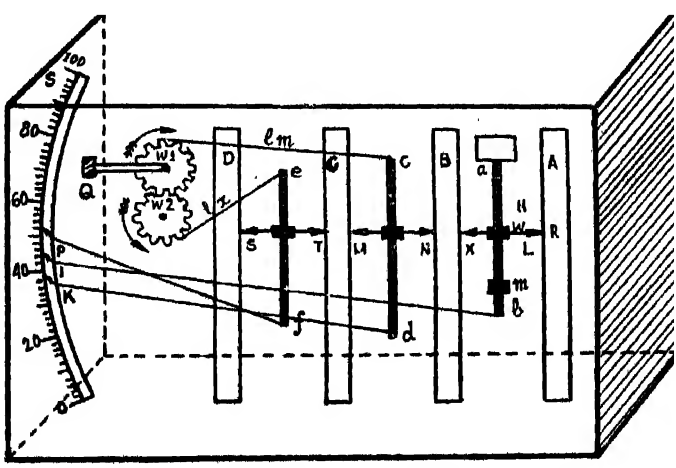

FIG. 1

Mahajan's maximum and minimum hygrometer. Type I (Inside).

line 5 cms apart from each other. Between the supports A and B, there is a revolving rod XR, between supports B and C the revolving rod MN and between supports C and D the revolving rod ST. The fine end of these revolving rods rest inside hollow grooves which are fitted with hard jewels. The rotation of the rod XR is controlled by the hair spring H, tied to the screw L. At right angles to this revolving rod XR there is a balancing rod ab rigidly fixed to it. On its end a there is a pan 3 cm × 3 cm × 0.5 cm, having a perforated bottom. The absorbing material as used in the Mahajan's Optical Hygrometer (Mahajan, 1941) is filled into it. The other end b of this rod is elongated into a thin rod having a fine pointer I which moves on the scale S marked on the dial.

Between the supports B and C, the revolving rod MN supports the balancing rod cd. Its end d is elongated into a pointer K which represents the minimum reading of the humidity. The rod cd is just below the rod bI. So when the humidity of the air decreases, the pan a goes up, and the end b goes down. Therefore the rod bI also goes down. It pushes the end d down, and hence the arm dk also goes down. When the humidity of air increases, the pan a on absorbing more moisture from air goes down, the end b moves up, and the rod bI also goes up. It does not disturb the lower rod cd. The pointer K remains unaffected. The end c is thick and heavy and so balances the longer arm dk.

Between the pillars C and D, the revolving rod ST supports the balancing rod ef. Its end e is thick and heavy. Its other end f is elongated into a pointer P, which represents the maximum percentage humidity of surrounding air. The pointer P stands on the upper side of the central pointer I. The rod ef is slightly above the arm bI. When the humidity increases, the material absorbes more moisture, and goes down. The rod end b and the arm bI move up. The arm bI pushes the end f of the rod ef and the arm fP upward. Hence the pointer P representing the maximum humidity, is pushed up. When the humidity of the surrounding air decreases the central pointer I goes down, but leaves the pointer P unaffected. It has no tendency to come back. If the humidity increases again and exceeds the previous limit, the central pointer pushes the pointer P still higher and on decrease of humidity comes back without disturbing the position of pointer P.

The resetting of the pointer P and K for observations of next 24 hours, is done with the help of two cogged wheels W_1 and W_2. The wheel W_1 has a knob Q which controls its clockwise or anticlockwise movements. On rotation of wheel W_1, the other wheel W_2 rotates in opposite direction. There are two levers Lm and Lx. One end of each lever rests on the toothed wheel and the other end touches the corresponding balancing rod. Thus by revolving the knob Q the pointers P and K are reset for next observations.

This whole apparatus is enclosed inside a wooden case of dimensions 15 × 10 × 10 cm. (Fig. 2). In order to have a free circulation of air inside

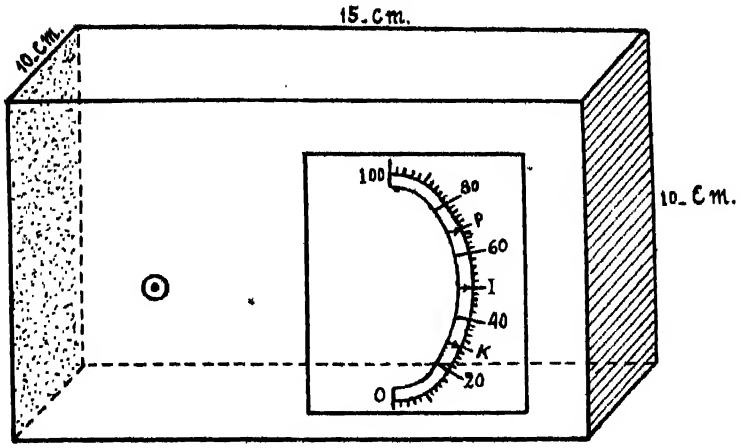

FIG. 2

Mahajan's maximum and minimum hygrometer. Type I (covers)

the instrument, its top is perforated with small holes and the sides are ventilated like the Stevenson screen.

The scale *S* is calibrated in percentage humidity with the help of a standard wet and dry bulb hygrometer.

CONSTRUCTION OF DEVICE II

In the slit of the Mahajan's Hummeter, two riders of the shape given in Fig. 3*a*, are inserted. One is above the pointer *I* (Fig. 3*b*) and the other

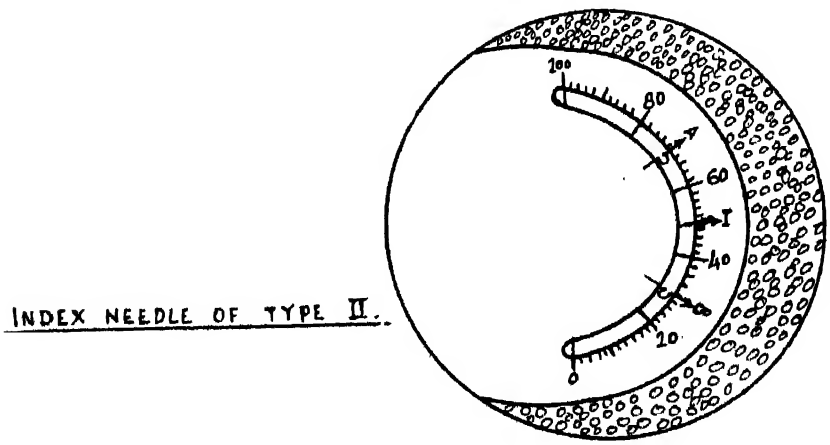

(*a*) (*b*)

FIG. 3

Mahajan's maximum and minimum hygrometer. Type II

is below it. They are made of any metal but are light in weight and elastic in property. They fit well into the slit and do not move by air or wind but only by a push of the pointer *I*.

When the pointer moves upward, it pushes the rider A which represents the maximum % humidity. But when the humidity decreases, the pointer *I* moves down without affecting the rider *A*, and pushes the rider *B* downward. When the humidity increases again, the pointer moves up without affecting the rider *B*. Thus the rider *A* represents the maximum humidity and *B* the minimum humidity during any interval of time. Therefore this device also serves well the purpose of the maximum and minimum Hygrometer.

The instruments are in the making and further details will be published in due course.

THEORY

Both these devices work on the principle of the Mahajan's optical hygrometer.

ACKNOWLEDGMENT

The author is indebted to the Government of the Union of Patiala and East Punjab States for providing facilities for conduct of research work in the Research Laboratory, Patiala.

RESEARCH LABORATORY,
PATIALA.

REFERENCES

Mahajan, L. D , 1946. *Ind. Jour. Phy.*, **20**, 214.
Mahajan, L. D., 1941, *Ind. Jour. Phy.*, **15**, 425.

ABSORPTION AND REFLEXION OF U. H. F. WAVES (300-500 Mc/s) BY SEAWATER

BY S. K. CHATTERJEE AND B. V. SREEKANTAN

(*Received for publication, Jan.* 17, 1949)

ABSTRACT. The present paper deals with the absorption and reflexion suffered by a plane electromagnetic wave (300-500 Mc/s) while travelling a solution of a mixture of electrolytes simulating sea water. Experimental results indicate maximum absorption at 380 Mc/s and very little variation of the reflexion coefficient over the frequency range in question. It has also been observed that dielectric constant and conductivity increase with increasing frequency of the incident wave.

INTRODUCTION

The solution of many problems of radio wave propagation, especially at ultra-high freqencies requires a knowledge of the absorption and reflection taking place at a earth and water surface. The propagation of ultra short wave, for which the ionosphere plays a negligible part, over both land and sea and at distances both within and beyond optical range has been investigated by a number of workers, but there still appears to be a paucity of available published data for the frequencies in question. The data reported here will serve tentatively to fit into certain gaps in the experimental information already available. The present experiment relates to the study of absorption and reflexion of u. h. f. waves (300-500 Mc/s) in sea water. Sea water (Int. Crit. Table 1928) varies in its salt content at different places and times from 0.15 to 4.15%. In order to obtain definite information as regards the behaviour of sea water at ultra high frequencies, experiment has been carried out in the laboratory with a mixture (Dorsey, 1940) of 26.9 gms/kg of sodium chloride. 3.2 gms/kg of magnesium sulphate, 3.2 gms/kg of magnesium chloride, and 1.4 gms/kg of copper sulphate in aqueous solution to simulate sea water. The results as regards reflexion coefficient will differ under practical conditions, as due to the presence of, crest and though of waves and varying ridges with place and time, there will be diffuse reflexion, whereas, in the present experiment, the reflexion may be regarded as specular.

EXPERIMENTAL

Attenuation Coefficient.—

The method of measurement employed is the free space wave method. A parallel beam of radiation emanating from a dipole aerial placed at the

focus of a parabolic cylindrical reflector, being reflected by another plane reflector placed at 45°, passes through a cell containing sea water and the intensity of the transmitted beam picked up by a detector is studied. The experimental arrangement is the same as reported elsewhere (Chatterjee and Sreekantan, 1948). If the intensity of the beam incident at the liquid surface be I_0 the attenuation coefficient α at any frequency can be found from the decrease of transmitted wave intensity I varying with the depth x of the liquid according to the following relation

$$\alpha = \frac{2.303}{x} \log \frac{I_0}{I}$$

provided the decay in intensity follows a simple exponential law. But due to high refractive index of the liquid under investigation multiple reflexion takes place inside the liquid giving rise to a transmission percentage vs depth of the liquid curve of wavy nature (Fig. 1). The increase of direct beam

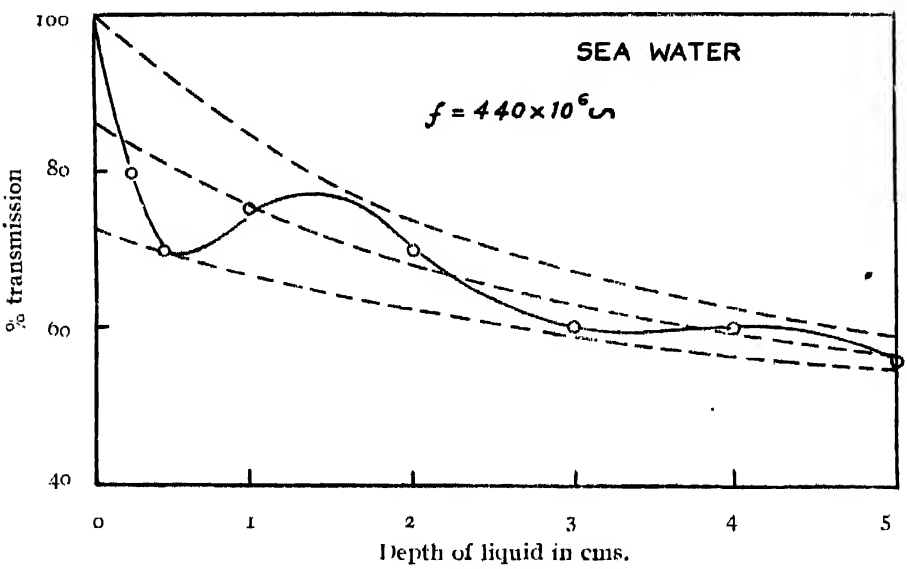

FIG. 1

intensity due to secondary reflexion may be avoided if the liquid layer is sufficiently thick to absorb secondary beam, or if the liquid possesses very high absorption index. Generally the application of a simple exponential law will introduce considerable error in the calculation of α.

When a plane wave is incident normally on the air-liquid surface, a portion of it will be reflected back into air and will constitute the useful energy for propagation purposes. The rest of it will penetrate the liquid layer and a portion of it passes the liquid glass surface and will reach the detector directly, and another portion will reach the detector after suffering multiple reflexion inside the liquid layer. If E_0 represents the amplitude of the electric vector and ω the angular frequency, the electric component

of the incident wave may be represented by $E_0 e^{i\omega t}$. Neglecting number of reflexions undergone, inside the liquid beyond the fourth and assuming the liquid layer to be of uniform thickness and that no energy is refracted back into the liquid from the glass air surface, it can be shown (Knerr, 1937) that the average energy at the input of the detector is given by the following relation.

$$Energy = B.[e^{-2\alpha x} + 2RR'e^{-4\alpha x}\cos\phi + R^2R'^2 e^{-6\alpha x} + 2R^2R' e^{-6\alpha x}\cos 2\phi + 2R^3R'^3 e^{-8\alpha x}\cos\phi + R^4R'^4 e^{-10\alpha x}]$$

where α the attenuation coefficient is given by $\frac{2\pi nK}{\lambda}$ involving n the refractive index and, K the absorption index. The phase factor is represented by ϕ and B is a constant, involving E_0 and the amplitude of transmission factors at the air-liquid and liquid-glass surface. The amplitude of reflexion factors in the liquid at the upper and lower surfaces are R and R' respectively. It is evident from the energy expression that the terms involving $e^{-6\alpha x}$. $\cos\phi$ becomes maximum when the term involving $e^{-4\alpha x}$. $\cos\phi$ becomes maximum and minimum. The result is that the maxima and minima are shifted depending upon x the thickness of the liquid layer. Therefore the values of n cannot be determined from the ratio of the free space wavelength and that determined from the distance between two consecutive peaks.

Attenuation coefficient has been determined as reported elsewhere (Chatterjee and Sreekantan, 1948). The value of α corresponding to 2-3 cms. depth of the liquid has been reported in Fig. 3.

The voltage developed at the input of the detector is proportional to the square root of the energy reaching the detector. For a square law detector the change in plate current being proportional to the square of the input voltage, is proportional to the energy received by the detector. The detector is of the resonant line type (Chatterjee, 1948).

Refractive Index.—

The oscillator is coupled to the lecher wire system (Fig. 2) by means of a loop near the shorting bridge 2. The coupling loop can be moved

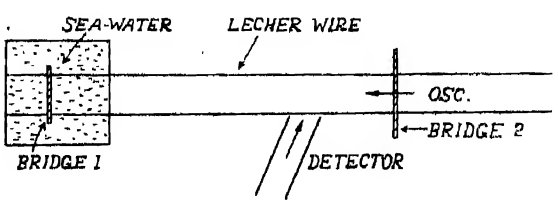

FIG. 2

Arrangement for determining refactive index

with the bridge 2. The adjustment consists in shifting the shorting bridge 1 as far deep in the liquid as possible and then adjusting the bridge 2

to make the detector reading maximum. The detector is then shifted to position for maximum deflection. Next procedure is to shift the first bridge inside the liquid towards the detector, thus varying the thickness of the liquid travelled by the wave and plotting the detector reading against the thickness of the liquid. For each position of the first bridge, the energy reaching the detector will be contributed by the electric component of the direct wave and also the component of the wave entering the liquid and reflected back into the air and so on. The resultant electric component E of the wave at the detector may be represented by the following expression (Cooper, 1946)

$$E = a + b\ e^{-\alpha x} e^{-j(2\beta x - \gamma)}$$

where β is the phase constant of the liquid path and γ represents the phase factor of the reflected and transmitted wave. The factors a and b involve amplitudes of the transmission and reflexion factors and the electric field strength of the initiating wave at the detector. The detector being a square law type the the above expression for the field strength produces a plate current change in the detector proportional to

$$a^2 + b^2\ e^{-4\alpha x} + 2ab\ e^{-2\alpha x} \cos(2\beta x - \gamma)$$

The distance between two consecutive peaks of the curve relating the detector deflexion and thickness of the liquid x gives half the wavelength in the liquid.

REFLEXION COEFFICIENT

The ratio of the reflected to incident intensity for normal incidence is given by Fresnel's expression $(N-1)/(N+1)$ which can be written equal to $(n-1-jk)/(n+1+jk)$. On squaring, we get the reflection coefficient R as follows

$$R = \frac{(n-1)^2 + K^2}{(n+1)^2 + K^2}$$

The variation of R over the frequency range is given in Fig. 3. Values of the absorption index K are obtained from the following relation $K = (\alpha\gamma/2\pi n)$.

DISCUSSION

The vibration of the attenuation coefficient with frequency (Fig. 3) indicates maximum absorption at 380 Mc/s. The relaxation time τ corresponding to the peak absorption can be calculated from the Debye (Debye, 1929) relation $\omega\tau = 1$, to be equal to 4.18×10^{-10} seconds.

The reflection coefficient shows very little variation over the frequency range under investigation (Fig. 3). The refractive index of the solution

indicates increasing values with frequency increasing. The electrical behaviour of the solution may also be studied in terms of the complex

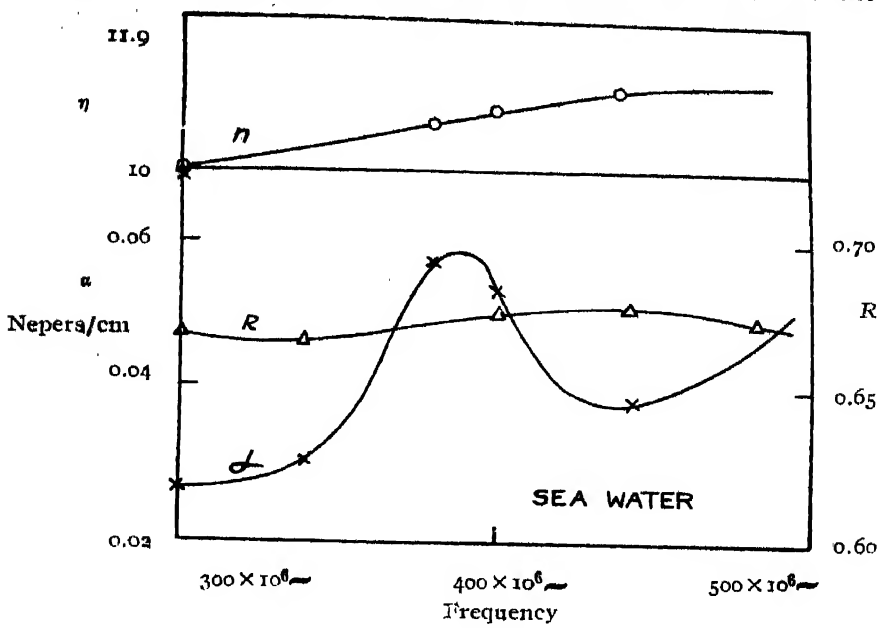

FIG. 3

dielectric constant $\epsilon - j\frac{2\sigma}{f}$ where ϵ is the dielectric constant, σ is the conductivity and f is the frequency in c. p. s. Since the complex index of refraction $N = n(1 - jk)$ is equal to the square root of the complex dielectric constant, it can be written that

$$\epsilon = n^2(1 - K^2) \quad \text{and} \quad \sigma = \frac{n\alpha}{60\pi} \quad \frac{mhos}{cm}$$

Variation of $\tan \sigma = \epsilon''/\epsilon'$ where $\epsilon' = n^2$ and $\epsilon'' = 2n^2K$ and σ with frequency can be studied from Fig. 4.

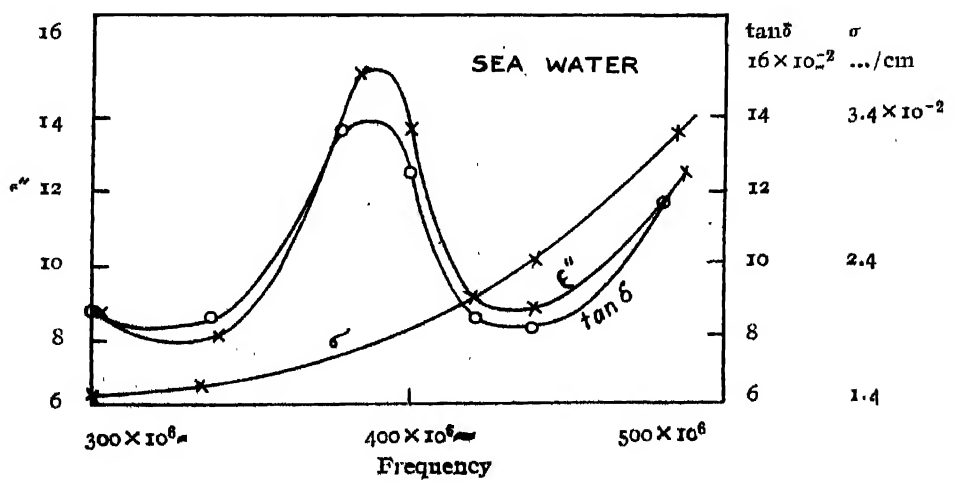

FIG. 4

The rise of conductivity with frequency may be explained in the following way. The present case is similar to that of finding the conductivity of a solution containing per cm^3, $(n_1\ n_2,\ n_3 \ldots n_s)$ ions of species $(1, 2, 3, \ldots s)$ with charges $(e_1, e_2, e_3 \ldots e_s)$ e.s.u. per ion. The frequency dependence of the conductivity of a mixture of strong electrolytes has been investigated by Falkenhagen and Fischer (1932) and also by Onsoger and Fuoss (1932). The conductance of the *jth* species of ions in a mixture of s different kinds of ions is given by the following expression (Onsager and Fuoss, 1932)

$$\Lambda_j = \Lambda_j^0 - \left[\frac{1.97 \times 10^6}{DT^{3/2}} \cdot \Lambda_j^0 \cdot Z_j \sum_{n=0}^{\infty} C_n \gamma_j^{(n)} + \frac{26.98}{\eta (DT)^{1/2}} \cdot Z_j \right] \cdot \Gamma^{1/2}$$

where Λ_j^0 represents the conductance at infinite dilution. The relaxation term inside the parenthesis depends on the square root of the total ionic strength Γ and on the mobility ratios and on the ratios in which the various ions are present. The term due to the electrophoretic effect involves only the square root of total ionic strength and viscosity.

To evaluate the above expression a knowledge of viscosity is essential. If the composition of a mixture of electrolytes of concentration c is given by the mole fractions x, y and $(1-x-y)$ and if η', η'', η''' represent the relative viscosities of solutions of pure salts of concentration c the relative viscosity η of the mixture is given (Ruby and Kawai, 1926) by the following expression

$$\eta = x\eta' + y\eta'' + (1-x-y)\eta'''$$

The total ionic concentration of the mixture of electrolytes forming sea water is 34.7 gm/kg of sea water. Then taking the viscosity values for the respective salts (Int. Crit. Tables, 1929) as follows

$$\eta NaCl = 1.0456$$

$$\eta MgCl_2 = 1.1500$$

$$\eta MgSO_4 = 1.1800$$

$$\eta CuSO_4 = 1.1500$$

the relative viscosity of sea water is 1.0688. The viscosity of pure water at 25°C being 8. 94 millipoises, the viscosity of sea water at 25° C is 9.557 millipoises. Calculating the dielectric constant D from the values of n (Fig.3) the values for relaxation and electrophoretic correction terms at different frequencies have been determined and tabulated below :

TABLE I

f in Mc/s	$\frac{1.971 \times 10^6}{(DT)^{3/2}}$	$\frac{28.98}{\eta (DT)^{1/2}}$
300	0.3832	17.57
400	0.3407	16.90
500	0.3217	16.58

So the expression for the conductivity at different frequencies can be written as follows

$$\Lambda_j^{300} = \Lambda_j^0 - \left[0.3832 \Lambda_j^0 . Z_j^1 \sum_{n=0}^{\infty} C_{n-j}^{(n)} \gamma + 17.57 Z_j \right] . \Gamma^{\frac{1}{2}}$$

$$\Lambda_j^{400} = \Lambda_j^0 - \left[0.3407 \Lambda_j^0 . Z_j^1 \sum_{n=0}^{\infty} C_{n-j}^{(n)} \gamma + 16.90 Z_j \right] . \Gamma^{\frac{1}{2}}$$

$$\Lambda_j^{500} = \Lambda_j^0 - \left[0.3217 \Lambda_j^0 Z_j^1 \sum_{n=0}^{\infty} C_{n-j}^{(n)} \gamma + 16.58 Z_j \right] . \Gamma^{\frac{1}{2}}$$

It will be evident from the above table that the correction terms due to relaxation and electrophoretic effects decrease with increasing frequency. So the value for conductivity increases with increase of frequency over the range in question.

ACKNOWLEDGMENT

The authors express their grateful thanks to the Head of the Department for giving facilities for carrying out the investigation.

Department of Electrical Communication Engineering,
Indian Institute of Science, Bangalore.

REFERENCES

Chatterjee S. K., and Sreekantan B. V., 1948, *Ind. Jour. Phys.*, **22**, 229.
Chatterjee S. K., and Sreekantan B. V., 1948, *Ind. Jour. Phys.*, **22**, 233.
Chatterjee S. K., 1948, *Ind. Jour. Phys.*, **22**, 157.
Cooper R., 1946, J. I. E. E., 93, Part III, 69.
Debye P., 1929, 'Polar Molecules', Chemical Catalog Co., New York.
Dorsey N E, 1940, "Properties of Water Substance", 651, Reynold Publishing Co., New York.
Falkenhagen H., and Fischer W., 1932, *Physik. Z.*, **33**, 941.
International Critical Tables, 1928, **3**, 100.
International Critical Tables, 1929, **6**, 15.
Knerr, H. W., 1937, *Phy. Rev.*, **51**, 1054.
Onsager L., and Fuoss, R. M., 1932, *Jour. Phy. Chem.*, **36**, 2689.
Ruby C. E., and Kawai J., 1926, *Jour. Amer. Chem. Soc.*, **48**, 1119.

THE NEAR ULTRA-VIOLET SPECTRA OF BENZENE PART III. FERMI RESONANCE IN THE EMISSION SPECTRUM OF BENZENE

By R. K. ASUNDI and M. R. PADHYE

ABSTRACT. A large number of Fermi doublets have been discovered in the emission spectrum of benzene. These are due to accidental degeneracy in the vibrations 1596 $e_{''}^{+}$ and 1598 $e_{''}^{+}$ (combination of 606 $e_{''}^{+}$+992 $a_{1''}$) further superposed by several quanta of 992 $a_{1''}$ vibration and involving also 923 $a_{1''}$ excited frequency in addition to series of 160 difference frequency. The magnitude of doublet interval with increasing excitation of the vibrations is well represented by an expression derivable from considerations of the first order perturbation in the potential function of the molecule.

INTRODUCTION AND RESULTS

Fermi resonance in the case of benzene seems to have been first discovered by Wilson (1934). The Raman spectrum of benzene shows two strong lines at a frequency difference of 1584 and 1606 instead of one calculated at 1596.* These have been explained as Fermi doublets due to resonance between (1596) $e_{''}^{+}$ and (606 $e_{''}^{+}$ + 992 $e_{1''}$ = 1598) $e_{''}^{+}$.

In the Raman spectrum, lines involving higher vibrational quanta are usually too weak to observe and these vibrations are inactive in the infrared spectrum. Hence Fermi doublets involving overtones or combination tones have not been recorded. In the absorption spectrum similarly only the fundamental Fermi doublet is observed but since absorption can go to different vibrational levels in the excited electronic state, two more doublets have been recorded both of which, however, involve the same fundamental Fermi doublet. In the high pressure fluorescence spectrum (Ingold and Wilson, 1936), there is evidence of not only the fundamental Fermi doublet but also two more doublets involving one and two quanta of 992 superposed on the Fermi doublet.

In the case of the emission spectrum, in addition to the fundamental doublet, four more Fermi doublets are found involving one to four quanta of 992 successively added to both components of the doublet. Each of these is further developed into series involving the 160 difference frequency. Some of them also develop into progressions involving the 923 frequency in the excited state overlapped by the 160 difference frequency. The wavenumbers on these doublets ovserved in the course of an investigation on the emission

* All frequencies are given in wavenumbers in cm^{-1} units.

spectrum of benzene§ are collected together in Table I, in which also the bands observed in absorption and fluorescence are suitably indicated.

The Table shows two parallel series of bands termed α and β which involve these doublets. The fundamental doublet frequencies obtained from the value for the mean of the five bands that occur in the 160 series superposed over the fundamental doublet is 1585 and 1602. Similarly the positions from the ground state of the doublets involving 1 to 4 quanta of 992 are obtained as mean values from the corresponding 160 progressions. These data on observed mean frequencies are given in Table III. They enable us to study the Fermi interaction with increasing quanta of vibrations as in CO_2 or H_2O. It must, however, be remembered that the differences in the present case are obtained from the band head data which are themselves subject to an error of about ± 3 cm^{-1}.

DISCUSSION OF RESULTS

The case of accidental degeneracy here met with falls to a certain extent in the same class as of CO_2, which has been fully worked out by Dennison (1932: 1940) and Adel and Dennison (1933). The interaction is treated as a perturbation brought about by anharmonicity. The first order perturbed energies are obtained by solving the secular determinant $|A^r_s - \lambda W_1 \delta^r_s| = 0$. The roots of this determinant λW_1 furnish the required perturbed energies. The quantity A^r_s is the matrix element of the perturbing function $T_1 + \lambda U_1$. The first order perturbation should give the magnitude of the interaction correctly. This is nearly but not wholly borne out by experiment. The agreement between theory and experiment becomes, however, more complete if the second order perturbation is also employed. A complete theory of Fermi resonance for CO_2 is hence given by Dennison and Adel and Dennison, which is further extended by Darling and Dennison (1940) with suitable alterations to H_2O. The accuracy of experimental data available in both these molecules is superior to that in our experiments on benzene. Here we do not observe the band origins as in CO_2 or H_2O particularly in their infrared data but only band heads. It is, therefore, thought that the first order perturbation alone need be considered. The case of methyl halides which is analogous to CO_2 is in this respect particularly interesting and has been worked out by Adel and Barker (1934). Using only the first order perturbation, they obtain expressions for $W\alpha$ and $W\beta$ which are separations from the unperturbed levels including the constant shift $\frac{\Delta}{2}$ due to the ground level. Thus,

$$W\alpha = \Delta + \left[\frac{\Delta^2}{4} + \frac{nb^2}{2} \right]^{\frac{1}{2}}$$

§ For details of experimental procedure, etc., refer to the paperon the Emission Spectrum of Benzene in the near ultraviolet Part I of this series.

and $$W_\beta = \Delta - \left[\frac{\Delta^2}{4} + \frac{nb^2}{2} \right]^{\frac{1}{2}}$$

where Δ is the displacement of the calculated frequency from the mean of the observed doublet, b^2 is given by $\left(\frac{\Lambda^2 - \Delta^2}{2} \right)$ where Λ is the doublet separation and n takes values 1, 2...etc., b is a measure of the anharmonicity appearing in the cubic part of the potential function.

In benzene, the fundamental perturbation occurs between the singly excited $e_{\prime\prime}^{+}$ vibration and the single excited composite vibration 1598 $e_{\prime\prime}^{+}$ (formed by 992 a_{1g} + 606 $e_{\prime\prime}^{+}$). In other words, the degeneracy is between two doubly degenerate vibrations. For single excitation, the degeneracy is not removed both and vibrations have the same l value namely 1. In this respect the fundamental degeneracy in benzene differs from that in CO_2 or the methyl halides where the fundamental degeneracy is between a singly excited non-degenerate vibration and a doubly excited degenerate vibration. The l value for the non-degenerate vibration being always 0, only the component having $l=0$ of the doubly excited non-degenerate vibration enters into interaction whereas the component having $l=2$ is unaffected.

The observed excited Fermi doublets in benzene arise on account of superposition of a non-degenerate totally symmetrical vibration which has no influence on the l value. The vibration quantum numbers of the frequencies giving rise to the doublets are shown in Table II. Among such doublets found in CO_2, there are similarly those which arise by superposition of a non-degenerate vibration. These considerations lead us to adopt expressions for W_α and W_β similar to those used by Adel and Barker. The value for the component vibrations thus calculated are given in Table III along with the observed values. The agreement is considered satisfactory.

Note added on January 12, 1949.—

In a recent paper which reached us last month, Garforth and Ingold (1948) have made a detailed analysis of the fluorescence bands of benzene. From a re-examination of the spectrograms and micro-photograms of the bands previously reported by Ingold and Wilson (1936), they have recast the data on band maxima and recorded similar resonance doublets. Although there is some discrepancy in the wavelength data it is satisfactory to find that the doublet separations are exactly identical with those recorded here.

TABLE I

Series*	ν_{vac}	Int.**	Series	ν_{vac}	Int.
a_0^0	36504††	8	β_0^0	36486††	8
a_0^1	36343+††	4·5	β_0^1	36325+††	5
a_0^2	36182††	2·5	β_0^2	36166††	3
a_0^3	36023††	1	β_0^3	36006††	1·5
a_0^4	35871	1	β_0^4	35848††	0
a_{-1}^0	35517††	5	β_{-1}^0	35492††	7
a_{-1}^1	35356††	3	β_{-1}^1	35330††	4·5
a_{-1}^2	35193††	1	β_{-1}^2	35169††	4·5
a_{-1}^3	35038††	2	β_{-1}^3	35007	1
a_{-1}^4	34877††	·5			
a_{-2}^0	34530††	3	β_{-2}^0	34501††	4·5
a_{-2}^1	34371††	3	β_{-2}^1	34338††	3
a_{-2}^2	34208††	1	β_{-2}^2	34176††	3
a_{-2}^3	34046	1·5	β_{-2}^3	34018††	0
a_{-3}^0	33549	1·5	β_{-3}^0	33512††	3
a_{-3}^1	33384	2·5	β_{-3}^1	33347	0
			β_{-3}^2	33189	0
			β_{-4}^0	32524	1·5
			β_{-4}^1	32351	1
			β_{-4}^2	32210	0
a_{1-1}^0	36442	2	β_{1-1}^0	36421+	3·5
a_{1-1}^1	36276	1	β_{1-1}^1	36257	2
			β_{1-1}^2	36097	2
a_{1-2}^0	35455	3·5	β_{1-2}^0	35425	4(?)
a_{1-2}^1	35393	1	β_{1-2}^1	35264	2(?)
a_1^0	37427	0			
a_2^0	38353†	2 (?)			

† These are also present in the absorption spectrum Radle and Beck, (1940).
†† These are also present in the fluorescence spectrum Ingold and Wilson (1936).
* The notation followed is the one given in Part I of the series, namely, negative subscripts for superposition of 992 quanta in the ground state and the superscript denoting the quanta of the difference frequency 160 superposed
** The intensities are those visually estimated relative to the intensity of the strongest band B_0^0 as 10.

The complete table given in Part I of the series gives some more bands as belonging to α and β series but since the assignment is not unique, they are not included in this table.

TABLE II

Doublet No.	V_1 606 e_g^+	V_2 992 a_{1g}	V_3 (1596) e_g^+
I	1	1	0
	0	0	1
II	1	2	0
	0	1	1
III	1	3	0
	0	2	1
IV	1	4	0
	0	3	1
V	1	5	0
	0	4	1

TABLE III

$\Delta = R - (\nu_2 + \nu_8) = 1593.5 - 1598 = -4.5$ cm^{-1}

$b^2 = \left\{ \frac{\Lambda^2 \mp \Delta^2}{\quad} \right\} = 134.4$

$$W_{\alpha\beta} = \Delta \pm \left\{ \frac{\Delta^2}{4} + \frac{nb^2}{2} \right\}^{1/2}$$

Doublet No.	Series	Frequencies observed mean values	Frequencies calculated	Values $W_{\alpha,\beta}$	O−C
I	α_0^0	1585	(1585)	−13	0
	β_0^0	1602	(1602)	+ 4	0
II	α_{-1}^0	2572	2574	−16.3	− 2
	β_{-1}^0	2598	2597	+ 7.3	1
III	α_{-2}^0	3559	3563	−18.9	− 4
	β_{-2}^0	3590	3592	+ 9.9	− 2
IV	α_{-3}^0	4542	4553	−21.1	−11
	β_{-3}^0	4579	4586	+12.1	− 7
V	α_{-4}^0	—	5543	−23	—
	β_{-4}^0	5566	5580	+14	−14

BENARES HINDU UNIVERSITY.

REFERENCES

Adel and Barker, 1934, *J. Ch. Phys.*, **2**, 627.

Adel and Dennison, 1933, *Phys. Rev*, **43**, 716.

Darling and Dennison, 1940, *Phys. Rev.*, **57**, 128.

Dennison, 1932, *Phys. Rev.*, **41**, 304.

,, 1940, *Revs. Mod. Phys.*, **12**, 175.

Garforth and Ingold, 1948, *J. C. S.*, p. 427.

Ingold and Wilson, 1936, *J. C. S.*, pp. 941 and 1210.

Radle and Beck, 1940, *J. Ch. Phys.*, **8**, 507.

Wilson, 1934, *Phys. Rev.*, **46**, 146.

THEORY OF DOUBLET SPECTRA UNDER MAGNETIC PERTURBATION

By S. SENGUPTA

(*Received for publication, Dec. 16, 1948*)

ABSTRACT. The problem of a spinning electron moving round the nucleus in the presence of an external magnetic field has been considered from the wave-statistical point of view. The general expressions for energies and wave functions in any field strength have been obtained. The problems of no field, weak field (Zeeman effect) and strong field (Paschen-Back effect) are considered as special cases. The results for the no field case are identical with those obtained in the earlier paper (Kar and Sengupta, 1919). Other results also agree with the well-known spectroscopic formulæ.

In a recent paper the energies and intensities of doublet spectra have been calculated by Kar and Sengupta (1949) by the usual wave-statistical method without splitting the second order wave equation into two linear equations as has been done by Dirac. In the above paper the effect of the external magnetic field has not been considered. Further, although a spin function with half harmonic value is introduced, no generalised wave equation for the spin and revolving motion of the electron is given. Moreover, in that paper the idea of vector coupling between L and S and the formation of the coupled states defined by J and M has been used.

In the present paper we shall dispense with the above idea and shall give a general treatment of the problem taking into account the effect of external magnetic field. We shall at first calculate the energy values and wave functions of a spinning electron moving round a nucleus and under the influence of an external magnetic field. The problems of (*a*) no field (*b*) weak field and (*c*) strong field will then be considered as special cases.

Before we actually go into the problem it may be useful to give a short summary of the previous works on the subject. As early as 1926 Heisenberg and Jordon (1926) first discussed the problem using matrix mechanics. Later on Condon and Shortley (1935) arrived at the same result by a somewhat similar method. Again on starting from Dirac's equations for hydrogenic atom, Darwin (1928) and subsequently Bose and Bose (1944) using Sonine's polynomials, obtained the same general expression for the energy of the spinning electron in any field strength.

The complete wave function for the spinning electron moving round the nucleus is given by (vide Kar and Sengupta *loc. cit.*).

$$\chi_{nlm_l m_s} = \chi_{nlm_l} . \chi'_{m_s}$$

where χ_{nlm_l} and χ'_{m_s} are the orbital and spin wave functions. If we assume the spinning electron to be equivalent to a rotator of mass m_0 and radius a, where a is the radius of gyration of the electron about its centre, then the wave equation satisfied by χ'_{m_s} is the same as that of a rotator. It can be easily shown that the complete function $\chi_{nlm_lm_s}$ satisfies the wave equation,

$$\Delta\chi_{nlm_lm_s}+\frac{8\pi^2 m_0}{h^2}(E_{nls}-V)\chi_{nlm_lm_s}=0 \qquad \ldots \quad (1.1)$$

where $$\Delta=\left(\frac{1}{r^2}\frac{\partial}{\partial r}r^2\frac{\partial}{\partial r}+\frac{1}{r^2\sin\theta}\frac{\partial}{\partial\theta}\sin\theta\frac{\partial}{\partial\theta}+\frac{1}{r^2\sin^2\theta}\frac{\partial^2}{\partial\phi^2}\right)$$

$$+\frac{1}{a^2}\left(\frac{1}{\sin\theta'}\frac{\partial}{\partial\theta'}\sin\theta'\frac{\partial}{\partial\theta'}+\frac{1}{\sin^2\theta'}\frac{\partial^2}{\partial\phi'^2}\right) \qquad \ldots \quad (1.2)$$

and $$E_{nls}=E_{nl}+E_s \qquad \ldots \quad (1.3)$$

E_{nl} being the well known relativistic orbital energy and E_s the spin energy obtained by solving the wave equation for χ'_{m_s}. Thus for the spinning electron moving round the nucleus we get the wave equation, wave functions and energy values respectively from (1.1), (1) and (1.3).

It is evident that the wave function $\chi_{nlm_lm_s}$ is $2(2l+1)$-fold degenerate with respect to m_l and m_s. Now, since any linear combination of these is also a solution of the wave equation, we write for the general wave function

$$\chi_{nl}=\sum_{m_l=-l}^{+l}\sum_{m_s=-\frac{1}{2}}^{+\frac{1}{2}}\alpha_{m_lm_s}\chi_{nlm_lm_s} \qquad \ldots \quad (2)$$

where $\alpha_{m_lm_s}$'s are arbitrary constants. It is easily seen that χ_{nl} satisfies the same wave equation as $\chi_{nlm_lm_s}$ viz., equation (1.1).

We shall now consider the effect of the spin-orbit and magnetic perturbations on this system. The spin-orbit perturbation is given by (Thomas (1926))

$$E_{s-0}=\frac{Ze^2}{2m_0^2c^2}\cdot\frac{(LS)}{r^3} \qquad \ldots \quad (3)$$

where L and S represents the orbital and spin angular momentum vectors of the electron. Other symbols have their usual meaning. Now,

$$(LS)=L_xS_x+L_yS_y+L_zS_z$$

$$=\tfrac{1}{2}\{(L_x+iL_y)(S_x-iS_y)+(L_x-iL_y)(S_x+iS_y)+2L_zS_z\}=-\frac{h^2}{8\pi^2}\cdot$$

operator ... (3.1)

where, $$\text{operator}=e^{i(\phi-\phi')}\left(\frac{\partial}{\partial\theta}+i\cot\theta\frac{\partial}{\partial\phi}\right)\left(\frac{\partial}{\partial\theta'}-i\cot\theta'\frac{\partial}{\partial\phi'}\right)+$$

$$e^{-i(\phi-\phi')}\left(\frac{\partial}{\partial\theta}-i\cot\theta\frac{\partial}{\partial\phi}\right)\left(\frac{\partial}{\partial\theta'}+i\cot\theta'\frac{\partial}{\partial\phi'}\right)+2\frac{\partial^2}{\partial\phi\partial\phi'} \qquad \ldots \quad (3.2)$$

which is obtained by introducing the well known operators associated with L_x+iL_y etc.

Thus the spin-orbit interaction energy becomes,

$$E_{s-0} = -\frac{Ze^2}{m_0^2c^2}\cdot\frac{h^2}{16\pi^2r^3}\cdot \text{ operator} \qquad \ldots \quad (4)$$

Now the orbital magnetic moment of the electron is

$$M_l = \frac{e}{2m_0c}L$$

and the spin magnetic moment

$$M_s = \frac{e}{m_0c}S$$

Hence the total magnetic interaction energy in an external magnetic field H along the $z\rightarrow$ axis, is given by

$$\begin{aligned} E_H &= \frac{e}{2m_0c}(LH + 2SH) \\ &= a(m_l + 2m_s) \end{aligned} \qquad \ldots \quad (5)$$

where

$$a = \frac{ehH}{4\pi m_0c} \qquad \ldots \quad (5.1)$$

Thus the total perturbation energy is

$$E_{s-0} + E_H = -\frac{Ze^2}{m_0^2c^2}\cdot\frac{h^2}{16\pi^2r^3}\text{ operator } + a(m_l + 2m_s) \qquad \ldots \quad (6)$$

We shall now apply the general method of perturbation for degenerate systems to find the change in energy and wave function. Let the changed energy and wave function be,

$$\left.\begin{aligned} E &= E_{nls} + \varepsilon \\ \chi &= \chi_{nl} + \psi \end{aligned}\right\} \qquad \ldots \quad (7)$$

where ε and ψ represent small changes in energy and wave function. The wave equation for the perturbed state is given by (Kar and Sengupta *loc. cit.*)

$$\Delta\chi + \frac{8\pi^2m_0}{h^2}\{E - (V + E_{s-0} + E_H)\}\chi = 0 \qquad (8)$$

On substituting from (7) in (8) and remembering the relation (1.1), we get neglecting second order terms,

$$\Delta\psi + \frac{8\pi^2m_0}{h^2}(E_{nls} - V)\psi = \frac{8\pi^2m_0}{h^2}(E_{s-0} + E_H - \varepsilon)\chi_{nl} \qquad (8.1)$$

If we express ψ as a function of the unperturbed wave functions χ_{nl}'s then

$$\psi = \sum_{n'}\sum_{l'} A_{n'l'}\chi_{n'l'} \qquad \ldots \quad (8.2)$$

where $A_{n'l'}$'s are small constants. On substituting (8.2) in (8.1) we get

$$\sum_{n'}\sum_{l'}(E_{nls} - E_{n'l's})A_{n'l'}\chi_{n'l'} = (E_{s-0} + E_H - \varepsilon)\chi_{nl} \qquad \ldots \quad (9)$$

It is evident that if we multiply both sides of (9) by any of the $2(2l+1)$ functions $\chi_{nlm_l m_s}$ and integrate throughout the five dimensional q-space then the left hand side will vanish due to the orthogonality of the wave functions $\chi_{nlm_l m_s}$. Therefore we get $2(2l+1)$ equations of the type

$$\int (E_{s-0} + E_{II} - \varepsilon)\chi_{n'l'} \chi_{nlm_l m_s} d\tau = 0$$

Or from (2)

$$\sum_{m'_l} \sum_{m'_s} \alpha_{m'_l m'_s} \int (E_{s-0} + E_{II} - \varepsilon)\, \chi_{nlm'_l m'_s}\, \chi_{nlm_l m_s}\, d\tau = 0 \quad \ldots \quad (10)$$

Now it may be easily shown that the well known relations between the associated Legendre functions

$$e^{i\phi}\left(\frac{\partial}{\partial\theta} + i\cot\theta\,\frac{\partial}{\partial\phi}\right) P_l^{m_l} e^{im_l\phi} = -\sqrt{(l-m_l)(l+m_l+1)}\, P_l^{m_l+1} e^{i(m_l+1)\phi}$$

$$e^{-i\phi}\left(\frac{\partial}{\partial\theta} - i\cot\theta\,\frac{\partial}{\partial\phi}\right) P_l^{m_l} e^{im_l\phi} = \sqrt{(l+m_l)(l-m_l+1)}\, P_l^{m_l-1} e^{i(m_l-1)\phi}$$

are also valid for $P_s^{m_s}$ with $s=\frac{1}{2}$ and $m_s = \pm\frac{1}{2}$. On using the above relations we get,

$$E_{s-0}\chi_{nlm_l m_s} = -\frac{Ze^2}{m_0^2c^2}\,\frac{h^2}{16\pi^2 r^3}\Big\{\sqrt{(l+m_l)(l-m_l+1)}\,\chi_{nlm_l-1,m_s+1} + \sqrt{(l-m_l)(l+m_l+1)}\,\chi_{nlm_l+1,m_s-1} + 2m_l m_s \chi_{nlm_l m_s}\Big\} \quad \ldots \quad (11)$$

On integrating (10) with the help of (11) we can write out the $2(2l+1)$ equations for different values of m_l and m_s. For $m_s=\frac{1}{2}$ we get $(2l+1)$ equations of the type,

$$\alpha_{m_l\frac{1}{2}}\left\{\frac{b}{2}m_l + a(m_l+1) - \varepsilon\right\} + \alpha_{m_l+1,-\frac{1}{2}}\,\frac{b}{2}\sqrt{(l-m_l)(l+m_l+1)} = 0 \quad \ldots \quad (12)$$

and for $m_s=-\frac{1}{2}$ we get $(2l+1)$ equations of the type,

$$\alpha_{m_l,-\frac{1}{2}}\left\{-\frac{b}{2}m_l + a(m_l-1) - \varepsilon\right\} + \alpha_{m_l-1,\frac{1}{2}}\,\frac{b}{2}\sqrt{(l+m_l)(l-m_l+1)} = 0 \quad (12.1)$$

where $$l \geq m_l \geq -l$$

and $$b = \frac{Ze^2}{m_0^2c^2}\cdot\frac{h^2}{8\pi^2}\int_0^\infty \frac{R^2(nl)}{r^3}\cdot r^2 dr = \frac{Rhc\alpha^2z^4}{n^3 l(l+1)(l+\frac{1}{2})} \quad \ldots \quad (12.2)$$

Perturbation energy.—

The $2(2l+1)$ equations given by (12) and (12.1) contain $2(2l+1)$ constants. By eliminating them and solving for ε we get in general $2(2l+1)$

roots of ε. We shall now find out these roots. We take the lth equation of (12) obtained by putting $m_l = l$,

$$\alpha_{l,\frac{1}{2}}\{\tfrac{1}{2}bl + a(l+1) - \varepsilon\} = 0 \qquad (13)$$

and $-l$th equation of (12.1)

$$\alpha_{-l,-\frac{1}{2}}\{\tfrac{1}{2}bl - a(l+1) - \varepsilon\} = 0 \qquad (13.1)$$

From these we get the two roots,

$$\left.\begin{aligned} \varepsilon &= a(l+1) + \tfrac{1}{2}bl \\ \varepsilon &= -a(l+1) + \tfrac{1}{2}bl \end{aligned}\right\} \qquad (14)$$

To get the other $4l$ roots we take the m_{l+1}th equation of (12.1),

$$\alpha_{m_l,\frac{1}{2}}\cdot\tfrac{1}{2}b\sqrt{(l-m_l)(l+m_l+1)} + \alpha_{m_l+1,-\frac{1}{2}}\{-\tfrac{1}{2}b(m_l+1) + am_l - \varepsilon\} = 0 \ldots \quad (15)$$

If we eliminate $\alpha_{m_l,\frac{1}{2}}$ and $\alpha_{m_l+1,\,-\frac{1}{2}}$ from (15) and (12), we get solving for ε,

$$\varepsilon = a(m_l+\tfrac{1}{2}) - \frac{b}{4} \pm \frac{1}{4}\sqrt{b^2(2l+1)^2 + 4a^2 + 8ab(m_l+\tfrac{1}{2})} \quad \ldots \quad (15.1)$$

Thus here we get two energy values for each value of m_l. Since m_l here can take up $2l$ values from $l-1$ to $-l$ corresponding to the $2l$ equations of (12), (the lth equation being already considered) we get in all $4l$ values of ε from (15.1) Again from (14) we get two more values of ε. Thus we have altogether $4l+2$ values of ε.

These $4l+2$ values of ε however can be arranged in two groups. It is seen from (14) and (15.1) that when $a=0$ *i.e.*, in the absence of any magnetic field, all the $4l+2$ different energy levels merge into two, ε_1 and ε_2 where,

$$\left.\begin{aligned} \varepsilon_1 &= \tfrac{1}{2}bl \\ \varepsilon_2 &= -\tfrac{1}{2}b(l+1) \end{aligned}\right\} \quad \ldots \quad (16)$$

Since both levels given by (14) merge to ε_1, it is easily seen that of the $(4l+2)$ levels $(2l+2)$ merge to ε_1 and the remaining $2l$ to ε_2. Thus we see that in the absence of a field a particular level E_{nls} will break up into two under spin-orbit interaction. Their perturbed energies are given by (16). on application of the field ε_1 splits up into $(2l+2)$ different levels. Two of these are given by (14) and the other $2l$ levels are obtained from (15.1) with the positive sign before the radical. They are,

$$\varepsilon_1^{m_l} = a(m_l+\tfrac{1}{2}) - \frac{b}{4} + \frac{1}{4}\sqrt{b^2(2l+1)^2 + 4a^2 + 8ab(m_l+\tfrac{1}{2})} \quad \ldots \quad (17)$$

where $$l-1 \geq m_l \geq -l$$

It is interesting to note that for $b(2l+1) > 2a$ *i.e.*, for weak field, the energies given by (14) are obtained by putting $m_l = l$ and $-l-1$ respectively in (17). Thus in this case all the $(2l+2)$ energy values are obtained from (17) for $\geq m_l \geq -l-1$, which may be conveniently represented by $\varepsilon_1^{l}, \varepsilon_1^{l-1} \ldots \varepsilon_1^{-l}, \varepsilon_1^{-l-1}$.

The other level ϵ_2 splits into $2l$ different levels whose energies are obtained from (15.1) with negative sign before the radical, namely,

$$\epsilon_2^{m_l} = a(m_l + \tfrac{1}{2}) - \frac{b}{4} - \frac{1}{4}\sqrt{b^2(2l+1)^2 + 4a^2 + 8ab(m_l + \tfrac{1}{2})} \quad \ldots \quad (17.1)$$

where $$l - 1 \geq m_l \geq -l$$

Wave function.—

Let us next proceed to find out the wave functions associated with these energy values. We shall throughout neglect ψ, the small correction in the wave function due to perturbation. However, the perturbation also affects the degeneracy of the wave functions and as such modifies the unperturbed wave functions. The modification of this type is often called the zero order correction of the wave function due to perturbation. It may be calculated in the following way.

We have taken the unperturbed wave function in the general form χ_{nl} given in (2), in which $\alpha_{m_l m_s}$'s are arbitrary constants. Thus the problem of finding out the zero-order-corrected wave functions reduces itself to finding the values of $\alpha_{m_l m_s}$'s for different perturbed energy values. To do this we substitute any particular value of ϵ from (17) or (17.1) in the $(4l+2)$ equations of (12) and (12.1). Then we get $(4l+2)$ equations connecting $(4l+2)$ arbitrary constants $\alpha_{m_l m_s}$'s. On combining these equations with the general averaging condition

$$\sum_{m_l} \sum_{m_s} \alpha^2_{m_l m_s} = 1 \quad \ldots \quad (18)$$

we can easily find out the values of these constants.

If we take the energy values given in (17) and substitute them in equations (12) and (12.1), we see that all $\alpha_{m_l m_s}$ except $\alpha_{m_l \frac{1}{2}}$ and $\alpha_{m_l+1, -\frac{1}{2}}$ vanish. For these two we get from (12)

$$\frac{\alpha_{m_l \frac{1}{2}}}{\alpha_{m_l+1, -\frac{1}{2}}} = -\frac{\frac{1}{2}b\sqrt{(l-m_l)(l+m_l+1)}}{\frac{1}{2}bm_l + a(m_l+1) - \epsilon_1^{m_l}} \quad \ldots \quad (19)$$

utilising the relation (18) and after some work we get,

$$\left.\begin{aligned} \alpha^2_{m_l \frac{1}{2}} &= \frac{-\frac{1}{2}b(m_l+1) + am_l - \epsilon_1^{m_l}}{-\frac{1}{2}b + a(2m_l+1) - 2\epsilon_1^{m_l}} \\ \alpha^2_{m_l+1, -\frac{1}{2}} &= \frac{\frac{1}{2}bm_l + a(m_l+1) - \epsilon_1^{m_l}}{-\frac{1}{2}b + a(2m_l+1) - 2\epsilon_1^{m_l}} \end{aligned}\right\} \quad \ldots \quad (19.1)$$

Thus the wave functions associated with the given energy values $\epsilon_1^{m_l}$'s are,

$$\chi_{nl\epsilon_1 m_l} = \alpha_{m_l \frac{1}{2}} \chi_{nlm_l \frac{1}{2}} + \alpha_{m_l+1, -\frac{1}{2}} \chi_{nlm_l+1, -\frac{1}{2}} \quad \ldots \quad (20)$$

where $$l \geq m_l \geq -l-1$$

and $\alpha_{m_l\frac{1}{2}}$, $\alpha_{m_l+1,-\frac{1}{2}}$ are given by (19.1). Similarly if we take the energy values given in (17.1) and substitute them in the equations (12) and (12.1) we get as before for the non-vanishing coefficients $\alpha_{m_l\frac{1}{2}}$ and $\alpha_{m_l+1,-\frac{1}{2}}$,

$$\frac{\alpha_{m_l\frac{1}{2}}}{\alpha_{m_l+1,-\frac{1}{2}}} = \frac{-\frac{1}{2}b\sqrt{(l-m_l)(l+m_l+1)}}{\frac{1}{2}bm_l+a(m_l+1)-\epsilon_2{}^{m_l}} \qquad \ldots \quad (21)$$

and

$$\left.\begin{aligned} \alpha^2_{m_l\frac{1}{2}} &= \frac{-\frac{1}{2}b(m_l+1)+am_l-\epsilon_2{}^{m_l}}{-\frac{1}{2}b+a(2m_l+1)-2\epsilon_2{}^{m_l}} \\ \alpha^2_{m_l+1,-\frac{1}{2}} &= \frac{\frac{1}{2}bm_l+a(m_l+1)-\epsilon_2{}^{m_l}}{-\frac{1}{2}b+a(2m_l+1)-2\epsilon_2{}^{m_l}} \end{aligned}\right\} \qquad \ldots \quad (21.1)$$

Thus the wave functions associated with the energy values $\epsilon_2{}^{m_l}$'s are,

$$\chi_{nl\epsilon_2{}^{m_l}} = \alpha_{m_l\frac{1}{2}}\chi_{nlm_l\frac{1}{2}} - \alpha_{m_l+1,-\frac{1}{2}}\chi_{nlm_l+1,-\frac{1}{2}} \qquad \ldots \quad (22)$$

where $$l-1 \geq m_l \geq -l$$

and $\alpha_{m_l\frac{1}{2}}$, $\alpha_{m_l+1,-\frac{1}{2}}$ are given by (21.1). Here we have taken $\alpha_{m_l+1,-\frac{1}{2}}$ negative, for it can be easily shown from (17.1) that $\epsilon_2{}^{m_l} < \frac{1}{2}bm_l + a(m_l+1)$ and so from (21) the ratio $\alpha_{m_l\frac{1}{2}}/\alpha_{m_l+1,-\frac{1}{2}}$ should be negative.

Thus the equations (17), (17.1), (20) and (22) give the general values of the energies and wave functions of the electron in any field strength. From these we can calculate the frequencies and intensities of the lines resulting from any transition. The general expression for the intensity of the line in any field strength is rather complicated. We shall, however, consider a simple case and calculate the intensities of the ten components of sodium D_1 and D_2 lines in any field strength. But before that we shall consider some special cases.

No field case.—

As already pointed out for $H=0$ *i.e.*, $a=0$ the $(2l+2)$ levels of energies $\epsilon_1{}^{m_l}$'s given in (17) merge into one level ϵ_1 given by (16). Similarly the $2l$ levels given by (17.1) merge into another level ϵ_2. The total energies of these two levels are given by (*vide* equations (7) and (1.3))

$$\left.\begin{aligned} E_1 &= E_{nl} + E_s + \epsilon_1 \\ E_2 &= E_{nl} + E_s + \epsilon_2 \end{aligned}\right\} \qquad (23)$$

Scince E_s is constant, it will not affect the calculation of frequencies of different lines. Neglecting it and substituting the values of E_{nl}, ϵ_1 and ϵ_2 it may be easily seen that (23) is identical with the well known spin-relativity formula.

It is evident that ϵ_1 and ϵ_2 levels are now $(2l+2)$- and $(2l)$- fold degenerate. The associated wave functions can be easily found from (20) and (22) by putting $a=0$. Thus the $(2l+2)$ wave functions for ϵ_1 are given by,

$$\chi_{nl\epsilon_1}^{m_l} = \sqrt{\frac{(l+m_l+1)}{2l+1}}\chi_{nlm_l\frac{1}{2}} + \sqrt{\frac{(l-m_l)}{2l+1}}\chi_{nlm_l+1,\,-\frac{1}{2}} \quad \ldots \quad (24)$$

where $$l \geq m_l \geq -l-1$$

and the $2l$ wave functions for ϵ_2 level are given by

$$\chi_{nl\epsilon_2}^{m_l} = \sqrt{\frac{(l-m_l)}{2l+1}}\chi_{nlm_l\frac{1}{2}} - \sqrt{\frac{(l+m_l+1)}{2l+1}}\chi_{nlm_l+1,\,-\frac{1}{2}} \quad \ldots \quad (24.1)$$

where, $$l-1 \geq m_l \geq -l$$

If we write $m=m_l+m_s$ remembering that m has the value $m_l+\frac{1}{2}$ for both the functions on the right hand side of (24) and (24.1) then it is easily seen that they are identical with the wave functions given in the earlier paper (Kar-Sengupta *loc. cit.*) for the states $j=l+\frac{1}{2}$ and $j=l-\frac{1}{2}$. Thus the different lines and their intensities can now be calculated in the same way as before.

Weak field case (Zeeman effect).—

In this case $b>>a$, since H is small. Hence we neglect a^2 compared to b^2. Thus from (17) we get

$$\epsilon_1^{m_l} = \frac{b}{2}l + ag(m_l+\tfrac{1}{2});\ g=\frac{2l+1}{2l+1} \quad \ldots \quad (25)$$

where $$l \geq m_l \geq -l-1$$

and g is the Lande factor for doublets with $j=l+\frac{1}{2}$. Similarly from (17.1) we get,

$$\epsilon_2^{m_l} = -\frac{b}{2}(l+1) + ag(m_l+\tfrac{1}{2});\ g=\frac{2l}{2l+1} \quad \ldots \quad (25.1)$$

where $$l-1 \geq m_l \geq -l$$

and g is the Lande factor for doublets with $j=l-\frac{1}{2}$. If we write $m=m_l+\frac{1}{2}$ then it is easily seen that (25) and (25.1) are identical with Lande's formula for Zeeman separations. For vanishingly small fields, the wave functions associated with (25) and (25.1) are still same as in the no field case and are given by (24) and (24·1) respectively. We shall now calculate the intensities of the Zeeman components of the lines resulting from any transition $nl \rightarrow n'l'$

($l'=l-1$). For no field we get in general three lines from the above transition. They are,

$$(1)\quad nl\epsilon_1 \rightarrow n'l'\epsilon'_1$$

$$(2)\quad nl\epsilon_2 \rightarrow n'l'\epsilon'_1$$

$$(3)\quad nl\epsilon_2 \rightarrow n'l'\epsilon'_2$$

The fourth line as was shown in the previous paper will have zero intensity. In a weak magnetic field both ϵ_1, ϵ_2 and ϵ'_1, ϵ'_2 break up into several levels, their energies being given by (25) and (25·1). From any one of these initial levels $\epsilon_1^{m_l}$ or $\epsilon_2^{m_l}$ in general three different transitions may occur. These are characterised by three different values of Δm_l, *viz.*, $\Delta m_l = 0, \pm 1$. For the transitions with $\Delta m_l = 0$, only the Z-component of the electric moment (M_z) exists. Hence the resulting vibrations are along the Z-direction and we get the π-components of the Zeeman pattern. For $\Delta m_l = \pm 1$ we get the σ-components. Since in transverse observation intensities of the lines are proportional to the square of the moments, we shall have to calculate M_x, M_y and M_z for different transitions from the wave functions (24) and (24·1). Calculations are same as in the previous paper (Kar-Sengupta *loc. cit.*) and we shall only give the results here.

(1) For the line $nl\epsilon_1 \rightarrow n'l'\epsilon'_1$

$$\left.\begin{aligned} &\Delta m_l = 0 \qquad M_z^2 = \frac{(l-m_l)(l+m_l+1)}{(2l+1)^2} R^2(nl;\ n'l-1) \\ &\Delta m_l = \pm 1 \quad M_x^2 = M_y^2 = \frac{1}{4}\frac{(l\mp m_l)(l\mp m_l\mp 1)}{(2l+1)^2} R^2(nl;\ n'l-1) \end{aligned}\right\} \quad \ldots \quad (26)$$

(2) for the line $nl\epsilon_2 \rightarrow n'l'\epsilon'_1$

$$\left.\begin{aligned} &\Delta m_l = 0 \qquad M_z^2 = \frac{(2m_l+1)^2}{(4l^2-1)^2} R^2(nl;\ n'l-1) \\ &\Delta m_l = +1,\ M_x^2 = M_y^2 = \frac{(l-m_l-1)(l+m_l+1)}{(4l^2-1)^2} R^2(nl;\ n'l-1) \\ &\Delta m_l = -1,\ M_x^2 = M_y^2 = \frac{(l+m_l)(l-m_l)}{(4l^2-1)^2} R^2(nl;\ n'l-1) \end{aligned}\right\} \quad \ldots \quad (26.1)$$

(3) for the line $nl\epsilon_2 \rightarrow n'l'\epsilon'_2$

$$\left.\begin{aligned} &\Delta m_l = 0 \qquad M_z^2 = \frac{(l+m_l)(l-m_l-1)}{(2l-1)^2} R^2(nl,\ n'l-1) \\ &\Delta m_l = +1,\ M_x^2 = M_y^2 = \frac{1}{4}\frac{(l-m_l-1)(l-m_l-2)}{(2l-1)^2} R^2(nl;\ n'l-1) \\ &\Delta m_l = -1,\ M_x^2 = M_y^2 = \frac{1}{4}\frac{(l+m_l)(l+m_l-1)}{(2l-1)^2} R^2(nl;\ n'l-1) \end{aligned}\right\} \quad \ldots \quad (26.2)$$

If we write $m = m_l + \frac{1}{2}$ and $j = l + \frac{1}{2}$ for the initial state ϵ_1 and $j = l - \frac{1}{2}$ for the initial state ϵ_2 then the above formulæ reduce to the well known relations for the intensities of the Zeeman components first derived empirically by Ornstein and Burger (1924).

Strong field case (Paschen-Back effect).

In this case $a >> b$. Hence we get from (17), neglecting b^2 compared with a^2,

$$\epsilon_1^{m_l} = a(m_l + 1) + \tfrac{b}{2} m_l \qquad \ldots \quad (28)$$

where $$l - 1 \geq m_l \geq -l$$

Similarly from (17.1) we get,

$$\epsilon_2^{m_l} = a m_l - \tfrac{b}{2}(m_l + 1) \qquad \ldots \quad (28.1)$$

where $$l - 1 \geq m_l \geq -l$$

The remaining two energy values ϵ_1^l and ϵ_1^{-l-1} are given by (14). The wave functions can be easily calculated from (20) and (22). They are,

$$\left.\begin{aligned} &\chi_{nl\epsilon_1^{m_l}} = \chi_{nlm_l\frac{1}{2}} \quad \text{for } l \geq m_l \geq -l \\ \text{and} \quad &\chi_{nl\epsilon_1^{-l-1}} = \chi_{nlm_l = -l, -\frac{1}{2}} \end{aligned}\right\} \qquad \ldots \quad (29)$$

giving the $(2l+2)$ wave functions associated with $(2l+2)$ energy values $\epsilon_1^{m_l}$. Similarly the wave functions associated with $\epsilon_2^{m_l}$'s are given by,

$$\chi_{nl\epsilon_2^{m_l}} = \chi_{nlm_l+1, -\frac{1}{2}} \qquad \ldots \quad (29.1)$$

where $$l - 1 \geq m_l \geq -l$$

with the above results we can calculate the different lines and their intensities in the Paschen-Back limit. It is easily seen that all the energies given by (28) and (28.1) can be incorporated in the single formula.

$$\epsilon = a(m_l + 2m_s) + b m_l m_s \qquad \ldots \quad (30)$$

where $$m_s = \pm\tfrac{1}{2} \text{ and } l \geq m_l \geq -l$$

and the corresponding wave functions are given by $\chi_{nlm_l m_s}$. Equation (30) gives the most commonly used form for the energy in the Paschen-Back limit. It is easily seen on comparing the energies in the weak (vide (25) and (25.1)) and strong (vide (28) and (28.1)) magnetic fields that in both the cases $\epsilon_1^{m_l} > \epsilon_2^{n}$. Evidently this is also true for any intermediate field strength (vide (15.1)). This explains the well known empirical rule that no two levels in the Zeeman and Paschen-Back limits with the same value of m cross each other. If we neglect b compared to a in (30), then for allowed transitions we have,

$$\Delta\epsilon = a\Delta m_l$$

where $$\Delta m_l = 0, \pm 1;$$

This gives three lines exactly as in Lorentz triplet. Calculations of the intensities for this case also give the same value for the three lines as is to be found in the so called normal triplet, namely, the outer component has half the intensity of the middle one.

Calculation of the intensities of the ten components of sodium D-lines in any field strength.—

The sodium D_1 line results from the transition $3^2P_{\frac{1}{2}} \rightarrow 3^2S_{\frac{1}{2}}$, which breaks up into six components in a magnetic field. The D_2-line results from the transition $3^2P_{\frac{3}{2}} \rightarrow 3^2S_{\frac{1}{2}}$, which breaks up into four components in a magnetic field.

Energies and wave functions for the initial states $3^2P_{\frac{1}{2}}$ and $3^2P_{\frac{3}{2}}$.—

$^2P_{\frac{3}{2}}$ level breaks up into four different levels in a magnetic field H. They are obtained by writing $m_l = 1, 0, -1$ and -2 respectively in (17). Thus,

$$\epsilon_1^1 = 2a + \frac{b}{2}; \quad \epsilon_1^0 = \frac{a}{2} - \frac{b}{4} + \frac{\Delta}{2}; \quad \epsilon_1^{-1} = -\frac{a}{2} - \frac{b}{4} + \frac{\Delta'}{2}; \quad \epsilon_1^{-2} = -2a + \frac{b}{2} \qquad \ldots (31)$$

where

$$\left.\begin{aligned} \Delta &= \tfrac{1}{2}\sqrt{9b^2 + 4a^2 + 4ab} \\ \Delta' &= \tfrac{1}{2}\sqrt{9b^2 + 4a^2 - 4ab} \end{aligned}\right\} \qquad \ldots (31.1)$$

The four associated wave functions are given by, (vide (20) and (19.1))

$$\left.\begin{aligned} \chi_{31\epsilon_1^1} &= \chi_{311\frac{1}{2}} \\ \chi_{31\epsilon_1^0} &= A_{0\frac{1}{2}}\chi_{310\frac{1}{2}} + A_{1,-\frac{1}{2}}\chi_{311,-\frac{1}{2}} \\ \chi_{31\epsilon_1^{-1}} &= A_{-1\frac{1}{2}}\chi_{31,-1\frac{1}{2}} + A_{0,-\frac{1}{2}}\chi_{310,-\frac{1}{2}} \\ \chi_{31\epsilon_1^{-2}} &= \chi_{31,-1,-\frac{1}{2}} \end{aligned}\right\} \qquad \ldots (32)$$

where,

$$\left.\begin{aligned} A_{0\frac{1}{2}} &= \sqrt{\frac{1}{2}\left(1 + \frac{a+\frac{b}{2}}{\Delta}\right)}; \quad A_{-1,\frac{1}{2}} = \sqrt{\frac{1}{2}\left(1 + \frac{a-\frac{b}{2}}{\Delta'}\right)} \\ A_{1,-\frac{1}{2}} &= \sqrt{\frac{1}{2}\left(1 - \frac{a+\frac{b}{2}}{\Delta}\right)}; \quad A_{0,-\frac{1}{2}} = \sqrt{\frac{1}{2}\left(1 - \frac{a-\frac{b}{2}}{\Delta'}\right)} \end{aligned}\right\} \qquad \ldots (32.1)$$

$^2P_{\frac{1}{2}}$ level breaks up into two levels in a magnetic field. They are obtained by writing $m_l = 0, -1$ in (17.1). Thus,

$$\epsilon_2^0 = \frac{a}{2} - \frac{b}{4} - \frac{\Delta}{2}; \quad \epsilon_2^{-1} = -\frac{a}{2} - \frac{b}{4} - \frac{\Delta'}{2} \qquad \ldots (33)$$

Δ and Δ' being given by (31.1). The associated wave functions obtained from (22) and (21.1) are,

$$\left.\begin{aligned} \chi_{31\epsilon_2^0} &= A_{0\frac{1}{2}}\chi_{310\frac{1}{2}} - A_{1,-\frac{1}{2}}\chi_{311,-\frac{1}{2}} \\ \chi_{31\epsilon_{2m}^{-1}} &= A_{-1\frac{1}{2}}\chi_{31,-1\frac{1}{2}} - A_{0,-\frac{1}{2}}\chi_{310,-\frac{1}{2}} \end{aligned}\right\} \qquad \ldots (34)$$

where,

$$\left.\begin{aligned} A_{0\frac{1}{2}} &= \sqrt{\frac{1}{2}\left(1 - \frac{a+\frac{b}{2}}{\Delta}\right)}; \quad A_{-1,\frac{1}{2}} = \sqrt{\frac{1}{2}\left(1 - \frac{a-\frac{b}{2}}{\Delta'}\right)} \\ A_{1,-\frac{1}{2}} &= \sqrt{\frac{1}{2}\left(1 + \frac{a+\frac{b}{2}}{\Delta}\right)}; \quad A_{0,-\frac{1}{2}} = \sqrt{\frac{1}{2}\left(1 + \frac{a-\frac{b}{2}}{\Delta'}\right)} \end{aligned}\right\} \qquad \ldots (34.1)$$

Energies and wave functions for the final state $3^2S_{\frac{1}{2}}$.—

Here energies are obtained as before from (17). They are,

$$\epsilon_1^0 = a + b'\,;\quad \epsilon_1^{-1} = -a + b' \qquad \ldots\ (35)$$

b' is the value of bl for $l=0$ (vide (12.2)). The associated wave functions are given by (vide (20)).

$$\left.\begin{aligned} \chi_{30\epsilon_1^0} &= \chi_{300\frac{1}{2}} \\ \chi_{30\epsilon_1^{-1}} &= \chi_{300,-\frac{1}{2}} \end{aligned}\right\} \qquad \ldots\ (36)$$

we shall now calculate the intensities of the six lines resulting from the transition $3^2P_{\frac{3}{2}} \rightarrow 3^2S_{\frac{1}{2}}$. We have here

four initial levels ——→ $\epsilon_1^1 \quad \epsilon_1^0 \quad \epsilon_1^{-1} \quad \epsilon_1^{-2}$

two final levels ——→ $\epsilon_1^0 \quad \epsilon_1^{-1}$

Since for allowed transitions we must have $\Delta m_l = 0, \pm 1$ we get altogether six lines as shown by the arrows. The transitions $\epsilon_1^0 \rightarrow \epsilon_1^0$ and $\epsilon_1^{-1} \rightarrow \epsilon_1^{-1}$ give the π-components. Other transitions give rise to the σ-components. The respective moments and hence the intensities can be easily calculated from the wave functions already given. Thus we get for the two π-components,

$$\left.\begin{aligned} &(1)\quad \epsilon_1^0 \rightarrow \epsilon_1^0 \qquad M_z^2 = \frac{R^2(31;30)}{6}\left(1 + \frac{a+\frac{b}{2}}{\Delta}\right) \\ &(2)\quad \epsilon_1^{-1} \rightarrow \epsilon_1^{-1} \qquad M_z^2 = \frac{R^2(31;30)}{6}\left(1 - \frac{a-\frac{b}{2}}{\Delta'}\right) \end{aligned}\right\}$$

and for the four σ-components,

$$\left.\begin{aligned} &(3)\quad \epsilon_1^1 \rightarrow \epsilon_1^0 \qquad M_x^2 = M_y^2 = \frac{R^2(31;30)}{6} \\ &(4)\quad \epsilon_1^0 \rightarrow \epsilon_1^{-1} \qquad M_x^2 = M_y^2 = \frac{R^2(31;30)}{12}\left(1 - \frac{a+\frac{b}{2}}{\Delta}\right) \\ &(5)\quad \epsilon_1^{-1} \rightarrow \epsilon_1^0 \qquad M_x^2 = M_y^2 = \frac{R^2(31;30)}{12}\left(1 + \frac{a-\frac{b}{2}}{\Delta'}\right) \\ &(6)\quad \epsilon_1^{-2} \rightarrow \epsilon_1^{-1} \qquad M_x^2 = M_y^2 = \frac{R^2(31;30)}{6} \end{aligned}\right\} \qquad (37)$$

The intensities of four lines resulting from the transition $3^2P_{\frac{1}{2}} \rightarrow 3^2S_{\frac{1}{2}}$ can be similarly calculated.

Here we have,

two initial levels ——→ $\epsilon_2^0 \quad \epsilon_2^{-1}$

two final levels ——→ $\epsilon_1^0 \quad \epsilon_1^{-1}$

The resulting transitions are shown by arrows. We get for the two π-components,

$$\left.\begin{aligned}
&(1)\quad \epsilon_2^0 \rightarrow \epsilon_1^0 \qquad M_z^2 = \frac{R^2(31;30)}{6}\left(1 - \frac{a+\frac{b}{2}}{\Delta}\right)\\
&(2)\quad \epsilon_2^{-1} \rightarrow \epsilon_1^{-1} \qquad M_z^2 = \frac{R^2(31;30)}{6}\left(1 + \frac{a-\frac{b}{2}}{\Delta'}\right)
\end{aligned}\right\} \qquad \ldots \quad (38)$$

and for the two σ-components,

$$\left.\begin{aligned}
&(3)\quad \epsilon_2^0 \rightarrow \epsilon_1^{-1} \qquad M_x^2 = M_y^2 = \frac{R^2(31;30)}{12}\left(1 + \frac{a+\frac{b}{2}}{\Delta}\right)\\
&(4)\quad \epsilon_2^{-1} \rightarrow \epsilon_1^0 \qquad M_x^2 = M_y^2 = \frac{R^2(31;30)}{12}\left(1 - \frac{a-\frac{b}{2}}{\Delta'}\right)
\end{aligned}\right\}$$

Since for transverse observation the intensities are proportional to M_z^2 and M_x^2, equations (37) and (38) give the relative intensities of the ten components of sodium D-lines in any field strength. As already pointed out these equations have also been derived by Heisenberg and Jordon (1926) from matrix mechanics.

In conclusion we may note that the whole theory given above is based on the introduction of half-harmonic for representing the spin motion of the electron. There are, however, two difficulties in taking half-harmonic in the spin function. Firstly, it makes the wave function double valued and secondly there is no apparent reason why the electron should have the spin quantum number s always equal to $\frac{1}{2}$ and not other half integral values *viz.*, $\frac{3}{2}$, $\frac{5}{2}$ etc. The first question has already been discussed in the previous paper (Kar-Sengupta *loc. cit.*). The second objection may be removed if we remember the condition of boundedness of the wave functions. It is well known that for physically valid solutions the probability density

$$\rho = X'_{m_s}{}^2 d\tau = (P_s^{m_s})^2 \sin^2\theta' d\theta' d\phi'$$

should be both single valued and bounded *i.e.*, it must have finite values throughout the q-space. The values of the half-harmonic Legendre functions can be obtained by solving the well known wave equation for the rotator by the usual power series method. The two functions with $S = \frac{1}{2}$, are

$$P_1^{\frac{1}{2}} = \sin^{\frac{1}{2}}\theta' \quad \text{and} \quad P_{\frac{1}{2}}^{-\frac{1}{2}} = \frac{\cos\theta'}{\sin^{\frac{1}{2}}\theta'}$$

It is easily seen that though the second half-harmonic Legendre function is not bounded, the probability density for both the functions are bounded. Thus the above half-harmonic functions with $s = \frac{1}{2}$ give physically valid solutions. However, if we write out the four half-harmonic functions with $s = \frac{3}{2}$ and $m_s = \pm\frac{1}{2}, \pm\frac{3}{2}$, then it will be evident that the first three satisfy the condition of boundedness of the density function, but the fourth function

with $m_s = -\frac{3}{2}$ does not. Thus with $S = \frac{3}{2}$, the allowed half-harmonic values of m_s are $\pm\frac{1}{2}, +\frac{3}{2}$, while the value $-\frac{3}{2}$ is forbidden. But this non-symmetry in the values of m_s appears to be physically untenable, for there is no fundamental difference between the positive and negative values of m_s. This argument also applies to other higher half-harmonic functions. Thus we may conclude that half-harmonic values of S higher than $\frac{1}{2}$ are really forbidden. They do not give a set of physically valid solutions.

ACKNOWLEDGMENTS

I am grateful to Prof. K. C. Kar, D.Sc., of Presidency College, Calcutta for suggestion of the problem and helpful criticisms throughout the progress of the work.

Finally, I must thank the Government of West Bengal for awarding a research scholarship and giving me other facilities.

PHYSICAL LABORATORY,
PRESIDENCY COLLEGE, CALCUTTA.

REFERENCES

Bose, S. N. and Bose, K., 1944, *Ind. Jour. Phys.*, **17**, 301.

Condon, E. U. and Shortley, G. H., 1935, Theory of Atomic spectra (Camb.).

Darwin, C. G., 1928, *Proc. Roy. Soc.* A, **118**, 664.

Heisenberg, W. and Jordon, P., 1926, *Zeit. f. Phys.*, **37**, 263.

Kar, K. C. and Sengupta, S., 1949, *Ind. Jour. Phys.*, **23**, 19.

Ornstein, L. S. and Burger, H. C., 1924, *Zeit. f. Phys.*, **29**, 241.

Thomas, L. H., 1926, *Nature*, **117**, 514.

EMISSION SPECTRA OF THE DIATOMIC HALIDES OF MANGANESE. PART I—MnCl

By P. TIRUVENGANNA RAO

(*Received for publication, Dec. 3, 1938*)

Plate XII

ABSTRACT. Violet-degraded and double-headed bands attributed to the diatomic molecule MnCl between $\lambda 3500-\lambda 3900$ have been photographed in emission in a heavy current discharge from a D. C. generator. They consist of seven well-separated groups. A vibrational analysis is suggested on the basis that the system is due to the transition $^1\pi-{}^1\Sigma$ and the following formula is derived,

$$\nu = 26887.1 + [413.3u' - 1.2u'^2] - [385.6u'' - 0.8u''^2]$$

The chlorine isotopic components are detected in the (1, 0) sequence.

The possibility of an electronic transition involving higher multiplicity terms is indicated.

INTRODUCTION

Band spectra of diatomic molecules of the heavier elements, nickel, iron, cobalt, manganese, and chromium (other than the oxides) have been the subject of a number of investigations in recent years. The hydrides of these elements were reported by Pearse and Gaydon (1938) to give characteristic emission bands, when excited under special conditions, such as a high tension arc in a flame of burning hydrogen or in a specially designed discharge tube using a 5000 volt, 7½ KVA transformer. Heimer (1936) obtained bands of the hydrides of cobalt, iron and manganese and reported their rotational structure. The study of the halides of these elements was also attempted. Mesnage (1937) recorded characteristic bands of molecules in emission in a high frequency discharge with external electrodes. A brief analysis of some of them appears to have been proposed by him as quoted in the "Identification of Molecular Spectra" by Pearse and Gaydon. But no details of such analysis on any molecule as done by him are available in the literature. More (1938) reported four systems of NiCl and three of CoCl and suggested their vibrational analysis.

For MnCl, band heads were measured in two regions; (1) visible from $\lambda 5043-\lambda 4331$ consisting of 12 strong heads, some degraded to red, some to violet and others being headless; (2) ultra-violet, from $\lambda 3770-\lambda 3658$ comprising of violet degraded and marked sequences of close double headed

bands. The wavelengths of five of the outstanding heads and their vibrational assignment were quoted by Pearse and Gaydon. Muller (1943) investigated the MnCl spectrum in absorption of the vapour at high temperatures and interpreted an ultra-violet system between $\lambda 3500-\lambda 4000$ as due to the transition ${}^7\pi-{}^7\pi$, the (0, 0) bands of which are arranged in quadratic multiplet schemes.

Work on the other halides was due to Mesnage (1937), Muller (1943) and Rochester and Olsson (1939). The general observational data on these molecules are still meagre and it is believed that further investigation is needed in view of the importance of the knowledge of the constants for these molecules for a clearer understanding of the general problem of binding forces in diatomic molecules.

In this paper,* the constants will be reported for the MnCl molecule as obtained from an investigation of the ultra-violet system in the region $\lambda 3700$.

EXPERIMENTAL

The usual transformer and a low power (5 to 10 watts.) high frequency discharge through the vapour, which have been used by us, generally have proved unsuccessful for the excitation of the emission bands of halides of such refractory metals as manganese. Mesnage, who reported the appearance of the bands in high frequency discharges should have used a high power oscillator of the order of 250-500 watts. The type of arc and discharge tube described by Pearse and Gaydon for NiH and MnH bands suggested to us the possibility of exciting the bands by a high tension, direct current generator, intended for use in connection with hollow cathode sources. Preliminary attempts showed that the necessary conditions for producing the halide bands like the hydride bands, should be really positive column conditions in which a high partial pressure of the halide vapour or the metallic vapour mixed with halogen is maintained with a high current density.

The generator employed is (made by Siemens-Schuckert, Germany) capable of delivering a current of one ampere at 2000 volts. It is separately excited and run by a three-phase induction motor. The generated voltage can be regulated over a range 600 to 2000 volts by a series resistance in the field circuit. With this type of generator, no specially designed discharge tube was needed. An ordinary tube of quartz about 10″ long and 0.5″ in diameter, provided with side-tubes for the electrodes and vacuum pump connection, served the purpose well. The electrodes were short cylinders of pure nickel sheet, the distance between them could not be set greater than about one inch; to avoid melting of the sealing wax joint, the arrangement, shown in Fig. 1, was adopted in which these joints were fairly remote from the cylindrical electrodes; water cooling of the discharge tube was

* A brief report was published in 'Current Science'—July, 1948.

TABLE I

Manganese Chloride Bands ($\lambda 3500 - \lambda 3800$)

Wave length	Int.	Wave number	Classification.	Wave length	Int.	Wave number	Classification.
3532.98	1	28296.7	13,10	3687.82	2	27108.6	
35.11	1	28279.6	12,9	89.43	4	27096.8	8,8
37.05	1	28264.1	11,8	90.42	1	27089.5	
38.59	1	28251.8	10,7				
40.69	1	28235.0	9,6	3691.96	2	27078.2	7,7
42.80	1	28218 2	8,5				
44.37	1	28205 7	7,4	94.04	3	27063.0	(P_5)
				95.80	3	27050.0	6,6
81.79	2	27911.1	12,10	96.45	1	27045.3	
83.49	2	27897.8	11,9				
85.32	2	27883.6	10,8	98.48	3	27030.5	5,5
87.76	2	27864.6	9,7				
90.35	2	27844.5	8,6	3700.18	3	27018.1	(P_4)
91.87	2	27832.7		02.22	5	27003.2	4,4
92.90	2	27824.8	7,5				
96.37	2	27797.9	6,4	04.96	3	26983.2	(Q_3)
98.17	2	27784.0	5,3	06.35	4	26973.1	3,3
3600.31	2	27767.5	4,2				(P_3)
02.18	3	27753.1		07.27	1	26964.5	
03 81	2	27740.5	3,1	08.90	4	26954.5	2,2
05.51	3	27727.5					
03.81	1	27718.5	2,0	10.89	4	26940.1	(Q_2)
				12.70	4	26926.9	1,1 (P_2)
28.50	1	27551.8					
29.92	2	27541.2	11,10	15.87	2	26904.0	
				17.02	3	26895.7	0,0 (Q_1)
31.60	2	27528.3					
33.04	2	27517.3	10,9	3736.93	3	26752.4	10,11
				38.09	1	26744.1	
3634.82	3	27503.9		36.93	3	26754.6	9,10
35.70	2	27497.2	9,8				
				40.66	2	26725.7	
38 82	2	27473.6		42.17	1	26714.9	8,9
39.50	2	27468.5	8,7				
				43.09	2	26708.3	
40.59	2	27460.3		44.55	2	26697.9	7,8
41.76	3	27451.5	7,6				
				47.21	2	26678.5	6,7
44.02	2	27454.4					
45.04	3	27426.8	6,5	49.03	2	26666.0	
46.14	1	27418.5		51.57	2	26648.0	5,6
47.28	2	27409.9		3753.68	2	26633.0	
48.10	3	27403.8	5,4	55.43	3	26620.6	4,5
49.11	2	27396.2					
				56.67	1	26611.8	
50.03	3	27389.3		58.11	2	26601.6	3,4
51.19	4	27380.6	4,3				
52.11	2	27373.7		59.79	2	26589.7	
				62.09	2	26573.4	2,3
3654.00	4	27359.5					
55.24	3	27350.2	3,2	64.13	1	26559.0	
56.08	1	27343.9		66.16	1	26544.7	1,2
56.98	3	27337.2		68.83	1	26525.9	
58 00	2	27329.6	2,1	70.79	1	26512.1	0,1
60 11	2	27313.8		3785.29	1	26410.6	
61.35	1	27304.6	1,0	87.61	2	26394.4	10,12

TABLE I (*contd.*)

Wave length	Int.	Wave number	Classification.	Wave length	Int.	Wave number	Classification.
3790.47	3	26374.5	9,11	3845.56	1	25996.7	
				47.32	2	25984.8	8,11
91.97	2	26364.1					
94.26	3	26348.2	8,10				
				50.28	2	25964.8	
96.59	3	26332.0	7,9	51.93	2	25953.7	7,10
98 81	3	26316.6					
3800.82	3	26302.7	6,8	53.50	1	25943.1	
				55.10	2	25932.3	6,9
03.19	3	26286.3					
05.28	3	26271.9	5,7	57.00	2	25919.6	
				60.25	1	25897.7	5,8
08.52	2	26249.5	4,6				
				61.69	1	25888.1	
11.77	2	26227.1	3,5	63.69	1	25874.7	4,7
14.64	2	26207.4		65.25	1	25864 2	3,6
16.57	2	26194.1	2,4				
				70 54	1	25828.9	
18.79	2	26178.9		72.90	1	25813.2	2,5
20.75	2	26165.5	1,3				
				74 09	1	25805.2	
22.45	1	26153.8		75 98	1	25792.6	1,4
25.43	1	26133.5	0,2				
				79.70	1	25767.9	
42.47	1	26017.6	9,13	81.45	1	25756 3	0,3

not found necessary. In the absence of long quartz tube even an alternative arrangement consisting of shorter straight vitreosil tube, just long enough to extend beyond the cylindrical electrodes only, with a pyrex tube connection at either ends sealed on to it, proved sufficient. The generator leads are connected to aluminium electrodes in the side-tubes to the pyrex ends.

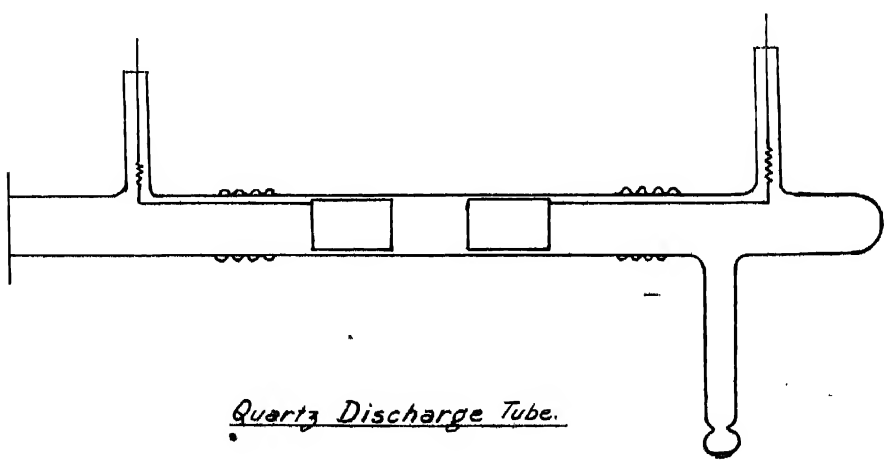

FIG. 1

The substance was spread at the centre between the electrodes and also sprinkled inside the nickel cylinders. When the generator voltage is applied,

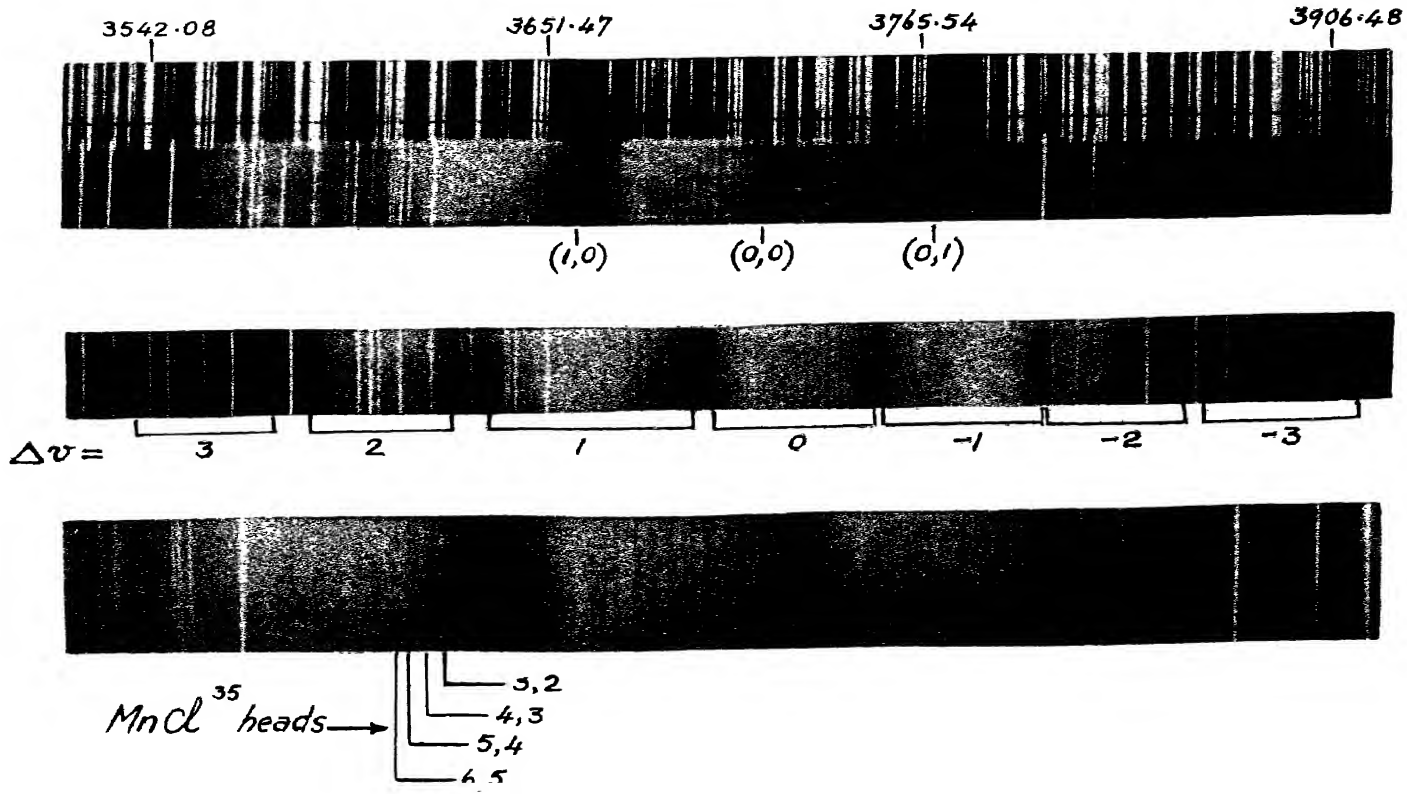

Fig. a.

Fig b

Fig c.

Manganese chloride bands (Quartz Littrow spectrograph).

the condition in the tube is best described as an arc discharge. With an ammeter and voltmeter in the circuit; the voltage is gradually increased from about 600 until the discharge starts. An optimum current condition is found to exist for each substance at which the discharge can be maintained without a break-down. For MnCl, a current of about 0.6 of an ampere at 1500 volts proved satisfactory for the excitation of the bands very strongly. The discharge was intense and the kathode presented a strong glow across its entire section, very much similar to that in a hollow kathode source. The spectrum was photographed with a Hilger quartz Littrow spectrograph (type E 1.) and also in the first order of a 10 ft. cancave grating on Ilford special rapid plates. Short exposures of about 2 to 4 minutes were quite adequate to give good spectra on account of the high intensity of the discharge.

DESCRIPTION OF THE SPECTRUM AND ANALYSIS

The bands are reproduced in Plate XII in three strips; (*a*) for a short exposure, and (*b*) for a long exposure to bring out the higher sequences distinctly. Strip (*c*) is a higher enlargement of the central sequences to indicate the intensity variations in them, and to bring out $MnCl^{35}$ isotopic leads in the (1,0) sequence. The ordinary typical appearance of well-separated close sequences is evident. As observed by Mesnage, the bands are double-headed and degraded to the violet and extend from $\lambda 3800 - \lambda 3500$. Some of them, chiefly of the (0,0) sequence, are line-like. In addition to the band system, the arc lines of manganese are also excited in the source. But the overlapping is so little that the bands could be easily distinguished. Table I gives the wavelength and other data of the entire system.

In attempts to arrive at the vibrational structure of the bands, two considerations were mainly taken into account; (1) the apparent sequence structure of the bands, (2) the nature of the electronic states involved in the emission of the system.

Rochester and Olsson suggested $^1\Sigma - {}^1\Sigma$ as a probable transition for one of the band systems in manganese fluoride. If a similar $^1\Sigma$ may be considered as a possible ground state for the observed MnCl bands the electronic transition of the system may be $^1\pi - {}^1\Sigma$. The doublet characteristic of the bands may be assumed to arise from the expected P, Q components. A vibrational scheme can be developed on this basis and the bands arranged in a quadratic array; the seven groups being regarded as seven sequences, with the strongest of them at $\nu = 26895.7$ as the (0,0) band of the $\Delta v = 0$ sequence; 10 to 14 members are assigned in each sequence. From such an interpretation the usual formula calculated from the wave numbers of the less refrangible components of the doublets is

$$\nu = 26887.1 + [413.3u' - 1.2u'^2] - [385.6u'' - 0.8u''^2]$$

with $\omega' > \omega''$, consistent with the violet degradation of the bands. This classification is shown in column 4 of Table I. Support for this vibrational

scheme is obtained by the detection of the chlorine isotopes for four members of the (1,0) sequence as shown in Table II below :

TABLE II

Band	Calc. isotropic shift	Obs. isotropic shift
(3,2)	7·7	6.3
(4,3)	8.0	6.9
(5,4)	8.2	7.6
(6,5)	8.4	8.3

Further support is obtained from a comparison of the ground state frequency of MnCl with the corresponding values of the chlorides of the elements in the first transition group of the periodic table, as far as they are known. These values are shown in Table III.

TABLE III

Ground state frequencies of the chlorides.

			Ti		Mn	Fe	Co	Ni
Cu	Zn	Ga		Ge				
417	391	365	456	403	386		421	418

One main difficulty, however, in the above interpretation of the bands has been the intensity peculiarities in the heads forming the $\Delta v = 0$ sequence. It is seen from the reproduction of the spectrum that the intensity variations are normal in all the sequences but they are certainly abnormal in the (0,0) sequence. This would suggest a more complex structure than that arising from a simple electronic transition $^1\pi - {}^1\Sigma$. The large number of unclassified bands, shown separately in Table IV and occurring in the same regions as the well developed groups, would also lead to a similar view. Muller considered the existence of high multiplicity terms in molecular spectra from the conception that the total spin of a molecule is composed of the spin vectors of the separate atoms. Terms of such high multiplicity as $^7\pi$ were suggested for MnCl and MnBr. Unfortunately, the original paper of Muller was not accessible to the author. It was read only in abstract (Science abstracts, 1948). A $^7\pi - {}^7\pi$ transition giving 19 band systems was reported.

But it would seem that the bands do not appear to be as complicated as they would have been if both the upper and lower states involved π terms

TABLE IV

Unclassified Bands.

Wave-length	Int.	Wave-number	Wave-length	Int.	Wave number
3557.92	1	28098.3	35.72	1	26761.0
59.97	1	28082.1	45.79	1	26689.1
61.99	1	28066.2	63.34	1	26564.6
64.02	1	28050.2	77.05	1	26468.2
67.59	1	28122.2	79.00	1	26453.9
89.46	2	27851.4	81.21	0	26439.1
3620.83	1	27610.1	86.27	1	26403.7
22 32	1	27598 8	88.65	2	26387.2
24 52	0	27582.0	3826.99	2	26108.5
25.37	1	27575.6	30.42	2	26099.4
27.22	1	27561 5	32.09	1	26088.1
37.68	1	27482.4	36.81	1	26056.0
43.35	1	27439.5	38.49	1	26044.6
53.17	1	27365.7	68.69	1	25841.2
69.08	1	27247.1	71.73	1	25821.0
70 55	1	27236 2	77.60	1	25781.3
72.37	1	27223 7	82.79	1	25747.4
74.25	2	27208.7	84.33	1	25737.2
76 01	1	27195.7	86.09	1	25725.2
77.87	1	27181.9			
79.74	2	27168.1	87.91	1	25713.5
81,63	3	27154.2	89.95	1	25700.0
83.60	1	27139 1	91.64	1	25688.9
85.62	2	27124.8	93.12	1	25679.1
3703.53	1	26993.6	94.68	1	25668.1
30.53	1	26999.7	95.99	1	25660.2
32 51	1	26784.0	98.43	1	25644.1
34.50	1	26769.8	3900.18	1	25632.6

of multiplicity seven; further in MnF, Rochester and Olsson's systems indicate Σ as a probable lower state. The observed complexity may perhaps be due to a high multiplicity π term for the upper state, the lower state being a $^7\Sigma$. If this view is correct, an alternative classification would be to regard the successive doublets in any particular sequence as P, Q components of the structure arising from an upper $^7\pi$ term. The fainter unclassified heads may form the heads of the other component systems. Such a possible assignment is indicated in brackets for some of the heads in the $\Delta v = 0$ sequence. A detailed study of the bands on this basis is being made along with that of the structure of similar bands which the author succeeded in obtaining in the case of MnBr add MnF. A discussion of these will be presented in a succeeding communication.

While a detailed study of the bands on the basis of a $^7\pi - {}^7\Sigma$ transition was in progress Bacher published in *Hel. Phy. Acta.* a comprehensive and interesting paper on the same system of MnCl and other analogous systems in the remaining halides of manganese attributing them to the transition $^7\pi - {}^7\Sigma$. The author has since confirmed Bacher's analysis by extending

it to higher sequences in MnCl and MnBr systems. A brief report of this work has already appeared in *Curr. Sci.* (1949) while a detailed paper is in the course of publication in the Indian Journal of Physics.

ACKNOWLEDGMENT

The author is indebted to Prof. E. Miescher for sending the reprints of all the related papers.

The author expresses his thanks and gratitude to Prof. K. R. Rao for his interest and guidance.

ANDHRA UNIVERSITY
WALTAIR

REFERENCES

Heimer, 1936, *Nature*, **24**, 521.
Mesnage, 1937, *Compt. Rend.*, **204**, 761.
More, 1938, *Phy. Rev.*, **54**, 122.
Muller, 1943, *Hel. Phy. Acta.*, **16**, 1.
Pearse and Gaydon, 1938, *Phy. Soc. Proc.*, **50**, 201.
Rochester and Olsson, 1939, *Zeit. f. Physik.*, **114**, 495.

THE PRINCIPAL MAGNETIC SUSCEPTIBILITIES OF SINGLE CRYSTALS OF RARE EARTH SALTS AT LOW TEMPERATURES. PART II. PRASEODYMIUM SALTS

By A. MOOKHERJI

(*Received for publication, June 27, 1949*)

ABSTRACT. The principal susceptibilities of praseodymium salts have been measured from room temperature down to liquid air temperature. The results are discussed in terms of the crystalline electric field theory. It is found that (1) on the basis of a single suitable cubic field the observed magnetic moment at all temperatures in the range studied can be explained satisfactorily. (2) The observed large anisotropies of the crystals point to the existence of strongly asymmetric rhombic field. (3) a rough estimate of the rhombic part of the field shows that the splitting by it is by no means small and compares favourably with the cubic splitting. (4) The χ_1-axis of praseodymium sulphate rotates by about 63 degrees in the range studied.

INTRODUCTION

Following Van Vleck (1932), Penney and Schlapp (1932) if one attributes all the observed deviations in the magnetic properties of the rare earth ion, Pr^{+++} from the ideal free ion behaviour, to the splitting of the energy levels of the Pr^{+++} ion, under the influence of strong and generally asymmetric crystalline fields, one should expect the mean of the three principal susceptibilities to be determined almost wholly by the cubic part of the field. The rhombic part will have very little effect on the mean of the three susceptibilities though the individual susceptibilities will be affected considerably. This conclusion has been verified satisfactorily in the case of cerium salts (Mookherji, 1949).

Though in most of the crystals the crystalline fields are predominantly cubic in symmetry, the small deviations from the cubic part of the field produce nearly as great an effect on the susceptibilities as cubic parts. On the other hand if we consider the mean of the three principal susceptibilities of the crystal, which is the one measured with crystal powder, the effect of the non-cubic part is not so conspicuous, owing to averaging out of the effect along the three principal axes, which are not all of the same sign (Mookherji 1946; Bose, 1948). The measurements on powder will reveal only the effects of the cubic part of the field whereas measurement with single crystal can reveal the effects of both the cubic and the non-cubic part. That is why measurements on the principal susceptibilities of single crystals

are much more informative than the usual measurements, namely, on the crystal powder.

It is true that the axes of the crystal fields associated with the different paramagnetic ions in crystals will not in general be parallel to one another and even in an anisotropic crystal there is a partial averaging out of the contributions of the non-cubic parts of the crystalline electric field associated with different paramagnetic ions. But even so, such anisotropy as is left over can supply much information regarding the asymmetric part of the crystalline field and the influence on the magnetic properties (Krishnan and Mookherji, 1936).

In this communication the results of magnetic measurements on single crystals of salts of Pr^{+++} ions from room temperature down to liquid air temperature are discussed from the point of view of the splitting of the energy levels by the cubic as well as the non-cubic part of the field and ultimately of the magnetic behaviour of the ion.

EXPERIMENTAL

The experimental methods used in these measurements were the same as described in our previous paper (Mookherji, 1949) on cerium salts.

Specimens of praesodymium salts in these investigations were of high purity and were made available through the kindness of Professor Trombe' of Paris University to whom we take this opportunity to express our thanks.

RESULTS

The results of measurements are collected in Tables I to IV. The same notations and diamagnetic corrections as adopted in the previous paper (Mookherji, 1949) are used in the present communication. Figs. 1 to 5 show the nature of variation of magnetic anisotropy and square of principle moments with temperature.

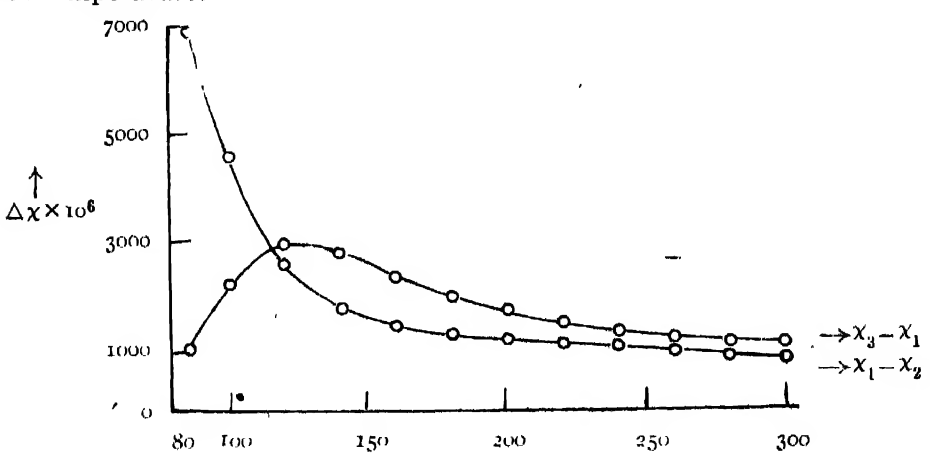

Fig. 1

$Pr_2(SO_4)_3.8H_2O$

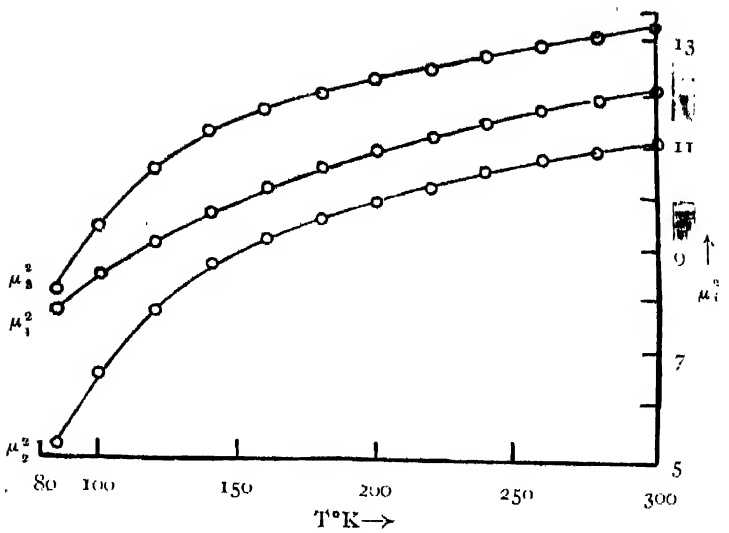

Fig. 2

$Pr_2(SO_4)_3.8H_2O$

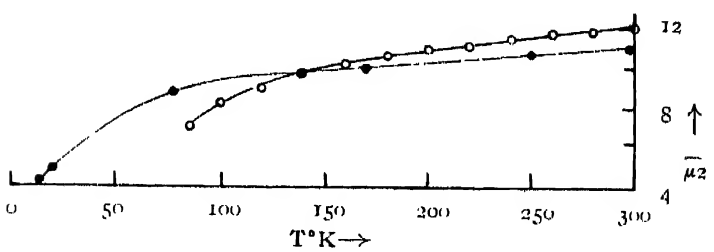

Fig. 3

$Pr_2(SO_4)_3.8H_2O$

Gorter—O

Present author— . .

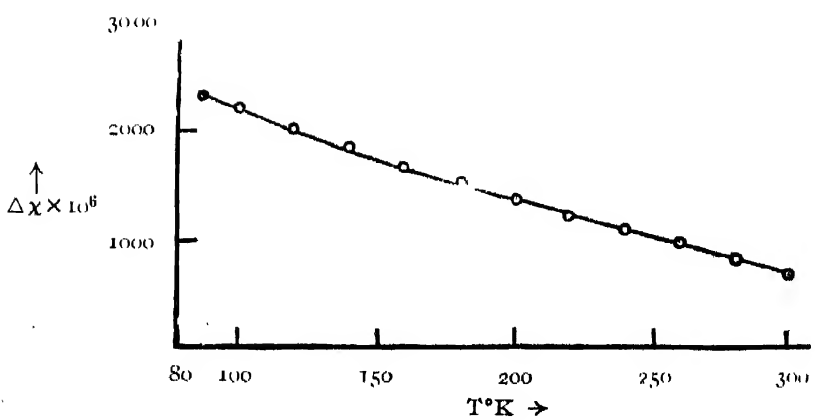

Fig. 4

$Pr_2Mg_3(NO_3)_{12}.24H_2O$

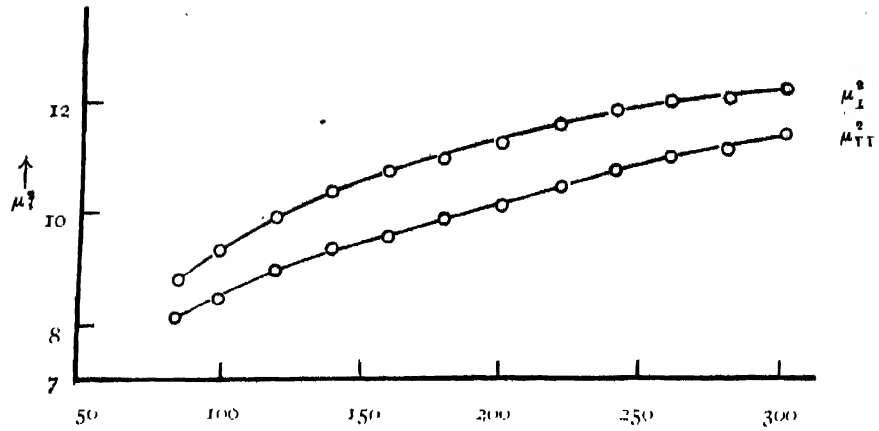

Fig. 5

$Pr_2Mg_3(NO_3)_{12}.\ 24H_2O$

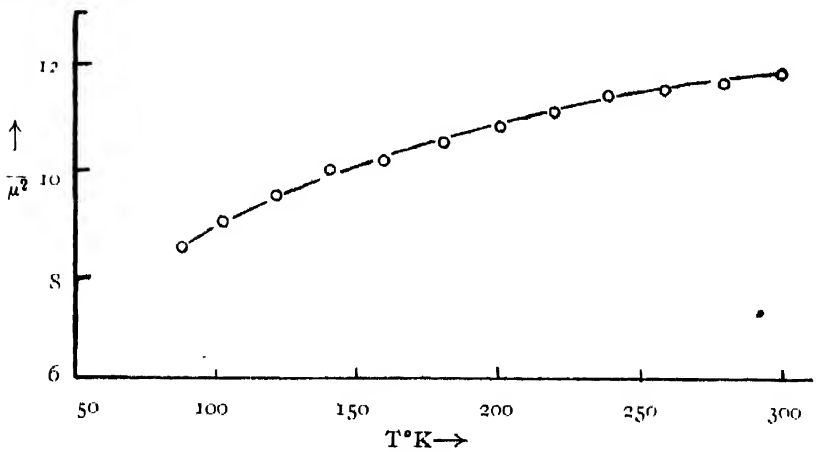

Fig. 5a

$Pr_2Mg_3(NO_3)_{12}.\ 24H_2O$

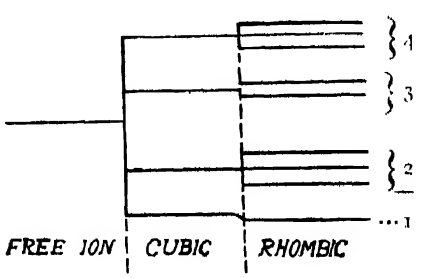

Fig. 6

THE MEAN MAGNETIC MOMENT AND THE CUBIC PART OF THE FIELD

The ground state of the Pr^{+++} ion is $^3H_4$. The next higher level namely the $^3H_5$ is removed by about 2100 cm^{-1} and hence at all ordinary temperatures

the influence of the latter level on the magnetic behaviour of the ion will be negligible. The splitting of the ground level of Pr^{+++} ion under electric fields is given in Fig. 6 above.

TABLE I

Magnetic anisotropy at 30°C.

Crystal	Crystallographic data	Mode of suspension.	Orientation in the field.	$\Delta\chi$	Magnetic Anisotropy
$Pr_2(SO_4)_3.8H_2O$	Monoclinic prism $a:b:c$ 2.986:1:1.99 $\beta=118°$	'b' axis vertical 'a' axis vertical (001) plane horizontal	$\theta=+2°.1$ 'b' axis along field 'b' axis along field	795 1006 1800	$\chi_1-\chi_2=795$ $\chi_3-\chi_1=1005$ $\psi=+25°.9$ Cal. $\psi=+26°.0$
$Pr_2Mg_3(NO_3)_{12}.24H_2O$	Trigonal	Trigonal axis horizontal	Trig. axis normal to field.	636	$\chi_\perp-\chi_\parallel=636$

TABLE II

Absolute susceptibility along a convenient direction

Crystal	Direction along which susceptibility was measured.	Temp. °C	Density of the crystal	Volume susceptibility.	Corresponding gm. mol. susceptibility.	Corresponding gm. mol. susceptibility at 30°C.
$Pr_2(SO_4)_3.8H_2O$	Along χ_1-axis	28.5	2.837	38.47	9,680	9,640
$Pr_2Mg_3(NO_3)_{12}.24H_2O$	Normal to Trigonal axis	30.5	2.182	13.49	9,430	9,450

We have already mentioned that the mean of the three principal susceptibilities is determined to a close approximation by the cubic part of the field alone. Taking the cubic part of the field b to be of the fourth order, the energy levels will be given by (Penney and Schlapp. 1932) the following equation (1)

$$\begin{aligned} W_1 &= 672a \\ W_2 = W_3 = W_4 &= 336a \\ W_5 = W_6 &= 96a \\ W_7 = W_8 = W_9 &= -624a \end{aligned} \qquad (1)$$

and the corresponding energy separations are $0, -336a, -576a$ and $-1296a$, where 'a' is a constant determined by the magnitude of the cubic field, the

TABLE III

Temperature variation of Magnetic Anisotropy

Crystal	Temp. °K	Suspension used for measurement		$\chi_3-\chi_1$	θ
		'b' axis vertical	'a' axis vertical		
		$\chi_1-\chi_2$	$\chi_3-\chi_1\cos^2\theta-\chi_2\sin^2\theta$		
$Pr_2(SO_4)_3.8H_2O$	300	800	1010	1010	+2.1
	280	868	1070	1070	2.1
	260	937	1170	1170	2.5
	240	1010	1320	1310	4.0
	220	1100	1500	1480	6.7
	200	1200	1780	1720	12.5
	180	1320	2120	1970	19.5
	160	1480	2670	2340	28.0
	140	1740	3460	2770	32.0
	120	2620	4590	2960	52.0
	100	4590	5710	2250	60.2
	85	6880	6750	1060	62.5
		Trigonal axis horizontal			
		$\chi_\perp-\chi_\parallel$			
$Pr_2Mg_3(NO_3)_{12}$ $_{24}H_2O$	300	660			
	280	802			
	260	949			
	240	1080			
	220	1220			
	200	1380			
	180	1520			
	160	1690			
	140	1860			
	120	2020			
	100	2210			
	85	2340			

TABLE IV

Temperature variation of principal susceptibilities

Crystal and direction along which measurement was taken	Temp. °K	χ'_1	χ'_2	χ'_3	$\bar{\chi}'$	μ_1^2	μ_2^2	μ_3^2	$\overline{\mu^2}$
	300	9960	9160	10970	10030	12.05	11.08	13.27	12.13
	280	10500	9630	11570	10570	11.82	10.87	13.06	11.92
	260	11140	10290	12300	11240	11.67	10.70	12.89	11.78
	240	11770	10760	13080	11870	11.39	10.42	12.66	11.49
	220	12470	11370	13960	12500	11.06	10.09	12.38	11.18
$Pr_2(SO_4)_3 8H_2O$	200	13390	12190	15110	13560	10.80	9.830	12.18	10.90
Along χ_1-axis	180	14380	13060	16350	14600	10.43	9.482	11.87	10.59
	160	15530	14050	17870	15800	10.02	9.070	11.53	10.21
	140	16900	15160	19670	17280	9.540	8.560	11.10	9.730
	120	18510	15890	21460	18690	8.960	7.681	10.39	9.010
	100	20360	16000	22870	19830	8.330	6.450	9.23	8.003
	85	22360	15480	22420	20420	7.66	5.137	8.03	7.00
		$\chi'_\perp$	$\chi'_\parallel$	$\bar{\chi}'$	$\mu_\perp^2$	$\mu_\parallel^2$	$\overline{\mu^2}$		
	300	10110	9450	9890	12.23	11.43	11.96		
	280	10610	9810	10340	11.98	11.08	11.68		
	260	11390	10440	11080	11.91	10.04	11.61		
	240	12190	11110	11830	11.80	10.75	11.45		
	220	12970	11750	12570	11.50	10.42	11.14		
$Pr_2Mg_3(NO_3)_{12}$ $_{24}H_2O$	200	13830	12450	13370	11.15	10.04	10.78		
Along $\chi_\perp$ – axis	180	15040	15520	14540	10.91	9.810	10.54		
	160	16550	14860	15990	10.68	9.585	10.32		
	140	18400	16540	17780	10.39	9.337	10.04		
	120	20550	18530	19880	9.920	8.964	9.000		
	100	23090	20880	22350	9.310	8.420	9.010		
	85	25900	23560	33750	8.880	8.076	8.610		

mean of the three principal susceptibilities will then be given by

$$\bar{\chi}=\frac{2Ng^2\beta^2}{a}[(.0092e^{13\nu}+.0333e^{-2\nu}-.0227e^{-7\nu}-.0199e^{-14\nu})$$

$$+(.1302e^{13\nu}+.0052e^{-7\nu})]\div[3e^{13\nu}+2e^{-2\nu}+3e^{-7\nu}+e^{-14\nu}] \qquad (2)$$

Where $\nu=\frac{48a}{kT}$, and hence conversely from the observed mean of the three principal susceptibilities at any given temperature we can calculate the field constant. It is gratifying that over the whole of the temperature range studied by us, the observed magnetic data for the mean susceptibility fit well with the value $a=-.585$ cm^{-1}. The observed values of $\bar{\mu^2}$ and those calculated on the assumption of a cubic field of the fourth order with $a=-.585$ cm^{-1} are given in Table V.

TABLE V

$Pr_2(SO_4)_3.8H_2O$

$a=-.585$ cm^{-1}

Temp. °K	$\bar{\mu^2}$	
	Calculated	Observed
300	11.74	12.1
200	10.86	10.9
100	8.19	8.01
85	7.18	7.0

The corresponding values for the $Pr_2Mg_3(NO_3)_{12}.24H_2O$ are given in Table VI.

TABLE VI

$Pr_2Mg_3(NO_3)_{12}24H_2O$

$a=-.508$ cm^{-1}

Temp. °K	$\bar{\mu^2}$	
	Calculated	Observed
300	11.95	11.96
200	10.85	10.78
100	8.89	9.01
85	8.05	8.62

Thus the magnetic data for the mean susceptibility for both the crystals can be satisfactorily explained on the basis of a suitable cubic field. The magnitudes of the cubic field required for this purpose are reasonable since they will correspond to an overall separation of 756 cm^{-1} in the sulphate and 661 cm^{-1} in the double nitrate. These are of the order of separation in the absorption spectra.

For the octahydrated sulphate data for the mean susceptibility at low temperature are available from the measurements of Görter and de Haas (1931). Their values are given in Table VII, for comparison

TABLE VII

Temp. °K	288	249.3	169.6	137.9	77.53	20.4	14.39
μ^2	11.03	10.83	10.1	9.66	8.72	4.8	4.24

Among the other prasoedymium salts for which magnetic data at low temperatures are available are :—

(1) $Pr_2(C_2H_5SO_4)_6\ 18H_2O$.....Faraday rotation of this crystal has been studied by Becquerel (1936).

(2) The anhydrous sulphate whose meen susceptibility in the powder state has been measured by Görter and de Haas (1931).

In both these salts the temperature variation of $\overline{\mu^2}$ is nearly the same as in the hydrated sulphate, which point to a crystalline field of nearly the same magnitude in all of them. This is to be expected since in all of them the field is presumably due to an octahedron of six negatively charged oxygen atoms, surrounding the Pr^{+++}ion, belonging to the water molecules in one case and to SO^{--4} groups in the other; but their distances from the ion will be nearly the same in both the cases.

We have seen that the cubic part of the field determines to a first approximation the mean square moment $\overline{\mu^2}$, *i.e.*, its deviation from the free ion value of 12.81, of Hund, and that the rhombic part will have very little effect on $\overline{\mu^2}$, though the whole of observed anisotropy is due to it.

In the above discussions we have for simplicity taken the cubic field to be of the fourth degree. This is justifiable at least in the case of Ce^{+++}ion (Mookherji, 1949). In Pr^{+++} ions also the sixth degree terms of the cubic field, of any reasonable magnitude that may be present will not much affect the mean magnetic moment. This can be seen from the following Table VIII taken from a paper by Kynch (1937) which gives the energy levels under a cubic field involving respectively (1) the fourth degree terms only, (2) the fourth and sixth degree terms, the magnitudes of these two groups being chosen on the basis of the known distance of the negatively charged atoms surrounding the ion in the crystal.

TABLE VIII

Only Fourth degree terms	0_1	101.8	174.5	392.7	cm^{-1}
Sixth degree terms also included	0_1	116.7	200	403.3	

It will be seen that the two sets of values are not very different, showing that the effect of the sixth degree terms on the energy levels and hence on the magnetic moment is quite small.

It is observed that χ_1 – axis of $Pr_2(SO_4)_3\ 8H_2O$ rotates through about 63° as the temperature is lowered from 300 to 85 degrees Kelvin.

MAGNETIC ANISOTROPY AND THE RHOMBIC PART OF THE FIELD

Though the rhombic part of the field does not to a first approximation affect the mean susceptibility, it is the rhombic that is responsible for the observed anisotropy of the crystal, and from the known anisotropy it should be possible with suitable simplifying assumptions to estimate the rhombic part. The assumptions referred to are :—

(1) The principal axes of the rhombic field concide with those of the cubic field

(2) The field axes associated with different paramagnetic ions in the unit cell are all oriented parallel to one another.

(3) That the rhombic terms which can be put in the usual form

$$V_r = Ax^2 + By^2 - (A+B)z^2 \qquad (3)$$

have either

(*a*) Some symmetry, corresponding, say to the two constants A and B being equal in which case the expression for V_r reduces to

$$V_r = A(x^2 + y^2 - 2z^2) \qquad (4)$$

Or

(*b*) Extreme asymmetry, corresponding to the coefficient of z^2 being zero, in which case the expression for V_r reduces to

$$V_r = A(x^2 - y^2) \qquad (5)$$

We shall refer to these two alternatives as case (*a*) and case (*b*) respectively.

With these assumptions, as Penney and Kynch (1939) have shown, the separations of the energy levels produced by the rhombic field will be as given in Fig. 7

Case (*a*)—Denoting by numbers 1 to 4, the four split levels split by the cubic part of the field as shown in Fig. 7, the overall splitting produced by

the rhombic part will be $28m$ for level (2) and $8m$ for level (4), where m is

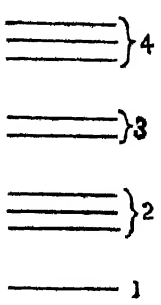

FIG. 7

a constant determined by the rhombic field. The corresponding expressions for the principal susceptibilities at room temperature will be

$$\left.\begin{aligned}\mu_x^2=\mu_y^2&=12.14+.058m\\ \mu_z^2&=12.14-.116m\end{aligned}\right\} \qquad (6)$$

Case (*b*)—Here the overall separations of (2) and (4) will be $28m$ and $8m$ respectively. The susceptibility at room temperature is given by

$$\left.\begin{aligned}\mu_x^2&=12.14+.058m\\ \mu_y^2&=12.14-.058m\\ \mu_z^2&=12.14\end{aligned}\right\} \qquad (7)$$

12.14 represents the mean susceptibility of the crystal at room temperature. It is independent of m and is determined by the cubic field alone.

In actual crystals the simplifying assumptions (1) to (3) will not hold at all. But the order of magnitude of the rhombic part of the field can still be estimated roughly.

From equations (6) and (7) it will be seen that $\Delta\mu^2$ is equal to $0.174\ m$ in case of (*a*) and equal to $0.116m$ in case of (*b*). In both cases the separations are equal to $28m$ and $8m$ respectively for levels (2) and (4). For any rhombic field in general, we may calculate the order of magnitude of the separations by taking $\Delta\mu^2$ to be of the order of $0.15m$, and the separations to be of the order of $10m$. Now in $Pr_2(SO_4)_3 8H_2O$, $\bar{\mu}^2$ is about 12 cm^{-1} and the anisotropy $\frac{\Delta\mu^2}{\bar{\mu}^2}$ is about 0.2 from which we obtain $\Delta\mu^2=2.5$ cm^{-1}. Since $\Delta\mu^2 \sim 0.15m$, this gives $m \sim 0.16$ cm^{-1}, and the separation produced by the rhombic field, which we have taken to be of the order $10m$, should be about 160 cm^{-1}. This is not much smaller than the separations by the cubic part of the field.

ACKNOWLEDGMENT

The work was carried out at the laboratories of the Indian Association for the Cultivation of Science, Calcutta, and the author wishes to express

his thanks to its committee of management for affording all facilities. The author also expresses his thanks to Sir K. S. Krishnan, Kt., D.Sc., F.R.S., F.N.I., for his keen interest and valuable help and advice. Thanks are also due to Dr. A. Bose, D.Sc., for his valuable discussions.

REFERENCES

Bacquerel, J. 1936, *Physics* **3**, 705.

Bose. A, 1948, *Ind. Jour. Phys.*, **22**, 195.

Gorter C. J. and de Haas, W. J, 1931, *Proc. Roy. Acad. Ams.*, **24**, 1249

Jackson L. C., 1939, *Proc. Roy. Soc. A.*, **170**, 266.

Krishnan, K. S. and Mookherji, A. 1936, *Phill. Trans Roy. Soc. A.*, **237**, 135

Kynch J. G., 1937, *Trans. Farad. Soc.*, **33**, 1402

Mookherji A., 1946, *Ind. Jour. Phys.*, **20**, 9.

,, , 1949, *Ind. Jour. Phy,*. **23**, 217.

Penney W. G. and Kynch, 1939, *Proc. Roy. Sco. A.*, **170**, 112.

Penney, W. G. and Schlapp. R, 1932, *Phys, Rev.* **41**, 194.

1932, ,, ,, **42**, 666.

Van Vleck J. H., 1932, The Theory of Electric and Magnetic Susceptibilities, Oxford, Clarendon Press, Chapter XI.

THE EMISSION SPECTRUM OF LEAD IODIDE

By P. TIRUVENGANNA RAO

(*Received for publication, Jan. 3, 1949*)

Plate XIII

ABSTRACT. An extensive system of bands, attributed to the diatomic molecule PbI in the visible region extending from λ6400–λ4350 has been obtained for the first time in a high frequency discharge. The bands are photographed with a Hilger constant deviation and a Fuess glass spectrographs. Some of the bands have sharp heads and are clearly degraded towards the red while some are diffuse and headless. About 130 bands in all could be measured and a vibrational analysis has led to the following quantum formula for the band heads.

$$\nu = 19509.6 + (119.5u' - 0.25u'^2) - (156.6u'' - 0.30u''^2)$$

The intensity distribution in the system is analogous to that in the emission bands of PbCl. By analogy with the corresponding systems of the related halide molecules, the band system has been interpreted as due to the high frequency component of a $^2\Delta - ^2\pi$ electronic transition.

INTRODUCTION

The absorption spectrum of lead chloride was first reported by Baratt (1929) without analysis. The fluorescent spectrum of PbCl has been photographed and partly analysed by Popov and Neujmin (1932) using spectrographs of low dispersion (20-80A per mm.). In the course of a series of investigations on the band spectra of the halides of groups IV and V of the periodic table, Howell and Rochester (1934) reported that high frequency discharges through the vapours of the lead halides, PbF, PbCl and PbBr excited in each case a large system of bands degraded towards the red. Later, Rochester (1936) analysed the spectra of two of the halides of lead PbF and PbCl and showed that Popov and Neujmin's analysis of PbCl was incorrect. He derived the following vibrational formulæ for the two molecules.

$$\text{PbF} \quad \nu = 22566.6 + 397.75(v' + \tfrac{1}{2}) - 1.77(v' + \tfrac{1}{2})^2 - 507.5(v'' + \tfrac{1}{2}) + 2.32(v'' + \tfrac{1}{2})^2$$

$$\text{PbCl} \quad \nu = 21863.1 + 228.8(v' + \tfrac{1}{2}) - 0.795(v' + \tfrac{1}{2})^2 - 303.6(v'' + \tfrac{1}{2}) + 0.875(v'' + \tfrac{1}{2})^2$$

Morgan (1936) independently reported the analysis of PbF and PbCl bands observed by him in absorption. His analysis was found to be entirely in agreement with that of Rochester in each case. In addition, Morgan reported

the analysis of PbBr bands observed in absorption and derived the following quantum formula for the band heads.

$$\nu = 20844.3 + [152.5u' - 0.40u'^2 - 0.028u'^3] - (207.5u'' - 0.50u''^2)$$

The spectrum of the remaining halide molecule of lead, namely PbI, does not appear to have been studied as yet either in absorption or in emission. As part of a series of investigations into the molecular spectra of the iodides of heavy elements thallium, lead and bismuth which lie in the same horizontal row of the periodic table, the results of a study of the spectrum of thallium iodide have already been reported by the author and K. R. Rao (1948). In continuation of this work which is intended to establish and compare the ground state frequencies of these molecules, the spectrum of lead iodide has been excited in emission in a high frequency discharge. Characteristic bands in the region $\lambda 6400 - \lambda 4350$ have been obtained. The object of this paper is to interpret these bands and derive the vibrational constants for this molecule.

The experimental set up for this investigation is the same as that employed by the author in similar investigations and described in detail previously. The spectrum is excited in the electrodeless H. F. discharge and also by a 1/4 kilowatt transformer. For a good development of the system, the excitation from a low power H. F. oscillator is found to be more favourable. Considerable difficulty, however, was experienced by the author in suppressing the emission bands of iodine which unfortunately lie in a large region of overlap with the bands of lead iodide itself. As the discharge tube is being continuously evacuated by a high vacuum pump, the substance was heated strongly till it begins to sublime when the discharge was found to be intense white in colour. Under these conditions, the emission bands of iodine in the visible region were not observed, owing probably due to the predominance of the vapour pressure of lead iodide over that of free iodine formed invariably as a decomposition product. Intermittent heating at intervals of five seconds was found necessary to maintain the characteristic white discharge. After a number of attempts, it was found that the overlapping continuous spectrum could be reduced to a minimum by optimum heating and minimum exposure with a sharply focused spectrograph with a fine slit. The bands due to lead iodide were clearly brought out under these conditions free from any trace of iodine bands.

In taking a photograph of the spectrum, two instruments were chiefly used. (1) Hilger constant deviation spectrograph (2) a Fuess glass instrument with a dispersion of 24 A per mm. at $\lambda 4500$. It was found that a higher dispersion instrument was unsuitable for obtaining a good photograph of the bands as they appear hazy under high dispersion, as in the case of thallium iodide bands. Exposures on the constant deviation spectrograph

varied from 30 to 45 minutes while with the Fuess instrument an exposure of 20 minutes is found to be sufficient using Ilford Special Rapid Panchromatic plates. Measurements of the band heads were made with a comparator and were reduced to wavelengths using iron arc wavelength standards. In addition to the bands of lead iodide, some lead and iodine lines were also recorded on the plates. From a close scrutiny of the plates, these were distinguished from the bands.

DESCRIPTION OF THE SPECTRUM

Photographs of the spectra have been reproduced in Plate XIII in two strips (*a*) and (*b*). Strip (*a*) is an enlargement of the spectrum in the region λ6400—λ4500 taken on a constant deviation spectrograph. The reproduction shows no trace of the emission spectrum of iodine in the visible region. Some of the bands have sharp heads around λ5800 and are clearly degraded towards the red, while some are diffuse and headless. Strip (*b*) is an enlargement of a portion of the spectrum between λ5500—λ4300 taken on a Fuess glass spectrograph. Owing to the poor intensity of the spectrum below λ5000, bands in this region are better brought out on the Fuess instrument owing to its high light gathering power. Some of the bands in this reproduction appear red degraded, though many of them appear diffuse and headless on the violet end. Besides the PbI bands, the two reproductions show a large number of lines. The intensities of the bands are visual estimates on a 0—5 scale.

RESULTS

Table I is a catalogue of the band heads assigned to a single system. The table is self-explanatory.

TABLE I

Lead iodide bands.

Wave-length	Int	Wave number	Classification.	Wave-length	Int.	Wave number	Classification.
6357.3	2	15725.6	2,27	6165 2	3	16215 6	0,22
45.1	2	15755.9	1,26	11.1	5	16359.2	0,21
18.4	1	15822.4	3,27	6096.7	1	16397.8	
04.1	3	15858.3	2,26	71.2	2	16466.7	2,23
6287.0	5	15901.5	1,25	44.6	2	16539.1	
74.3	5	15933.6	0,24	5984.1	3	16706.3	2,20
49.6	2	15996.6		51.3	5	16798.4	0,18
6190.6	3	16149.1	2,24	28.9	2	16861 9	2,19

TABLE I (*contd.*)

Wave-length	Int.	Wave number	Classification.	Wave length	Int.	Wave number	Classification.
5910.9	3	16913.2	1,18	5273 3	3	18958.2	2,5
5873.4	3	17021.2	2,18	64.2	2	18991.0	1,4
51.1	5	17086.1	0,16	58.0	1	19013.4	0,3
35.6	3	17131.5	3,18	50.9	1	19039.1	4,6
02.2	5	17230.1	0,15	39.6	2	19080.1	3,5
5787.9	2	17272.7	3,17	31.2	2	19147.4	1,3
76.9	2	17305.5	2,16	15.0	2	19170.1	0,2
65.5	3	17339.8	1,15	5189.1	3	19265.8	2,3
51.4	5	17382.3	0,14	80.2	3	19298.9	1,2
39 9	2	17417.1	3,16	72 7	1	19326.9	0,1
29.9	2	17447.5	2,15	5147.4	3	19421.9	2,2
13 6	4	17497.3	1,14	30.4	2	19486.2	0,0
03 6	5	17527.9	0,13	5095.5	1	19619.7	
5692.1	3	17563.4	3,15	76.4	2	19693.5	3,1
79.0	3	17603.9	2,14	5065.7	2	19735.1	2,0
5666.8	4	17641 8	1,13	52.7	2	19785.9	5,2
55.2	3	17678.0	0,12	46.0	2	19812.2	4,1
5588.5	2	17888.9	2,12	36.3	3	19850.3	3,0
75 2	2	17931.6	1,11	22.7	1	19904 1	
60.7	4	17978.4	0,10	12.4	2	19945.0	
5472.6	3	18267.8	0,8	4997.1	1	20006 0	7,2
53.6	2	18344.2	2,9	88.6	4	20040.1	6,1
06.0	2	18492.8	2,8	79.1	4	20078.9	5,0
5386.1	3	18561.2	0,6	68.3	2	20122.0	8,2
67.9	2	18624.6		59.8	2	20156.5	7,1
50.7	3	18684.0	1,6	50.2	2	20195.6	6,0
43.1	3	18710.5	0,5	40.5	3	20235.2	9,2
26.4	2	18769.2	3,7	31.5	2	20272.2	8,1
16.3	2	18804.9	2,6	23.2	2	20306.3	7,0
07.2	3	18837.1	1,5	02.2	2	20393.3	9,1
5291.4	2	18893.4	4,7	4875.6	2	20504.6	10.1
83.9	1	18920.2	3,6	65.6	2	20546.7	9,0

Fig. *a*.

Fig. *b*.

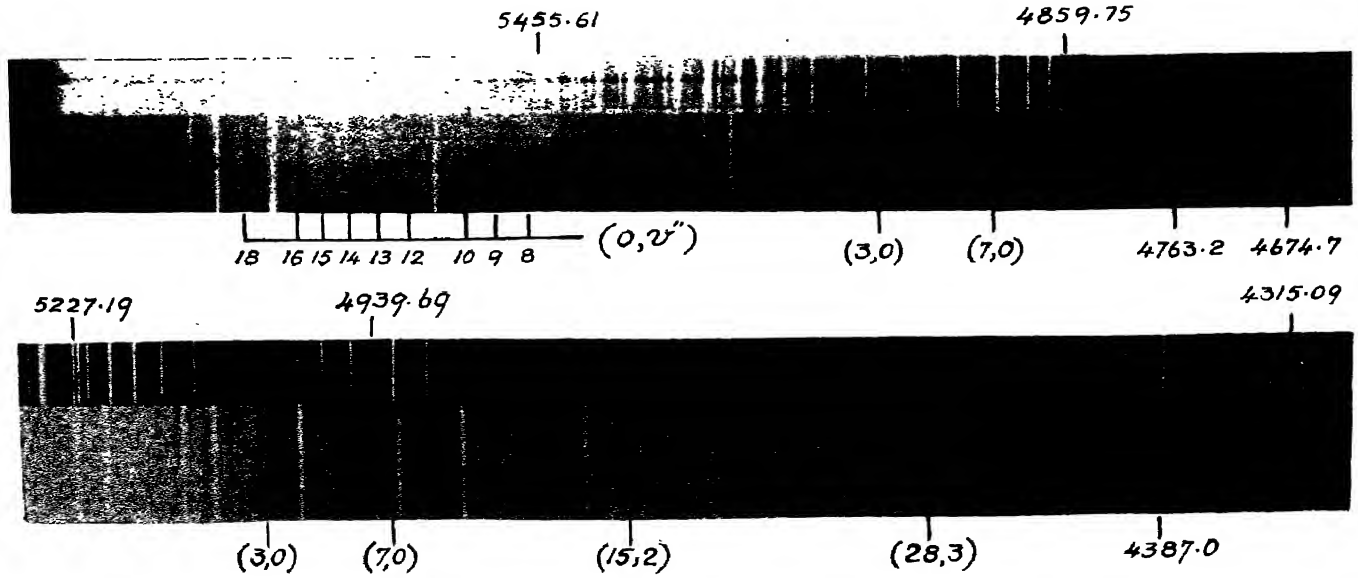

Lead iodide emission bands.

(*a*) Constant deviation.
(*b*) Fues spectrograph.

TABLE I (*contd.*)

Wave-length	Int.	Wave number	Classification.	Wave-length	Int.	Wave number	Classification.
4855.1	0	20591.2	12,2	4576.5	3	21844.7	27,4
41.1	2	20650.7	14,3	67.5	1	21887.7	26,3
30.0	3	20698.2	13,2	63.1	1	21908.8	
19.0	3	20745.4	12,1	56.8	3	21939.1	28,4
14.2	3	20766.1	15,3	48.8	1	21977.7	
10.2	3	20783.4	11,0	41.0	3	22015.4	27,3
05.9	2	20802.0		33.3	2	22052.8	29,4
4789.1	3	20874.9	16,3	24.1	3	22097.7	28,3
4784.1	2	20896.8	12,0	14 1	1	22146.6	
78.1	1	20923.0	15,2	07 6	3	22178.6	27,2
67.4	2	20970.0	14,1	00.9	4	22211.6	29,3
54.1	2	21028.6	16,2	4481.9	1	22305.7	33,5
47 3	1	21058 7		79.9	2	22360.6	32,4
4742.3	4	21080.9	18,3	66.5	1	22382.6	
39.3	1	21194.3		59.8	2	22416.3	31,3
29.7	3	21137.1	17,2	47.5	3	22478.8	30,2
22.8	1	21168.0		41.1	3	22510.7	32,3
07.3	3	21237.7	18,2	4434.7	3	22543.1	
4699.3	2	21237.8	20,3	30.6	2	22564.0	34,4
85.8	2	21335.1	19,2	22.9	1	22603.3	33,3
64.2	3	21433.9	20,2	16.9	2	22634.0	
58.0	1	21462.5		12.2	1	22658.1	32,2
4651.0	2	21494.8	22,3	4407.6	2	22681.7	
37.6	1	21556.9		4399.2	3	22725.0	
11.2	3	21680.3	24,3	95.6	3	22743.7	
04.9	1	21709.9		91.7	3	22763.9	36,4
00.3	4	21731.6	26,4				

Vibrational Analysis and Intensity Distribution.

The clearly, well separated, prominent band heads between λ 6000 – λ 5400 marked on the reproduction (*a*) represent unambiguously a long progression, which served as a starting point in the analysis. The order of $\Delta G(v)$ interval

in this progression is 150 cm^{-1}. At this stage a comparison is made of the ground state frequencies of the halides of the elements in the same horizontal row of the periodic table as shown in Table II below.

TABLE II

Ground state frequencies.

	Hg.	Tl.	Pb.	Bi.
F	490.8	475.0	506.9	512.0
Cl.	293.4	287.5	304.2	308.4
Br.	186.3	192.1	207.5	209.5
I.	125.7	121.0		163.9

It can be seen from the table that the ω_e'' value generally decrease though slightly, from Hg. to Tl but increase as we pass from Pb to Bi. The close similarity of the ω''_e values of the lead and bismuth halides in particular call be seen from the above table. In view of this, a value of ω_e'' which is aproximately equal to that of BiI, appears highly probable for lead iodide. This suggested that the above mentioned progression is to be regarded as a v'' progression. Since these bands are degraded towards the red, the few fainter components lying on the longer wave-length side of some of them are to be regarded as sequence members. With the help of the few v'' progressions thus developed, the order of the relative values of ω_e' and ω_e'' were ascertained. The vibrational matrix, shown in Table III in which the intensities of bands have only been represented, has been built up to include most of the band heads in the spectrum. The classification of the bands is shown in the last column of Table I.

Each of the other halides of lead is known to give large system of bands in the visible region and this system of PbI occuring in the same region is to be regarded as a system resulting from a similar electronic transition. A comparison is therefore made of the ground and excited state constants of these molecules as shown in Table IV.

Table IV shows that ν_e for PbI shifts to the red which is to be expected as the lead iodide is the heaviest molecule. Bands of PbI in the region around the system origin are comparitively less intense as in the other halides of lead. The other vibrational constants obtained for PbI, are seen to be entirely in keeping with those of the remaining halides of lead.

Further confirmation of the analysis by means of the isotope effect has not been possible since iodine has no isotopes. But lead, the other constituent of the PbI molecule, has got three isotopes of masses 206, 207, and 208. The calculated separations of the fainter components 206 and 207

TABLE III

Intensity distribution in PbI bands.

v″ \ v′	0	1	2	3	4	5	6	7	8	9	10	11	12	13	14	15	16	17	18	19	20	21	22	23	24	25	26	27
0	2		2	1	†	3	3	*	3	4	4	*	5	5	5	5	5		5	*	*	5	3	*	5	5	2	
1			3	2	1	3	3					2		4	4	3			3									
2	2		3	3		3	2		2	2			2		3	2	2		3	2	2		2		3		3	2
3	3	2				2	1	2								3	2	2	3									1
4		2					1	2																				
5	4	†	2																									
6	2	4																										
7	2	2	1																									
8		2	2																									
9	2	2	3																									
10		2																										
11	3																											
12	2	3	0																									
13			3																									
14		2		2																								
15			4	3																								
16			2	3																								
17			3																									
18			3	4																								
19			2																									
20			3	2																								
21																												
22				2																								
23																												
24				3																								
25																												
26				1	4																							
27				3	3																							
28				3	3																							
29				4	2																							
30																												
31				2																								
32				3	2																							
33				4		1																						
34					2																							
35																												
36					3																							

* Bands superposed by lines † Bands too faint to be measured accurately.

TABLE IV

Vibrational constants of Pb halides.

Molecule	ν_e	ω'_e	$x'_e\omega'_e$	ω''_e	$x''_e\omega''_e$
PbF	22565.2	397.8	1.77	506.9	2.29
PbCl	21866.9	228.6	0.76	304.2	0.89
PbBr	20884.3	152.5	0.40	207.5	0.50
PbI*	19509.6	119.5	0.25	156.6	0.30

* Values for PbI shown in this table are those obtained in the present work.

for the most favourable bands on the longer wavelength side are of the order of a few wavenumber units. Moreover, they occur on the red side of the most abundant molecule Pb^{208} I^{127} and since the bands are red-degraded, any possible observation of the isotope effect under the dispersion used in the present work can be ruled out. But for the bands on the more refrangible end of the spectrum the fainter isotopic heads should lie on the shorter wavelength side of the most abundant molecule. The theoretical separations for some suitable bands being of the order of 4 wavenumber units, only diffuseness was observed which might be an unresolved isotope effect.

The vibrational constants have been calculated from the usual $\Delta G(v) - v$ graphs. The $\Delta G(v)$ values are found to be regular for band heads for which measurements on different plates seldom differed by more than 2 or 3 wavenumber units. Only these band head data were used in the evaluation of the vibrational constants. Diffuse and faint bands for which measurements differed by as much as 5 wavenumber units were also classified though their values were not used in the calculations. The following quantum formula has been derived for the band heads.

$$\nu = 19509.6 + (119.5u' - 0.25u'^2) - (156.6u'' - 0.30u''^2)$$

The intensities of the bands shown in vibratonal matrix are assigned visually on a 0–5 scale. It is to be noticed that the condon curve is a wide open parabola which is analogous to that obtained in the case of the emission bands of PbCl analysed by Rochester. The curve obtained in the present case is what is to be expected for a band system with such relative ω_e values. In fact, such a wide open parabola seems to be the general feature of most of the halide molecules.

Electronic Transition

Each of the monohalides of tin is found to give doublet systems of bands with a lower state $^2\pi$ separation of 2360 cm^{-1} found in SnCl (Jevons, 1926). Since both tin and lead occur in the same subgroup in the periodic

table, the halides of lead might be expected to have a $^2\pi$ lower state. Each of the other halides of lead give a large system of bands in absorption in the visible region and hence it is probable that $^2\pi$ is the ground state of these systems. In PbF, Rochester (1938) analysed two systems designated by him as B_1 and B_2 involving a $^2\pi$ ground state. He reported that the ground state has a width of 8270 cm^{-1}, the largest separation so far recorded. With this $^2\pi$ separation he calculated that the other component A_2 of the system designated by him as A_1 occurring in the visible region should lie in the region around λ 7000. He also suggested that by analogy with the $^2\Delta - ^2\pi$ system found in the spectrum of SnCl by Ferguson (1928), system A_1 is to be regarded as the high frequency component of a $^2\Delta - ^2\pi$ transition. In lead iodide then, the present system is analogous to system A_1 in PbF and has therefore to be regarded as the high frequency component of a $^2\Delta - ^2\pi$ transition. The other compotent may therefore be expected at wave-lengths higher than λ 7000, as PbI is a heavier molecule than PbF.

ACKNOWLEDGMENT

The author is grateful to Prof. K. R. Rao, D.Sc. for his interest in the work.

ANDHRA UNIVERSITY WALTAIR.

REFERENCES

Baratt, 1920, *Trans. Faraday. Soc*, **25**, 758.
Ferguson, 1928, *Phys. Rev.*, **32**, 607.
Howell and Rochester, 1934. *Proc. Univ. Durham. Phil. Soc.*, **9**, 126.
Jevons, 1926, *Proc. Roy. Soc.*, **110**, 365.
Morgan, 1936, *Phys, Rev.*, **49**, 47
Popov and Neujmin, 1932, *Phys. Z. Sowjet*, **2**, 394.
Rao, P. T. and Rao K. R., 1948, *Curr. Sci.*, **17**, 121.
Rochester, 1936, *Proc Roy. Soc.*, **153**, 407.
Rochester, 1938, ,, ,, ,, **167**, 567.

ERRATA

1. Part 3, Vol 23.

In page 111, line 8, insert "$X\phi > X90$, (b) and (c)" after (c)

,, ,, 112, ,, 19 read "less than" for greater

,, ,, 112, ,, 22 ,, "decreases" for increases

,, ,, 112, ,, 25 ,, "$X\phi$" for X

,, ,, 113, ,, 1 ,, "X_{90}" for X_{90}
(col. 9)

,, ,, 113, last row, ,, "4.17" for 4.74
(col. 6.)

,, ,, 116, ,, 32 ,, $I\phi$ for I

,, ,, 117, ,, 1, ,, $X\phi$ for X

2. Part 4, Vol 23.

In page 170, Table V, Remarks column, the numerical values of first quantum number in the brackets are to be increased by 2 ; *e.g.* (0.0), (2.0) etc. should be read as (2,0), (4,0) etc. *Ref.* Asundi (1940), *Proc. Acad. Sc. A*, **12**, 491.

THE NEAR ULTRA-VIOLET SPECTRA OF TOLUENE PART I. THE ABSORPTION BANDS WITH PARTICULAR REFERENCE TO THE NEW BANDS OBSERVED.

By M. R. PADHYE

(*Received for publication, Nov. 5, 1948*)

Plate XIV

ABSTRACT. The absorption spectrum of toluene has been studied between the temperatures 0°C and 250°C and different initial vapour pressures. It was only after the investigations were being undertaken that a paper by Ginsberg, Matsen and Robertson appeared. These authors have recorded and analysed a large number of bands. In addition to these bands, about twenty new bands on the longer wavelength side are also recorded on our plates. These bands have been tabulated and analysed. The main results of the work are as follows:

(1) The bands involve a combination of two or more quanta of vibrations in the ground state.

(2) The intensity consideration leads to the classification of the band at 35202 cm^{-1} as due to the excitation of a single quantum of vibration with frequency 2273. Thus a new vibration frequency is proposed.

(3) Some bands are classified as due to the excitation of the non-totally symmetrical frequencies not included in the analysis of the previous workers.

(4) Incidentally a complete analysis of the already known absorption bands is also given and the results are discussed.

INTRODUCTION

The absorption spectrum of toluene recorded by Savard (1929) was first suggestively analysed by Sponer (1942) who gave also a theoretical discussion. The analysis comprises only a few bands. Sometime after an experimental investigation on these bands was undertaken by us, a paper dealing with the same subject was published by Ginsberg, Matsen and Robertson (1946). They have recorded a large number of absorption bands of toluene. They also give a detailed analysis of the bands observed by them which confirms the first suggestive analysis by Sponer. The wavelength data recorded by them go up to 2760Å. In our experiments we have obtained the data extended on the longer wavelength side up to 2891Å at higher temperatures thus recording 20 new bands. As they were thought likely to yield more informations regarding the vibrational levels in the ground state of the molecule, they are measured and reported here. The bands observed by Ginsberg and others are also recorded on our plates but they have not been measured.

EXPERIMENTAL

An all-quartz absorption cell of 10 cms. length was used. A few drops of the liquid were put in the cell which was then evacuated and sealed off.

For the development of the bands on the longer wavelength side, the cell was sealed off when there was a small amount of liquid still left in it at room temperature (28°C). It was not possible to estimate the exact pressure of the vapour in the cell but no bands on the longer wavelength side of the already known bands were recorded at room temperature. The cell was then enclosed in an electric furnace. When the temperature of the cell was in the range of 90°C – 150°C the band-system developed new bands towards the longer waves. At still higher temperatures, continuous absorption sets in. Toluene supplied by the Fine Chemicals Section of this University was used without further purification. A Hilger medium quartz spectrograph was the recording instrument and Eastman III-O and Kodak Special Rapid plates were employed.

The source of continuous radiation was a locally prepared π type hydrogen discharge tube run on a transformer delivering about 6,000 volts.

Two suitable plates were measured on a Hilger comparator (least count .0001 cm.), one of them twice, and the data presented in Table I are the mean of the three values thus obtained for each band. The intensity data are those visually estimated relatively on the basis of the 0,0 band at 37475* taken as 10. From the average difference in wavenumbers found in the three readings, it is estimated that the values of wavenumbers recorded are correct to within ± 3.

THEORY OF THE SPECTRUM

Due to the substitution of CH_3 in place of one of the H atoms of benzene, the symmetry D_{6h} is reduced to C_{2v}. This group has three elements of symmetry namely the two-fold axis and a plane of reflection perpendicular to the molecular plane. There can be only four different kinds of vibrations possible ; one, a_1, being totally symmetrical and the others a_2, b_1 and b_2 being non-totally symmetrical. All the vibrations are non-degenerate. The transition $A_{1g} - B_{2u}$ of benzene in this symmetry becomes $A_1 - B_1$ and is allowed, as also the transitions involving a_1 vibrations which have the transition moment lying in the plane of the ring in a direction perpendicular to the $C-CH_3$ bond. The direct product Table shows that transitions involving b_1 and a_2 types of vibrations are also allowed since the direct product transforms like a translation but the moments in this case lie in the other two perpendicular directions and hence these transitions give rise to weak bands. The symmetry considerations show that the transitions involving single excitation of b_2 vibration should be forbidden since the transition integral is not invariant for any of the three moments.

Since this point group has no degenerate vibrations, most of the degenerate vibrations of benzene are split up into one totally symmetrical a_1 and one non-totally symmetrical vibrations. As in benzene, it can be expected that these large number of a_1 vibrations will give rise to intense bands due

* Positions of bands are given in units of cm^{-1} in this paper.

to 1-0 or 0-1 transition and also the combinations of these vibrations. Theoretically we can expect to find weaker bands due to non-totally symmetrical vibrations of the type a_2 and b_1. An interesting feature of this part of the spectrum is that there is comparatively a strong band corresponding to the frequency of 620.* This vibration has been classified as the b_1 part of the split 606 e_g^+ vibration of benzene. In most of the mono-substituted benzenes so far studied, this is the only non-totally symmetrical vibration which has been found to be prominently excited. The other totally symmetrical frequencies are superposed on this. This part of the spectrum is quite analogous to that of benzene and the intensity of this transition shows the extent to which the substitution has brought about perturbation in the six-fold symmetry of the ring. This also shows that some of the characteristics of the benzene spectrum are still carried in the spectra of its mono-substituents.

REMARKS ON THE ANALYSIS OF THE ABSORPTION BANDS OF TOLUENE

Pitzer and Scott (1943) classified the fundamental frequencies of toluene, as obtained from investigations of infra-red and Raman spectra, according to the various symmetry classes appropriate to the structure of the molecule and have compared the frequencies with corresponding ones of benzene. From the analysis of its absorption spectrum, Ginsberg *et al* (1946) have proposed values for the frequencies in the excited state of the molecule. They find that of the ground state frequencies, six a_1 vibrations are given by the absorption spectrum and in the excited state five of these are obtained. These five ground state vibrations which can also be recognised in the excited state with altered frequencies are 514, 785, 1003, 1012 and 1212. The 1176 vibration does not seem to have its excited frequency represented in the absorption spectrum.

Among the non-totally symmetrical vibrations in the ground state, a frequency of 620, classified as corresponding to e_g^+ 606 frequency of benzene, is found to be very prominent. Its value in the excited state as identified by Ginsberg is 528. Superimposed on the $0-1$ and $1-0$ transitions of this vibration appear the already mentioned totally symmetrical vibrations. The analysis of the absorption spectrum shows that some more non-totally symmetrical frequencies are also probably excited. Ginsberg found that the frequencies 845, 988 a_2 and 1062 b_1 were detectable in the spectrum. But since the bands involving these frequencies also afford a possible analysis in terms of totally symmetrical vibrations, the latter classification is preferred by them.

Ginsberg (1936) and others have classified some bands as due to intercombination of these frequencies. They also note that the stronger bands are

* Frequencies are given in cm^{-1} units.

accompanied towards the longer wavelengths, by fairly intense bands at spacings of 59 and 178. These are suggested to be due to difference frequencies. The high intensity of the bands involving these difference frequencies probably indicates that the bands arise in low frequency vibration. They have thus classified a large number of bands measured by them. Still some intense bands are left over and in an attempt to classify them we find that some of them involve as high as four quanta of different a_1 vibrations. It is also possible to account for some more bands on the assumption that they involve other non-totally symmetric vibrations. Such new assignments for the recorded bands of Ginsberg are included in Table II.

The excitation of the totally symmetric part of the $e_{\parallel}^{\dagger}$ frequency 514 whose value in the excited state falls to 456 shows some characteristic differences from other substituted benzene spectra (Sponer and Wollman, 1941; and Wollman, 1946). In the case of halogen derivatives it is found that the $0-1$ transition is very weak. But in the case of toluene as also aniline and phenol it is found that $0-1$ and even $0-2$ transitions are fairly intense. Similarly the halogen derivatives the $0-1$ transition corresponding to b_1 frequency 620 is weaker than $0-2$ transition but in toluene reverse is true. Sponer (1941) has explained these characteristics of the halogen derivatives on theoretical grounds.

NEW BANDS AND THEIR CLASSIFICATION

Twenty new bands have been measured on our spectrograms which were not recorded by Ginsberg *et al* (1946). The wavenumbers, intensity and the possible assignment is given in Table I. As the bands can only be observed at higher temperatures, it is probable that the higher ground level frequencies may be involved in these bands. Analysis indeed shows that in some cases the ground level has to be loaded with four quanta of different vibration frequencies to account for the bands.

In the present experiments the band at 35202 is the strongest in this part of the spectrum. It is possible to classify it as due to the excitation of 1062 b_1 together with 1212 a_1 vibration in the ground state. An alternative classification can be, excitation of two quanta of 620 b_1 with two quanta of 514 a_1. Its high intensity is, however, incompatible with any of these classifications since both involve the excitation of non-totally symmetric frequencies b_1 which ought to be weak. In the second alternative two quanta of non-totally symmetrical vibrations are excited and the intensity of such a transition is expected to be weak since the non-totally symmetrical vibrations have their minima one above the other. Hence we are inclined to regard the band as due to a fundamental frequency of 2273 in the ground state. The band at 36160 and 36050 can then be classified as due to superposition of 932 and 964 a_1 frequencies in the excited state over this transition.

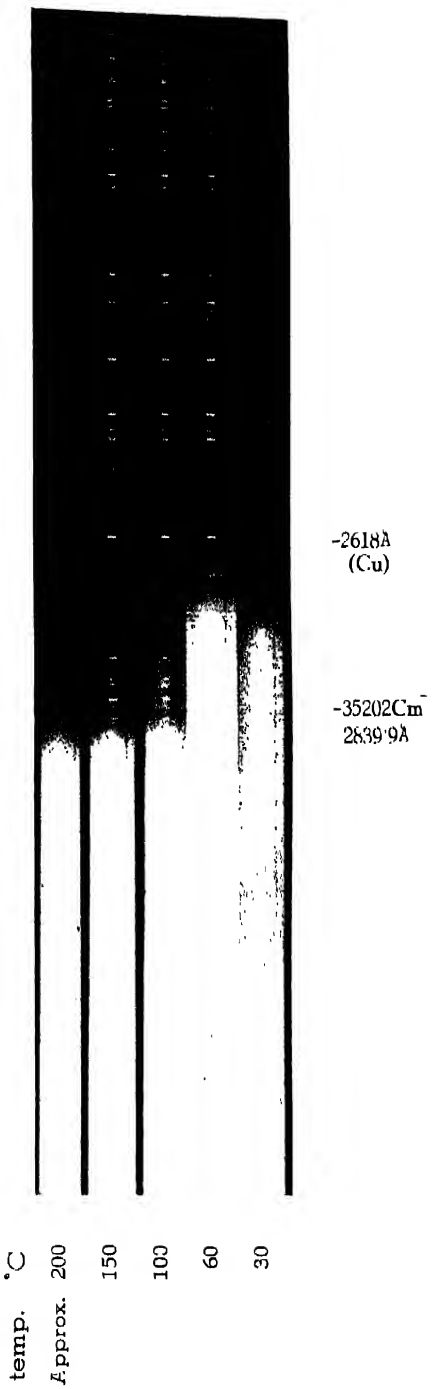

Fig. 1.

The bands next in intensity are 35087 and 35604. The one at 35087 involves an excitation of 1176 and 1212 a_1 in the ground state. There are also bands corresponding to further loading of 620 b_1 and 514 a_1 on this transition. The band at 35604 which is 1871 wavenumbers distant from the o,o band is also one which does not afford a convincing classification. It can be due to excitation of three quanta of 620 b_1 frequency but intensity considerations do not support such a classification. The alternative is the excitation of 1178 a_1 and 1212 a_1 in the ground state with 528 in the excited state. The discrepancy between the observed and calculated values in this case is, however, large.

The band at 35496 is in a similar category. It can be regarded as due to excitation of two quanta of 998 a_2 vibration but its fairly high intensity suggests the alternative classification of two quanta of 1212 a_1 in ground state with 456 in the excited state. Here also the numerical agreement is not satisfactory.

In considering the intensity distribution in this part of the spectrum, it must be borne in mind that this part of the spectrum is developed only at higher temperatures. The intensity, therefore, corresponds to this temperature.

There are also a number of bands due to combination of 514 a_1 with 620 b_1 frequencies and also with other totally symmetric vibrations. The complete analysis is shown in Table I.

TABLE I

New Bands in the Absorption Spectrum of Toluene

ν_{vac} cm^{-1}	Int.	Assignment proposed	Alternative assignments
34574	0	−1176−1212−514	
34658	1	−1176−1012−620	
34764	2	−1176−1012−514	
34876	1.2	−2×1212+456−620	−2×988−620
34983	3	−2×1212+456−514	−2×988−514
35087	5	−1176−1212	−2×1176−785+751
35202	8	−2273	−1062−1212
			−2×620−2×514
35288	4	−1176−1012	
35409	2	−2×1003−1012+964	−2×1030
35496	2.5	−2×1212+456	−2×988
35604	5	−1176−1212+528	−3×620
35687	0	−1003−785	
35720	1	−514−2×620	
35756	1.5	−1212−514	
35827	0	−620−2×514	
35893	0	−1586 (b_1)	
36012	1.5	−1176−1212+932	
36050	3	−1176−1212+564	
36160	3	−2273+964	−1062−1212+964
			−2×620−2×514+964
36568	0	−785−2×59	

TABLE II

Extended analysis of the Absorption Bands of Toluene
+ Bands already analysed by Ginsberg

ν_{vac} cm^{-1}	Int.	Assignments	ν_{vac} cm^{-1}	Int.	Assignments
36268$^+$	*vvw*	−1212	37329	*vw*	−620+528−59
36301$^+$	,,	−1176, −1003−178	43	*vvw*	+932−1062
36415$^+$	,,	−1003−59	56$^+$	*w*	−2 × 59
65$^+$	*vvwBD*	−1012	60	*w*	
74$^+$	,,	−1003	81$^+$	*w*	−620+528
93	,,	−988	84	*w*	
36517$^+$	,,	−785−178	93	*vvw*	+932−1012
71	,,	−785−2 × 59	37418$^+$	*ms*	−59
36631$^+$	*vvw*	−785−59	21	*ms*	
76$^+$	,,	−620−178	32$^+$	*vvw*	−1003+964
92$^+$	*w*	−785	66$^+$	*s*	−9
36729$^+$	*vvw*	−1212+456	70	*s*	
35	,,	−620−2 × 59	37477$^+$	*vvs*	(0−0)
63	,,	−2 × 620+528	37480	*s*	+528−514
84$^+$	*vw*	−514−178	95	*vw*	+528−2×178, −1189−1012
96$^+$	,,	−620−59	37649	,,	−620+964−2 × 59
36857$^+$	*w*	−620	37706$^+$	*vvw*	+456−178
72	*vvwB*	−1062+456	60$^+$	*vw*	+932
36903$^+$	*vvw*	−514−59	85$^+$	*vvwBD*	−620+964
63$^+$	*w*	−514	37823$^+$	*w*	+520−178
37121$^\pm$	*vvw*	−2 × 178	28$^+$	*w*	−2 × 1003−2 × 1189
51$^+$	,,	−456−785	31	*w*	
37191	*vvw*	+932−1212	50	*vvwBD*	+456−59
37206	,,	−620+528−178	59	*vw*	+1189−785
45$^+$	*vw*	−178−59	72	*vw*	−620+2×528
37299 / 37302 $^+$	*ms*	−178	75$^+$	,,	−514+964
37304$^+$	*vw*	−3×59	37913	*wBD*	+456
15	,,	−620+456	24$^+$	,,	+528−59
25	,,	−1212+2×528	33$^+$	*s*	+528−9
			36$^+$	*m*	
			48$^+$	*w*	
			53	*m*	
			93$^+$	*s*	
			98	*s*	

TABLE II (*contd.*)

ν_{vac} cm^{-1}	Int.	Assignments	ν_{vac} cm^{-1}	Int.	Assignments
38005$^+$	*vs*	0+528	38738	*m'*	
08	*vs*		49$^+$	*wBD*	+751+528−9
10	*vs*		57$^+$	*m*	+751+528
80	*vwBD*	+932−334	59	*m*	
38173$^+$	*vw*	+751−59	94	*vw'*	+964+528−178
38212	*wD*	+2×456−178	38805	*vvwBD*	+456+932−59, +2×751−178
28$^+$	*m*	+751	40	*m*	+3×456
31	*m*		38869$^+$	*m'*	+456+932
33$^+$	*m'*	+932−178	81	*w*	+932+528−59
59$^+$	*w*	+964−178	38932$^+$	*w'*	+932+528−9
63	*w*		41$^+$	*s*	+932+528
82	*vw*	+528+456−178	60$^+$	*wBD*	+964+528−9
93$^+$	,,	+932−2×59	72$^+$	*s'*	+964+528
38317$^+$	*vvw*	+3×456−3×178	84$^+$	*w*	+751+932−178, 2×751
21	,,	+964−2×59	39065$^+$	*vvw*	+456+1189−59, +3×528
38342	*vwD*	−1003+2×932	99	*vw*	+751+932−59,
51$^+$	*m*	+932−59	39124$^+$	*wBD*	+456+1189
54	*w*		44$^+$	*vw*	+2×456+751, +456+528+751−59
82$^+$	*mBD*	+964−59	47	*vw*	
91$^+$	*vw*	+2×456	62$^+$	*m*	+751+932
38402$^+$	*mBD*	+932−9	39204$^+$	*s*	+1189+528
09$^+$	*vs*	+932	39335$^+$	*vw'*	+456+3×528−178, +456+932+528−59
11	*vs*		41$^+$	*m*	+2×932
31$^+$	*mBD*	+964−9	43	*m*	
41$^+$	*s*	+964	67$^+$	*mBD*	+932+964−9
44	*m*		75$^+$	*msD*	+932+964
56	*vwBD*	456+528	77	*w*	
86	,,	+1189−178, +3×456−2×178	91	*wB*	+456+528+932
38539$^+$	*vvw*	+2×528	39406$^+$	*m'*	+2×964
47$^+$	*vvwBD*	+1189−2×59	52	*vw*	964+1189−178
77	,,	+528+751−178	39513$^+$	*vwBD*	+2×751+528, +456+3×528
38601$^+$	*wBD*	+1189−59			
10	*wBD*				
66$^+$	*s'*	+1189			
72	*ms*				

TABLE II (*contd.*)

ν_{vac} cm^{-1}	Int.	Assignments	ν_{vac} cm^{-1}	Int.	Assignments
39543	*vw*	+932+1189−59	39903^{+}	*s'*	+932+964+528
39602^{+}	*ms'*	+932+1189	30^{+}	*wD*	+2×964+528
39636^{+}	*s'*	+964+1189	45^{+}	*vwBD*	+2×751+964, +751+1189+528
62	*vw*	+751+964+528−59	40135^{+}	*w'*	+932+1189+528
72	*vwBD*	+3×751−59	66^{+}	*w'*	+2×751+1189
39693^{+}	*m'*	+751+932+528	40306^{+}	*wBD*	+2×932+964
39725^{+}	*w*	+3×751, +528+751+964	22	*wD*	+2×1189+528−59
82	*vw*	+3×456+932	37^{+}	*wBD*	+2×964+932
39800^{+}	*w'*	+2×932+456	49^{+}	*vvwBD*	+751+932+1189
11^{+}	*vwD*	+456+751+1189−59	84^{+}	,,	+2×1189+528
35^{+}	*w'*	+751+932+964	40555	*s'*	
53^{+}	*wD*	+2×1189	65^{+}	*vw*	+932+964+1189
72^{+}	*m'*	+456+751+1189, +528+2×932	40816	*vw*	+2×1189+964
			41030	*vvw*	+3×1189

ACKNOWLEDGMENTS

In conclusion, the author wishes to express his sincere thanks to Prof. R. K. Asundi for his valuable guidance and encouragement. Thanks are also due to Mr. B. Bhattacharyya for his help in analysing the recorded data on the absorption of toluene and to Dr. Majumdar of Allahabad University, for permission to use the Comparator.

BENARES HINDU UNIVERSITY

REFERENCES

Ginsberg, Matsen and Robertson, 1946, *J. Chem. Phy.*, **14**, 511
Pitzer and Scott, 1943, *J. Am. Chem. Soc.*, **65**, 803.
Savard, 1929, *Ann. de Chemie.*, **11**, 287.
Sponer, 1942, *J. Chem. Phy.*, **10**, 672.
Sponer and Teller, 1941, *Rev. Mod. Phy.*, **13**, 119.
Sponer and Wollman, 1941, *J. Chem. Phy.*, **9**, 816
Wollman, 1946, *J. Chem. Phy.*, **14**, 123.

THE NEAR ULTRA-VIOLET SPECTRA OF TOLUENE PART II. THE EMISSION BANDS

By R. K. ASUNDI and M. R. PADHYE

(*Received for publication, Nov. 8, 1948*)

PLATE XV

ABSTRACT An emission spectrum of toluene in the near ultraviolet is excited by a transformer discharge through flowing vapour. This spectrum, which was previously observed by Stewart *et al* in Tesla discharge and mentioned by Kistiakowsky and co-workers in resonance fluorescence, has been considerably extended and studied in greater detail. Most of the bands are those observed already in absorption but there are a few which have not been recorded in the absorption spectrum. A complete analysis of the emission bands which is in agreement with the one for absorption bands is proposed. The general appearance of bands and their intensities are compared with those of the corresponding emission bands of benzene. A fairly strong continuous emission band with a sharp short wavelength limit coinciding with the origin of the emission band system has also been recorded.

INTRODUCTION

The spectra of aromatic molecules have attained significance in recent years owing to the theoretical advances that have been successfully made in the interpretation of the spectra of benzene and some of its mono-derivatives. Recently we reported on the emission spectrum of benzene (Asundi and Padhye, 1945 and 1949). In this paper we communicate results on the emission spectrum of one of its mono-derivatives—toluene whose absorption spectrum has been recently analysed (Ginsberg, Matsen and Robertson, 1946) and also extended (Padhye, 1949) and whose Raman and infra-red spectra (Pitzer and Scott, 1943) are fairly well understood.

Stewart and collaborators (1930) were the first to excite the emission spectrum of toluene by the Tesla discharge through flowing vapour. They have observed about twenty-three bands, whose wavenumbers are recorded correct to four places only. It appears that they have observed also a fairly strong continuous background. Cuthbertson and Kistiakowsky (1936) have attempted to excite resonance fluorescence of toluene which even at 0.01 mm. pressure emit spectra which, by using a spectrograph with a resolving power of better than 25000, appear nearly continuous. At ordinary pressures and with illumination by the 2536A line, toluene emits a strong fluorescence consisting of mainly a continuum with a few faint and indistinct bands which become even fainter upon lowering the pressure. They do not record any numerical data.

The emission spectrum of toluene, which has been excited in the present investigation by high frequency as well as ordinary uncondensed transformer

discharge in flowing vapour, shows that the bands of toluene are indeed superposed by a continuous spectrum but the intensities of the two spectra being nearly of the same order with that of the continuum being uniformly slightly less than that of the bands, it has been possible to measure the heads of the emission bands. They are, however, not sharp like the benzene band heads but look rather diffused, probably on account of the continuum in which they are situated.

EXPERIMENTAL PROCEDURE AND RESULTS

The experimental methods both for h. f. discharge and trrnsformer discharge are exactly similar to those employed in the case of benzene (Asundi and Padhye, 1945 and 1949). Since the spectrnm was devoloped with greater intensity in transformer discharge like in benzene, it was photographed under this discharge only using both the medium Hilger and E_1 Hilger quartz Littrow spe trographs described elsewhere. Iron and copper arc lines were used for standard wavelengths. Three plates, Kodak Special Rapid, taken on the E_1 Littrow instrument were selected for measurement with a Hilger Comparator reading upto 0.0001 mm. The bands were measured by focusing the cross wires on the visually estimated maximum intensity part near the heads. The entire region, in which the bands lie, is occupied also by a continuum which is mentioned above. This circumstance renders the weaker bands liable to be less accurately measured than the stronger ones. The three values measured did not differ by more than 3 cm^{-1} and 7 cm^{-1} for the stronger and weaker ones respectively. The intensities represent visual estimates taking the most intense band at 37474* to be 5. The toluene employed was the one supplied by the Fine Chemicals Section of this University (b-p.110.8°C).

The bands extend from 2667Å to 2900Å and are in the body of a continuum which also starts practically with its maximum intensity from 2667Å and extends towards the longer waves. It appears to have a sharp short wavelength limit at 2667Å. Also in a few spectrograms there could be seen a slight trace of its extention with weak intensity falling towards the shorter waves upto about 2603Å. No sharp limit has been observed on the long wave side, although the intensity shows a drop at about 3500Å. The data on the band heads reduced to wavenumbers in vacuo by the use of Kayser's Tabellen are given in Table I, along with the possible corresponding bands recorded by Stewart (1930). It also contains the visually estimated intensity values and the assignments in terms of the analysis proposed. Corresponding values, wherever observed in the absorption spectrum, are also included. These prove that the emission bands are the counterparts of the known absorption bands. The bands are reproduced in Plate XV.

* Unless otherwise stated, the position of the bands is always given in this paper in wavenumbers per cm.

ANALYSIS

It is seen that the electronic transition responsible for the ultraviolet bands of benzene is a forbidden one. The symmetry character of this transition, $A_{1g}-B_{2u}$ is calculated on the assumption of a six-fold D_{6h} symmetry for benzene molecule. Mono substitution by any atom or radical destroys this six-fold symmetry and reduces it to one of C_{2v} type to which therefore the toluene molecule belongs. This symmetry has one two-fold axis in the molecular plane and a plane of reflection perpendicular to it. Considerations of the energy states of the molecule closely follow that for benzene. As a matter of fact, in calculating the benzene levels a mean value of resonance energy given by thermo-chemical data on benzene, toluene, ethyl benzene and propylbenzene have been utilised (Pauling and Sherman, 1933) to evaluate the energy levels. Thus not only are the characters of the electronic states of toluene similar to those of benzene but to a first approximation even the energy values are the same. This is corroborated by the fact that the bands, *e.g.*, those in the near ultraviolet, lie in nearly the same region of the spectrum. On these considerations, the lowest state of toluene, as in benzene, is one of total symmetry *viz.*, A_1, corresponding to A_{1g} in benzene The excited state of benzene is anti-symmetrical to the two-fold axis and to the plane of reflection which in the case of C_{2v} is the B_1. Hence the transition now is the A_1-B_1 which is an allowed one with the transition moment lying in the plane of the molecule in the y direction, *i.e.*, the direction perpendicular to the $C-CH_3$ bond.

The absorption spectrum of toluene is thus different from that of benzene in so far as the latter is due to a forbidden transition while the former to an allowed one. This circumstance renders particularly the vibration structures in two cases to be very different. Thus the o−o band which is absent in the case of benzene at ordinary temperatures should be present in the case of toluene with considerable intensity. The totally symmetrical a_1 vibrations should be directly superposed over the o−o transition and should be very intense.

The components of the electric moment in two other directions (other than those due to A_1-B_1) do not occur in this transition. But the product table shows that b_1 and a_2 vibrations, where superposed, should give rise to weak bands with transition moment in these two directions and that the b_2 vibration should not occur in the spectrum. An important class of transitions amongst this type found in all mono-substituted benzenes is the one due to the non-totally symmetrical b_1 part of the split up 606 e_g^+ frequency which makes the benzene transition allowed. This non-totally symmetrical vibration is found to be very prominent. Many of the previous investigators on the absorption spectrum of substituted benzenes have, after Sponer (1942), called the first part due to a_1 vibration the allowed part, and the latter coming in due to superposition of the non-totally symmetrical vibrations the forbidden

part. Thus the spectrum due to a molecule with C_{2v} symmetry should consist of these two parts. The third possible transition that can be allowed is the $1-1$ transition of any vibration even including b_2. The bands due to the $1-1$ transition of non-totally symmetrical vibrations will be very weak and scarcely observable.

As the symmetry table shows there can be only four types of vibrations possible in the C_{2v} symmetry, *viz.*, a_1 totally symmetrical and a_2, b_1 and b_2 non-totally symmetrical, all non-degenerate. Hence the degenerate vibrations of benzene will split into two, most of them giving one totally symmetric

TABLE I

Emission Bands of Toluene

ν cm^{-1} (Stewart)	ν_{vac} cm^{-1} (Authors)	Int.	Assignment	Absorption bands Ginsburg *et al*
	37475	5	0,0	37477
	37452	1	0+1189−1212	
	37416	1.5	0−59	37418
	37379	1	0+528−620	37381
	37354	0	0−2×59	37356
	37320	1	0+456−620	37319
3728	37299	2.5	0−178	37299
3721	37244	2	0−59−178	37245
	37199	1.5	0−2×620+964, 0+932−1212	37191, 37206
3713	37130	0	0−340 (b_1) *, 0−2×178 (?)	37121
3697	36960	2	0−514	36963
3686	36888	.5		
	36851	2.5	0−620	36857
3679	36785	2	0−514−178	36784
3668	36688	4	0−785	36690
	36657	0	0−2×1003+1189	
3662	36625	.5	0−785−59, 0−842 (a_2)	36631
	36529	0		
	36514	0	0−785−178	36517
	36494	0	0−985 (a_2)	36493

* The symmetries of vibrations other than a_1 are indicated in brackets.

—2618·39Å
(Cu)
—37475
(0,0)
2667·64Å
2824·4Å
(Cu)

TABLE I (*contd.*)

ν cm^{-1} (Stewart)	ν_{vac} cm^{-1} (Authors)	Int	Assignment	Absorption bands Ginsbarg *et al*
3647	36467	2	0 − 1003	36465
3641	36430	0	0 − 2 × 1003 + 964, 0 − 985 − 59	
	36415	0	0 − 1003 − 59, 0 − 1060 (b_1)	36115
	36403	0	0 − 2 × 1003 + 932, 0 − 1070 (b_1)	
	36307	1	0 − 1176	36301
3628	36293	0	0 − 1003 − 178	
	36281	0		
3623	36263	1	0 − 1212	36268
	36205	0	0 − 1212 − 59	
3590	35842	.5	0 − 1012 − 620, 0 − 1630 (b_1)	
3583	35733	0		
3567	35681	1	0 − 620 − 1176, 0 − 1003 − 785	35687
3548	35469	0	0 − 2 × 1003	
	35421	0		
3528	35296	0	0 − 1003 − 1176	35288
3507	35068	0	0 − 2 × 620 − 1176	
3486	34842	0	0 − 2 × 1003 − 620	
3465	34680	1	0 − 2 × 1003 − 785	
3425	34265	0		
	34202	0		

and one non-totally symmetric vibrations. Further calculations show that toluene should have 14 of a_1 type; 4 of a_2, 13 of b_1, and 8 of b_2 type vibrations. In the table given by Pitzer and Scott (1943), one a_2 vibration has been listed in b_2 making the former 3 and latter 13. Table II gives a list of the totally symmetric vibrations as given by these authors. These are all Raman lines active and polarised.

The above mentioned theoretical considerations are well borne out in the analysis of the absorption spectrum of toluene. Some strong absorption bands were analysed by Sponer (1942) identifying some totally symmetric vibration frequencies in the upper state. The symmetry proposed was C_s. But later analysis of the absorption spectrum and theoretical considerations prove that the symmetry should be the same as other mono-substituted

TABLE II.

Totally symmetrical a_1 vibrations of Toluene

Raman spectrum	Absorption spectrum	
	Normal state	Excited state
1002	1003	932
521	514	456
1210	1212	1189
1603	.....	.....
1175	1176	.....
785	785	756
1030	1012	964
1483	.....	.....
1380	.....	.....
2950	.....	.....

N. B. Vibrations in this Table as in the rest of the paper are given in wavenumbers per cm.

benzenes, namely, C_{2v}. The absorption spectrum of toluene has been investigated by Ginsberg, Matsen and Robertson (1946). They have analysed the bands as due to superposition of a_1 vibrations on the 0–0 transition and also the 1–1 transition of these vibrations. Some bands are also analysed as due to superposition of the totally symmetrical vibrations on the non-totally symmetrical part corresponding to the $e_{''}^{+}$ frequency of benzene. A more detailed analysis shows that other characteristics of the transition in question are also satisfied. An extension of the absorption bands towards longer waves, described elsewhere, gives further evidence in support of these considerations.

In the case of emission, the most characteristic features have already been put down. The continuum spreads over the whole of the region starting with 0–0 band. The first and the strongest band at 37475 is the 0–0 band. A number of totally symmetric a_1 vibrations are superposed over this transition, the strongest being the 785 at 36688. The other vibrations observed are 514, 1176, 1003 and 1212. The corresponding bands are quite intense. The frequency of the a_1 vibration, classified by Pitzer and Scott as 1030, has been found to be 1012 in the absorption by Ginsberg, Matsen, and Robertson (1946). In the present experiments also a band corresponding to 1030, could not be found and it is likely that the band at 36467 whose distance from the 0–0 band is 1008 is due to the blending of two bands due

to 1003 and 1012. The frequency 1003 is also excited by 2 quanta and band at 35469 is classified as such. There are also some differences in other frequencies considered *e.g.*, the frequency tabulated by Pitzer and Scott as 521 is found to be 514 both in absorption and emission. These frequencies are tabulated in Table II together with the excited state frequencies found in absorption spectrum.

The other part which is called the forbidden part of the spectrum is also developed in emission. The band at 36851 is analysed as $0-620$ where 620 is the non-totally symmetrical b_1 part of the e_g^1 frequency 606. The intensity of this band is rather large for the non-totally symmetrical vibration. It appears therefore to indicate the importance of the mechanism which makes the spectrum of benzene allowed, and hence the weakness of the substituent in destroying the six-fold symmetry of benzene. There are some totally symmetrical vibrations superposed over this transition. There are also bands which can be classified as possibly due to the excitation of b_1 vibrations or a_2 vibrations but there are in most cases other alternatives also possible for them and it is not possible to make a conclusive choice.

The emission spectrum differs rather widely, as it should, from the absorption spectrum even in appearance. The absorption spectrum has a number of bands lying to the short wavelength side of the $0-0$ band, whereas in emission there are none But on the longer wavelength side of the $0-0$ band both in emission and absorption there are about 18 bands in common which are similarly classified. These are all due to excitation of the totally symmetric ground state frequencies and those due to the further superposition of difference frequencies of 59 and 178 on them. The analysis of the absorption spectrum also gives 59 and 178 as difference frequencies involved in the spectrum. The same frequencies are also found in emission associated with the transitions involving a_1 vibrations. These low frequencies must be due to $1-1$ transition of a frequency which is quite low as the intensity of the band suggests. In benzene such a difference frequency of 160, which was due to the ground state e_u^1 404 frequency, dropping to 240 in the upper state. The e_u^1 frequency is split into 405 a and 467 b_2 in the present case. The assignment to either is not possible since a_2 is not excited in the ground state or in the excited state in either spectrum and the other single quantum excitation is not allowed.

It will be interesting to compare the spectrum with the emission spectrum of benzene. The transition involved in the case of benzene is a forbidden one. The spectrum of benzene even then shows a large number of bands which are quite intense and quite sharp involving a number of vibrations in keeping with the selection rules for the forbidden transition. But the transition in toluene is an allowed one. One would expect a spectrum consisting of a large number of bands involving the totally symmetrical frequencies which in number are many more than in benzene. It would have also been expected that the spectrum should be more intense than the benzene spectrum. These conditions are partly fulfilled in the case of absorption

spectrum but in emission the experimental facts are quite the opposite. In all there are very few bands and these have no sharp heads. The total intensity of the spectrum as a whole including the continuum is also less than in benzene as far as could be judged. This can be understood on the following considerations.

A comparative study of the total intensity of absorption due to different substituents has been done by Sklar (1939) and Mulliken (1939). Sklar has treated toluene as one substitution. Theoretically it is found that large intensification is closely associated with large directing power which in its turn is associated with the induction effect or migration effect between the ring and the substituent. The induction effect has very small influence and much less when the substituents are not of a polar character. The migration effect is attributed to the non-bonding type of the p_z electrons of the substituent. Thus large intensification ought to be expected in those cases where the substituent has low ionisation potential, a pair of unbound p_z electrons and small ring-radical distance. Since these are not favourable in the case of the CH_3 radicle, the intensification expected was small and actually the absorption spectrum of toluene is found to be only twice as intense as benzene. If the same considerations hold in the case of emission and if these are the only corresponding emission spectra, then the intensity of emission, which ought to have been larger in toluene than in benzene, is actually smaller. Probably an explanation of this anomally is to be sought in the nature of the excited states in the two molecules.

ACKNOWLEDGMENTS

We desire to record our thanks to Prof. Sir K. S. Krishnan and Prof. Dr. N. R. Dhar of Allahabad University for permission to one of us (M. R. P.) to work in their laboratories and to use the E_1 quartz Littrow spectrograph.

Benares Hindu University

REFERENCES

Asundi and Padhye, 1945, *Nature*, **156**, 368
" " " , 1949, *Ind. Jour. Phys.*, **23**, 199
Cuthbertson and Kistiakowsky, 1936, *J. Chem. Phy.*, **4**, 9
Ginsberg, Matsen and Robertson, 1946, *J. Chem. Phy.*, **14**, 507
Mulliken, 1939, *J. Chem. Phy.*, **7**, 353
Padhye, 1949, *Ind. Jour. Phys.*, **23**, 331
Pauling and Sherman, 1933, *J. Chem. Phy.*, **1**, 679.
Pitzer and Scott, 1943, *J. Am. Chem. Soc.*, **65**, 803.
Sklar, 1939, *J. Chem. Phys.*, **7**, 984.
Sponer, 1942, *Rev. Mod. Phy.*, **14**, 224.
" " , 1942, *J. Chem. Phy.*, **10**, 672.
Stewart, 1930, Recent Advances in Physical and Inorganic Chemistry, p. 356.

EVALUATION OF SPECTROGRAMS OF HIGH SPEED STEELS FOR MINOR ELEMENTS. PLATE CALIBRATION METHOD

By B. N. BHADURI

(Received for publication, June 16, 1949)

ABSTRACT. Minor elements occurring in high speed steels do not exceed a total of two per cent. Such steels of our Works manufacture designated as T.H.S.2 are of the conventional type 18-4-1. The time-scale method of plate calibration due to Smith has been adopted and applied to the ferrous analysis of the above samples; the spectra evaluated and compared with the usual method of log ratio of galvanometer deflections against composition. The elements receiving attention were manganese, silicon and vanadium. Conventional spark technique for exciting spectra was used. The standard deviations of results which have been computed, do not exceed 2 to 3 per cent of contents.

INTRODUCTION

The method of plate calibration for the evaluation of spectrograms can best be carried out in case of alloying elements occurring in small percentages. A method given by Smith (1945) of the British non-ferrous metals Research Association has been used in the analyses of non-ferrous alloys. The method is being adopted and applied to the analysis of ferrous samples such as high speed steels. The elements considered are manganese, silicon and vanadium, the total contents of which do not exceed two per cent in the given alloys.

The basis of method of plate calibration arises out of known relative intensities of manganese triplets 2949.2, 2939.3 and 2933.1. These values were derived from a consideration of "statistical weights" and given by D. M. Smith as 7 : 5 : 3. The ratios are independent of the source of excitation.

As applied to ferrous analysis, it was, however, not possible to include Mn 2949.2 owing to its own interference with an iron line having the same length (Fe II 2949.205). In what follows, therefore, two lines, Mn 2939.3 and Mn 2933.1 formed the calibration pair.

PROCESS

Technique : The apparatus used in exciting the spectra and in the photometric work and the processing of plates is described underneath :

Volts	—	230 A. C.
Condenser	—	0.005 μF
		15,000 V spark
		22,000 V wave peak.

Transformer		1/4 KVA tapping from 15,000 V
Added inductance		Nil
Spark gap	-	2 mm.
Electrodes	-	Samples, chill-cast, flat surface.
Counter electrode	-	H. S. brand carbon also flat surface,
Pre-sparking	-	3 mins.
Spectrograph	-	E 478 Littrow
Sp. phic slit	-	7 divs (=0.0175 mm)
Photometer slit	-	8 divs (=0.016 mm)

The apparatus are all of Hilger's specification and of Hilger manufacture.

Photographic plates	—	Ilford Process
Developer	—	ID 13 No. 1 and 2 in equal proportions.
Development	—	4 mins.

Flat surface technique of spark excitation with a condensed spark of routine type was used.

Reproducibility : In order to test the reproducibility of spectral intensities a continuous spark of 25 secs. duration on a chosen sample against carbon was given with spectra distributed throughout the plate. The data are given in Table I.

TABLE I

	Mn 2939 Deflection	Density D 2939	$D-\text{Av}$ (d)		Mn 2933 Deflection	Density D 2933	$D-\text{Av}$ (d)	
1	67	0.80	−0.01		120	0.54	0.00	
2	69.5	0.78	−0.03		127.5	0.52	−0.02	
3	66	0.80	−0.01		121	0.54	0.00	
4	65.5	0.81	0.00		120	0.54	0.00	
5	70	0.78	−0.03	$\Sigma d^2 = .0100$	126	0.52	−0.02	$\Sigma d^2 = .0047$
6	69	0.78	−0.03	Std. deviation	125.5	0.52	−0.02	Std. deviation
7	66	0.80	−0.01		120	0.54	0.00	
8	63	0.82	0.01	$\sigma = \sqrt{\frac{\Sigma d^2}{n}}$	117.5	0.55	0.01	$\sigma = \sqrt{\frac{\Sigma d^2}{n}}$
9	63	0.82	0.01	=0.023	117	0.55	0.01	=0.016
10	66.5	0.80	−0.01	in %	127	0.52	−0.02	in %
11	65	0.81	0.00	2.8%	119.5	0.55	0.01	3%
12	58.5	0.86	0.05		113	0.57	0.03	
13	62.5	0.83	0.02		117.5	0.55	0.01	
14	62.5	0.83	0.02		116.5	0.56	0.02	
15	62	0.83	0.02		117	0.55	0.01	
16	58	0.86	0.05		113.5	0.57	0.03	
17	62	0.83	0.02		116.5	0.56	0.02	
18	63	0.82	0.01		122	0.54	0.00	
	Mean 0.81				Mean 0.54			

Clear plate Av. 420 mm.

The deflections are the mean of two readings obtained by measuring the line each way as the plate is moved from one side to the other. The standard deviations of densities as obtained was 2.8% for Mn 2939.1 and 3% for Mn 2933.1.

EXPERIMENTAL

A series of three plates A, B and C was used for making the blackening curves. As the distribution of spectra over the plate was of some consequence in sampling, spectra were distributed evenly and were noted. The sequence is shown in Table II

TABLE II

Distribution of spectra

Plate	Alloy used	Exposure	Time of exposure
A.	(13)	1-3	Sec. 10
		4-6	,, 15
		7-9	,, 20
		10-12	,, 30
		13-15	,, 45
		16-18	,, 60
		19,20	,, 90
B & C.	(13)	1-4	,, 10
		5-8	,, 15
		9-12	,, 20
		13-16	,, 25
		17-20	,, 30
		21-24	,, 45
		25-28	,, 60
D.	(13)	1-10	,, 25
		20-29	,, ,,
		11-13	,, 10
		14-16	,, 20
		17-19	,, 30
E.	(13)	1,2,12,13,23,24	,, 10
		3,4,14,15,25,26	,, 20
		5,6,16,17,27,28	,, 30
	(3)	7,18	,, 25
	(4)	8,19	,, ,,
	(7)	9,20	,, ,,
	(30)	10,21	,, ,,
	(42)	11,22	,, ,,
F.	(6)	1-4	,, 25
		13-16	,, ,,
		25-28	,, ,,
	(13)	5,22	,, 10
		6,23	,, 20
		7,24	,, 30
	(3)	8,17	,, 25
	(4)	9,18	,, ,,
	(7)	10,19	,, ,,
	(30)	11,20	,, ,,
	(42)	12,21	,, ,,

The table shows the distribution for all the plates used in the experiment. The spectra are numbered serially from top to bottom.

Spectra with exposure time of 10, 15 etc. to 60 secs. were photographed. The spark used was continuous with pre-sparking as described. The number of spectra of each duration in case of a plate is given in Table II. All such results are included in the table.

BLACKENING CURVES

Blackening curves were drawn from data given in Table III, where mean values of densities and deflections for manganese lines from the three plates A, B and C are given, the density (Sug. Def. Glas., 1946) being defined as

$$D = \log d_0/d$$

where d_0 is the deflection obtained from clear plate, *i.e.*, base plus unexposed processed emulsion and d, deflection due to the line. Such blackening curves are shown plotted in Fig. 1. The plot is of densities against log time of

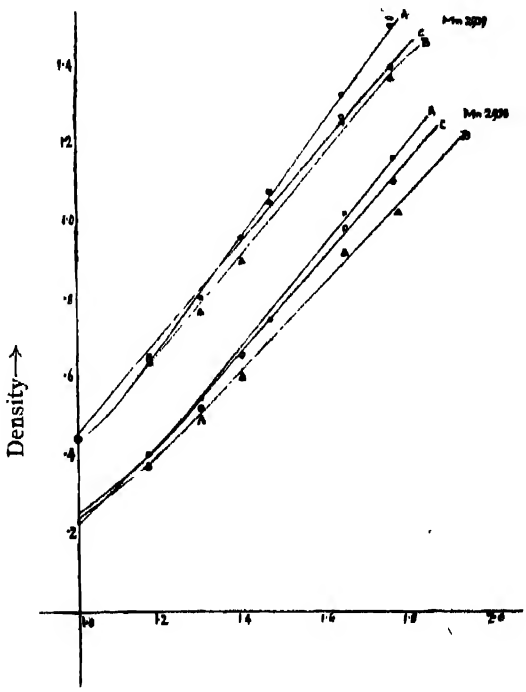

FIG. 1
Blackening curves

exposure. The separation of curves along axes parallel to abscissa are measured giving $\Delta\epsilon$ (log exposure time ratio) for different values of densities. This is shown in Table III. The mean of log exposure time ratio ($\Delta\epsilon$) thus measured gives, attributing a value 100 to the photographic intensity of Mn 2939, a value equal to 60.3 for Mn 2933; Baly's value on a consideration of statistical weights being 60.1. No correction for background was made but the agreement afforded was excellent.

TABLE III

Time of exposure	I = 100 (Mn 2939) Deflection	Density	I = 60.3 (Mn 2933) Deflection	Density
10″	A 153	0.44	238	0.23
	B 152.5	0.44	237	0.25
	C 144.4	0.44	222	0.26
	Mean 150	0.44	232.3	0.25
	Log *It*	3.00		2.78
15″	A 89	0.65	159	0.40
	B 79.5	0.63	177	0.37
	C 90.9	0.64	157	0.40
	Mean 86.46	0.64	164.3	0.39
	Log *It*	3.176		2.96
20″	A 62.7	0.80	116.2	0.54
	B 72.4	0.76	137	0.48
	C 67.0	0.75	122	0.51
	Mean 67.3	0.77	125.1	0.51
	Log *It*	3.301		3.081
25″	—	—	—	—
	B 51.2	0.92	103.2	0.61
	C 44.2	0.95	86	0.65
	Mean 47.7	0.94	94.6	0.63
	Log *It*	3.398		3.178
30″	A 36	1.04	73	0.74
	B 35.5	1.07	74.5	0.75
	C 34.1	1.07	66	0.78
	Mean 35.2	1.06	71.2	0.76
	Log *It*	3.477		3.257
45″	A 19	1.32	39	1.01
	B 24	1.25	51	0.91
	C 22	1.26	42.4	0.97
	Mean 21.7	1.28	44.1	0.96
	Log It	3.653		3.433
60″	A 12.5	1.50	28	1.15
	B 18.2	1.36	41.2	1.01
	C 16.0	1.39	32.5	1.09
	Mean 15.6	1.42	33.9	1.08
	Log *It*	3.778		3.558

D (Density)	Plate A	Plate B	Plate C
0.5	—	2.58	2.25
0.6	2.40	2.50	2.20
0.7	2.25	2.40	2.25
0.8	2.20	2.35	2.20
0.9	2.10	2.35	2.20
1.0	2.10	2.30	2.20
1.1	2.15	—	2.15
1.2	2.18	—	
$\Delta\epsilon$	0.22	0.24	0.22

Mean $\Delta\epsilon$ 0.22
Antilog 0.78

Photographic Intensity

Mn 2229 100
Mn 2933 60.3

Data according to Baly
Mn 2939 100
Mn 2933 60.1

Clear plate Av. 406 mm.

In all subsequent experiments a calibration pattern as described above was included in the plate. Blackening curves were drawn in each case. Data for D, E and F plates are given in Table IV-VI.

TABLE IV

Time of exposure	Mn 2939		Mn 2933		Density	Plate D
	Deflection	Density	Deflection	Density		
10″	128	0.42	193	0.24	0.5	2.20
	124	0.44	192	0.25		
	114	0.47	186.5	0.26	0.6	2.45
Mean	123	0.44	190.5	0.25	0.7	2.70
20″	53	0 54	98.5	0.54		
	53	0.53	99.5	0.53	Mean	2.45
	54	0.52	102	0.52	Δe	0.245
					Antilog	0.755
Mean	53.3	0.53	100	0.53		
					Photographic Intensity	
30″	32	1.03	64.5	0 72		
	36	0.97	72	0.67		
	34.5	0.99	70	0.68	Mn 2939	100
					Mn2933	56.9
Mean	34.2	1.00	68.8	0.69		

Clear plate Av. 338 mm

TABLE V

Time of exposure	Mn 2939		Mn 2933		Density	Plate F
	Deflection	Density	Deflection	Density		
10″	177.5	0.35	251	0.20	0.4	2.55
	183.0	0.34	261.5	0.19		
	171.5	0.37	251.5	0.20	0.5	2.32
Mean	177.3	0.35	255.0	0.20	0.6	2.15
20″	117.5	0.53	190	0.32	0.7	2.20
	91.5	0.64	159.7	0.40	Mean	2.28
	81.2	0.69	149	0.43	Δe	0.228
Mean	96.7	0 62	166.2	0.38	Antilog	0.772
30″	57.7	0.84	110.2	0.56	Photographic Intensity	
	59.0	0.83	112.7	0.55		
	52.5	0.88	103.2	0.59		
					Mn 2939	100
Mean	56.4	0.85	108.7	0.57	Mn 2933	59.2

Clear plate Av. 400 mm.

TABLE VI

Time of Exposure	Mn 2939		Mn 3939		Density	Plate F.
	Deflection	Density	Deflection	Density		
	(Mean)		(Mean)			
10″	172.8	0.36	258.7	0.44	0.4	2.40
20″	81.7	0.69	152.7	0.42	0.5	2.13
30″	48	0.92	100.2	0.60	0.6	2.00
					0.7	2.00
					0.8	2.03
					Mean	2.11
					$\Delta\epsilon$	0.211
					Antilog	0.789
					Photographic Intensity	
					Mn 2939	100
					Mn 2933	61.5

Clear plate Av. 400 mm.

Giving the photographic intensity a value 100 for Mn 2939, the values were 56.9, 59.2 and 61.5 respectively for Mn 2933 for plates D, E and F.

Having constructed the blackening curves for plates A, B and C (Fig. 1) and obtained the mean $\Delta\epsilon$, a second plot was made with log *It* as one axis and deflection the other. This shows little scatter. The data are taken out of Table III. The calibration curve so obtained is shown in Fig. 2.

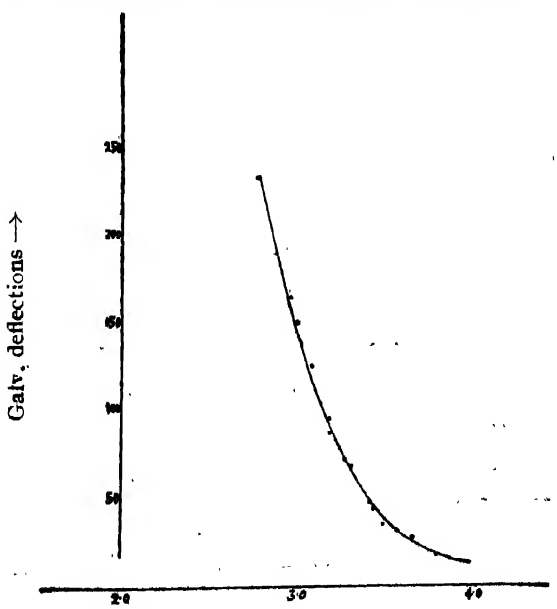

FIG. 2

Calibration curve

We now come to a stage of drawing intensity-calibration curves. As in all cases of high speed steel analysis exposures having been standardised at a fixed value of 25 secs., a parameter log I_{25} derived from log It-log 25 was used instead of log It in plotting intensity-calibration curves. Such a curve is shown plotted in Fig. 3, for plate D. The data are from Table VII.

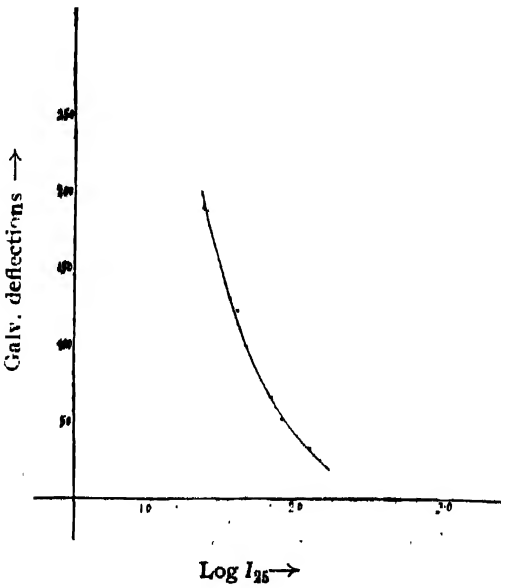

FIG. 3
Intensity calibration curve

TABLE VII

Time of exposure	Mn 2939		Mn 2933	
	Deflections	Log I_{25} (log It-log 25)	Deflections	Log I_{25} (log It-log 25)
Plate D. 10″	123	1.602	190.5	1.357
20″	53.3	1.903	100	1.658
30″	34.2	2.079	68.8	1.834
Clear plate Av. 338 mm.				
Plate E. 10″	177.3	1.602	255	1.374
20″	96.7	1.903	166.2	1.675
30″	56.4	2.079	108.7	1.851
Clear plate Av. 400 mm.				
Plate F. 10″	172.8	1.602	258.7	1.391
20″	81.7	1.903	152.7	1.692
30″	48.0	2.079	100.2	1.868
Clear plate Av. 400 mm.				

Verification of results.—

Suggestion arising out of Smith's paper for verification of variation with time of the intensity of emission was tried. No systematic variation was evident and no generalisation was possible as with Smiths. The result for plate D is tabulated in Table VIII.

TABLE VIII

Plate D

Exp. No.	Mn 2939		Mn 2933		Exp. No.	Mn 2939		Mn 2933	
	log I_{25}	I_{25}	log I_{25}	I_{25}		log I_{25}	I_{25}	log I_{25}	I_{25}
1	1.93	85.1	1.68	47.9	20	2.00	100.0	1.73	53.7
2	1.90	79.4	1.63	42.7	21	1.98	95.5	1.72	52.5
3	1.92	83.2	1.66	45.7	22	1.99	97.7	1.72	52.5
4	1.99	97.7	1.72	52.5	23	1.98	95 5	1.72	52.5
5	1.96	91.2	1.71	51.3	24	2.02	104.7	1.74	55.0
6	2.01	102.3	1.75	56.2	25	1.98	95.5	1.70	50.1
7	1.99	97.7	1.71	51.3	26	1.93	85 1	1.65	44.7
8	1.99	97 7	1.71	51.3	27	1.93	85.1	1.63	42.7
9	1.96	91.2	1.70	50.1	28	1.94	87.1	1.66	45.7
10	1.98	95.5	1.71	51.3	29	1.93	85.1	1.64	43.7

Av. on 100% basis.

100 :53.6

In a following table is shown the results of chemical analysis and the uses to which the alloys are put. Useful line pairs (Harrison, 1939) for purposes of calibration and for analysis and internal standards are shown in Tables IX and X.

TABLE IX

Chemical analysis

Sample No.	Use	Mn	Si	V	Cr	W
(3)	Standard	0.22	0.17	1.17	4.27	18.64
(4)	Standard ... —	0.20	0.22	1.22	4.42	18.84
(6)	Test alloy	0.21	0.16	1.22	4.35	19.05
(7)	Standard	0.20	0.14	1.26	4.40	19.83
(13)	Calibration	0.24	0.20	1.44	4.70	20.79
(30)	Standard	0.30	0.16	1.33	4.27	17.98
(42)	Standard	0.25	0.23	1.40	3.60	19.39

TABLE X

Line pairs

Calibration	Mn 2939.30	Mn 2933.06
Analysis	Mn 2933.06 Si I 2881 58 VII 3062.70	
Internal Standard	Fe I 2936.90 Fe II 2885.93 Fe II 3062.23	

Calibration curves.—

Two series of plates E and F are taken to include calibration patterns distributed evenly over the plate as also exposures from standards. Plate E includes exposures from a test alloy. Results from plates E and F are shown in Tables XI and XII. The results include the usual log R, ratio.

TABLE XI

Plate E

Mn Chart

Sample No.	Mn 2933 deflection	Fe 2937 Deflection	$R = \frac{Mn}{Fe}$	log R	log I_{Mn}	log I_{Fe}	log ratio of Ints. (+)
(3)	115.7	39.5	2.92	0.465	1.81	2.15	0.34
(4)	115.0	36.0	3.19	0.504	1 82	2.18	0.36
(7)	115.0	35 5	3.24	0.511	1.82	2.18	0.36
(30)	80.0	37.0	2.16	0.335	1.96	2 17	0.21
(42)	83.0	37.7	2.20	0.342	1.95	2.16	0.21

V Chart

Sample No	V3063 Deflection	Fe 3062 Deflection	$R = \frac{V}{Fe}$	log R	log I_V	Tog I_{Fe}	log ratio of Ints. (+)
(3)	66.7	35.5	1 88	0 27	2 03	2.18	0 15
(4)	49.2	29.7	1.66	0.22	2.11	2.21	0.10
(7)	42.7	27.7	1 54	0 18	2.14	2.22	0.08
(30)	48.7	28 2	1.73	0.24	2.11	2.21	0.10
(42)	42.5	29	1.46	0.16	2.14	2.21	0.07

TABLE XI (*contd.*)

Si Chart

Sample No.	Si 2881 Deflection	Fe 2886 Deflection	$R = \frac{Si}{Fe}$	log R	log I_{Si}	log I_{Fe}	log ratio of intensities (+)
(3)	187	150	1.25	0.097	1.56	1.68	0.12
(4)	158.5	135.5	1.19	0.075	1.65	1.74	0.09
(7)	162.2	132.5	1.22	0.086	1.64	1.75	0.11
(30)	142.7	136.5	1.04	0.017	1.71	1.73	0.02
(42)	131 5	133.7	0.98	0.01	1.75	1.74	−0.01

TABLE XII

Plate F

Mn Chart

Sample No.	Mn 2933 Deflection	Fe 2937 Deflection	$R = \frac{Mn}{Fe}$	log R	log I_{Mn}	log I_{Fe}	log ratio of intensities (+)
(3)	109.2	42.5	2.57	0.41	1.82	2 11	0.29
(4)	112.5	36.75	3.07	0.49	1.80	2.14	0.34
(7)	123.2	41 5	2 97	0.47	1.77	2 11	0.34
(30)	85 7	46 2	1 85	0 27	1.91	2 09	0 18
(42)	79.2	42.5	1.86	0.27	1.94	2.10	0 16

V Chart

Sample No	V 3063 Deflection	Fe 3062 Deflection	$R = \frac{V}{Fe}$	log R	log I_V	log I_{Fe}	log ratio of intensities (+)
(3)	62	34.2	1 81	0.26	2.01	2.15	0.14
(4)	50.2	31.5	1.595	0.20	2.08	2.17	0.09
(7)	55.2	35 7	1.55	0.19	2.05	2.14	0.09
(30)	49.2	34 0	1.45	0.16	2.08	2.15	0.07
(42)	37.5	26.7	1.405	0.15	2.13	2.20	0.07

TABLE XII (*contd.*)

Si Chart

Sample No.	Si 2881 Deflection	Fe 2886 Deflection	$R = \frac{Si}{Fe}$	log R	log I_{Si}	log I_{Fe}	log Ratio of intensities (+)
(3)	169.5	130.5	1.30	0.11	1 63	1 74	0.11
(4)	145 0	120.7	1.20	0.08	1.69	1.78	0.09
(7)	152.7	130	1.17	0 07	1 67	1.74	0.07
(30)	132.2	136.2	0 971	0.01	1.73	1.72	0.01
(42)	123 0	122.5	1.003	0.00	1.77	1.77	0.00

deflection due to analysis line to that due to internal standard and log I_{25} values and their differences derived from appropriate calibration curves E and F (not shown) for elements manganese, silicon and vanadium. Calibration curves were plotted with log R and log ratio of intensities against composition. Such curves for elements manganese, silicon and vanadium are shown plotted in Fig. 4. Discussion of results follows. Plate F includes a test alloy. From the appropriate intensity calibration curve (F), compositions of Mn, Si, and V were derived. Values are tabulated in Tables XIII, XIV and XV).

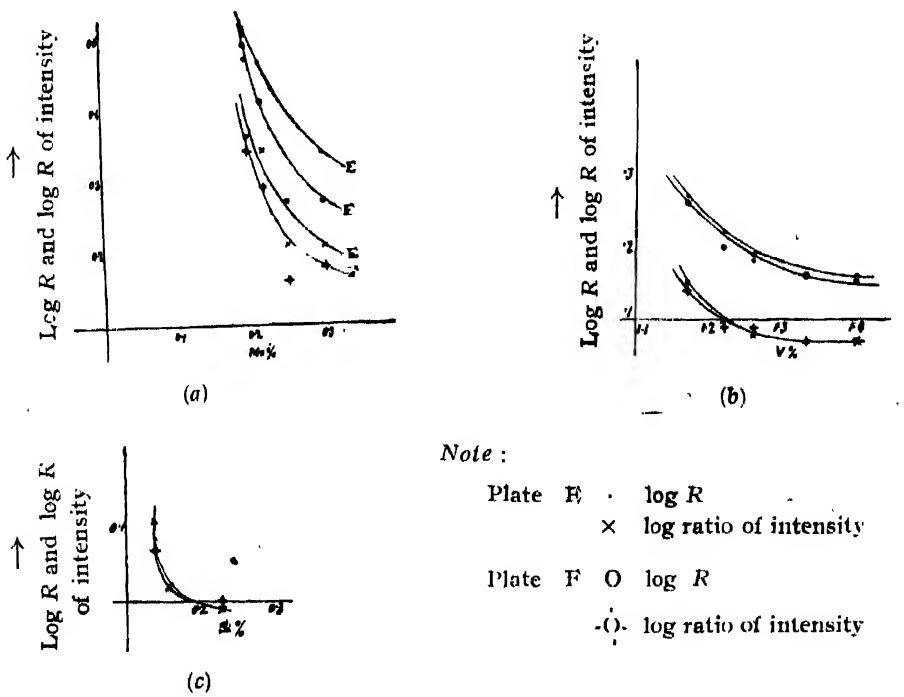

FIG. 4

TABLE XIII

Readings for Sample (6)

Mn

(0.21)

	Fe I 2937 Deflection	Mn 2933 Deflection	$R=\frac{Mn}{Fe\ I}$	log R	% (Calculated)	$I_{Fe\ I}$	Mn	log ratio of Ints.	% Calculated (b)	Diff. b Av$_b$ (d)	Sq. of Diffs. $\times 10^{-6}$
1	41.5	178.5	3.10	0.49	0.200	2.11	1.75	0.36	0.198	−0.004	16
2	40	122	3.05	0.48	0.200	2.12	1.77	0.35	0.200	−0.002	4
3	46.5	128.5	2.76	0.44	0.210	2.09	1.75	0.34	0.202	0.000	—
4	38	120	3.16	0.50	0.197	2.13	1.78	0.35	0.200	−0.002	4
13	45	128.5	2.86	0.46	0.205	2.10	1.75	0.35	0.200	−0.002	4
14	45.5	128	2.81	0.45	0.208	2.09	1.75	0.34	0.202	0.000	—
15	38.5	114.5	2.98	0.47	0.202	2.13	1.79	0.34	0.202	0.000	—
16	35	112	3.20	0.50	0.197	2.15	1.81	0.34	0.202	0.000	—
25	40	115	2.87	0.46	0.205	2.12	1.79	0.33	0.206	0.004	16
26	48.5	126	2.60	0.42	0.214	2.08	1.76	0.32	0.208	0.006	36
27	41.5	126.5	3.05	0.48	0.200	2.11	1.75	0.36	0.198	−0.004	16
28	52.5	135	2.57	0.41	0.218	2.06	1.73	0.33	0.206	0.004	16
					Σ2.456				Σ2.424		Σ112
					Mean 0.205				Mean 0.202		

Standard deviation. $\sigma=\sqrt{\frac{\Sigma d^2}{n}}$ = 1.5% of content.

Table XIV

Readings for Sample (6)
Si
(0.16)

Exp. No.	Fe II 2886 Deflection	Si I 2881 (Deflection)	$R=\frac{\text{Si I}}{\text{Fe II}}$	log R	% (Calculated)	$I_{\text{Fe II}}$	$I_{\text{Si I}}$	log ratio of Ints.	% (Calculated) b	Diff. b-Av. (d)	Sq of Diffs. $\times 10^{-6}$
1	126	150	1.19	0.08	0.139	1.75	1.68	0.07	0.140	−0.001	1
2	118	144.5	1.22	0.09	0.137	1.78	1.70	0.08	0.140	−0.001	1
3	119	149.5	1.255	0.10	0.136	1.78	1.68	0.10	0.140	−0.001	1
4	125	154	1.23	0.09	0.137	1.76	1.67	0.09	0.140	−0.001	1
13	131	157.5	1.20	0.08	0.139	1.74	1.66	0.08	0.140	−0.001	1
14	123.5	150.5	1.22	0.09	0.137	1.76	1.68	0.08	0.140	−0.001	1
15	118.5	149	1.26	0.10	0.136	1.78	1.68	0.10	0.140	−0.001	1
16	112.5	143.5	1.275	0.11	0.135	1.80	1.70	0.10	0.140	−0.001	1
25	134.5	159	1.18	0.07	0.140	1.73	1.66	0.07	0.140	−0.001	1
26	148	168	1.14	0.06	0.141	1.69	1.64	0.05	0.142	0.001	1
27	156.5	173.5	1.11	0.05	0.142	1.66	1.62	0.04	0.144	0.003	9
28	161.5	184	1.14	0.06	0.141	1.65	1.60	0.05	0.142	0.001	1
					Σ 1.660				Σ 1.688		Σ20
					Mean 0.138				Mean 0.141		

Standard deviation $\sigma=\sqrt{\frac{\Sigma n^2}{n}}$ < 1% of content.

TABLE XV

Readings for Sample (6)

V

(1.22)

Exp. No.	VII 3063 (Deflection)	Fe II 3062 Deflection	$R = \frac{\text{VII}}{\text{Fe II}}$	log R	% Calculated	I VII	I Fe II	log ratio of Ints.	% Calculated (b)	Diff. b-Av$_s$ (d)	Sq. of Diffs. $\times 10^{-6}$
1	75	50	1.50	0.18	1.271	1.96	2.07	0.11	1.203	−0.014	196
2	55	36	1.53	0.18	1.271	2.05	2.14	0.09	1.242	0.025	625
3	51	30	1.70	0.23	1.200	2.07	2.18	0.11	1.203	−0.014	196
4	50	29	1.72	0.24	1.190	2.07	2.18	0.11	1.203	−0.014	196
13	50	30.5	1.64	0.21	1.220	2.07	2.17	0.10	1.220	0.003	9
14	57	34.5	1.65	0.22	1.210	2.04	2.15	0.11	1.203	−0.014	196
15	48.5	32	1.515	0.18	1.271	2.08	2.16	0.08	1.280	0.063	3969
16	46.5	27	1.725	0.24	1.190	2.09	2.19	0.10	1.220	0.003	9
25	52	30.5	1.70	0.23	1.200	2.06	2.17	0.11	1.203	−0.014	196
26	52.5	53	1.59	0.20	1.238	2.06	2.16	0.10	1.220	0.003	9
27	58	34	1.70	0.23	1.200	2.04	2.15	0.11	1.203	−0.014	196
28	59	36	1.56	0.19	1.254	2.03	2.14	0.11	1.203	−0.014	196
					Σ 14.715				Σ 14.603		Σ 4993
					Mean 1.226				Mean 1.217		

Standard deviation $\sigma = \sqrt{\frac{\Sigma d^2}{n}}$ = 1.5% of content.

The standard deviations of 12 results are :

1.5 for Mn
< 1.0 for Si
1.5 for V.

The accuracy obtained is comparable to usual log *R* method.

DISCUSSION OF RESULTS.

In the calibration curves given by the two methods (Fig. 4) accuracy obtained was nearly constant. Calibration did not usually produce a single curve applicable to the two plates. This is the more remarkable in the case of manganese. For silicon, however, a single curve suffices. For vanadium two curves are given form sets of closely lying parallel curves.

On the application of background correction it can be said that no standard critique of spectral background evaluation exists; the emphasis is laid on having a clean plate with little background. Background calculation adds materially to time, a fact which militates against ordinary routine business. No attempt was thus made to calculate this factor. These facts point to a conclusion that plate calibration does not usually compensate for responses of plates. Nonetheless, the method described is simple and can be of general use. Further work might also give better corroborative results.

ACKNOWLEDGMENT.

The author gratefully acknowledges to the authorities of the Tata Iron Steel Co, Ltd. for permission to publish the paper.

R & C Laboratories,
TISCO. Jamshedpore

REFERENCES

Harrison, G. R., 1939, M.I.T., Wavelength Tables.
Smith, D. M., 1945, Collected papers, B.N.F.M.R.A.
Sp. phic Discussion Group, 1946, Suggested Definitions, Glass; ow.

A STUDY OF A WILSON'S CLOUD CHAMBER WITH LARGE SENSITIVE TIME AND OF ITS APPLICATION IN MEASURING RANGE OF α-PARTICLES EMITTED BY Pu^{239}

By H. P. DE

(*Received for publication, July 8, 1949*)

Plate XVI

ABSTRACT. A brief description of a cloud chamber with long sensitive time has been given. Three different methods of determination of sensitive time have been described. The range of particles emitted from a specimen supposed to contain Pu^{239}, has been determined.

A Wilson cloud chamber was constructed with a large sensitive time in order to photograph tracks of ionising particles emitted during events of rare occurrence. In the present instance, the object of investigation was the measurement of the track length of α-particles emitted from a precipitate supposed to contain transuranic elements. The precipitate was separated by Dr. S. D. Chatterjee from a sample of uranite, a very old uranium containing mineral. The U_{238} portion of the uranium by absorption of cosmic neutrons or neutron produced during spontaneous fission of U_{235}, is expected to produce transuranic elements according to the following reaction

$$U^{238} + n_0^1 \longrightarrow U^{239} \xrightarrow{\beta^-} Np^{239} \xrightarrow{\beta^-} Pu^{239}$$

Pu^{239} is an α-particle emitter, with a half life of 24000 years. The sample supplied was of such feeble radioactivity, that ordinary ionisation method was not sensitive enough to detect its activity. When the sample after dissolution was spread over photographic emulsion C_2 of Ilford, several tracks could be observed on developing the plate after two weeks exposure. It was thought worthwhile to use a portion of the sample as a source of α-particles to measure their track lengths in the Wilson cloud chamber, and by comparison with the track lengths of α-particles emitted under identical conditions from a polonium source in the same cloud chamber, to determine the track length of the unknown source under standard conditions of temperature and pressure, and if possible from such measurements to identify its origin.

In Table I, we give the energy and range of α-particles emitted from Pu^{239} and from two other α-particle emitter of approximately the same

TABLE I

Source	Energy of α-particles in Mev.	Range in cms at 15°C-760 mm of Hg	Half life
$_{84}Po^{210}$	5.298	3.842	140 days
$_{94}Pu^{239}$	5.144	3.675	24000 yrs.
$_{90}$Rd. Th^{228}	5.335	3.88	1.9 yrs.

track lengths. The aim of our investigation by the method employed was (1) to establish whether the precipitate supplied was α-emitter, and (2) if so, to establish the identity of the emitting source from the range of the α-particles measured.

The present paper contains a description (*i*) of the Wilson cloud chamber of long sensitive time constructed in the workshop of the Institute, (*ii*) of the methods used to determine the sensitive time during expansion and the pressure variation within the chamber and (*iii*) of the method used for measuring the length of the α-particle tracks emitted by the given precipitate in terms of that from polonium.

(*i*) *Cloud Chamber.*—The diameter of the chamber is 15 cms., depth 2 cms., expansion is produced by the displacement of a movable diaphragm closing the lower side of the chamber; the latter consists of a brass plate fixed at the centre of a rubber diaphragm. The rubber sheet is attached by means of the plate to a lever actuated by a cam and which is put under compression by a suitable steel spring. The under side of the diaphragm is filled with water on which a circular block of paraffin floats, such that the upper side of the paraffin is on a line with the water level—in fact, during expansion very little air current is produced.

The sensitive time is prolonged by producing first a rapid expansion to attain the necessary degree of supersaturation, and then to maintain the degree of supersaturation by further slow expansion. This end was achieved by cutting the slope of the cam controlling the expansion as shown in the diagram (Fig. I*a*); simultaneous with the movement of the diaphragm, air in the lower chamber gets compressed, so a flow of air takes place through the orifice of the stopcock producing a prolongation of the state of supersaturation as desired. To produce the desired effect, opening of the stopcock needs adjustment [figure of the Chamber and manometer, Figs. (*a*) and (*b*)].

A detailed study of the change of pressure was made by a manometer as described below. The accompanying figure (Fig. I*b*) gives a detail of the manometer which is attached to the cloud chamber. A small circular rubber membrane is cemented to the end of a side tube connected with the mano-

meter and a small mirror M movable about axis X has its other end resting on the centre of the rubber membrane : a beam of light reflected from the

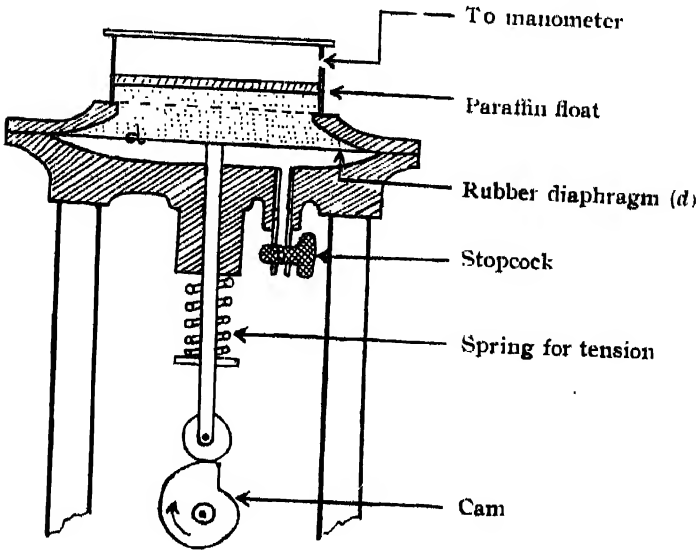

FIG. 1(*a*)

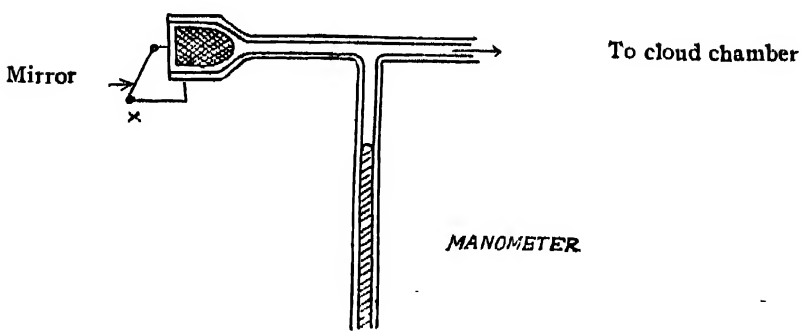

FIG. 1(*b*)

mirror falls on a scale placed at a distance of about 3 metres from the mirror, in order that a small change in the pressure in the expansion chamber may be determined with fair degree of accuracy. With this arrangement, a relative change of pressure up to about one per cent of the total change which was about 20 cms. of Hg could be determined. It may be added that we are not interested in the absolute value of the pressure at different moments, but only on the variation of pressure as the expansion progressed. The image of the spot of light is photographed with a standard Cine camera taking 24 pictures per sec. on a 35 mm film, thus changes of pressure can be observed at intervals of 0.04 sec. It may be argued that as there is a time lag between the pressure attained within the chamber and that indicated by the motion of the rubber membrane attached to the manometer, the latter does not, therefore, record the actual pressure in the chamber at the time of record. The lag being a constant common

factor, the motion of the spot of light does give a true picture of the change of pressure with time, within the chamber. A plot of the time variation of the image or the spot of light has been given in Fig. 2.

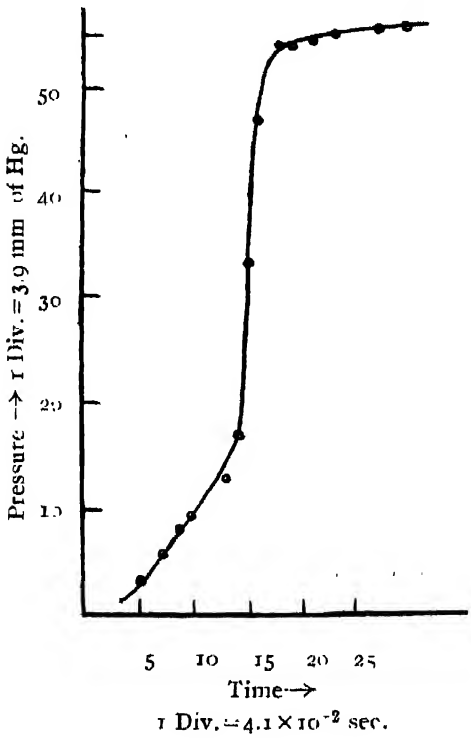

FIG. 2

(ii) Sensitive time —The study of sentitive time has been described in a paper by Hazen (1942) where details about the sensitive time and its dependence on various factors has been fully discussed ; here only the relevant points in the paper are discussed and utilized.

The sensitive time can be increased by (1) increasing the time for completion of the expansion and (2) also by increasing the ratio of the volume to the surface of the cloud chamber. Time duration of the expansion must be of the same magnitude as the sensitive time before the latter is appreciably lengthened. In our case, this condition is fulfilled as the time duration has been lengthened by the arrangement already described above; in addition, by increasing the ratio of volume to surface i.e. by using chamber of greater depth, the sensitive time can be increased ; but then it is not possible to illuminate the whole depth of the cloud chamber ; in our case the ratio of volume to the surface was, slightly greater than unity.

Actual period over which the state of supersaturation persisted was measured by three independent methods, each method yielding a sensitive time of about one second.

(a) In the first method a simple experimental device is adopted for roughly estimating the sensitive time of the cloud chamber. A weak radioac-

Fig. a.

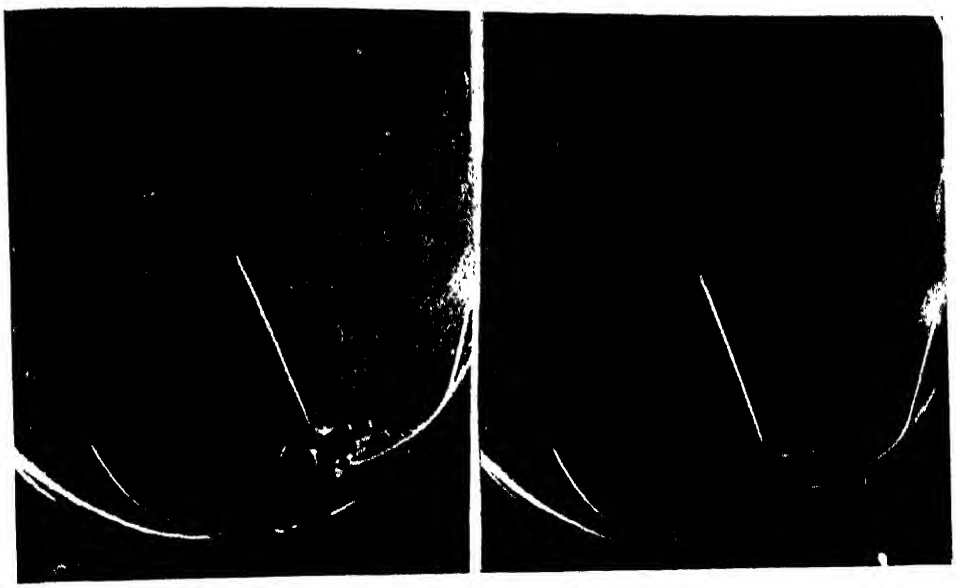

Stereo-picture of α-particle emitted from Pu^{239}.

Fig. b.

Stereo-picture of a diffuse long-range α-particle track, possibly emitted from the other isotope of Pu. Only one picture was recorded out of about 8000 photographs.

tive source is placed inside a massive block of lead, 10 cms. from the cloud chamber; the lead block contains a cylindrical hole of 0.5 cm. diameter; in front of this lead block a massive lead wheel, 4 cms. thick, revolves slowly at a rate of 1 revolution in 11.5 secs. The rotating wheel contains a 4 mm hole and the wheel is so oriented that in a complete revolution the hole in the wheel comes once in line with the hole in the block of lead. On the wheel there is a graduation at intervals of 5° marking with 0, the position of alignment of the two holes.

Operation for expansion was started by rotating the handle attached to the cam controlling the motion of the diaphragm of the cloud chamber, for different possitions of the wheel with respect to the fixed 0 mark, named as the point of observation in the Fig. 3. Thus 0 in the table shows that the operation starts when holes are in alignment, expansion corresponding to 5° means that after 0.16 sec. alignment occurred between two holes, and so on.

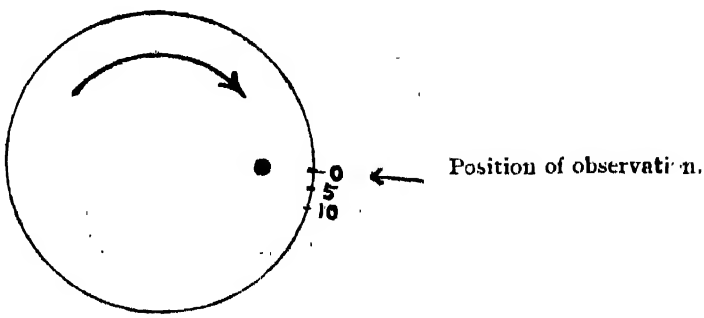

FIG. 3(*a*)

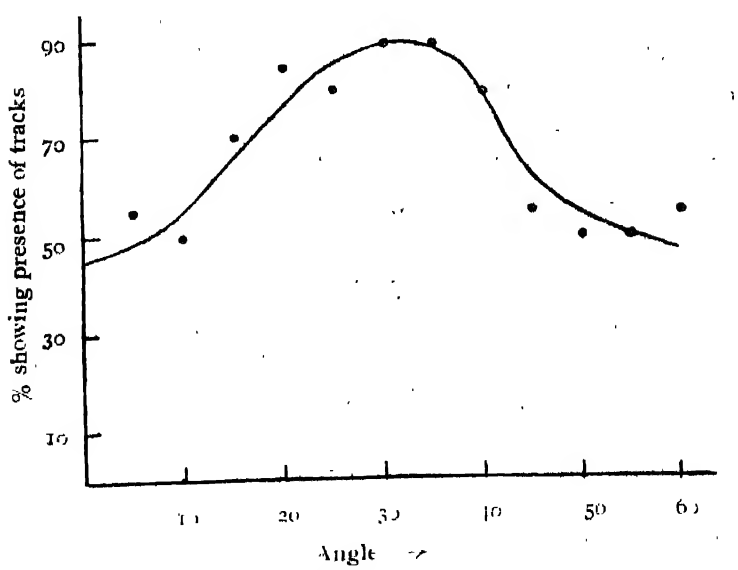

FIG. 3(*b*)

Table II, along with the graph, shows that for an angular width of about 25° on the lead wheel, the chamber must have remained in a state for

receiving the impression of ion trails. Now, 25° on the lead wheel corresponds to 0.8 sec. — the sensitive time of the cloud chamber.

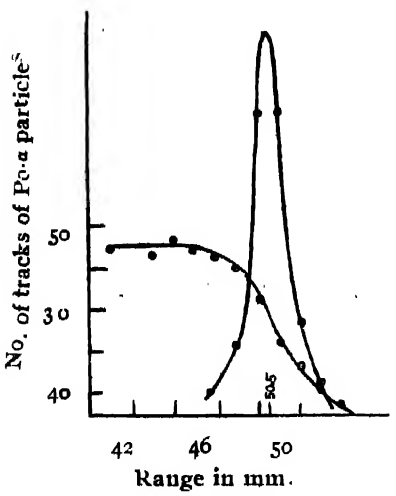

FIG. 4

TABLE II

Angle in degrees	Percentage of total expansion giving the presence of tracks
0	45
5	55
10	50
15	70
20	85
25	80
30	90
35	90
40	80
45	55
50	50
55	50
60	55

(*b*) In the second method, the sensitive time was estimated from the cinematographic picture extending over the period taken to perform the act of expansion; photographs are taken of several expansion at the rate of 24 pictures per sec. During the course of one of the expansions, two different tracks at different places in the chamber were observed after an interval of 20 pictures; this observation leads to the conclusion that during above period at least the chamber must have remained sensitive. It was noticed that the number of droplets formed per c.c. in the expanded volume was never more than 1 or 2 on an average; a larger number of droplets per c.c. generally shortens the sensitive time by denuding the volume of supersaturated vapour by causing a growth in the size of the droplets at the expense of the state of supersaturation.

(*c*) In the third method, William's formula, connecting the sensitive time and the number of cosmic particles recorded per expansion, was utilized in finding the sensitive period of the chamber. Average number of cosmic ray tracks per expansion is given by the expression

$$t_s.j.x.d$$

where j is about 0.03 — number of cosmic particles per cm^2 per second.

d = diameter of the chamber in cm.

x = depth of illumination

t_s = sensitive time.

Observation extending over a thousand expansions revealed that on an average 0.5 was the number of cosmic ray track per expansion; since $d=13$ cms., $x=1$ cm., on substitution, the sensitive time comes out to be a little over one second.

(*iii*) *Measurement of length of α-particle tracks.*—The main objective for the construction of this chamber was to find the range of the α-particles emitted from a precipitate extracted from an uranium ore of Indian origin and supposed to contain plutonium 239. Usually a very small quantity of Pu is found to be present in the ore. In the method of separation employed Pu was extracted with a rare earth tracer from the ore; a small fraction of the extract was smeared on the surface of a brass disc placed inside the chamber. The content of Pu on the specimen was so small that out of 2,000 photographs taken, only 36 tracks of α-particles emitted from the source were obtained; amongst them were some tracks which were diffused and some of them ended outside the region of illumination.

Some of these tracks are reproduced in Plate XVI.

In order to obtain a correct length of the tracks, the stereoscopic pictures were built up in space with the same camera arrangement used for photographing them under identical conditions. By this method the lengths of α-particle tracks as built up in space were determined.

TABLE III

Range in mm.	No. of particles
43	44
44	45
45	43
46	47
47	44
48	42
49	40
50	32
51	21
52	16
53	10
54	6

Similarly, a large number of photographs of tracks of α-particles emitted from polonium source were taken under identical conditions. These tracks

were also built up in space and from the measurement of their lengths an estimate of the average track length was obtained by using the above method.

A comparison of this average length of α-particle track from Po as deduced from graph was made with the length of the longest Pu α-track. (FIG. 4).

This method was found necessary since total number of plutonium α-particle tracks were only 88. With such a meagre number, extra-polation was not possible without incurring a large amount of statistical error. (*vide* Plates)

The results on measurement of the track lengths are given below:

Average range of Po-α = 50.5 mm.

Maximum range of Pu-α = 46 mm.

Whence the range of Pu-α = 3.5 cms. under normal conditions.

The range thus determined gives a value smaller than that found by other authors, but as no other α-particle of this range have been observed for α-particle emitting sources belonging to the three principal radioactive series occurring in nature, the observed particles may be attributed to Pu^{239}. In the Radio Chemical laboratory of the Institute, attempts are being made to isolate this element from a larger quantity of pitchblende obtained from Canada. When the isolated precipitate is ready the investigation with the Wilson chamber will again be resumed.

ACKNOWLEDGMENT

In conclusion it gives a great pleasure to the author to express his sincere thanks to the Director of the Institute, Dr. D. M. Bose, M.A., Ph.D., F.N.I., for his valuable discussion and help in writing this paper. In building up the details of the apparatus the author wishes to express his sincere thanks to Dr. J. P. Sircar for his constant help and mature suggestions towards improvement. Thanks are also due to Mr. S. P. Dutt, M.Sc., for his assistance during photographic work.

BOSE INSTITUTE,
93, UPPER CIRCULAR ROAD, CALCUTTA.

REFERENCE

Hazen, 1942, *Rev. Sc. Inst.* **18**, 217.

INDIAN TROPICAL STORMS AND ZONES OF HEAVY RAINFALL

By S. MULL and Y. P. RAO

(*Received for publication, March 22, 1949*)

ABSTRACT. The accepted explanation for the heavy rainfall in southwest monsoon depressions in India on the basis of frontal structure is not supported by radio-sonde data. An alternative explanation on the basis of convergence derived from the isobaric patterns is offered. It has also been applied to satisfactorily explain the distribution of heavy rain in the post-monsoon depressions.

It is well known that in the southwest monsoon depressions, widespread and heavy rain is confined to the southwest sector. This was explained by Ramanathan and Ramakrishnan (1944) as due to the ascent of old monsoon air over the fresh monsoon air as illustrated in Fig. 1. According to them the fresh monsoon air behaves as a cold airmass relative to the old monsoon air. A front therefore develops in the Western sector between the two air masses and it slopes up towards the south. Consequently the rainfall due to the upglide of the old monsoon air occurs in the southwest sector of the depression.

Examination of radio-sonde ascents in the southwest sector, however, showed that the existence of the front was doubtful as no marked temperature discontinuities were noticed. A depression devoloped in the NE Bay of Bengal on 1. 7. 45 and intensified into cyclonic storm by 0230 hrs. G.M.T. of 2. 7. 45. Widespread and heavy rain occurred in the southwest quadrant of the storm as will be seen from Fig. 2, which shows the isobaric distribution

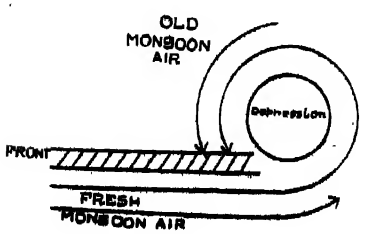

FIG. 1

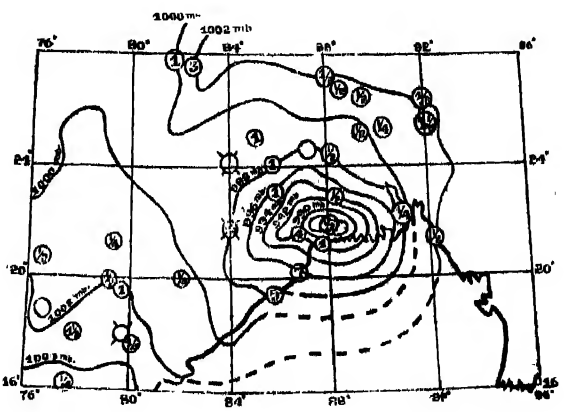

FIG. 2

Rainfall shown in circles.

at 0200 hrs. G.M.T. of 2. 7. 45 and the rainfall amount in the preceding twentyfour hours. Cuttack situated in the southwest section, recorded seven inches of rain during the period. In Fig. 3 is given the radio-sonde ascent of 1300 hrs. G.M.T. of 1. 7. 1945. It will be seen that the ascent curve does not show the existence of two airmasses and hence the above explanation does not seem to be satisfactory. An alternative explanation for the rainfall in the southwest sector of monsoon depressions is given below :—

The equation for gradient wind is :

$$V = \frac{1}{\rho\lambda^2}\frac{\partial p}{\partial n} + \frac{1}{\lambda}\frac{V^2}{r} \qquad \ldots \quad (1)$$

where V is the gradient wind and the other terms have their usual significance. r is positive for anticyclonic flow and negative for cyclonic. We proceed to find the horizontal divergence in the area $ABCD$ (Fig. 4) where AB and CD are two successive isobars of values p_0 and $p_0+\Delta p$ and AC and BD are respectively the wedge and trough lines. Due to the gradient flow which is along the isobars, the horizontal divergence, termed as longitudinal divergence by Bjerknes and Holmboe (1944) is :

$$V_2BD - V_1AC = \left[\frac{1}{\rho_2\lambda_2}\left(\frac{\partial p}{\partial n}\right)_2 BD - \frac{1}{\rho_1\lambda_1}\left(\frac{\partial p}{\partial n}\right)_1 AC\right] + \left[\frac{1}{\lambda_2}\frac{V_2^2}{r_2}BD - \frac{1}{\lambda_1}\frac{V_1^2}{r_1}AC\right]$$

$$= \Delta p\left[\frac{1}{\rho_2\lambda_2} - \frac{1}{\rho_1\lambda_1}\right] + \left[\frac{1}{\lambda_2}\frac{V_2^2}{r_2}BD - \frac{1}{\lambda_1}\frac{V_1^2}{r_1}AC\right] \qquad \ldots \quad (2)$$

Subscript 1 and 2 refer respectively to the values at AC and BD. As AC is to the north of BD, $\lambda_1 > \lambda_2$, while r_2 which refers to cyclonic flow is negative. The first term is therefore divergent while the second term is convergent. We have neglected variations in density which are generally small, particularly in barotropic conditions as in tropics. It can be shown that the net flow is longitudinally convergent when

r_1 is the critical radius of curvature for anticyclonic flow

r_2 = 900 kms

$\frac{dp}{dn}$ $\frac{1}{150}$ mb/km

$AC = BD = 300$ kms

and λ_1 and λ_2 correspond respectively to 25°N and 15°N.

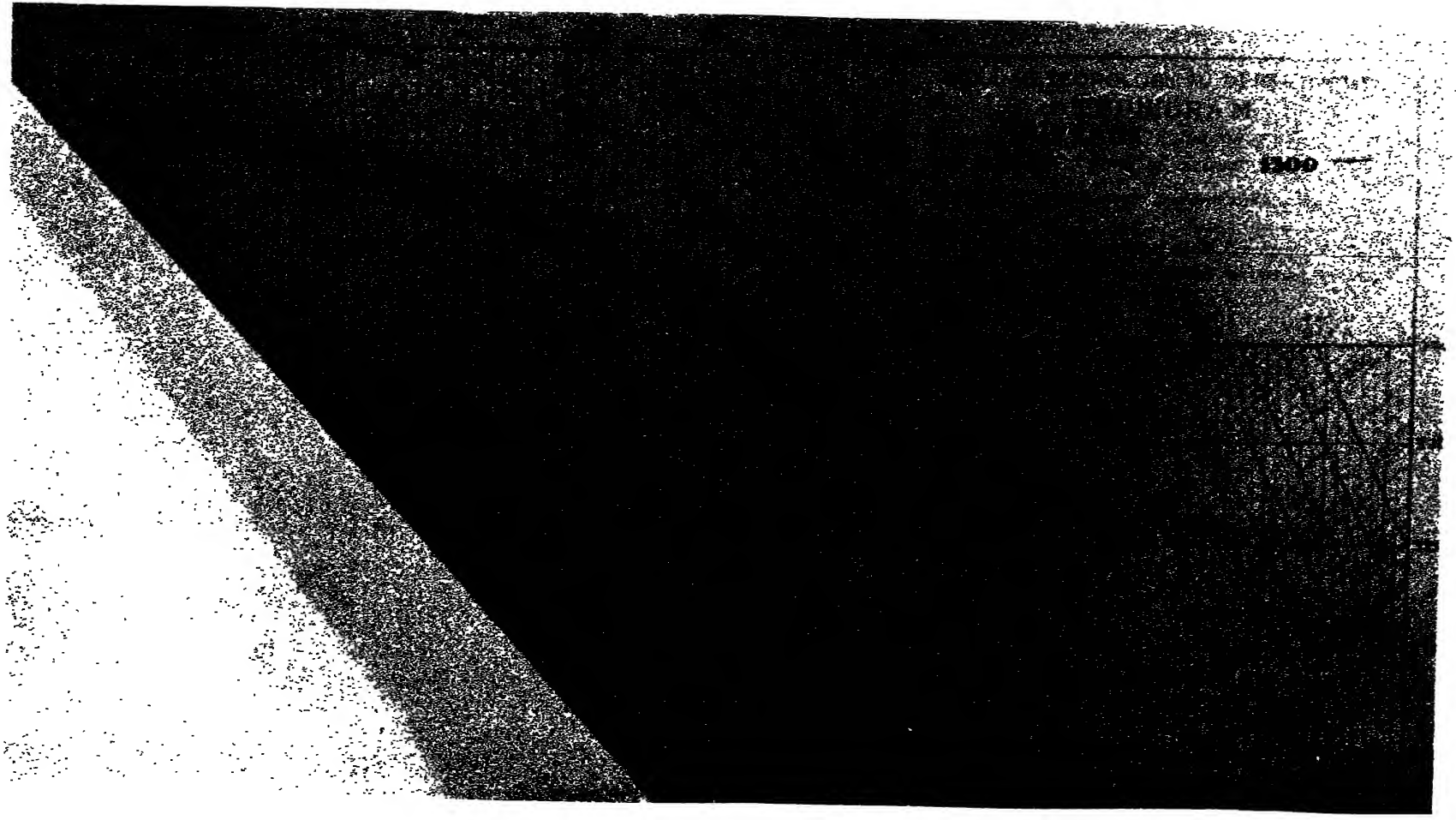

Fig. 3.

The above values of variables have been so chosen as to approximate to the conditions in the SW monsoon depressions in India. Thus under such conditions the airflow is longitudinally convergent from a high to low and by similar reasoning longitudinally divergent from a low to high.

Let us now briefly consider the case when the air flow is from east to west. As before, the divergence is:

$$V_2.BD - V_1AC = \left[\frac{1}{\rho_2\lambda_2}\left(\frac{\partial p}{\partial n}\right)_2 BD - \frac{1}{\rho_1\lambda_1}\left(\frac{\partial p}{\partial n}\right)_1 AC\right] + \left[\frac{1}{\lambda_2}\frac{V_2^2}{r_2}BD - \frac{1}{\lambda_1}\frac{V_1^2}{r_1}AC\right]$$

$$= \Delta p\left[\frac{1}{\rho_2\lambda_2} - \frac{1}{\rho_1\lambda_1}\right] + \left[\frac{1}{\lambda_2}\frac{V_2^2}{r_2}BD - \frac{1}{\lambda_1}\frac{V_1^2}{r_1}AC\right] \quad \ldots \quad (2)$$

In the present case λ_1 corresponds to a more southerly latitude than λ_2 and hence $\lambda_1 < \lambda_2$. r_2 is negative as it corresponds to cyclonic circulation. Thus for easterly flow from a high to a low both the terms are negative and there is longitudinal convergence. Similarly in an easterly current the air flow is divergent from a low to a high. The above points are illustrated in Fig. 6.

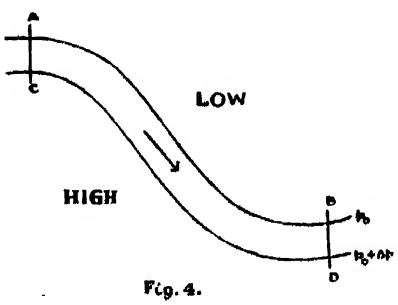

Fig. 4.

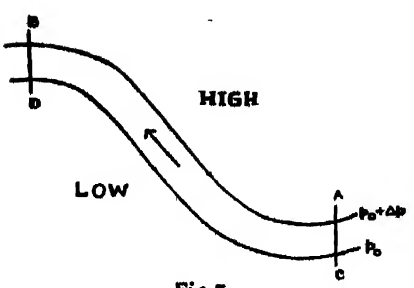

Fig. 5.

FIG.

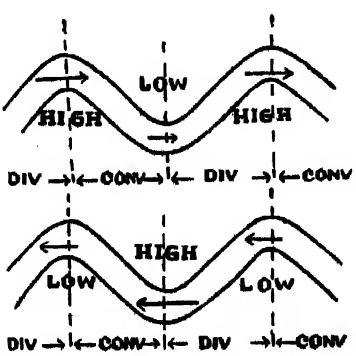

FIG. 6

Bjerknes and Holmboe (1944) have termed the divergence due to the cross-isobar wind component which arises owing to tangential acceleration as Transverse Divergence. V_t, the cross isobar component, is given by

$$V_t = \frac{1}{\lambda} v \frac{\partial v}{\partial s}$$

where s is measured along the isobar. The flow across the isobar is thus :

$$\int_{v_1}^{v_2} v_t . ds = \int_{v_1}^{v_2} \frac{1}{\lambda} v \, dv = \tfrac{1}{2}\left[\frac{v_2^2}{\lambda_2} - \frac{v_1^2}{\lambda_1} \right] \quad \ldots \quad (3)$$

This is the transverse flow at an isobar. The transverse divergence in the area $ABCD$ will be given by the difference between the flow at two successive isobars. This will be zero when the successive isobars are parallel. We may compare the quantity

$$\tfrac{1}{2}\left[\frac{v_2^2}{\lambda_2} - \frac{v_1^2}{\lambda_1} \right]$$

with the second term

$$\left[\frac{v_2^2}{\lambda_2} \frac{BD}{r_2} - \frac{v_1^2}{\lambda_1} \cdot \frac{AC}{r_1} \right]$$

in equation (2). BD or AC and r_2 or r_1 are generally comparable quantities. Hence BD/r_2 and AC/r_1 will not be too small. For instance, in the numerical example given previously $-(BD/r_2) = \frac{1}{3}$. As r_2 has opposite sign to r_1 in the flow from a trough to a ridge or viceversa, the term for cross-isobar flow and the cyclostrophic component of longitudinal convergence (*i.e.* second term of equation (2) will respectively represent the sum and difference of nearly equal terms. Hence the transverse divergence (which is given by the difference between the cross-isobar flow at two successive isobars) may be neglected as compared with the longitudinal divergence (to which the main contribution is due to the cyclostrophic component). If the gradient is less in the ridges and more at the troughs, the difference between v_2^2 and v_1^2 will be negligible and hence in such cases transverse divergence can be neglected. As in tropical cyclones, the isobars open out at the ridges and come closer at the troughs, we are justified in taking account of the longitudinal divergence only.

We now consider the longitudinal divergence in a system of closed isobars moving west. $ABCD$ is a line dividing the low into eastern and western halves, (Fig. 7). The net divergence in the eastern half is :

$$v_1 AB - v_2 CD = \Delta p \left[\frac{1}{\rho_1 \lambda_1} - \frac{1}{\rho_2 \lambda_2} \right] + \left[\frac{v_1^2}{\lambda_1} \frac{AB}{r_1} - \frac{v_2^2}{\lambda_2} \cdot \frac{CD}{r_2} \right] \quad \ldots \quad (4)$$

Here subscripts 1 and 2 refer respectively to AB and CD and $\lambda_1 > \lambda_2$. If the consecutive isobars are concentric, both the terms are negative and there

is convergence in the eastern half and divergence in the western half. But in a depression moving to west $r_1 > r_2$ and this can cause V_1 to be sufficiently greater than V_2 for the second term to become positive. In such cases, the longitudinal divergence is probably small enough to be neglected. Where this difference in the radii of curvature r_1 and r_2 is not sufficient to make the second term compensate the first, in equation (4), it is necessary, as shown by Bjerknes and Holmboe (1944), that the circular isobars should be closer to the south than to the north for the resulting flow to be non-divergent.

The isobaric pattern with a southwest monsoon depression is shown in Fig. 3. The airflow between the two isobars P_1 and P_2 is from anticyclonic

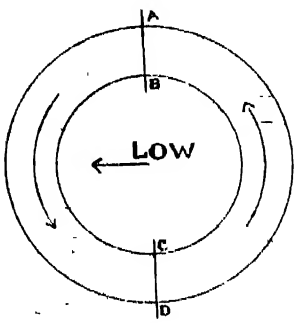

FIG. 7

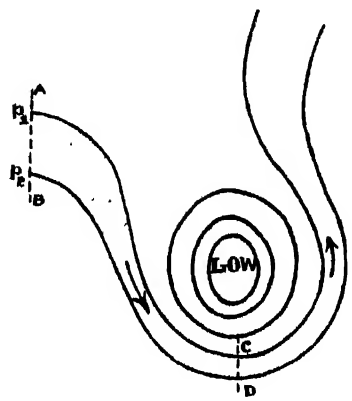

FIG. 8

curvature at AB to cyclonic curvature at CD and hence convergent, as shown before. It is apparent that the airflow between the isobars P_1 and P_2 is not appreciably convergent in any other portion. The values of the various variables, used for discussion in the earlier para, correspond to the conditions met in this case. But owing to the movement of the whole pattern to the west along with the motion of the depression, the curvature of the airpath is, however, greater than that indicated by the isobars. Correspondingly the contribution of the second term in equation (2) is greater and hence the longitudinal convergence is also greater. For reasons explained in the discussions of longitudinal divergence in closed isobars, the flow in the portion of the closed isobars seems non-divergent. Probably this is partly obtained by the slight crowding of isobars to the south in the closed system. As we recede away to the south from the centre of the depression, the perturbation, due to the depression on the normal west to east isobars, decreases and hence the convergence also diminishes. It will thus be seen that the area of maximum convergence is in the southwest sector of the depression but somewhat away from the centre. As convergence leads to rainfall, the occurrence of widespread and heavy rain in the southwest sector of southwest monsoon depressions is explained. As an illustration we give in Fig. 9 the isobaric map of 0230 hrs. G.M.T. on 30. 6. 1930, the rainfall distribution during the

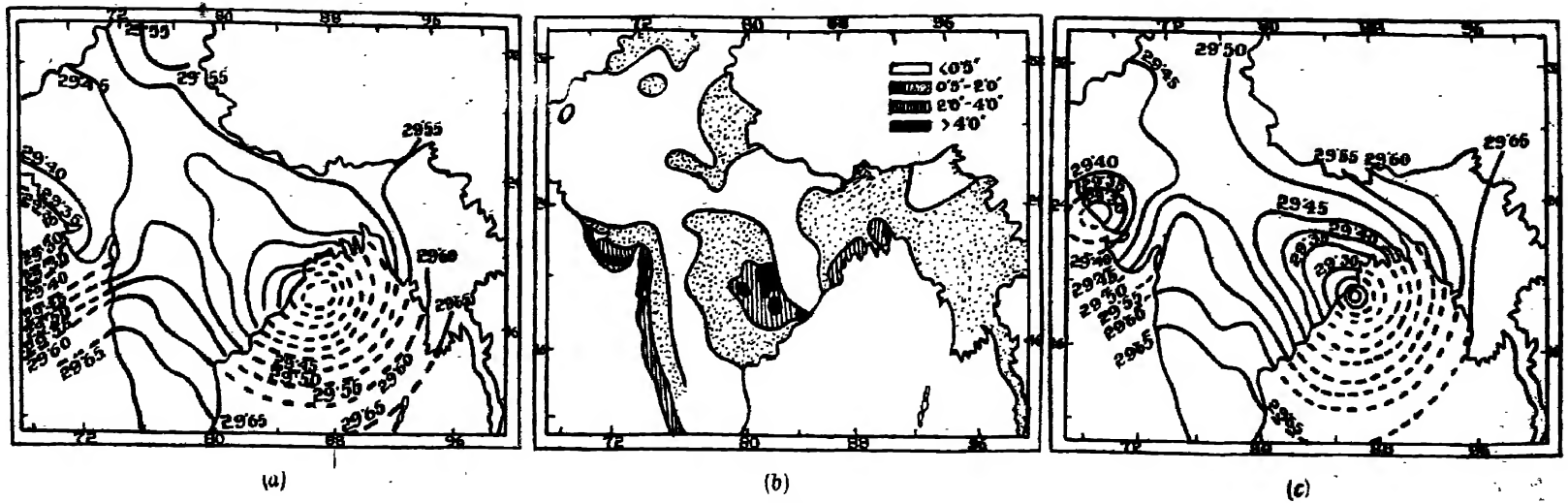

FIG. 9

(*a*) Isobars at 0800 Hrs. I.S.T. of 30.6.1930.

(*b*) Rainfall from 0800 Hrs. I.S.T. of 30.6.1930 to 1.7.1930.

(*c*) Isobars at 0800 Hrs. I.S.T. of 1.7.1930.

following twentyfour hours, and the isobaric map of 0230 hrs. G.M.T. on 1. 7. 1930.

In the post-monsoon depressions, the northeast sector gets the heavy rain. The distribution of isobars with such a depression is shown in Fig. 10. By reasoning similar to the preceding case, it can be seen that the area of convergence is only in the northeast sector, and hence heavy rain is confined to that area.

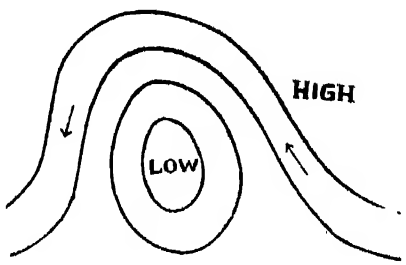

FIG. 10

The above discussion brings out how the rainfall distribution in tropical depressions affecting India can be explained from the zones of convergence derived from the isobaric patterns.

REGIONAL METEOROLOGICAL CENTRE,
NAGPUR.

REFERENCES

Bjerknes, J. and Holmboe, 1944, *Journal of Meteorology*, **1**, 1.

Ramanathan, K. R. and Ramakrishnan, K. P., 1944. *Ind. Met. Memoirs*, **26**, Pt. II.

THE EMISSION SPECTRUM OF BISMUTH IODIDE

By P. TIRUVENGANNA RAO

(*Received for publication, February, 7,1949*)

Plate XVII

ABSTRACT. The spectrum of bismuth iodide has been photographed in emission in a high frequency discharge using a Fuess spectrograph. A new band system between λ 5900−λ 5600, consisting of four marked groups of bands, some of which are degraded towards the red, is obtained in addition to the band system between λ 4300−λ4150, analysed by Morgan. Vibrational analysis of this new system has led to the determination of the following constants

$$w_e' = 195.0 \qquad w_e'' = 167.9$$

$$\nu_e = 17216.0 \quad x_e'w_e' = 1.0 \qquad x_e''w_e'' \sim 0.3$$

The lower state is considered common to both the systems. By analogy, the new system may correspond to the low frequency system observed in the other bismuth halides The electronic states in the halides of bismuth are briefly discussed

INTRODUCTION

In the course of a series of investigations on the molecular spectra of the halides of the elements of groups IV and V of the periodic table, Howell and Rochester (1934) reported that high frequency discharges through the vapours of the halides of lead and bismuth excited in each case large systems of bands degraded towards the red. Later, Howell (1936) published the analysis of a band system between λ5100−λ4150, attributed to the diatomic molecule, BiF. The band spectra of BiBr, BiCl, BiF and BiI have been examined by Morgan (1936) in absorption and a vibrational analysis given for each of the observed systems. For BiBr, two systems for each of the isotopes $Br^{79}Cl^{35}$ and $Br^{81}Cl^{37}$ with origins at λ 4045.7 A and λ 4869.1 A, were analysed. In BiCl, a band system lying between λ 4000−λ 3600 has been found for each of the isotopes Cl^{35} and Cl^{37} in addition to the system at λ5500−λ4300 reported by Saper (1931). The vibrational analyses in the above two cases have been confirmed by the respective isotope shifts. One band system between λ4900 and λ4150 for BiF has been analysed. The analysis of this system is entirely in agreement with that reported by Howell for BiF in emission. Morgan also reports another system for BiF, on the shorter wave-length side of the above system, but no analysis is given as it is too weak for measurement. Rochester (1937) reports a triplet system

for BiF in the ultraviolet between λ 3050−λ 2250 with wide multiplet separations of 7300cm^{-1} and 4800cm^{-1}. In the case of BiI, only one band system between λ 4300−λ5150 has been observed. It corresponds to the high frequency system observed in the other bismuth halides. The bands, which are about 22 in all, are arranged in marked sequences but the direction of degradation of the bands is uncertain. The following quantum formula has been derived by Morgan to represent the bands:

$$\nu = 23388.9 + (198.6u' - 1.44u'^2) - (163.9u'' - 0.31u''^2)$$

Morgan suggested that the low frequency system, corresponding to the one observed in the other halides of bismuth, might have been either lost in the overlapping diatomic bismuth bands occurring in the same region, or altogether absent because of the probable decomposition of BiI, at the high temperatures used in his experiment. No previous work on the emission spectrum of this molecule appears to have been published so far.

As a continuation of his work on the molecular spectra of such a series of molecules as TlI, PbI the author investigated the emission spectrum of BiI, excited by a low-power H.F. Oscillator. A new band system attributed to the diatomic molecule BiI, which corresponds to the low frequency system observed in the other bismuth halides has been obtained in addition to the system λ 4300−λ 4150 reported by Morgan in absorption. The object of this paper is to report the analysis of the new system.

The experimental method for this investigation also is the same as the one employed by the author in the case of TlI and described in detail elsewhere (Rao and Rao, 1949). Working with the iodides of heavy elements, it has been the experience of the author that the emission bands and continuum of iodine, which is invariably present in the discharge tube as a decomposition product, could be eliminated by a careful heating of the substance and by giving minimum exposure with a sharply focussed spectrograph. With BiI, continued heating was found necessary for maintaining a characteristic discharge which is bluish violet in colour. In photographing the spectrum a Fuess glass spectrograph was mainly used. The advantage of using this instrument was the short interval of time during which optimum conditions for reproducing the spectrum could be maintained. An exposure of 5 minutes duration was found sufficient using Kodak-panchromatic plates. In addition to the bands, some bismuth lines were also excited. Measurements were made on a Hilger comparator and were reduced to wavelengths by using iron arc standards. Band head data obtained from different plates seldom differed by more than 2 wave-number units.

DESCRIPTION OF THE SPECTRUM

The spectrum is reproduced in two strips in Figs. *a* and *b* (Plate XVII). Strip *a* is an enlargement of the system between λ5900−λ5650 newly obtained

in the present investigation. The bands are arranged in four distinct groups. Some of the bands appear clearly red-degraded while the direction of degradation of some others is uncertain. Strip *b* is a reproduction of the system between $\lambda 4300 - \lambda 4150$ analysed by Morgan. The bands are clearly red-degraded, while the sequence degradation is towards the violet. But Morgan reports that the direction of degradation of these bands obtained by him in absorption is uncertain. This system is reproduced here to show that the bands appear more prominently in emission than in absorption.

Table I gives the wavelength, intensity and other data of the new system.

TABLE I

(Bismuth iodide bands)

Wavelength	Int.	Wavenumber	Classification	Obs. – Calc
5859.9	6	17060.4	0,1	−1.6
50.3	5	17088.4	1,2	0.1
41.2	4	17115.0	2,3	1.8
33.2	2	17138.5	3,4	1.8
5802.2	10	17230.1	0,0	0.8
5794.4	4	17256.6	1,1	1.6
37.8	8	17423.5	1,0	1.2
30.2	4	17446.6	2,1	0.6
23.6	1	17466.7	3,2	−1.6
5676.6	4	17611.3	2,0	−2.0
68.9	3	17635.2	3,1	0.2

Vibrational Analysis and Intensity Distribution

The bands are arranged in four marked groups. The relative intensities of bands in each group suggest that each group is obviously to be regarded as a sequence. Intensity considerations point to the group of bands at λ 5800 as being the $\Delta v = 0$ sequence. The group lying on its longer wavelength side is then to be identified as the (0,1) sequence. From intensity considerations the most intense band in this sequence is to be classified as the (0,1) band. The intensities of the higher sequence members gradually fall off. A similar feature is observed in all the other sequences. Some of the higher sequence members present a line like appearance as their direction of degrada-

tion is uncertain. The (0,0) band appears clearly red degraded while the direction in which the (1,0) band is degraded is uncertain. It is to be noted that in all cases, the sequence degradation is towards the violet, though some of the bands are clearly degraded towards the red. The vibrational matrix shown in Table II is built up to include all the band heads. As the number of bands observed in the system is small, only two $\Delta G(v'')$ values are obtained and of these two the first is probably more reliable. Since the direction of degradation of some of the bands is uncertain, the breadth of such bands being of the order of 5 wavenumber units, the lower state vibrational frequency suggested here may be regarded as approximately equal to that of the other system analysed by Morgan. Hence the lower state appears to be common to both the systems. The upper state vibrational frequency obtained here is also of the same order as that of the other system. By analogy, this system may correspond to the low frequency system observed in the other bismuth halides. The following vibrational constants are suggested for the system

$$\omega'_e = 195.0 \qquad \omega''_e = 167.9$$

$$\nu_e = 17216.0$$

$$x'_e\omega'_e = 1.0 \qquad x''_e\omega''_e = 0.3$$

It is to be noted that while in the corresponding systems of the bismuth halides $\omega_e' < \omega_e''$, in this system $\omega_e' > \omega_e''$.

The intensity distribution in the system is shown in Table III. The intensity in each sequence shows a gradual fall as we pass from first to higher sequence members. The Condon curve that can be drawn through the strongest bands is of the type which is to be expected with such relative values of ω as occur here.

TABLE II

Vibrational Analysis of BiI bands

v' \ v''	0	1	2	3	4	$\Delta G(v')$
	169.7					
	17230.1	17060.4				194.8
0	*193.4*	*196.2*				
	166 9	*168.2*				
	17423.5	17256.6	17088.4			
1	*187.8*	*190.0*				188.9
	17611.3	17446.6		17115.0		
2	*165.7*					
		188.6				188.6
		17635.2	17466.7		17138.5	
3			*168.5*			
$\Delta G(v'')$	167.4	168.4				

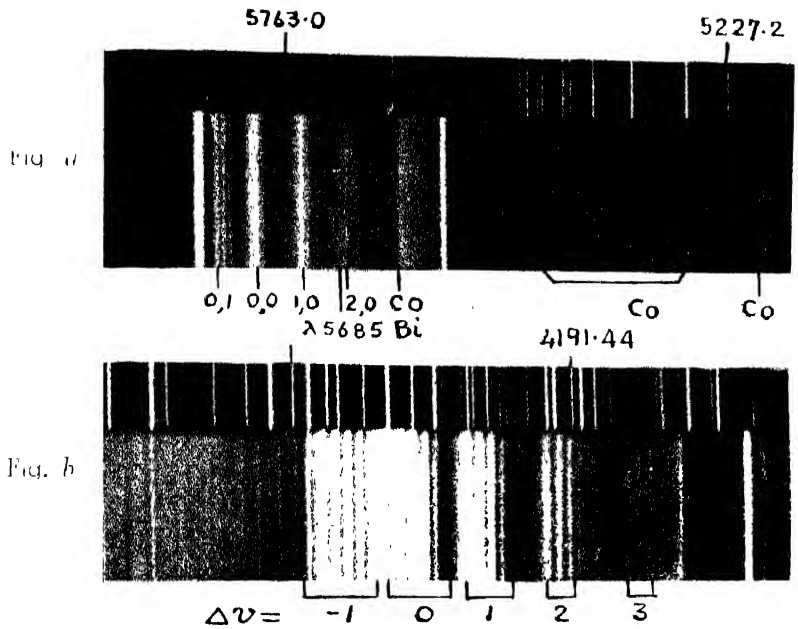

Bismuth iodide bands.

(*a*) New system.

(*b*) Morgan's system.

TABLE III

Intensity Distribution in the System

v' \ v''	0	1	2	3	4
0	10	6			
1	8	4	5		
2	4	4		4	
3		3	1		2

MORGAN'S SYSTEM

As in the other system, the bands in this system appear clearly degraded towards the red while in all the sequences the sequence degradation is towards the violet. All the bands recorded by Morgan are obtained here together with 3 new bands, whose wavelength, intensity and other data are shown in the Table IV.

TABLE IV

Wavelength	Int.	Wavenumber	Classification
4160.4	2	24029.4	5,2
68.0	3	23985.6	3,0
4246.2	1	23543.9	5,5

ELECTRONIC STATES IN BISMUTH HALIDES

Investigations on the halides of the related elements N, P, As, etc. are few. A band system between λ 6550—λ 5456 attributed to the molecule NBr is known from the work of Eliott (1939). Band spectra of the halides of phosphorus and arsenic are not so far known. Of the halides of antimony, Howell and Rochester (1939) analysed a triplet system of SbF in the visible region between λ 5200—λ 3600, which was suggested as due to a transition between triplet electronic levels. They also analysed a similar triplet system in the ultraviolet between λ 2700 – λ 2200. The final state is common in both the triplet systems and is suggested to be a probable $^3\pi$. They stated that the multiplet separations of the states are not known nor is the nature of other electronic levels. Two band systems between λ 5600 – λ 4600 attributed to SbCl have been analysed by Ferguson and Hudes (1940). In any of the

above investigations, however, no definite information regarding the electronic states of the halides of these elements is available in order to identify by comparison the electronic states of bismuth halides. But an idea of the electronic states of the halides of bismuth can be obtained from a knowledge of the electronic states of the BiH molecule. Heimer (1935) established two systems in BiH with a common $^1\Sigma$ upper state as due to the transitions $^1\Sigma - {}^1\Sigma$ and $^1\Sigma - {}^1\Pi$, the lower $^1\Sigma$ being the ground state. Hence the ground state of the halides of bismuth may, in all probability be a $^1\Sigma$. A consideration of the ground state configurations of the halides of the elements Hg, Tl, Pb etc., lying in the same horizontal row of the periodic table would also lead to the same view. The ground state of the mercury halides can be written as $\sigma^2\Pi^4\sigma$, $^2\Sigma^+$. By the successive addition of one electron to the above configuration, the ground state configurations of the halides of the other elements are

$\sigma^2\pi^4\sigma^2$, $^1\Sigma$ (thallium halides)

$\sigma^2\pi^4\sigma^2\pi$, $^2\pi_{(r)}$ (lead ,,)

$\sigma^2\pi^4\sigma^2\pi^2$, $^1\Sigma$, $^1\Delta$ and $^3\Sigma^-$ (bismuth ,,)

By analogy with the $^1\Sigma$ ground state established in the halides AlCl ; Holst, (1934) and AlBr (Jennergreen, 1948), Howell (1937) suggested that the ground state of the thallium halides is a $^1\Sigma$. Ferguson (1928) analysed two systems of SnCl with a common lower state with a separation of 2360 cm., while Rochester (1938) established a $^2\Pi$ ground state in the spectrum of PbF with a doublet separation of 8270 cm^{-1}. This indicates that $^2\Pi$ may probably be the ground state of lead halides. With the exception of BiF, each of the other halides of bismuth is known to give two systems of bands which have a common ground state. The simple, well marked rotational structure observed in the low frequency system of BiF indicates, as Howell remarked, that the transition involved may be between singlet levels. Hence the ground state of bismuth halides is most probably $\sigma^2\ \pi^2$, $^1\Sigma$. Excitation of the π electrons of the normal configuration into the next higher orbits gives the electronic states

$\sigma^2\pi^4\sigma^2\pi\sigma$, $^1\Pi {}^3\Pi_{(r)}$

and $\sigma^2\pi^4\sigma^2\pi^0\sigma^2$, $^1\Sigma^+$

The $^1\Pi$ and $^1\Sigma^+$ states are most probably the upper levels of the two observed band systems in bismuth halides.

$\pi\sigma_1\ ^1\Pi \longrightarrow \pi^2$, $^3\Sigma$ (low frequency system)

σ^2, $^1\Sigma^+ \longrightarrow \pi^2$, $^1\Sigma$ (high ,, ,,)

The first two excited states of BiH molecule also $^1\Pi$ and $^1\Sigma$ established from a study of the rotational structure of the bands, which probably gives further

justification for the proposed identification of the energy states in the case of bismuth halides. The transition $^3\Pi_{(r)} - {}^1\Sigma$ may be weak and lie in the near infra-red.

One might also regard the two systems in bismuth halides as due to the transitions $^3\Pi_0 - {}^1\Sigma$ and $^3\Pi_1 - {}^1\Sigma$, the other component $^3\Pi_2 - {}^1\Sigma$ lying probably in the infra-red. But the simple marked rotational structure observed by Howell in BiF bands indicates clearly that the transition may be between singlet levels. This supports the assignment of the two systems to the transitions $^1\Pi - {}^1\Sigma$ and $^1\Sigma - {}^1\Sigma$.

As the energies of dissociation cannot be extrapolated with accuracy in these halides, no attempt has, therefore, been made to correlate the above electronic states with those derivable from the most probable products of dissociation.

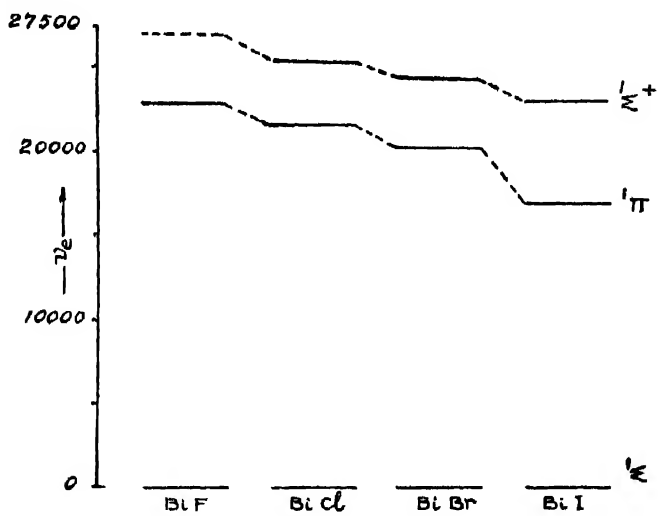

ELECTRONIC ENERGY LEVELS IN BISMUTH HALIDES.

FIG. 1

An energy level diagram for the halides of bismuth is given in Fig. 1. A glance at this diagram shows that the corresponding energy levels are lower, the heavier the molecule, which is to be expected.

ACKNOWLEDGMENTS

The author desires to express his grateful thanks to Prof. K. R. Rao and Mr. C. Ramasastry for valuable discussions in the course of the work.

REFERENCES

Eliott, 1939, *Proc. Roy. Soc.*, **169**, 469.

Ferguson, 1928, *Phy .Rev.*, **32**, 607.

Ferguson and Hudes, 1940, *Phy. Rev.*, **57**, 705.

Heimer, 1935, *Zeit. f. Physik.*, **95**, 328.

Holst, 1934, *Zeit f. Phys.*, **93**, 65.
Howell, 1936, *Proc. Roy. Soc.*, **155**, 141.
,, ,1937, ,, ,, ,, **160**, 242.
Howell and Rochester, 1934, *Univ. Durham. Phil. Soc. Proc.*, **9**, 126.
,, ,, , *Phy. Soc. Proc* , **51**, 329.
Jennergreen Carl Gustav, 1948, *Nature*, **161**, 315.
Morgan, 1936, *Phy. Rev.*, **49**, 47.
Rao, Tiruvenganna and Rao, K. R., 1949, *Ind. Jour. Phy.*, **23**, 185.
Rochester, 1937, ,, ,, **51**, 146 A.
,, 1938, *Proc. Roy. Soc.*, **164**, 567
Saper, 1931, *Phy. Rev.*, **37**, 1710A.

FORTY ONE ELECTRON SYSTEM OF MOLYBDENUM—Mo II

By V. RAMAKRISHNA RAO

(Received for publication, March 22, 1949)

Plates XVIIIA and B

ABSTRACT. Analysis of the spectrum of Mo II is extended to include the identification of nearly all the sextet terms. Detection of the inter-combinations lines led to the derivation of a connected system of atomic energy levels. About eighty lines have been newly classified.

INTRODUCTION

In a previous paper the author (1949) reported the identification of the fundamental multiplets of Mo III, due to the combination of $4d^3(^4F)5s\ ^5F$ with $4d^3(^4F)5p^5(G,\ D,\ F)^0$ terms. In a brief review therein of our knowledge of the different spectra of Mo, it was indicated that while the structure of Mo III was completely unknown, that of Mo II is very meagre. The present work is an attempt to extend the latter spectrum corresponding to the forty one electron configuration.

The experimental work and the method of assigning the lines due to Mo I, II and III were already described. The general observation might be mentioned that Mo III lines are absent altogether in the arc, and much enhanced in the condensed spark: Mo II lines do occur in the arc but are much less enhanced. Lines strong in arc and weakened in condensed spark are assignable to Mo I.

ANALYSIS

The ionised atom of Mo, iso-electronic with the neutral atom of columbium has five outer electrons giving rise to the optical spectrum. The chief electron configurations that may be expected are summarised in Table I.

TABLE I

Even	Odd
$4d^5$	$4d^4 5p$
$4d^4 5s$	
$4d^3 5s^2$	$4d^3 5s 5p$

Meggers and Kiess (1926) were the first to report two sextet and three quartet groups due to transition $d^4s - d^4p$. Schauls and Sawyer (1940) detected what may be called the resonance group of Mo II involving the deepest configuration $4d^5$, and also suggested a modification of one of the sextets identified by Meggers and Kiess. The author's first attempt in extending this scheme was to establish the intercombination lines. In the course of this, one observation in the existing regularities proved very fruitful. With Sawyer's modification of the $^6D - {}^6D^0$ multiplet, the intervals between $4d^4 5p\ {}^6D^0_{\frac{1}{2}}\ {}^6D_{1\frac{1}{2}}$, ${}^6D^0_{2\frac{1}{2}}$ are seen to be same within limits of experimental error as the intervals of $4d^4\ 5p\ {}^4D^0_{\frac{1}{2}}$, ${}^4D^0_{1\frac{1}{2}}$ and ${}^4D^0_{2\frac{1}{2}}$, derived from the group $d^4s\,{}^4D - d^4p\,{}^4D^0$ as identified by Meggers and Kiess. This suggested the probability of the latter being the intercombination group $d^4s^4D - d^4p\ {}^6D^0$. Scrutiny of the plates strengthened this suggestion. (Ref: Plate XVIIIA, B While the group $^4D - {}^4F^0$ was unmistakable on the spectrum the $^4D - {}^4D^0$, multiplet is too faint to be classified as such. The relative magnitude of the term values d^4p $^4P^0$, $^4D^0$, and $^4F^0$ is also inconsistant: it is not in correspondence with the analogous spectra of V I, Cr II, and Cb I as shown in Table II for the $^4D^0$ term has the largest value in these spectra while in Meggers and Kiess's identication $^4F^0$ is higher than $^4D^0$.

TABLE II

Term	V I	Cr II	Cb I	Mo II
P	25130	49707	23684	37219.6
F	26172	51944	26440	41401.8
D	26480	54787	27507	* 43504.5A 39394.7M

* A—Author's value M—Megger's value.

Consideration of the Zeeman effect data published by Wilhelmy (1926) is not conclusive but it may be significant that the Zeeman splitting jusiifies the classification of the $^6D - {}^6F^0$ and $^4D - {}^4F^0$ and $^4D - {}^4P^0$ groups and a similar confirmation is not obtained either for $^6D - {}^6D^0$ or $^4D - {}^4D^0$ as given by Meggers. The above considerations led to the adoption of Meggers and Kiess's $^4D - {}^4D^0$ group as intercombinations. A scheme of quartet and sextet multiplets based on this view is obtained and given in Tables III and IV. The intensity of the new group $^4D - {}^4D^0$ is normal: the relative order of magnitude of the terms referred to above is consistent (cf. Table II). The table shows all the groups obtained in the spectrum. Symbol 'M' in place of wave-number denotes that Meggers and Kiess's identification is retained. 'S' signifies Schauls and Sawyer's classification. At all other places where numerical values of the wave-numbers are given, the analysis is due to the author. The intensity values given are entirely from the present

TABLE III

Multiplets in Mo II

	$a\ {}^6D_{\frac{1}{2}}$	${}^6D_{1\frac{1}{2}}$	${}^6D_{2\frac{1}{2}}$	${}^6D_{3\frac{1}{2}}$	${}^6D_{4\frac{1}{2}}$	$a\ {}^4D_{\frac{1}{2}}$	${}^4D_{1\frac{1}{2}}$	${}^4D_{2\frac{1}{2}}$	${}^4D_{3\frac{1}{2}}$
$z\ {}^6P_{1\frac{1}{2}}$	$S_{(20)}$	$S_{(20)}$	$S_{(15)}$						
${}^6P_{2\frac{1}{2}}$		$S_{(20)}$	$S_{(20)}$	$S_{(3)}$					
${}^6P_{3\frac{1}{2}}$			$S_{(20)}$	$S_{(20)}$	$S_{(18)}$				
								25189.0(3)	
$x\ {}^6D_{\frac{1}{2}}$	$M_{(15)}$	$M_{(20)}$				25577.4(3)	25290.2(3)		
${}^6D_{1\frac{1}{2}}$	$M_{(20)}$	381.57.8(12)	$M_{(20)}$				25532.7(3)	25079.7(6)	
${}^6D_{2\frac{1}{2}}$		$S_{(4)}$	38160.0(6)	$S_{(20)}$			25918.5(3)	25465.5(2)	24763.6(1)
${}^6D_{3\frac{1}{2}}$			38288.0(2)	$S_{(20)}$	$S_{(20)}$				
${}^6D_{4\frac{1}{2}}$				$S_{(15)}$	$S_{(20)}$				
$y\ {}^6F_{\frac{1}{2}}$	$M_{(20)}$	$M_{(20)}$							
${}^6F_{1\frac{1}{2}}$	$M_{(20)}$	$M_{(20)}$	$M_{(20)}$						
${}^6F_{2\frac{1}{2}}$		$M_{(20)}$	$M_{(20)}$	$M_{(20)}$					
${}^6F_{3\frac{1}{2}}$			$M_{(20)}$	$M_{(20)}$	$M_{(15)}$				
${}^6F_{4\frac{1}{2}}$					$M_{(20)}$			22119.9(2)	
${}^6F_{5\frac{1}{2}}$					$M_{(20)}$				
$z\ {}^4P_{\frac{1}{2}}$	35422.5(3)	35172.8(20)				M	M		
${}^4P_{1\frac{1}{2}}$	36240.8(18)	35989.0(11)	35607.0(20)				M	M	
${}^4P_{2\frac{1}{2}}$		36968.5(3)	36585.2(3)				M	M	M
$y\ {}^4F_{\frac{1}{2}}$							$M_{(15)}$	$M_{(15)}$	
		39340.7(1)				$M_{(20)}$		$M_{(15)}$	$M_{(10)}$
${}^4F_{2\frac{1}{2}}$							$M_{(20)}$		$M_{(12)}$
${}^4F_{3\frac{1}{2}}$			39801.1(3)	39317.4(20)	38757.7(5)			$M_{(20)}$	
${}^4F_{4\frac{1}{2}}$									$M_{(25)}$
$y\ {}^4D_{\frac{1}{2}}$	41602.8(0)					29014.2			
${}^4D_{1\frac{1}{2}}$			41244.0(5)				29000.7(20)	28547.0(10)	
${}^4D_{2\frac{1}{2}}$							29659.4(15)	29207.2(20)	
${}^4D_{3\frac{1}{2}}$					41828.2(8)			30176.0(18)	29473.2(20)

TABLE III (*contd.*)

	$a\ ^6D_{\frac{1}{2}}$	$^6D_{1\frac{1}{2}}$	$^6D_{2\frac{1}{2}}$	$^6D_{3\frac{1}{2}}$	$^6D_{4\frac{1}{2}}$	$a\ ^4D_{\frac{1}{2}}$	$^4D_{1\frac{1}{2}}$	$^4D_{2\frac{1}{2}}$	$^4D_{3\frac{1}{2}}$
$z\ ^6D_{\frac{1}{2}}$	30986.2(12)								
$^6D_{1\frac{1}{2}}$		31021.4(13)			—				
$^6D_{2\frac{1}{2}}$		31470.1(2)	31087.0(20)	30604 3(15)					
$^6D_{3\frac{1}{2}}$			31844.8(2)	31361.6(20)	3082.5(10)				
$^6D_{4\frac{1}{2}}$				32271.1(6)	31710.3(20)				
$z\ ^6F_{\frac{1}{2}}$	28336.5(5)	28084.8(8)							
$^6F_{1\frac{1}{2}}$		28679.4(8)	28295.9(6)						
$^6F_{2\frac{1}{2}}$			29002.6(20)	28518.9(4)					
$^6F_{3\frac{1}{2}}$				29378 4(20)	28816.6(4)				
$^6F_{4\frac{1}{2}}$					30367.8(20)				
$^6F_{5\frac{1}{2}}$									
$y\ ^6P_{1\frac{1}{2}}$	39879.5(6)	39628.6(8)	39244.7(15)			27290.07(1)			
$^6P_{2\frac{1}{2}}$			39801.1(3)	39317.4(20)			27559.6(5)	27105 4	
$^6P_{3\frac{1}{2}}$			40427.3(3)	39943.7(3)	39383.6(20)				
$y\ ^6D_{\frac{1}{2}}$									
$^6D_{1\frac{1}{2}}$	37877.5(1)	37626.7(14)				25288 8(3)			
$^6D_{2\frac{1}{2}}$		38135.8(10)	37751.6(12)	37270.1(6)			25509.7(2)	25056.7	24355 0(2)
$^6D_{3\frac{1}{2}}$			38551.3(10)	38069.1(15)	37507.7(1)			25856.4(1)	
$^6D_{4\frac{1}{2}}$				39336.8(2)	38774.9(18)				26421.6(15)

Additional Combinations

	$a\ ^6S_{2\frac{1}{2}}$
$z\ ^6P_{1\frac{1}{2}}$	S(25)
$^6P_{2\frac{1}{2}}$	S(26)
$^6P_{3\frac{1}{2}}$	S(25)
$x\ ^6D_{1\frac{1}{2}}$	—
$^6D_{2\frac{1}{2}}$	S
$^6D_{3\frac{1}{2}}$	S
$^6F_{1\frac{1}{2}}$	46148.3(7)
$^6F_{2\frac{1}{2}}$	46514.4(2)
$^6F_{3\frac{1}{2}}$	47231.2(1)

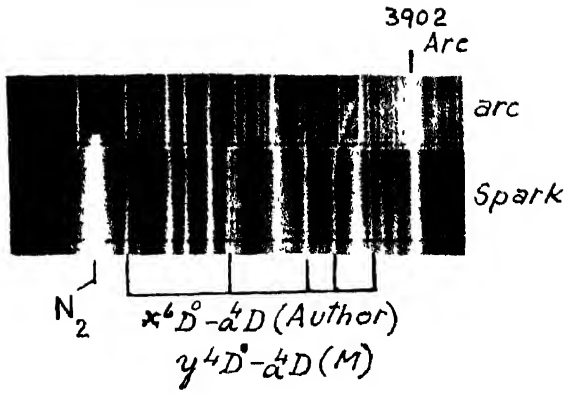

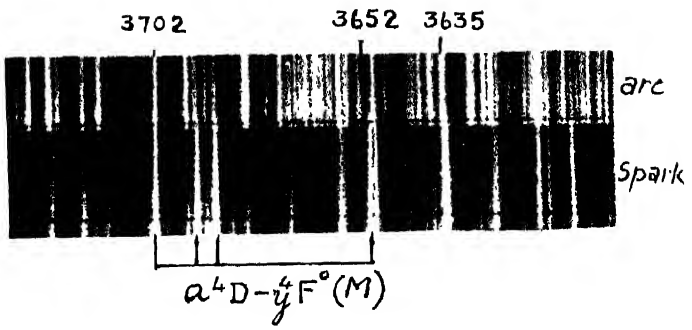

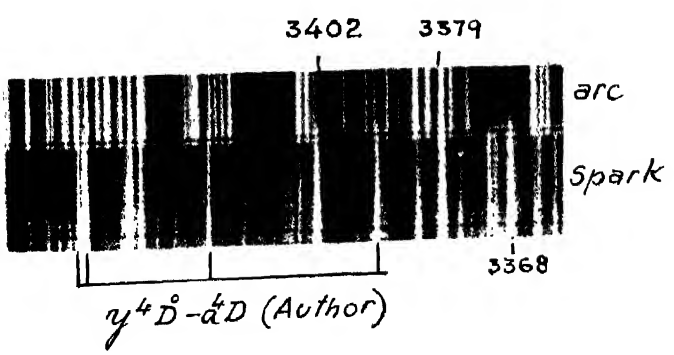

Quartets in Mo II.

RAO

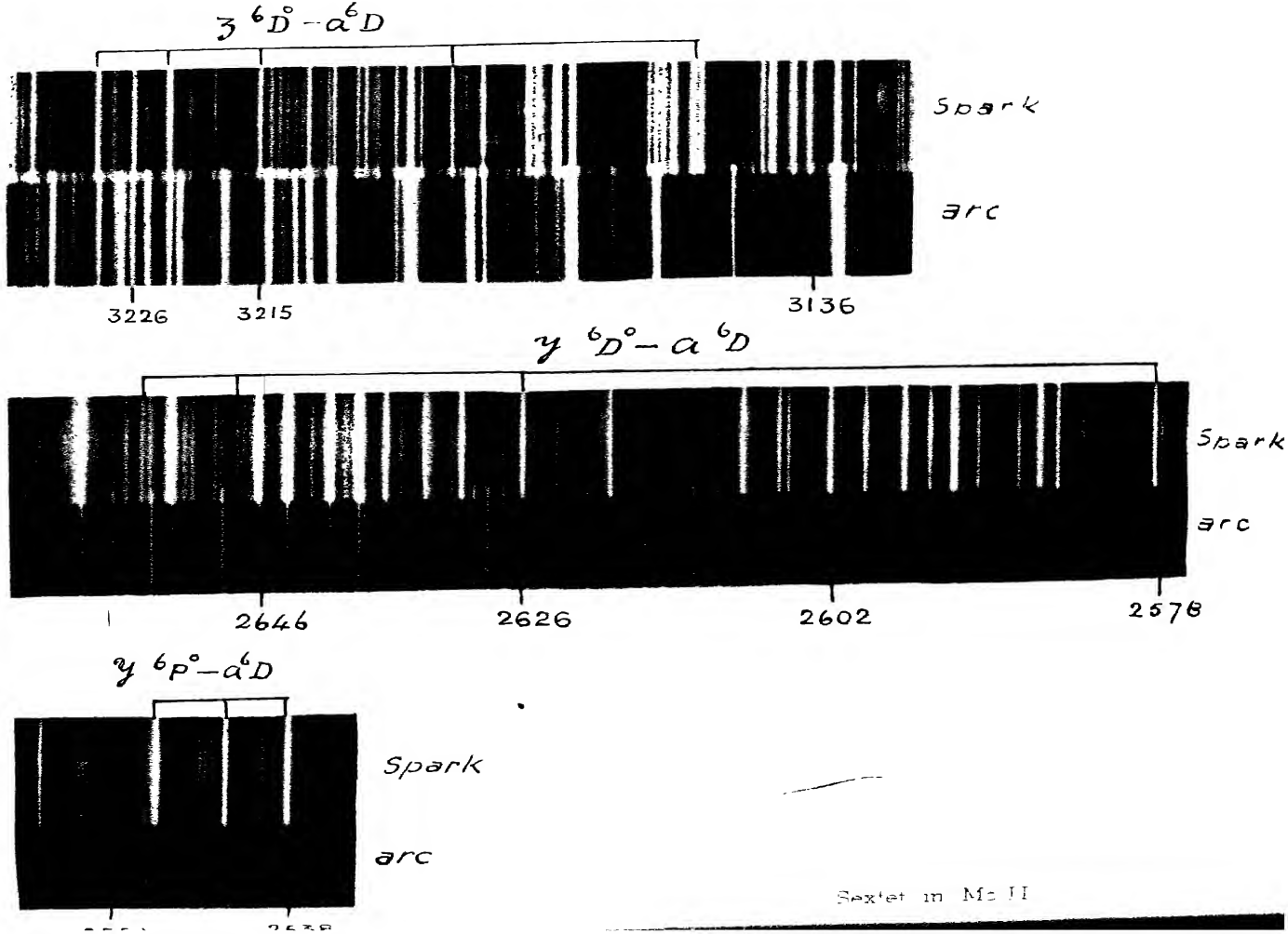

Sextet in Mn II

TABLE IV

Term Values

Electron configuration	Term symbol	Mo II		Cb I	
		Term value	Intervals	Term value	Intervals
$4d^5$	$a\ ^6S_{2\frac{1}{2}}$	−11783.7		11344.70	
$4d^4 5s(^5D)$	$a\ ^6D_{\frac{1}{2}}$	0		0	
	$a\ ^6D_{1\frac{1}{2}}$	250.7	250.7	154.19	154.19
	$a\ ^6D_{2\frac{1}{2}}$	633.85	383.2	391.99	237.80
	$a\ ^6D_{3\frac{1}{2}}$	1116.7	482.9	695.15	303.26
	$a\ ^6D_{4\frac{1}{2}}$	1677.21	560.5	1050.26	355.01
$4d^4 5s(^5D)$	$a\ ^4D_{\frac{1}{2}}$	12588.6		8410.90	
	$a\ ^4D_{1\frac{1}{2}}$	12875.8	287.2	8705.32	294.42
	$a\ ^4D_{2\frac{1}{2}}$	13328.8	453.0	9043.14	337.82
	$a\ ^4D_{3\frac{1}{2}}$	14030.3	701.5	9497.52	454.38
$4d^4 5p(^5D)$	$z\ ^6P_{1\frac{1}{2}}$	37257.3		24283.34	
	$z\ ^6P_{2\frac{1}{2}}$	37825.3	568.0	24543.13	259.79
	$z\ ^6P_{3\frac{1}{2}}$	38519.0	693.7	24904.86	361.73
	$x\ ^6D_{\frac{1}{2}}$	38166.0		26552.40	
	$x\ ^6D_{1\frac{1}{2}}$	38408.5	242.5	26713 32	160.92
	$x\ ^6D_{2\frac{1}{2}}$	38793.9	385.4	26983.34	270.00
	$x\ ^6D_{3\frac{1}{2}}$	38921.9	128.0	27427.07	443.73
	$x\ ^6D_{4\frac{1}{2}}$	37697.3	−1224.6	27974.87	547.80
	$y\ ^6F_{\frac{1}{2}}$	34069.7		23984.87	
	$y\ ^6F_{1\frac{1}{2}}$	34364.6	294.9	24164.79	179.92
	$y\ ^6F_{2\frac{1}{2}}$	34830.7	466.1	24396.80	232.01
	$y\ ^6F_{3\frac{1}{2}}$	35448.5	617.8	24769.91	373.11
	$y\ ^6F_{4\frac{1}{2}}$	36215.9	767.4	25199.81	429.90
	$y\ ^6F_{5\frac{1}{2}}$	37176.2	960.3	25680.36	480.55
$4d^4 5p(^5D)$	$z\ ^4P_{\frac{1}{2}}$	35424.7		22006.74	
	$z\ ^4P_{1\frac{1}{2}}$	36239.8	815.0	23006.86	1000.12
	$z\ ^4P_{2\frac{1}{2}}$	37219.6	979.8	23684.44	677.58
	$y\ ^4F_{1\frac{1}{2}}$	39590.8		25936.01	
	$y\ ^4F_{1\frac{1}{2}}$	39949.0	358.2	26060.65	130.64
	$y\ ^4F_{3\frac{1}{2}}$	40434.5	485.5	26175.79	105.14
	$y\ ^4F_{4\frac{1}{2}}$	41401.8	967.3	26440.33	274.54
	$y\ ^4D_{\frac{1}{2}}$	41602.8		26717.73	
	$y\ ^4D_{1\frac{1}{2}}$	41877.2	274.4	26936.86	219.13
	$y\ ^4D_{2\frac{1}{2}}$	42535.0	658.4	27859.70	422.84
	$y\ ^4D_{4\frac{1}{2}}$	43504.5	968.9	28096.74	237.04
$4d^3 5s5p(^5F)$	$z\ ^6D_{\frac{1}{2}}$	30986.2		19623.96	
	$z\ ^6D_{1\frac{1}{2}}$	31272.1	285.9	19765.15	141.22
	$z\ ^6D_{2\frac{1}{2}}$	31720.9	448.8	19993.78	228.6
	$z\ ^6D_{3\frac{1}{2}}$	32478.4	757.5	20315.74	321.96
	$z\ ^6D_{4\frac{1}{2}}$	33387.5	909.1	20733.88	418.14
	$z\ ^6F_{\frac{1}{2}}$			18791.09	
	$z\ ^6F_{1\frac{1}{2}}$	28336.5		19036.55	245.46
	$z\ ^6F_{2\frac{1}{2}}$	28930.1	593.6	19427.90	391.35
	$z\ ^6F_{3\frac{1}{2}}$	29636.5	706.4	19916.69	438.79
	$z\ ^6F_{4\frac{1}{2}}$	30495.2	858.7	20432.11	515.42
	$z\ ^6F_{5\frac{1}{2}}$	32045.0	1549.8		

TABLE IV (*contd.*)

Term Values

Electron configuration	Term symbol	Mo II		Cb I	
		Term value	Invervals	Term value	Intervals
$4d^4 5s 5p (^5p)$	$y\ ^6P_{1\frac{1}{2}}$	39878.6		28278.25	
	$y\ ^6P_{2\frac{1}{2}}$	40434.6	556.0	28652.66	374.41
	$y\ ^6P_{3\frac{1}{2}}$	41061.0	626.4	28973.12	0.4326
	$y\ ^6D_{\frac{1}{2}}$			25879.81	
	$y\ ^6D_{1\frac{1}{2}}$	37877.4		26067.06	187.25
	$y\ ^6D_{2\frac{1}{2}}$	38385.5	508.1	26386.36	319.30
	$y\ ^6D_{3\frac{1}{2}}$	39185.6	800.1	26832.43	446.07
	$y\ ^6D_{4\frac{1}{2}}$	40452.0	1266.4	27419.62	587.19

plates by visual estimation. The table comprises of the additional sextet-sextet groups which are established from the usual general considerations such as relative intensities of lines, intervals and magnitude of the terms and a comparative study of the similar spectra. The detection of all the sextet terms due to the comfigarations mentioned in Table I is now complete : with the exception of just two terms $4d^3 5s\ (^5P)\ 5p\ ^6S$ and $(^5F)^6G$.

In Table IV all the term values are collected and compared with corresponding values of Cb I. For this purpose the alphabetical prefixes a, b, c and x, y, z, etc., for the terms are retained as in Cb I. The general consistency in the term scheme is taken as a justification of the analysis. One difference between Cb I and Mo II may be emphasised. The deepest term is due to the $4d^5$ instead of $4d^4\ 5s$. This feature may be normally expected as arising in a row of iso-electronic atomic systems where the addition of md and $(m+1)s$ electrons are concerned.

ACKNOWLEDGMENT

It is a great pleasure to thank Dr. K. R. Rao under whose guidance this work has been taken up.

REFERENCES

Meggers and Kiess, 1926, *Jour. Opt. Soc. Amer.*, **12**, 417, 432.
Meggers and Humphreys, 1945, *BSJ. America*, **34**, 477.
Rao. V. R., 1949, *Ind. J. Phy.*, **23**, 258.
Schauls and Sawyer, 1940, *Phy. Rev.*, **58**, 781.
Wilhelmy, 1926, *Ann. Der. Phy.*, **80**.

NEW BAND SYSTEMS OF THE TlCl MOLECULE

By P. TIRUVENGANNA RAO

(*Received for publication, Feb. 7, 1949*)

Plate XIX

ABSTRACT. The spectrum of thallium chloride is photographed in a high frequency discharge in the first order of a 10 ft. concave grating, having a dispersion of 5.7 Å/mm. Two new systems of bands, one between λ 4300—λ 4150 designated here as *A*, and the other between λ 4150—λ 3800 designated as *B*, have been obtained in addition to the ultraviolet system around λ 3200 analysed by Howell and Coulson. System *B* consists of about 75 bands in all, which are degraded in either directions while a few of them are headless and diffuse. System *A* consists of about 18 bands which are mostly degraded towards the red, while a few of them are violet-degraded. The vibrational analyses of these two systems have shown that the lower state, which is found to be common to both of them, is the upper state of the ultraviolet system, $^3\Pi—^1\Sigma^+$. Predissociation, similar to that found in the upper state of the ultraviolet system, is observed in the lower state of both the systems at $v''=5$. The following vibrational constants have been determined for the two systems.

		$\omega_e'=101.3$	$\omega_e''=205.5$
System *B*	$\nu_e=24683.3$	$x_e'\omega_e''=0.1$	$x_e''\omega_e''=6.5$
System *A*	$\nu_{0,0}\sim24040$	$\omega_e'\sim100$,	$\omega_e''\sim206$

The chlorine isotope effect observed in some bands in the two systems supports the vibrational analyses.

The close proximity of these two systems suggests that the upper levels may form an electronic doublet.

INTRODUCTION

The early work on this molecule was due to Butkow (1929) who recorded bands in absorption in the region λ 3400—λ 3200 using a dispersion of 17 Å/mm. He measured 49 bands in all and ascribed them to the molecules $TlCl^{35}$ and $TlCl^{37}$. He proposed an analysis of these bands fitted into the following quantum formula :—

$$\nu=31036.0—283.7n''+1.10n''^2+428.5n'—202.6n'^2+50.6n'^3—4.85n'^4.$$

Howell and Coulson (1938) photographed the spectrum of thallium chloride both in emission and absorption on a Hilger E_1 spectrograph having a dispersion of 6 Å/mm. at λ 3200. Excluding isotopic heads and diffuse bands, they measured 59 bands and showed that Butkow's analysis is incorrect. They were able to identify and measure the positions of the band orignis and the following formulae have been derived for the *Q* and *R* heads.

$$\nu_Q=31054.2—287.(v''+\tfrac{1}{2})+1.24(v''+\tfrac{1}{2})^2+216.91(v'+\tfrac{1}{2})—6.80(v'+\tfrac{1}{2})^2.$$

$$\nu_R=31079.6+204.0u'—5.15u'^2—284.8u''+0.9u''^2.$$

Confirmation of their analysis was obtained by the variation of the $\nu - \nu_0$ interval in the bands in accordance with theoretical expectations and also from the chlorine isotope shifts observed in 38 bands. Neujmin (1934) reported diffuse bands and a continuum in absorption around λ 2510 and measured 13 bands on the red edge of this continuum and 4 on the violet side of the band system analysed by Howell and Coulson. He interpreted them as due to transitions from successive v'' levels to two unstable electronic levels. The existence of these bands in absorption was also confirmed by Howell and Coulson.

In the course of a series of investigations on the molecular spectra of the diatomic halides of thallium, the author photographed the spectrum of thallium chloride in emission in a high frequency discharge. The following results have been obtained: (*a*) the band system between λ 3500—λ3150 analysed by Howell and Coulson, (*b*) a continuum and diffuse bands around λ2500 observed by Neujmin, (*c*) two new systems of bands, one between λ 4150—λ 3800 and the other between λ 4300—λ 4150 not recorded in any previous investigation (See note at the end). The present paper reports the vibrational analysis of these two systems attributed to the TlCl molecule.

The experimental method for developing the emission spectrum of thallium chloride is the same as that for the other halides of thallium and described in detail previously (Rao and Rao, 1949). The spectrum was excited by a low power high frequency oscillator using external electrodes. The discharge was bright green in colour due to the intense λ 5350 Tl line. Intermittent heating at regular intervals was found necessary to maintain the discharge.

The spectrum was photographed on a number of spectrographs. (1) Hilger constant deviation (2) Hilger glass Littrow (8—12 Å/mm. in the region covered by the band systems) (3) Hilger quartz Littrow (11 A/mm. at λ 3900) (4) 10 ft. concave grating with a dispersion of 5.7 A/mm. in the first order. An exposure of 45 minutes was found sufficient with Hilger constant deviation spectrograph using Ilford Selochrome plates. Exposures varying from 1 to 2 hours were given on Ilford special rapid plates while using the other spectrographs.

Measurements were made on the band heads; the type of band origins similar to those observed by Howell and Coulson in the main system are not observed in the new systems. The iron arc lines served as wavelength standards for reducing the plates. The plates taken on all the spectrographs were measured, though band data measured from the grating plates were finally adopted, owing to its high dispersion. About 18 bands in the less refrangible system which may be designated as system *A* and 75 in the other system *B* could be measured in all.

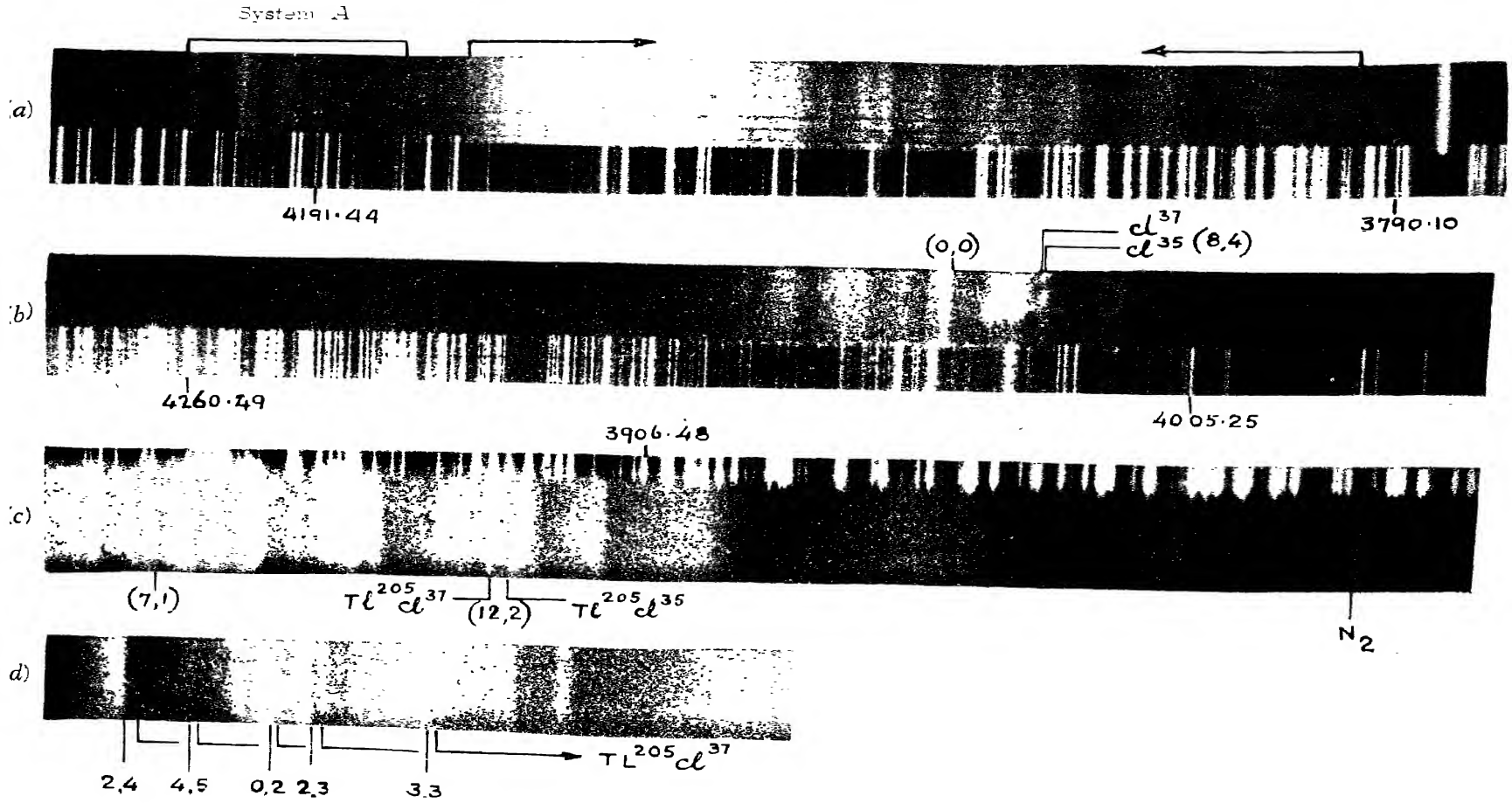

Thallium chloride bands.

(*a*) Quartz Littrow, (*b*) Glass Littrow (*c*) and (*d*) Concave grating spectrograms.

DESCRIPTION OF THE SPECTRUM

Photographs of the spectra illustrating their main features taken on the various instruments are reproduced in Plate XIX in four strips. Strip (*a*) is an overall picture of the two systems of bands in the region λ 4300—λ 3800 taken on the quartz Littrow spectrograph. System *A* consists mostly of bands clearly degraded towards the red, while a few of them are violet-

TABLE I

TlCl bands. System *B*

Wavelength	Int.	Wavenumber	Classification	Wavelength	Int.	Wavenumber	Classification
4124.91	2	24236.1		3981.88 R	2	25106.7	13, 5
21.53 V	2	24256.0	3, 4	77 73 R	3	25132.9	5, 0
19.65 V	4	24267.1	0, 2	76.46 R	3	25140.9	7, 1
15.45	2	24291.9	..	73.37	3	25160.5	9, 2
11.37 V	3	24316.0	5, 5	70 43 R	4	25179.1	..
07.93 R	5	24336.3	...	68.35	3	25192 3	11, 3
04.24 D	2	24358.2	4, 4	61.70	5	25234.6	6, 0
00.66 R	5	24379.5	1, 2	57.87	1	25259.0	10, 2
4096.52 R	6	24404.1		55.38	2	25274.9	...
94.70 R	3	24415.0	3, 3	50.87	2	25303.8	15, 5
92 61 D	2	24427.4	6, 5	47.38	3	25326.1	...
90.47 V	4	24440.2	...	44.41 R	3	25345 2	9, 1
85 30 V	7	24471.1	0, 1	41.65	1	25362.9	11, 2
79.45 R	6	24506.2	2, 2	37.85	0	25387.4	13, 3
68.69 R	4	24571.0	4, 3	35.94	2	25399 7	16, 5
64.32 V	5	24597.4	3, 2	30.22 R	1	25436.7	8, 0
59.31 R	10	24627.8	5, 3	28.45 V	2	25448.2	12, 2
57.03 R	2	24641.6	0, 0	27.01	1	25457.5	...
55.24 R	2	24652.5	2, 1	3925.38 V	5	25468.1	12, 2
52.70	1	24668.0	7, 4	21.16 V	1	25495.5	17, 5
50.48 V	5	24681.5	4, 2	16.55	1	25525.5	...
47.70 V	2	24698.4	6, 3	13.82 V	3	25543.3	9, 0
45.13 V	6	24714.1	9, 5	11.84 R	4	25556.0	13, 2
41.82	2	24734.4	1, 0	10.30 R	2	25566.3	...
39.09	3	24751 1	8, 4	09.05	2	25574 5	15, 3
38 40 V	7	24755.3	8, 4	02.76 V	3	25615.7	...
31.77	2	24796.0	7, 3	3898.72 V	3	25642.2	10, 0
27.69	2	24821.1	10, 5	89.74	2	25701.4	19, 5
4024 00 D	5	24843.9	4, 1	86.56 R	3	25722.4	...
20.21 D	5	24867.3	6, 2	83.10 V	4	25745.4	11, 0
15.13 R	4	24898.8	8, 3	79.00 D	2	25770 6	17, 3
08.39 R	3	24940.7	5, 1	73.46 V	2	25809.4	...
05.10	2	24961.1	7, 2	67.49 V	3	25849.3	12, 0
00.71	4	24988.5	...	63.92 R	3	25873.1	...
3998.16 R	3	24998.2	9, 3	61 07 V	3	25892.2	20, 5
96.61	1	25014.2	12, 5	35.99	3	26061.5	20, 3
91.75	3	25044.6	6, 1	32.88	4	26082 7	22, 5
84.04 R	2	25093.1	10, 3	28.16 R	2	26114.8	21, 4
				23.51 V	1	26146.6	15, 0

R indicates that the band is red-degraded
V ,, ,, is violet-degraded
D ,, ,, is diffuse
the degradation of the other bands is uncertain.

degraded. The other system *B* consists of bands degraded either way, though a few of them are diffuse and headless. Bands belonging to this system are very intense between λ 4100—λ 4000 and these are separately shown in strip (*b*) which is an enlargement taken on the glass Littrow instrument. Strip (*c*) is a reproduction of a portion of system *B* between λ 4000—λ 3800 taken on the 10 ft. concave grating. Strip (*d*) is an enlargement of system *A* taken on the grating.

The intensities of the bands are assigned visually on a 0—10 scale.

RESULTS

Table I gives the wavelength, intensity and other data of system *B* and Table II gives the data for the other system *A*. The tables are self-explanatory.

TABLE II

TlCl bands. System *A*

Wave-length	Int.	Wave-number	Classification	Wave-length	Int.	Wave-number	Classification
4244.21 R	3	23554.9	2, 4	4210.29 V	3	23744.7	4, 4
41.97	1	22567.3	2, 4^1	04.21 R	2	23779.0	1, 4
34.45	1	23609.2	1, 5	00.50 R	1	23800.0	3, 3
33.04	0	23617.1	4, 5^1	4199.18	1	23807.5	3, 3^1
27.13 V	2	23650.1	3, 4	94.28	1	23835.3	5, 4
23.31 R	8	23671.5	0, 2	88.45 R	3	23868.5	2, 2
21.82	3	23679.8	0, 2^1	84.75	1	23889.6	4, 3
17.43 R	5	23704.5	2, 3	81.58 V	4	23907.7	7, 5
15.45	2	23715.6	2, 3^1	57.65	2	24045.3	3, 1

VIBRATIONAL ANALYSIS OF SYSTEM *B*

The band system presents a complicated appearance owing to the absence of conspicuous sequences or progressions. Though most of the bands are clearly red-degraded, some of them are degraded towards the violet, while others are headless and diffuse but intense. Such a feature is usually observed in the case of band systems for which the vibrational frequencies of the upper and lower states are of the same order of magnitude. But this would mean that discrete close sequences should be noticed, which is not at all a prominent feature of the system. The complicated appearance, then, may be due to overlapping sequences due possibly to fairly large difference between the vibrational frequencies of the upper and lower states. Such relative values of ω'_e and ω''_e should give rise to large chlorine isotopic separations while

most of the bands are not accompanied by the weaker isotope heads. But, this, however, is not a serious difficulty, as the isotopic shifts depend also upon the vibrational quantum numbers of the bands.

As a first step, an attempt is made to pick out progressions with an interval of about 287 cm.$^{-1}$ which is the ground state frequency established from the analysis of the main band system between λ 3500—λ 3150, but this proved futile. The failure to build up the analysis on this basis seemed reasonable as the band system has not been obtained in absorption in any previous investigation. The possibility of analysing the red-degraded bands into one system and the violet-degraded bands into another was also tried but without success. After a number of attempts, it was found that an interval of approximately 100 wavenumber units is found to occur between many bands in the system. A few progressions with this interval could thus be built up which are arranged in a Deslander's scheme. The intervals between the vibrational levels of the lower state of this system are found to be of the same order of magnitude as those of the upper state of the main system. Hence it was considered that the upper state of the main system may be the lower state of the present system. On this basis, the vibrational matrix shown in Table III could be built up to include almost all the bands in the system. The classification of the bands is shown in the last column of Table I. The most intense band in the spectrum is classified as the (0,0) band but the

TABLE III

Vibrational Analysis of TlCl Bands (System *B*)

v' \ v''	0	1	2	3	4	5	6	
0	24627.8	24440.2	24267.1					
1	24734.4							$\Delta G(v')$
2		24641.6	24471.1					
3			24571.0	24404.1	24256.0			
4		24843.9	24668.0	24506.2	24358.2			100.4
5	25132.9	24940.7	24765.7	24597.4		24316.0		97.3
6	25236.6	25044.6	24867.3	24698.4		24415.0		102.1
7		25140.9	24961.1	24796.0	24652.5			95.9
8	25436.7			24898.9	24755.3			100.2
9	25543.3	25345.2	25160.5	24998.2		24714.1		99.3
10	25642.2		25259.0	25093.1		24821.1		97.4
11	25745.4		25362.9	25192.3				
12	25849.3		25468.1			25014.2		
13			25556.0	25387.4		25106.7		
14								
15	26146.6			25574.5		25303.8		
16						25399.7		
17				25770.6		25495.5		
18				25873.1				
19						25701.4		
20				26061.5		25892.2		
21					26114.5			
22						26082.7		
$\Delta G(v'')$	193.2	178.5	166.5	148.1				

TABLE IV

Intensity Distribution in System *B*.

v' \ v''	0	1	2	3	4	5
0	10	4	4			
1	2					
2		2	7			
3			4	6	2	
4		5	1	6	2	
5	3	3	1	5		
6	5	3	5	2		
7	3	3	2	2	2	
8	1			4	7	
9	3	3	3	3		6
10	3		1	2		2
11	4		1	3		
12	3		5			1
13			2	0		2
14						
15	1			2		2
16						2
17				2		1
18				3		
19						2
20				3		3
21					2	
22						4

abnormal intensity of this band may partly be due to the superposition of the (0,3) band at λ 4059.4 of the second positive system of N_2. Some bands in the (v', 0) progression can as well be fitted in the (v', 1) progression since in this region of the table the upper state vibrational level interval is about one-half of that of the lower state. The absence of some bands in the (v', 4) progression is probably due to the overlapping of some of the bands of the (v', 1) progression.

Since band origins similar to those observed in the main system are not observed in the present system, the wavenumber data for the band heads (R or P) only are represented in the scheme. The differences between R—R heads and P—P heads were used in the evaluation of the vibrational constants taking band head data for which accurate measurements have been possible. The ν_e values calculated from bands distributed all over the scheme are found to be fairly consistent. The band heads can be represented by the following quantum formula

$$\nu = 24683.3 + (101.3\ u'. - 0.1\ u'^2) - (206.5\ u'' - 6.5\ u''^2)$$

The following points lend support to the analysis proposed here.

(1) The absence of bands with $v'' > 5$ indicates a clear case of predissociation in the lower state of this system. This gives further justification for identifying this level with the upper state of the main system in which such a predissociation was also noticed by Howell and Coulson at $v'' = 5$. Thus one of

the electronic levels involved in the emission of this band system is one which is well established for this molecule.

(2) The intensity distribution in the system is shown in Table IV. It can be seen that the locus of the strongest bands falls on a typical condon curve which is to be expected with such relative values of ω_e as occur here. The curve is neither a narrow parabola which means that ω_e values are of the same order nor a wdie open parabola in which case ω_e of one state is a small fraction of that of the other.

(3) The isotopic shifts for Tl^{205} Cl^{37} molecule are calculated with the help of the formula

$$\nu_i - \nu = (\rho - 1)\ (\omega_e' u' - \omega_e'' u'') - (\rho^2 - 1)\ (x_e' \omega_e' u'^2 - x_e'' \omega_e'' u''^2)$$

In spite of the large difference between ω_e' and ω_e'', the expected separations in many cases are small, for the relative values of v' and v'' are such that the main term in the above equation becomes small. In such cases, the isotopic heads must have been either unresolved or lost in the degradation of the main bands. However, for bands involving high v' values, the predicted separations are indeed large ; but such bands are either faint or the calculated positions of the isotopic components coincide with neighbouring main bands. The following two favourable bands for which isotopic heads have been observed with certainty, show separations which are in agreement with the predicted values, as shown in Table V.

TABLE V

Band	Calc. isotopic separation	Obs. isotopic separation
8,4	4.2	4.2
12,2	18.4	19.9

VIBRATIONAL ANALYSIS OF SYSTEM *A*

This system occuring between λ 4300-λ 4150 consists mostly of bands degraded towards the red, though a few of them are violet-degraded. A prominent feature which distinguishes this system from the other is the appearance of the chlorine isotopic heads. For about five bands the Tl^{205} Cl^{37} isotopic components could be detected with certainty. The most intense band at $\nu = 23671.5$ cannot be regarded as the (0,0) band, since with such a classification it was not possible to account for the isotope splitting of the order of 8 wavenumber units. A close examination of the system revealed that the prominent bands at λ 4188.45, 4217.43, 4244.21 form an obvious progression. The order of the $\Delta G(v)$ intervals between these bands suggested that the lower state of this system is the same as that of the other system. On this basis, the quantum array shown in Table VI is built up. The classification of the bands is shown in the last column of Table II.

TABLE VI

v' \ v''	0	1	2	3	4	5
0			23671.3			
			107.5			
1			23779.6*			
			89.5			
2		24045.3	23868.5	23704.5	23554.9	
		176.8	*164.0*	*95.5*	*149.6* *95.2*	
3				23800.0	23650.1	
				89.6	*149.9* *94.6*	
4				23889.6	23744.7	23609.4
					144.9 *90.6*	
5					23835.3	
6						
7						23907.7

* Measurement uncertain

The $\Delta G(v')$ intervals suggest that the upper state frequency of this system is of the same order of magnitude as that of the upper state of system *B*. As the number of bands is less, the vibrational constants cannot justifiably be determined. The following values may, however, be suggested

$\nu_{0,0} \sim 24040\ \text{cm}^{-1}$. $\omega_e' \sim 100$, $\omega_e'' \sim 206$ (same as for system *B*).

Considering that the lower state is common to both the systems and that the upper vibrational constants are approximately equal, the approximate predicted Tl^{205} Cl^{37} isotopic separations may be compared with those observed in 5 bands, as shown in Table VII.

TABLE VII

Band	Approx.-calc. isotopic separation	Obs isotopic separation
0,2	9.1	8.3
3,3	7.4	11.1
2,4	10.0	12.4
3,3	5.0	7.5
4,5	7.1	7.9

This table shows that the observed separations are of the same order as the predicted values calculated from approximate values of vibrational constants. The absence of bands with $v'' > 5$ is noteworthy, which indicates a clear case of predissociation in the lower state of this system. This is a further justification for the identification of this level with the lower state of the other system. It is probable that there is predissociation in the upper state also as the number of v' levels observed is limited. This explains why a few bands alone are observed in the system. The intensity distribution in the

bands is shown in Table VIII. As the separation of the (0,0) bands of these two systems is approximately 580 cm^{-1}, it is very probable that the upper levels may form an electronic doublet.

TABLE VIII

	0	1	2	3	4	5
0			8			
1			2			
2		1	3	5	3	
3				4	2	
4				1	3	1
5					1	
6						
7						

ELECTRONIC TRANSITIONS IN TlCl

The electronic states of the related group III elements Al, Ga, In, etc. have been discussed by Miescher and Wehrli (1934 & 1935), Howell and others. Holst (1934) and Jennergren (1948) have established the ground states of the molecules AlCl and AlBr as $^1\Sigma^+$. By analogy, the other molecules may in all probability be a similar $^1\Sigma^+$. Miescher and Wehrli consider that the doublet systems observed in the Ga and In halide spectra are due to forbidden transitions between the ground level and certain components of a triplet level. Both of these systems have a common lower state $^1\Sigma^+$ arising from the electron configuration $\sigma^2\pi^4$. The excitation of one of the π electrons produces the configuration $\sigma^2\pi^3\sigma$ giving rise to the molecular states $^1\Pi$, $^3\Pi_0^+$, $^3\Pi_0^-$, $^3\Pi$, and $^3\Pi_2$ (inverted) Howell suggested that the doublet system in TlF may be identified as due to a forbidden transition $^3\Pi_0$—$^1\Sigma^+$ and $^3\Pi_1$—$^1\Sigma^+$, and the singlet system occurring on the violet side as due to the transition $^1\Pi$—$^1\Sigma^+$. In TlCl, Howell and Coulson found only one component of the doublet system which was identified as due to the transition $^3\Pi_1$—$^1\Sigma^+$. They also suggested that the diffuse bands and continuum in TlCl around λ 2500 may be due to the transition $^1\Pi$—$^1\Sigma^+$. The vibrational analysis of the two new systems analysed in the present work have shown that the lower state of these two systems is the upper state of the system $^3{}_1\Pi$—$^1\Sigma^+$. Hence the lower state of the two systems is a $^3\Pi_1$. To identify the upper states, it is necessary to examine the next higher states resulting from the configuration $\sigma^2\pi^3\pi$. This configuration will give rise to states $^3\Sigma^+$, $^1\Sigma^+$, $^1\Sigma^-$, $^1\Delta$, $^3\Sigma^-$ and $^3\Delta$. The close proximity of the two systems suggests that the upper states may

form an electronic doublet. Hence the upper states are to be identified as two members of a triplet level. Since the lower state is a $^3\Pi_1$, the upper states may be the members of either $^3\Delta$ or a $^3\Pi$ term. Since the doublet separation is only of the order of 580 cm.$^{-1}$ it appears more probable that the upper states may be two members of a $^3\Delta$ term, which is one of the excited states of the electron configuration $\sigma^2\pi^3\pi$.

The author has recently received from Prof. E. Miescher (1941) the reprint of his paper on band spectrum of thallium chloride, in which he recorded some of the bands in both the systems reported here, but no analysis was presented for these bands.

ACKNOWLEDGMENTS

The author is grateful to Mr. C. Ramasatry for giving helpful suggestions in the course of the work and to Prof. K. R. Rao for his interest and guidance, and to Prof. E. Meischer for sending him the reprint of his paper referred to above.

REFERENCES

Butkow, 1929, *Zeit. f. Physik.*, **58**, 232.
Holst, 1934, „ „ **93**, 65.
Howell, 1937, *Proc. Koy. Soc.*, **160**, 242.
Howell and Coulson, 1938, *Proc. Roy. Soc.* **166**, 238.
Jennergren Carl Gustav, 1948, *Nature*, **161**, 315.
Miescher and Wehrli, 1934, *Helv. Phys. Acta.*, **7.3**, 298.
„ „ 1935, „ „ **8**, 279.
Miescher 1941, *Helv. Phy. Acta.*, **14**, 148.
Neujmin, 1934, *Phys. Zeit. Sowjet.*, **5.4**, 580.
Rao Tiruvenganna and Rao K. R., 1949, *Ind. Jour. Phy.*, **23**, 185.

RADIATION RESISTANCE OF SKEW-WIRE RADIO FREQUENCY TRANSMISSION LINES

By S. S. BANERJEE and R. R. MEHROTRA

(*Received for publication, April 19, 1949*)

ABSTRACT. An equation has been developed for calculating the radiation resistance of skew-wire high frequency transmission lines, by the method of 'induced e.m.f.' It has been shown that the general formula derived can be applied for any orientation of the transmission lines with respect to each other. In view of the practical layout design of transmission lines, six special cases of orientation of the lines have been considered, for which the expressions for radiation resistance have been deduced mathematically and verified by independent process. Finally, for practical verification of the expressions obtained, the variation of radiation resistance of skew-wire transmission lines without taper when the angle of elevation of one of the wires is increased, has been experimentally determined.

INTRODUCTION

The study of the radiation resistance of transmission lines has recently gained considerable importance due to their wide applications at very high frequencies. Radiation resistance of parallel and coplanar tapered-wire in high frequency transmission lines and the effects of bends and curves of various types on the same have been studied by one of us (Banerjee, 1935; Banerjee and Singh, 1936) previously. It may be mentioned however, that the transmission lines instead of always being coplanar may happen to be skew owing to the unavoidable layout of the transmission lines. In the present communication we have developed a general formula for the calculation of radiation resistance for half wave length long skew-wire transmission lines, with any kind of orientation of the two wires with respect to each other. For the practical use of the problems six special cases have been considered for different orientations of the lines for which the expressions for radiation resistance have been deduced from the general equation and verified independently by the method of 'induced e.m.f.'

THEORETICAL CONSIDERATIONS

Let BP and CR in Fig. 1 represent two skew-wires half wavelength long. The total radiation resistance R_T of the two wires of transmission lines when the currents in them are in antiphase is given by

$$R_T = 2(R_{11} - R_{12}) \qquad (1)$$

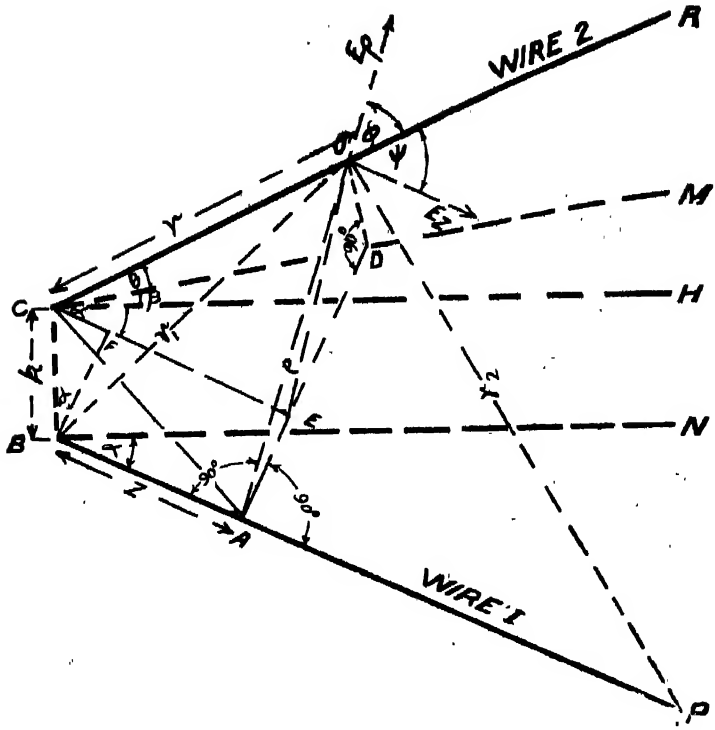

FIG. 1

where R_{11} is the radiation resistance of one of the wires and R_{12} is the radiation resistance of one wire due to the other. R_{11} can be calculated after Pistolkors (1929) and Banerjee (1935). R_{12} can be calculated from the relation,

$$R_{12} = -\int^{l} \frac{E_r}{I} \sin(mr)dr \qquad (2)$$

where E_r is the value of electric field at any point O along the wire 2 due to the current in the wire 1 (Fig. 1). For the calculation of E_r we have to find out the value of electric intensity E_z parallel to the wire 1, and E_ρ perpendicular to this direction as shown in Fig. 1. We will then have,

$$E_r = E_z \cos\psi + E_\rho \cos\phi \qquad \ldots (3)$$

where ψ is the angle between E_z and the wire 2, and ϕ is the angle between E_ρ and the same wire. By evaluating E_z and E_ρ after Carter (1932) it may be shown that

$$R_{12} = 30\int_{o}^{l} \frac{\sin m r_2}{\gamma_2} \cos\psi \sin(mr)dr + 30\int_{o}^{l} \frac{\sin m r_1}{\gamma_1} \cos\psi \sin(mr)dr$$

$$-30\int \frac{\sin m r_2}{r_2} \cdot \frac{Z-l}{\rho} \cdot \cos\phi \sin(mr)dr$$

$$-30\int \frac{\sin m r_1}{r_1} \cdot \frac{Z}{\rho} \cos\phi \sin(mr)dr. \qquad \ldots (4)$$

where $m = 2\pi/\lambda$, l = length of the wires, Z and ρ are the coordinates of the point O with reference to wire 1, and r_1 and r_2 are the distances of the point O from the input and output ends respectively of wire 1. Thus, knowing the values of Z, ρ, r_1, r_2, ϕ and ψ from the orientation of the lines, the radiation resistance, can be calculated with the help of equation (4). For representing the orientation of the lines for the general case of skew-wires a reference plane is taken which is defined as the plane containing one wire and the line joining the input ends of the wires. The angle which the other wire makes with the reference plane is the angle of elevation. The reference plane mentioned above is the plane of the paper in Fig. 1. Wire 1 lies on this plane and wire 2 makes an angle of elevation θ with this plane. CM represents the projection of wire 2 on the reference plane and therefore angle MCR = angle θ. The tapering angles for these wires may be represented by the angles which these wires, or their projections on the reference plane, make with the lines drawn on the reference plane perpendicular to the line joining the input ends of the transmission lines. In Fig. 1, angle PBN and angle MCH, represented by α and β respectively, are the tapering angles of wires 1 and 2.

Now, for evaluating Z, ρ, r_1, r_2, ϕ and ψ take any point O on the wire 2, at a distance r from the input end of this wire. From O draw a line OA perpendicular to wire 1. AD is the projection of the line OA on the reference plane. Draw CE perpendicular to AD and BF perpendicular to CE. It will be seen from the diagram that $\angle CBF = \angle ECH = \angle\alpha$.

Now $$Z = AB = CE - CF = CD\cos(\alpha+\beta) - k\sin\alpha,$$

and, as $$CD = r\cos\theta,\ Z = r\cos\theta\cos(\alpha+\beta) - k\sin\alpha \quad \ldots (5)$$

$$\rho = OA = \sqrt{AD^2 + OD^2} = \sqrt{(AE+ED)^2 + OD^2}$$

As $AE = BF = k\cos\alpha$, and $ED = CD\sin(\alpha+\beta) = r\cos\theta\sin(\alpha+\beta)$

we get $$\rho = \sqrt{\{r\cos\theta\sin(\alpha+\beta) + k\cos\alpha\}^2 + r^2\sin^2\theta} \quad \ldots (6)$$

$$r_1 = OB = \sqrt{\rho^2 + Z^2} \quad \ldots (7)$$

$$r_2 = OP = \sqrt{\rho^2 + (l-Z)^2} \quad \ldots (8)$$

For calculating the angles ϕ and ψ, join AC and OE. In the ΔACO the angle $AOC = \phi$ and

$$\cos\phi \quad \frac{r^2+\rho^2-AC^2}{2r\rho},$$

Now $$AC^2 = CB^2 + BA^2 - 2CB.BA\cos(CBA) = k^2 + Z^2 + 2kZ\sin\alpha$$

$$\phi = \cos^{-} \quad \frac{r^2+\rho^2-k^2-Z^2-2kZ\sin\alpha}{2r\rho} \quad \ldots (9)$$

For calculating ψ triangle CEO is considered in which angle $OCE = \psi$

$$\therefore \quad \cos\psi = \frac{OC^2 + CE^2 - OE^2}{2.OC.CE} = \frac{r^2 + r^2\cos^2\theta\cos^2(\alpha+\beta) - OD^2 - DE^2}{2r^2\cos\theta\cos(\alpha+\beta)}$$

$$= \frac{r^2 + r^2\cos^2\theta\cos^2(\alpha+\beta) - r^2\sin^2\theta - r^2\cos^2\theta\sin^2(\alpha+\beta)}{2r^2\cos\theta\cos(\alpha+\beta)}$$

$$= \cos(\alpha+\beta)\cos\theta$$

$$\therefore \quad \psi = \cos^{-1}[\cos(\alpha+\beta)\cos\theta] \qquad \ldots \quad (10)$$

The six special cases mentioned previously have been considered below for calculation of radiation resistance. It may be mentioned, however, that as r_1 and r_2 are functions of ρ and Z, we will consider the expressions for Z, ρ, ϕ and ψ only in the following cases.

Case 1. Skew wires with single taper, ($\alpha = 0$).

Substituting $\alpha = 0$ in equations (5), (6), (9) and (10) we get

$$Z = r\cos\theta\cos\beta$$

$$\rho = \sqrt{[r\cos\theta\cos\beta + k]^2 + r^2\sin^2\theta}$$

$$\phi = \cos^{-1}\left[\frac{r^2 + \rho^2 - k^2 - Z^2}{2r\rho}\right]$$

$$\psi = \cos^{-1}[\cos\beta\cos\theta]$$

Case 2. Skew-wires without taper.

For this case, $\alpha = \beta = 0$, which gives from the same equations as mentioned in case 1,

$$Z = r\cos\theta$$

$$\rho = \sqrt{k^2 + r^2\sin^2\theta}$$

$$\phi = \cos^{-1}\left[\frac{r\sin^2\theta}{\rho}\right], \quad \text{and } \psi = \theta$$

Case 3. Coplanar tapered wire.

For coplanar wires $\theta = 0$ and substituting this in equations (5), (6), (9) and (10) we get,

$$Z = r\cos(\alpha+\beta) - k\sin\alpha$$

$$\rho = k\cos\alpha + r\sin(\alpha+\beta)$$

$$\phi = [\pi/2 - (\alpha+\beta)] \text{ and } \psi = (\alpha+\beta)$$

Case 4. Coplanar wires with equal taper.

In this case $\theta = 0$ and $\alpha = \beta$ and we have

$$Z = r \cos 2\alpha - k \sin \alpha$$

$$\rho = r \sin 2\alpha + k \cos \alpha$$

$$\phi = (\pi/2 - 2\alpha) \quad \text{and} \quad \psi = 2\alpha$$

Case 5. Coplanar wires with single taper ($\theta = \alpha = 0$).

This will give,

$$Z = r \cos \beta, \; \rho = k + r \sin \beta$$

$$\phi = \pi/2 - \beta \quad \text{and} \quad \psi = \beta$$

Case 6. Parallel wires.

This is obtained by making $\theta = \alpha = \beta = 0$ which leads to the usual expressions given as,

$$Z = r, \; \rho = k, \; \phi = \pi/2 \quad \text{and} \quad \psi = 0$$

values of Z, ρ, ϕ and ψ obtained in the above equations have been verified by evaluating them from their actual orientations, the diagramatic representations of which have not been shown separately.

EXPERIMENTAL

The radiation resistance of skew wire transmission lines with any orientation can be determined experimentally by the method adopted by Banerjee (1935) and subsequently by Banerjee and Singh (1936) for measuring the radiation resistance of parallel and coplanar tapered transmission lines. In the present communication, however, the variation of radiation resistance of untapered skew-wires as described in case 2, in the previous section, has been experimentally determined, when the angle of elevation of one of the wires is increased.

In the case of skew-wires the mean radiation resistance per unit length is obtained from the relation

$$R = 2\alpha \sqrt{L/C},$$

where α is the attenuation constant, and, L and C are the mean values of inductance and capacity per unit length of the wires. The mean value of $\sqrt{L/C}$ can be written as,

$$\frac{120}{\sqrt{2l^2(1-\cos\theta)+k^2}-k} \int_k^{\sqrt{2l^2(1-\cos\theta)+k^2}} \log_e \frac{2x}{d} dx$$

where d is the diameter of the wire and x is the separation between the wires, denoted by the distance between any two points on the two transmission lines which are equidistant from their respective input ends. After integrating the above expression, we get,

$$\sqrt{L/C} = \frac{120}{\sqrt{2l^2(1-\cos\theta)+k^2}-k}\left[\sqrt{2l^2(1-\cos\theta)+k^2}\left(\log_e\frac{2\sqrt{2l^2(1-\cos\theta)+k^2}}{d}\right)\right.$$

$$\left.-\sqrt{2l^2(1-\cos\theta)+k^2}-k\log_e\frac{2k}{d}+k\right]$$

The attenuation constant α is determined experimentally as stated above, by drawing resonance curves obtained by noting the deflections in a sensitive galvanometer at the input end of the transmission lines as a short circuiting bridge is moved along the lines. It should be mentioned, however, that the short circuiting metal bridge is moved along the length of the wires in such a way that the points of contact of the bridge with the wires may be equidistant from their respective input ends. Thus finding out α and the mean value of $\sqrt{L/C}$, radiation resistance is obtained for various angles of elevation of one of the wires.

TABLE I

Wavelength—254.0 cm.

Distance between input ends—5.0 cm.

Angle of elevation	Total radiation resistance in ohms (observed)	Total radiation resistance in ohms (calculated)
0°	5.96	5.92
2°	10.49	10.19
4°	14.11	14.01
6°	15.39	15.34

Table I shows the radiation resistance of untapered skew-wire transmission lines half wave-length long when angle of elevation, θ, of one of the lines is increased. Column 2 contains the experimentally observed values of radiation resistance and column 3 gives the calculated values for comparison. It may be mentioned, however, that as the experimentally observed values of radiation resistance include the ohmic resistance of the lines, the values shown in column 2 contain the sum of radiation resistance calculated from equation (4) and the high frequency ohmic resistance of the lines. Fig. 2 shows the variation of radiation resistance of untapered skew-wire transmission lines, as the angle of elevation of one of the lines is increased. The dotted line shows the calculated variation of radiation resistance and the continuous one represents the experimental variation.

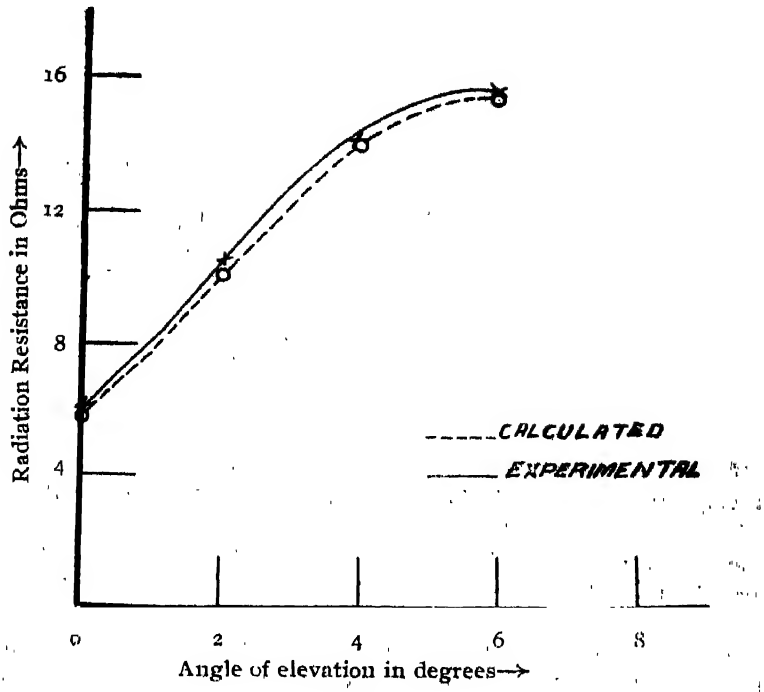

FIG. 2

SUMMARY AND CONCLUSION

A general formula for calculating radiation resistance of skew-wire radio-frequency transmission lines has been obtained by the method of 'induced e.m.f.' It has been shown that with the help of this formula radiation resistance can be calculated for any orientation of the transmission lines with respect to each other, and equation for six special cases of orientation of the lines have been derived from the general formula and verified independently. For the sake of practical interest, the variation of radiation resistance in one of the above cases, namely, for skew-wire transmission lines without taper, when the angle of elevation of one of the wires is increased, has been verified experimentally.

ACKNOWLEDGMENTS

In conclusion the authors have pleasure to record their sincere thanks to Principal M. Sengupta and Prof. G. C. Mukerjee for their kind interest in the above investigation.

SECTION OF COMMUNICATION
ENGINEERING AND APPLIED PHYSICS
ENGINEERING COLLEGE,
BENARES HINDU UNIVERSITY.

REFERENCES

Banerjee, S. S., (1935), *Phil. Mag.*, **19**, 787.
Banerjee, S. S. and Singh, B. N., (1936), *Phil. Mag.*, **22**, 955.
Carter, P. S., (1932), *Proc. Inst. Rad. Eng.*, **20**, 1004.
Pistolkors, A. A., (1929), *Proc. Inst. Rad. Eng.*, **17**, 562.

THE PRINCIPAL MAGNETIC SUSCEPTIBILITIES OF SINGLE CRYSTALS OF RARE EARTH SALTS AT LOW TEMPERATURES. PART III—NEODYMIUM SALTS

By A. MOOKHERJI

(Received for publication, June 27 1949)

ABSTRACT. The principal susceptibilities of neodymium salts have been measured from room temperature down to liquid air temperature. The results are discussed in terms of Crystalline Field Theory. It is found that (1) though the mean susceptibility can be explained satisfactorily on the basis of a single cubic field even of the fourth degree, the absolute magnitude of the fourth order cubic field estimated in this manner from the magnetic data will not be correct, (2) the cubic part of the field in the various neodymium salts estimated from magnetic data on the assumption that the cubic part of the field is wholly of the fourth degree, is found to vary markedly from crystal to crystal. (3) The influence of the fourth and six degree terms of the cubic field on the Stark splitting of the rare earth ions and in crystals, and their large magnetic anisotropy go to show that the low lying energy levels as observed in absorption spectra cannot be attributed to cubic field alone. (4) The χ_1–axis of neodymium sulphate rotates by about 7° in the range studied.

INTRODUCTION

Penney and Schlapp (1932) have attempted to estimate the character and the size of the crystalline electric field acting on the Nd^{+++}ion in crystals. They find that a cubic field of fourth degree represented by $D(x^4+y^4+z^4)$ gives quite a good agreement with the measurement of $Nd_2(SO_4)_3 8H_2O$ by Gorter and de Haas (1931). These values of magnetic measurements give a crystalline electric field which is about three times higher than the field estimated from the magnetic measurements of Zernicke and James (1926) and St. Meyer (1925). In spite of these discrepancies one fact stands out clearly that the effective mean square moment as determined by each set of workers can be explained on the assumption of a single suitable cubic field (different for different workers) which is the same at all temperatures in the range studied.

The cubic field referred to is generally regarded as of the fourth degree and though the mean of the three principal susceptibilities can be explained satisfactorily on the basis of such a field—but the absolute magnitude of this fourth degree field as estimated by Penney and Schlapp and others (Spedding, 1937) will not be correct, since the sixth degree terms of the cubic field also influences the susceptibility of the Nd^{+++}ion, and the magnitudes of the fourth degree and six degree terms in the crystals of Nd^{+++}ions are not known.

In this communication is reported the magnetic measurements on single crystals of neodymium salts from room temperature to liquid air temperature. The results are discussed in terms of the ground level split by the cubic field of fourth and sixth degrees. The calculations of the low lying energy levels from the measurements on absorption spectra of the rare earth ions in crystals are also discussed.

EXPERIMENTAL

Crystals were grown out of aqueous solution of highly pure rare earth specimens, a gift from Professor Trombé of Paris University.

The experimental methods used in these measurements were the same as adopted in our previous measurements on cerium salts (Mookherji, 1949).

RESULTS

The results of measurements are collected in Tables I to IV. The nature of variation of magnetic anisotropy and of the square of the principal moments with absolute temperatures are shown in Figs. 1 to 5.

Notations and diamagnetic corrections used in this paper are the same as adopted in our previous paper on cerium salts.

MAGNETIC BEHAVIOUR OF Nd^{+++} ION IN FOURTH AND SIXTH DEGREE CUBIC FIELD

The ground state of the Nd^{+++} ion is $^4I_{9/2}$. The next higher level is separated from it by about 2510 cm^{-1} and hence in neodymium salts at all ordinary temperatures, the higher level will have very little influence on the magnetic properties.

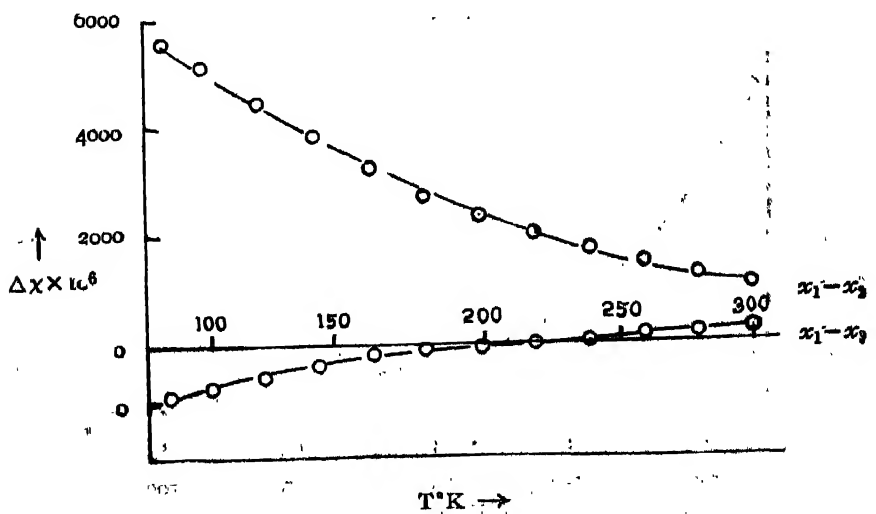

FIG. 1

$Nd_2(SO_4)_3, 8H_2O$

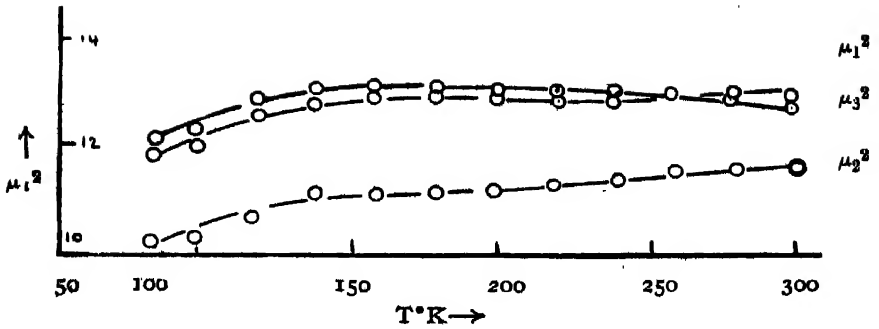

FIG. 2
$Nd_2(SO_4)_3, 8H_2O$

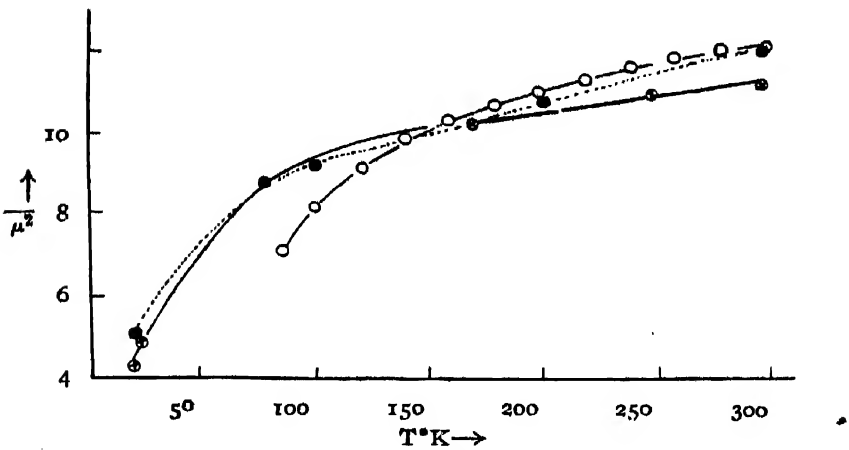

FIG. 3
$Nd_2(SO_4)_3, 8H_2O$
• — Gorter
× — Jackson
o — Author

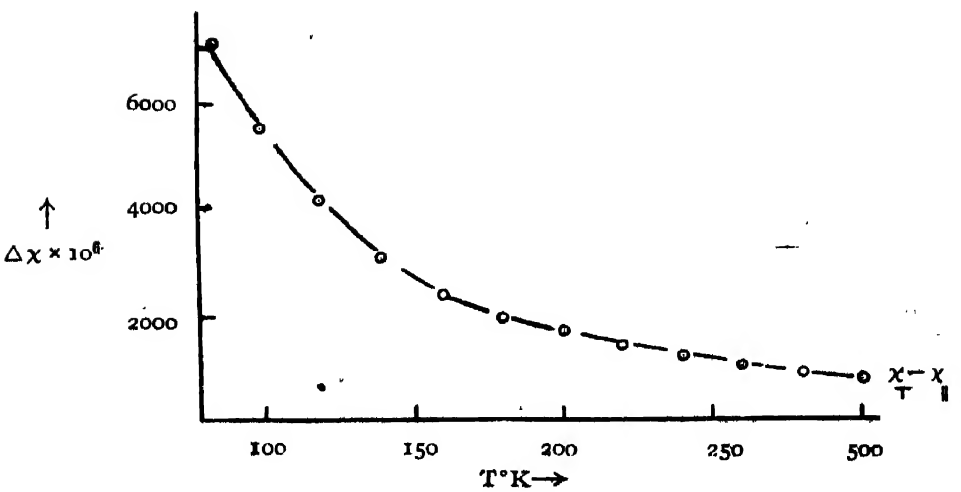

FIG. 4
$Nd_2Mg_3(NO_3)_{12}, 24H_2O$

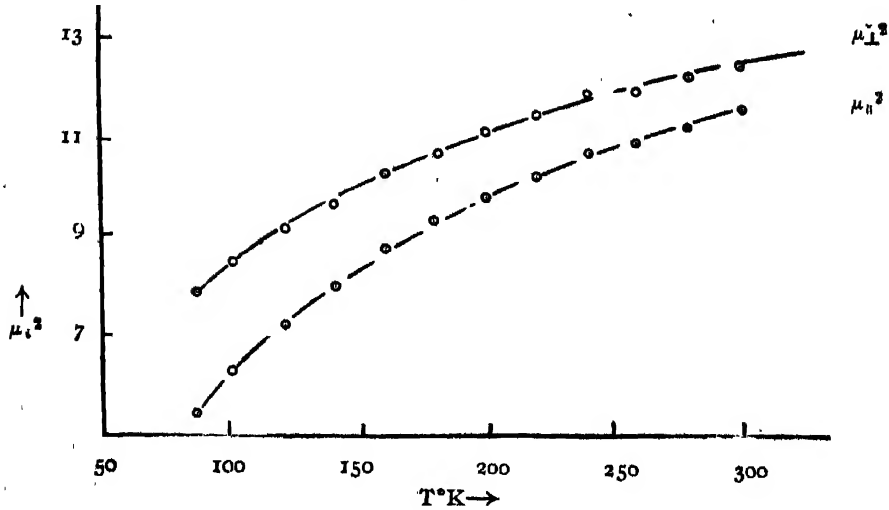

FIG. 5

$Nd_2Mg_3(NO_3)_{12}$, $24H_2O$

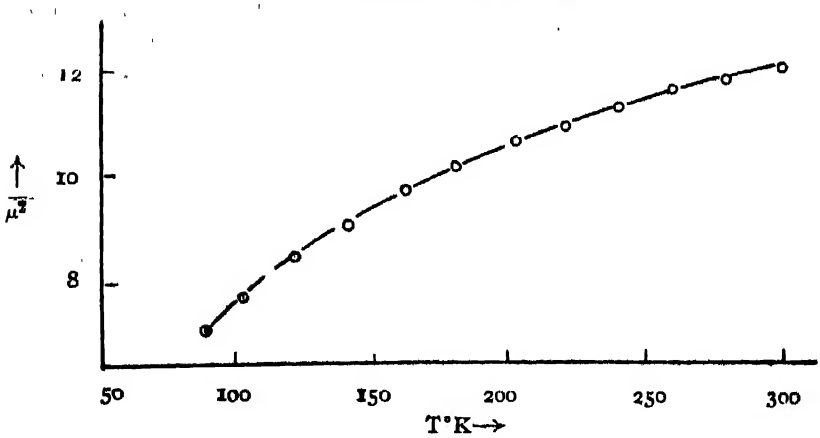

FIG. 6

$Nd_2Mg_3(NO_3)_{12}$, $24H_2O$

TABLE 1

Magnetic Anisotropy at 30°C

Crystal	Crystallographic data	Mode of suspension	Orientation in the field	$\Delta\chi$	Magnetic Anisotropy
$Nd_2(SO_4)_3$, $8H_2O$	Monoclinic prism $a:b:c$ 2.983 : 1 : 1.997 $\beta = 118°8'$	'b' axis vertical	$\theta = +14.6$	960	$\chi_1 - \chi_2 = 960$
		'a' axis vertical	'b' axis along field	188	$\chi_1 - \chi_2 = -122$
		(001) pl. hor.	'b' axis along field	1016	$\psi = 13.5$ Cal $\psi = 12.9$
$Nd_2Mg_3(NO_3)_{12}$, $24H_2O$	Trigonal	Trig. Axis horizontal	Trig. Axis normal to field	636	$\chi_\perp - \chi_\parallel = 636$

TABLE II

Absolute Susceptibility along a convenient direction

Crystal	Direction along which susceptibility was measured	Temp. °C	Density of the crystal	Vol. Susceptibility	Corresponding gm. mol. sucept.	Corresponding gm. mol. sucept. at 30°C
$Nd_2(SO_4)_3, 8H_2O$	Along χ_1–axis	30.5	2.988	41.93	10110	10130
$Nd_2Mg_3(NO_3)_{12}, 24H_2O$	Normal to Trig. axis	28.0	2.185	12.67	9610	9550

Unlike cerium, and praseodymium, the splitting of the energy levels of Nd^{+++}-ion in a cubic field depends on whether the cubic field involves only the fourth degree terms or, in addition, terms of the sixth degree also. This is particularly so with the separations of the lower levels as will be seen from Table V taken from a paper by Kynch (1937) which gives the energy levels, under a cubic field involving fourth degree terms only and also under a cubic field involving both fourth degree and sixth degree terms. The magnitudes of these two groups being chosen on the basis of known distance of the negatively charged atoms surrounding the Nd^{+++}-ion in the crystal.

Hence in neodymium salts the estimate of the magnitude of the cubic part of the field from the observed mean susceptibility data will be very different according as we choose fourth degree terms alone or include sixth degree terms also. Taking, for example, $Nd_2(SO_4)_3, 8H_2O$ in which the crystalline field in the neighbourhood of Nd^{+++}-ion cannot be much different from that in the neighbourhood of Pr^{+++}-ion in the crystal of $Pr_2(SO_4)_3, 8H_2O$, since the two crystals are isomorphous, we find that, with a cubic field of the fourth degree, the energy levels will be given by (Penney and Schlapp, 1932)

$$\left.\begin{aligned} W_1 &= 20.95A \\ W_2 = W_3 &= 9.11A \\ W_4 = W_5 &= 19.59A \end{aligned}\right\} \quad (1)$$

where 'A' is a constant of the fourth degree cubic field. If the fields are exactly the same in the praseodymium and neodymium salts, A_{Nd}/a_{Pr} should be equal to 17.8 according to the calculation of Penney and Kynch (1939).

Now assuming a purely fourth degree cubic field for neodymium, the mean of the three principal susceptibilities will be given by (Penney and Schlapp, 1932)

$$\begin{aligned} \bar{\chi} = \frac{2Ng^2\beta^2}{A}\,[&(.1483e^{19.59\nu} + .239e^{-9.11\nu} - .3879e^{-20.95\nu}) \\ &+ (6.065e^{19.39\nu} + 4.031e^{-9.11\nu} + 1.68e^{-20.95\nu})] \\ &+ [2e^{19.55\nu} + 2e^{-9.11\nu} + e^{-20.95\nu}] \end{aligned} \quad (2)$$

where $\nu = A/kT$

TABLE III

Temperature variation of Magnetic Anisotropy

Crystal	Temp. °K	Suspension used for measurement		$\chi_3-\chi_1$	θ'
		'b' axis vertical	'a' axis vertical		
		$\chi_1-\chi_2$	$\chi_3-\chi_1\cos^2\theta-\chi_2\sin^2\theta$		
$Nd_2(SO_4)_3, 8H_2O$	300	998	1040	103	+14.6
	280	1190	1160	41	14.4
	260	1410	1340	9	13.95
	240	1680	1540	− 45	13.6
	220	1980	1780	− 87	13.6
	200	2300	2040	−128	13.6
	180	2700	2360	−194	13.6
	160	3200	2810	−221	13.25
	140	3880	3270	−428	12.4
	120	4540	3730	−636	11.3
	100	5200	4260	−790	9.6
	85	5670	4660	−918	7.0
		Trigonal axis horizontal			
		$\chi_\perp-\chi_\parallel$			
$Nd_2Mg_3(NO_3)_{12}, 24H_2O$	300	668			
	280	807			
	260	965			
	240	1150			
	220	1360			
	200	1620			
	180	1930			
	160	2360			
	140	3080			
	120	4120			
	100	5440			
	85	7040			

TABLE IV

Temperature variation of Principal Susceptibilities

Crystal and direction along which measurement was taken	Temp. °K	χ'_1	χ'_2	χ'_3	$\bar{\chi}'$	μ_1^2	μ^2_2	μ^2_3	$\bar{\mu^2}$
$Nd_2(SO_4)_3\ 8H_2O$, Along χ_1 – axis	300	10520	9520	10620	10220	12.73	11.52	12.89	12.36
	280	11460	10270	11500	10740	12.94	11.60	12.98	12.50
	260	12400	11000	12410	11600	13.00	11.52	13.01	12.50
	240	13400	11720	13350	11940	12.96	11.34	12.91	12.42
	220	14590	12610	14500	13900	12.94	11.19	12.86	12.33
	200	16020	13720	15890	15210	12.92	11.07	12.81	12.27
	180	17960	15250	17760	16990	13.03	11.08	12.89	12.33
	160	20270	17070	20050	19130	13.07	11.01	12.91	12.33
	140	23280	19400	22850	21840	13.14	10.95	12.91	12.33
	120	26550	22010	25910	24820	12.84	10.64	12.54	12.01
	100	30310	25110	29520	28310	12.22	10.12	11.91	11.75
	85	35350	29680	34430	33820	12.12	10.17	11.80	11.36
		$\chi_\perp$	$\chi'_\parallel$	$\bar{\chi}'$	$\mu_\perp^2$	$\mu_\parallel^2$	$\bar{\mu^2}$		
$Nd_2Mg_3(NO_3)_{12}$, $24H_2O$ Along χ_1 – axis	300	10290	9620	10070	12.45	11.63	12.18		
	280	10790	9980	10520	12.18	11.15	11.84		
	260	11350	10380	11030	11.99	10.88	11.56		
	240	12260	11110	11880	11.87	10.75	11.50		
	220	12840	11840	12840	11.39	10.18	10.99		
	200	13740	12120	13200	11.08	9.772	10.64		
	180	14730	12800	14090	10.69	9.287	10.22		
	160	15880	13520	15090	10.24	8.722	9.733		
	140	17110	14030	16080	9.658	7.980	9.076		
	120	18830	14710	20400	9.722	7.120	8.450		
	100	20900	15460	26050	8.427	6.233	7.690		
	85	22900	15860	28190	7.898	5.466	7.050		

TABLE V

Only Fourth degree terms	0, 63.8 278.6 cm^{-1}
Sixth degree terms also included	0, 33.7 204.8 cm^{-1}

The value of A which fits best with experimental data is $A = -7.0$ cm^{-1} ; the observed and calculated values are shown in Table VI.

TABLE VI

$A = -7.0$ cm^{-1}

Temperature °K	$\overline{\mu^2}$	
	Calculated	Observed
300	12.7	12.5
200	12.6	12.3
100	11.8	11.8
85	11.6	11.4

This value of A will correspond to $a = -.393$ for Pr^{+++} ion in the same field, whereas the actual value of 'a' for Pr^{+++} ion deduced directly from the magnetic data for $Pr_2(SO_4)_3$, $8H_2O$ is $-.585$ cm^{-1} (Mookherji, 1949).

The discrepancy is evidently due to the occurrence of the sixth degree terms in the actual fields (the second degree terms, which represent the rhombic part of the field, will not affect the mean square moment appreciably).

The discrepancy is even more striking in $Nd_2Mg_3(No_3)_{12}$, $24H_2O$ of which A calculated from the magnetic measurements on the assumption of fourth degree cubic terms alone come out as $A = -32$ cm^{-1} which will be equivalent to $a = -1.8 cm^{-1}$ for Pr^{+++} ion in the same field, whereas the value of 'a' calculated directly from the magnetic measurements on $Pr_2 Mg_3 (NO_3)_{12}$, $24H_2O$ (Mookherji, 1948) in which the crystal field is presumably the same as in $Nd_2Mg_3(NO_3)_{12}$, $24H_2O$ is $a = -0.508$ cm^{-1}.

It is clear from the foregoing discussions that while in cerium, and to a good approximation in praseodymium also, the estimate of the cubic field, assumed to be wholly of the fourth degree, from the magnetic data will be of correct magnitude, it will not be so in Nd^{+++} ion, and hence any estimate of the cubic field from the magnetic data will be unreliable in the absence of previous knowledge regarding the relative magnitudes of the two types of terms.

This is evidently the explanation of the enormous variation in the magnetic behaviour of Nd^{+++} ion in different salts of neodymium ; whereas in cerium and praseodymium salts the magnetic behaviour does not show

such marked variations : this is due to the fourth degree terms of the cubic field being of nearly the same order in all salts but not the sixth degree terms.

For the octahydrated sulphate magnetic data at very low temperatures are available for the mean susceptibility from the measurements of Görter and de Haas (1931) on the powder crystal and for the principal susceptibilities from those of Jackson (1939) on single crystals. These data are given in Tables VII and VIII for comparison.

It has been observed that χ_1—axis of $Nd_2(SO_4)_3$, $8H_2O$ crystals rotate through 7 degrees as the temperature is lowered from 300°K to 85°K.

TABLE VII

T°K	300	288.5	200	100	20.4
$\bar{\mu}^2$	11.5	11.4	10.7	9.1	4.86

TABLE VIII

T°K	290	230	170	120	90	75	65	20
μ_1^2	13.36	12.96	12.40	11.47	10.54	9.78	9.39	7.06
μ_2^2	11.95	11.33	10.38	9.13	8.56	8.12	7.76	4.08
μ_3^2	12.86	12 63	11.89	10.86	9.98	9.32	8.75	5.33
$\bar{\mu}^2$	12.72	12.30	11.59	10.49	9.69	9.07	8.63	5.49

THE ABSORPTION SPECTRA IN RELATION TO THE SEPARATION OF LEVELS IN A CUBIC FIELD

Extensive measurements have been made on the absorption spectra of the rare earth salts, both in solid state and in aqueous solutions, particularly by Spedding (1937) and Freed (1931) and their collaborators. From the absorption measurements the low lying energy levels of the various rare earth ions, M^{+++} have been deduced. Now the number of these levels, and their relative separations are found to accord closely with what one should expect to occur in a cubic field of the fourth degree, and furthermore the overall separations in isomorphous salts of different rare earths are of magnitudes to be expected from nearly the same magnitude of the cubic field. These results are strikingly illustrated by the following Table IX taken from a recent paper by Penney and Kynch (1939) in which the calculated values refer to a cubic field of the fourth degree of the same magnitude in all cases, the magnitude of the field being so chosen as to give in Nd^{+++} the observed overall splitting of 260 cm^{-1}. The agreement between the observed and the calculated values is indeed very impressive.

From this close fit, Spedding concludes that the absorption measurements can give the energy levels much more accurately than the magnetic data—which is readily conceded, since the calculations from the magnetic data are based on the observed deviations of $\overline{\mu^2}$ from the Hund value and these deviations are in most cases small. For the same magnitude of the cubic field, the energy separations involve factors proportional to $Z^4_{\text{effective}} = (Z-\sigma)^4$, where Z is the nuclear charge of the paramagnetic atom, and σ is the screening constant for the $4f$ electrons responsible for the observed magnetic moment of the ion. Since the energy levels can be deduced accurately from the absorption measurements, it should be possible to utilise this data to calculate the precise values of σ, which are not so easily evaluated even from the emission spectroscopic data for the ionized atom.

TABLE IX

Ion	Levels in cm^{-1}	
	Observed	Calculated
Pr^{+++}	0, 110, 235, 500	0, 121, 207, 467
Nd^{+++}	0, 77, 260	0, 76, 260
Er^{+++}	0, 19, 41, 85	0, 19, 38, 85, 89
Dy^{+++}	0, 22, 57, 80, 112	0, 53, 57, 84, 107

In spite of the close inter-consistency of the arguments and the experimental fit, one should view with scepticism the separation of levels as deduced from the absorption spectra as representing the separation produced by a cubic field alone, and that of the fourth degree. Firstly we know that most of these salts are strongly anisotropic magnetically, and the anisotropy of the individual ions should be greater than that of the crystal, since what is observed as the anisotropy of the crystal as a whole is merely an averaged effect of the anisotropies of the differently oriented individual groups. In any case the anisotropy of the individual ions cannot be less than that of the crystal, and even such anisotropy as has been observed for the Pr^{+++} ion (Mookherji 1949) should correspond to a separation which is not much less than that produced by the cubic part of the field. Though the rhombic part of the field has little influence on the mean of the three principal susceptibilities of the crystal, its effect on the separation of the levels is quite large.

Moreover, even if the effect of the rhombic part of the field on the separation of the levels is neglected for the purpose of argument, the cubic part of the field cannot be regarded as consisting of the fourth degree terms alone. At least in the case of Nd^{+++} ion the effect of the sixth degree terms is considerable; whereas the experimental fit suggested by the data given

in Table IX is nearly as good in neodymium salts as in the salts of Pr^{+++}, for example, in which the sixth degree terms are not so effective as in Nd^{+++}.

Lastly the observed absorption spectrum of $Gd_2(SO_4)_3$, $8H_2O$ (Nutting, and Spedding, 1937), is by no means as simple as one should expect from the splitting in the crystalline field. The ground state of Gd^{+++} ion is an *S*-state, ${}^8S_{7/2}$. The splitting in the crystalline field even in strong and asymmetric ones will be quite small, of the order of a few cm^{-1}. Whereas absorption spectra suggest a complicated and widely separated set of energy levels, near the ground level. All of which show that in spite of the apparent coincidence of the energy levels, the low lying energy levels observed in absorption spectra cannot be attributed to the cubic field alone. They may be electronic levels, as influenced by vibrational levels, which in the rare earth salts may be separated by energy differences of the order of a few hundred cm^{-1}.

The evidence from specific heat data is more decisive regarding the separations of the lowest levels, but can give no more information regarding the origin of the separation of levels than absorption measurements.

ACKNOWLEDGMENTS

The work was carried out at the laboratories of the Indian Association for the Cultivation of Science, Calcutta, and the author wishes to express his thanks to its Committee of Managment for affording all facilities. The author also wishes to express his thanks to Sir K. S. Krishnan Kt., D.Sc., F.R.S., F.N.I., for his keen interest and valuable advice and help. Thanks are also due to my friend, Dr. A. Bose, D.Sc., for his valuable discussions and to Prof. Trombé for his gift of pure rare earth specimens.

REFERENCES

Freed, S., 1931, *Phys. Rev.*, **38**, 2122.
Görter, C. J. and de Haas W. J., 1931, *Proc. Roy. Acad. Am.*, **34**, 1249.
Jackson, L. C., 1939, *Proc. Roy. Soc.*, A 170, 266.
Kynch, J. G., 1937, *Trans. Farad. Soc.*, **33**, 1402.
Meyer, St.. 1925, *Z. Phys.*, 26, **51**, 478.
Mookherji, A, 1949, I. *Ind. Jonr. Phys.*, **23**, 207, 309.
Nutting, G. C. and Spedding F. H., 1937, *J. Chem. Phys.*, **5**, 33.
Penney, W. G. and Kynch J. G., 1939, *Proc. Roy. Soc.*, A, **170**, 112.
Penney, W. G. and Schlapp R, 1932, *Phys. Rev.*, **41**, 194.
,, ,, ,, ,, ,, ,, **42**, 666.
Spedding, F. H., 1937, *J. Chem. Phys.*, **5**, 316.
Spedding, and Howe, 1937, *J. Chem. Phys.*, **5**, 415.
Spedding, Hamlin and Nutting, 1937, *J. Chem. Phys.*, **6**, 191.
Zernicke, J. and James, 1926, *Amer. Chem. Soc.*, **48**, 2827.

A NOTE ON THE COMPARISON BETWEEN EMISSION AND FLUORESCENCE SPECTRA (ULTRAVIOLET) OF BENZENE

By R. K. ASUNDI and M. R. PADHYE

(*Received for publication, March 23, 1949*)

ABSTRACT. In the present paper a comparison of a new modified analysis of fluorescence bands and emission bands of benzene in the ultra violet region has been made.

After our work on the emission bands of benzene (Asundi and Padhye, 1949) was completed we got a paper of Garforth and Ingold (1948) kindly sent to us by Professor Ingold, dealing with the fluorescence spectrum of benzene. A preliminary report of our analysis of the emission bands was published in Nature (Asundi and Padhye, 1945) where the fluorescence data then available (Ingold and Wilson, 1936, and Wilson, 1936) were used for a comparison of the spectrum in emission and fluorescence. Garforth and Ingold have now revised the original data of Ingold and Wilson (1925). The list of bands now given by them differs from the original list of band maxima given by Ingold and Wilson (1936) both with respect to the frequencies and intensities, particularly for the weaker bands. A complete analysis of the absorption bands recorded by Radle and Beck (1940) has also been given by them (1948). This agrees closely with the analysis of the same bands done by us also. Hence the main interest now is in the comparison of the new modified analysis of the fluorescence bands and the emission bands of benzene. The fluorescence spectrum, as it is set forth by Garforth and Ingold, is now more similar than before to the emission spectrum of benzene obtained by transformer discharge through flowing benzene vapour. Emission data, however, do not support certain classifications proposed by Garforth and Ingold. A few relevent observations on the comparison between emission and fluorescence spectra are therefore necessary. This is given below in terms of the different series of bands involved.

Series *A*, *B*, *C*, *D* and *F* are common to the two analyses. The *E* series of which there are but two weak bands in fluorescence is not represented in emission at all.

The bands which Garforth and Ingold include among the *G* series are present in emission but are designated by us as the β^0_{1-1} series for reasons which will be clear later. In emission is also observed a series of bands not recorded in fluorescence designated by us as α^0_{1-1}.

According to Garforth and Ingold two distinct series of Fermi doublets occur. One is that due to degeneracy between B^0_{-1}, F^0_0 ; B^0_{-2}, F^0_{-1} etc. This doublet series is also observed in emission where we prefer to designate the bands as α^0_0, β^0_0 ; α^0_{-1}, β^0_{-1} etc. In this series the doublet separation increases from 27, 31, 37 to 39 with the loading of successive quanta of 992 cm^{-1}, and finds an explanation as given in our paper (Asundi and Padhye, 1949*a*).

The second series is given by Garforth and Ingold as due to D^0_{-1}, G^0_0 ; D^0_{-2}, G^0_{-1} etc. In this series only the first pair occurs as two distinct bands with the expected doublet separation of 27 cm^{-1}. Further members of the series are no longer doublets but are represented by only a single band. This would mean that the doublet separation has diminished to zero already with the loading of one more quantum of 992 cm^{-1}. The emission data do not support this interpretation. We prefer to leave the *D*-series undisturbed by Fermi degeneracy.

There is, however, another series of Fermi doublets brought about by bands of *G* series which are designated by us as β^0_{1-1} series and which resonate with bands recorded only in emission (but probably not in fluorescence) and designated by us α^0_{1-1} etc. On this interpretation the Fermi doublet separation again increases, as it should, and in the same way as in the first series when successive quanta of 992 cm^{-1} are loaded on α^0_{1-1}, β^0_{1-1}.

Series *H*, *I*, *J*, and *W* of Garforth and Ingold are also present in emission and are included in our analysis without, however, being so designated. The H^0_{-1} band has for its ground state the Fermi degenerate level α^0_0, β^0_0 (or B^0_{-1}, F^0_0 according to Garforth and Ingold). Accordingly, there are two bands which in our analysis are indicated as $\alpha^0_0 + (2 \times 240)$ and $\beta^0_0 + (2 \times 240)$.

In fluorescence one band each is observed for *M* and *O* series. The *O*-series is present in emission. The *M* band has not been recorded in emission and probably it is masked by the strong C^1_0 band near it.

The *N*-series of Garforth and Ingold has been classified as a part of *C*-series by us. But the relatively greater intensity of the bands as well as the comparatively greater activity of $e_g^-(H)$ frequencies indicate that the classification of Garforth and Ingold is the more likely.

The *Q*-series of Garforth and Ingold coincides with what has been called the *K*-series by us. The frequency of $e_g^+(H)$ vibration, which is determined by this series is according to Garforth and Ingold 3060 cm^{-1}, the corresponding Raman frequency for liquid benzene is 3047 cm^{-1} and our data give 3051 cm^{-1}. Garforth and Ingold suggest that this discrepancy is probably due to a resonance, (due to internal forces in liquid state, Fermi resonance being otherwise forbidden) of this vibration with $a_{1g}(H)$ 3062 in the liquid resulting in an alteration of e_g^+ vibration to 3047 cm^{-1}. We remark,

however, that the bands of this series are all weak and the accuracy obtained by us is not greater than ± 6 cm^{-1}.

The case of the *Y*-series is rather interesting. In our opinion the emission data as well as the principles which govern Fermi interaction are definitely against the classification proposed by Garforth and Ingold. According to us the *Y*-series is represented by a single band (Y''_0) which is weak and is not accompanied by the usual 161 cm^{-1} progression. The bands designated by Y^2_{-1}, Y^2_{-2}, which are already doubtful according to Garforth and Ingold, are clearly to be classified as bands of the *N*-series. We classify the bands Y^0_{-1}, Y^0_{-2} etc. as A'^0_0, A'^0_{-1} etc. Our reasons are the following :—

(*a*) Corresponding bands associated with *B* series, *i.e.*, B'^0_0 etc. are definitely present in the emission spectrum though there is considerable overlap between them and members of the *D*-series. This is discussed in the paper (Asundi and Padhye, 1949).

(*b*) The positions of the bands follow a regular course and there is no evidence of resonance perturbation with the α, β doublet.

(*c*) The Fermi interaction giving rise to α, β doublets is satisfactorily explained on the basis of the first order perturbation theory for two interacting vibrations.

(*d*) That there is no perturbation is further evident from the fact that the overall separation between the triplets remains practically constant with increasing quanta of vibrations. This would not be so if Fermi resonance occurred between this vibration and vibrations giving rise to α, β doublet. There is sufficient outside evidence to show that the interaction apparently increases if the degenerate levels are loaded with quanta of vibrations which are contesting in Fermi resonance. This is experimentally recorded as the increase in doublet separation with added quanta of contesting vibrations. On the other hand, if the Fermi-split levels are loaded with the third non-contesting vibration the separation of the two levels remains the same with successive loading on of the doublet levels with quanta of non-contesting vibrations.

(*e*) With the present interpretation the intensities observed are normal and do not need any explanation.

Apart from these bands which are common to fluorescence and emission spectra, there are over forty additional weak bands recorded in emission only and which find place in our analysis in conformity with selection rules. They have not been assigned to any series but are suitably indicated in our paper by numbers denoting the frequencies of vibrations involved. The maximum vibrational energy in the upper electronic state observed in the emission spectra is slightly greater than that in fluorescence. The extensive-

ness of the data indicates that this method of excitation of polyatomic molecules, if it could be used, has some advantage over the optical method of excitation.

SPECTROSCOPY DEPARTMENT
COLLEGE OF SCIENCE
BENARES HINDU UNIVERSITY

REFERENCES

Asundi and Padhye, 1945, *Nature*, **156**, 368.

Asundi and Padhye, 1949, *Ind. Jour. Phys.*, **23**, 199, 237, 281.

Asundi and Padhye, 1949a, *Ind. Jour. Phys.*, **23**, 281.

Garforth and Ingold, 1948, *Jour. Chem. Soc.*, p. 427.

Ingold and Wilson, 1936, *Jour. Chem. Soc.*, p. 941.

,, ,, 1948, ,, ,, ,, p. 417.

Radle and Beck, 1940, *Jour. Chem. Phys.*, **8**, 507

Wilson, 1936, *Jour. Chem. Soc.*, p. 1210

NEW BANDS IN THE SPECTRUM OF THALLIUM BROMIDE

By P. TIRUVENGANNA RAO

(*Received for publication, Feb. 22, 1949*)

Plate XX

ABSTRACT. The spectrum of thallium bromide is photographed in emission in a high frequency discharge in the first order of a 10 ft. concave grating and also on a quartz Littrow spectrograph. About 40 new bands between λ 4050—λ 3800, attributed to TlBr, have been recorded which are classified into three v′ progressions in the vibrational scheme of the main system $^3\pi - {}^1\Sigma$ given by Howell and Coulson. The observed bromine isotope separations support the analysis. A revised analysis of the brief system of bands between λ 4000 –λ 3950 is given. The lower state of this system is considered the same as the upper state of the main system.

INTRODUCTION

In a previous communication, the author (Rao, 1949) established for the first time the existence of Tl^{203} isotope from a study and measurement of some bands in the main system of thallium bromide, using a dispersion of 5.7 Å/mm. It was also stated that the brief system of bands around λ 3950 observed only in emission by Howell and Coulson (1941) has been obtained together with a set of new bands between λ 3980—λ 3800. The analysis of the brief system of bands around λ 3950 attributed to TlBr has been given by Howell and Coulson in a fragmentary quantum array, which indicated that the lower state of this system is the upper state of the main system. Their analysis was supported by the observed predissociation in both the states which are crossed by two repulsive states. Measurements of these bands with intensities, assigned visually on a 0 - 10 scale, by the author revealed that the intensity of the bands as given in the quantum array by Howell and Coulson differ widely from those assigned by the author. The object of this paper is (1) to interpret the new set of bands between λ 4050—λ 3800 and (2) to re-examine the brief system of bands between λ 4000—λ 3950.

The spectrum has been photographed both on a quartz Littrow spectrograph with a dispersion of about 12 Å/mm. at λ 3950 and in the first order of a 10 ft. concave grating. An exposure of one hour was found sufficient for the development of the brief system using the quartz Littrow instrument, while the additional bands between λ 4050—λ 3800 were photographed on the grating by giving an exposure of 3 hours' duration using Ilford Special rapid plates. The brief system appears with much better contrast when photographed on the quartz Littrow spectrograph than on the grating and therefore an enlargement taken from the former is reproduced in Fig. (*a*), Plate XX. Members of this system appear much more intense than those of the main system in this region of the spectrum. The bands are clearly degraded towards the red. This feature alone serves to distinguish

them from these of the main system. Fig. (*b*) Plate XIX is a reproduction of the additional bands between λ 4050—λ 3860 taken on the grating. These bands are comparatively less intense than those of the main bands in this region of the spectrum and are somewhat diffuse. In view of the diffuse nature of the bands, measurements on their intensity maximum differed by as much as 3 to 4 wavenumber units. Some of these bands above λ 3950, occur in an overlapping region with the brief system. In Fig (*b*) the shorter limbs represent the $TlBr^{79}$ heads and the longer ones, the head of $TlBr^{81}$.

Vibrational analysis of the new bands (λ 4050 – λ 3800)

These bands occur in between prominent groups of the main system in this region of the spectrum. A recurrence of a wavenumber interval of 175 among these bands suggested that they can be interpreted as forming part of the main system. The band at $\nu = 26260$ could be classified as the (3,17) band in Howell and Coulson's scheme for $TlBr^{81}$ and thus the $v' = 3$ progression could be extended up to (3,22), to include the (3,18) and (3,19) bands classified by Howell and Coulson. Two of the bands, viz. (3,21) and (3,22) in this progression are superposed by N_2 bands and hence they appear very intense. As has already been pointed out by the author in a previous paper, the values of v' from (3,20) upwards in Howell and Coulson's classification should be increased by one. Hence the (3,20), (4,20), etc., become (4,20), (5,20), etc. Adopting this new numbering, the $v' = 4$ progression in Table I consists of bands observed by Howell and Coulson. Two more new $v' = 5$ and $v' = 6$ progressions could be built up which include about half of the additional bands obtained in the present work. The remaining bands are interpreted as the $TlBr^{79}$ heads corresponding to those classified in the $v' = 3$, $v' = 5$ and $v' = 6$ progressions. The $v' = 5$ and $v' = 6$ progressions start in Howell and Coulson's classification at values of $v'' > 30$. The $\Delta G(v')$ intervals obtained by them in this region are found to be in keeping with those obtained here. It is to be noted that the $\Delta G(v')$ interval of about 70 between the levels $v' = 2$ and $v' = 3$ falls rapidly to about 40 between the levels $v' = 3$ and $v' = 4$. Some of the bands which occur in a region of overlap with the brief system are also classified, since these could be distinguished by their diffuse appearance from the members of the brief system, which are clearly degraded towards the red. The vibrational analysis of all the new $TlBr^{81}$ bands together with those observed by Howell and Coulson up to λ 4500 is shown in Table I, which starts from the (3,15) band. The high frequency part of the scheme is given in Howell and Coulson's paper. For all the bands between λ 3800—λ 4050, the author's measurements have been used though some of the bands are observed by Howell and Coulson. The $TlBr^{79}$ isotopic separations observed agree fairly well with those to be expected from theory and are of the same order as those observed by Howell and Coulson in this region, The observed separations

are shown in column 6 of Table II; which gives the other data. For comparison, the isotopic separations for the common bands observed by the author and Howell and Coulson are given in column 7. The classification of the bands is shown in the last column of the table.

TABLE II :—TlBr bands

$TlBr^{81}$		$TlBr^{79}$					
Wave-length	Wave-number	Wave-length	Wave-number	Int.	$\Delta\nu$ (observed)	$\Delta\nu$ (H & C)	Classification.
3807.0	26260	3811.3	26230	5	30		3,17
14.0	26212	17.4	26188	2	24		6,18
20.8	26165	24.3	26141	2	24		5,18
26.9	26124	30.3	26100	5	24	26	4,18
33.4	26079	37.4	26052	5	27	30	3,18
40.3	26032	43.5	26011	3	21		6,19
46.5	25990	50.5	25963	2	27		5,19
53.0	25947	56.5	25923	5	24	28	4,19
59.3	25904	63.8	25874	5	30	28	3,19
66.9	25853	70.5	25829	3	24		6,20
73.0	25812	77.0	25786	2	26		5,20
79.4	25770	83.2	25745	5	25	26	4,20
86.1	25726	87.2	25696	4	30		3,20
93.0	25680	97.1	25653	3	27		6,21
99.9	25634	3903.3	25612	2	22		5,21
3905.9	25595	09.9	25569	5	26	30	4,21
12.6	25551	17.7	25518	4	33		3,21
19.4	25507	23.8	25479	3	28		6,22
26.5	25461	30.7	25434	2	27		5,22
33.2	25418	37.4	25391	5	27	34	4,22
40.1	25373	45.0	25341	4	32		3,22
—*	—	50.2	25308	4			6,23
54.2	25283	*		3			5,23
67.3	25199	*		3			3,23
87.4	25074	92.5	25040	3	34	38	4,24
94.5	25027	4000.0	24993	3	34		3,24

Bands obscured by the brief system.

THE BRIEF SYSTEM (λ 4000—λ 3930)

Howell and Coulson measured 6 bands in all and gave a fragmentary quantum array, which led to the conclusion that the lower state of this system is the upper state of the main system. An examination of the reproduction of this system given by them has revealed that the $v'=0$ progression in their quantum scheme is not the same as the $v'=0$ progression marked on the enlargement. It is, therefore, considered desirable to remeasure the bands of this system. It was found that the bands with intensities given in brackets at λ 3945.18 (10), λ 3960.20 (8) λ 3973.80 (6), λ 3984.5 (2), constituting the $v'=0$ progression in their scheme, are obtained in the present work as 3944.86 (4), 3960.07 (6), 3973.96 (10), 3984.72 (5). Hence it is clear that while the bands in this progression are the same in both cases, the intensities of the bands assigned by the author differ widely from those given by them. The intensity estimates of the author coincide with those assignable to those present in Howell and Coulson's reproduction. The bands of this system are clearly degraded towards the red and hence they could be distinguished from those of the main system occuring in this region. Bands with $v'=1$ progression in Howell and Coulson's scheme at λ 3930.75 (8) and λ 3949.1 (4) belong to the main system and are not regarded here as forming part of the brief system. In the present work, two more new bands at λ 3977.12 (4), λ 3966.70 (3) could be assigned with certainty to this system. Apart from those that are assigned to the main system, only 6 bands could be identified as forming members of this brief system. As this system is obtained here free from the emission continuum, the assignment of bands to either of the two systems is considered reliable. For the brief system, measurements were made from the plate taken on the quartz Littrow spectrograph. Judging from intensity considerations, one may perhaps suggest the following scheme for the brief system, with the most intense band as the (0,0) band.

TABLE III

v' \ v''	0		1		2
0	25156.7	(10)	25088.8	(5)	
	46.1	*67.9*	*47.9*		—
1	25202.8	(3)	25136.7	(4)	
	42.2	*66.1*			
2	25245.0	(6,			
3	—				
4	25342.3+	(4)			

+ Superposes over (3,22) $TlBr^{79}$ band.

But such an analysis with $\omega' \sim 47$ and $\omega'' \sim 67$ throws doubt on the emitter of the system. It may perhaps have to be attributed to either a $TlBr^+$ or to a

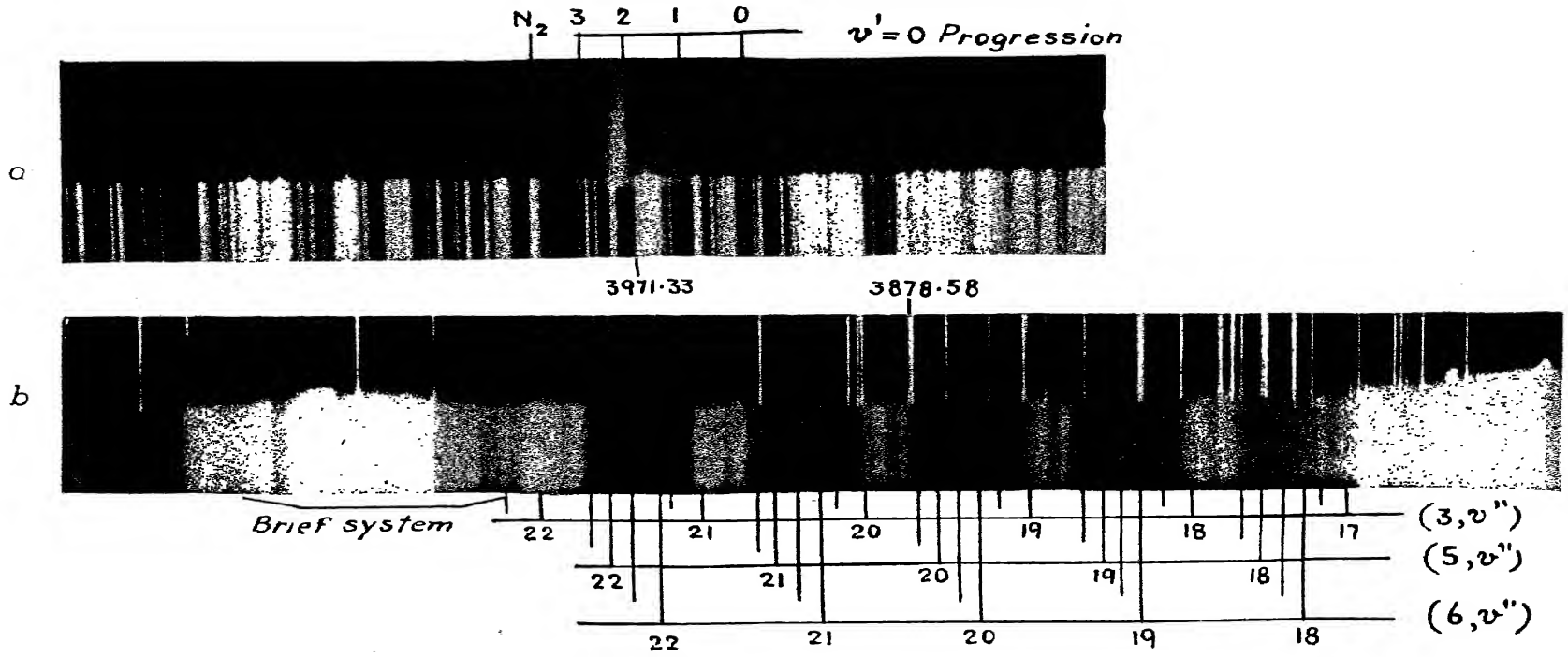

Thallium bromide bands.

foreign molecule. With the low power H. F. oscillator used in the present investigation, the former is improbable while it is also inconceivable that a pure sample of thallium bromide obtained from B. D. H. should give rise to bands of a foreign molecule with such high intensity. Hence the quantum scheme given by Howell and Coulson with the new $v'=1$ progression appears more probable.

TABLE IV

v' \ v''	0		1		2		3	
0	25342.3+	(4)	25245.0	(6)	25156.7	(10)	25088.8	(5)
		97.3		88.3	46.1	67.9	47.9	
1					25202.8	(3) 66.1	25136 7	(4)

+ Superposes over (3,22) $TlBr^{79}$ band.

The intensity distribution in the system now corresponds to what is to be expected with ω values so unequal. The lower state of the system, therefore, as suggested by Howell and Coulson, is the upper state of the main system. The two continua observed by them at λ 1900 and λ 3300 arising from two unstable levels are, as suggested by them, responsible for the observed predissociation in both the states. Further, in TlCl, the author (1949 a) reported the analysis of a doublet system whose lower state is the upper state of the main system $^3\Pi—^1\Sigma$, with ω values differing considerably from each other. This gives additional support to the conclusion that the brief system with widely differing ω values has its lower state as the upper state of the main system.

ACKNOWLEDGMENT

The author is indebted to Frof. K.R. Rao for his interest in the work.

REFERENCES

Howell and Coulson, 1941, *Proc. Phy. Soc.*, **53**, 706.
Rao, Tiruvenganna, 1949, *Ind. Jour. Phy.*, **23**, 265.
„ 1949 a, „ „ „ **23**, 393

PRELIMINARY STUDY OF SOME METALLIC OXIDE SMOKES WITH ELECTRON MICROSCOPE

By A. K. CHAUDHURY and M. L. DE

(*Received for publication, Aug. 31, 1949*)

Plate XXI

ABSTRACT. The structures of the oxide smokes of magnesium, zinc, molybdenum and tungsten have been directly examined under electron microscope. An attempt has been made to correlate the results obtained from electron microscopical observations with those obtained from X-ray studies.

INTRODUCTION

Within a rather short career of sixteen years, the electron microscope has become an indispensable adjunct to the older methods of investigation, such as optical microscopy, X-ray analysis, etc. Due to its extremely high resolution the electron microscope is specially suited for the direct observation of the size and shape of such fine particles as are present in smokes, mining dusts, pigments, etc. In X-ray diffraction experiments, the crystal structure is not directly apparent, the structure has to be computed from the experimental observations. The electron microscope on the other hand offers unique opportunities for a direct vision of the crystalline structure up to the order of 100 Angstrom units. The interfacial angles of the orthographic projection of the crystals as seen through the electron miscroscope, can be directly measured and compared with those calculated from X-ray data. In this way the identity of the crystals may be established. The axial element and interfacial angles of unknown crystals, can also be directly determined by this method (Kirkpatrick and Davis, 1948).

In the present investigation, oxide smokes of magnesium, zinc, molybdenum and tungsten were studied with the electron microscope recently installed at the Institute of Nuclear Physics, Calcutta University (Dasgupta et al, 1948), using electrons of 50 ekv energy.

METHOD OF SPECIMEN PREPARATION

All the specimens were prepared by collecting the oxide-smoke on a blank 200 mesh steel grid without any nitrocellulose film. This was possible because of the tendency of the oxide particles to form chains reaching far out into the open mesh space. As no further support of the nitrocellulose film was necessary, lack of resolution and contrast due to the additional thickness of the supporting film was not encountered. This meant much increase in the

practical value of the resolution and contrast. This is an advantage of this method, since the particles are so small that their electron-scattering is almost of the same order as that of the film.

Magnesium oxide was prepared by burning magnesium ribbon in air. Zinc oxide smoke was prepared by burning the pure metal in oxy-coal gas flame. The oxides of molybdenum and tungsten were prepared by heating the pure metals electrically in air.

DISCUSSION OF RESULTS

Fig. 1 (Plate XXI) shows the electron-micrograph of magnesium oxide. It is known from X-ray analysis that MgO crystallises in the cubic lattice of the NaCl type structure. The shapes of the MgO smoke particles, as can be seen in the electron-micrograph, can be derived from cubes of equal sides, the actual shape depending on the orientation of the particles with respect to the photographic plate. Under optimum operating conditions the three dimensional geometry of the particles is clearly brought out in relief. This indicates that MgO crystals grow uniformly in all directions, and retain the internal symmetry of the unit crystal during the process of growth.

The relative orientations of two big crystals of MgO in Fig. 1 have been diagrammatically represented in Fig. 2.

Fig. 3. shows the electron micrograph of zinc oxide smoke at microcrystalline stage. From X-ray analysis it is known to crystallise in the hexagonal system. But the oxide particles here show a striking peculiarity in having formed skeletal tetrahedrons with four legs. Barnes and Burton (1941) ascribe this phenomenon to a growth of the crystal along the preferred direction of the zinc-oxygen tetrahedral configuration. Fuller (1944) also made a detailed study of ZnO smoke by taking stereo-electron-micrographs and determining the spatial angles among the four legs. He concludes that the ZnO smoke particles consist of four needle shaped crystals united at a common juncture. From X-ray analysis the dimension of the unit crystal of ZnO is of the order of 3 Angstrom units, while the legs of the tetrahedrons taper down to a thickness of the order of 100 Angstrom unit. Hence the needles, as shown in the micrographs, have been formed by the superposition of many unit crystals along the preferred directiones.

Fig. 4 shows the electron micrograph of molybdenum oxide. From X-ray analysis it is known that the phase MoO_2 is tetragonal in structure with axial ratios:

$a : a : c = 4.86 : 4.86 : 2.79$ while the phase MoO_3 is orthorhombic with axial ratios $a : b : c = 3.92 : 13.94 : 3.66$. The electron-micrographs of molybdenum oxide smoke presented in Fig. 4 show clearly that the phase MoO_3 predominates in the smoke.

Figures 5 and 6 show the electron-micrographs of tungsten oxide smoke. The square shape is due to the phase WO_2 which is known to crystallise in

tetragonal form with axial ratios:

$$a : a : c = 4.86 : 4.86 : 2.77.$$

The rhombic shape is produced by WO_3 which is pseudo-monoclinic in structure (Brakken, 1931) with axial ratios: $a : b : c = 7.48 : 7.48 : 3.82$. This indicates that both the phases are produced in the smoke when metallic tungsten is electrically heated in air under atmospheric pressure. The spherical particles are droplets of the molten metal which settle on the steel grid support along with the oxide smoke.

ACKNOWLEDGMENTS

The authors are indebted to Prof. M. N. Saha, F.R.S., and to Dr. N. N. Das Gupta for kindly providing laboratory facilities and for constant encouragement during the progress of the work. Thanks are also due to Mr. D. L. Bhattacharya for assistance given on numerous occasions during the course of the work. The authors also take this opportunity for acknowledging the financial aid given by Dr. B. C. Law for the installation of the electron-microscope with which this research was carried out.

REFERENCES

Barnes, R. B. and Burton, C. J., 1941, *Amer. Chem. Soc.*, **19**, 965.

Brakken, H., 1931, *Z. Kryst.*, **78**, 487.

Das Gupta, N. N., De, M. L., Bhattacharya, D. L., and Chaudhury, A. K., 1948, *Ind. Jour. Phys.*, **22**, 497.

Fuller M. L., 1944, *Jour Appl. Phys.*, **15**, 164.

Kirk-patrick, A. F., and Davis, E. G., 1948, *Analytical Chemistry*, **20**, 965.

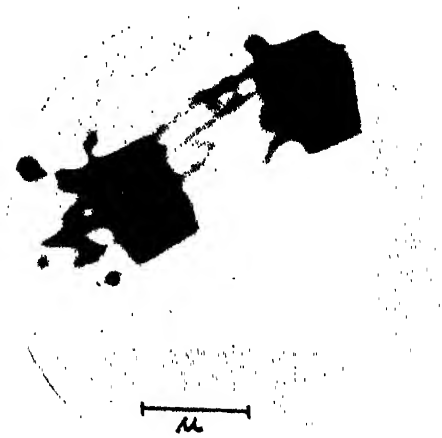

Fig. 1

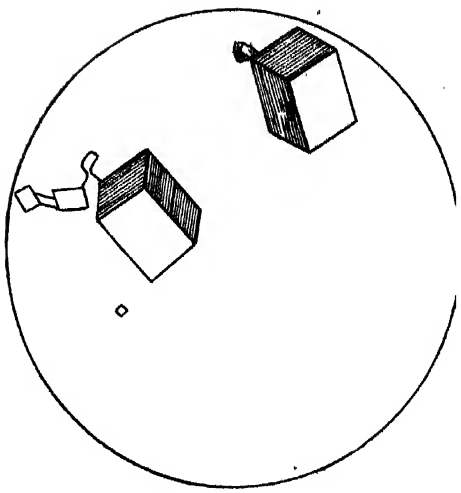

Fig. 2

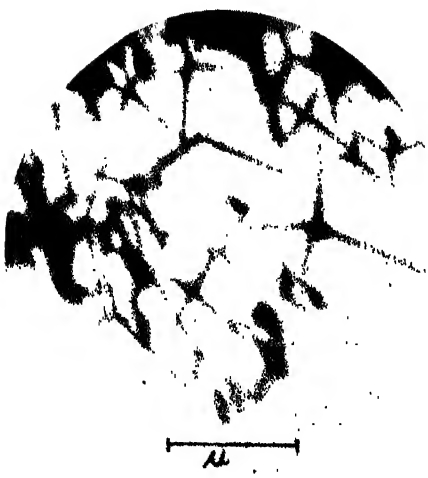

Fig. 3

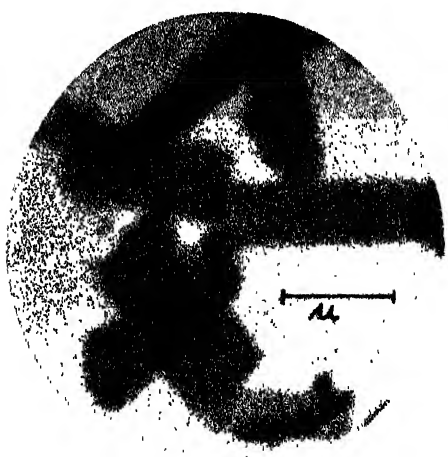

Fig 4

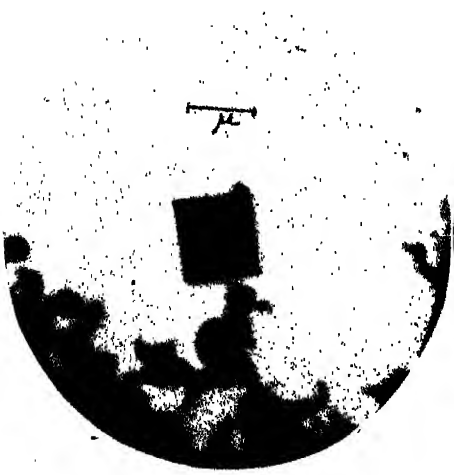

Fig. 5

Fig. 6

A MULTI-STAGE TURBO-EXPANDER AIR LIQUEFIER

By AKSHAYANANDA BOSE

(*Received for publication, July 22, 1949*)

ABSTRACT. A new type of air liquefier, depending upon the adiabatic expansion of the compressed gas in a multi-stage turbine of low speed, is described. The actual method of liquefaction depends on precooling a suitable fraction of the compressed gas in a heat exchanger, by the other part of the gas cooled by its expansion below the critical point in the turbine, when the former liquefies under its own pressure. The great advantage of such a method is discussed. Preliminary calculations for a small liquefier gives a practical efficiency of about 0.6 kwh. per kgm of liquid air.

INTRODUCTION

In the year 1937, while the author was engaged in developing cryogenic techniques in these laboratories, it occurred to him that a turbine could be used as a refrigerator. Following this, he calculated the details of working of such a turbo-refrigerator as may be used profitably for the liquefaction of air. The author, however, had to leave the construction of the air liquefier unfinished, due to the lack of proper facilities. Recently, owing to the kind facilities offered to the author by the authorities of the Indian Association for the Cultivation of Science, he has been able to take up the work again. On looking through the literature, however, he finds that in the mean time Prof. P. Kapitza has published a paper (Kapitza, 1939) in which he has described the construction of a similar air liquefier in actual action, which has, to a large extent, fulfilled the present author's expectations. The original paper of Prof. Kapitza is not available to the author so that he cannot exactly compare the details of working of Kapitza's machine with his own. It appears, however, from English abstracts of the paper published between 1939-42 that Kapitza's machine is a single stage expansion turbine. The air is compressed to about 6 or 7 atmospheres with the help of a 50 H. P. compressor and after passing through water and air cooler, without any necessity of previous purification, passes into the turbine. This runs at 40,000 r. p. m. and develops about 4 H. P. The pressure of the air drops about 75 per cent in its passage through the turbine and the air entering the turbine, pre-cooled in the last stage to about $-158°C$, emerges at about $-187°C$ and in the liquid state. The weight of the turbine is only about 250 gms. and it deals with about 600 cu. m. of air per hour, producing about 30 kgms. of liquid air per hour, liquefaction beginning within 20 minutes of starting. The efficiency of the liquefier as claimed by Kapitza is about 80 per cent. Hausen, in a subsequent paper (Hausen, 1941) criticises Kapitza's method

and says that as regards weight, space occupied and efficiency this machine is in no way superior to the existing Linde and Claude-Heylandt machines. This paper also is not available to the present author so that he cannot discuss the contradictory claims of these two authors, though it would appear from our experience that Hausen's criticism will not most probably be tenable in our case. In any case, one sees clearly the stamp of the typical genius of Prof. Kapitza in the development of this machine.

From what follows, it will be seen that though the principle of Kapitza's new liquefier and that undertaken by the present author are primarily the same, *the details are fundamentally different.* Further, the present author can claim to have *independently* undertaken the project *as early as 1937.* We shall discuss the merits and demerits of various machines in their proper places but it may even now be mentioned that a Kapitza machine, from what meagre description is available, evidently depends on a *single expansion de Laval impulse turbine,* whereas, the present author uses the *principle of multiple expansion* and various other devices to be mentioned later, which according to thermodynamic principles, is more efficient and at the same time avoids unduly high blade speed, which must be a great drawback of the Kapitza machine. For these reasons author thinks it useful to publish the work undertaken by him, particularly because even after the lapse of 10 years he does not find any attempt by Kapitza to make any further improvement in his machine, which must obviously follow the line suggested by the present author.

From the principles of thermodynamics it is well known that in the production of cold, our aim should be to approximate the ideal reversible isentropic process. Of the two processes at present in use for air liquefaction, the Linde method is essentially irreversible and the maximum performance is about 0.9 kwh. per kgm. of liquid air produced. The Claude-Heylandt method is an attempt towards realising the isentropic method. Unfortunately, due to difficulties of lubrication at low temperatures between the piston and the cylinder in this method, the performance is about the same as in the Linde method. Kapitza has done away with the need of lubrication in his piston-cylinder helium liquefier (Kapitza, 1934) by keeping a very minute clearance between the piston and the cylinder, but this machine can be used only for very small scale generation of cold because of the difficulties in construction of large machines of this type. We know, however, that in a turbine the question of lubrication in the expansion chamber does not arise and a turbine is now a practical success wherever generation of large power is concerned and a large amount of gas is to be dealt with. Thus, in view of the very large demand of liquid air for various laboratories, industrial and other purposes, *e.g.*, scientific investigations at extreme low temperatures, production of oxygen for medical, aviation and submarine breathing purposes, welding, high temperature furnaces, blasting of rocks, etc., and also nitrogen for the manufacture of chemical fertilizers,

explosives, etc., it is worthwhile to develop the turbine method of liquefaction of air. In 1926 world's consumption of manufactured oxygen was 80 million cu. m. and of nitrogen 200 million cu. m. In the last two decades the air liquefaction and rectification industry has expanded by leaps and bounds. The by-products of the industry, neon and argon gases are also in great demand.

THERMODYNAMIC PRINCIPLES INVOLVED

Now, let us consider the thermodynamical theory of a heat engine acting as a refrigerator. In an ordinary heat engine a quantity of heat is supplied by the boiler to the working substance at high temperature and a fraction of it is taken up by the condenser at lower temperature as the working substance is made to pass through the complete reversible cycle. The balance of the heat is converted into work done by the engine during the complete cycle. The ideal efficiency is defined by

$$\eta = \frac{W}{Q_1} = \frac{Q_1 - Q_2}{Q_1} = \frac{T_1 - T_2}{T_1} \tag{1}$$

where Q_1 and Q_2 are the amount of heat taken up at the higher temperature T_1 and delivered at the lower temperature T_2 respectively and W is heat equivalent of the work done during the cycle. Also,

$$W = \frac{Q_1 (T_1 - T_2)}{T_1} = \frac{Q_2 (T_1 - T_2)}{T_2} \tag{2}$$

In a refrigerator, on the other hand, we take up an amount of heat Q_2 at the lower temperature T_2 of the condenser, and discharge Q_1 amount of heat at a higher temperature T_1, and in order to do this we have to do work W. Thus, the total energy $Q_2 + W$ supplied $= Q_1$ the amount of heat delivered at the higher temperature and the performance of the refrigerator is

$$\Phi = \frac{Q_2}{W} = \frac{Q_2}{Q_1 - Q_2} = \frac{T_2}{T_1 - T_2} = \frac{1}{\eta} - 1, \tag{3}$$

also,

$$W = \frac{Q_2 (T_1 - T_2)}{T_2} \tag{4}$$

Thus, the greatest amount of work that is theoretically available in letting a quantity of heat Q_2 pass from a higher temperature to a lower is also the least amount of work that is needed to "pump up" the same quantity of heat through the same range of temperature, the work done depending on temperature as shown. From these considerations it is possible to deduce in a very simple manner many results for a refrigerator by analogy with the existing results for an ordinary heat engine.

It is well known that no engine works in the strictly reversible manner and the "efficiency ratio" is a measure of this deviation from the ideal. The

ideal Carnot cycle requires that all the operations upon the working substance should take place in a single vessel so that the entire amount of heat is taken up at a single high temperature. But when the engine is separated into parts, as is done in practice, the last stage of Carnot cycle, *i.e.*, the adiabatic compression from T_2 to T_1, is replaced by a direct heating by the source of heat. In refrigerators, however, this difficulty does not arise. There the performance, as defined by Q_2/W, is increased by taking up heat by the exhaust gas successively at different temperatures and a strict analogy is to be found in the cycle of steam engines with superheating. The total work done in adiabatic expansion is measured by the drop in the total heat or enthalpy, I, during the adiabatic expansion when the gas is admitted at the initial pressure expanded adiabatically and discharged at the final pressure. This measures the amount of cold generated by the machine. The actual work done by the adiabatic expansion is, however, equal to the change of internal energy under adiabatic conditions. The two are denoted by $\int v.dp$ and $\int p.dv$ respectively, where $p.v^{\gamma}=$constant, if the working substance is an ideal gas. The net work done upon the working substance in the cycle is given by the area of the cycle (see Fig. 1)

$$abcd = eabcdf - cadf = (I_b - I_c) - (I_a - I_d)$$

$$= \delta I_1 - \delta I_2 = \int^{b} v.dp - \int^{a} v.dp \qquad (5)$$

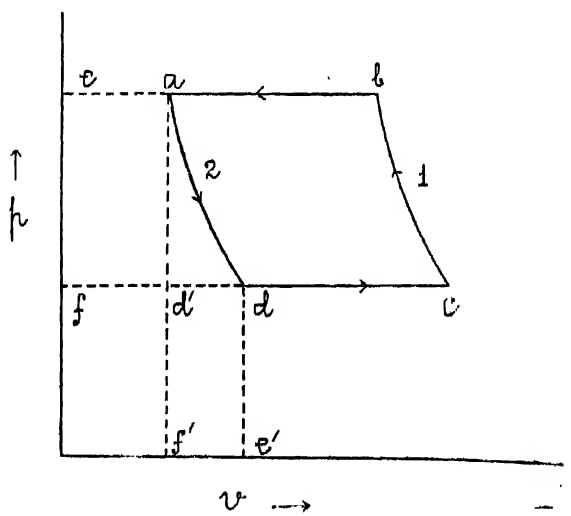

FIG. 1

The cold produced is measured by the change in enthalpy during adiabatic expansion from a to d, *i.e.*, by the area $cadf = \int_{d}^{a} v.dp$ ... (6)

The performance

$$\phi = \frac{Q_2}{W} = \frac{eadf}{abcd} = \frac{\delta I_2}{\delta I_1 - \delta I_2} \qquad \ldots (7)$$

ADVANTAGES AND DISADVANTAGES OF DIFFERENT TYPES OF EXPANSION ENGINES USED AS REFRIGERATORS

From thermodynamical theories it is evident that for an increased performance of the engine, the heat should be taken up by the expanded gas in stages rather than all being taken up at the lowest temperature. This usually happens in refrigerators by the use of pre-cooling in a counter-current heat exchanger (Ruhemann, 1937). It may also be realised by expanding the gas in multiple stages in two or more expansion machines: Multiple expansion is also closer to the ideal process since the temperature-fall in any particular stage is smaller and the exchange of heat with the engine parts, in consequence, smaller. As is known, this principle of multiple expansion is a necessary condition for the successful working of a turbine from quite different considerations.

To increase the performance of an adiabatic expansion machine, far greater advantage is obtained by reducing the exhaust pressure than increasing the initial pressure, not only because the mechanical difficulties of production and handling of high pressure increases rapidly with increasing pressure but also the works in actual machines corresponding to isothermal compression and adiabatic expansion deviate from the ideal value more at high pressures than at moderately low pressures. Of course, the expansion ratio and the enthalpy change are decreased by using a moderate initial pressure but these may be easily compensated by using a suitable, low exhaust pressure. A further advantage of using lower initial as well as final pressure, is the possibility of using a better heat-exchanger system.

To secure the full benefits of low exhaust pressure, however, the friction between the parts of the expansion machine has to be minimised to the least possible amount so that the expansion may be carried down to the lowest back pressure in the condenser. This is not possible in cylinder and piston engines, not only because (1) the friction of piston against cylinder is quite large, but also (2) the volume becomes excessive. In the turbine these considerations do not arise. Thus, considering (2) first the expansion is carried in stages so that the volume for each expansion is provided in that stage and the turbine blades continuously move on to make space for the expanded gas. On the other hand, the friction occurs only at the shaft bearings which need not be at a low temperature and hence may be properly lubricated. Indeed, the friction is so small that the shaft of a turbine set in motion has been known to revolve for several hours before coming to rest unless a load is put on. Thus, in this way also a turbine from its very construction is eminently suitable as a gas liquefying machine.

The main disadvantage in a turbine is the leakage over the tips of the blades. But this is negligible for large turbines and particularly if moderate initial pressure is used. Use of moderate pressure is thus advantageous not

only for reasons mentioned earlier but also in minimising blade leakage. Hence, use of moderate pressure, like multiple expansion, is an essential condition for the efficient working of a turbine, and this restriction instead of proving to be disadvantageous, really improves the efficiency of the machine over that of high pressure machines, in every way, so much so that no piston and cylinder machine can compare with it. This will be readily seen in the case of "exhaust turbines," so called because they work with the exhaust gas from the piston-cylinder engines and produce nearly as much work.

Another difficulty in a single stage turbine, as used by Kapitza, is the high blade speed, corresponding to about 40,000 r.p.m. But this may be successfully tackled by providing multi-expansion so that the speed is quite moderate, between 2,000-4,000 r.p.m. or even less. At the same time, for reasons mentioned earlier, this multistage expansion should serve to increase the performance as a liquefier. Even this reduced speed may appear very high compared to piston-cylinder engines, but this creates no appreciable mechanical difficulty and is rather useful in reducing the heat leakages by rapid sweeping out of the expanded gases. The turbines are also more efficient than the piston-cylinder engines in this that there are no periodic fluctuations of temperatures in turbine expansion chamber.

The really important loss in a turbine is that due to fluid friction and turbulent motion while the gas passes through the nozzles and the blades and these may be considerable at such high velocities at which the gas passes. Another point to be considered is that turbines can be most profitably used only for really large scale liquefaction of gases. A turbine, handling the same amount of gas as a piston and cylinder machine, has a very much smaller size. This is no doubt very advantageous as regards weight, space occupied by the machine and losses of heat through surface area. But this smaliness in size will lead to real difficulty in manufacturing the various parts of the machine when small scale liquefaction is contemplated. For example, if we use a compressor, of capacity 30 cu. m. of air per hour compressed to 50 atmospheres, necessary for the liquefaction of a few litres of liquid air per hour, the size of the cross-section of the turbine nozzle has to be made as small as about 0.01 sq. cm. and the other dimensions of the turbine on a similar scale.

GENERAL PROCESSES AND ARRANGEMENT OF THE METHOD OF LIQUEFACTION

Now, we shall discuss the actual processes of liquefaction with the help of the expansion engine. Since the pressures involved are not high, turbo-compressors capable of delivering large quantities of air may be used with great advantage. The best method of liquefaction appears to us to be cooling down a part of the compressed gas thus obtained, by expansion in a turbine to such a temperature that the other part of the gas, cooled by counter-current heat

exchange to this temperature, liquefies under its own pressure. Thus, the final step in liquefaction by Joule-Thomson expansion, as is done by many people but which is an essentially irreversible process and also is not suitable for the low initial pressure used for turbines, is avoided. Liquefaction in the turbine itself as done by Kapitza (1939) would also lead to complications, for example, due to (1) the liquid friction, (2) the high centrifugal force produced by the liquid on the blades and (3) the too low temperatures within the turbine. The amount of cold which has to be generated by the machine to liquefy each kilogramme of air starting from room temperature, say 300°K, is theoretically about 97.6 kilo-calories. The pressure between which we should work is primarily determined by the effective limits of turbine design and also by the lowest temperature we intend to reach in the turbine. This lowest temperature from previous considerations must be above the boiling point of air under the final exhaust pressure but sufficiently below the critical point of air. The diagram of the liquefaction circuit used by us is essentially as shown in Fig. 2, and the various processes of the complete cycle of operations may be very conveniently represented by a temperature-entropy diagram as in Fig. 3.

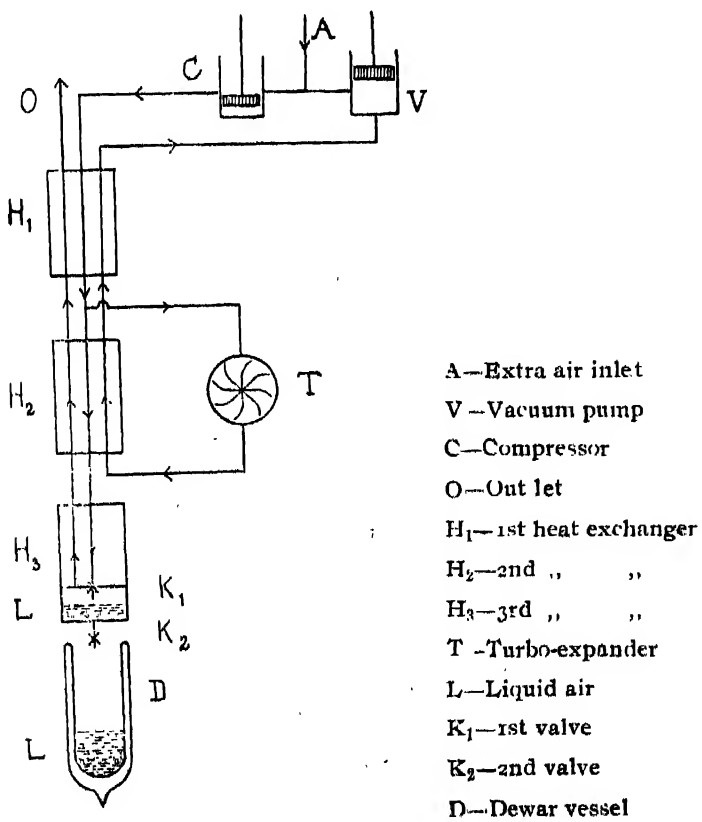

FIG. 2

Diagram of liquefier. Arrows mark the passage of air

Supposing that the gas obeys the adiabatic law $pv^{\gamma}=$constant, down to the lowest temperature, the cold developed per unit mass in an "equivalent" single stage expansion, by utilising the kinetic energy of the expanding gas in producing work, is given by

$$\Delta i'.J=\eta.p_1v_1\frac{\gamma}{\gamma-1}\left[1-\left(\frac{p_2}{p_1}\right)^{\frac{\gamma-1}{\gamma}}\right] \quad \ldots \quad (8)$$

where $\Delta i'$ is the adiabatic change of enthalpy in the process and η is the "efficiency ratio" *i.e.*, the ratio of the work done by the actual and the ideal engine. The total change of enthalpy in our arrangement is

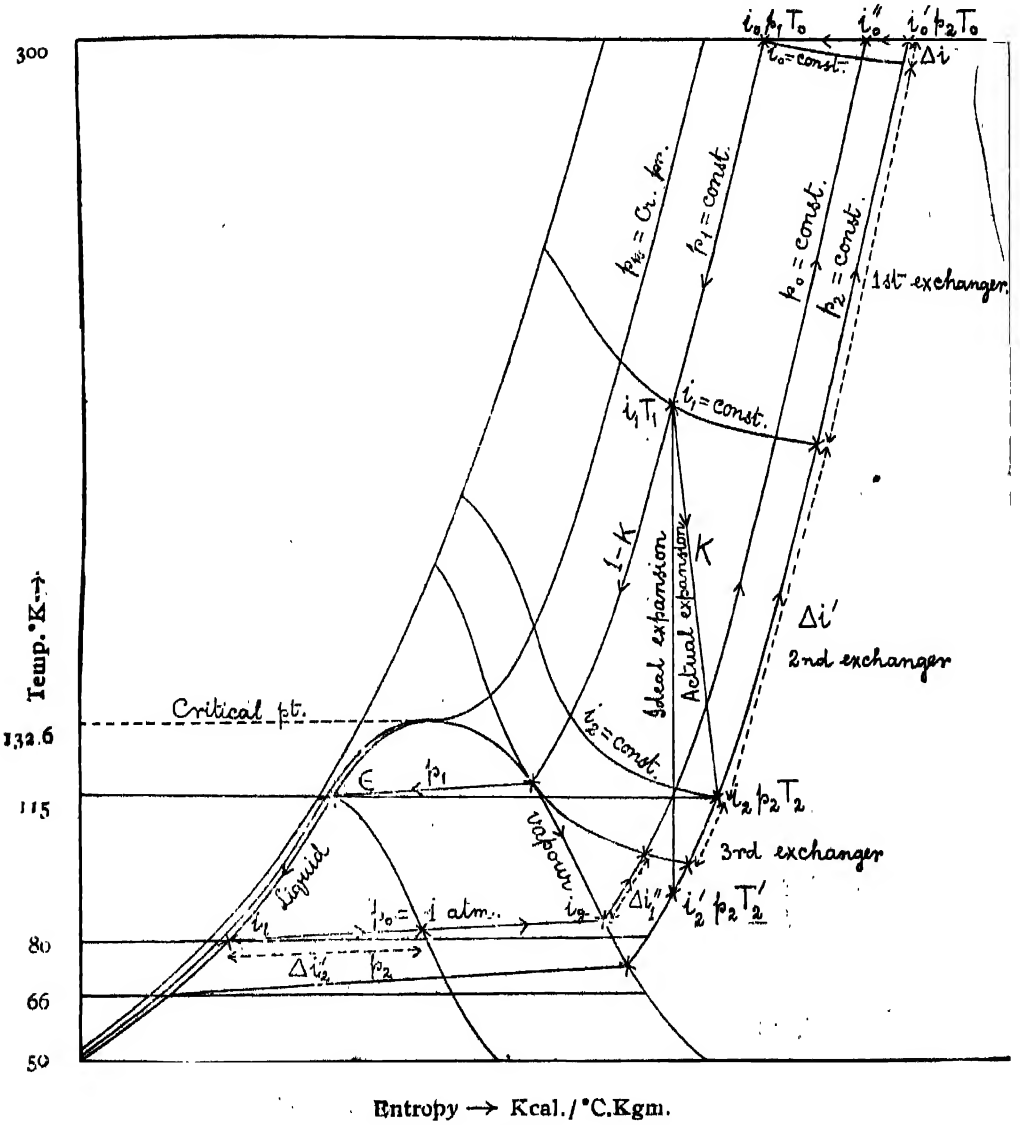

Entropy → Kcal./°C.Kgm.

FIG. 3

Entropy-temperature diagram of the turbine air liquefier
(Not drawn to scale)

$Q = \Delta i + K.\Delta i'$, where K is the fraction of air going through the expansion engine, Δi is the isothermal change of enthalpy in compressing the gas at room temperature. (This is, however, only a convenient idealisation).

There is a further amount of change of enthalpy and corresponding cold generated, $(1-K)\Delta i'' = (1-K-\epsilon).\Delta i''_1 + \epsilon.\Delta i''_2$, where ϵ is the fraction of the whole becoming liquid, when the vapour and the liquid phases obtained under high pressure is allowed to pass from pressure p_1 to atmospheric pressure accompanied by enthalpy changes $\Delta i_1''$ and $\Delta i_2''$ respectively, so that really, $Q = \Delta i + K\Delta i' + (1-K)\ \Delta i''$.

If the mixture of vapour and liquid, however, be throttled down to atmospheric pressure through a valve, then of course this last term should be omitted, which will obviously mean a loss of available cold. But at the same time a part of Δi corresponding to change of enthalpy in compressing this part of the gas from atmospheric pressure to pressure p_1 will be made available. This quantity, however, is comparatively small and as we have indicated, we should avoid throttling though we cannot utilize Δi thereby. If we know K, the expanded fraction, and also ϵ, the liquefied fraction, we can easily calculate $(1-K)\Delta i''$ since $\Delta i''$ consists of two parts $\Delta i_1''$, due to change of pressure of the vapour and $\Delta i_2''$ due to that of liquid.

If the gas had obeyed the perfect gas law we might have calculated the amount of cold $K.\Delta i'$, easily. But since this is not so, the quantity is rather difficult to determine. This amount of cold depends in a complicated manner upon the temperature T_1 at which the gas enters the turbine, the initial pressure p_1 and the fraction K, for given values of the efficiency ratio, the final temperature and the pressure. General thermodynamic principles show that the higher the temperature T_1, the larger is the amount of cold, generated by the machine. It is, however, obviously not profitable to make T_1, higher than room temperature. It is to be noted, further, that the higher the final temperature T_2, at the exit of the turbine the higher will T_1 be and less the difference between T_2 and T_0 the initial temperature before entering the heat-exchanger I. Now, the part of the air expanded in the machine must give the whole of its cold to the incoming high pressure air, for which it is necessary that there should exist the least temperature gradient from T_0 to T_2, but this condition may not be fulfilled if $T_0 - T_2$ is too small, so that cold will be lost at the end of the exchanger I. In actual practice this exchanger will be omitted altogether so that $T_0 = T_1$, so that our exchanger-loss consideration will refer to heat-exchanger II. The fraction expanded in the turbine evidently determines the main amount of cold generated and this amount should be only that much as can be efficiently exchanged for a given temperature gradient.

In the ideal case the expansion engine would have taken us to the state i_2', p_2, T_2', from the state i_1, p_1, T_1 but due to losses we reach only i_2, p_2, T_2

and the efficiency ratio is given by

$$\eta = \frac{i_1 - i_2}{i_1 - i_2'} \qquad \ldots \quad (10)$$

If we pass M kilograms of air through the liquefier of which a fraction K goes through the turbine, the amount of cold generated here is given by $MK\eta\,(i_1 - i'_2)$ of which a part is lost in the heat exchangers I and II. There is an additional loss in exchanger III. If the efficiency of the heat exchangers is denoted by ψ then total loss representing the cold taken away by the outgoing gas is given by $MK(1-\psi)(i'_0 - i_2) + M(i'_0 - i_o) + M(1-\epsilon-K)(1-\psi)(i_0 - i_g)$, the first term denoting the loss of cold of the gas passing through the turbine, the last term that of the vapour coming out of the liquefaction chamber and the middle term corresponding to the loss due to the difference of enthalpies at pressures p_1 and p_2 at temperature T_0.

If λ be the amount liquefied by the machine the liquefaction fraction as defined by

$$\epsilon = \frac{\lambda}{M} = \frac{K[\eta(i_1 - i_2') - (1-\psi)\,(i_0' - i_2)] - (i_0' - i_0) - (1-\epsilon-K)\,(1-\psi)\,(i_0 - i_g)}{L + i_0' - i_g} \qquad (11)$$

where L = the latent heat and i_g the enthalpy of the vapour at the boiling point under atmospheric pressure, when the expansion engine alone is producing the cold. There should, however, be another positive added term in the numerator which is due to the change of enthalpy of the liquid-vapour mixture as its pressure changes from p_1 to p_0. This amount is just enough to maintain the vapour-liquid equilibrium while the mixture is passed along the saturation curve so that the amount of gas liquefied remains the same (this is not strictly true for a mixture like air) but may be much more if an additional isentropic expansion is used here. For an accurate calculation of ϵ an elaborate temperature-entropy diagram in which isobars and isenthalps are drawn is necessary and p_1, T_1, K have to be determined empirically. It is obvious that T_2 in our case must be fairly below 132.6°K (critical temperature of air). p_1 not more than about about 40 atmospheres (critical pressure) consistent with good working of the turbine, is then sufficient for liquefaction.

Starting from a given initial state if the value of T_2 is reduced, $i_1 - i_2'$ must diminish and in the expression for ϵ the liquefaction fraction, K increases till the product reaches the maximum value giving the maximum production for the liquefier for this value of temperature T_2. Now, if $M(1-K)$ kgm of air be cooled down by heat exchangers at pressure p_1 from T_0 to T_g, the temperature of liquefaction under this pressure, the amount of cooling of the gas is $M(1-K)\psi(i_0 - i_g)$. Hence,

$$\epsilon = \frac{\lambda}{M} = \frac{(1-K)\psi(i_0 - i_g)}{L + i_0' - i_g} \qquad \ldots \quad (12)$$

From these two equations K can be obtained as a function of temperature T_2.

If the efficiency ratio of the machine is known we can also find out $i_1 - i_2'$ as a function of temperature T_2. The efficiency of heat exchangers are usually about 90%. From the entropy temperature diagram it is not difficult to find out by trial the values of various quantities appearing in the previous equations which give the best performance of the machine. The work supplied to the machine is obtained on the assumption that the compression is isothermal and the gas obeys the Boyles's law during the process (or more accurately from the temperature-entropy diagram).

The consumption of work consists of two parts namely:

(1) compressing the fraction K from pressure p_2 to p_0

(2) and compressing the whole from p_0 to p_1.

If the fraction liquefied be ϵ then it is evident that for the liquefaction of 1 kgm of air $1/\epsilon$ kgm of air must be compressed to the desired pressure. Hence, work consumption,

$$W = \frac{1}{\epsilon}\left[RT(\log p_1/p_0 + K \log p_0/p_2) - K\left(\frac{p_1v_1 - p_2v_2}{\gamma - 1}\right)\right] \quad \ldots \quad (13)$$

where the negative term takes into account the work recovered from the turbine. Otherwise, the net work consumption may be found out by measuring the area of the temperature-entropy diagram. As K changes the work consumption also changes for given values of p_1 and p_2. The minimum value of work consumption may be calculated from this.

From a rough calculation we see that for an expansion from 10 to .03 atmospheres the suitable initial temperature is about 300°K for a ratio $K = 0.5$. The work consumption is then minimum at $K = 0.5$ and is about 0.6 kwh per kgm of liquid air produced. Actually a transition from 10 atmospheres isobar to 1 atmosphere ought to reach this work consumption at $K = 0.9$ but this is not so due to losses. The final temperature at the exit of the machine is somewhat above 90°K. This rough calculation of the performance compares very favourably with those of other types of machines and with the ideal performance. There is no doubt with further investigations which are in progress in this laboratory, much improvement can be brought about in the machine and there will be no rival to a turbo-liquefier in the field of large scale production of liquid air.

ACKNOWLEDGMENTS

The author takes this opportunity of expressing his gratefulness to the authorities of the Indian Association for the Cultivation of Science for all

facilities provided, to Prof. S. N. Bose for valuable discussions and to Prof. M. N. Saha, D.Sc., F.R.S. and Prof. K. Banerjee, D.Sc. for their encouragement in reviving interest in this line of work.

INDIAN ASSOCIATION FOR THE
CULTIVATION OF SCIENCE,
210, BOWBAZAR STREET,
CALCUTTA

REFERENCES

Crowther, J. G. 1942, *Jour. App. Phys.*, **13**, 475

Hausen, H. 1941, *Z. ges. Kalte. Ind.* **48**, 24.

Kapitza, P. 1934, *Proc. Roy. Soc. A*, **147**, 189.

,, ,, 1939, *Novosti, Tekhniki*, No. **11-12**, 40.

,, ,, 1939, *Jour. Tech. Phys. (U. S. S. R.)* **9**, 99.

,, ,, 1939, *Jour. Phys. (U.S.S.R)*, **1**, 7.

,, ,, 1939, *Planovoe Khoz*, No. **2**, 73.

,, ,, 1939, *Khim. Referat. Zhur*, No. **6**, 91.

Ruhemann, M. & B., 1937, Low Temperature Physics. (Cambrdge Univ. Press)

Lenz, H , 1939, Handbuch der Experimental Physik, Band IX, teil 1.
Wien Harms, (Akademische Verlagsgesellschaft, Leipzeig).

THE PRINCIPAL MAGNETIC SUSCEPTIBILITIES OF SINGLE CRYSTALS OF RARE EARTH SALTS AT LOW TEMPERATURE. PART IV—SAMARIUM SALTS

By A. MOOKHERJI

(*Received for publication, June 23, 1949*)

ABSTRACT. The principal susceptibilities of samarium salts have been measured from 300°K to 85°K. The results are discussed in the light of crystal field theory. It has been found that the magnetic anisotropy of cerium, prasaeodymium and neodymium salts increases as temperature is lowered whereas in samarium salts it increases at first, then passing through a maximum decreases.

INTRODUCTION

A survey of the experimental results on the paramagnetic behaviour of solids—namely the salts of the rare earths or of the iron group of elements—reveals considerable deviations from Curie's Law. It is only in a few of these solids that the observed deviations can be attributed to the overlapping of J-levels. This is evidently the case with the salts of trivalent samarium. From knowledge of the separation between the lowest of the multiplet levels and its immediately higher level, the temperature variation of the magnetic moment of Sm^{+++} ion was computed by Miss Frank (1932). Later on, in order to explain the deviations from the theory at low temperatures, as revealed by Freed's (1930) measurements, she (1938) worked out the effect of the crystalline field on the Sm^{+++} ion following Van Vleck (1932), Penney and Schlapp (1932).

In this communication is reported the temperature variation of the principal susceptibilities of single crystals of Sm^{+++} ion and discussed in the light of the work of Frank.

EXPERIMENTAL

Crystals were grown out of aqueous solution. Specimen of rare earth used is of high purity. The experimental methods used for the measurement were the same as in previous paper by the author . (Mookherji, 1948.)

RESULTS

Results of measurements are collected in Tables I to IV and illustrated in Figs. 1-5. Notations and diamagnetic corrections used in this paper are the same as adopted in previous papers. (Mookherji, 1948.)

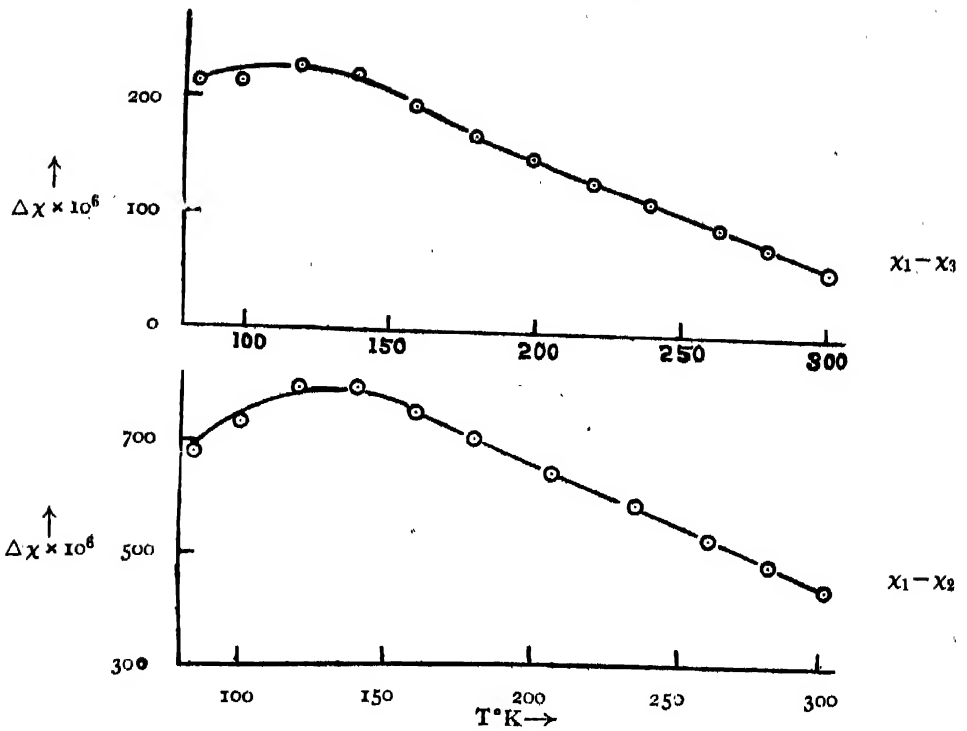

FIG. 1
$Sm_2(SO_4)_3, 8H_2O$

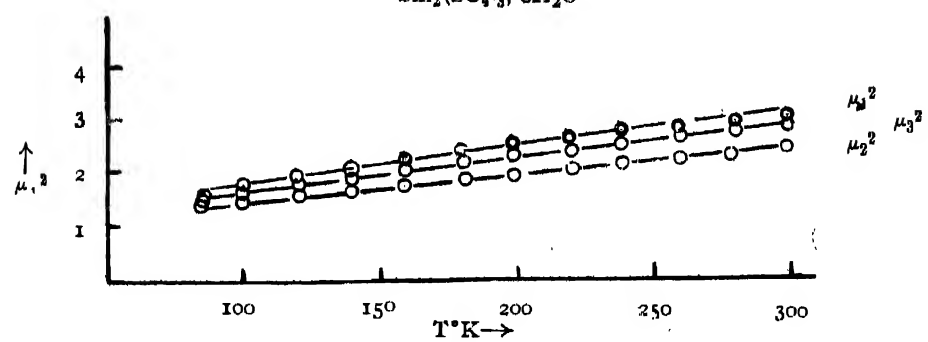

FIG. 2
$Sm_2(SO_4)_3, 8H_2O$

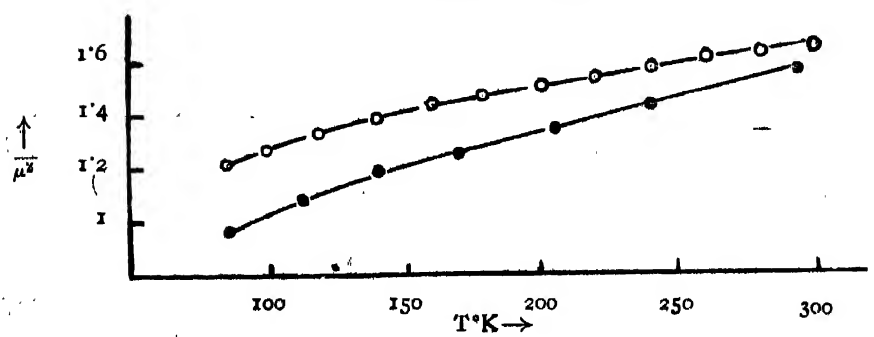

FIG. 2a
$Sm_2(SO_4)_3, 8H_2O$
• — Freed o — anth

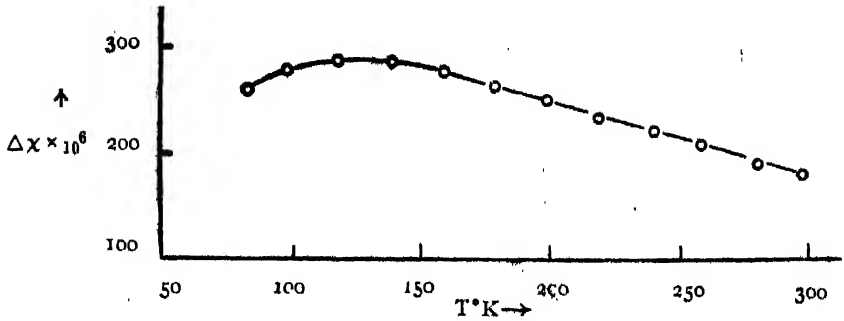

FIG. 3
$Mg_3Sm_2(NO_3)_{12}$, $24H_2O$

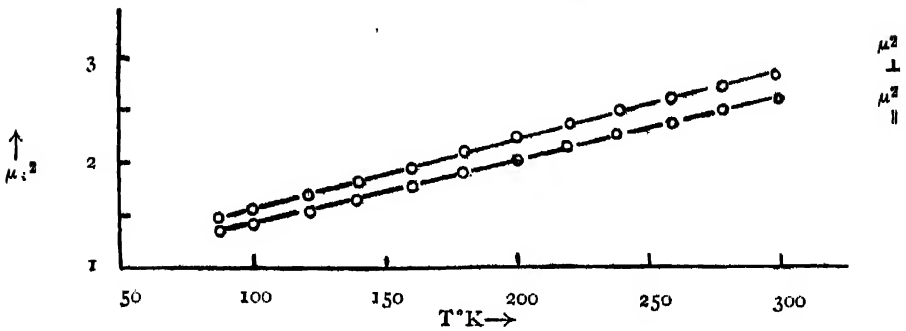

FIG. 4
$Sm_2Mg_3(NO_3)_{12}$, $24H_2O$

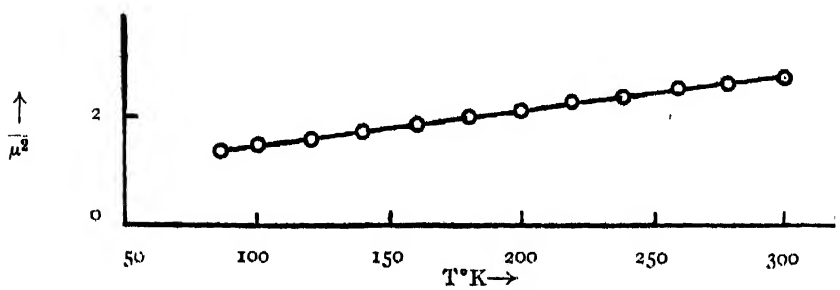

FIG. 5
$Sm_2Mg_3(NO_3)_{12}$, $24H_2O$

TABLE I

Magnetic Anisotropy at 30°C

Crystal	Crystallographic data	Mode of suspension.	Orientation in the field.	Δχ	Magnetic Anisotropy.
$Sm_2(SO_4)_3$, $8H_2O$	Monoclinic prism $a:b:c$ 3.003 : 1 : 2.002 $\beta = 118°16'$	'b' axis vertical	$\theta = -24.4$	441	$\chi_1 - \chi_2 = 441$
		'a' axis vertical	'b' axis along field	22	$\chi_1 - \chi_3 = 55$
		(001) plane horizontal	'b' axis along field	310	$\psi = +52.7$ Cal. $\psi = +52.4$
$Sm_2Mg_3(NO_3)_{12}$, $24H_2O$	Trigonal	Trigonal axis horizontal	Trig. axis normal to field.	176	$\chi_\perp - \chi_\parallel = 176$

TABLE II

Absolute Susceptibility along a convenient direction

Crystal	Direction along which susceptibility was measured.	Temp. °C	Density of the crystal.	Volume susceptibility.	Corresponding gm. mol. susceptibility.	Corresponding gm. mol susceptibility at 30°C.
$Sm_2(SO_4)_3$, $8H_2O$	Along χ_1-axis	27.4	2.970	9.07	2220	2700
$Sm_2Mg_3(NO_3)_{12}$, $24H_2O$	Normal to Trigonal axis	30.1	2.164	2.527	1810	1810

DISCUSSIONS

The ground state of the samarium ion, Sm^{+++}, is ${}^6H_{5/2}$, unlike the other rare earth ions that we have considered, the immediately higher level, namely ${}^6H_{7/2}$, is separated by only 930 cm^{-1}; so that even at room temperature, the effect of the ${}^6H_{7/2}$ level cannot be neglected. Since the magnetic moment of the higher level is much larger than that of the ground level, the effective moment per ion will naturally increase with the rise of temperature and the consequent increase in the number of ions occupying the higher level. The increase is indeed so marked that the susceptibility, which to a first approximation is proportional to μ^2_{eff}/T, and which at first diminishes with rise of temperature, as in typical paramagnetic substances, becomes stationary and then actually increases with further increase in temperature.

In calculating the effect of the crystalline field, however, on the mean moment the splitting of the ${}^6H_{5/2}$ level will naturally have a much larger effect than the splitting of ${}^6H_{7/2}$ levels. The effect of the crystalline field on the susceptibility of samarium salts and in particular of $Sm_2(SO_4)_3$, $8H_2O$ which has been measured in the powdered state by Freed (1930) over a wide range of temperatures has been discussed in detail by Frank (1938). The splitting of the levels ${}^6H_{5/2}$ and ${}^6H_{7/2}$ is given by the following scheme :—

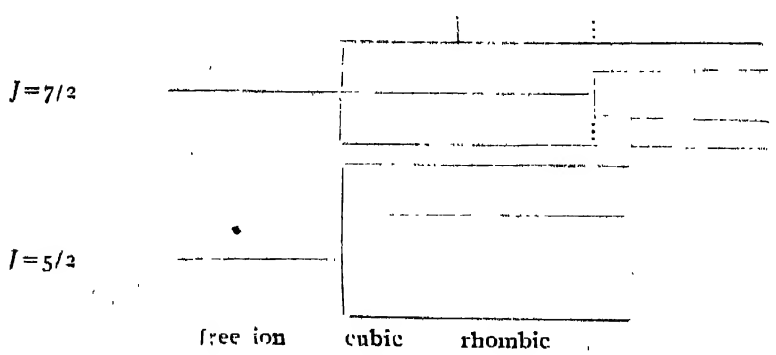

FIG. 6

Principal Magnetic Susceptibilities of Samarium

TABLE III

Temperature variation of Magnetic Anisotropy

Crystal	Temp. °K	Suspension used for measurement		$\chi_1 - \chi_2$	θ
		'b' axis vertical	'a' axis vertical		
		$\chi_1 - \chi_2$	$\chi_3 - \chi_1 \sin^2\theta - \chi_2 \cos^2\theta$		
$Sm_2(SO_4)_3,8H_2O$	300	449	313	59	−24.4
	280	494	329	81	,,
	260	537	345	100	,,
	240	582	362	121	,,
	220	625	378	140	,,
	200	670	395	161	,,
	180	713	412	180	,,
	160	759	423	206	,,
	140	799	425	238	,,
	120	799	322	241	,,
	100	738	386	227	,,
	85	681	335	229	,,
		Trigonal axis horizontal			
		$\chi_\perp - \chi_\parallel$			
$Sm_2Mg_3(NO_3)_{12},24H_2O$	300	179			
	280	193			
	260	208			
	240	223			
	220	236			
	200	251			
	180	265			
	160	279			
	140	290			
	120	288			
	100	276			
	85	26			

TABLE IV

Temperature variation of principal susceptibilities

Crystal and direction along which measurement was taken	Temp. °K	χ'_1	χ'_2	χ'_3	$\overline{\chi'}$	μ_1^2	μ_2^2	μ_3^2	$\overline{\mu^2}$
$Sm_2(SO_4)_3,8H_2O$ Along χ_1-axis	300	2490	2040	2430	2320	3.009	2.464	2.937	2.803
	280	2580	2090	2500	2390	2.912	2.355	2.820	2.689
	260	2710	2170	2610	2500	2.839	2.273	2.734	2.677
	240	2820	2240	2700	2590	2.729	2.165	2.611	2.501
	220	2950	2330	2810	2700	2.617	2.070	2.492	2.393
	200	3130	2450	2960	2840	2.518	1.977	2.387	2.290
	180	3280	2570	3100	2980	2.383	1.805	2.253	2.167
	160	3340	2780	3330	3220	2.281	1.793	2.148	2.074
	140	3720	2930	3480	3380	2.099	1.648	1.964	1.904
	120	4000	3200	3760	3650	1.934	1.547	1.818	1.766
	100	4310	3570	4080	3990	1.738	1.441	1.646	1.608
	85	4620	4040	4390	4350	1.583	1.384	1.504	1.490

		$\chi'_\perp$	$\chi'_\parallel$	$\overline{\chi'}$	$\mu_\perp^2$	$\mu_\parallel^2$	$\overline{\mu^2}$
$Sm_2Mg_3(NO_3)_{12},24H_2O$ Along $\chi_\perp$-axis	300	2400	2220	2340	2.095	2.690	2.833
	280	2460	2270	2400	2.783	2.564	2.710
	260	2540	2330	2470	2.662	2.445	2.589
	240	2630	2410	2560	2.545	2.330	2.473
	220	2740	2500	2660	2.424	2.218	2.392
	200	2850	2600	2770	2.295	2.094	2.220
	180	2950	2690	2860	2.144	1.951	2.080
	160	3090	2820	3000	1.996	1.817	1.936
	140	3240	2950	3140	1.827	1.663	1.772
	120	3470	3180	3380	1.678	1.539	1.598
	100	3890	3620	3800	1.570	1.459	1.533
	85	4240	4080	4190	1.454	1.349	1.419

Frank finds that a fourth degree cubic field producing a separation of about 200 cm^{-1} explains satisfactorily the observed deviation of μ^2 of $Sm_2(SO_4)_3$, $8H_2O$ at different temperatures from the free ion value. She further finds that a rhombic field, large enough to separate the upper level by as much as 65 cm^{-1} which is nearly a third of the separation produced by the cubic field, does not affect appreciably the mean susceptibility—as indeed we should expect.

We may also in this connection point out that, just as in Ce^{+++}, and unlike in Nd^{+++}, the sixth degree terms of the cubic field have no effect at all on the splitting or on the magnetic susceptibility.

In Fig. 3 are plotted the values of Freed for the mean susceptibility of $Sm_2(SO_4)_3$ $8H_2O$, along with the author's values. It will be seen from Fig. 3 that present values for $\overline{\mu^2}$ are uniformly higher, and hence closer to the free ion value, than Freed's. This will correspond to an appreciably smaller cubic field than that required to explain Freed's values.

This is satisfactory, since assuming the field to be of the same magnitude as in the octahydrated sulphates of the other rare earth ions like praseodymium and neodymium (Mookherji, 1949) which are isomorphous, one should expect a splitting of about 180 cm^{-1} instead of 210 cm^{-1} found by Frank to fit with Freed's data. The splitting 180 cm^{-1} will fit satisfactorily with present values for the mean of the three principal susceptibilities.

There is one other important feature of Sm^{+++} ion, which distinguishes it from the rare earth salts like cerium, praseodymium and neodymium considered previously and which is associated with the level ${}^6H_{7/2}$ of the free ion of Sm^{+++} not being sufficiently high. The separation is only about 930 cm^{-1}, whereas RT even at room temperature is about 200 cm^{-1}. For the free ion the upper level corresponds to an effective square moment, $\overline{\mu^2}_{upper}$ equal to 10.8, and lower one to $\overline{\mu^2}_{ground}$ equal to 0.72 ; so that even if a small percentage of the ions occupy the upper level, the contribution from it to the susceptibility will be considerable. Indeed, at room temperature, when both the levels are occupied under equilibrium conditions determined by the temperature, the average square moment of the free Sm^{+++} ion is about 2.5 showing that the contribution from the ${}^6H_{7/2}$ level is even more than that of the lower level. Now from disposition of the split levels of ${}^6H_{7/2}$ and ${}^6H_{5/2}$ under a non-cubic field given in Fig. 6 , it can be seen that for a given asymmetric field the contribution from the upper level to the susceptibility will be much more anisotropic than the contributions from the lower levels. Thus as we go to low temperatures, the population in the ${}^6H_{7/2}$ levels diminishes progressively according to the Boltzmann Law, and it will be not merely the mean square moment $\overline{\mu^2}$, that will diminish rapidly but also the anisotropy. This diminution of anisotropy with fall of temperature is indeed so large that it more than compensates the natural increase of $\Delta\mu^2/\overline{\mu^2}$ which accompanies the fall of temperature in any typical paramagnetic substance. This explains

why in Sm^{+++} ion the effect of the upper level not only compensates this rise, but actually makes $\Delta\mu^2/\overline{\mu^2}$ decrease with fall of temperature whereas in praseodymium, neodymium and cerium salts the anisotropy $\Delta\mu^2/\overline{\mu^2}$ increases with fall of temperature which is the normal behaviour. This will be clear from Table V which gives the values of $\Delta\mu^2/\overline{\mu^2}$ ($\Delta\mu^2$ referring to the difference in values for the two extreme principal susceptibilities) at room temperature and at 85°K, for the isomorphous hydrated sulphates and also for the hydrated double nitrates.

TABLE V

$M_2(SO_4)_3\ 8H_2O$, M =		Ce*	Pr	Nd	Sm
$\Delta\mu^2/\overline{\mu^2}$ at	300°K	09	.18	.11	.19
	85°K	.23	.34	.17	.15
$M_2Mg_3\ (NO_3)_{12}\ 24H_2O$, M =		Ce	Pr	Nd	Sm
$\Delta\mu^2/\overline{\mu^2}$ at	300°K	.16	.07	.07	.11
	85°K	.79	.09	.34	.07

* Crystal measured was $Ce(NH_4)(SO_4)_2,\ 4H_2O$.

ACKNOWLEDGMENTS

The work was carried out at the laboratories of the Indian Association for the Cultivation of Science, Calcutta, and the author wishes to express his thanks to its Committee of Management for affording all facilities. The author also wishes to express his thanks to Sir K.S. Krishnan, Kt., D.Sc., F.R.S., F.N.I., for his keen interest and, valuable advice and help. Thanks are also due to Dr. A. Bose, D.Sc. for his valuable discussions.

The author is indebted to Profesor Trombe for the gift of the rare earth.

REFERENCES

Frank. A., 1932, *Phys. Rev.*, **39**, 119.
,, ,, 1938, ,, **48**, 765.
Freed. S., 1930, *J.Am. Chem. Soc*, **52**, 2702.
Penney and Schlapp, R, 1932, *Phys Rev.*, **41**, 194.
,, ,, ,, 1932, ,, **42**, 666,
Mookherji, A., 1949, I *Ind. Jour. Phys.*, **23**, 309 and 46.
Van Vleck, 1932, The Theory of Electric and Magnetic Susceptibilities Chap. XI.

BAND SPECTRUM OF CADMIUM BROMIDE

By C. RAMASASTRY

(*Received for publication, Feb. 15, 1949*)

Plates XXIIA and B

ABSTRACT. The H. F. emission spectrum of cadmium bromide molecule is reinvestigated *P*, *Q* component head splitting is presented for the (0, 0) and (1, 1) bands of the main system and a few additional bands are assigned to this system. A new group of bands is interpreted as forming the counterpart of the main system which arises from $^2\Pi - {}^2\Sigma$ transition. About 50 bands are measured in the visible region and regularities shown.

INTRODUCTION

In the early work of Walter and Barratt (1929) on the absorption spectra associated with various compounds of zinc, cadmium and mercury, about 12 bands were listed in the region $\lambda 3551$ to $\lambda 3407$ as belonging to (Cd + Br). But the wavelengths of these bands agree closely with the TlBr absorption band heads obtained later by Butkow (1931) and so the bands are considered by Pearse and Gaydon (1941) as really belonging to TlBr but not to Cd Br. Recent investigations of Oeser (1935) on the absorption and fluorescent spectra of the halides of zinc and cadmium did not reveal any discrete bands of the CdBr molecule. The high frequency emission spectrum of cadmium bromide vapour was studied by Wieland (1929) who analysed a system of violet degraded bands of high intensity, lying in the region $\lambda\lambda 3250 - 3120$, as consisting of six sequences with the (0, 0) band placed at $\lambda 3176.65$, ν 31470.5. He also listed three unclassified bands at $\lambda 3395.1(3)$, 3092.5(1), 3075.4(0). The existence of diffuse bands in the visible region from $\lambda 6400 - \lambda 3300$ was just mentioned by him but no measurements were given. Howell (1943) considered, from an analogy with the band systems of the other halide molecules of Zn, Cd, and Hg, that the system analysed by Wieland should be one of the components of $^2\Pi - {}^2\Sigma$ transition; but the other component system could not be established. The present work is taken up with a view to finding out this missing component system and to search for other band systems of CdBr which would correspond to the various known systems of the related molecules.

EXPERIMENTAL

The discharge tube is of thick-walled pyrex glass with external electrodes, the source of excitation being a H. F. oscillator constructed by the

author. Heating is done by an etna burner until the colour of the discharge becomes intense white. Ilford Selo chrome and Special rapid plates are employed for photographing the bands. Preliminary investigation is carried out with Hilger small and medium quartz spectrographs using plates sensitised for the far ultra-violet.

RESULTS

(*a*) No bands are obtained in the region $\lambda 3000 - \lambda 1850$ but four broad and ill-defined continua are recorded extending over regions (*i*) $\lambda\lambda 2500 - 2550$ (*ii*) $\lambda\lambda 2610 - 2660$ (*iii*) $\lambda\lambda 2700 - 2785$ and (*iv*) $\lambda\lambda 2875 - 2930$.

(*b*) The visible bands, clearly red-degraded, occur in the region $\lambda 4000 - \lambda 3850$. Of these, those lying between $\lambda 4100$ $\lambda 4000$ are of greater intensity than the rest. There is also a strong general continuum overlying the visible bands. This continuum gradually fades away to shorter wavelengths and is practically imperceptible at about $\lambda 3350$.

(*c*) An isolated violet degraded band at $\lambda 3208.1$ and another faint band at $\lambda 3324$, obviously related to the former, could be definitely observed.

(*d*) The Wieland system occurs in the region $\lambda 3250 - \lambda 3100$. This consists of the most intense bands of the entire spectrum.

(*e*) A few faint bands in the $\lambda 3000$ region could be detected in the rotational structure of the OH band, $\lambda 3064$.

SYSTEM *D*

Wieland's system (system *D*.) is photographed by the author on the Hilger quartz Littrow spectrograph. Lighter exposures showed that the (0, 0) and (1, 1) bands are split up into two component heads (Plate XXIIA, Fig. *a*). Such double heads are not observed for any of the remaining bands of the system. Hence the above components cannot be due to bromine isotope effect but are to be considered as *P* and *Q* heads. Details of measurements are given below :

TABLE 1

(v', v'')	ν Wieland	ν Author	$\Delta\nu$
0, 0	31170.5	31170.7	3.2
		31173.9	
1, 1	31491.0	31493.1	2.8
		31496.2	

The number of component heads observed in each band gives the conclusive evidence for the consideration that the system is due to $^2\Pi - ^2\Sigma$ transition. Then the other component system should also be present, from the analogy of the spectra of the corresponding molecules. The three unclassified bands of Wieland in the λ3095 region cannot form the missing component system, for (*i*) they give 840 cm^{-1} for the $^2\Pi$ width which is too small compared with the expected value of 1140 cm^{-1} derived from the ^2P separation of the Cd atom (*ii*) there are no regularities among the bands In the region of these faint bands listed by Wieland, a few more bands also could be measured in the present work ; the presence of a band is suspected wherever there is a shading of the rotational lines of the OH band (Plate XXIIA, Fig. *b*). This fragmentary group can be interpreted as forming the higher members of the Wieland system and the bands are classified accordingly in Table II.

TABLE II

Additional Bands in the *D*-system of CdBr

Wieland λ (Int.)	Author λ (Int.)	ν_{obs}	ν_{cal}	(v', v'')
3095.1(3)	3095.0(3)	32301	32300.3	(7, 4)
3090.5(1)		32352	32351.3	(9, 6)
	3080.7(0)	32458	32480.2	(12, 9)
3075.1(0)	3075.0(1)	32505	32508.8	(6, 2)
	3072.0(0)	32536	32536.1	(7, 3)
			32513.3	(8, 4)
	3068.1(0)	32583	32571.1	(10, 6)
			32591.3	(11, 7)
	3061.1(0)	32657	32628.1	(13, 9)

The positions of the various bands is calculated with the help of the formula

$$\nu = 31458.3 + 254.5(n' + \tfrac{1}{2}) - 230.0(n'' + \tfrac{1}{2})$$

$$0.75(n' + \tfrac{1}{2})^2 + 0.50(n'' + \tfrac{1}{2})^2$$

which was derived by Wieland (1920) to represent the *D*-system. The above bands form a continuation of the intensity parabola when arranged in a Deslandre's table, thus supporting their positions in the vibrational scheme.

SYSTEM *C*

With the bands on the short wavelength side of the *D*-system having been classified as above, the only alternative left is to identify the two

isolated bands at λ3298.1 (3) and 3323.7 (1) as the other component of the doublet system $^2\Pi - {}^2\Sigma$. These bands are shown in Plate XXIIB, Fig. *c*. As is expected from what is found in the corresponding band systems of CdCl and CdI, this system is fragmentary and occurs on the long wavelength side of the fully developed counterpart component analysed by Wieland. The bands are arranged as hereunder giving a lower state first difference of 234 units which compares well with the ground state vibrational frequency of 230 units which is established from the analysis of the *D*-system.

TABLE III

C-system of CdBr Bands

v'' / v'	0		1
0	λ 3298.1 (3) ν 30312	234	3323.7 (1) 30078

Further, the separation between the (0,0) band of this system and that of the *D*-system is 31470 − 30312 = 1158 cm.$^{-1}$ which is in such excellent agreement with the predicted 1140 units that one can confidently consider the missing component of the $^2\Pi - {}^2\Sigma$ transition as established.

VISIBLE SYSTEM

In none of the investigations on the spectrum of the CdBr molecule are measurements available for the bands in the visible region. In the present work, these bands are photographed on a Fuess glass spectrograph. At higher dispersions the band heads became diffuse. Wavelengths, visual estimates of intensities and wavenumber data of about 50 bands are given in Table IV.

Plate XXIIB, Fig. *d* shows an enlargement of the Fuess spectrogram. The bands are clearly red degraded. The heads are single. They are almost equally spaced. The separation of bands is about 110 cm.$^{-1}$. Assuming that the lower state of the visible bands of CdBr is identical with its ground state ($\omega_e'' = 230$), these bands can be arranged into long progressions. Each progression consists of alternate bands and gives a first difference of about 220 cm.$^{-1}$ for the lower state. These regularities are shown in Table V. If the scheme is correct, there is predissociation in the upper state at $v' = 2$.

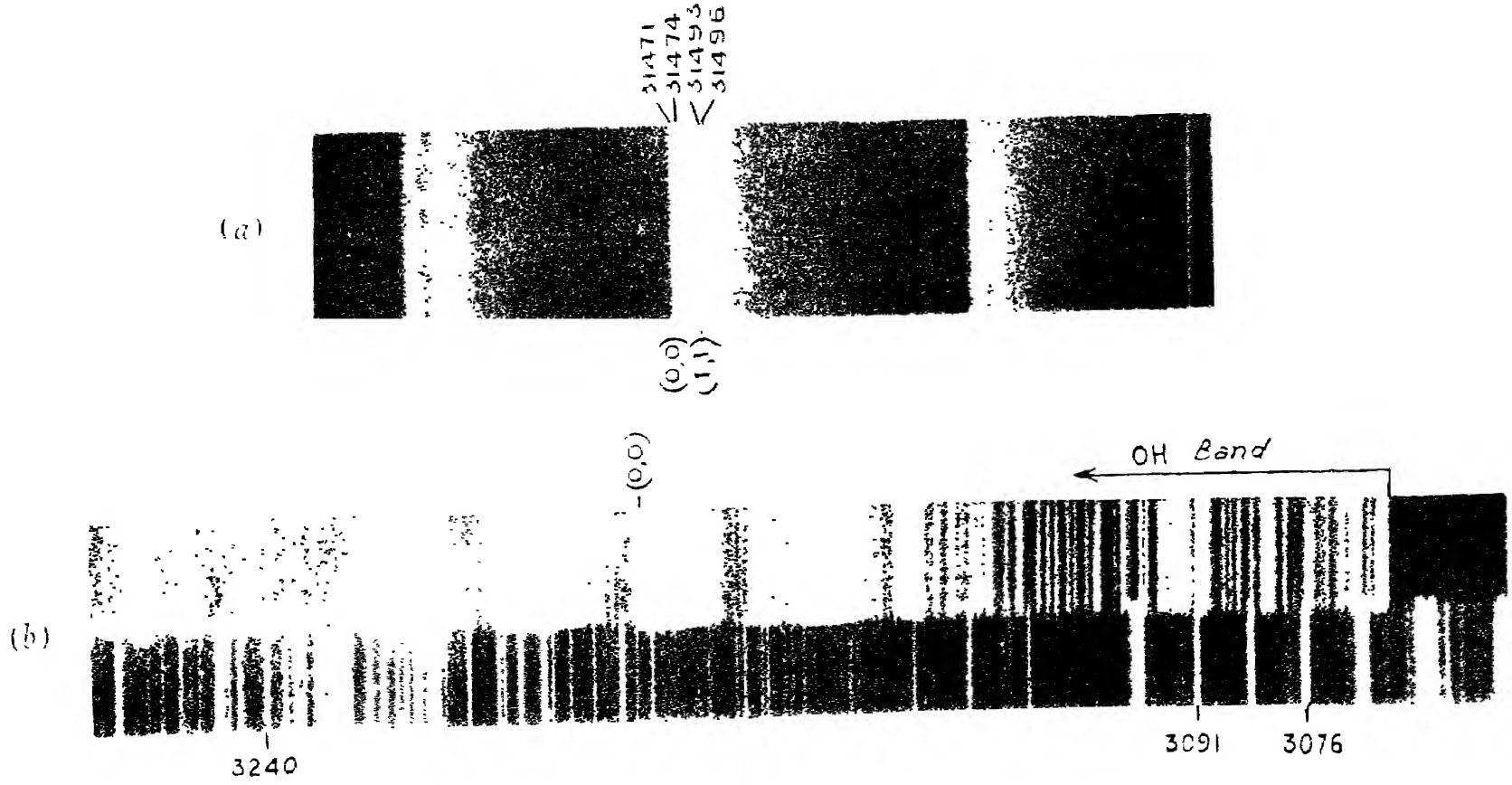

Emission bands of Cr Pt

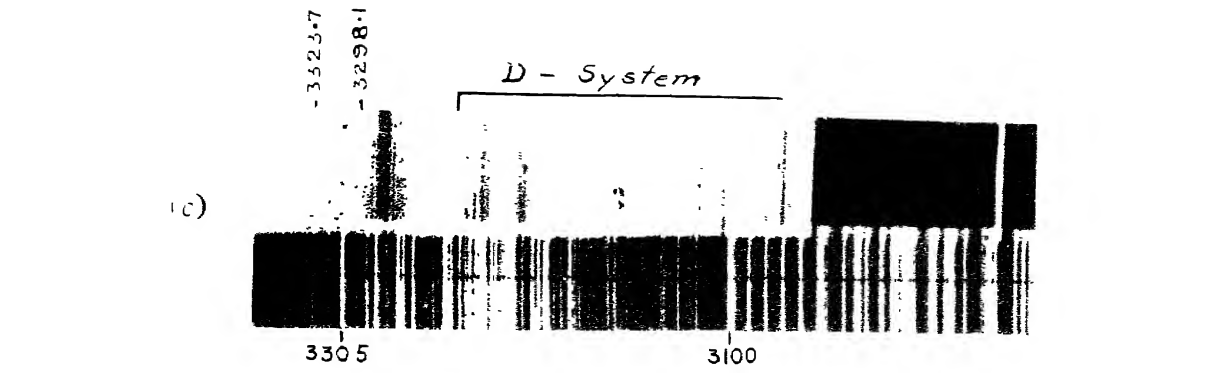

Emission bands of Cd Br

TABLE IV

CdBr Visible Bands

λ	Int.	ν_{vac}	λ	Int	$\nu_{vac.}$
3928.4	r	25448	4355.4	3	22954
			4376.2	3	22844
3944.3	r	25346			
3962.4	2	25230	4398.1	3	22731
			4418.5	3	22626
3978.4	2	25130			
3997.3	2	25010	4438.0	1	22524
			4461.7	2	22407
4013.6	1	24908			
			4484.0	4	22295
4030.6	3	24803	4504.4	5	22194
4048.4	2	24694			
			4525.6	5	22090
4067.2	2	24586	4548.4	5	21979
4085.7	3	24469			
			4570.4	5	21874
4103.2	3	24361	4594.5	4	21758
4121.4	3	24257			
			4613.0	3	21668
4139.8	4	24149	4619.0	3	21644
4158.7	4	24039	4638.0	3	21555
			4643.8	3	21531
4175.6	6	23942			
4195.9	5	23826	4661.0	3	21444
			4680.4	4	21319
4214.2	4	23723			
4234.5	4	23609	4712.4	2	21215
4254.8	3	23496	4733.5	1	21120
4274.2	3	23390	4757.5	1	21014
4294.7	3	23278	4782.1	1	20905
4306.7	3	23213	4807.0	1	20793
4315.0	3	23168	4831.6	1	20691
4335.8	2	23057			

ELECTRONIC STATES.

Four band systems are established in the case of each one of the molecules CdCl and CdI, one in the visible, two in the ultraviolet and one in the far ultraviolet. [Wieland (1929), Howell (1943), Ramasastry and Rao (1946), Ramasastry (1947)]. There is good evidence to consider the two near u.v. systems as due to $^2\Pi - {}^2\Sigma$ transition. The visible system, however, is probably due to $^2\Sigma - {}^2\Sigma$ transition. The corresponding systems of CdBr also can be interpreted accordingly. The far u.v. system of CdCl and CdI have their (0,0) bands at λ2205 and λ2387 respectively. But in the case of CdBr no such band system is obtained in this region of the emission spectrum excepting a continuum from λ2550−λ2500. If, in spite of the disagreement in the region of occurrence, this continuum is supposed to correspond to the far u.v. systems of CdCl and CdI, the difficulty still remains because this upper state of CdBr is repulsive giving rise to continuum

instead of being stable as in CdCl and CdI molecules. In CdF also (Rochester and Olsson, 1939) the corresponding system is not observed but this region of the CdF spectrum is not yet systematically investigated owing to experimental difficulties and in all probability a band sytem of CdF should exist round about $\lambda 2100$. On analogy with Zn halides (Ramasastry, 1948) one more band system is to be expected for cadmium halides also between the far ultra violet and $^2\Pi - ^2\Sigma$ systems. But no definite evidence is as yet available as regards their existence, though about twenty diffuse bands are observed in the expected region (author's unpublished work on CdI). Probably the level is repulsive in Cd halides and one of the observed near u.v. emission continua of CdBr may as well be due to such an unstable level of this molecule.

ACKNOWLEDGMENT

The author is grateful to Prof. K. R. Rao, for his kind interest in the work.

REFERENCES

Butkow, 1931, *Zeits. F. Phys.*, **71**, 678.
Howell, 1943, *Proc. Roy. Soc.* **A182**, 95.
Oeser, 1935, *Zeits. f. Phys.*, **95**, 699.
Pearse and Gaydon, 1941, Identification of Molecular Spectra, pg
Ramasastry, 1947, *Ind. Jour. Phys.*, **21**, 367.
Ramasastry, 1948, *Ind. Jour. Phys.*, **22**, 119
Ramasastry and K.R.Rao, 1946, *Ind. Jour. Phys.*, **20**, 100.
Rochester and Olsson, 1939, *Zeits. f. Phys.*, **114**, 495.
Walter and Barratt, 1929, *Proc. Roy. Soc.*, **A122**., 201
Wieland, 1929, *Helv. Phy. Acta*, **2**, 46 & 77.

STUDIES OF A SCHRAGE THREE-PHASE SHUNT COMMUTATOR MOTOR

II. Behaviour of the motor running super-synchronous on no-load and sub-synchronous on load for identical brush position.

By H. P. BHATTACHARYYA

(*Received for publication, Aug. 15, 1949*)

ABSTRACT. This paper deals with the vector and locus diagrams of a Schrage three-phase shunt commutator motor when its brushes are set in such a way that while the speed is super-synchronous on no-load, it becomes sub-synchronous on load.

INTRODUCTION

In a brush-shifting commutator motor it is well known that the slip, which is assumed positive when it runs at a sub-synchronous speed, becomes negative when the speed becomes super-synchronous owing to the rotation of air-gap flux in the latter case being opposite to that in the former. In both the cases the impressed voltage from the brushes shall oppose the voltage induced in the stator and this explains why the brushes have to be crossed over in order to make the motor run at super-synchronous speeds. The voltage induced in the stator varies with slip while the magnitude of the brush voltage depends only on the number of the commutator segments between each pair of half-brushes that may be connected to the two terminals of a stator phase. This is, briefly speaking, the internal behaviour of the machine in the two distinct speed ranges, namely, the range of speed with the slip varying from 0 to +1 and that with slip varying from 0 to −1. Vector and locus diagrams for each such speed range have already been obtained by Arnold (1926), Conrad and others (1911)and by Bhattacharyya and Deb (1949), assuming the impressed voltage from the brushes and that induced in the stator to be in opposition.

It is, however, likely that under certain brush settings the motor will run at a super-synchronous speed on no-load and at sub-synchronous speeds on load that may be well within the full load capacity of the machine. This is, therefore, a new running condition where the slip becomes negative on no-load and positive on load. This interesting case has not been dealt with so far by previous workers in the line. The author, therefore, thought it desirable to undertake a study of the motor under such brush settings in order to derive suitable vector and locus diagrams to represent its action.

VECTOR DIAGRAM

Since the no-load speed is super-synchronous, the brushes are definitely crossed over. But as soon as a suitable load slows down the machine to some sub-synchronous speed, the rotation of air-gap flux becomes opposite to that at no-load so that the voltage induced in the stator changes sign, while the voltage from the brushes remains exactly the same as at the no-load condition. Hence these two voltages become now additive instead of being

subtractive. The vector and locus diagrams under this condition will thus be entirely diffrent from those hitherto obtained for the speed ranges of the motor with the slip varying from o to +1 or from o to −1.

Fig. 1 gives a schematic representation of the vector diagram when the

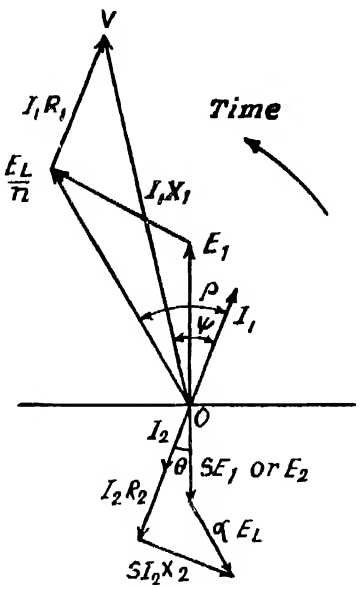

FIG. 1
Vector diagram

slip of the motor varies from negative on no-load to positive on load. It can be easily seen that the resultant voltage on the secondary side is now the vector sum of the voltages SE_1 and αE_L. The secondary current I_2 is thus considerably larger than what would be for the motor running at a sub-synchonous speed for similar brush spread with SE_1 and αE_L opposing each other. The reflection of I_2 on the primary side is still larger than that of an equal current when passing through a similar secondary with SE_1 and αE_L opposing each other, because the whole of the stator and lap winding ampere-turns are now demagnetising with respect to the primary ampere-turns, whereas, in the ordinary sub-synchronous condition (SE_1 opposing αE_L) the stator ampere-turns are demagnetising and the lap winding ampere-turns are magnetising with respect to the primary.

CIRCLE DIAGRAM

The circle diagram can be obtained either directly from the vector diagram already obtained or by considering separately the circle diagrams of the currents I_L and I_S on the secondary side and reflecting these on the primary.

In the former case referring to Fig. 1, the following relation can be obtained.

$$SE_1 = I_2R_2 \cos\theta + SI_2X_2 \sin\theta - \alpha E_L \cos(\rho - \theta) \quad \ldots \quad (1)$$

From Fig. 1, we also get

$$S=\frac{\frac{1}{n}E_1 \sin(\rho-\theta)+I_2R_2\sin\theta}{I_2X_2\cos\theta} \quad \ldots \quad (2)$$

$$(E_1/n)\sin(\rho-\theta)=I_1X_1\cos\theta \quad \ldots \quad (3)$$

$$(E_1/n)\cos(\rho-\theta)=E_1+I_1X_1\sin\theta \quad \ldots \quad (4)$$

From equations (2) and (3) we obtain

$$S=\frac{pI_1X_1}{I_2X_2}+\frac{R_2}{X_2}\tan\theta \quad \ldots \quad (5)$$

Since in our present case SE_1 and $\frac{1}{n}E_1$ are additive, the standstill relation between I_1 and I_2 will be $I_1=-I_2(1+p)$. But at any slip S this relation changes to $I_1=-I_2(s+p)$. Substituting therefore $I_1=-I_2(S+p)$ in equation (5) we get

$$S=\frac{R_2}{X_2}\tan\theta-\frac{p(s+p)X_1}{X_2},$$

so that
$$p(S+p)X_1=R_2\tan\theta-SX_2 \quad \ldots \quad (6)$$

and finally,

$$S=\frac{R_2\tan\theta-p^2X_1}{X_2+pX_1} \quad \ldots \quad (7)$$

From Fig. 1, we have

$$E_1\cos\theta=V\cos\psi-R_1I_1 \quad \ldots \quad (8)$$

$$E_1\sin\theta=V\sin\psi-I_1X_1 \quad \ldots \quad (9)$$

From equations (1) and (4)

$$SE_1=I_2R_2\cos\theta+SI_2X_2\sin\theta-p\{E_1+I_1X_1\sin\theta\}$$

Substituting for $I_1=-I_2(S+p)$ we get

$$SE_1=I_2R_2\cos\theta+SI_2X_2\sin\theta-p\{E_1-I_2(S+p)X_1\sin\theta\}$$

$$=I_2R_2\cos\theta+SI_2X_2\sin\theta-pE_1+I_2\sin\theta\{p(S+p)X_1\}$$

Substituting for $p(S+p)X_1$ from equation (6) we get

$pE_1+SE_1=I_2R_2\cos\theta+I_2R_2\sin\theta\tan\theta.$

Substituting for S from equation (7)

$$pE_1+\frac{R_2\tan\theta-p^2X_1}{X_2+pX_1}E_1=I_2R_2\cos\theta+I_2R_2\sin\theta\tan\theta.$$

Hence,

$$E_1\cos\theta(R_2\tan\theta-p^2X_1)+E_1\cos\theta(X_2+pX_1)p=I_2R_2(X_2+pX_1) \quad \ldots \quad 10$$

From equations (8), (9) and (10)

$$(V\cos\psi-R_1I_1)\left\{R_2\frac{V\sin\psi-I_1X_1}{V\cos\psi-R_1I_1}-p^2X_1\right\}+(V\cos\psi-R_1I_1)(pX_2+p^2X_1)$$

$$-I_2R_2(X_2+pX_1)$$

Then,

$$V\sin\psi(R_2)+V\cos\psi(pX_2)=I_1R_1(pX_2)+I_2R_2(X_2+pX_1)+I_1X_1R_2 \quad \ldots \quad (11)$$

This equation (11) follows directly from equation (10) which can be regarded as an equivalent transformer equation of the motor, as I_2 has been expressed in terms of E_1.

Therefore in equation (11) we can write $I_1 = -I_2(1+p)$ and we get

$$\sin\psi\,(V - R_2) + \cos\psi\,(V - pX_2) = I_1\left\{R_1pX_2 + X_1R_2 - \frac{R_2(X_2+pX_1)}{1+p}\right\}$$

For a constant applied voltage the quantities within brackets are constant and substituting L, K and M respectively for them, we get

$$L\sin\psi + K\cos\psi = MI_1$$

Putting $I_1\sin\psi = x$; and $I_1\cos\psi = y$

$$L\frac{x}{I_1} + K\frac{y}{I_1} = MI_1$$

Or,
$$Lx + Ky = M(x^2+y^2) \qquad \ldots \quad (12)$$

which is an equation of a circle whose centre is the point $\left(\frac{L}{2M}; \frac{K}{2M}\right)$ and whose radius is A, where,

$$A = \left\{\left(\frac{L}{2M}\right)^2 + \left(\frac{K}{2M}\right)^2\right\}^{1/2}$$

Now taking OV as the Y-axis and substituting for L, K and M as follows,

$$L = V - R_2$$

$$K = V - pX_2 \text{ and}$$

$$M = \left\{R_1pX_2 + X_1R_2 - \frac{R_2(X_2+pX_1)}{1+p}\right\},$$

the circle diagrams can be drawn for different values of p.

Alternatively we can proceed as follows. It is known that the resultant current on the secondary side I_2 is the vector sum of I_L and I_S due to the voltages αE_L and SE_1 taken seperately, where,

$$I_L = \frac{\alpha E_L}{\sqrt{(R_L+R_S)^2 + (SX_2)^2}} \qquad \ldots \quad (13)$$

and
$$I_S = \frac{SE_1}{\sqrt{(R_L+R_S)^2 + (SX_2)^2}}$$

also
$$I_S = \frac{E_1}{\sqrt{\left(\frac{R_L+R_S}{S}\right)^2 + (X_2)^2}} \qquad \ldots \quad (14)$$

from equations (13) and (14) it is evident that each of I_L and I_S has a circle locus and Fig. 2, shows how they are related.

T' and N' are respectively therefore the loci of I_L and I_S and their reflection on the primary side are T and N. The resultant reflected primary current will have another circle locus given by the resultant of T and N, whose centre will lie at the intersection of the perpendicular bisectors of OA and OB and whose radius will be the distance from O to the centre.

It may be noted that each of T and N will be $(1+\rho)$ times T' and N' respectively. The total primary current is, however, given by adding the magnetising current to the reflected current from the secondary.

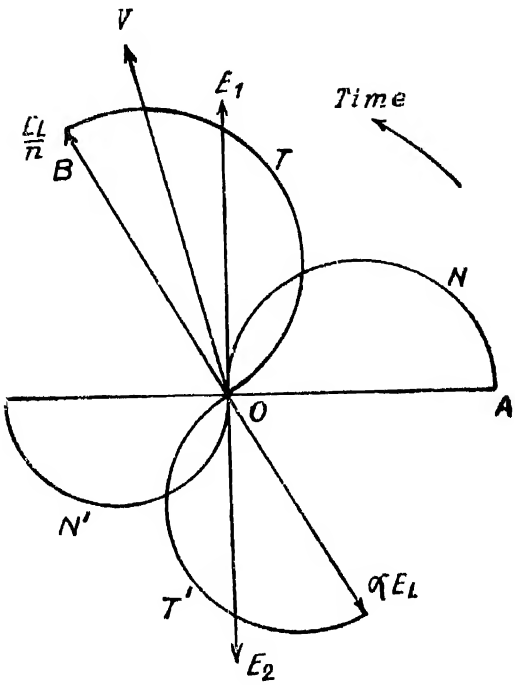

Fig. 2
Circle diagram

DISCUSSION

In the above treatment a symmetrical brush position has been assumed. It may, however, be noted that with unsymmetrical brush positions, only the inclination of the brush voltage with the voltage induced in the stator will change. As a result the resultant voltage on the secondary side will change, but even then the motor can run at a super-synchronous speed on no-load and at sub-synchronous speed on load for identical brush settings. It is to be noted further that for a different brush position or no-load speed, there will be a different locus diagram and each such diagram will give the locus of only those loads that can reduce the speed of the machine below synchronism.

In addition to a symmetrical brush position, it has been assumed further that the primary leakage reactance and the resistance of the secondary-lap circuit are constant and that there is no leakage between the primary and the lap winding. These assumptions if not realised in practice may lead to a discrepancy between the experimental and theoretical locus diagrams. But the preliminary results of measurements made on a B. T. H. brush shifting shunt commutator motor show good agreement between the two. A detailed report of the experimental investigation will be communicated in due course.

NOTATIONS USED

(These refer to per-phase values and it is assumed that the ratio of turns of the rotor primary and the stator secondary is unity.)

V = Primary applied voltage.
E_1 = Primary induced voltage from the stator at standstill.
S = Fractional slip.
n = Ratio of effective lap turns for 180 electrical degrees brush displacement to effective stator turns.
α = Ratio of effective lap turns for brush displacement of β electrical degrees to the effective lap turns for brush displacement of 180 electrical degrees, where, $\alpha = \sin \beta/2$.
SE_1 = Stator induced voltage at the slip S.
E_L = Voltage induced in the lap winding between a pair of half-brushes when they are separated by 180 electrical degrees.
E_L/n = Lap induced voltage on the primary.
αE_L = Voltage injected from lap to secondary.
I_1 = Primary current.
I_2 = Secondary stator-lap combination current.
R_1 = Primary resistance.
X_1 = Primary leakage reactance at supply frequency.
R_2 = Effective stator-lap combination resistance.
X_2 = Effective stator leakage reactance at supply frequency.
θ = Angle of lag of I_2 from SE_1
ρ = Angle of lag of I_1 from E_L/n
ψ = Angle of lag of I_1 from V
$p = \alpha n$
R_L = Lap winding resistance.
R_S = Stator winding resistance.
I_L = Current in the stator-lap combination circuit due to voltage αE_1.
I_S = Current in the stator-lap combination circuit due to voltage SE_1.

ACKNOWLEDGMENT

The author is indebted to Dr. A. K. SenGupta, Lecturer-in-charge of the Electrical Machines Laboratory and to Professor. Dr. P. C. Mahanti, Head of the Department, for their helpful discussions and for giving all facilities to carry out the work.

ELECTRICAL MACHINES LABORATORY, DEPARTMENT OF APPLIED PHYSICS.
UNIVERSITY COLLEGE OF SCIENCE & TECHNOLOGY, CALCUTTA.

REFERENCES

Arnold, A. H. M. 1920, *J. I. E. E.*, **64**, 1139-51.
Bhattacharyya, H. P., and Deb, S. B. (1919), *Ind. Jour. Phys.*, **23**, 93-6.
Conrad, A. G., Zweig, F., and Clark, J. G. (1941), *Trans, A, I. E. E.*, **60**, 829-33.

ON THE RAMAN SPECTRA OF SOLID CH_3Cl AND CH_2Cl_2*

By N. C. MAJUMDAR

(*Received for publication, Aug 3, 1949*)

Plate XXIII

ABSTRACT. The Raman spectra of methyl chloride and methylene chloride in the solid state at $-160°C$ have been investigated and compared with those for the liquid and gaseous states. In the former case the frequency shifts of almost all the Raman lines are observed to diminish when the change either from gaseous to liquid state or from liquid to solid state takes place. In the latter case, however, such changes in the frequencies of the Raman lines are smaller and only those of the deformation oscillations are found to diminish considerably. No new lines in the low frequency region have been observed in the case of any of these two substances in the solid state.

INTRODUCTION

Raman spectra of many simple molecules such as HCl, CO_2, CS_2 and H_2S have been investigated in all the three states—gaseous, liquid and solid. It has been observed that in some of these cases some changes take place in the frequencies of some of the Raman lines and these changes may be due to changes in the configuration of the molecules. Such data, therefore, are helpful in understanding the influence of intermolecular field in the state of aggregation on the structure of the molecule. Data for the solid state, however, are not available for many other simple molecules. With a view to obtaining such data in the case of a series of such molecules, a programme of investigations has been undertaken and in the present investigation the results obtained in the case of methyl chloride and methylene chloride in the liquid state at the room temperture and in the solid state at about $-160°C$ have been discussed.

EXPERIMENTAL

The liquids used in the present investigation were obtained from an old stock of Kahlbaum's sealed bottles. Mythyl chloride was used in its original round bottomed sealed tube and was not redistilled. Methylene chloride was redistilled in vacuum. In order to study the Raman spectra of these two substances in the solid state, the low temperature technique used previously (Majumdar, 1948) was employed. A Fuess glass spectrograph having a dispersion of about 12.5 A.U. in the 4046 Å region was used for photographing the Raman spectra.

* Communicated by Prof. S. C. Sirkar

RESULTS AND DISCUSSION

The spectrograms for the liquid and solid states are reproduced in Plate XXIII. The frequency shifts of the Raman lines are given in Tables I and II along with those for the vapour state for comparison. The data for the vapour state are those reported by Nielsen and Ward (1942). The data for the liquid state reported by Wagner (1938, 1939) are also included to show how far the Raman spectra of the liquids recorded in the present investigation agree with the latest of those reported by the previous workers.

TABLE I

CH_3Cl

Vapour	Liquid at 30°C		Solid at −160°C
Nielsen and Ward (1942)	Wagner (1938)	Present author	Present author
$\Delta\nu$ in cm^{-1}	$\Delta\nu$ in cm^{-1}	$\Delta\nu$ in cm^{-1}	$\Delta\nu$ in cm^{-1}
726 (10)	709 (10)	712 (5) ; ±e, k	695 (3) ; e, k
	1016 (d 0)	1016 (0 b) ; e, k	1016 (0 b) , e, k
	1106 (d 0)	-	-
	1370 (d 0)	—	—
	1446 (d ½)	1415 (0 b) ; e, k	1139 (1) ; e, k
	2683 (d 00)	—	—
	2861 (2)	2861 (2) ; k	2853 (0) ; e
2968 (7)	2955 (11)	2957 (10) e, i, k	2948 (5) ; e, i, k
	3036(b 2)	3040 (2b) ; e, k	3032 (2) ; e, k

TABLE II

CH_2Cl_2

Vapour	Liquid at 30°C		Solid at 160°C
Nielsen and Ward (1942)	Wagner (1939)	Present author	Present author
$\Delta\nu$ in cm^{-1}	$\Delta\nu$ in cm^{-1}	$\Delta\nu$ in cm^{-1}	$\Delta\nu$ in cm^{-1}
281 (5)	283 (0)	285 (5) ; ±e, i, ±k	293 (3) ; e, k
712 (10)	700 (12)	705 (10) ; ±e, i, k	702 (5) ; e, k
	736 (4)	737 (4) ; e, k	730 (0) ; e, k
	1148 (1)	1160 (2) ; e, k	1164 (1) ; e, k
	1255 (00)	—	—
	1417 (3)	1424 (3) ; e, k	1413 (2) ; e, k
	2822 (00)	—	—
	2985 (8)	2986 (10) ; e, i, k	2982 (5) ; e, k
5002 (5)			
	3045 (3)	3056 (3b) ; e, k	3058 (2) ; k

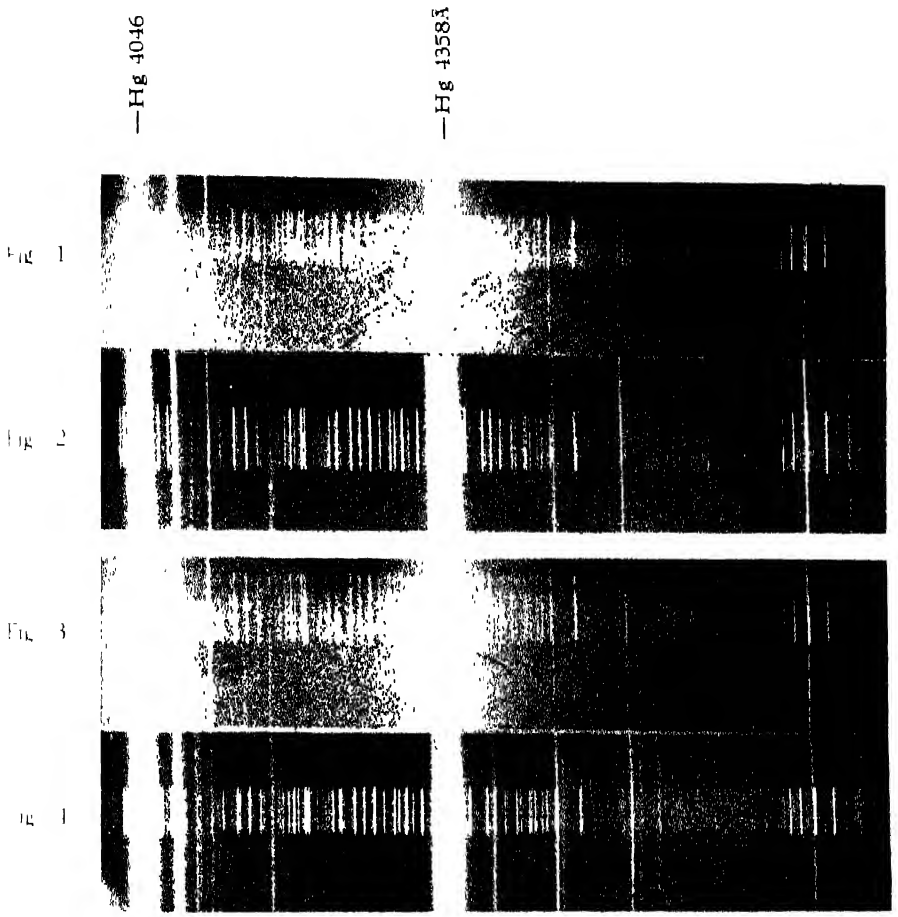

Raman Spectra.

Fig. 1 — CH_3Cl, Solid at −160°C

Fig. 2. — „ Liquid at 30°C

Fig 3. — CH_2Cl_2, Solid at −160°C

Fig. 4. — „ Liquid at 30°C

Methyl Chloride.—It will be seen from Table I that in the case of methyl chloride the frequency-shift of the line due to C-Cl valence oscillation diminishes considerably when the substance passes either from the vapour to the liquid state or from the liquid to the solid state. The value of the frequency-shift for the vapour is 726 cm^{-1} which diminishes to 709 cm^{-1} in the case of the liquid according to Nielsen and Ward (1942). In the present investigation this is observed to change finally to 695 cm^{-1} in the case of solid at $-160°C$ and $\Delta\nu$ for the liquid state was found to be 712 cm^{-1}. Thus the strength of the bond seems to be weakened by the influence of molecular field. The frequencies of the lines due to C-H valence and deformation oscillations also diminish slightly with the change of state, but this change is a little less than that observed in the case of C-Cl valence oscillation. The spectrogram for the solid state, however, did not show any new line in the neighbourhood of the Rayleigh line. The changes in the frequencies of the Raman lines, and consequently, in the strength of the C-Cl and C-H bonds which take place with the change of state and temperature of the substance are thus due to the presence of the large permanent electric moment in the molecule. It is quite evident that in the state of aggregation in the liquid the intermolecular field is strong enough to affect the strength of the bonds and when the molecules further come closer together in the solid state the strength of the intermolecular field increases considerably and the strengths of the bonds are diminished appreciably.

Methylene chloride.—The data for the vapour, liquid and solid states given in Table II show that the major change occurring in the Raman spectrum of the substance with its solidification at low temperature is the splitting of the line 737 cm^{-1} into two lines at 730 and 745 cm^{-1}. This line is totally depolarised according to Trumpy (1934), and therefore, it represents the antisymmetric valence oscillation of the CCl_2 group. The splitting of the line into two components shows that the unit cell contains at least two molecules, the influence of molecular field on one being slightly different from that on the other. Evidently, the lattice differs from a cubic one. The crystal structure of solid methylene chloride has not yet been investigated and therefore no definite information regarding the actual structure is available.

The frequency of the line 285 cm^{-1} due to deformation oscillation of the CCl_2 group increases and that of the deformation oscillation of CH_2 group diminishes a little when the liquid is solidified. The strengths of the C-Cl and C-H bonds, however, do not seem to diminish considerably with the solidification of the substance as can be inferred from the fact that the frequencies of the symmetric valence oscillations diminish very slightly. By comparing these results with those for methyl chloride it is seen that a smaller value of the permanent electric moment in the present case produces such a distribution of intermolecular field in the solid state as affects considerably the frequencies of only particular modes of vibration, *e.g.*, the deformation C-Cl and C-H oscillations ; but this change is an increase in the

former case and a diminution in the latter case. This again may be due to a non-cubic intermolecular field in the crystal.

There is no indication of any new line in the low frequency region in the spectrogram due to solid methylene chloride, although the rotational oscillation of the molecule in the lattice, as postulated by Kastler and Rousset (1941), can take place in this case about a line bisecting the Cl-C-Cl angle. On the other hand, all the bonds are single in both methyl chloride and methylene chloride molecules and there is very little tendency for dimer formation. Therefore if the new lines in the neighbourhood of the Rayleigh line in some other cases be attributed to oscillations in dimers in the solid state, the absence of such lines in these two cases can be easily understood. The formation of loose associated molecules will not produce any sharp new Raman line, but it may produce very broad band in the low frequency region. In the case of methylene chloride there seems to be a continuous wing extending from the edge of the Rayleigh line up to about 90 cm^{-1} from it and this may be due to the vibrations of loosely associated molecules against each other in the solid state.

ACKNOWLEDGMENT

The author is indebted to Prof. S. C. Sirkar for his kind interest and guidance throughout the progress of the work and to the authorities of the Indian Association for the Cultivation of Science for kindly providing all facilities for the work.

INDIAN ASSOCIATION FOR THE
CULTIVATION OF SCIENCE,
210, BOWBAZAR STREET,
CALCUTTA.

REFERENCES

Kastler, A. and Rousset, A., 1941, *C. R. Acad. Sc.*, **212**, 645; *Jour. de Physique*, **2**, 49.
Majumdar, N. C., 1948. *J. Sc. Indust. Research*, **8B**, 25.
Nielsen, J. Reed and Ward, N. E., 1942, *J. Chem. Phys.*, **10**, 81.
Trumpy, B., 1934, *Z. f. Phys.*, **88**, 226.
Wagner, 1938, *Zeit f. Phys. Chem. B.*, **40**, 36.
Wagner, 1939, *Zeit f. Phys. Chem. B.*, **45**, 69.

PLAUSIBLE SPEED LIMIT FOR METALLIC PROJECTILES

By K. R. DIXIT

(Received for publication, Aug. 18, 1950)

ABSTRACT The flight of a metallic projectile is discussed in two separate cases (*i*) in the Earth's atmosphere and (*ii*) in the interstellar space. It is shown that in the Earth's atmosphere 7 Mach numbers appear to be the plausible speed limit for long duration flight. In the interstellar space it is shown that when flying with a speed, which is greater than the velocity of escape from the surface of the Earth, the body will be warmed up in a short interval of time by the power plant to such an extent that we have to apply to it the equations governing the stability of hot bodies in interstellar space. Here we find that our metallic projectile is too small to be stable. Lastly, starting from the equations of Wigner and Seitz (1934) and considering the connection between the elastic properties of ordinary metals and the velocity of sound in those metals, it is shown that at speeds greater than the velocity of sound in metals, the Fermi energy of the electron cloud will become very large and thus make the metal relatively less stable in this state.

The flight of metallic projectiles at high speeds is assuming increasing importance. In the consideration of the movement of such projectiles two separate cases have to be considered; (1) the flight in the Earth's atmosphere and (2) the flight in the interstellar space. We shall consider these two in that order. Further, as the velocity of sound in a metal is connected with the elastic properties, some new phenomena might be expected to occur when the metal object moves with a velocity comparable with the velocity of sound propogation in the metal. Some aspects of this are considered in the last section.

1. FLIGHT IN THE EARTH'S ATMOSPHERE

We are quite familiar with the laws which govern the movement of ordinary propeller planes moving at speeds of about 500 m.p.h. and we are gradually gaining some knowledge of the flight at higher speeds. In this connection we often hear of supersonic speeds, that is speeds which are greater than the speed of sound in air at N.T.P., namely 700.5 m.p.h. When a plane travels at a speed greater than this, it is travelling faster than the pressure waves and would be able to catch them up. This results in a furious clash of air-currents, which throws the whole plane into violent vibrations. As a result of these vibrations some conventional planes have been actually torn apart. Wind tunnel experiments have been made going up to Mach number 4.4, (4.4 times the velocity of sound in air). Experiments at higher speeds, with air rushing past a model at one mile per second and more, have not yet been performed. It is, however, possible to draw some conclusions

from our knowledge of the meteoric flights, about what we may expect to happen, when a projectile is moving very fast in the atmosphere of the Earth. In this connection it must be remembered that a meteor does not require a power plant for its propulsion. The presence of the power plant and the heat produced by it will introduce more complications. We shall have to consider these, specially in the case of interstellar flight, where no cooling effect will be produced by the air currents and the cooling due to radiation becomes appreciable only at very high temperatures.

Meteors usually come from distances beyond the Moon and have velocities of about 20 miles per second at the time of entering the ionosphere. The motion of the meteors is produced by gravity, and their temperature is very low, a few degrees absolute, at the time of entering the Earth's atmosphere. The meteors during their flight become visible at a height of about 100 kilometres above the surface of the Earth. At this height the air pressure is of the order of 10^{-3} mm. of Hg and the temperature is about -100°C. Thus the meteor up to the time it becomes visible, has been flying only for a few seconds through cold rarefied atmosphere; and yet it is warmed up to such an extent as to become visible. The high temperature is the result of the movement of the meteor. The meteor is moving faster than the air molecules, it therefore traps and compresses the slow moving air molecules in front of it. A cap of compressed air is created in front of the meteor. Such a cap of compressed air becomes intensely hot and melts the surface material of the meteor. The behaviour of the meteor is not so very peculiar, as any projectile moving through air with a speed, which is greater than the speed of sound in air, will be trapping air in front of it. These trapped molecules will be pushed from behind by the projectile and will acquire the velocity of the projectile. This is an additional velocity acquired by the molecules. The effect of the added velocity is to increase the kinetic energy and hence raise the temperature of the trapped air molecules. By applying the laws of the kinetic theory of gases, we find that a projectile moving with a speed of 11 metres per second, will increase the temperature of the molecules trapped in front of it by 1°C. The increase in the temperature of the cap, as determined by the kinetic theory, is proportional to the square of the velocity and we could expect that the temperature of the aircap trapped in front of a projectile, moving with the speed of sound in air would be about 70°C. Thus we could expect a jet plane moving at a speed of 760.5 m.p.h., to be preceded by an aircap, whose temperature is greater than the temperature of the surrounding air by about 70°C. The projectile is in contact with the aircap and hence its temperature could also be expected to be greater than that of the surrounding by 70°C. The large amount of fuel consumed in a jet plane will further increase the temperature, but it may to some extent be compensated for by the partial vacuum and the corresponding cooling created behind the projectile. There will also be loss of energy due to radiation, calculations are made for such changes in the next section, but in general the cooling

produced by radiation for a flight in the Earth's atmosphere will be smaller than the cooling produced by other causes.

To the same approximation, the temperature of a projectile made up of thin sheets of metal, and moving at a speed which is 3.5 times the speed of sound in air, the increase in temperature above the surroundings would be $70^{\circ}C \times 3.5^2 = 850^{\circ}C$. If the temperature of the surrounding air is $-100^{\circ}C$, temperature of the projectile would be $750^{\circ}C$; and if made of aluminium it would melt before this speed is reached. Thus 3.5 Mach numbers appear to be the speed limit, for a flight of thin aluminium projectile, even through rarefied air, for an interval sufficiently long for the establishment of equilibrium conditions. There will be a slightly higher speed limit for other metals.

Thus we are forced to conclude, that it would be almost impossible to have a metal projectile, flying for an appreciable distance at speeds represented by Mach numbers beyond 7, without deformation of the projectile caused by melting of some of its parts. Such deformation changes the shape of the fins of the projectile and reduces the speed. It should be pointed out that these calculations consider the warming up due to compression of air in front of the projectile, partial cooling due to the vacuum created at the back and the increase in temperature due to the combustion of the fuel. These considerations, therefore, apply to the flight in the Earth's atmosphere, be it in troposphere, stratosphere or ionosphere. To this approximation there must be a plausible speed limit, about 7 Mach numbers, for long duration ($\sim$100 seconds) flights, even in a rarefied atmosphere (pressure $\sim 10^{-3}$ mm. of Hg).

2. INTERSTELLAR FLIGHT

In the case of flight in interstellar space, we have not to consider the warming or cooling of the aircap or the airtail. We have to consider the warming up of the plane by the combustion of the fuel and the radiation of heat, to and from the projectile. But in order to reach interstellar space, it is necessary for a projectile to acquire a speed which is greater than, (at least equal to) the velocity of escape from surface of the Earth. This velocity is given by the relation, $V = (2GM/a)^{\frac{1}{2}}$, where G is the universal constant of Gravitation, M is the mass of the Earth and a the radius. This velocity is about 7.1 miles or 11.3 kilometres per second, and is about 2.2 times the velocity of sound in metals like aluminium and steel. But the velocity of sound in a metal is connected with the elastic properties and some new phenomena might be expected to occur, when a metal object moves first through air and then in interstellar space with a velocity comparable with the velocity of sound propagation in the metal. We shall defer this theoretical discussion to the next section. Here we shall assume that such speeds are permissible without producing an elastic deformation of the metallic object, and proceed to consider the thermal conditions governing the flight in interstellar space.

Let us consider a metallic projectile, mass 10 tons (10,000 kilograms) and surface area 100 square metres. This projectile starts from rest on the surface of the Earth and acquires a speed of 11·3 kilometres per second before it leaves the Earth's atmosphere, in about 100 seconds. During this period it has acquired a kinetic energy $\sim 6.4 \times 10^{18}$ ergs. This energy is supplied by the rapid combustion of the fuel. Now every unit of fuel utilised may be split up in two parts, a and b. a is used in producing motion and in imparting kinetic energy $\frac{1}{2}mv^2$, whereas b is wasted in producing an increase of temperature. The ratio $a/a+b$ is known as the efficiency of the fuel. The ratio $a : b$, is independent of the velocity, but it may be slightly modified by the temperature of the fuel, which modifies the properties of the fuel and hence its efficiency. But to a first approximation we may assume that the ratio $a : b$ is constant, then the increase of temperature of the object, will be proportional to b and hence to a and thus to the square of the velocity. Even the best fuel is not 100% efficient and a certain percentage of it will be wasted in heating the power plant and our projectile, and to a first approximation the change of temperature produced by this wasteful combustion can be taken proportional to the square of the velocity. It should be noted that this heating is not the same as produced by frictional resistance, which is not proportional to the square of the velocity at high velocities.

To get an idea of the changes of temperature produced, by the heat supplied or radiated, let us calculate the energy required to heat the projectile from 300°K to 1000°K. The average specific heat of the projectile could be assumed to be 0·2 calories per degree C. The required energy will be $0.2 \times 700 \times 10^3 = 1.4 \times 10^5$ calories or 5.9×10^{12} ergs, which is only one per cent of the kinetic energy, and could be easily supplied even by a fuel with an efficiency of 99%. But no fuel has reached this efficiency, and the actual heating produced while imparting the kinetic energy corresponding to the velocity of escape would be much greater than that indicated by the range 300°K to 1000°K.

Let us now consider the radiation to and from the plane. The radiation received by the plane depends on the solar constant and the surface area. For the surface area of 100 sq. metres it is 1.35×10^{12} ergs per second and is negligible as compared to 5.9×10^{16} ergs. The loss of heat by radiation is governed by the Stefan's law and would depend on the temperature of the projectile. For an object at 1000°K and 100 sq. metres surface area it would be 5.73×10^{13} ergs per second, which means that only a thousandth part of the heat produced (5.9×10^{16} ergs) by a fuel which is 99% efficient, is lost in one second by radiation. The radiation loss per second will be comparable with the heat produced by the wasteful combustion of the fuel only at very high temperatures, comparable with the surface temperature of the stars. In interstellar space the loss of heat due to radiation is the only means available for reducing the temperature

of the projectile. As seen above the rediation loss at low temperatures ($\sim$1000°K) is negligible as compared to the heat produced by the wasteful combustion of the fuel. Hence the temperature of the projectile will go on increasing until equilibrium conditions are established at very high temperatures. But long before this happens, the entire material of our projectile would be vaporised; we shall have to consider this object as a small hot gaseous body and apply to it equations similar to those given by S. Chandrasekhar, (1939)

$$\frac{d}{dr}(p_g + p_r) = -\frac{GM\rho}{r^2}$$

This is the equation of hydrostatic, radiative equilibrium of a spherically symmetrical distribution of matter (Where p_g is the gas pressure, p_r, the radiation pressure, G, the constant of gravitation, $M(r)$ the mass enclosed inside r and ρ the density).

It will be seen from the equation, that the radiation pressure for our object will be large compared with the gravitational attraction, and the system will not be stable. In fact in an attempt to establish a state of equilibrium by making the loss of energy due to radiation equal to the heat produced, our projectile lands itself into a state, where it fails to satisfy the conditions of stability for heated bodies in interstellar space. Thus it appears that in interstellar space, the flight of a metallic object with a power plant, at speeds greater than the velocity of escape, for an appreciable time, will result in the deformation and the possible destruction of our object. But no object can reach the interstellar space, unless it has acquired in the Earth's atmosphere a velocity greater than the velocity of escape from the surface of the Earth. Even if it were possible to do so (and this is rather unlikely as 7 Mach numbers is a plausible speed limit for atmospheric flight of about 100 seconds duration), a flight in interstellar space with such a velocity for an appreciable time, will result in the deformation and possible destruction of the metallic object with a power plant. Thus even in interstellar space there appears to be a plausible speed limit (for a metallic object with a power plant), which must be less than the velocity of escape and hence must be comparable with the limit of about 7 Mach numbers for atmospheric flight of appreciable duration. The impossibility of interstellar flight at speeds less than the velocity of escape, need not concern us while considering the conditions of thermal equilibrium. Both these conditions, however, taken together give us the plausible speed limit as already mentioned.

3. THE VELOCITY OF SOUND IN A METAL AND ITS COHESIVE PROPERTIES

The first successful calculation of the cohesive forces in metals was made by Wigner and Seitz (1933) who obtained wave functions for electrons in metallic sodium and lithium by numerical integration. Wigner and Seitz

divide the lattice into polyhedra, one polyhedron surrounding each atom. The wave functions of the valence electrons extend throughout the whole lattice and have periodic properties. This leads to boundary condition for the wave function at the boundary of any atomic polyhedron, $d\psi/dn=0$, where the differentiation is normal to the boundary. Fröhlich (1937) replaced the atomic polyhedron by a sphere of equal volume and radius r_0, so that,

$\frac{4}{3}\pi r_0^3=\Omega=$ the atomic volume, or the volume of the atomic polyhedron.

The polyhedron having been replaced by the sphere, the boundary condition assumed is that $\frac{d\psi}{dn}$ vanishes everywhere on the surface of the sphere. Within this sphere $V(r)$ is taken as the potential energy of an electron in the field of the ion. If $E(r_0)$ is the energy of an electron in the lowest state in the lattice : $E(r_0)$ is given by the Schrödinger equation,

$$\frac{d^2\psi}{dr^2}+\frac{2}{r}\frac{d\psi}{dr}+[E(r_0)-V(r)]\psi=0$$

with the boundary condition,

$$\frac{d\psi}{dr}=0 \text{ for } r=r_0$$

Frohlich has calculated the values of $E(r_0)$ subject to certain simplifying assumptions (Hume-Rothery, 1947). He writes

$$E(r_0)=E_0+E_1+E_2$$

In this equation E_0 is the work required to break up into free electrons and positive ions a hypothetical crystal in which all the electrons are in the lowest energy state : E_1 is the mean Fermi energy and in a free electron model it is the kinetic energy of the motion of translation of the electrons, whereas in the zone theories E_1 is that part of the energy which is associated with the motion of the electrons in the periodic field of the lattice ; and E_2 is the ionisation potential of a free atom and is constant for any given metal.

Thus it will be seen that $-(E_0+E_1+E_2)$ is the work required to evaporate the electrons and ions from the crystal and convert them into neutral atoms; or the energy of the crystal relative to the free atom is $+(E_0+E_1+E_2)$. Large values of this expression tend to make the energy of the crystal greater than that of free atoms and hence the crystal relatively less stable. E_1 is the constant of the free atoms, while both E_0 and E_2 are functions of the distance between the atoms. Frohlich assumed that the electron clouds do not overlap and that E_1 is the same as given by the free electron theory ; and calculated E_0+E_1 for different values of r_0. The curve for E_0+E_2 passes through a minimum. The minimum indicates the equilibrium value of r_0, ($\frac{4}{3}\pi r_0^3=$ the atomic volume) or the lattice spacing and the

curvature in the region of the minimum permits a calculation of the compressibility K,

$$\frac{1}{K} = -v\left(\frac{dp}{dv}\right) = v\left(\frac{d^2E}{dv^2}\right)_{v=\Omega}$$

where E is the total energy.

Fuchs (1936) has shown that the mutual attraction between the ionic cores cannot be neglected. Only by taking this into account it is possible to explain satisfactorily the elastic properties of the noble metals. But once this is done, the nature of the curve showing total energy as a function of r_0, is similar to the curve obtained by Fröhlich. Here also the minimum gives the equilibrium value of r_0 and the lattice spacing, the curvature as before gives the compressibility. This then may be assumed to be the general property for all metals, even aluminium and iron for which no exact calculations are available.

We now proceed to establish relations between the elastic properties as defined above with the velocity of sound in a metal.
We know that

$$V = \text{the velocity of sound} = \sqrt{\frac{\text{elasticity}}{\text{density}}} = \sqrt{\frac{\text{the Young's modulus}}{\text{density}}}.$$

We also know, that if K is the compressibility, k is the bulk modulus, Y is the Young's modulus and σ is the Poisson's ratio which is nearly equal to $\frac{1}{3}$ for most metals, then we have

$$k = \frac{Y}{3(1-2\sigma)} \simeq \frac{Y}{3(1-2/3)} \simeq Y.$$

This gives us the relation,

$$K = \frac{1}{k} \simeq \frac{1}{Y} \text{ or } V^2 = \frac{Y}{\rho} \simeq \frac{1}{K\rho}.$$

Hence we get,

$$\frac{1}{K} \simeq V^2\rho = V^2 \frac{\text{atomic weight}}{\text{atomic volume}} = V^2 \cdot \frac{1}{\Omega},$$

but

$$\frac{1}{K} = \frac{1}{9\Omega} r_0^2 \left(\frac{d^2E}{dr^2}\right).$$

Therefore we finally come to the expression that

$$V \propto r_0 \left(\frac{d^2E}{dr^2}\right)^{1/2}.$$

That is the velocity of sound in a metal is a function of the distance at which the total energy becomes a minimum (or the lattice spacing), as well as the curvature of the energy curve at that place. This will be strictly correct for the ideal metals of Fröhlich, for changes in which the atomic volume remains

unaltered, and for metals for which the Poisson's ratio is about $\frac{1}{3}$; for all other metals we may assume it to be a good enough first approximation.

The question now arises as to what we might expect to happen when the metal begins to move with a velocity which is greater than the velocity of sound in that metal. As seen above the velocity of sound in a metal represents the minimum of the energy curve and the value of k_1 for which it is stable. When the velocity of a metal increases, it also increases the velocity of the electron cloud associated with it. As the velocity passes beyond the limit given by the velocity of sound in that metal, the Fermi energy k_1 of the electron cloud will begin to increase above the limit given by the minimum energy and the stability. Greater the deviation from the velocity of sound, the greater will be the increase in k_1 and greater will be the instability that results. This also appears to point out that the flight of a pure metallic object at velocities greater than that of sound in that metal increases the energy of the associated electron cloud and makes the metallic object relatively less stable.

The plausible speed limit suggested by these theoretical considerations is comparable with that given in sections 1 and 2. In this connection we should remember that meteors are not pieces of pure metals and hence their stability will be governed by other causes than the Fermi energy. For example, at velocities greater than the velocity of sound in a solid we can expect the characteristic frequencies, the Debye characteristic temperature and the melting point to be altered. We shall, however, defer this discussion to a later paper.

Royal Institute of Science,
Bombay, India.

REFERENCES

Chandrasekhar, S., 1939 'An Introduction to the Study of Stellar Structure', p. 216, Chicago.

Frohlich, H., 1937, *Proc. Roy. Soc.*, A, **158**, 97

Fuchs, K., 1936, *Proc. Roy. Soc. A.*, **153**, 622

Hume-Rothery, W., 1017, 'Atomic Theory for Students of Metallurgy', pp. 417-424, London.

Wigner, E. and Seitz, F., 1933, *Phys. Rev.*, **43**, 804

THE SPECTRO-CHEMICAL DETERMINATION OF CARBON IN FERROUS ALLOYS

By K. C. MAZUMDER and M. K. GHOSH

(*Received for publication, April 10, 1949*)

ABSTRACT. It has been possible to determine carbon spectro-chemically. The determination up to 0.30% C can be carried out exactly in the same way and under similar conditions as that of the metallic elements present in the ferrous alloys. Beyond this range it has been found necessary to use a nitrogen draught directed against the spark gap. The calibration curves obtained are smooth and the accuracy is within ±0.02. An explanation is suggested for the above peculiarity.

INTRODUCTION

In recent years spectroscopes have been extensively used for the quantitative determinations of the alloying and the impurity metallic elements in both ferrous and non-ferrous alloys. The presence of carbon in ferrous alloys is of fundamental importance but its response to the spectro-chemical method of evaluation of its amounts present in steel has been extremely poor. Several attempts have been made during the past few years and that too, under very special types of excitation for determining carbon by spectroscopes. In most of the cases the workers could not observe any reliable concentrational variation of the intensity of the carbon lines and thus quantitative estimation of carbon was not possible; [*vide* Emery and Booth (1935)]. Only Convey and Oldfield (1945) achieved some success in determining carbon spectroscopically. None of these earlier workers has, however, described the nature and extent of the irregularities nor has suggested the reasons thereof. We have been working on this problem for the last few years and have succeeded in establishing the real nature of the failure of the carbon estimation by spectroscope. We are also offering an explanation for this peculiar behaviour of carbon existing in the ferrous alloys; this will be presently discussed.

The successful adaptation by Mazumder and Ghosh (1948) of the medium quartz spectorscope for the determination of the metallic elements found in steel encouraged us to try to estimate carbon also by the same instrument. The carbon lines appear brightly on the plates with a sparking voltage of 10,000 or so; but they do so in such a crowded condition together with the lines belonging to the rest of the elements present in the sample that reliable quantitative estimations of the carbon contents have not been possible. The only alternative left is to try the larger instrument generally

used for ferrous analyses. The conditions under which these analyses are carried out, have also been retained in the present case excepting the change of the spectral range from $\lambda 4200-2600$Å to $\lambda 3000-2200$Å. This is necessary for having the only uncontaminated carbon line -2296.89Å photographed on the plate. Under similar conditions of excitation but with slightly longer exposures, the 2296.89 line appears on the plate with photometrically measurable blackening for as low a percent as 0.10. The curve in Fig. 1, is seen to be very smooth and the accuracy is within ± 0.02. On repeating the work over and over it has been found that up to about 0.40%; the calibrations curves obtained are smooth and so, the estimation was reliable but for percentages higher than the above, smooth curves can not very often be obtained. The curve in Fig. 2 shows that the points beyond 0.40% lie very irregularly and no accurate estimation is at all possible from the curves of this nature. The reason for such selective spectro chemical response of carbon *i.e.*, the regularity up to 0.40%, is to be found in its metallurgical behaviour with respect to iron. "In steel containing small proportions of carbon, the ferrite forms a continuous net work, shown to consist of distinct grains by etching but from 0.40 percent C onwards, the ferrite grains are isolated and surrounded by pearlite" (Metallography by Desh). The Fe-atoms in the completely isolated grains of ferrite will be easily detached and ionized and to a comparatively greater extent conduct the current in the spark. The sparking points will thus be confined mostly to the ferrite grains. The stable cementite molecules Fe_3C in the pearlite grains will not so easily be affected by the spark and the observed irregularities in the carbon estimation will be the result. This spectroscopic observation corroborates in an interesting way the results of the microscopic studies obtained long ago.

Two methods suggest themselves for obviating these troubles about the carbon estimation. One is to have a more forcible discharge in the spark by inserting in the secondary circuit an auxiliary spark gap, preferably of the rotating type, and the second is to have an N_2 draught directed against the spark gap for removing the metallic ions which generally persist in carrying the current at the expense of those of the metalloids or non-metals like carbon, phosphorus, etc. even when the sparking potential has considerably died down. The nitrogen draught thus induces fresh ions to be formed and the carbon atoms have then more chances to participate in the conduction. The effective sparking potential also is enhanced to a certain extent as in the case of the first method. Both of these methods have been employed by different workers on different occasions for steadying the sparking potentials and thereby obtained more consistent results by the spectro-chemical analysis. We also tried these methods. The draught was of nitrogen from a cylinder. But no decisively increased accuracy in the spectro-chemical estimation of the metallic elements with which we were concerned at that time was observed.

The inclusion of an auxiliary spark gap in the circuit, rotating or non-rotating, does not also materially improve the accuracy of the estimation of the metallic elements. In the case carbon also the auxiliary spark gap has not been found to improve the consistency. The nitrogen draught, however, at a pressure of 2mm. to 3mm. of water, effects a decisive improvement. The irregularities beyond 0·10% C, observed previously, completely disappears with the nitrogen draught. The calibration curves are now smooth and regular and the accuracy is generally of the same order as in the chemical method. It should be noted that in the formal spectroscopic work the so called vacuum arc is only an arc in reduced pressure of air or nitrogen obtained from a cylinder. This gives a much clearer plate and also produces change in the relative intensity of the spectral lines. By blowing nitrogen against the sparking gap we have also noticed an improved cleanliness of the plate and an enhancement of the intensity of the carbon line. Convey and Oldfield (1915) obtained consistent results in the carbon estimation by sending an air draught against the spark gap by means of an aspirator and an air drier. We have also repeated their work and obtained better results than those obtainable without nitrogen or air draught. But the nitrogen draught is easier to produce and yields more consistent results; the drying of the draught by $CaCl_2$ can also be dispensed with, if found inconvenient.

EXPERIMENTAL

Hilger large quartz spectrograph has been used for photographing the spectra. The following are the conditions for exciting the spectra.

Voltage – 15,000
Capacity – 0.005 μF.
Inductance Nil
Spark gap – 2.0 mm.
Upper electrodes – pointed Cu-rods.
Lower ,, conical samples with flat top, 2 mm. dia.
With and without nitrogen draught at 2 inches of water.

The samples were all collected from the Tata Steel of graded carbon contents necessary for drawing calibration curves. In the beginning both the electrodes were of steel of the same composition; the results obtained were not very consistent. Pointed At-rods were then tried as upper electrodes, still there was not noticed any pronounced improvement in the result. Copper rods were then used for the upper electrodes and all the subsequent investigations have been carried out with copper in the upper position. The initial experiments were done with the simple sparking

circuit used generally for the spectro-chemical analysis of steel. When it was found that beyond 0.40% C, the calibration curves were not always regular, a nitrogen draught at 2 inches of water was directed against the spark gap. The nitrogen was obtained from a cylinder and dried by passing through a system of $CaCl_2$ tubes. The method and the apparatus used for measuring the intensity of the spectral lines are the same as were described by Ghosh and Mazumder (1918) in connection with their work on "The spectro-chemical analysis of the Bearing Alloys". The corrections obtained by the emulsion calibration have not, however, been always carried out in the present work.

RESULTS

It has been found that with an exposure of one minute the carbon line 2296.89A, even for a sample of carbon contents, 0.10%, appears with sufficient blackening to permit of accurate photometric measurement. The curves in Fig. 1 and Fig. 2 have been obtained from spectrograms taken

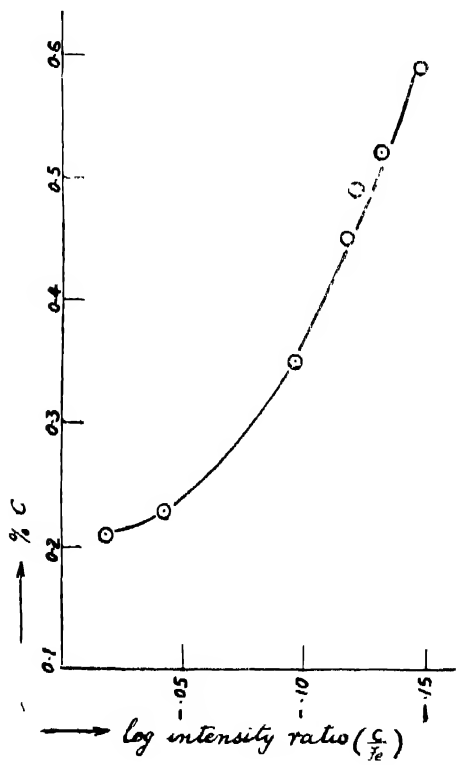

FIG. 1
C in steel without N_2 draught

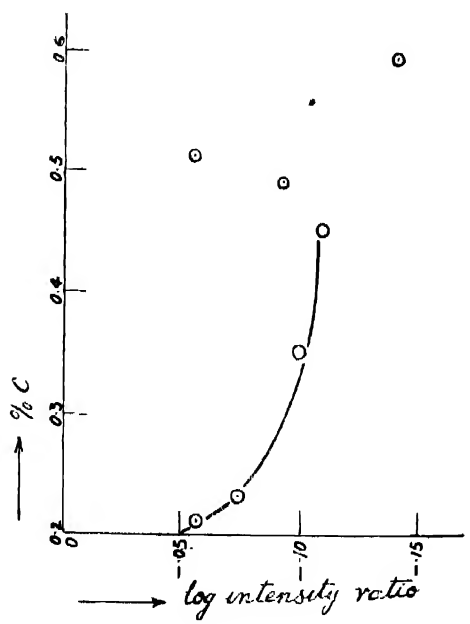

FIG. 2
C in steel without N_2 draught

without nitrogen draught. The curve in Fig. 1 is smooth and regular but that in Fig. 2 is extremely irregular beyond 0.40% carbon though both plates have been taken under exactly the same conditions. From several

plates taken without nitrogen draught we can conclude that the results obtained up to 0.40 % C are reliable and beyond this range regular curves

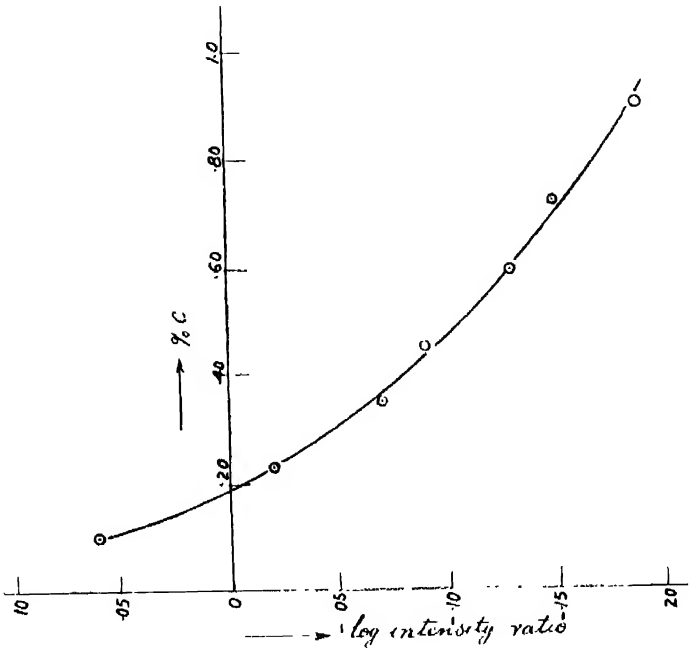

FIG. 3
C in steel with N_2 draught

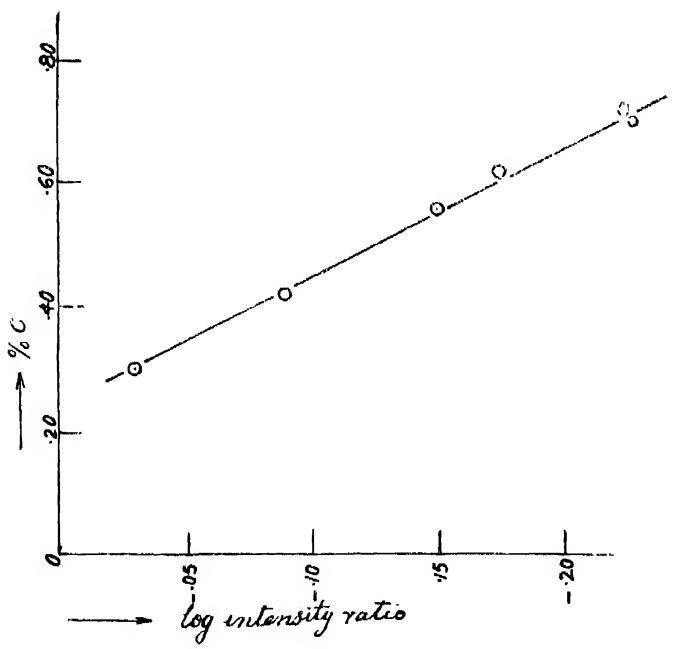

FIG. 4
C in high speed steel with N_2 draught

can only occasionally be obtained. With a nitrogen draught directed against the spark gap these irregularities completely disappear and carbon

contents of various ferrous alloys can reliably be estimated by spectroscope. The curves in Fig. 3 and Fig 4 have been obtained from plates taken with a nitrogen draught; the former is for ordinary carbon steel and the latter, high speed steel. The spectra photographed in this way, have always been found to give smooth curves. It can then be said that the carbon in steel can be spectro chemically determined but for the range beyond 0 40% a nitrogen draught should be used.

ACKNOWLEDGMENTS

The writers take this opportunity to thank the Tata Management and to Dr. J. C. Ghosh, Chief Chemist, for facilities given to carry out the investigation.

New Research Laboratory
T. I. S. Co., Jamshedpore.

REFERENCES

Convey, J. and Oldfield, J. H., May, 1915, *J Iron and Steel Institute.*
Emery, F. H and Booth, H S., 1935, *Ind* and *Eng Chem.*, **7**, 410
Mazumder, K. C and Ghosh, M K , 1948, *Ind. J Phys.*, **22**, 501
Ghosh, M. K. and Mazumder, K. C., 1948, *Ind. J Phys* , **22**, 409.

VARIATION OF INTENSITY OF DISTANT ATMOSPHERICS WITH FREQUENCY CHANNELS

By S. R. KHASTGIR and ASIT SEN

(Received for publication, Aug. 15, 1950)

ABSTRACT. The results of an investigation carried out with a cathode-ray tube direction-finder on the intensity of distant atmospherics as received on a limited range of frequency 170-204 Kc/s (corresponding to the wavelength range, 1470-1760 metres) are given in the present paper. The following types of intensity variation with frequency were observed.

(1) During the day time and occasionally at night, the intensity of distant atmospherics, as received within the experimental range of frequency, was found to vary inversely as the cube of the frequency.

(2) Usually at night, the intensity of the distant atmospherics, within the frequency range, was found to decrease exponentially with the increase of frequency.

(3) During the day or night, the intensity of the distant atmospherics, within the same frequency range, was found to vary in a manner suggesting a combination of the first two types of intensity variation.

From theoretical considerations the following conclusions are drawn:

(*i*) The first type of intensity variation with frequency prevails, whenever, (whether during day or night) the source of atmospherics is not very distant and the atmospherics pulse reaches the receiving point by the ground path.

(*ii*) The second type is associated with sky-waves only and is observed almost invariably during the night hours with fairly distant atmospherics.

(*iii*) The third type which is a combination of the first two types is observed when the source of atmospherics is not too distant and yet not too close so that ground and sky waves are both present.

INTRODUCTION

Some measurements of the intensity of atmospherics received in medium radio frequency channels (250/2000 Kc/s) were made by Khastgir and Rao (1940) following the Warbler method. Similar measurements were carried out by Khastgir and Ray (1950) over the same frequency range following the peak method of measurements of Potter (1931). These measurements were later extended to still higher frequencies (2 to 20 Mc/s) by Khastgir and Ali (1942). Although these previous experiments, where a large frame aerial was used, gave field strengths of atmospheric pulses coming primarily in a direction parallel to the plane of the frame aerial, the atmospheric pulses coming from other directions also had their contribution. To find exactly the manner in which the intensity of the received atmospherics

varied with the frequency to which the receiver was tuned, a cathode-ray tube direction-finder was therefore used in the present investigation. This enabled determinations of the intensity of individual atmospheric pulses coming from sources situated in specific directions with reference to the receiving point. A limited range of frequencies, *viz.*, 170-204 Kc/s (corresponding to a wavelength range 1470-1760 metres) was investigated and measurements of the intensity of distant atmospherics in definite directions were made both during day and night.

The subject of frequency distribution of atmospherics has been reviewed theoretically and the theoretical findings regarding the intensity variation of the distant atmospherics for different frequencies under different conditions of propagation were found to agree well with the experimental results.

CATHODE-RAY TUBE D/F EQUIPMENT

The cathode-ray tube D/F equipment consisted of the following :

(1) *Aerial System.*—A pair of 'crossed' loop aerials, 6 ft. square with 10 turns of 7/22 stranded copper wire was installed, the plane of one aerial being in the north-south direction and that of the other in the east-west direction. Each aerial could be tuned to the desired range of frequencies.

(2) *H/F Amplifier Units.*—The two loop aerials were connected to two similar H/F amplifier units. In each amplifier, two screen-grid valves with earthed cathodes were used in push-pull in the first stage which was followed by a pentode valve in the second stage. The push-pull circuit in the first stage necessitated the use of two similar ganged condensers in each aerial for tuning purposes, one plate of each condenser being connected to the earth-point and the other plates being joined in the usual way to the grids of the two valves working in push-pull. For tuning each aerial to the different frequencies, it was necessary to insert in parallel with each variable aerial tuning condenser one or another of a set of fixed condensers of requisite values by switching in steps. For tuning the first stage, a similar set of fixed condensers with a similar switching arrangement was used in parallel with the variable condenser across the secondary of the inter-stage transformer. The pentode valve in the second stage was followed by an output transformer, the secondary of which was tuned in the same manner by a similar set of fixed condensers inserted in parallel to the vairable condenser across it by similar switching arrangement.

(3) *Oscillograph Unit.*—A Cossor oscillograph was used. The output of one amplifier was connected to the vertical pair and that of the other to the horizontal pair of the deflecting plates of the oscillograph.

The deflection-sensitivity of the oscillograph spot was found to be linear over a wide range of A/C voltage applied to either pair of the deflecting plates.

The calibration of the oscillograph sweep-length in terms of the R/F voltage applied to the input of either amplifier was effected with the help of the deflection-sensitivity curve and the gain characteristics of the H/F amplifier for specified frequencies within the desired range. The gain *vs.* input voltage curves were constructed in the usual way for the specified frequencies. From the gain characteristics data, the gian *vs.* frequency curves were also obtained for definite input voltages. The amplifier gain which was found to decrease slightly with frequency, could be regarded as practically constant over the limited frequency range under investigation. The circuit diagram of the D/F equipment is shown in Fig. 1.

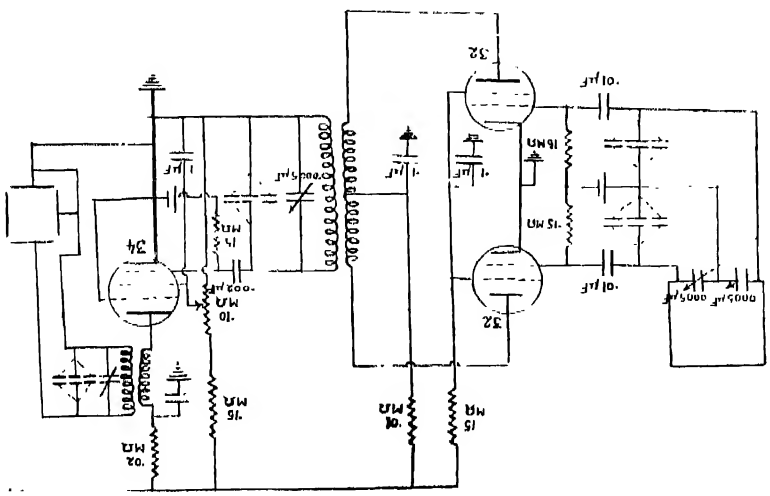

FIG. 1

EXPERIMENTAL PROCEDURE

When the atmospheric pulse was received by the aerial system, currents were induced into the two loop aerials, each tuned to any frequency in the desired range. The voltages developed across the tuning condensers were then amplified by the two H/F amplifier units and the tuned amplified voltages applied across the two pairs of the deflecting plates of the oscillograph yielded a straight line response on the oscillograph screen. The inclination of the straight line gave the direction of arrival of the atmospherics. In the experimental arrangement, the straight line sweep on the oscillograph screen in the vertical direction indicated 0°. The orientation of the line in the clockwise direction indicated increasing angles towards the east-west direction. The usual adjustments for the 45°-alignment were made each time before a set of observations was taken.

The directional observations of atmospherics were made on days when there was no local thunderstorm and at times when the distant atmospherics were found to be fairly frequent and uniform over an interval of time covering about 10-15 minutes When such conditions were found to prevail, observations of the direction and strength of atmospherics were made on each frequency channel for 2 minutes taking about 10-15 minutes for four different frequencies. The average length of the linear responses due to atmospheric pulses during this short time was then found for each frequency in any particular direction. From the calibration curve, the voltage across the aerial tuning condenser corresponding to this average sweep-length was obtained. Knowing this voltage, field strength of the atmospherics for 2 minutes on any frequency and for any particular direction was calculated from the standard formula.

EXPERIMENTAL RESULTS

The experimental results on the intensity of atmospherics as received on different frequencies are as follows:

A. The field strength of the distant atmospherics as received in the frequency range of 170 to 204 Kc/s was found to be inversely proportional to the cube of the frequency.

Denoting the field strength by E and the frequency by f, the field strength was found to obey the relation:

$$E \propto \frac{1}{f^3}$$

This relation was found to hold mostly during day and only occasionally during night. It is to be noted that in the report by Dellinger (1933) on radio propagation data, an inverse square relotion $E \propto \frac{1}{f^2}$ was found to prevail during the day time. The inverse square relation during the day was also observed (Khastgir and Ali, 1942) on a wide range of frequencies (2-20 Mc/s) and was shown to be due to ground wave propagation only.

B. The field strength of the distant atmospherics in the same frequency range was found to decrease exponentially with the increase of frequency.

This type of intensity variation with frequency would be represented by:—

$$E \propto e^{-mf}, \quad \text{where } m \text{ is a constant}$$

or,
$$\log E = \text{const.} - \text{const.} f.$$

This relation was found to hold almost invariably during the night time.

The exponential decrease of the intensity of atmospherics with the increase of frequency had been previously observed at night by Espenchied, Anderson and Bailey (1926). Our previous work (1940, 1942) on 250-2000 Kc/s and also on 2-20 Mc/s confirmed this feature regarding atmospherics received during night.

C. The field strength of the distant atmospherics in the same frequency range was found to vary in a manner suggesting a combination of the first two types of field strength variation.

The inverse cube law of variation of field strength of atmospherics with frequency within the experimental range 170-204 Kc/s is illustrated in Fig. 2 which represents typical sets of day-time observations. Some of the occasional night-time observations which showed the same type of field strength variation within the same frequency range are shown in Fig. 3. Some typical night-time experimental results showing exponential decrease of intensity with the increase of frequency within the range are illustrated in Fig. 4.

Typical experimental results showing the mixed type of intensity variation with frequency are shown in Figs. 5, 6 and 6a. The day-time results shown in Fig. 5 clearly indicates that the field strength of the atmospherics does not increase proportionately with the inverse cube of the frequency but increases somewhat exponentially with some inverse power of frequency.

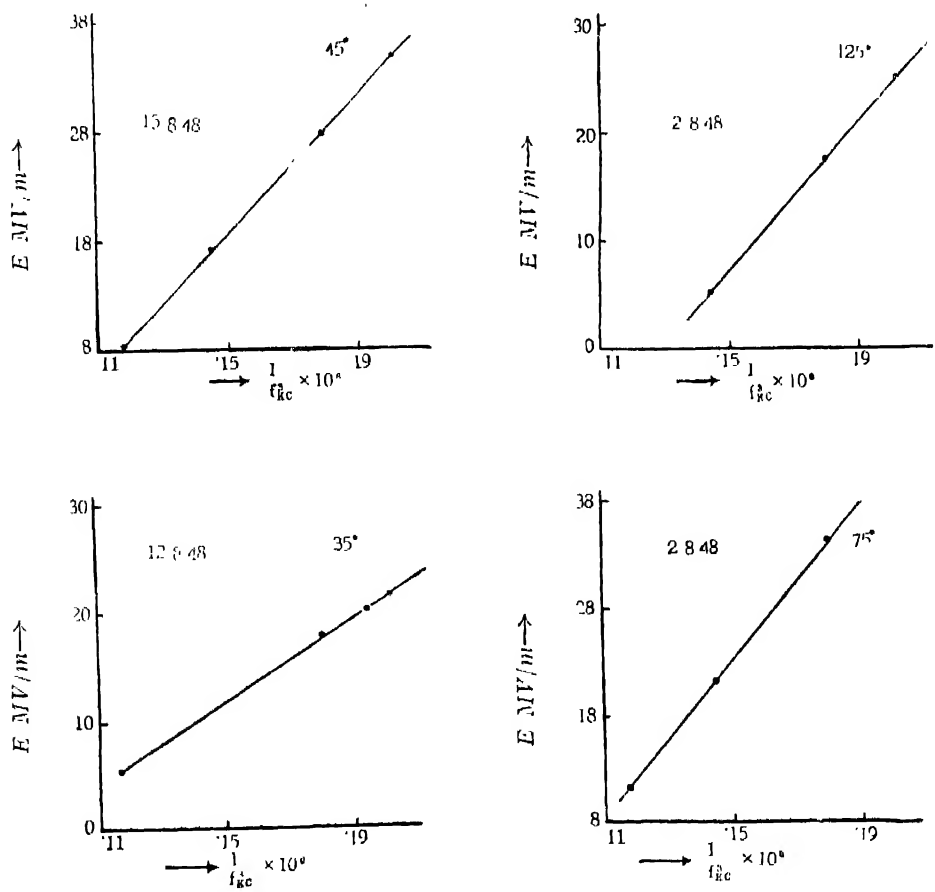

FIG. 2

Day-time observations.

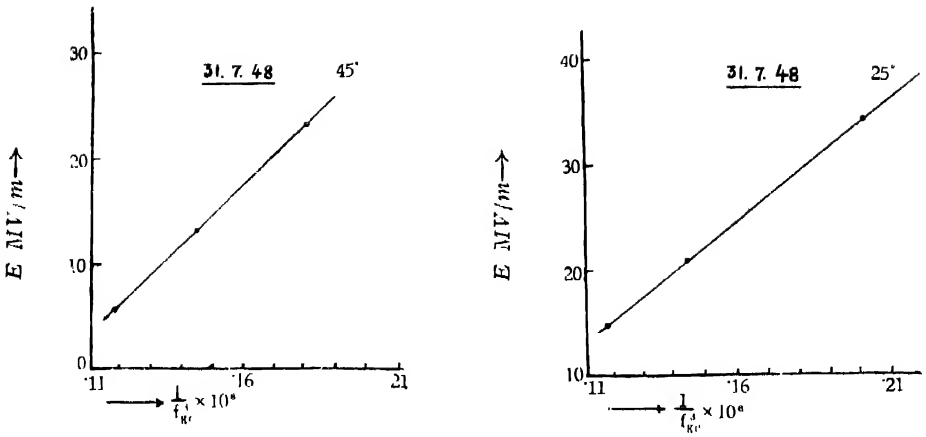

FIG. 3
Night-time observations.

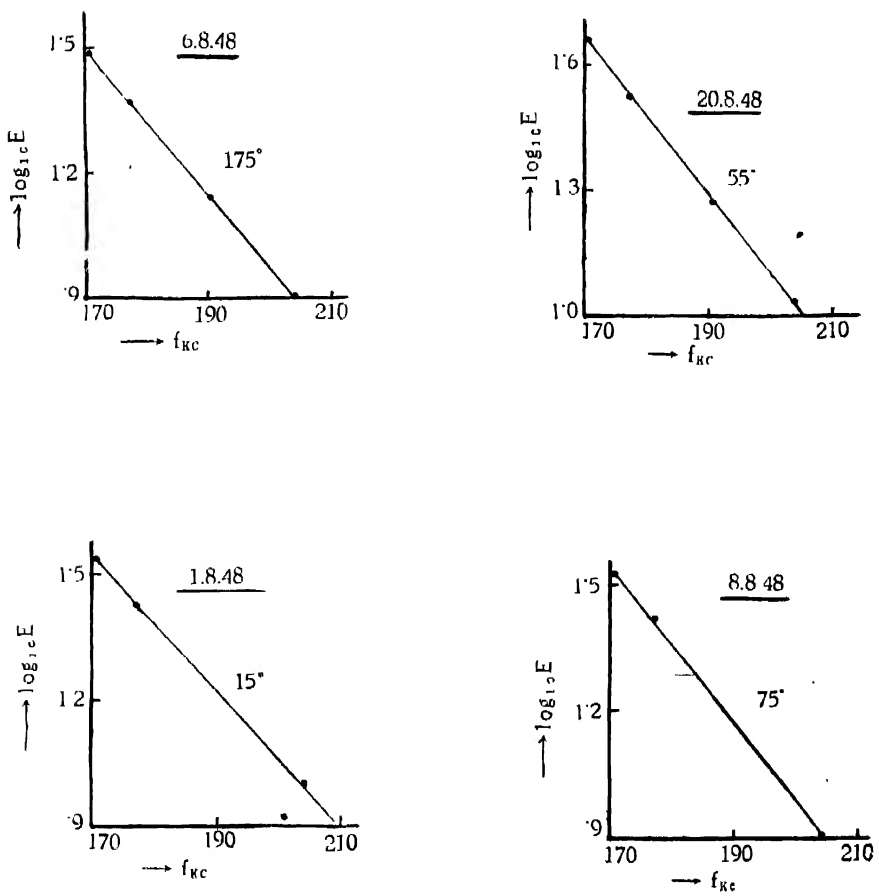

FIG. 4
Night-time observations.

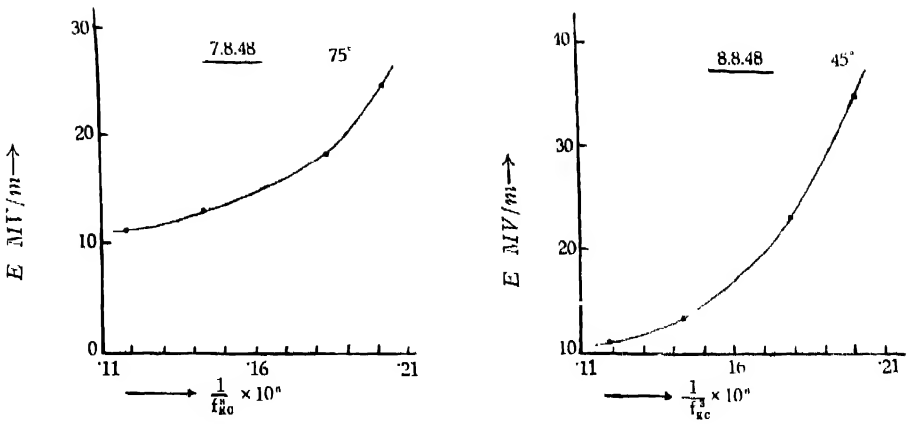

FIG. 5

Day-time observations.

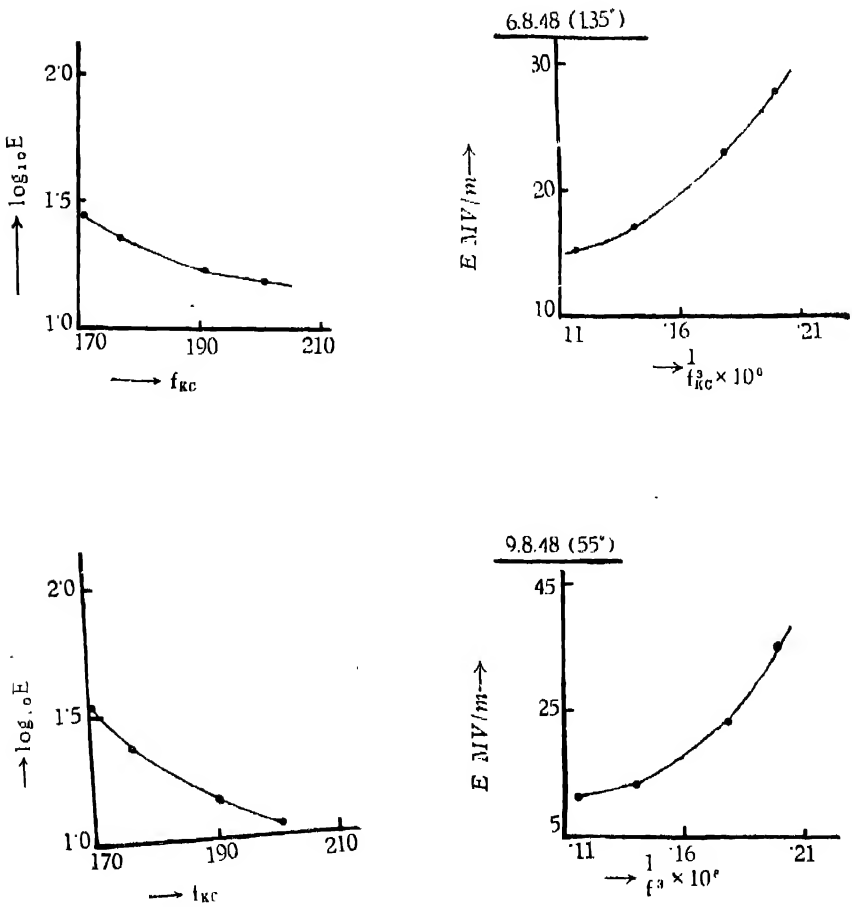

FIG. 6

Night-time observations.

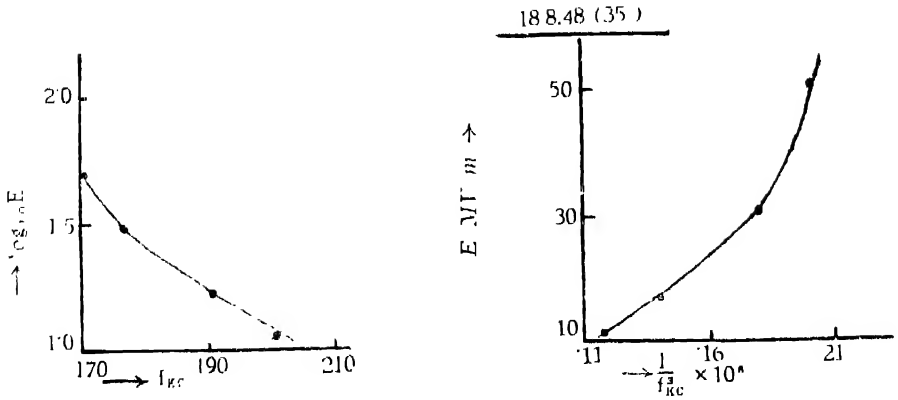

FIG. 6a
Night-time observations.

The night-time results illustrated in Fig. 6 and 6*a* show that the logarithm of the field strength of the distant atmospherics does not decrease linearly with the increase of frequency. They also show that the field strength does not increase proportionately but increases somewhat exponentially with the inverse cube of frequency.

In all the graphical representations of the field strength of distant atmospherics as a function of frequency, the directions of arrival of the atmospherics (having the 180°-ambiguity) have been indicated.

THEORETICAL CONSIDERATIONS

At large distances from the lightning discharge, outside the electrostatic and induction fields, the wave-form of the radiation field is of a damped sinuous type and can be represented by $E_0.e^{-\alpha t}.\sin qt$ with suitable values for E_0, α and q.

The effect of a highly damped sinuous atmospheric pulse on the receiving circuit was examined theoretically by Moullin (1924) and Turner (1931). We shall however, make use of the Fourier analysis by Burch and Bloemsma (1925) of the common pulse forms. Representing a non-periodic disturbance by $E=f(t)$ from $t=0$ to $t=\infty$ and expressing it as a Fourier series they showed that for an exponentially damped sinuous pulse represented by, $E_0.e^{-\alpha t}.\sin qt$, the amplitude of a Fourier component of frequency $p/2\pi$ would be given by

$$X_p \quad \sqrt{(\alpha^2+q^2-p^2)^2+4\alpha^2p^2} \qquad (1)$$

In the range of radio frequencies, $p \gg q$ or α, so that

$$X_p \Big| = \frac{q.E_0}{p^2}$$

Replacing the angular frequency p by $2\pi f$ where f is the frequency to which the receiver is tuned, the amplitude of the received atmospheric pulse would be

$$N_f = \frac{A}{f^2} \qquad \ldots (2)$$

where A is a constant.

The above conclusion has to be considered in finding an expression for the field strength of an atmospheric pulse received at some distance. Neglecting any kind of attenuation, the field strength is given by

$$E = K.f \qquad (3)$$

where K is some constant for the same source of atmospherics and the same receiving point. In view of (2), the field strength of the Fourier component of frequency f will be represented by

$$E = \frac{A}{f^2}.K.f = \frac{AK}{f} \qquad (4)$$

I *Ground Waves*

When the atmospheric pulse reaches the receiving point along the ground path alone, the field strength of the distant atmospherics received on frequency f should be obtained from

$$E = \frac{A.K}{f}.A_1$$

where A_1 is the flat-ground attenuation factor.

Accepting Norton's formula for ground attenuation, it was shown by Khastgir and Ali (1942) that for distant atmospherics

$$E = \frac{A.K.a.c}{f}\left(1 + \frac{1}{a^2 f^2}\right)^{\frac{1}{2}} \qquad (5)$$

where $a = \epsilon + 1/2\sigma$

ϵ = dielectric constant of the ground ($\approx$ 10 e.s.u.)

σ = electrical conductivity of the ground ($\approx 10^7$ e.s.u.)

c = velocity of light

Case *A*. For frequencies of the order of 10^7 cycles/sec., when $a.f >> 1$, we can neglect $1/a^2f^2$ and write

$$E = \frac{A.K.a.c}{f^2} \propto \frac{1}{f^2} \quad \ldots \quad (6)$$

This inverse square relation which had been actually found to hold for higher frequencies should thus be associated with ground-wave propagation only.

Case *B*. For frequencies of the order of 10^5 cycles/sec., as employed in the present investigation, when $a.f << 1$, we can write

$$E = \frac{A.K.c}{f^3} \propto \frac{1}{f^3} \quad \ldots \quad (7)$$

II *Sky waves*

When the source of the atmospheric pulse is so distant that the pulse cannot reach the receiving point by the ground path and is received only after reflexion from the ionosphere, it had been already shown (Khastgir and Ali 1942) that for medium and short radio waves, the field strength of the distant atmospherics received on frequency f would be

$$E = \frac{M}{f} \cdot e^{-m.f} \quad \ldots \quad (8)$$

where M and m are constants. Thus we get $\log E + \log f = \text{const.} - m.f$.

As the frequency is of a high order, the variation of $\log f$ with f is negligible in comparison with the variation of $\log E$ with f in the limited range of frequencies. We can thus write

$$\log E = \text{constant} - \text{constant}.\ f \quad \ldots \quad (9)$$

III *Combination of Ground and Sky waves*

Considering the particular case when the phase-difference between the ground wave and the sky wave is an even multiple of π, the field strength of the atmospherics would be represented by

$$E = \frac{D}{f^3}\left(1 + b.f^2.e^{-m.f}\right) \quad \ldots \quad (10)$$

where D, b and m are constants. Putting $\Delta = D(1 + b.f^2e^{-m.f})$ in (10), we get: $E = \Delta/f^3$.

From the relevant experimental data it was found that $m.f > 2$. It is evident from (10) that under such condition the slope of the curve $E \sim 1/f^3$ which is given by Δ, would increase with the increase of $1/f^3$. Taking the variation of Δ with f to be of the form: $\Delta = \Omega . e^{s.f}$, (where Ω and s are constants) it is evident that when both ground and sky waves are present we get the relation

$$E + 3 \log f = k_1 + (k_2/f^n),$$

where k_1 and k_2 are constants

or approximately

$$\log E = k_1 + (k_2/f^n) \qquad (11)$$

CONCLUSIONS

In the light of the above theoretical considerations, the experimental results given in the paper lead to certain definite conclusions. According to (7), in the frequency range under investigation, the field should vary as the inverse cube of frequency, provided there is only the ground wave propagation. Thus whenever, whether during day or night, the field strength of the distant atmospherics was found to vary proportionately with the inverse cube of frequency, it should be concluded that the source of atmospherics was not distant and the atmospheric pulse must have reached the receiving point by the ground path only. In the case of sky-wave propagation only, we find again, according to (9) that the field strength should decrease exponentially with the increase of frequency. It is therefore concluded that whenever the intensity of the distant atmospherics was found to follow this exponential law, the source of atmospherics should be considered as sufficiently distant so that the atmospheric pulse reached the receiving point by the sky-path only. Since the sky-wave which is extremely feeble during day increases in strength considerably during night, the exponential decrease of intensity with frequency is associated with the night-time observations of fairly distant atmospherics.

Whenever there is a departure from the inverse-cube law or from the exponential law of decrease of intensity with frequency, it can be inferred that the source of atmospherics is not too distant and yet not too close so that the pulse could reach the receiving point by both the sky and ground paths. Under such circumstances the curve showing E against $1/f^3$ is expected to be in accordance with (10), having a slope increasing with the increasing value of $1/f^3$. The logarithm of the field strength should also vary according to (11) with some inverse power of frequency.

ACKNOWLEDGMENT

In conclusion, we sincerely thank Mr. S. C. Mitra, M.Sc. for technical help during the investigation.

REFERENCES

Burch, C. R. and Bloemsma, J., 1925, *Phil. Mag.*, **49**, 480.

Dellinger, 1933, Report on Radio propagation data, *Proc. I.R.E.*, **21**, 1419.

Espenschied, Anderson and Bailey, 1926, *Proc. I.R.E.*, **14**, 7.

Khastgir, S. R. and Ali Md. Innas, 1942, *Ind. Jour. Phys.*, **16**, 399.

Khastgir, S. R. and Rao, K., 1940, *Proc. I.R.E.*, **28**, 511.

Khastgir, S. R. and Ray, A. K., 1940, *Science and Culture*, **5**, 773.

Moullin, E. B., 1924, *Jour. Inst. Elec. Engrs.*, **62**, 356.

Potter, R. K., 1931, *Proc. I.R.E.*, **12**, 1731.

Turner, L. B., 1931, Wireless, p. 513.

ON THE ABSORPTION OF U. H. F. RADIO WAVES IN ORGANIC LIQUIDS AT DIFFERENT TEMPERATURES*

By S. N. SEN

(*Received for publication, 21, Sept., 1939*)

ABSTRACT. The absorption of U. H. F. radio waves of wave lengths ranging from 55 cms upto 1 metre in acetone, methyl ethyl ketone and ether at different temperatures has been investigated. Absorption maxima have been observed for different frequencies in the case of all the three liquids at temperatures above 0°C and it has been observed that these maxima shift to lower frequencies with the lowering of the temperatures of the liquids as observed in the case of alcohols by previous workers. A new hypothesis has been put forward to explain the occurrence of such absorption maxima. In this hypothesis it has been assumed that permanent electric moment of the molecule fluctuates as the molecule executes rotatory oscillation in the intermolecular field.

INTRODUCTION

Investigations on the measurement of refrective indices of liquids with very short electric waves having wavelength of the order of a few centimetres and even sometimes a few millimetres were first carried out in 1896 by several authors such as Lampa (1896), Lang (1896), and others and the results showed that the values of n were nearly equal to those for wavelength in the visible region. Drude (1897) first discovered that on changing the wavelength the dielectric constant changes rapidly in some cases in the region of wavelengths of about 75 centimetres and pointed out that this abrupt diminution in the dielectric constant with increase in the frequency of applied oscillating field indicated an anomalous absorption of electric waves. Work in this line received an impetus when Debye (1913) proposed his theory about premanent electric moments of molecules and the dependence of the dielectric constants on the relaxation time of the molecules in the liquid. Numerous papers have been published on this subject verifying Debye's theory. Among these mention may be made of the work done by Mobius (1920), who investigated the dispersion of electric waves in water and ethyl alcohol between wavelengths, 4 millimetres and 0.3 millimetres. Later, Mizushima (1927) undertook a systematic programme of investigation in order to verify Debye's theory. He measured the dielectric constants for different wavelengths ranging from 3.08 metres upto about 50 metres. He investigated the dielectric constant of various alcohols at different temperatures ranging from about 65°C to upto about −68°C for wavelengths 3.08 metres, 6.1 metres, 9.5 metres and 50 metres. In the case of all these alcohols he observed that the dielectric

* Communicated by Prof. S. C. Sirkar

constants diminished suddenly on increasing the frequency of the oscillating field, the actual region in which such a discontinuity takes place depending on the temperature and the nature of the liquid. It was observed that the region of anomalous dispersion shifts towards longer wavelengths as the temperature of the liquid is lowered. At any particular temperature, however, the position depends on the moment of inertia of the molecules, for molecules with higher moment of inertia the frequencies of the region of anomalous dispersion being lower than those for molecules with lower moment of inertia. In the case of acetone and ether, however, he did not observe any anomalous dispersion in this region. He also concluded that the results observed in the case of alcohols were in agreement with those predicted by Debye's theory. Later on, Mizushima (1929) used still shorter wavelength of the order of about 58 centimetres and investigated the dielectric constant of a few alcohols at different temperatures. He observed that in the case of methyl alcohol anomalous dispersion occurs at a temperature lower than -60°C, for ethyl alcohol absorption takes place at about -30°C and for higher alcohols such absorption takes place at higher temperatures for the particular wavelengths used. Such investigations were also carried out more recently by several workers confirming Mizushima's work. Mention may be made of the work by Malsch and Keutner (1935), who investigated the dielectric constants of alcohols at a particular temperature for wavelengths ranging from 50 cm upto 10 metres. Ardenne and Otterbein (1936) carried out similar investigations in the case of glycerine, ethyl alcohol, methyl alcohol and water, using wavelengths ranging from 13.45 centimetres upto 55.5 centimetres and obtained results similar to those reported by previous workers.

In Debye's theory it has been postulated that the rotation of the molecules in the liquid can take place only with particular frequencies, because the rotation of molecule is influenced by the moment of inertia of the molecule and the viscosity of the liquid. When the frequency of the incident electric field applied to measure the dielectric constant coincides with natural frequency of free rotation of the molecules inside the liquid the molecule can follow oscillations of the field. Thus some amount of work is done by the electric field and absorption of electric energy takes place. Mizushima (1928) pointed out that the absorption in the region of about 58 cms might be due to rotational transitions of the molecules in the liquid. His main argument in favour of such a hypothesis was based on the facts that in case of water vapour absorption is observed in the region between 9μ to 300μ, and according to Debye's theory, the relaxation time of the water molecule in the vapour state would correspond to 126μ in vacuum. Since the absorption bands observed in the infra-red region are due to rotational transitions of the water molecule it is inferred that the free rotation of the molecules in the dielectric postulated by Debye would also correspond to such rotational transitions as produce infra-red absorption spectra.

The question whether the anomalous absorption of electric waves in the case of alcohols and other liquids is due to rotational transition of the molecules in the liquid state has not been discussed in detail by any subsequent worker after the suggestion was put forward by Mizushima (1929). Also definite conclusion can be arrived at only by carrying out further experimental investigations of this problem. If rotational transitions would be responsible for such anomalous absorption, certainly the number of rotating molecules and the probability of rotational transitions would increase with the increase of temperature of the liquid. This question has not been investigated carefully by any previous worker. An alternative explanation of the phenomenon can also be offered. An extra oscillating part of the dipole moment may be created by the inter molecular field in a liquid having polar molecules if the molecule executes damped oscillations in the liquid, and the frequency of such oscillations can be deduced from the time of relaxations given in Debye's theory. If this latter hypothesis would be true the effect of the intermolecular field would increase at lower temperatures, and therefore the intensity of absorption of electric waves would also increase with the lowering of temperature of the liquid. It has been proposed to investigate absorption of ultra high frequency radio waves by optical method in a large number of organic liquids having polar molecules in order to find out which of the two explanations mentioned above is correct, and the present paper deals with results of preliminary investigations on such absorption in acetone, ether and methyl ethyl ketone.

EXPERIMENTAL

As a source of U. H. F. radio waves a G. R. 857-A U. H. F. oscillator was used. It gave radio waves of frequencies ranging from 100 Mc/sec. to 525 Mc/sec. Acetone and ether were chosen as two of the liquids studied, because Mizushima had not observed any anomalous absorption in the case of these two liquids in the region from 3.08 metres upto 50 metres even when the liquids had been cooled to $-69°C$. Methyl ethyl ketone was the third liquid investigated, and this liquid was chosen to find out the change in the nature of absorption with the addition of CH_2 group in the acetone molecule. All these liquids were chemically pure and were distilled before use. Vertical aerials having lengths suitable for different wavelengths were fixed with the output terminal and a small cylindrical parabolic reflector was placed behind the aerial and it was observed that when the body of the oscillator was earth-connected, the direct current in the detector was not influenced by movement of any conductor in its neighbourhood. First, a rectangular glass cell with stoppered mouth was placed between the tuned detector and the aerial and the diminution in the current after the detector had been tuned again was noted. The liquid to be investigated was then put in the cell and after tuning the detector, further diminution in the current was again noted. This was repeated for the liquid heated to different temperatures and also cooled to about $0°C$. In each case the absorption was investigated for a

wide range of frequencies. The current in the detecting circuit with the empty glass cell between the circuit and the aerial was taken as I_0 and that with the cell filled with the liquid at a particular temperature was taken as I, and the attenuation co-efficient was calculated from these data.

RESULTS AND DISCUSSION

The results obtained for the three liquids at different temperatures are given in Tables I, II and III and they have also been plotted in Figs 1, 2 and 3.

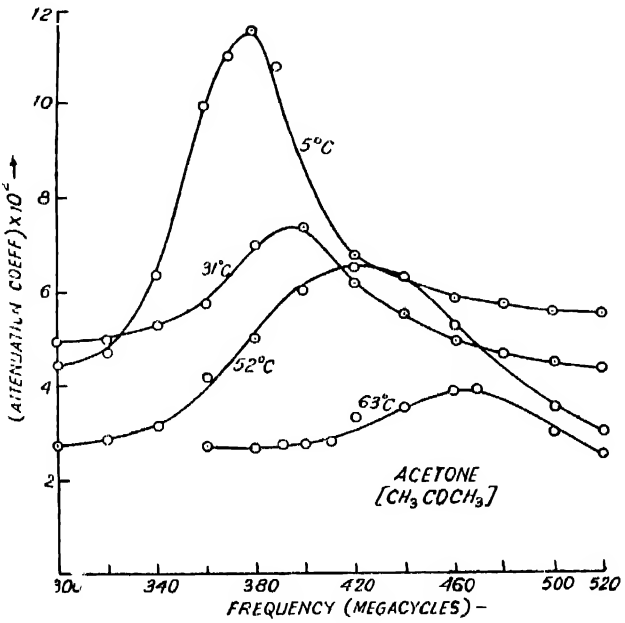

FIG. 1

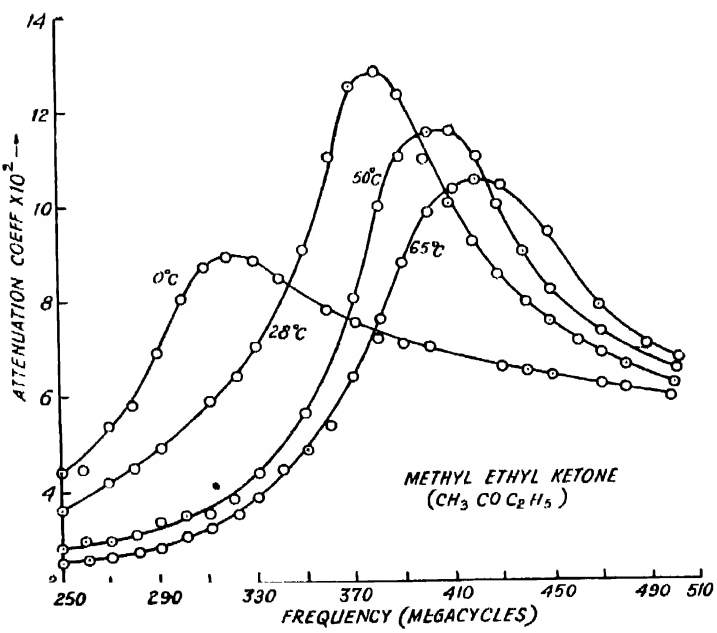

FIG. 2

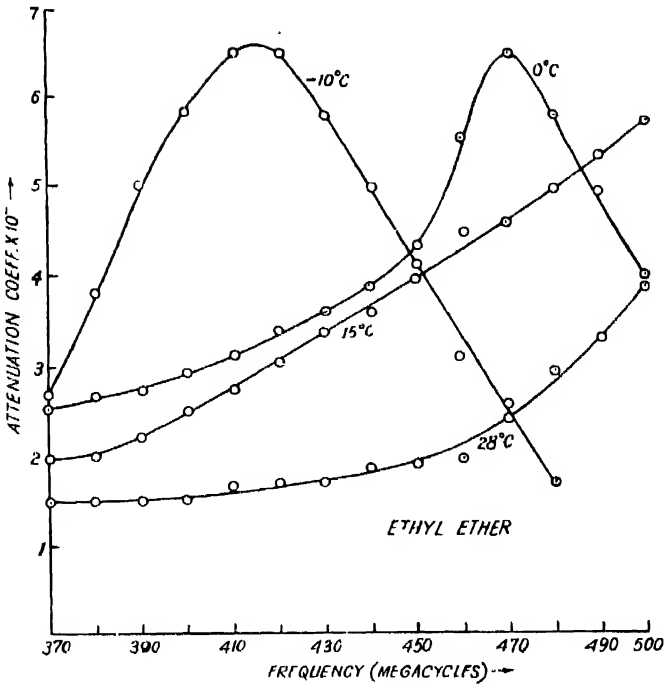

FIG. 3

TABLE I

Attenuation co-efficient of Acetone ($CH_3C().CH_3$) at different temperatures.

Temperature / Frequency in mega-cycles per sec.	5°C	31°C	52°C	63°C
300	.011	.030	.027	
320	.017	.040	.028	
340	.033	.052	.031	
360	.090	.056	.042	.026
370	.110		.045	.026
380	.115	.071	.049	.026
390	.107		.050	.027
400	.075	.075	.061	.028
410			.063	.029
420	.065	.061	.067	.033
430			.060	.034
440	.063	.054	.053	.037
450				.037
460	.058	.049	.045	.039
470				.038
480	.057	.046	.039	.038
490				.027
500	.056	.041	.036	.026
510		.038	.035	.026
525	.055	.032	.031	.026

TABLE II

Attenuation co-eff. of methyl ethyl ketone ($CH_3CO.C_2H_5$

Temperature / Frequency in mega-cycles per sec.	0°C	28°C	50°C	65°C
250	015	.030	.029	.026
260	015	.030	.030	026
270	055	.011	.036	.029
280	058	.015	031	.029
290	060	051	.033	.020
300	070	056	.035	.030
310	086	061	.035	.032
320	000	.066	.038	.034
330	088	.069	043	.038
340	085	079	.048	.042
350	078	.090	.056	040
360	070	.115	.066	053
370	076	.121	.086	063
380	072	.128	.090	.075
390	072	.121	.110	.088
400	072	.114	.115	.099
410	068	.103	.115	.103
420	067	.090	.110	.105
130	066	.078	.100	.104
440	066	.075	.080	.100
450	061	.070	.081	.095
160	063	.070	.076	.085
170	062	.067	073	.078
480	061	065	070	.073
490	061	.063	069	.070
500	061	.063	.065	.069

It will be seen from these results that in the case of acetone the height of the peak of absorption increases as the temperature of the liquid is lowered and at the same time the position of maximum absorption shifts towards the lower frequencies. In the case of methyl ethyl ketone, however, the shift of the maximum is similar to that observed in the case of acetone up to about 28°C. As the liquid is further cooled to 0°C, a large shift in the position of the maximum and also an abrupt diminution in its height take place. In the case of ether no maximum in absorption is observed when the liquid is at temperatures, 28°C and 15°C, although the absorption co-efficient increases rapidly with increase in the frequency of the incident waves. When, however, the liquid is cooled to 0°C an absorption peak is observed with its maximum at 470 Mc/sec and this shifts to 415 mc/sec and the integrated absorption increases when the liquid is further cooled to −10°C. Mizushima (1927) did not observe any absorption maximum in the case of acetone and ether for wavelengths ranging from 3.08 upto 50 metres, but in the present investigation we see that such an absorption takes place when still shorter wavelengths are used. Hence this phenomenan is not a characteristic of alcohols alone, but it is exhibited probably by all polar molecules only if suitable wavelengths are used and the liquids are maintained at

TABLE III

Attenuation co-efficients of ethyl ether at different temperatures.

Temperature / Frequency in Mega-cycles per sec.	−10°C	0°C	15°C	28°C
350	.017	.013		.010
360	.020	.015		.013
370	.027	.020	.010	.014
380	.030	.022	.019	.014
390	.050	.023	.023	.016
400	.058	.030	.025	.016
410	.060	.031	.028	.017
420	.006	.035	.030	.018
430	.058	.036	.035	.018
440	.051	.040	.030	.019
450	.043	.041	.040	.019
460	.032	.050	.045	020
470	.026	.060	046	.025
480	.018	.050	.050	.030
490		050	.053	.036
500		.041	.056	.030

suitable temperatures. The shift of the maximum in the absorption observed in the present investigation can be explained by Debye's theory as has been done by Mizushima, but the change in the height of the peak with the change of the temperature of the liquid observed in the case of acetone cannot be explained by the hypothesis that this absorption is due to rotational transitions of the molecules in the liquid, because if the absorption were due to such rotations it would increase with the increase of temperature of the liquid. Contrary to such expectations we see that not only the height of the peak increases with the lowering of the temperature, but it also becomes smaller in the case of acetone and ether with the rise of temperature. Methyl ethyl ketone, however, behaves in a similar manner only up to a temperature of 28°C, and there is some abrupt diminution in the height of the peak when the liquid is cooled to 0°C, and this may be due to some change in the structure of the molecule which may occur in this temperature range. In the case of ether the integrated absorption in the peak increases with the lowering of temperature.

These facts may be explained if we postulate the hypothesis that the incident waves initiate rotational oscillations of the molecules in the liquid and the frequency of these oscillations coincide exactly with that corresponding to the relaxation time given by Debye's theory, and also that the intermolecular field produced by the surrounding molecules has an effect on the permanent electric moment of the molecule. Probably, the value of the permanent electric moment changes periodically as the molecule executes rotatory oscillation, because the shape of the molecule is not exactly spherical and the cavity in which it executes the oscillation has not got any spherical symmetry. If this hypothesis be true absorption

may take place for frequencies corresponding to the relaxation time and this has been found to be true in the case of large number of molecules by Mizushima (1927). The frequency corresponding to rotational transition, on the other hand, would be different from this frequency deduced from the relaxation time. Secondly, the degree of fluctuation in the permanent electric moment of the molecule produced by its rotatory oscillation would increase at lower temperatures, because the molecules surrounding the particular molecule in question come nearer together and the inter-molecular field becomes stronger. At higher temperatures, however, owing to thermal agitation, the intermolecular field acting on different molecules at different places of the liquid at any instant is not exactly identical, and therefore, the fluctuation in the permanent electric moment is due to the oscillation of the molecule in a field which has a range of values instead of a particular fixed value. Hence it is expected, according to such a hypothesis, that the absorption peak will be broader and broader as the temperature of the liquid is raised. The results for acetone seem to be in agreement with such a hypothesis. This was pointed out earlier by Sirkar and Sen (1940). The results for methyl ethyl ketone and ether obtained in the present investigation also seem to support this hypothesis, if it is assumed that below 28°C the molecules of methyl ethyl ketone become associated to a higher degree, which results in a diminution in the effective permanent electric moment, and also in an abrupt increase in the viscosity of the liquid. No general conclusion regarding the correctness of this alternative explantion of the absorption of electric waves by organic liquids can be drawn before results have been obtained for a large number of liquids. The investigations are, therefore, being continued with other liquids.

ACKNOWLEDGMENT

The author is indebted to Prof. S. C. Sirkar for his kind interest and guidance during the progress of the work and to Prof. S. K. Mitra of the University College of Science, Calcutta for the loan of a crystal detector.

INDIAN ASSOCIATION FOR THE CULTIVATION OF SCIENCE,
210, BOWBAZAR STREET, CALCUTTA 12.

REFERENCES

Ardenne, Von and Otterbein, G., 1936, *Phys. Zeits.*, **37**, 533.
Debye, P. 1913, *Verh. Deut. Phys.*, **15**, 770.
Drude, 1897, *Zeits. Phys. Chem.*, **23**, 308.
Lampa, 1896, *Wien Ber.*, **105**, 587. 1040.
Lang, 1896, *Wein Ber.*, **105**, 253.
Malsch, J. and Kentner, E., 1935, *Phys. Zeits.*, **36**, 588.
Mizushima, S. 1927, *Sc. Paper. Insti Phys. & Chem. Research Japan*, **5**, 201.
,, , *Sc. Paper. Insti. Phys. & Chem. Research Japan.*, **9**, 292.
Mobius, W., 1929, *Ann. der Phys.*, **32**, 293.
Sirkar, S. C. and Sen, S.N., *Science & Culture* **15**, in press.

ESTIMATION OF SOLVATION OF IONS IN A SOLUTION FROM KINETIC THEORY *

BY H. MUKHERJEE

(*Received for publication, Nov. 1, 1949*)

ABSTRACT. By assuming that a point particle, having the same mass and charge as a solvated ion, can represent the ion as far as its motion in an electric field is concerned, Drude's relation connecting the velocity of a free electron in an electric field with the mass and other quantities associated with the motion of the electron has been applied to the motion of the ion; and it has been shown that the formula gives the degrees of hydrations of ions relative to the hydration of the H^+ ion in close agreement with Washburn's experimental values.

THEORETICAL

The motion of an electrically charged particle in an electric field conforms, to a first approximation, to the equation

$$u = \frac{u}{X} = \frac{e\lambda}{2mc} \qquad \ldots \quad (1)$$

where u = velocity of the particle in an electric field of X (E.M. Units)

λ = mean free path of the particle

e, m = charge and mass respectively of the particle

c = mean thermal velocity of the particle

In deriving the above equation it has been assumed that

(*i*) the particle and the molecules among which it moves are hard spheres,

(*ii*) the particle comes to rest at each collision with the molecules,

(*iii*) the time, λ/c, is large in comparison with the duration of a collison

i.e., the size of the particle is small in comparison with the mean free path.

The value of λ when a number of charged particles are moving through molecules of different kinds, is given by Jeans (1935) as

$$\lambda = \frac{1}{\sqrt{2}\pi\nu\sigma^2 + \Sigma\pi\nu_s\left(\frac{\sigma+\sigma_s}{2}\right)^2\sqrt{1+m/m_s}} \qquad \ldots \quad (2)$$

where ν, σ = number and diameter respectively of the moving particles.

ν_s, σ_s, m_s = number, diamater and mass respectively of the molecules among which the particles are moving.

* Communicated by Prof. S. N. Bose

If ν is negligible in comparison with ν_1, ν_2 etc., and if σ is negligible in comparison with σ_1, σ_2 etc.,

$$\lambda = \frac{1}{\Sigma \pi \sigma_s^2 \nu_s \sqrt{1 + m/m_s}} \quad \ldots \quad (3)$$

The equation of motion of the ions formed by the dissociation of an electrolyte in a solvent is, though of the type of equation (1), very complicated; for firstly, the solvent being a liquid, its molecules are very close together and secondly, the ions being solvated, have a rather large size; consequently, the mean free path, if any, is comparable with or even smaller than the diameter of the ions. The collision will certainly be more than binary and there will arise complications due to mutual attractions and repulsions. When the solution is dilute, there is practically no interaction between ions and ions and the equation of motions will be somewhat less complicated. If besides, the ions have negligible size, the equation would be reduced to the simple form (eq. 1).

Let it be assumed that in a dilute solution it is possible to represent the ions by indefinitely small particles as regards change, mass and velocity in an electric field. We shall call these particles the 'representative particles.' If m is the mass and c, the average velocity of a representative particle, we have from the kinetic theory,

$$\bar{c} = \sqrt{\frac{8}{3\pi}} C = 0.921C$$

where C is that root mean square velocity of the particle ;

and $\frac{1}{2}mC^2 = E$ = the average kinetic energy of thermal motion,

so that $$2m\bar{c} = 1{\cdot}842\sqrt{2m\bar{E}}$$

Whether a solvent is composed of molecules of one kind or a mixture of associated and unassociated molecules can be determined with the aid of the formula

$$S\left(\frac{m_s}{\rho_s}\right)^{\frac{2}{3}} = K(T_0 - T) \quad \ldots \quad (4)$$

where S = surface tension of the solvent at the temperature T^0K

m_s = average molecular weight of the associated and unassociated molecules

ρ_s = density of the solvent at T^0K

T^0 = temperature at which the surface tension is zero

K = 2.12, for associated liquids.

Assuming that a solvent is composed of only two kinds of molecules, we write equation (3) as

$$\lambda = \frac{1}{\pi v_2 \sigma_2^2 \left[\left(1 + m_1/m_2\right)^{\frac{1}{2}} + \frac{v_1}{v_2} \cdot \frac{\sigma_1^2}{\sigma_2^2}\left(1 + m/m_1\right)^{\frac{1}{2}}\right]}$$

$$= \frac{1}{\pi v_2 \sigma_2^2 \sqrt{m}\left[\left(\frac{1}{m} + \frac{1}{m_2}\right)^{\frac{1}{2}} + \frac{v_1}{v_2} \cdot \frac{\sigma_1^2}{\sigma_2^2}\left(\frac{1}{m} + \frac{1}{m_1}\right)^{\frac{1}{2}}\right]} \quad \ldots \quad (5)$$

From (1), and (5)

$$u_1 = \frac{Ae}{Q}$$

$$\text{or } \log u_1 = \log A + \log e - \log Q \quad \ldots \quad (6)$$

where $A = \frac{1}{1.842\sqrt{2E.\pi v_2 \sigma_2^2}}$, $Q = m\left[\left(\frac{1}{m} + \frac{1}{m_2}\right)^{\frac{1}{2}} + \frac{v_1}{v_2} \cdot \frac{\sigma_1^2}{\sigma_2^2}\left(\frac{1}{m} + \frac{1}{m_1}\right)^{\frac{1}{2}}\right]$

For another kind of ions

$$\log u'_1 = \log A + \log e' - \log Q' \quad \ldots \quad (6')$$

$$\therefore \quad \log Q' = \log \frac{u_1}{u'_1} + \log Q + \log \frac{e'}{e} \quad \ldots \quad (7)$$

APPLICATION TO THE CASE OF IONS IN WATER

In order to apply (7) to the case of ions in water at 18°C, firstly we have to determine the average molecular weight of water with the aid of equation (4).

At 18°C, $S = 73$ dynes per cm., $T_c = 647°K$, $T = 291°K$ and $\rho_s = 1$. Therefore equation (5) gives $m_s = 33.24$. Assuming water to consist of (H_2O) and $(H_2O)_2$ molecules, we have, therefore,

$$v_1 : v_2 = 1 : 5.521$$

If the $(H_2O)_2$ molecules are supposed to be hard spheres

$$\sigma_1 : \sigma_2 = 1 : 2^{\frac{1}{3}}$$

$$\therefore \quad \frac{v_1}{v_2} \cdot \frac{\sigma_1^2}{\sigma_2^2} = \frac{1}{5.521} \cdot \left(\frac{1}{2}\right)^{\frac{2}{3}} = 0.1141$$

Table I gives the values of $\log Q$ for different values of m—the temperature being 18°C :

TABLE I

m	$\log Q$	m	$\log Q$	m	$\log Q$	m	$\log Q$
0	$-\infty$	70	1.2168	200	1.6213	360	1.8625
10	0.6053	80	1.2655	220	1.6599	380	1.8849
15	0.7167	90	1.3097	240	1.6954	400	1.9064
20	0.8007	100	1.3495	260	1.7279	420	1.9268
30	0.9263	120	1.4183	280	1.7583	440	1.9462
40	1.0206	140	1.4795	300	1.7863	460	1.9649
50	1.0969	160	1.5332	320	1.8134	480	1.9824
60	1.1607	180	1.5791	340	1.8388	500	2.0000
		19	0.7854	37	0.9947		

Supposing that the hydrogen ion is solvated by either one or two molecules of water, we have, in the former case, $(m)_h' = 19$, and in the latter case, $(m)_h' = 37$. Correspondingly, log Q = either 0.7854 or 0.9947. The velocity of the ion or the particle representing it is 3.24×10^{-4} cm. per sec., for a potential-fall of 1 volt per cm.

The velocity of the particle representing the lithium ion is 3.4×10^{-4} cm. per sec. For this particle, therefore,

$$\frac{u_1}{u_1'} = \frac{324}{34} \; ; \text{ i.e. } \frac{t_1}{t_1'} = 0.9790; \; e = e'$$

If $(m)_{h'} = 19$, we should have

$$\log Q' = 0.7854 + 0.9790 = 1.7644.$$

The mass of the particle must, therefore, lie between 280 and 300. Using the method of proportional parts, the mass is calculated to be 284.4. Actual calculation will give the value 284.1. If this is taken as the mass of the solvated Li^+ ion, the number of water-molecules attached to the Li^+ ion is

$$(284.1 - 7) \div 18 = 15.4$$

If the degree of hydration of H^+ be 2, $(m)_{h'} = 37$. Calculating in the manner just shown, the degree of hydration of the Li^+ is found to be 25.7.

Table II gives the values of the hydrations of some ions. Below the calculated values are given the values experimentally obtained by Washburn and Millard (1915) with 1.25N solution.

TABLE II

H^+	Li^+	Na^+	K^+	Cl^-	
1	15.4	10.4	5.5	5.5	(calculated)
	14	8.4	5.1	4	(observed
2	25.7	18.2	10.8	10.1	(calculated)
	25.3	16.6	10.5	9	observed)

DISCUSSION

Although the calculated values are satisfactorily close to the experimental values, the former are consistently too high. This is not unexpected, for equation (7), based on a simple assumption, cannot presume to represent the actual state of things accurately. The closeness of the calculated values to the experimental values, however, shows that the assumption is not very wrong. At any rate, with its help, an approximate idea of the solvation of an ion can be obtained provided the degree of solvation of any other ion is known. It is also possible that the hydration valves of Li^+, etc., in a solution more dilute than 1.25N is somewhat higher (Baborovsky, 1927).

Descrepancies perhaps occur when heavier molecules are dealt with. In the case of caesium, calculation shows that if H^+ is supposed to be associated with one molecule of water, Cs^+ will be unhydrated and if H^+ is associated

with two molecules, C_s' will have 5 molecules; on the other hand, the observed values are 4.7 and 9.9 respectively. It is, however, obvious that the velocity depends on the mass, being smaller if the mass is larger. It is not therefore clear how K' with mass $(40+5.4\times18)$ or 137 can have velocity smaller than C_s' with mass $(133+4.7\times18)$ or 218.

It may be argued that the water molecules are not detached from, or independent of, one another; and so more than one molecule is likely to react to a collision. The values of m_1 and m_2 should, therefore, not be 18 and 36, but larger. But since equation (7) refers to point-masses, collision is considered to take place with one molecule of water at a time and the duration of collision is extremely small; also the molecules of water are in a quasi-bound state. Hence we may suppose that during a collision, only one molecule is affected.

Lastly, although the assumption has been that water is composed of simple and binary molecules, the possibility of the existence of trinary and higher molecules cannot be altogether ruled out.

ACKNOWLEDGMENTS

The author records thanks to Dr. S. R. Palit and Prof. S. N. Bose for their helpful criticism, and to the Surendranath College authorities for affording him facilities for work and to the Government of Bengal for financial help for conducting research work.

PHYSICS DEPT.,
SURENDRANATH COLLEGE,
CALCUTTA

REFERENCE

Baborovsky, 1927, *Zeit. Phys. Chem.*, **129**, 129.
Jeans, 1935, Introduction to Kinetic Theory of Gases - Chap.V.
Washburn and Millard, 1915, *J. A. C. S.*, **37**, 694.

THE COMPLEX SPECTRUM OF THE DIATOMIC MOLECULE OF CHROMIUM CHLORIDE (CrCl)

By V. RAMAKRISHNA RAO and K. R. RAO

(*Received for publication, April 11, 1949*)

Plate XXIV

ABSTRACT A band system attributed to CrCl molecule is obtained in emission in a heavy current discharge from λ 6300—5700. The bands occur in five groups and appear analogous to the manganese halide bands. The system is interpreted as due to the electronic transition $^6\Pi - ^6\Sigma$ involving high multiplicity terms.

INTRODUCTION

With the analysis of the band spectrum of manganese hydride (Nevin, 1942, 1945) and the manganese halides (Muller, 1943; Bacher, 1948 and Rao, 1948) the postulates of hitherto unknown high multiplicity terms in band spectra are being developed in analogy with the complex spectra of atoms. For manganese an electronic transition $^7\Pi - ^7\Sigma$ has been established. Similar theoretical considerations should lead us to expect a $^6\Pi - ^6\Sigma$ transition in the case of the hydride and halides of chromium which just precedes manganese in the periodic table. To verify this prediction the spectrum of chromium chloride has been investigated.* An extensive band system is obtained in the region λ6400—5700, which exhibited a characteristic line-like appearance with an unusual intensity distribution. The theoretical postulates and the interpretation of the band system are described in the succeeding sections.

EXPERIMENTAL

The chromium chloride used in this investigation was specially prepared for this purpose by heating chromium in an atmosphere of dry chlorine. A very pure Kohlbaum specimen of the metal is finely powdered and heated in a hard glass tube while passing dry chlorine over it. Violet scales of chromium chloride volatalise and deposit on the sides. The anhydrous chloride thus obtained is cooled in a current of dry carbon dioxide and finally scraped off.

For the excitation of the bands the method developed in our laboratory and used successfully for Mn-halides (Rao, 1948) is employed for the CrCl bands as well. The anhydrous salt which vaporises at 1065°C is placed in a discharge tube of simple design shown in Fig. 1. The tube, nine inches long and about one inch in diameter, is made of quartz capable of withstanding a heavy current discharge. Any ordinary pyrex H-shaped dis

* A preliminary report has appeared in Current Science, 1949

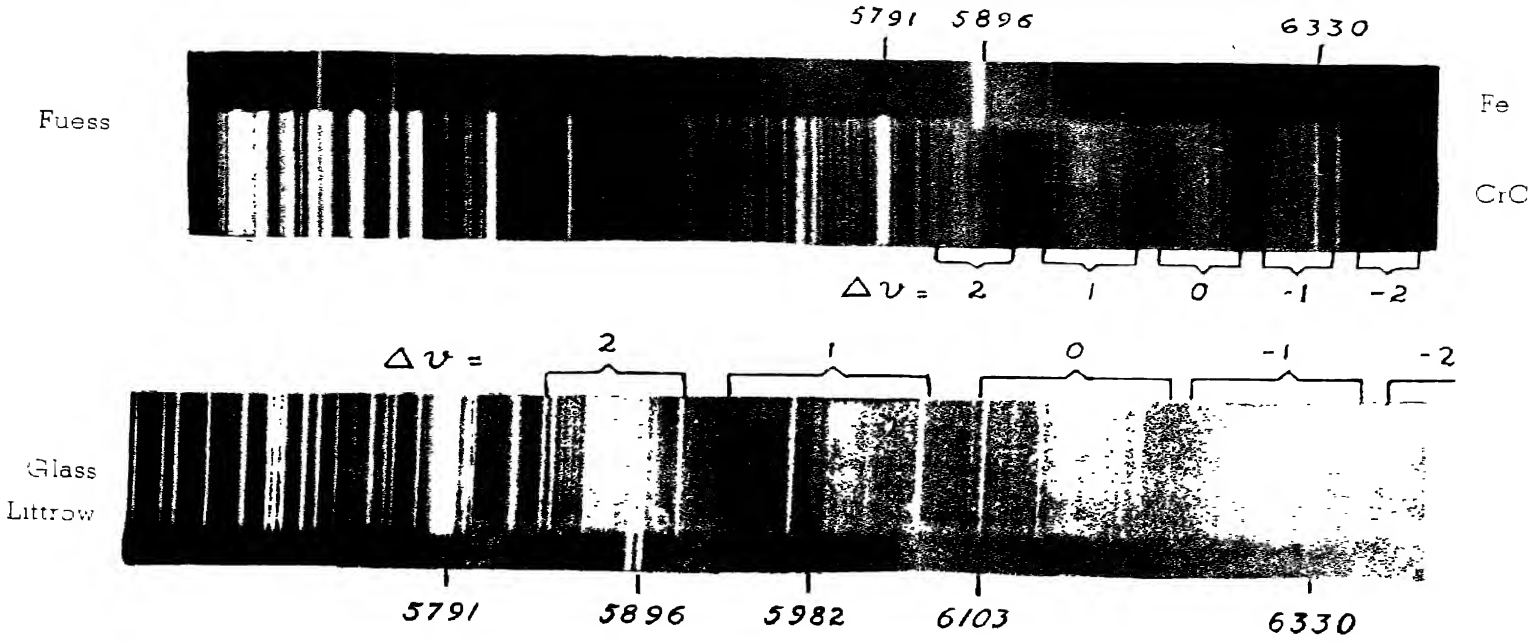

Chromium chloride bands.

charge tube is divided into two halves by a cut in the middle; the two portions

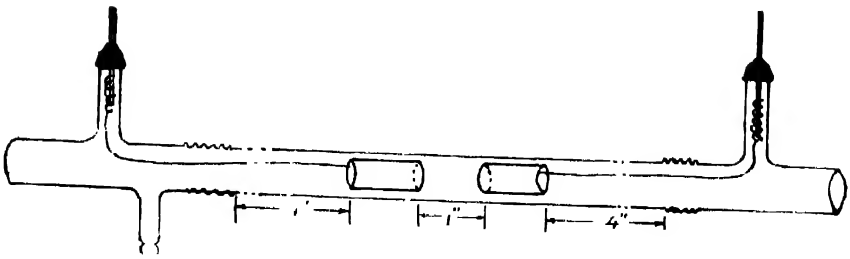

FIG. 1
Heavy current discharge tube

are attached with shellac one at each end of the quartz tube. The electrodes are short cylinders of pure nickel and inserted into the middle of the tube such that they rest in the middle quartz portion of the tube at a distance of about one inch from each other. A small quantity of the substance is placed in between the electrodes. The tube is continuously evacuated and excited by a 2 K.W., D. C. generator developing 2000 volts. A characteristic discharge of very bright greenish blue colour is obtained at 1200V and 1 amp. Photographs are taken on special rapid panchromatic plates with a Hilger large glass Littrow spectrograph of high resolution and light gathering power and also with a Fuess instrument. Exposures of five and one minutes respectively were sufficient.

DESCRIPTION OF THE SPECTRUM

No characteristic spectrum definitely ascribed to the diatomic CrCl molecule is known till now. Mesnage (1935) observed about 15 red-degraded bands in the region 2600 in a H. F. discharge through a heated quartz tube containing CrCl vapour. An analysis of these bands was also presented and vibrational constants $\omega_e' = 33$ and $\omega_e'' = 117$ cm^{-1} were suggested. The values as indicated by Pearse and Gaydon (1938) are not in consonance with the corresponding values in analogous spectra. Even the origin of the bands was questioned by the above authors who attributed them to the AlCl molecule. In the visible region Eder and Valenta's Atlas of typical spectra contains a photograph of CrCl. It shows in the region λ 6500—5800 a few continuous patches. Mesnage also reported diffuse bands in about the same region but no discrete structure was reported. The bands obtained by us are in five groups with line like structure but they are very different in appearance from the actual lines of chromium and should be definitely considered as bands. Each group gives the impression of a sequence with a particular Δv value. The intensity distribution in each sequence is unlike the usual Franck-Condon types. It resembles very much the band spectra of manganese chloride obtained in emission by Muller (1943) and Rao (1948). These features have led us to the assumption that the bands are due to an electronic transition involving high-multiplicity terms, as in the case of manganese halide bands. The multipli-

city obviously should be even, considering the total number of the electrons. Pearse and Gaydon (1937) casually suggested the possibility of a transition $^6\Pi - {}^6\Sigma$ for CrH band at λ 3650. A simillar transition seemed most likely for Cr-halide bands as well.

The chromium atom with 24 electrons and the chlorine atom with 17 electrons have the following electornic configurations.

Cr: $1s^2\ 2s^2\ 2p^6\ 3s^2\ 3p^6\ 3d^5\ 4s$ giving a ^7S as ground term,

Cl: $1s^2\ 2s^2\ 2p^6\ 3s^2\ 3p^6$ giving a ^2P as ground term.

The incomplete $3d^5\ 4s$ and $3p^5$ groups give rise to the respective atomic energy states. In the process of formation of the molecule the following electron configuration may be imagined on account of the particular stability of the d^5 core (Laporte) to give rise to the moleculer terms.

$$\sigma^2\pi^4, \quad \sigma\pi^2\delta^2$$

With the spins all parallel, the total spin is 5/2, giving a multiplicity 6.

When the spins are parallel the λ values, being of opposite sign according to Pauli's exclusion principle, make $\Sigma\lambda = 0$, resulting in a Σ state. An upper sextet Π state may arise from the configuration

$$\sigma^2\pi^4, \ \pi^2\delta^2\pi. \longrightarrow {}^6\Pi$$

It is easy now to formulate the possible rotational heads for the transition $^6\Pi - {}^6\Sigma$. The ground state Σ (with $\Lambda = 0$) must correspond to the coupling type, Hund's case *b*. In a $^6\Sigma$ state [$(\Lambda = 0)$ and $(S = 2\frac{1}{2})$] there is a spin splitting of each rotational level, *i.e.*, for each value of K there will be six component level, with J lying between $K - S$ and $K + S$, which, following Mulliken, may be designated as F_6, F_5, F_4 ....F_1, respectively. These levels have very small separations and ordinarily, are not resolvable.

The upper $^6\Pi$ state may approximate to case *a* or case *b*, or may represent any state intermidiate between the two. In fact for higher values of K it approaches case (*b*) and for low values of K, case (*a*). No meaning can be attached to K in the former and to Ω in the latter. The calculation can be made for higher values of K and reduced to the low values. Combining Λ and Σ we get 6 values giving $^6\Pi_{-1\frac{1}{2}}$, $^6\Pi_{-\frac{1}{2}}$ etc. to $^6\Pi_{3\frac{1}{2}}$ which we might denote as F_6, F_5,...F_1. Whatever stage of coupling the state represents the rotational energy term is given by equation (72), Jevons' "Report" page 124.

A schematic diagram for the transition $^6\Pi - {}^6\Sigma$ representing the various observable branches is represented in Fig. 2. The form of the branches is indicated, in the usual notation, as T, S, R...N according to the corresponding ΔK values 3, 2, etc, -3,; changes of K by $0, \pm 1$, etc., being permitted. The rotational lines would be represented by the formula :

$$\nu = \nu_0 + F'(K) - F''(K) = \nu_0 + B'K'(K'+1) - B''K''(K''+1),$$

ν_0 represents the frequency of the nul-line of the band. The formula for the indivitual forms are :

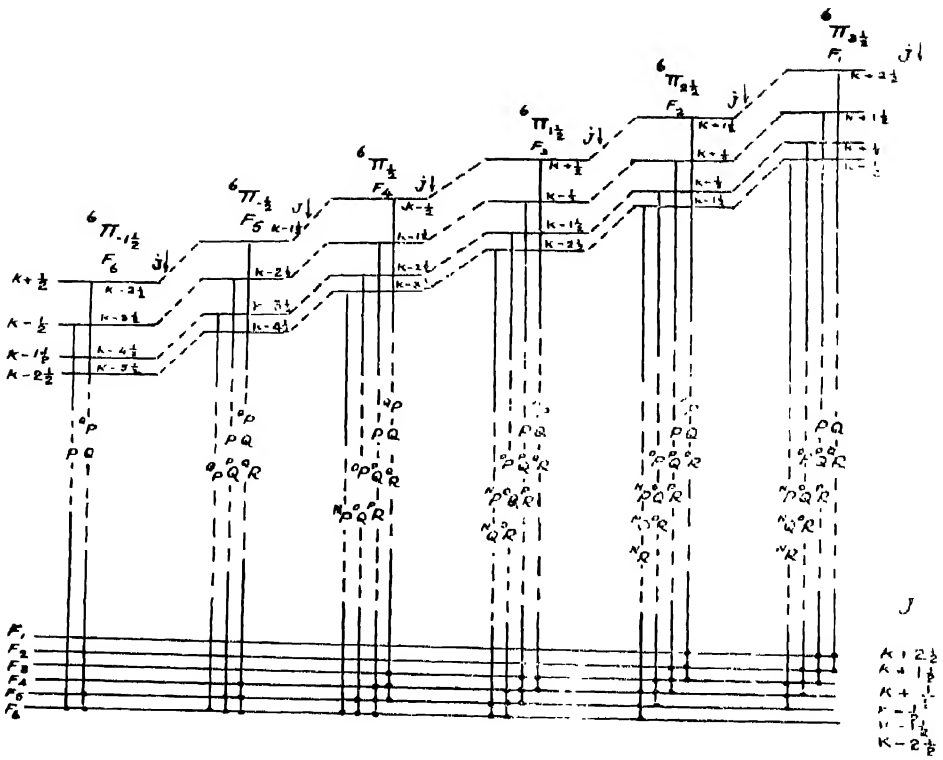

FIG. 2
Transitions in CrCl.

Form	ΔK	
T	$+3$	$\nu=\nu_0+F'(K+3)-F''(K)$
		$=\nu_0+12B'_v+(7B'-B'')K+(B'-B'')K^2$
S	$+2$	$\nu=\nu_0+F'(K+2)-F''(K)$
		$=\nu_0+(1)6B'+(5B'-B'')K+(B'-B'')K^2$
R	$+1$	$\nu=\nu_0+F'(K+1)-F''(K)$
		$=\nu_0+2B'+(3B'-B'')K+(B'-B'')K^2$
Q	0	$\nu=\nu_0+F'(K)-F''(K)$
		$=\nu_0+(B'-B'')K+(B'-B'')K^2$
P	-1	$\nu=\nu_0+F'(K-1)-F''(K)$
		$=\nu_0-(B'+B'')K+(B'-B'')K^2$
O	-2	$\nu=\nu_0+F'(K-2)-F''(K)$
		$=\nu_0+2B'-(3B'+B'')K+(B'-B'')K^2$
N	-3	$\nu=\nu_0+F'(K-3)-F''(K)$
		$=\nu_0+6B'-(5B'+B'')K+(B'-B'')K^2$

Differentiating the above expressions with respect to K and equating to zero (the condition for head formation), we get the value of K at which the head is formed. For the case in which $B' > B''$ (violet degraded bands) K_h is negative for R, S, T forms and positive for the others. The K_h values for the latter are shown below :

ΔK	0	-1	-2	-3
Form	Q	R	0	N
K_h	-	$\frac{B'+B''}{2(B'-B'')}$	$\frac{3B'+B''}{2(B'-B'')}$	$\frac{5B'+B''}{2(B'-B'')}$

Hence in CrCl bands for which $\omega_e' > \omega_e''$ we expect only the Q, P, O, and N forms as head forming. These transitions are shown in Fig. 2.

TABLE I

List of the theoretical transitions.

$\Delta J-1$	0	-1	Symbol
P_6			A
$^QP_{65}$	Q_6		B
$^OP_{56}$			C
P_5	$^PQ_{56}$		D
$^QP_{54}$	Q_5	$^QR_{56}$	E
$^NP_{46}$			F
$^OP_{45}$	$^OQ_{46}$		G
P_4	$^PQ_{45}$	$^PR_{46}$	H
$^QP_{43}$	Q_4	$^QR_{46}$	I
$^NP_{35}$	$^NQ_{36}$		J
$^OP_{34}$	$^OQ_{35}$	$^OR_{36}$	K
P_{33}	$^PQ_{34}$	$^PR_{35}$	L
$^QP_{32}$	Q_{33}	$^QR_{34}$	M
$^NP_{24}$	$^NQ_{25}$	$^NR_{26}$	N
$^OP_{23}$	$^OQ_{24}$	$^OR_{25}$	O
P_2	$^PQ_{23}$	$^PR_{24}$	P
$^QP_{21}$	Q_{21}	$^QR_{23}$	Q
$^NP_{13}$	$^NQ_{14}$	$^NR_{15}$	R
$^OP_{12}$	$^OQ_{13}$	$^OR_{14}$	S
P_1	$^PQ_{12}$	$^PR_{13}$	T
	Q_1	$^QR_{12}$	U

TABLE II

Catalogue of CrCl band-heads

Wave-length	Wave-number	Int	v′, v″	Symbol.
6484.9	15416	1		
66.5	15460	2		
51.7	15496	3	0,2	*B*
40.7	15522	1	0,2	*D*
35.1	15536	2	0,2	*E*
27.2	15555	2	0,2	*G*
11.5	15593	1	0,2	*K*
6399.1	15621	1	0,2	*M*
78.9	15672	2		
71.6	15690	1		
51.4	15740	1		
39.6	15770	2	0,1	*B*
23.5	15810	1	0,1	*E*
15.0	15831	4	0,1	*G*
09.9	15844	3	0,1	*H*
06.9	15851	2	0,1	*I*
01.9	15864	1	1,2	*D*
6298.5	15873	3	1,2	*E*
89.5	15894	1	0,1	*M*
86.5	15903	2		
84.0	15909	1	1,2	*H*
79.0	15922	2	1,2	*I*
71.3	15940	2	0,1	*L*
65.6	15955	2	1,2	*L*
61.8	15965	3	1,2	*M*
59.4	15972	3		
56.7	15979	2		
52.4	15989	1	0,1	*S*
43.5	16011	1	1,2	*O*
38.0	16027	0		
32.6	16040	1	1,2	*U*
26.7	16056	1	1,2	*S*
24.9	16060	1	0,0	*B*
18.6	16076		0,0	*C*
11.4	16095		0,0	*D*
08.8	16102	1	0,0	*E*
05.0	16111	4	1,1	*A*
03.7	16115	2	1,1	*B*
00.4	16124	0	0,0	*G*
6295.3	16137	3	0,0	*H*
93.0	16142	3	0,0	*I*
89.9	16151	1	1,1	*D*
86.1	16161	1	0,0	*J*
79.6	16178	1	0,0	*K*
76.3	16187	1	0,0	*M*
72.6	16196	5	1,1	*I*
68.6	16207	1	0,0	*N*
65.0	16216	0	1,1	*K*
62.6	16222	5	0,0	*O*
58.6	16233	5	0,0	*Q*
56.6	16238	2	1,1	*M*
52.8	16248	1	0,0	*R*
49.4	16257	1	1,1	*P*
47.2	16263	0	0,0	*T*
40.5	16281	6bl	0,0; 1,1	*S,T,U*
30.6	16307	0	1,1	*T*
22.7	16329	2	1,1	*U*
16.5	16345	4		
14.1	16351	3		

TABLE II (*contd.*)

λ	ν	Int.	v′, v″	Symbol
6112.4	16356	2		
09.4	16364	1		
03.7	16379	8bl		
6096.0	16400	5bl	1,0	*A*
94.6	16404	2	1,0	*B*
87.8	16422	4	1,0	*C*
85.0	16429	0		
76.7	16452	1	1,0	*E*
54.7	16512	2	2,1	*H*
49.6	16526	2	1,0	*L*
47.8	16530	4	1,0	*M*
42.6	16545	1	2,1	*K*
40.4	16551	4	2,1	*L*
31.8	16574	1	1,0	*O*,*Q*
28.9	16582	1	2,1	*O*
22.1	16601	0		
20.2	16606	2	1,0	*R*
16.8	16615	2		
14.1	16623	0	1,0	*S*
08.9	16639	1	2,1	*S*
06.4	16644	3	2,1	*T*
5998.0	16664	4		
90.1	16681	1		
83.3	16709	0		
78.7	16721	1	2,0	*B*
72.9	16738	2		
70.7	16744	3		
67.1	16754	1		
64.6	16761	3	2,0	*E*
62.1	16768	0		
59.0	16777	3		
55.8	16786	1		
48.4	16807	0	2,0	*I*
36.1	16841	2		
35.2	16844	1		
33.3	16849	1	2,0	*M*
30.5	16857	1		
24.0	16876	1	2,0	*N*
08.4	16920	1	2,0	*R*
04.4	16932	0	2,0	*S*

TABLE. III

Vibrational differences in the *Q* heads.

v′,v″	Q_6		Q_5		Q_4		Q_3		Q_2		Q_1
0,0	16060	42	16102	42	16142	45	16187	46	16233	48	16281
0,1	15770	40	15810	41	15851	43	15894	43	15940	49	15989
ω_e''	290		292		291		293		293		292
1,0	16404		—		—		16530	44	16574	49	16623
0,0	16060		16102		16142		16187		16233		16281
ω_e'	344		—		—		343		342		342

TABLE IV

Difference scheme for the 0,0 group.

ΔK	$^6\Pi_{-2\frac{1}{2}}$	$^6\Pi_{-1\frac{1}{2}}$		$^6\Pi_{-\frac{1}{2}}$		$^6\Pi_{\frac{1}{2}}$		$^6\Pi_{1\frac{1}{2}}$		$^6\Pi_{2\frac{1}{2}}$
Q		42		42		45		46		48
			7		5		—		—	
P				42		—		—		—
			9		43		—		—	—
				48		11		41		45
O							17		15	—
								46		41
N										

ANALYSIS

With the above picture of expected transitions an analysis of the band groups has been attempted. As mentioned previously the bands occur in 5 groups. One of these extending from λ6230 – 6140 stands out prominently and is considered as $\Delta v = 0$ group. A detailed analysis has been suggested for three of these five groups. The outermost two groups are fainter and practically obliterated due to superposition of the lines. In Table, II, a catalogue of the wave-lengths together with the intensities and wave-numbers is given. The fourth column gives the vibrational assignment. The rotational designation of each head denoted arbitrarily for convenience by symbols *A*, *B*, *C*, . . . *U* is given in the last column. The meaning of the arbitrary symbols *A* to *U*, *i.e.*, the corresponding actual heads which they represent will be clear from Table I.

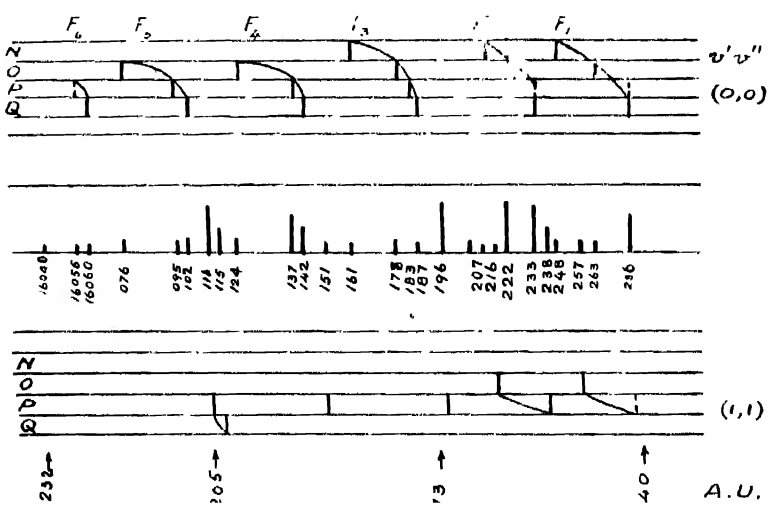

FIG. 3

Structure of (0,0), (1,1) bands. CrCl at λ6230

In order to bring out clearly the rotational structure obtained in each sequence a plot of all the band heads (about 25) measured in the $\Delta v = 0$ group is shown on a uniform frequency scale in Fig. 3. The height of each line in this figure indicates the intensity of the head. The rotational transition and the vibrational assignment of each band are also represented in the same diagram. The (0,0) bands are placed in the upper and the (1,1,) bands in the lower portion of the figure.

The scheme shows that practically all the heads have been interpreted on the assumption of the transition $^6\Pi - {}^6\Sigma$, and the manner in which almost all the important band heads seem to fit into the scheme and the close analogy of this molecule with the corresponding halides of Mn are taken to justify the interpretation of the structure presented in this paper.

The coupling constant has a value of about 46 cm^{-1} as calculated from the Q branch separations shown in Table III. which also gives the values of the vibrational constants $\omega_e' = 342$ and $\omega_e'' = 292$ cm^{-1}. The breadth of the multiplet is about $5 \times 46 = 230$ cm^{-1} ; it is just smaller than the gross structure given by the vibrational intervals. The result of this is that overlap of the groups need not be expected a feature which is evident from the reproduction. (Plate XXIV) Table IV presents the scheme of intervals in the (0,0) group. The separations in the components gradually increase from F_6 to F_1. A similar increase is observed in the separations between Q,P,O,N forms of the rotational branches.

ACKNOWLEDGMENT

Our thanks are due to Dr. Bh. S. V. Raghava Rao of the Chemistry department for his help in the preparation of the chromium chloride.

REFERENCES

Bacher, 1948, *Helv Phys. Acta.*, **21**, 379.
Pearse and Gaydon, 1937, *Nature*, **140**, 110
,, ,, ,, , 1938, *Nature*, **141**, 370
Laporte, *Hand Buch Der Astro. Phy Bd*, III, 692, 712
Mesnage, ,, 1935 *C. R. ACD. SCI.*, **201**, 380.
Muller, 1943, *Helv Phy. Acta.*, **16**, 1.
Nevin, 1942, *Proc. Roy. Irish, Acad.*, **48**, 1
,, , 1945, *Proc Roy. Irish, Acad.*, **50**, 123
Rao, P. T, 1948, *Curr. Sci.*, **17**, 209
,, , 1948, *Ind. J. Phy.*, **23**, 301.

EMISSION SPECTRA OF THE MANGANESE HALIDES

By P. TIRUVENGANNA RAO

(Received for publication, April 11, 1949)

Plates XXVA and B

ABSTRACT. Bacher's analysis of the MnCl bands in the region λ 3900–λ 3500, as arising from the electronic transition $^7\Pi-^7\Sigma$, is extended to the higher sequences $\Delta v=\pm 1$, ± 2, ± 3. A similar analysis is worked out for the $\Delta v=+1$ sequence of MnBr bands.

INTRODUCTION

In a short note, the author (Rao, 1948) reported characteristic bands in the region λ3900-λ3500 attributed to the diatomic molecule MnCl in a heavy current discharge. An analysis of these bands was communicated in a previous paper (1948 and 1949). Considering the previously published work of Rochester and Olsson (1939) on the band spectrum of MnF, the bands due to the MnCl molecule were attributed to the transition $^1\Pi-^1\Sigma$ and the vibrational constants $\omega'_e=413.3$ and $\omega''_e=385.6$ were estimated. It was, however, pointed out that there was the main difficulty in the above interpretation, namely, the very abnormal intensity peculiarity, chiefly, in the band heads forming the $\Delta v=0$ sequence. Mulier's (1943) suggestion of an electronic transition $^7\Pi-^7\Pi$ was also considered; but in view of the greater probability of a Σ-state as the ground state of the molecule, it was suggested that the observed complexity of the bands may be due to a high multiplicity Π term for the upper state only, the probable transition thus being $^7\Pi-^7\Sigma$. While a more detailed study of the bands, on this basis, of complex molecular terms was in progress, an interesting and comprehensive paper was published by Bacher (1948). This system of manganese chloride, designated by him, as system β, was obtained only in absorption. Besides this, the corresponding system in MnBr and MnI were also obtained in absorption. Emission bands were recorded only for manganese fluoride. In all these molecules the β system was attributed to the transition $^7\Pi-^7\Sigma$ similar to the one suggested by Pearse and Gaydon (1935) and established by Nevin (1948) in MnH. Bacher published an analysis completely for all the groups $\Delta v=0, \pm 1, \pm 2$, for the MnF molecule. In MnCl and MnBr, he gave the classification only for the $\Delta v=0$ sequence. Perhaps in the latter two molecules, since the absorption spectra alone were recorded, the groups with $\Delta v\neq 0$ might have been poorly developed. The emission spectra of these two molecules were obtained by the author in the present investigation with sufficient intensity

as to justify an extension of the scheme to the higher sequences as well. This extended analysis is presented in the following sections.

The experimental arrangement was described in detail previously. It will be seen that a discharge tube of quite a simple design without either external heating of the substance or water cooling of the discharge tube and circulation of the helium gas, as used by Bacher, is found sufficient for the excitation of all the halide bands The heavy current discharge itself produces enough local heating to vaporise the substance. In the case of MnF, the spectrum is obtained free from any trace of SiF bands. At a flash voltage of 1500 volts from a D. C. generator and with currents of 0.6, 0.5, and 0.3 amperes for MnF, MnCl and MnBr repectively, exposures of just 3 minutes' duration gave good spectra with a Hilger quartz Littrow spectrograph on Ilford S. R. plates. All the bands recorded by Bacher for the three molecules MnF, MnCl and MnBr have been obtained. But for the iodide, this experimental set-up was not suitable.

RESULTS

MnCl. Tables I to VI contain the observational data obtained with manganese chloride in the present work. They relate to the sequences $\Delta v = \pm 1, \pm 2, \pm 3$. The data on the $\Delta v = 0$ sequence is omitted as it was already completely reported by Bacher. The last two columns in these tables give the vibrational and the rotational assignments of the different heads. The classification is closely analogous to that determined for the $\Delta v = 0$ sequence by Bacher. The structure corresponds to the transition $^7\Pi = {}^7\Sigma$. For a full discussion of the multiplet analysis, reference may be made to Bacher's

TABLE I

MnCl bands $\Delta v = +1$ sequence.

λ	ν	I	v', v''	ΔJ		
				-1	0	$+1$
3663.17	27291.0	2	1,0	P_7		
62.36	27297.1	2			—	
61.55	27303.1	2	1,0	$^9P_{76}$	Q_7	
60.61	27311.1	3				
59.44	27318.8	2	1,0	$^9P_{67}$		
58.32	27327.2	3	2,1	$^9P_{76}$	Q_7	
57.45	27333.7	1	1,0	P_6	$^7Q_{67}$	

TABLE I (*contd.*)

MnCl bands $\Delta v = +1$ sequence.

λ	ν	I	v', v''	ΔJ		
				-1	0	$+1$
56.12	27311.1	2	1,0	$^{Q}P_{65}$	Q_6	$^{Q}R_{67}$
55.40	27318.6	5				
54.59	27355.1	5	2,1	P_6	$^{P}Q_{67}$	
53.85	27362.0	2	1,0	$^{O}P_{56}$	$^{O}Q_{57}$	
53.43	27371.3	3	2,1	$^{Q}P_{65}$	Q_6	$^{Q}R_{67}$
52.41	27378.9	5	1,0	P_5	$^{P}Q_{56}$	$^{P}R_{57}$
50.54	27385.4	1	1,0	$^{Q}P_{54}$	Q_5	$^{Q}R_{56}$
49.52	27393.1	3				
48.38	27401.7	5	2,1	P_5	$^{P}Q_{56}$	$^{P}R_{57}$
47.53	27408.0	5	1,0	$^{O}P_{45}$	$^{O}Q_{46}$	$^{O}R_{47}$
46.53	27415.6	3	2,1	$^{Q}P_{54}$	Q_5	$^{Q}R_{56}$
45.33	27424.6	6	1,0	P_4	$^{P}Q_{45}$	$^{P}R_{46}$
44.53	27430.6	2	1,0	$^{Q}P_{43}$	Q_4	$^{Q}R_{45}$
43.99	27434.7	5	1,0	$^{N}P_{35}$	$^{N}Q_{36}$	$^{N}R_{37}$
42.28	27447.5	6	2,1	P_4	$^{P}Q_{45}$	$^{P}R_{46}$
41.07	27456.7	6	1,0	$^{O}P_{34}$	$^{O}Q_{35}$	$^{O}R_{36}$
39.82	27466.1	4				
39.15	27471.1	4	1,0	P_3	$^{P}Q_{34}$	$^{P}R_{35}$
38.09	27479.1	6	2,1	$^{O}P_{34}$	$^{O}Q_{35}$	$^{O}R_{36}$
37.21	27485.8	3	1,0	$^{N}P_{24}$	$^{N}Q_{25}$	$^{N}R_{26}$
36.23	27493.2	4	2,1	P_3	$^{P}Q_{24}$	$^{P}R_{25}$
35.07	27502.0	6	1,0	$^{O}P_{23}$	$^{O}Q_{24}$	$^{O}R_{25}$
34.17	27508.8	3				
33.15	27516.5	4	1,0	P_2	$^{P}Q_{23}$	$^{P}R_{24}$
32.06	27524.8	5	2,1	$^{O}P_{23}$	$^{O}Q_{24}$	$^{O}R_{25}$
29.82	27541.8	6				
28.87	27549.0	4	1,0	$^{O}P_{12}$	$^{O}Q_{13}$	$^{O}R_{14}$
28.05	27555.2	3				
27.21	27561.6	3	1,0	P_1	$^{P}Q_{12}$	$^{P}R_{13}$

TABLE II

MnCl bands $\Delta v = +2$ sequence.

λ	ν	I	v′, v″	ΔJ		
				−1	0	+1
3606.67	27718.5	1	2,0	$^{o}P_{67}$		
05.51	27727.5	3	3,1	$^{o}P_{76}$	Q_7	
03.81	27740.5	2	2,0	P_6	$^{p}Q_{67}$	
02.18	27753.1	3	3,1	P_6	$^{p}Q_{67}$	
00.31	27767.5	2	2,0	$^{o}P_{56}$	$^{o}Q_{57}$	
3598.17	27781.0	2	2,0	P_5	$^{p}Q_{56}$	$^{p}R_{57}$
96.37	27797.0	2	3,1	P_5	$^{p}Q_{56}$	$^{p}R_{57}$
93.90	27824.8	1				
91.87	27839.7	2	3,0	P_4	$^{p}Q_{15}$	$^{p}R_{46}$
89.46	27851.4	2	3,1	P_4	$^{p}Q_{15}$	$^{p}R_{46}$
87.76	27861.0	1	2,0	$^{o}P_{35}$	$^{o}Q_{25}$	$^{o}R_{36}$
85.32	27883.0	2	3,1	$^{o}P_{34}$	$^{o}Q_{35}$	$^{o}R_{36}$
83.40	27897.8	2	3,1	P_3	$^{p}Q_{34}$	$^{p}R_{45}$
81.70	27911.1	2	2,0	$^{o}P_{23}$	$^{o}Q_{24}$	$^{o}R_{25}$
80.84	27918.5	2	2,0	P_2	$^{p}Q_{23}$	$^{p}R_{24}$
79.56	27928.5	2	3,1	$^{o}P_{24}$	$^{o}Q_{24}$	$^{o}R_{25}$
76.86	27949.5	1				
75.73	27958.1	1	2,0	$^{o}P_{12}$	$^{o}Q_{13}$	$^{o}R_{14}$

TABLE III

MnCl bands $\Delta v = +3$ sequence.

λ	ν	I	v′, v″	ΔJ		
				−1	0	+1
3545.99	28192.9	1	3,0	P_5	$^{p}Q_{56}$	$^{p}R_{57}$
44.37	28205.7	1	4,1	P_5	$^{p}Q_{56}$	$^{p}R_{57}$
42.80	28218.2	1	3,0	$^{o}P_{45}$	$^{o}Q_{46}$	$^{o}R_{47}$
40.69	28235.0	1	3,0	P_4	$^{p}Q_{45}$	$^{p}R_{46}$
38.59	28251.8	1	4,1	P_4	$^{p}Q_{45}$	$^{p}R_{46}$
37.05	28264.1	1	3,0	$^{o}P_{34}$	$^{o}Q_{35}$	$^{o}R_{36}$
35.11	28279.6	1	4,1	$^{o}P_{34}$	$^{o}Q_{35}$	$^{o}R_{36}$
32.08	28296.7	1	4,1	P_3	$^{p}Q_{24}$	$^{p}R_{35}$
30.40	28310.6	0	3,0	P_2	$^{p}Q_{23}$	$^{p}R_{24}$
28.9	28320.4	1	4,1	$^{o}P_{24}$	$^{o}Q_{24}$	$^{o}R_{25}$
27.63	28339.6	2				
25.83	28354.6	1	3,0	$^{o}P_{12}$	$^{o}Q_{13}$	$^{o}R_{14}$

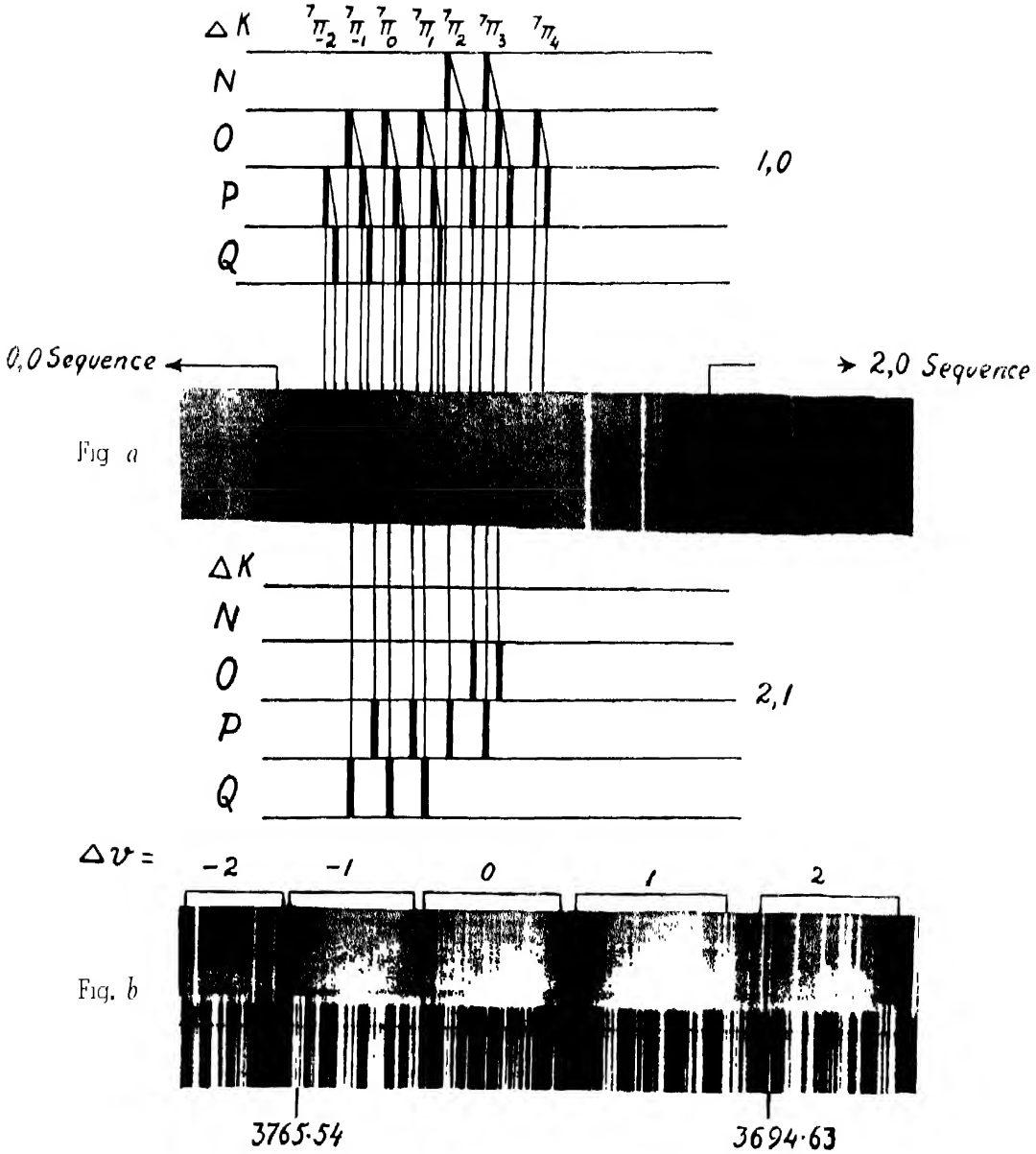

MnCl bands. Fig. *a*—(1,0) sequence, Fig. *b*—Overall picture.

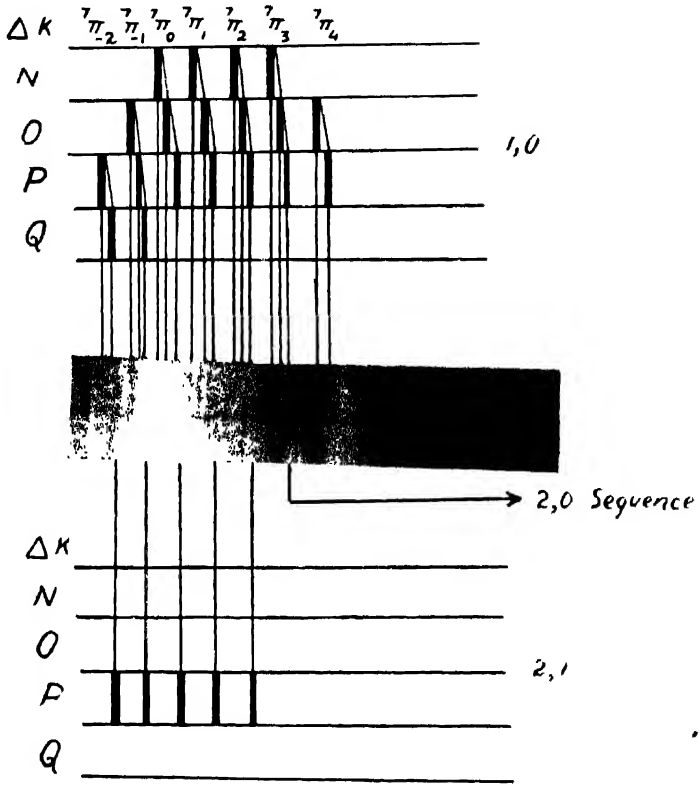

MnBr bands , structure of the (1,0) sequence

TABLE IV

MnCl bands $\Delta v = -1$ sequence.

λ	ν	I	v′, v″	ΔJ		
				−1	0	+1
3772.83	26497.8	2	0,1	P_7		
70.84	26511.8	3	0,1	$^{q}P_{76}$	Q_7	
69.71	26519.7	3				
66.38	26543.2	4	0,1	P_6	$^{q}P_{67}$	
64.64	26555.6	3	0,1	$^{q}P_{65}$	Q_6	$^{q}R_{67}$
63.72	26561.9					
62.11	26573.3	4	0,1	$^{o}P_{56}$	$^{o}Q_{57}$	
60.70	26582.9	2	1,2	$^{q}P_{65}$	Q_6	$^{q}R_{67}$
59.95	26588.0	4	0,1	P_5	$^{r}Q_{56}$	$^{r}R_{57}$
58.17	26601.2	6	0,1	$^{o}P_{54}$	Q_5	$^{q}R_{56}$
56.79	26610.9	2				
55.85	26617.6	7	0,1	$^{o}P_{45}$	$^{o}Q_{46}$	$^{o}R_{47}$
53.69	26632.9	7	0,1	P_4	$^{r}Q_{45}$	$^{r}R_{46}$
52.33	26642.6	2	0,1	$^{q}P_{43}$	Q_4	$^{q}R_{45}$
51.67	26647.3	7	0,1	$^{N}P_{35}$	$^{N}Q_{36}$	$^{N}R_{37}$
50.34	26656.7	3	1,2	P_1	$^{r}Q_{45}$	$^{r}R_{46}$
49.14	26665.2	6	0,1	$^{o}P_{31}$	$^{o}Q_{35}$	$^{o}R_{36}$
47.31	26678.3	7	0,1	P_3	$^{r}Q_{34}$	$^{r}R_{35}$
46.23	26686.0	3	0,1	$^{q}P_{32}$	Q_3	$^{q}R_{34}$
44.91	26695.4	6	0,1	$^{N}P_{24}$	$^{N}Q_{25}$	$^{N}R_{26}$
43.43	26706.0	3	1,2	P_3	$^{r}Q_{34}$	$^{r}R_{35}$
42.35	26713.6	1	0,1	$^{o}P_{23}$	$^{o}Q_{24}$	$^{o}R_{25}$
40.66	26725.7	4	0,1	P_2	$^{r}Q_{23}$	$^{r}R_{24}$
39.46	26734.3	4	0,1	$^{q}P_{21}$	Q_2	$^{q}R_{23}$
38.25	26742.9	4	1,2	$^{o}P_{23}$	$^{o}Q_{24}$	$^{o}R_{25}$
35.56	26762.5	3	0,1	$^{o}P_{12}$	$^{o}Q_{13}$	$^{o}R_{14}$
33.89	26774.3	2	0,1	P_1	$^{r}Q_{12}$	$^{r}R_{13}$
32.79	26782.0	1	0,1		Q_1	$^{q}R_{12}$

TABLE V

MnCl bands $\Delta v = -2$ sequence.

λ	ν	I	v′, v″	ΔJ		
				−1	0	+1
3820.75	26165.5	2	0,2	P_6	$^{r}Q_{67}$	
18.79	26178.9	2	0,2	$^{q}P_{65}$	Q_6	
16.57	26194.1	2	1,3	P_6	$^{r}Q_{67}$	$^{q}R_{67}$
14.64	26207.1	2	0,2	P_5	$^{r}Q_{56}$	
11.77	26227.1	2				$^{r}R_{57}$
08.52	26249.5	2	0,2	P_4	$^{r}Q_{45}$	
05.28	26271.9	3	0,2	$^{N}P_{35}$	$^{N}Q_{36}$	$^{r}R_{46}$
03.19	26286.3	3	1,3	P_4	$^{r}Q_{45}$	$^{N}R_{37}$
00.82	26302.7	3	0,2	P_3	$^{r}Q_{34}$	$^{r}R_{46}$
3798.81	26316.6	3	0,2	$^{N}P_{24}$	$^{N}Q_{25}$	$^{r}R_{35}$
96.59	26332.0	3	1,3	P_3	$^{r}Q_{34}$	$^{N}R_{26}$
94.26	26348.2	3	0,2	P_2	$^{r}Q_{23}$	$^{r}R_{35}$
91.97	26364.1	2	1,3	$^{o}P_{21}$	$^{o}Q_{24}$	$^{r}R_{24}$
90.47	26374.5	3	1,3	P_2	$^{r}Q_{23}$	$^{o}R_{25}$
87.61	26394.4	2	0,2	P_1	$^{r}Q_{12}$	$^{r}R_{24}$
85.29	26410.6	1				$^{r}R_{13}$

TABLE VI

MnCl bands $\Delta v = -3$ sequence.

λ	ν	I	v', v''	ΔJ		
				−1	0	+1
3863·69	25874·7	1	0,3	P_4	$^{1}Q_{45}$	$^{1}R_{46}$
61·99	25885·1	1				
60·25	25897·7	1	0,3	$^{N}P_{35}$	$^{N}Q_{36}$	$^{N}R_{37}$
57·00	25919·6	2	0,3	P_3	$^{1}Q_{34}$	$^{1}R_{35}$
55·10	25932·3	2				
53·50	25943·1	1	0,3	$^{N}P_{21}$	$^{N}Q_{25}$	$^{N}R_{26}$
51·93	25953·7	2	1,4	P_3	$^{1}Q_{34}$	$^{1}R_{35}$
50·28	25964·8	2	0,3	P_2	$^{1}Q_{23}$	$^{1}R_{24}$
47·32	25984·8	2	1,4	$^{0}P_{13}$	$^{0}Q_{24}$	$^{0}R_{25}$
45·50	25996·7	1	1,4	P_2	$^{1}Q_{23}$	$^{1}R_{24}$

excellent paper. Table VII briefly gives the different forms of branches expected in this system consisting of violet-degraded bands with $B^1 > B^{11}$, in conformity with the selection rules applicable to transitions between rotational energy levels ($\Delta J = 0$ or ± 1 excluding $0 \rightarrow 0$ and $\Delta K = 0, \pm 1, \pm 2$, etc.)

TABLE VII

ΔK	0	−1	−2	−3
"Form"	*Q*	*P*	*O*	*N*

As an illustration, a schematic diagram of the transitions is shown for the (1,0) sequence of MnCl in Plate XXV A Fig.(*a*). from which the classification of each band can be clearly understood.

Tables VIII and IX present the interval data between the component $^{7}\Pi$ terms for the (0,1) and (1,0) bands respectively. The intervals *Q*—*P*, *P*—*O*, *O*—*N* show the expected increase. The $^{7}\Pi$ intervals show a very slight increase

TABLE VIII

MnCl Differences between wavenumbers of (0,1) bands.

	$^{7}\Pi_{-2}$	$^{7}\Pi_{-1}$	$^{7}\Pi_{0}$	$^{7}\Pi_{1}$	$^{7}\Pi_{2}$	$^{7}\Pi_{3}$	$^{7}\Pi_{4}$
Q	43·8	45·6	41·4	13·4	48·3	47·7	
	14·0	12·1	12·0	9·7	7·7	8·6	7·9
P	45·1	45·4	44·3	45·4	47·4	48·1	
		15·3	13·3	13·1	12·1	11·6	
O			44·3	47·6	48·4	48·9	
			17·9	18·2			
N					48·1		

TABLE IX

MnCl Differences between wavenumbers of (1,0) bands

	$^7\Pi_{-2}$	$^7\Pi_{-1}$	$^7\Pi_0$	$^7\Pi_1$	$^7\Pi_2$	$^7\Pi_3$	$^7\Pi_4$
Q		38.3	4.0				
	12.1	7.7	6.5	6.0			
P		42.7	45.2	45.7	46.5	45.4	45.1
		14.9	16.0	16.6	14.1	14.5	12.6
O			41.1	45.1	48.7	45.3	47.0
					22.0	16.2	
N					51.1		

MnBr. The experimental data on the MnBr bands belonging to the $\Delta v = +1$ sequence and the classification of the individual heads are given in Table X. The transitions are reproduced in Plate XXVB.

Table XI gives the differences in MnBr similar to those shown in Tables VIII and IX for MnCl. The tables are self-explanatory.

TABLE X

MnBr bands $\Delta v = +1$ sequence

λ	ν	I	v', v''	ΔJ		
				-1	0	$+1$
3779.50	26451.0	4	1,0	$^qP_{76}$	Q_7	
77.76	26463.2	4	2,1	P_1		
76.14	26472.5	2	2,1	$^qP_{76}$	Q_7	
74.03	26489.1	3	1,0	$^oP_{67}$		
72.55	26499.8	10	1,0	P_6	$^PQ_{67}$	
71.50	26506.5	9	1,0	$^qP_{65}$	Q_6	$^qR_{67}$
70.15	26516.6	9	2,1	P_6	$^PQ_{67}$	
69.27	26522.8	8	2,1	$^qP_{65}$	Q_6	$^qR_{67}$
67.89	26532.5	6	1,0	$^sP_{57}$		
65.98	26546.0	6	1,0	$^oP_{56}$	$^oQ_{57}$	
63.96	26560.2	7	1,0	P_5	$^PQ_{56}$	$^PR_{57}$
62.13	26572.3	7	2,1	P_5	$^PQ_{56}$	$^PR_{57}$
59.75	26589.0	6	1,0	$^sP_{46}$	$^sQ_{47}$	
57.56	26605.5	7	1,0	$^oP_{45}$	$^oQ_{46}$	$^oR_{47}$
55.42	26620.6	6	1,0	P_4	$^PQ_{45}$	$^PR_{46}$
53.65	26633.2	6	2,1	P_4	$^PQ_{46}$	$^PR_{47}$
52.23	26643.3	4	1,0			
50.84	26653.2	6	1,0	$^sP_{35}$	$^sQ_{36}$	$^sR_{37}$
49.10	26665.5	5	1,0	$^oP_{34}$	$^oQ_{35}$	$^oR_{36}$
46.98	26680.6	7	1,0	P_3	$^PQ_{34}$	$^PR_{35}$
45.47	26691.4	5	2,1	P_3	$^PQ_{34}$	$^PR_{35}$
41.88	26717.0	5	1,0	$^sP_{24}$	$^sQ_{25}$	$^sR_{26}$
40.16	26729.3	6	1,0	$^oP_{23}$	$^oQ_{24}$	$^oR_{25}$
38.47	26741.3	4	1,0	P_2	$^PQ_{23}$	$^PR_{24}$
31.02	26794.7	7	1,0	$^oP_{12}$	$^oQ_{13}$	$^oR_{14}$
28.97	26809.5	10	1,0	P_1	$^PQ_{12}$	$^PR_{13}$

TABLE XI

MnBr Differences between wavenumbers of (1,0) bands.

	$^7\Pi_{-2}$		$^7\Pi_{-1}$		$^7\Pi_0$		$^7\Pi_1$		$^7\Pi_2$		$^7\Pi_3$	$^7\Pi_4$
Q	55.5											
		6.7										
P			59.4		60.1		60.0		60.1		68.2	
		10.1		11.2		15.1		15.1		12.0		11.8
O			50.6		59.5		60.0		63.8		65.4	
				13.5		15.5		12.3		12.3		
N					67.5		63.2		63.8			

ACKNOWLEDGMENT

The author desires to express his grateful thanks to Prof. K. R. Rao under whose guidance the work has been done.

ANDHRA UNIVERSITY
WALTAIR.

REFERENCES

Bacher, 1948, *Helv. Phy. Acta.*, **21**, 379
Muller, 1913, ,, ,, ,, **16**, 1.
Nevin, 1945, *Proc. Irish. Acad.*, **50**, 123.
Pearse and Gaydon, 1938, *Proc. Phys. Soc.*, **50**, 201.
Rao, Tiruvengadua, 1948, *Curr. Sci.*, **17**, 209
,, 1949, *Ind. Jour. Phy.*, **23**, 301
Rochester and Olsson, 1939, *Zeit. f. Physik.*, **114** 495

ON THE INFLUENCE OF SOLAR ACTIVITY ON THE INTENSITY OF COSMIC RAYS

By I. L. CHAKRABORTY AND S. D. CHATTERJEE*

(*Received for publication, Oct. 18, 1949*)

Plate XXVI

ABSTRACT. A report of a sudden increase in cosmic ray intensity following the solar flare on January 25, 1949 is given. It is accompanied by a rapid diminution in cosmic ray intensity and a slow recovery as a result of the concomitant magnetic storm. The relationship of the two processes with solar activity is discussed.

INTRODUCTION

The intensity of cosmic radiation at any place on the surface of the earth is subject to variations, which are, more or less, world-wide in character. These variations are of two kinds: periodic and non-periodic. The former type mainly consists of :

(*a*) The diurnal variation depending on solar time
(*b*) The diurnal variation depending on siderial time
(*c*) The seasonal variation and
(*d*) The 27-days period variation.

Most of these periodic variations have been accounted for, on theoretical grounds by Vallarta and Godart (1939), as being due to the relative change in the position and orientation of the magnetic dipoles of the Sun and the earth during their respective career.

Amongst the non-periodic variations the most important ones are

(*e*) magnetic storm effect as observed by Forbush (1937) and Hess and Demmelmair (1937), and
(*f*) Solar flare effect as reported by Forbush (1946), Duperier (1945), Dolbear and Elliott (1947) and Neher and Roesch (1948).

Both these non-periodic effects owe their origin to the same source, *viz.*, solar activity due to sunspots. From the observations enumerated above, it may be taken to be definitely established that on the Sun, sometimes active regions appear which are closely associated with sunspots and in which charged particles can be accelerated to energies of the order of $\sim 10^9$ e. v. The mechanism of such a process was first postulated by Swann (1933), who solved in relativistic mechanics, the problem of acquirement of cosmic rays

* Fellow of the Indian Physical Society

energies by charged particles, through the agency of magnetic fields associated with sunspots. A simpler model has been envisaged by Bagge and Biermann (1948) which readily shows that on account of the permanent magnetic field of the Sun, it is not possible for charged particles of energy $\sim 10^9$ e. v. to leave the Sun except in a very narrow band at high latitudes. This difficulty is sometimes surmounted in the following way :

A particle projected during a solar flare will come under the combined action of the Sun and the transient magnetic field of a pair of sunspots moving relative to one another. The latter provides a tunnel through the forbidden region of the permanent field through which charged particles can escape from the lower latitudes of the Sun. The existence of this tunnel depends on the relative strength and the orientations of the permanent and transient dipoles, and on the ratio of their field strengths as a function of the distance. If the charged particles which escape from the Sun are endowed with sufficient energy, they would cut across the barrier of the earth's magnetic field and reach its surface at particular places, causing local increase of cosmic rays intensity as observed in solar flare effects. Failing this, the particels would be deflected by the earth's magnetic field and move in trajectories which are crowded on either side of the magnetic equatorial plane at distances of the order of about three times the earth's diameter. The latter are responsible for the magnetic storm effect. Chapman (1937) has offered an explanation of this effect on the basis of Stormer's hypothesis, that a part of the earth's axial magnetic moment is caused by electronic ring currents as described above. If, during a solar flare, these electric ring currents are increased, the magnetic dipole of the earth is strengthened for regions outside of these ring currents, while inside, near the surface of the earth, the magnetic horizontal force is reduced. The increase of the earth's magnetic field in the outer space produces an increased deflection of the paths of the cosmic rays particles, thus reducing the observed cosmic ray intensity on the earth. As is well known, these trajectories have parabolic longitudinal sections. Thus generally, the charged particles emitted by the Sun, and directed towards the earth, will, if not provided with sufficient energy, return to infinity, following asymptotic paths. This explains why a magnetic storm, and the consequent change of cosmic rays intensity, starts suddenly with the initial phase of the storm, followed by a very slow recovery, extending over more than a week during the last phase of the storm. Under very special combination of circumstances more energetic particles are emitted from the Sun which can penetrate the earth's magnetic field and produce local increase in cosmic ray intensity. This, when it happens, precedes the former.

The possibility of charged particles endowed with cosmic rays energies being emitted from the Sun, has revived speculation regarding the origin of cosmic rays. Teller (1948) has advocated that cosmic rays are of solar origin and are kept relatively in the neighbourhood of the Sun by the action of

solar magnetic fields. This view has been amplified by Alfvén, Richtmyer and Teller (1949) who argue that the great total energy present in cosmic rays would require very efficient methods for the production of these rays if it be assumed that cosmic rays are spread uniformly throughout inter-galatic space. This difficulty can be somewhat side-tracked by assuming that the cosmic rays are generated on or in the neighbourhood of the Sun and are kept near the solar system by extended magnetic fields. According to this picture, cosmic rays circulate in the neighbourhood of the planetory system for thousands of years, during which time the radiation becomes isotropic. The validity of this solar theory can perhaps be tested by an analysis of a large number of data concerning magnetic storm and solar flare effects.

Since the magnetic storms and allied phenomena are closely associated with solar activity, their intensities and frequencies of occurrence wax and wane over the eleven year solar cycle. The present year, 1949, being situated at the crest of the eleven year-cycle, corresponding with maximum solar activity, it was considered desirable to undertake continuous cosmic rays intensity measurements throughout the year. The present paper, which is first of the series, describes some interesting results of measurements extending over one week following January 25th, 1949.

EXPERIMENTAL

For continuous measurement of cosmic rays intensity, especially extending over long periods of time, the pressure ionisation chamber is still perhaps the best available instrument. Standard ionisation chambers have been designed and described by Kolhröster (1926), Hoffmann and Lindholm (1928) Steinke (1928), Millikan and Cameron (1931) and Compton, Wollan and Bennett (1934). Our ionisation chamber assembly consists essentially of five parts. These are briefly described below :

(1) The collecting volume or ionisation chamber proper is a steel cylinder of 3 mm wall thickness with two hemispherical ends, welded with suitable

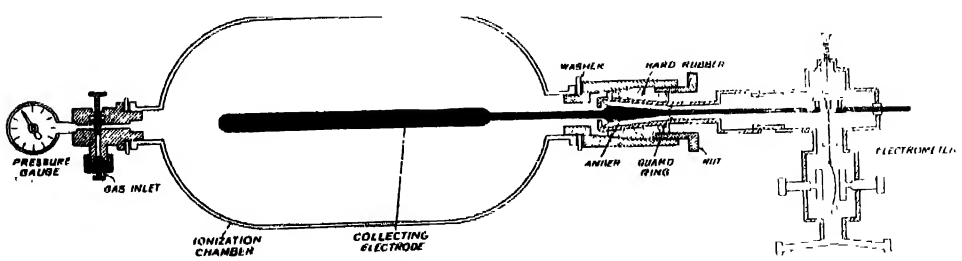

FIG. 1

flanges. One of the flanges is fitted with a gas inlet arrangement furnished with pressure gauge and needle valve while the other supports the highly insulated collecting electrode assembly and guard-ring. The volume of the chamber is five litres and is filled with argon at a pressure of 200 lbs per sq.

in. The vessel contains no network which, according to Steinke and and Schindler (1932) and Pfundt (1933), is unnecessary in high pressure chambers with a comparatively small electric field near the central electrode. In order to further suppress the radioactivity of the walls, the inside has been coated with a mixture of collodion and lamp-black to a thickness of 0.1 mm. This layer absorbs the α-particles. The vessel is insulated from its surroundings by an ebonite support.

(2) The guard-ring consists of a conical brass tube wedged between the hard-rubber and amber plugs. Suitable shields are screwed on both ends of the guard-ring, serving the following important functions :

(*a*) Protection of the collecting electrode from leakage currents which might flow across the insulation.

(*b*) Provision of electrostatic shielding for the electrode system.

(*c*) Elimination of the occurrence of the troublesome phenomena associated with the electrical polarisation of the insulators and their relaxation.

(3) A cylindrical brass rod, of five mm. diameter, and coaxial with the chamber, constitutes the inner collecting electrode. It is supported by being screwed into a small conical brass plug embedded in the insulator amber block. Screwed at the other end of the brass plug is a narrow brass rod, which is connected to the electrometer fibre and is "earthed" every hour by a phosphor-bronze strip operated by a clock-work arrangement.

(4) The measuring instrument is an unifilar electrometer of Wulf's type. The sensitive system consists of a Wollaston filament of 2μ thickness, attached by its lower end to a quartz spring bow. Suitable sensitivity is obtained by adjusting the tension of the filament and also varying the voltage or the position of the knife-edges. Like the apparatus of Hoffmann, Steinke or of Compton, the electrometer is placed outside the ionisation vessel. An extension of the guard-ring enclosing the space between the chamber and the electrometer is made air-tight. This space as well as the electrometer vessel are kept dry by means of phosphorus pentoxide.

(5) The recording apparatus consists of a camera with a cylindrical lens. Cinematographic film is wrapped round a drum mounted on ball-bearing pivots and slowly driven by a clock-work mechanism which is suitably geared to make one complete revolution in twenty-four hours.

The Wollaston filament is illuminated from behind and its image is thrown on the film with the help of a microscope as a dark line against a bright circular background. A sample strip, embodying hourly photographic records of the position of the filament, is shown in Fig. 3, Plate XXVI The slope of each line is a measure of the average cosmic-ray intensity during that hour.

The bottom and the four sides of the chamber are surrounded by lead bricks of 5 cms. thickness in order to cut down the local radiation. When

the top is covered with similar lead bricks, measurements are said to have been taken with closed shield. Otherwise, measurements have been taken with open shield.

A potential of +450 volts is obtained from three well insulated dry batteries and is laid directly on the wall of the chamber, so that the entire volume is used for the measured ionisation.

A schematic diagram of the arrangement is shown in Fig. 1, whilst a photograph of the ionisation chamber assembly is given in Fig. 2 of Plate XXVI.

The measurements were carried out in a small room situated on the top of the Bose Research Institute. The ceiling and one of the walls of the room consisted of thin cement asbestos sheets; the other three walls were constructed of slender masonary In order to minimise the temperature fluctuations, the outer walls and the roof were thickly coated with aluminium paint. Subsequently, the room has been thermally insulated by covering the floor with cork slabs while the walls and roof have been reinforced by double layer of tentest with cotton walls sandwiched between them. In order to keep the temperature and humidity of the room at constant controlled values, an air-conditioning unit is being installed.

RESULTS

If all the ions of one sign produced in a chamber of volume V are collected by the central electrode, then the ionization current observed can the written as

$$i = ePI_s V \qquad \ldots \quad (1)$$

where e = electron charge = 4.77×10^{-10} e.s.u.

P = pressure of the enclosed gas in atmospheres.

I_s = the number of pairs of ions produced per cc. per sec. per atmosphere

V = volume of the chamber in cc.

The rate of change of potential in volts per second is

$$d\phi/dt = 300\ ePI_s V/c \qquad \ldots \quad (2)$$

where c is the capacity of the central electrode system.

In our experimental arrangement,

$P = 13.3$ atmospheres (200 lbs per sq. inch.)

$V = 5000$ cc.

$c = 20.2$ cms.

and $d\phi/dt = 1.8 \times 10^{-3}$ volt per sec., the chamber being surrounded by lead bricks of 5 cms. thickness;

whence I_s is calculated out to be 3.9 ions per cc. per sec.

Now, the total ionization I_s is the sum of the ionizations due to cosmic rays and that due to local radiations.

$$i.e. \qquad I_s = C + L \qquad \ldots \quad (3)$$

These two components C and L have been differentiated adopting the method of Compton (1933). Following Compton, our ionisation chamber was shielded with lead bricks of thickness 2.5 cms and 5 cms in succession. Ionisation measurements were made in each of the above set-ups when no Ra source was in the neighbourhood. Next, a 1 mg Ra capsule, enclosed within a lead container, was placed at an approximate distance of one metre from the middle of the chamber and the ionisation measurements repeated. From these data, one can get C and L by the use of the formulas

$$C = [a/(a-b)](R_2 - bR_1)I_\gamma \qquad \ldots \quad (4)$$

$$L = R_2 I_\gamma - C \qquad \ldots \quad (5)$$

where $a = \dfrac{C_2}{C_1} =$ ionization due to cosmic rays through 5 cms. lead shield / ionization due to cosmic rays through 2.5 cms. lead shield

$$b = \frac{I_2}{I_1} = \text{ionization due to local-rays through 5 cms. lead shield} / \text{ionization due to local-rays through 2.5 cms. lead shield}$$

$$\text{and} \quad R_2 = \frac{i_2}{(i_r - i_2)} = \frac{i_2}{I_\gamma} \qquad \ldots \quad (6)$$

$$R_1 = \frac{i_1}{i_2} \cdot R_2 = \frac{i_1}{I_\gamma} \qquad \ldots \quad (7)$$

i_1 = ionization current through 2.5 cms. lead shield, radium absent.

i_2 = ionization current through 5 cms. lead shield, radium absent.

i_r = ionization current through 5 cms. lead shield, radium at 1 meter.

I_γ = ionization current through 5 cms. lead shield, due to local γ-rays alone.

From the above equations, we find

$$C = C_2 = 2.4 \text{ ions per c.c. per sec.}$$

$$L = I_2 = 1.4 \text{ ions per c.c. per sec.}$$

It may be mentioned, however, that the magnetic storm measurements described hereafter, were undertaken with the open shield, *i.e.*, with the top surface of ionization chamber uncovered.

Since cosmic ray intensity varies with change of barometric pressure, a correction for atmospheric pressure variation was necessary. Assuming that the ionization pressure relationship is linear, (Wollan, 1939) that there is a change of 2% in ionization per cm. change of pressure and that the barometric pressure coefficient is negative, all our data have been corrected for a constant barometric pressure of 1013 millibars.

Moreover, the temperature variation of the room in which the apparatus was housed, affected the sensitivity of the unifilar electrometer. This necessitated the determination of temperature coefficient of the instrument.

To do this the rate of change of sensitivity of the electrometer with temperature had to be determined. This was done by checking the deflection of the electrometer fibre for a constant voltage at different times of day and night in order to have sensitivity records at different temperatures. From the values of sensitivity thus obtained at different temperatures, the temperature coefficient of the instrument was calculated graphically and all the data were corrected for a mean temperature. The cosmic ray intensity measurements were first started in December, 1948, when a comet was visible. No appreciable change in intensity during the period of appearance of the comet could be detected.

Unfortunately, however, due to other pre-occupations no records could be taken during the week preceding January 25, 1949. A report of sunspots and radio fade-out appearing in the morning paper of January 25 prompted us to begin the measurements from the afternoon of that date. The result of measurements carried out during the following week is shown graphically in Fig. 4. Each point represents the average cosmic ray intensity at the corresponding hour, corrected for barometric pressure and room temperature. It will be noticed that an unusual increase of cosmic ray intensity, about 22% above the normal value was recorded at the very commencement of our measurements. This value rapidly diminished till it was about normal by the mid-day of the 26th and then climbed down to about 12% below normal when mid-night was reached. The subsequent course of the intensity curve is subnormal and jagged with a gradual upward tendency to attain the normal value which it did after twelve days.

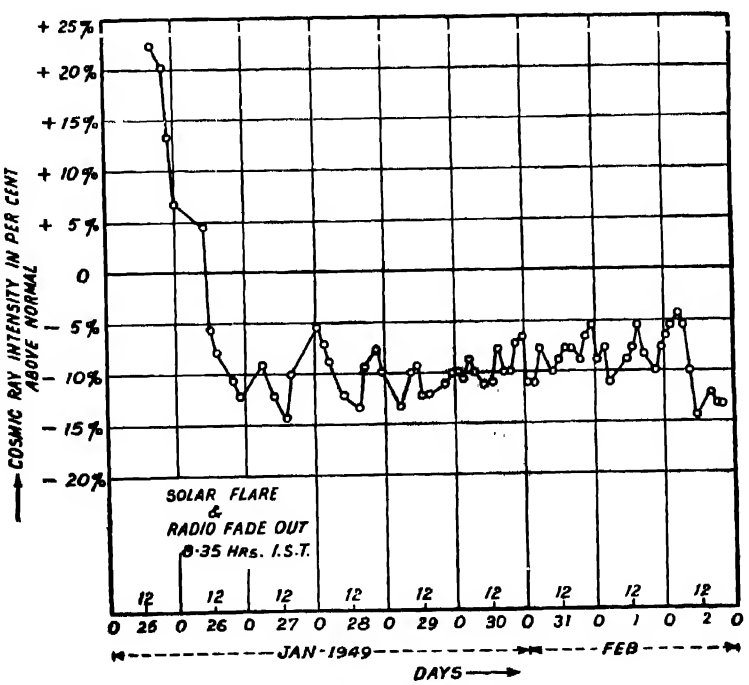

FIG. 4

Table I shows the list of solar flares observed at Kodaikanal during the month of January, 1949, whilst Table II gives the data of magnetic variations observed.

TABLE I

Month and date	Solar flares		Mean Lat.	Mean Longitude
	Time (I. S. T.)	Intensity		
January, 1949				
21st	8.15—8.40	slight	23° N	24° E
23rd	8.00—9 31	¡ reat	20° N (a)	5° W
			22° N (b)	5° E
25th	8.35—8.46	moderate	25° N	16° W

In addition to the above flares, observations showed disturbed or active regions around sunspot groups on the following days, *viz.*, February 1, 2, 3 etc.

TABLE II

Date	International character figure	Magnetic activity
January, 1949		
21st	0	Quiet
22nd	1	Slightly disturbed
23rd	1	Slightly disturbed; crochet at 13.29 hrs.
24th	1	Slightly disturbed; sudden commencement of severe storm at 23 58 hrs.
25th	2	Greatly disturbed; strom continued
26th	2	Greatly disturbed; storm continued till 18.28 hrs.
27th	1	Slightly disturbed
28th	0	Quiet

DISCUSSION OF THE RESULT

It is to be admitted that the result obtained by us, as outlined above is rather surprising. Forbush (1946) observed unusual increase in cosmic ray intensity, associated with solar flares at Cheltenham (geomagnetic latitude 50°N), Godhavn (78°N) and Christchurch (48°S), but not at Huancayo (1°S). It is, therefore, somewhat unusual that similar increase in cosmic ray intensity should have been observed at a place having low geomagnetic latitude as Calcutta (12°N). Moreover, it transpired, on enquiry, that no

Fig. 2

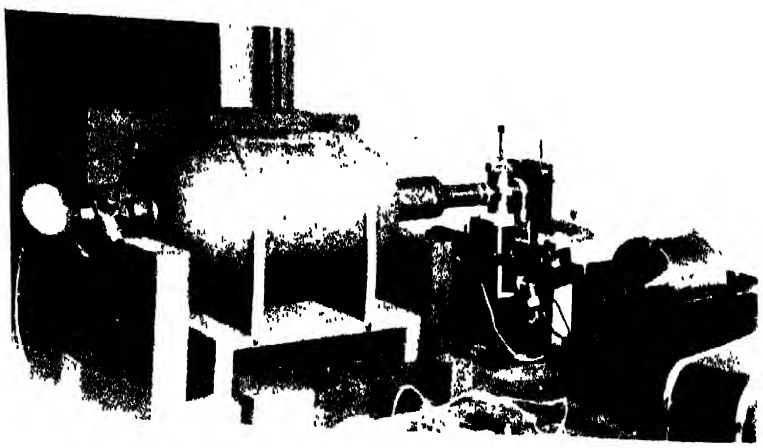

Fig. 3

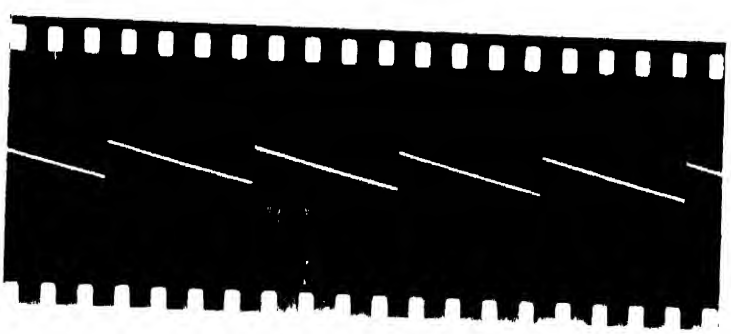

such increase was recorded this time at Washington or Manchester.* It is difficult to conceive why the observation of an increase in cosmic ray intensity due to a solar flare at a lower geomagnetic latitude should not be substantiated at a higher latitude. It might perhaps be mentioned in this connection that Sarna and Sharma (1946) got an abnormal increase in cosmic ray intensity at Lahore (21°N) on August 3, 1946, which was not corroborated by the record of Dolbear and Elliott (1947) at Manchester.† Such examples are, however, by no means rare. For example, the large increase in cosmic ray intensity observed by Forbush on February 28, 1942 at Cheltenham, and Godhavn as reported earlier, was not recorded by Duperier (1945), in London (70°N). On the other hand, the small increase observed by Forbush a few days later on March 7, 1942 at both the above places, was readily corroborated by Duperier. All these facts lend support to the hypothesis that the charged particles arrive at the earth only along certain directions after travelling through the magnetic field of the Sun, the earth and the transient sunspot field. Further, according to Forbush, Gill and Vallarta (1949), during solar flares accompanied by an increase of cosmic radiation, one would expect important departures from isotropy as observed at the earth. Such departures would occur only at certain points on the earth and only in certain directions. In a private communication, commenting on our results, Prof. Vallarta has remarked :

"It would not be a priori impossible for cosmic rays emitted from the Sun during a flare to reach the latitude of Calcutta, nor would it be ruled out that such rays would be observed there and not elsewhere, for instance in Cheltenham. The least latitude of arrival depends on the relative location of the tunnel and the earth." Prof. Vallarta has also kindly promised to get the relevant sunspot data from Mount Wilson and calculate whether the rays had required energy to reach the geomagnetic latitude of Calcutta. Even

* We are thankful to Dr. P. S. Gill and Dr. R. L. Sen Gupta for this information.

† The large increase of cosmic-ray intensity recorded on July 25, 1946 by Forbush, Dolbear and Elliott, and Neher and Roesch, has been associated with the intense solar flare observed on that date. None of the above observers could, however, detect a second increase on the following August 3, 1946, as reported by Sarna and Sharma. It occurred to us, that there might have been two successive active solar flares on these dates like those on February 28 and March 7, 1942 respectively. On looking through the data, kindly supplied by the Director of Solar Physics Observatory, Kodaikanal, on solar flares recorded during, that period in different places, it has come to our notice that an intense solar flare had actually been observed at Ondrejov (Prague) on August 3, 1946. The close simultaneity of the time of occurrence of the solar flare and the observation of increased intensity of cosmic rays by Sarna and Sharma leads us to believe that the two phenomena were perhaps interdependent. The relevant solar flare data are given below :

Observatory	Date 1946	Times (G. M. T.)		Co-ordination of Eruption		Importance
		Begin	End	Latitude	Longitude	
Ondrejov (Prague)	August 3	13. 11	13. 54	26 S	13 W	3

then, he says, it would not be possible for him to locate their exact place of arrival at the earth until the integrations of equations of motion was finished, which he hoped to do in near future.

It will be noticed that the increase of cosmic ray intensity was recorded at Calcutta on January 25, 1949, when, as shown in Table II, a severe magnetic storm was raging. This is, however, not very unusual. Corlin (1931) found that in 30 out of 32 cases there was an increase of ionisation after the beginning of the storm on an average 4.5% of the mean ionizations. It may also be mentioned that the increase in cosmic ray intensity observed on March 7, 1942 by Forbush and also by Duperier, occurred when the world had not fully recovered from the effect of the previous magnetic storm.

It is therefore likely that the aperture of the tunnel opened after the moderate solar flare of the January 25, when the world was passing through a magnetic storm in the wake of the great solar flare of January 23, 1949.

ACKNOWLEDGMENTS

The authors wish to express their sincere thanks to Dr. D. M. Bose, Director, Bose Research Institute for his keen insterest and helpful suggestions and to Prof. M. S. Vallarta for his kindly scrutinising our results. Thanks are also due to Dr. A. K. Das, Director, Solar Observatory, Kodaikanal for supplying the necessary solar flare and magnetic disturbances data and the Research Engineer, All-India Radio, Delhi, for information on radio fade-out. One of us (S. D. C.) is indebted to the National Institute of Sciences of India for the award of a Research Fellowship.

Bose Research Institute
Calcutta.

REFERENCE

Alfvén, Richtmyer and Teller, 1949, *Phys. Rev.*, **75**, 9[illegible].
Bagge and Bierman, 1948, *Naturwiss* **4**, 121
Chapman, 1937, *Nat.*, **140**, 123
Compton, 1933, *Phys Rev*, **43**, 387.
Compton, Wollan and Bennett, 1934 *Rev. Sci. Inst.*, **5**, 415
Corlin, 1931, *Lund. Obs Circ.*, No 1.
Dolbear and Elliott, 1947, *Nat*, **159**, 58.
Duperier, 1945, *Proc. Phys. Soc.*, **57**, 473.
Forbush, 1946, *Phys. Rev.*, **70**, 771.
Forbush, 1937, *Terr. Mag.*, **42**, 1.
Forbush, Gill and Vallarta, 1949, *Rev. Mod. Phys.*, **21**, 44
Hess and Demmelmair, 1937, *Nat.*, **140**, 316
Hoffmann and Lindholm, 1928, *Beitr Geophys.*, **20**, 12
Kolhörster, 1926, *Phys. Zeits.*, **27**, 62.
Millican and Cameron, 1931, *Phys. Rev.*, **37**, 237.
Neher and Roesch, 1948, *Rev. Mod. Phys*, **20**, 350
Pfundt, 1933, *Zeits. f. Physik.*, **86**, 439.
Sarna and Sharma, 1946, *Nat.*, **158**, 550
Steinke, 1928. *Z Phys*, **48**, 687.
Steinke and Schindler, 1932, *Naturwis*, **20**, 15.
Swann, 1933, *J Frank Inst.*, **215**, 273
Teller, 1948, Nuclear Physics Conference, Birmingham.
Wollan, 1939, *Rev. Mod. Phys.*, **11**, 160.
Vallarta and Godart, 1939, *Rev. Mod Phys.*, **11**, 180.

THE COMPLEX BAND SPECTRUM OF TITANIUM CHLORIDE (THE DIATOMIC MOLECULE, TiCl)

By V. RAMAKRISHNA RAO

(*Received for publication, July 27, 1949*)

Plate XXVII

ABSTRACT. The characteristic band spectrum of the titanium chloride molecule has been obatined more extensively than that recorded by More and Parker in a transformer discharge through the vapour. The bands are divided into two systems:

System I: from λ4206–4031

System II: „ λ4072–3787.

The systems are analysed on the assumption of the respective electronic transitions

$^4\Pi - ^4\Sigma$ and $\Sigma^4 - ^4\Sigma$

The approximate vibrational constants are:

	ν_e	ω_e'	$x_e'\omega_e'$	ω_e''	$x_e''\omega_e''$
System II	25000	474	4.4	455	3.8
System I	23810	531	1.5	458	3.8

INTRODUCTION

The prominent band at λ 4192 is known for a long time and was first reported by Fowler (1907) along with two others at λ 4199 and λ 4188, and ascribed to the molecule TiCl More and Parker (1937) recorded about 32 bands of this molecule in the region λ 4200–4000. They presented a fragmentary analysis of this group of bands assigning five bands to each of the 0,0 ; 1,1 etc., vibrational members. The heads are mentioned as forming either P_1 or P_2. Approximate vibrational constants are also suggested by them as $\omega_e' = 498.3$ and $\omega_e'' = 4.43$. Besides the violet of the above group of bands other groups were mentioned as occurring in fragmentary groups. For these even the wave-length data are not reported. Following the author's work on the complex band spectra chiefly of the halides of chromium, it is considered useful to study the band spectra of the halides of titanium which belongs to the same horizontal row as chromium. Vanadium occurs between Ti and Cr but the preparation of the halides has presented to us very serious difficulties, nor could these halides be supplied by Johnson and Mathey. A specimen of the chloride of Ti was available in a high degree of purity (supplied by Merck) and the band spectrum of this has been investigated. The results are described in this paper.

EXPERIMENTAL

More and Parker excited the bands in low and high frequency discharges through flowing vapour of $TiCl_4$. They found the high frequency discharge more intense than the low frequency one. In our work, the pure Merck product of $TiCl_4$ is introduced into the usual H-shaped discharge tube and a low frequency discharge from an ordinary 1/4 K.W. transformer is passed through the vapour. $TiCl_4$, being a liquid at room temperature (about 30°C), is placed in a container and is supplied in a regular stream controlled by a stopper from one end of the tube, while the tube is evacuated from the other end. As the vapour is corrosive a series of effective absorption towers are placed between the pump and discharge tube, partially to protect pump from the effect of chlorine or HCl. A characteristic bluish white discharge is obtained at a particular pressure which is maintained steadily by adjusting the stop-cock from time to time. Photographs are taken on the quartz Littrow spectrograph on Ilford special rapid plates. Exposures of 2 to 5 hours were given on account of the low intensity of the bands: good plates are obtained with 5 hours exposure. (Plate XXVII.)

DESCRIPTION OF THE SPECTRUM

The bands obtained by the author are in six groups and reproduced in Plate XXVII. The intensity distribution in each group is not as regular as might be expected in a simple structure. The bands are line-like as in the other complex halides. Of these six groups the one at λ 4192, as can be seen from the reproduction, is conspicuously intense and is the band that was first reported by Fowler. Another marked feature of this is that it is developed unusually long and definitely impresses as a long sequence structure. As mentioned by the previous authors it corresponds to the $\Delta v = 0$ group. Its intensity makes the identification unmistakable.

The other five groups occur to the violet of this prominent group and are of much less intensity. But there are no groups or bands towards the long-wavelength side of λ 4192. This feature is conspicuously different from the spectra of the chlorides of chromium and manganese in which there is a development of the groups on either side of the prominent one corresponding to $\Delta v = 0$. However, in general, an examination of the complex spectra has shown that the (1,0) group is of considerable intensity and even comparable with the (0,0) group while the $(\bar{0},1)$ group is much less intense. This might account for the absence of the groups on the red side of λ 4192 of TiCl. The (0,1) group is far too weak to be recorded.

All the six groups mentioned above could not be considered as belonging to one system. As we proceed from λ 4192 towards shorter wave-lengths we find the group at λ 3857 (the fourth group) shows a sudden rise in

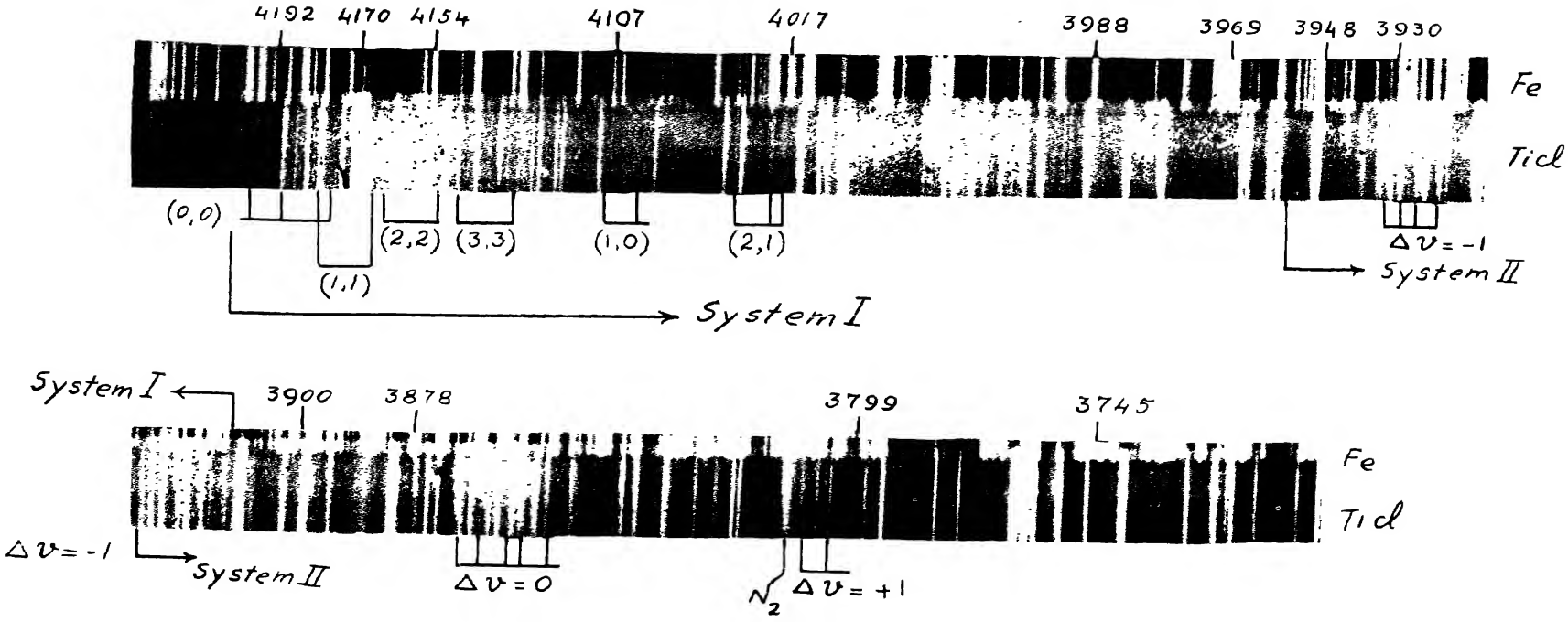

Titanium chloride bands.

intensity. This had to be regarded as the $\Delta v = 0$ group of another system. A similar feature is observed in the band groups of FeCl considered by Muller (1943) : a rise in intensity at a particular group being interpreted as a starting point of another system.

The characteristic bands of TiCl are hence divided into two different systems : λ 4192 being the (0,0) of system I and λ 3857, the corresponding number of system II.

STRUCTURE AND ANALYSIS OF THE BANDS

The structure of λ 4192 belonging to system I is much more complex than that of 3857 assigned to system II In order to interpret the structure of these two systems the following discussion may be helpful. In fact the analysis is suggested as a result of this discussion

Considering the total number of electrons in TiCl molecule, the multiplicity of the terms involved should be even: and as Ti atom has two electrons less than the Cr atom it is reasonable to expect the multiplicity to be four. The following variation of the multiplicities with atom may be instructive:

Molecule	Mnx	Crx	Vx	Tix	Scx	Cax	Kx
Multiplicity	7	6	5?	4	3	2	1

(x represents hydrogen or halogen atom.)

The titanium atom with 22 electrons and the chlorine atom with 17 electrons have the following electronic configurations:

Ti: $1s^2\ 2s^2\ 2p^6\ 3s^2\ 3p^6\ 3d^2\ 4s^2$ giving a ^3F term

Cl: $1s^2\ 2s^2\ 2p^6\ 3s^2\ 3p^5$ giving a ^2P term.

The incomplete $3d^2$ and $3p^5$ groups give rise to the respective atomic terms. In the process of formation of the molecule, the following electron configuration may be imagined :

$$\sigma^2\pi^4,\ \sigma\pi^5 \qquad {}^4\Sigma$$

With the spins all parallel, the total spin is 3/2 giving a multiplicity 4. When the spins are parallel the m_l values of the π electrons are of opposite sign according to Pauli's exclusion principle, and $\Sigma m_l = 0$, resulting in a Σ state. An upper state may arise from $\sigma^2\pi^4,\ \pi^3,\ \pi \longrightarrow {}^4\Pi$ by the elevation of the σ electron to a Π level.

It is easy now to formulate the possible rotational heads for the transition $^4\Pi - {}^4\Sigma$. The ground state $^4\Sigma$ must correspond to the coupling type, Hund's case (b). In a Σ state, ($\lambda = 0$), there is a spin splitting of each rotational level, *i.e.* for each value of K there will be component levels, with J lying between $(K-S)$ and $(K+S)$ which, following Mulliken, may be designated as (F_4, F_3, F_2, F_1) respectively. These levels have very small separations and ordinarily are not resolvable. The upper $^4\Pi$ state may

approximate to case (*a*) or case (*b*) or may represent any state intermediate between the two. In fact, in analogy with the CrCl transition, we have here the four levels F_4, F_3, F_2, F_1 corresponding to $\lambda+1\frac{1}{2}$ to $\lambda-1\frac{1}{2}$ (the Ω values).

A schematic diagram for the transitions $^4\Pi-{}^1\Sigma$ representing the various observable branches is given in Fig. 1. The form of the branches is indicated exactly as in the sextet transition of CrCl. For the rotational formula,

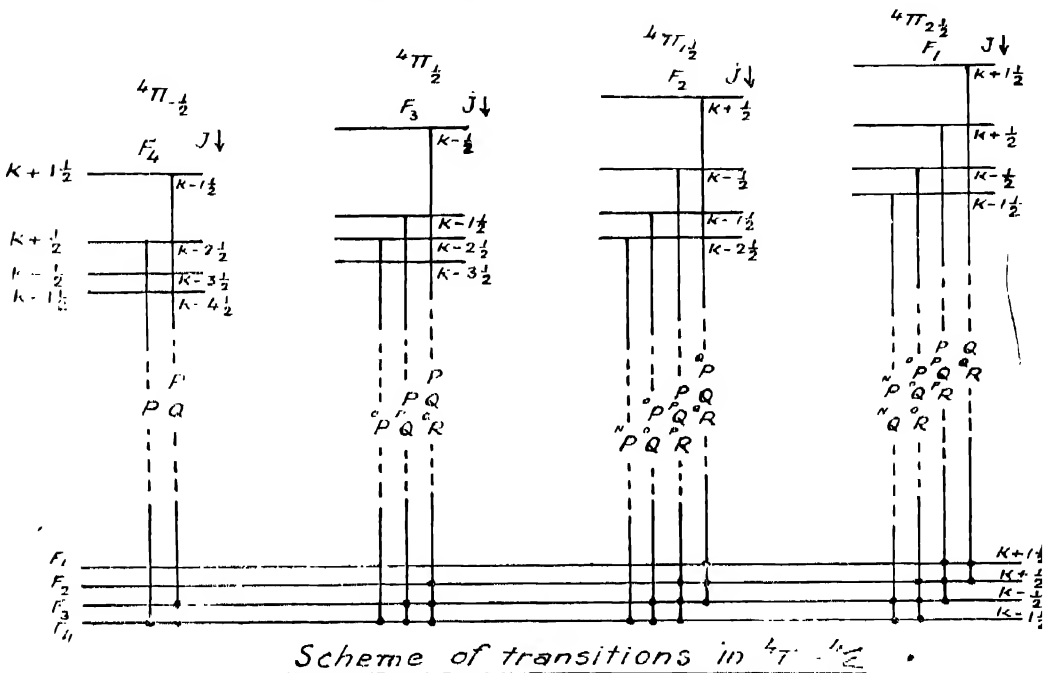

FIG. 1

etc.—reference may be made to our earlier discussion on the sextet transition (Rao and Rao, 1949).

As the bands of TiCl are conspicuously violet-degraded ($\omega_e' > \omega_e''$) we expect only the *Q*, *P*, *O*, and *N* forms as head-forming. These transitions only are shown in Fig. 1 and collected in Table I.

Another upper state can be postulated by imagining an electronic configuration

$$^2\pi^4,\pi^2\delta- \quad ^1\Sigma$$

in which one electron of the previous π^2 group is excited to a δ state. Here too the spins are parallel but while the m_l's are parallel for the π electrons that for the δ electron is anti-parallel, thus resulting in a Σ term again. Transitions between this state and the ground state should be naturally resulting in a simple band structure as both the states are $^1\Sigma$, and the bands should lie to the violet side of the previous group. System I is considered as probably due to the transition $^4\Pi-{}^4\Sigma$ and system II as $^1\Sigma-{}^1\Sigma$.

System II :— With the above picture of the expected transitions an analysis of the bands in system II is first attempted. In this process,

the vibrational constants given by More and Parker were helpful for preliminary attempts. (These constants were derived by them from the analysis of the group between λ4200 to 4000 *i.e.* of the system I)

TABLE I

List of Theoretical Transitions.

ΔJ −1	0	+1	Symbol.
P_4			A
$^{q}P_{43}$	Q_4		B
$^{o}P_{34}$			C
P_3	$^{r}Q_{31}$		D
$^{q}P_{32}$	Q_3	$^{q}R_{21}$	E
$^{N}P_{21}$			F
$^{o}P_{23}$	Q_{21}		G
P_2	$^{r}Q_{23}$	$^{r}_{m}R_{21}$	H
$^{q}P_{21}$	Q_2	$^{q}R_{21}$	I
$^{N}P_{13}$	$^{N}Q_{11}$		J
$^{o}P_{12}$	$^{o}Q_{11}$	$^{o}R_{11}$	K
P_1	$^{r}Q_{12}$	$^{r}_{m}R_{13}$	L
	Q_1	$^{q}R_{12}$	M

The group at λ 3867.9 is taken as a starting point as it is expected to correspond to the $\Delta v=0$ of system II due to the simpler transition $^4\Sigma-^4\Sigma$. With this start and with the help of the approximate ground state frequency 441, suggested by More and Parker, attempts have been made to detect regularities among these bands. They resulted in the identification of bands with simple sequence structure involving the interval difference of about 437, which is just very slightly different from the ground state frequency derived by More and Parker. The neighbouring groups fitted into a regular and simple sequences developing to large v',v'' values. The upper state has the first difference of 460 cm^{-1} which is of the proper order of magnitude. Most of the bands have entered into this analysis easily and the Deslander's scheme is given in Table II. By treating the system as a separate one, it is possible to explain easily the abnormal intensity of the group at λ 3867 which corresponds to the $\Delta v=0$ sequence. In manganese an analogous system is observed and analysed by Rochester and Olsson (1939) and is explained by Bacher (1948) as due to the $^7\Sigma-^7\Sigma$ transition. In the case of chromium the corresponding system has not been obtained as yet. As already pointed out earlier (Rao and Rao, 1949) the group at λ2600 region, reported by Nesnage has been identified by

TABLE II

Deslander's Scheme for TiCl System II

	0	(437.1)	1	(435.4)	2	(430.8)	3	(418.8)	4	(414.4)	5	(406.1)	6	(386.8)	7	(379.9)	8
0	25846.4(3)		25409.3(5)				24546.4(3)										
(460.1)	(460.8)	(437.1)	(459.5)														
1	26307.2(3)		25868.8(3)		25432.3(0)												
(458.5)		(438.4)	(457.3)	(435.5)	(459.6)												
2			26326.1(4b1)		25891.9(5b1)		25465.2(0,?		25039.5(0)		24627.4(1)						
(442)				(434.2)	(44 .6)				(443.4)	(412.1)	(442.0)	(405.9)					
3					26332.5.2)		25901.7(2)		25482.9(0)		25069.4.1)		24663.5(1)				
(435.8)						(430.8)	437.8)	(418.8)	(433.7)	(413.5)							
4							26337.5(b1)		25916.6(3						24700.1(9)		
(435)									(435.2)								
5									26351.8		25934.3(1)		25528.1(1)			24755.4(1)	
(430)										(417.8)	(430.2)	(406.2)	429.5				
6											26364.5		25957.6(3)		25570.2(0)		
(418)													(418.1)	(387.4)	(419.3)		
7													96375.7(3)		25989.5(5b1)		
8														(386.2)			

Gaydon (1927) as due to AlCl. Attempts by the author to obtain the group in CrCl have been inconclusive though it must be mentioned that there is a definite indication of the existence of the bands in the above region and quite distinct from the AlCl bands. However, the analysis of the bands of TiCl on the basis that they constitute two systems, is believed to be correct, and it is expected to be of a similar transition as the corresponding bands in other molecules.

Analysis of System I:—In the light of the postulates given earlier the 13 band heads belonging to the particular (v', v'') values align themselves thus (Table III).

TABLE III

	v''				
		F_1	F_2	F_2	F_1
	Q	B	B	I	M
v'	P	A	D	H	L
	O		C	G	K
	H			F	J

Having obtained the ground state difference for system II attempts are now made to build up the analysis of the first system. Values of ground state differences obtained by us are used for the identification of the sequence members. The band at λ 4192 is unmistakably the (0,0) band. In the (0,0) group regularities of the band heads of the order of about 30 cm^{-1} are observed. A comparison of the multiplet separations in CrCl and MnCl etc., gave 30 units as the approximate order of multiplet separations to be expected in the case of TiCl. Further, a study of the ^4P term in scandium I and Ti II and ^5P in Ti I, also gave a separation factor of the order of 30 cm^{-1}. This led us to attempt to secure regularities with about 30 as the multiplet separations, and so in each group are placed four members with that separation. These included most of the bands assigned by More and Parker to the (0,0) group. On building up the analysis we observed that the first vibrational difference in the upper state we obtained, was about 530 cm^{-1} whereas that due to More and Parker was 498 cm^{-1}; differing by 32 cm^{-1}. This is our multiplet separation, indeed. Evidently the previous authors did not chose the corresponding components in deriving the correct intervals. On a proper choice we arrive at the ground state difference 444, which also agrees very well with their values. This coincidence is taken as an additional support for our analysis. It is further gratifying to see that most of the bands assigned by More and Parker as belonging to a particular group (notably the 0,0 and 1,1 groups) go again into the same groups though the analysis is made from

a totally different view-point. Discrepancies are, however, noted and given in the catalogue of the wave-lengths with the assignments of the bands, in Table V. They might be attributed to the fact that our values differ from their values, and also we assign about 13 bands to each (v', v'') value. While the multiplet separations are found to be of the order of 30, the differences of the rotational heads are found to be of the order 7 to 12. The tendency for the separations to increase from F_1 to F_2 and also from Q to N branches is also brought out in Table IV.

The very considerable length of the (0, 0) group is a characteristic feature in the analysis ; it is a sequence developing up to high (v', v'') values. This feature is not present in CrCl and MnCl bands. This may explain why we do not get the other sequences so well developed in TiCl. Perhaps the entire intensity of the spectrum is thrown into the $\Delta v = 0$ sequence, as is also the case in system II, as can be seen from the picture. The (1,0) band of More and Parker is again one of the (1,0) group in our analysis. Two bands at ν 24069.4 and ν 24136.3 assigned by the previous authors do not find a place in our scheme ; the latter was not even observed on our plates.

In Table V a catalogue of the wave-lengths together with the intensities and wave-numbers are given. Column 5 gives the vibrational assignment. The rotational designation of each head, denoted arbitrarily for convenience by symbols A, B, C, etc., is given in the sixth column. The meaning of the arbitrary symbols A to H, is that, the corresponding actual heads which they represent will be clear from the Table I. The wave-numbers and intensities given in columns 7 and 8 are due to More and Parker and their assignment is also given for the purpose of comparison and clearness.

The scheme shows that practically all the bands have been interperted on the assumptions made; and the manner in which almost all the bands fit in, is taken as evidence in favour of our analysis. This interpretation places TiCl on a par with the corresponding halides in the horizontal row of the first transition group of elements, and brings out not merely the well-known law of alternating multiplicities but also one of progressive increase in multiplicities from group I to group VI elements.

As can be seen from the picture and analysis, one helpful factor in the complexity of the structure is that there is not much overlapping between members of the same sequence. The spread of the multiplet is 120 cms^{-1}, much smaller than the vibrational differences so that there is no overlap of members of different sequences.

The separation between the two systems is much smaller than what is observed in (Cr and) Mn halides.

More and Parker attributed three bands as due to an isotope of chlorine. A search for isotope effect in complex spectra of this type is not considered practicable, particularly under the dispersion we are able

Q | 23816.2(
(8.3)
P | 23807.9(3

O |

N |

24352.4(1)
(10.6)
24311.8(1)

O

N

530

Q

P

2

O

N

530

Q |

P |

3

O

N

5?3

Q

P

4

O

N

TABLE V

Author			Symbol	More and Parker		
Wave number	Int.	v′ v″		Wave number	Int.	v′ v″
23763.8	0					
23807.9	1	0,0	*A*	23805.6	1	0,0
23816.2	1	0,0	*B*			
23820.5	1			23844.5	10	0,0
23845.0	10		*E*			
23850.6	1	0,0	*F*			
23857.4	2	0,0	*G*			
23866.7	5	0,0	*H*	23864.8	4	0,0
23874.7	4	0,0	*I*	23871.3	8	0,0
23892.1	4	0,0	*K*	23890.8	6	0,0
23899.7	6	1,1	*A*	23899.1	0	1,1
23907.6	2	0,0	*M*	23906.4	5	0,0
		1,1	*B*			
23920.6	1	1,1	*C*	23920.5	4	1,1
23933.3	6	1,1	*D*	23930.8	8	1,1
23938.3	8	1,1	*E*			
23952.5	7	1,1	*G*	23949.3	5	1,1
23959.2	7	1,1	*H*	23961.3	0	2,2
23968.9	5	1,1	*I*	23965.1	3	1,1
23977.4	1	1,1	*J*			
23982.5	1	1,1	*K*	23983.4	4	2,2
23990.1	1	1,1	*L*			
23996.0	3	2,2	*A*	23995.6	7	2,2
24000.8	4	1,1	*M*			
24008.1	1	2,2	*B*			
24016.4	1	2,2	*C*	24013.5	5	2,2
24022.3	4					
24026.5	4	2,2	*D*			
				24030.1	6	3,3
24034.0	5	2,2	*E*	24033.7	bl	2,2
24041.3	5	2,2	*F*			
24051.4	3	2,2	*G*			
24056.7	3	2,2	*H*	24057.4	bl	3,3

TABLE V (*contd.*)

Author			Symbol	More and Parker		
Wave number	Int.	v' v''		Wave number	Int	v' v''
24063.6	3	2,2	*I*			
24069.4	3			24069.5	5	3,3
24075.1	2	2,2	*J*			
24084.4	8bl	2,2	*K*			
24090.1	3	2,2	*L*	24090.0	bl	3,3
24096.6	1	2,2	*M*			
		3,3	*A*			
24103.6	3	3,3	*B*	24106.8		4,4
24117.8	2					
24123.3	1	3,3	*C*			
24129.7	3	3,3	*D*			
				24136.3	3	4,4
24148.0	2	3,3	*E*	24147.4	2	4,4
24163.5	5bl	3,3	*H*			
24175.6	0	3,3	*I*	24178.3	1	4,4
24190.2	3bl	3,3	*L*	24191.7	bl	5,5
24198.7	3bl	3,3	*M*			
24209.5	5bl	4,4	*A*	24206.3		4,4
24219.4	5bl	4,4	*B*			
				24225.2	0	5,5
24230.7	1	4,4	*C*	24233.1	0	5,5
24242.8	6bl	4,4	*D*			
24251.9	3bl	4,4	*E*			
24262.9	1	4,4	*G*			
24284.0	0	4,4	*I*	24274.6	0	5,5
24320.0	0					
24326.6	1					
24341.8	1	1,0	*A*	24342.8	3	1,0
24352.4	1	1,0	*B*			
24358.3	1	1,0	*C*			
				24392.3	2	2,1

TABLE V (*contd.*)

List of unclassified bands

Wave number	Inten	Wave number	Intens
24474.6	1	25452.6	0
24769.6	2	25582.5	1
24884.7	1	25650.0	1
25046.5	1	25858.9	2
25082.8	2	25880.3	4b1
25294.0	0	25924.4	3
25307.1	1	26295.8	1
25340 7	2	26318.5	1
25358.9	2	26358.3	1
25385.4	4	26401 5	0
25417.8	1		

to use. The order of isotope shifts is the same as the order of separation of rotational heads and unless very accurate data are available, preferably quantitative microphotometric measurement of intensities and wave-lengths on spectra obtained under high dispersion, we cannot be very certain about the isotope effect.

The following approximate vibrational constants as obtained in the present investigation are collected in Table VI :

TABLE VI

	ν_e	ω_e'	$x_e'\omega_e'$	ω_e''	$x_e''\omega_e''$	A
System II	25900	474	4.4	455	3.8	—
System I	23810	534	1.5	455	3.8	30

ACKNOWLEDGMENT

It is a pleasure to thank Dr. K. R. Rao for his kind guidance during the progress of this work.

PHYSICS DEPARTMENT,
ANDHRA UNIVERSITY.
WALTAIR.

REFERENCES

Bacher, 1948, *Helv. Phys. Acta.*, **21**, 379.

Fowler, 1907, *Proc. Roy. Soc.* **A**, **79**, 509.

More and Parker, 1937, *Phy. Rev*, **52**, 1150.

Muller, 1913, *Helv. Phys. Acta*, **16**, 1.

Rao, V. Ramakrishna, and Rao, K. R., 1949, *Ind. J. Phy.* (in Press)

Rochester and Olsson, 1939, *Zs. f. Phy.*, **114**, 495.

THE WAVESTATISTICAL THEORY OF COMPLEX SPECTRA

By S. SENGUPTA

(*Received for publication, May 6, 1949*)

ABSTRACT. Wavestatistical representation of spin developed in two earlier papers of Kar-Sengupta (1949), and Sengupta (1949) are applied to the case of complex spectra. General formulae for the energy levels in the *sl* configuration are obtained. These formulae are same as those obtained previously by Houston. For *pl*-configuration, general formulae have been derived for the first time for the two limiting cases of *LS* and *jj* coupling. Applying the same method in the case of *N* electrons in any configuration, the well known Γ-and *g*-sum rules for the multiplets are derived. In addition, a new sum rule applicable to the electrostatic interaction energy has also been obtained. It has been called the δ-sum rule. The rule has been verified by taking the experimental results for a number of elements.

In two recent papers (Kar and Sengupta, 1949, and Sengupta, 1949) the wave statistical description of the spin motion has been given and with its help the energies and intensities of doublet spectra with and without the magnetic field have been calculated. In the present paper we shall apply the same method to the case of spectra of atoms with two or more valence electrons.

At first we shall derive in a simple way general expressions for the energy levels arising out of *sl*-configuration. These formulae, however, have also been obtained by Houston (1929) by use of complicated Pauli's equation for the spinning electron. For the next case of *pl*-configuration the general equation becomes very complicated as was first pointed out by Goudsmit (1930). However, in the present paper we shall extend our method and obtain for this configuration general solutions for the two limiting cases of *LS* and *jj* coupling. These formulae show the validity in this case of Lande interval rule for *LS* coupling and the Γ-sum rule for all coupling. Applying the same method to the case of *N* electrons in any configuration, we shall derive the well known Γ- and *g*-sum rules for the general case of multiplets. It is noteworthy that by so doing we get the theoretical basis of a new sum rule applicable to the electrostatic interaction energy. We shall call it the δ-sum rule. It may be noted that we do not find mention of this new sum rule in any of the current literatures on the subject so far available.

Let us first consider the case of two valence electrons occupying the n_1l_1 and n_2l_2 levels respectively. Using the principle of exchange degeneracy and remembering Pauli's exclusion principle, we can write out the complete wave function for the two electrons in the form,

$$\chi_{n_1 l_1 m_{l_1} m_{s_1}\ ;\ n_2 l_2 m_{l_2} m_{s_2}}$$

$$= \frac{1}{\sqrt{2}}\left(\chi^{(1)}_{n_1 l_1 m_{l_1} m_{s_1}} \cdot \chi^{(2)}_{n_2 l_2 m_{l_2} m_{s_2}} - \chi^{(2)}_{n_1 l_1 m_{l_1} m_{s_1}} \cdot \chi^{(1)}_{n_2 l_2 m_{l_2} m_{s_2}}\right) \quad \ldots \quad (1)$$

where, $\chi_{nlm_l m_s}$ can be split into the orbital and spin functions in the same way as in the previous papers. Since the above function is degenerate with respect to m_{l_1}, m_{s_1} and m_{l_2}, m_{s_2}, we get for the general wave function,

$$\chi_{n_1 l_1\ ;\ n_2 l_2} = \sum_{m_{l_1}} \sum_{m_{s_1}} \sum_{m_{l_2}} \sum_{m_{s_2}} \alpha_{m_{l_1} m_{s_1}\ ;\ m_{l_2} m_{s_2}} \cdot \chi_{n_1 l_1 m_{l_1} m_{s_1}\ ;\ n_2 l_2 m_{l_2} m_{s_2}} \quad \ldots \quad (1.1)$$

If we sum (1.1) with respect to m_{s_1} and m_{s_2}, we get four terms corresponding to $(m_{s_1}, m_{s_2}) = (+\frac{1}{2}+\frac{1}{2})$; $(-\frac{1}{2}-\frac{1}{2})$; $(+\frac{1}{2}-\frac{1}{2})$; $(-\frac{1}{2}+\frac{1}{2})$. By combining the last two terms suitably, we can write (1.1) in the following form without any loss of generality.

$$\chi_{n_1 l_1\ ;\ n_2 l_2} = \sum_{m_{l_1}} \sum_{m_{l_2}} \alpha_{m_{l_1} m_{l_2}} \psi^{(1)}_{m_{l_1} m_{l_2}} + \beta_{m_{l_1} m_{l_2}} \psi^{(2)}_{m_{l_1} m_{l_2}} + \gamma_{m_{l_1} m_{l_2}} \psi^{(3)}_{m_{l_1} m_{l_2}} + \delta_{m_{l_1} m_{l_2}} \psi^{(4)}_{m_{l_1} m_{l_2}} \quad \ldots \quad (2)$$

where,

$$\left.\begin{aligned}
\psi^{(1)}_{m_{l_1} m_{l_2}} &= \frac{1}{\sqrt{2}}\left(\chi^{(1)}_{n_1 l_1 m_{l_1}} \cdot \chi^{(2)}_{n_2 l_2 m_{l_2}} - \chi^{(2)}_{n_1 l_1 m_{l_1}} \cdot \chi^{(1)}_{n_2 l_2 m_{l_2}}\right) \chi^{(1)}_{\frac{1}{2}} \cdot \chi^{(2)}_{\frac{1}{2}} \\
\psi^{(2)}_{m_{l_1} m_{l_2}} &= \frac{1}{\sqrt{2}}\left(\chi^{(1)}_{n_1 l_1 m_{l_1}} \cdot \chi^{(2)}_{n_2 l_2 m_{l_2}} - \chi^{(2)}_{n_1 l_1 m_{l_1}} \cdot \chi^{(1)}_{n_2 l_2 m_{l_2}}\right) \chi^{(1)}_{-\frac{1}{2}} \cdot \chi^{(2)}_{-\frac{1}{2}} \\
\psi^{(3)}_{m_{l_1} m_{l_2}},\ \psi^{(4)}_{m_{l_1} m_{l_2}} &= \frac{1}{2}\left(\chi^{(1)}_{n_1 l_1 m_{l_1}} \cdot \chi^{(2)}_{n_2 l_2 m_{l_2}} \mp \chi^{(2)}_{n_1 l_1 m_{l_1}} \cdot \chi^{(1)}_{n_2 l_2 m_{l_2}}\right) \\
&\qquad \left(\chi^{(1)}_{\frac{1}{2}} \cdot \chi^{(2)}_{-\frac{1}{2}} \pm \chi^{(2)}_{\frac{1}{2}} \cdot \chi^{(1)}_{-\frac{1}{2}}\right)
\end{aligned}\right\} \quad \ldots \quad (2.1)$$

Now there are three different perturbing energies to be considered—

(1) The electrostatic interaction between the two electrones.

$$H_1 = \frac{e^2}{r_{12}} \quad \ldots \quad (3)$$

(2) The spin-orbit interaction of the two electrons

$$H_2 = \frac{Ze^2}{2m_0^2 c^2}\frac{(L_1 S_1)}{r^3} + \frac{Ze^2}{2m_0^2 c^2}\frac{(L_2 S_2)}{r^3} \quad \ldots \quad (3.1)$$

(3) The magnetic interaction of the two electrons

$$H_3 = a(m_{l_1} + 2m_{s_1} + m_{l_2} + 2m_{s_2}) \quad \ldots \quad (3.2)$$

where, $$a = \frac{ehH}{4\pi m_0 c}$$

Total perturbing energy $H = H_1 + H_2 + H_3$. If ϵ be the first order change in the energy of any level due to perturbation, then we get from the general theory of perturbation for degenerate states, (*vide*) Sengupta (1949)

$$\int (H - \epsilon) \chi_{n_1 l_1 ; n_2 l_2} \psi^{(i)}_{m l_1, m l_2} \, d\tau = 0 \qquad (4)$$

where $i = 1, 2, 3$ or 4.

For different values of m_{l_1}, m_{l_2} and i, equation (4) gives different equations. Evidently each equation will involve a number of terms associated with the co-efficients $\alpha_{m_{l_1} m_{l_2}}$, $\beta_{m_{l_1} m_{l_2}}$, $\gamma_{m_{l_1} m_{l_2}}$ and $\delta_{m_{l_1} m_{l_2}}$. Due to the well known characteristics of the perturbing energies, H_1, H_2, and H_3, all the terms of a particular equation shall have their $M = m_{l_1} + m_{l_2} + m_{s_1} + m_{s_2}$ same. Thus from (4), we get different equations for different values of M. Since a particular M can be realised in many ways, we get in general more than one equation for the same value of M. These equations involve the same co-efficients. Eliminating these co-efficients from the equations for a particular value of M, we get a determinantal equation, the solution of which gives the required values of ϵ for the states having the above value of M. Evidently the highest possible value of M is $l_1 + l_2 + 1$. For this the determinant consists of only one term and the corresponding energy is easily evaluated. But for smaller values of M, the order of the determinants increases rapidly and the solution becomes almost impossible. The solution can, however, be obtained for some simple special cases. We shall discuss in the following cases of *sl*- and *pl*-configurations.

sl-configuration.—

In this case one of the electrons is in the sth state, *i.e.*, $l_2 = 0$. The highest order of the determinant for any M value is four. Introducing the well-known operators for (LS) in H_2, integration in (4) can be easily performed (Sengupta, 1949). The required determinantal equation is,

$$
\begin{vmatrix}
\left(a(m_l+2)+\frac{b}{2}m_l+E-\epsilon\right) & \frac{b}{2\sqrt{2}}\sqrt{(l-m_l)(l+m_l+1)} & \frac{b}{2\sqrt{2}}\sqrt{(l-m_l)(l+m_l+1)} & 0 \\
\frac{b}{2\sqrt{2}}\sqrt{(l-m_l)(l+m_l+1)} & \left(a(m_l+1)+E-\epsilon\right) & -\frac{b}{2}(m_l+1) & \frac{b}{2\sqrt{2}}\sqrt{(l-m_l-1)(l+m_l+2)} \\
\frac{b}{2\sqrt{2}}\sqrt{(l-m_l)(l+m_l+1)} & -\frac{b}{2}(m_l-1) & \left(am_l+1+E'-\epsilon\right) & -\frac{b}{2\sqrt{2}}\sqrt{(l-m_l-1)(l+m_l+2)} \\
0 & \frac{b}{2\sqrt{2}}\sqrt{(l-m_l-1)(l+m_l+2)} & -\frac{b}{2\sqrt{2}}\sqrt{(l-m_l-1)(l+m_l+2)} & \left(am_l-\frac{b}{2}(m_l+2)+E-\epsilon\right)
\end{vmatrix} = 0 \quad (5)
$$

The M value of this determinant is $m_l + 1$. The symbol b denotes the constant of spin-orbit separations and is given by

$$b = \frac{Ze^2}{2m_0^2 c^2} \int \frac{R^2_{nl}}{r^3} \cdot r^2 dr. \qquad \ldots \quad (5.1)$$

and

$$\left.\begin{aligned} E &= \int \bar{\psi}^{(1)}_{m_1 m_s} H_1 \psi^{(1)}_{m_1 m_s} \, d\tau \\ E' &= \int \bar{\psi}^{(4)}_{m_1 m_s} H_1 \psi^{(4)}_{m_1 m_s} \, d\tau \end{aligned}\right\} \qquad \ldots \quad (5.2)$$

Thus E and E' are constants of electrostatic interaction energy.

Apart from some unimportant differences the above determinant is identical with that obtained by Houston (1929) by application of Pauli's equations for the spinning electron. It is not possible to solve equation (5) for the general case. Houston has given the solution for weak field only. We give here the solutions for both weak and strong fields. For weak field, the solutions, as given by Houston are,

$$\left.\begin{aligned} {}^3l_{l+1} &= E + \frac{b}{2}\, l + a\frac{l+2}{l+1}\, m \\ {}^3l_l &= E + \tfrac{1}{2}X - \tfrac{1}{4}b - \tfrac{1}{2}\sqrt{(X+\tfrac{1}{2}b)^2 + l(l+1)b^2} \\ &\quad + am\left\{1 + \frac{\sqrt{(X+\frac{1}{2}b)^2 + l(l+1)b^2} + X + \frac{1}{2}b}{2l(l+1)\sqrt{(X+\frac{1}{2}b)^2 + l(l+1)b^2}}\right\} \\ {}^3l_{l-1} &= E - \tfrac{1}{2}b(l+1) + a(l-1)/l.\ m \\ {}^1l_l &= E + \tfrac{1}{2}X - \tfrac{1}{4}b + \tfrac{1}{2}\sqrt{(X+\tfrac{1}{2}b)^2 + l(l+1)b^2} \\ &\quad + am\left\{1 + \frac{\sqrt{(X+\frac{1}{2}b)^2 + l(l+1)b^2} - X - \frac{1}{2}b}{2l(l+1)\sqrt{(X+\frac{1}{2}b)^2 + l(l+1)b^2}}\right\} \end{aligned}\right\} \qquad \ldots \quad (6)$$

For strong field we get,

$$\left.\begin{aligned} {}^3l_{l+1} &= E + \tfrac{1}{2}b(m-1) + a(m+1) \\ {}^3l_l &= E + am \\ {}^3l_{l-1} &= E - \tfrac{1}{2}b(m+1) + a(m-1) \\ {}^1l_l &= E + X + am \end{aligned}\right\} \qquad \ldots \quad (6.1)$$

where $m = m_l + 1$ and $\times = E' - E$

From (6.1) we note that in the strong field case the general formulæ are much simpler and the relative separations of the triplet levels do not depend on the electrostatic interaction energy, *i.e.*, on the coupling strength. Moreover it is seen that Γ-sum and g-sum (where Γ denotes the spin orbit interaction energy and g the Lande factor) for all levels of same m value

are 2 and 4 respectively which, as can be easily ascertained from (6), are identical with the corresponding sums in the weak field case. This shows that Γ-sum and g-sum are not only independent of coupling, as was shown by Houston, but also independent of field strength.

pl-configuration.—

Here one of the electrons is in the pth state, *i.e.*, $l_2=1$. This case, however, is much more complicated than the previous one. Here the highest order of the determinant to be solved is twelve. This seems to be an impossible task. But a solution can be obtained for the case when both the spin-orbit and electrostatic energies are small compared to the magnetic energy. But since this case is not of much importance, we do not give the solutions here. General solutions for weak field or no field case cannot be obtained. But for no field we can get the required formulae for the two extreme cases of LS and jj coupling.

LS coupling.—

Here the electrostatic interaction energy is much stronger than the spin-orbit interaction energy. Hence, we consider first the effect of the electrostatic energy $H_1=e^2/r_{12}$. This as may be easily seen from (4) and (2.1), splits the levels into three singlet terms $^1(l+1)$, $^1(l)$, $^1(l-1)$ and three triplet terms $^3(l+1)$, $^3(l)$, $^3(l-1)$. The wave functions for the singlets are given by $\psi^{(4)}_{m_1m_2}$ and for the triplets by $\psi^{(1)}_{m_1m_2}$, $\psi^{(2)}_{m_1m_2}$ and $\psi^{(3)}_{m_1m_2}$. The corresponding electrostatic energies can be easily calculated. The method of calculation is similar to that of Slater (1929), who has considered the effect of the electrostatic perturbation in detail. Slater, however, does not give the general energy values for the levels of pl-configuration. He has considered only some special cases. In the diagonal terms of the determinants set up from (4), the electrostatic portion of the energy involves integrations of the form,

$$E_{m_1m_2}=\int \bar{\psi}^{(i)}_{m_1m_2}\,\frac{e^2}{r_{12}}\,\psi^{(i)}_{m_1m_2}\,d\tau=\sum_{k=0}^{\infty}a^k(l_1m_1l_2m_2)F^k(n_1l_1n_2l_2)$$

$$\pm\sum_{k=0}^{\infty}b^k(l_1m_1l_2m_2)\,G^k(n_1l_1n_2l_2) \qquad \ldots\ (7)$$

where $i=1$, 2, 3 or 4 and

$$\left.\begin{aligned} a^k(l_1m_1l_2m_2)&=c^k(l_1m_1,\ l_1m_1).\ c^k(l_1m_2,\ l_2m_2)\\ b^k(l_1m_1l_2m_2)&=\lfloor c^k(l_1m_1l_2m_2)\rfloor^2\\ c^k(lm_ll'm'_l)&=\sqrt{\frac{2}{2k+1}}\int_0^{\pi}P_k^{m_l-m'_l}P_l^{m_l}P_{l'}^{m'_l}\sin\theta\,d\theta \end{aligned}\right\}\ \ldots\ (7.1)$$

The F^k's and G^k's are the well-known Slater-Condon notations. (For the meaning of these symbols *vide* Condon and Shortley (1935). For pl-configuration it can be shown that $k=0$ and 2 for a^k's and $k=l-1$. and $l+1$ for b^k's. Thus the electrostatic integrations in the diagonal terms of the determinants take the form,

$$Em_{l_1}m_{l_2}=(a^0F^0+a^2F^2)\pm(b^{l-1}G^{l-1}+b^{l+1}G^{l+1}) \qquad (7.2)$$

The a's and b's in (7.2) can be obtained with the help of the Gaunt's formula (Gaunt, 1929) for the integration of the product of three associated Legendre functions as in (7.1). The values of a^k's and b^k's for particular values of $l_1m_{l_1}l_2m_{l_2}$ have been given in tabular form by Slater (1929) and Shortley and Freid (1938). In Tables I and II we give the corresponding values for the pl-configuration.

TABLE I

$b^k\ (lm_l\ 1m'_l)$

In the third and fourth column are given the values of b^k for $k=l-1$ and $l+1$. The common denominator is written only for the term at the head of each column.

m_l	m'_1	$k=\ l-1$	$l+1$
l	1	$\frac{3l}{4l^2-1}$	$\frac{3}{(2l+3)^2(2l+1)}$
$l-1$	1	$3(l-1)$	9
l	0	0	$3(2l+1)$
$l-2$	1	$\frac{3(l-1)(2l-3)}{2l-1}$	18
$l-1$	0	3	$12l$
l	-1	0	$3(l+1)(2l+1)$
$l-3$	1	$\frac{3(2l-3)(l-2)}{2l-1}$	30
$l-2$	0	$\frac{12(l-1)}{2l-1}$	$9(2l-1)$
$l-1$	-1	0	$3l(2l+1)$

TABLE II

$a^k\ (lm_l\ 1m'_l)$

a^k's do not depend on the signs of m_l and m'_l. $a^0 = 1$ always. As before the common denominator is written only for the term at the head of the column.

$\lvert m_l \rvert$	$\lvert m'_l \rvert$	$k=2$
l	1	$\frac{l}{5(2l+3)}$
$l-1$	1	$l-3$
l	0	$-2l$
$l-2$	1	$\frac{2l^2-13l+12}{2l-1}$
$l-1$	0	$-2(l-3)$
$l-3$	1	$\frac{2l^2-19l+27}{2l-1}$
$l-2$	0	$-\frac{2(2l^2-13l+12)}{2l-1}$

With the help of the above tables the electrostatic interaction energies of the singlet and triplet terms can be easily determined. These energies are,

$$^1(l+1)\ ;\ ^3(l+1) = F^0 + \frac{l}{5(2l+3)}F^2 \pm \left(\frac{3l}{4l^2-1} G^{l-1} + \frac{3}{(2l+3)^2(2l+1)} G^{l+1} \right)$$

$$^1(l)\ ;\ ^3(l) = F^0 - \frac{1}{5}F^2 \pm \left(\frac{3}{(4l^2-1)} G^{l-1} - \frac{3}{(2l+3)(2l+1)} G^{l+1} \right)$$

$$^1(l-1)\ ;\ ^3(l-1) = F^0 + \frac{l+1}{5(2l-1)}F^2 \pm \left(\frac{3}{(4l^2-1)(2l-1)} G^{l-1} + \frac{3(l+1)}{(2l+3)(2l+1)} G^{l+1} \right)$$

We now consider the first order effect of the spin-orbit interaction on the above energy levels. On the singlet levels it may be easily shown that the spin-orbit interaction has no effect. The three triplet levels, however, split into nine different levels ${}^3(l+1)_{l+2,\ l+1,\ l}$; ${}^3(l)_{l+1,\ l,\ l-1}$; ${}^3(l-1)_{l,\ l-1,\ l-2}$. Energy values for these levels can be determined in the following way. By application of the perturbation theory, we have, as before, different determinantal equations for different values of M. For $M=l+2$, there is only one equation giving the energy of the ${}^3(l+1)_{l+2}$ level. This is,

$$ {}^3(l+1)_{l+2} = E_{l,1} + \frac{b_1}{2} l + \frac{b_2}{2} \qquad \ldots \quad (9) $$

Where $E_{l,1}$ is the electrostatic portion of the energy and is same as that given in (8). b_1 and b_2 are the constants of spin orbit separations for the l and p electrons respectively and are given by formulæ similar to (5.1). For $M=l+1$, we get a third order determinant whose roots are the three levels, ${}^3(l+1)_{l+2}$, ${}^3(l+1)_{l+1}$ and ${}^1(l)_{l+1}$. This determinantal equation is given by,

$$ \begin{vmatrix} \left(\frac{b_1}{2} l + E_{l,0} - \epsilon\right) & E^{l,0}_{l-1,1} & \frac{b_2}{2} \\ E^{l-1,1}_{l,0} & \left(\frac{b_1^{(l-1)}}{2} + \frac{b_2}{2} + E_{l-1,1} - \epsilon\right) & \frac{b_1\sqrt{l}}{2} \\ \frac{b_2}{2} & \frac{b_1\sqrt{l}}{2} & \left(E_{l,1} - \epsilon\right) \end{vmatrix} = 0 \ \ldots \quad (9.1) $$

where $E_{l,0}$ etc. are given by (7.2) and $E^{l,0}_{l-1,1}$ etc. are given by,

$$ E^{l,0}_{l-1,1} = \int \psi^{(1)}_{l-1,1} \frac{e^2}{r_{12}} \psi^{(1)}_{l,0} \, d\tau \qquad \ldots \quad (9.2) $$

The two unknown roots ${}^3(l+1)_{l+1}$ and ${}^1(l)_{l+1}$ are determined by using the two properties of the determinants obtained. These are, (1) sum of the roots are given by the sum of the diagonal terms of the determinants (diagonal sum rule) and (2). In the sum of the products of the roots taken two at a time, the portion depending linearly on the spin-orbit interaction terms is given by the linear terms in the sum of the products of the diagonal terms taken two at a time. The second property follows from the form of the particular determinants, which contain similar terms at the symmetrical positions. From these rules we get, (since the root ${}^3(l+1)_{l+2}$ is known) for the sum and product of the two unknown roots,

$$^1(l+1)_{l+1} + {}^3(l)_{l+1} = E_{l,0} + E_{l-1,1} + \frac{b_1}{2}(l-1)$$

$$^1(l+1)_{l+1} \cdot {}^3(l)_{l+1} = \frac{b_1}{2}\left(l E_{l,1} - E_{l,0} \right) + \frac{b_2}{2}\left(E_{l,1} - E_{l-1,1} \right) \quad \ldots \quad (9.3)$$

Since we are concerned only with the first order effect of the spin-orbit interaction, we take the solutions in the form,

$$\left.\begin{aligned} ^3(l+1)_{l+1} &= E_{l,1} + \alpha_1 \frac{b_1}{2} + \alpha_2 \frac{b_2}{2} \\ ^3(l)_{l+1} &= E_{l,0} + E_{l-1,1} - E_{l,1} + \beta_1 \frac{b_1}{2} + \beta_2 \frac{b_2}{2} \end{aligned}\right\} \quad \ldots \quad (9.4)$$

where the electrostatic portions are same as those given in (8) and α's and and β's are arbitrary constants. From (9.4) we get,

$$\left.\begin{aligned} ^3(l+1)_{l+1} + {}^3(l)_{l+1} &= E_{l,0} + E_{l-1,1} + \left(\alpha_1 + \beta_1\right)\frac{b_1}{2} + \left(\alpha_2 + \beta_2\right)\frac{b_2}{2} \\ ^3(l+1)_{l+1} \cdot {}^3(l)_{l+1} &= \frac{b_1}{2}\left\{\alpha_1\left(E_{l,0} + E_{l-1,1} - E_{l,1} \right) + \beta_1 E_{l,1}\right\} \\ &\quad + \frac{b_2}{2}\left\{\alpha_2\left(E_{l,0} + E_{l-1,1} - E_{l,1} \right) + \beta_2 E_{l,1}\right\} \end{aligned}\right\} \quad \ldots \quad (9.5)$$

Expressing the E's in terms of F's and G's with the help of (7.2) and Tables I and II and comparing (9.5) with (9.3) we get,

$$\alpha_1 + \beta_1 = l-1;\ \alpha_2 + \beta_2 = 0;\ -(2l+3)\alpha_1 + l\beta_1 = l^2 + 2l;\ -(2l+3)\alpha_2 + l\beta_2 = 3;$$

Solving these we get,

$$\alpha_1 = -\frac{l}{l+1};\ \alpha_2 = -\frac{1}{l+1};\ \beta_1 = \frac{l^2+l-1}{l+1};\ \beta_2 = \frac{1}{l+1} \quad \ldots \quad (9.6)$$

Substituting these values in (9.4) we get the required energy levels. In this way by solving different determinantal equations we get all the energy levels for the pl-configuration. We give in the following only the spin orbit portions of the energy. Electrostatic portions are already given in (8).

For singlets, as has been already pointed out, the spin-orbit portions of the energies are zero. It can be easily seen from (10), that the levels with same L and S value satisfy Lande interval rule. Further (10) also gives the separation factors for the different multiplets in terms of the single electronic parameters b_1 and b_2. For particular values of l these gives separation factors for special cases which are in agreement with those

$$
\begin{aligned}
{}^3(l+1)_{l+2} &= \frac{lb_1}{2} + \frac{b_2}{2}\,;\ {}^3(l+1)_{l+1} = -\frac{1}{l+1}\left(\frac{lb_1}{2} + \frac{b_2}{2}\right) \\
{}^3(l+1)_l &= -\frac{l+2}{l+1}\left(\frac{lb_1}{2} + \frac{b_2}{2}\right) \\
{}^3(l)_{l+1} &= \frac{1}{l+1}\left(\frac{(l^2+l-1)b_1}{2} + \frac{b_2}{2}\right)\,;\ {}^1(l)_l = -\frac{1}{l(l+1)} \\
&\left(\frac{(l^2+l-1)b_1}{2} + \frac{b_2}{2}\right)\,;\ {}^3(l)_{l-1} = -\frac{1}{l}\left(\frac{(l^2+l-1)b_1}{2} + \frac{b_2}{2}\right) \qquad \ldots \quad (10) \\
{}^1(l-1)_l &= \frac{l-1}{l}\left(\frac{(l+1)b_1}{2} - \frac{b_2}{2}\right)\,;\ {}^3(l-1)_{l-1} = -\frac{1}{l} \\
&\left(\frac{(l+1)b_1}{2} - \frac{b_2}{2}\right)\,;\ {}^3(l-1)_{l-2} = -\left(\frac{(l+1)b_1}{2} - \frac{b_2}{2}\right)
\end{aligned}
$$

given by Condon and Shortley (1935). As for the electrostatic portions of the energies, it can be easily shown that the general formulæ (8) yield those derived by Slater (1929) and by Shortley and Freid (1938) for special cases. It may be noted that Racah (1942) by calculating directly the matrix of P_k (cos w) in the $l_1 l_2 LM$ scheme and by use of Dirac's vector model has obtained lengthy general formulæ for the electrostatic energies of different levels for the two electron configuration $l_1 l_2$. For the special case of pl-configuration, his formula agrees with the electrostatic portions of the energies given in our formula (8).

jj coupling.—

In this case the spin-orbit interaction energies between the different electrons are much greater than the electrostatic interaction energies. Hence, we have to consider the spin-orbit interaction first. The effect is already known from previous works [Kar-Sengupta (1949) and Sengupta (1949)]. Each electron gives two levels corresponding to $j = l \pm \frac{1}{2}$, the spin orbit energies for which are $\frac{1}{2}l$ and $-\frac{1}{2}(l+1)$ respectively. The corresponding wave functions are,

$$
\left.
\begin{aligned}
\chi_{nljm} &= \sqrt{\frac{l+m+\frac{1}{2}}{2l+1}}\,\chi_{nlm-\frac{1}{2},\frac{1}{2}} + \sqrt{\frac{l-m+\frac{1}{2}}{2l+1}}\,\chi_{nlm+\frac{1}{2},-\frac{1}{2}} \quad \text{for } j = l+\tfrac{1}{2} \\
&= \sqrt{\frac{l-m+\frac{1}{2}}{2l+1}}\,\chi_{nlm-\frac{1}{2},\frac{1}{2}} - \sqrt{\frac{l+m+\frac{1}{2}}{2l+1}}\,\chi_{nlm+\frac{1}{2},-\frac{1}{2}} \quad \text{for } j = l-\tfrac{1}{2}
\end{aligned}
\right\} \qquad \ldots \quad (11)
$$

For pl-confiuration we get, therefore, in all four levels the spin-orbit energies for which are,

$$\left.\begin{aligned} j_1 = l + \tfrac{1}{2},\ j_2 = \tfrac{3}{2} \qquad & E = l\frac{b_1}{2} + \frac{b_2}{2} \\ j_1 = l + \tfrac{1}{2},\ j_2 = \tfrac{1}{2} \qquad & E = l\frac{b_1}{2} - b_2 \\ j_1 = l - \tfrac{1}{2},\ j_2 = \tfrac{3}{2} \qquad & E = -(l+1)\frac{b_1}{2} + \frac{b_2}{2} \\ j_1 = l - \tfrac{1}{2},\ j_2 = \tfrac{1}{2} \qquad & E = -(l+1)\frac{b_1}{2} - b_2 \end{aligned}\right\} \quad \ldots \quad (12)$$

The corresponding antisymmetric wave functions are,

$$\chi_{n_1 l_1 j_1 m_1 ;\, n_2 l_2 j_2 m_2} = \frac{1}{\sqrt{2}}\left(\chi^{(1)}_{n_1 l_1 j_1 m_1} \cdot \chi^{(2)}_{n_2 l_2 j_2 m_2} - \chi^{(2)}_{n_1 l_1 j_1 m_1} \cdot \chi^{(1)}_{n_2 l_2 j_2 m_2}\right) \quad \ldots \quad (12.1)$$

we next consider the effect of a small electrostatic perturbation on each of levels given in (12). This has been considered in detail by Inglis (1934). He has, however, considered only some special cases. We shall give here the general formulæ for the *pl*-configuration. The method of calculating the perturbation energies is same as that outlined in the beginning of the present paper. The final equation from which energy determinants are to be set up is of the form,

$$\int (H - \epsilon)\chi_{j_1 j_2} \cdot \chi_{j_1 m_1 j_2 m_2}\, d\tau = 0 \quad \ldots \quad (13)$$

where $H = e^2/r_{12}$. In the above, we have dropped n and l in the subscripts of χ for simplicity. The integrations involved in (13), though complicated can nevertheless be performed for the general case of *pl*-configuration, with the help of the Tables I and II. We denote the diagonal terms of (13) by $T\,(jm, j'm')$ and give in Table III, their values for the *pl*-configuration. Numbers given in the columns are to be used as coefficients to the integrals given at the head. To each T, F^0 must be added. The common denominator is given only for the first term of each column.

The twelve energy levels as determined with the help of Table III and diagonal sum rule are given in the following. For the individual levels we use the standard notation $(j_1 j_2)_J$ where J is the resultant angular momentum of the level and j_1 and j_2 are those of the individual electrons.

The above general formulæ give results identical with those obtained by Inglis (*l.c.*) for special cases. Racah (1942) by use of Tensor operators and Wigner's transformation formula for vector addition, has obtained general expression for the electrostaic energy for two electron configuration in the *jj* coupling. He has not, however, simplified his very complex formulæ for the special case of *pl*-configuration. Hence we are not able to compare our formula (14) with his results.

TABLE III

$T\,(jm\;j'm')$

j	m	j'	m'	F^2	$-G^{l-1}$	$-G^{l+1}$
$l+\frac{1}{2}$	$l+\frac{1}{2}$	$\frac{3}{2}$	$\frac{3}{2}$	$\frac{l}{5(2l+3)}$	$\frac{3l}{4l^2-1}$	$\frac{3}{(2l+3)^2(2l+1)}$
	$l+\frac{1}{2}$		$\frac{1}{2}$	$-l$	0	$-2(2l+1)$
	$l-\frac{1}{2}$		$\frac{1}{2}$	$\frac{l(2l-5)}{2l+1}$	$\frac{6l(l-1)}{2l+1}$	$\frac{18l}{2l+1}$
	$l-\frac{3}{2}$		$\frac{3}{2}$	$\frac{2l^2-11l+6}{2l+1}$	$\frac{3(l-1)(2l-3)}{2l+1}$	$\frac{18(2l-1)}{2l+1}$
	$l-\frac{1}{2}$		$\frac{1}{2}$	$-\frac{l(2l-5)}{2l+1}$	$\frac{6l}{2l+1}$	$\frac{(4l-1)^2}{2l+1}$
	$l+\frac{1}{2}$		$-\frac{1}{2}$	$-l$	0	$(l+1)(2l+1)$
	$l-\frac{5}{2}$		$\frac{5}{2}$	$\frac{4l^3-30l^2+53l-18}{4l^2-1}$	$\frac{6(l-1)(l-3)(2l-3)}{4l^2-1}$	$\frac{60(l-1)}{2l+1}$
	$l-\frac{3}{2}$		$\frac{3}{2}$	$-\frac{2l^2-11l+6}{2l+1}$	$\frac{18(l-1)}{2l+1}$	$\frac{24(l-1)^2}{2l+1}$
	$l-\frac{1}{2}$		$-\frac{1}{2}$	$-\frac{l(2l-5)}{2l+1}$	0	$2(l-1)^2$
	$l+\frac{3}{2}$		$-\frac{3}{2}$	l	0	0
$l+\frac{1}{2}$	$l+\frac{1}{2}$	$\frac{1}{2}$	$\frac{1}{2}$	$-(2l-1)$	0	0
	$l+\frac{1}{2}$		$\frac{1}{2}$	0	0	$2(l+1)(2l+1)$
	$l-\frac{1}{2}$		$\frac{1}{2}$	0	0	$2(2l+1)$
$l-\frac{1}{2}$	$l-\frac{1}{2}$	$\frac{1}{2}$	$\frac{1}{2}$	0	$(2l+1)$	0
	$l-\frac{1}{2}$		$-\frac{1}{2}$	0	0	0
	$l-\frac{3}{2}$		$\frac{1}{2}$	0	$\frac{3(l-1)(2l+1)}{2l-1}$	0
$l-\frac{1}{2}$	$l-\frac{1}{2}$	$\frac{3}{2}$	$\frac{3}{2}$	$\frac{(2l+3)(l-1)}{(2l+1}$	$\frac{3(l-1)}{2l+1}$	$\frac{9}{2l+1}$
	$l-\frac{1}{2}$		$\frac{1}{2}$	$-\frac{(l-1)(2l+3)}{2l+1}$	$\frac{2(l-1)^2}{2l+1}$	$\frac{18l}{2l+1}$
	$l-\frac{3}{2}$		$\frac{3}{2}$	$\frac{(l-1)(2l-7)(2l+3)}{4l^2-1}$	$\frac{6(l-1)(2l-3}{4l^2-1}$	$\frac{36}{2l+1}$
	$l-\frac{1}{2}$		$-\frac{1}{2}$	$-\frac{(l-1)(2l+3)}{2l+1}$	0	$9l$
	$l-\frac{3}{2}$		$\frac{1}{2}$	$-\frac{(l-1)(4l^2-8l-21)}{4l^2-1}$	$\frac{(l-1)(4l^2-20l+25)}{4l^2-1}$	$\frac{27(2l-1)}{2l+1}$
	$l-\frac{3}{2}$		$\frac{3}{2}$	$\frac{4l^3-24l^2-7l+57}{4l^2-1}$	$\frac{9(2l-3)(l-3)}{4l^2-1}$	$\frac{90}{2l+1}$

$$\left(l+\tfrac{1}{2},\tfrac{3}{2}\right)_{l+2} = \frac{lb_1}{2} + \frac{b_2}{2} + F^0 + \frac{l}{5(2l+3)}F^2 - \frac{3l}{4l^2-1}G^{l-1} - \frac{3}{(2l+3)^2(2l+1)}G^{l+1}$$

$$\left(l+\tfrac{1}{2},\tfrac{3}{2}\right)_{l+1} = \,,, \,,, + F^0 - \frac{l(2l+7)}{5(2l+1)(2l+3)}F^2 + \frac{9l}{(4l^2-1)(2l+1)}G^{l-1} - \frac{8l^2+20l-1}{(2l+3)^2(2l+1)^2}G^{l+1}$$

$$\left(l+\tfrac{1}{2},\tfrac{3}{2}\right)_{l} = \,,, \,,, + F^0 - \frac{(2l-3)(l+2)}{5(2l+1)(2l+3)}F^2 - \frac{9}{(4l^2-1)(2l+1)}G^{l-1} - \frac{4l^3+16l^2+7l-18}{(2l+3)^2(2l+1)^2}G^{l+1}$$

$$\left(l+\tfrac{1}{2},\tfrac{3}{2}\right)_{l-1} = \,,, \,,, + F^0 + \frac{l+2}{5(2l+1)}F^2 + \frac{9}{(4l^2-1)^2}G^{l-1} + \frac{3(l+2)}{(2l+3)(2l+1)^2}G^{l+1} \quad \Big\} \ \ldots \ (14)$$

$$\left(l+\tfrac{1}{2},\tfrac{1}{2}\right)_{l+1} = \frac{lb_1}{2} - b_2 + F^0 - \frac{1}{(2l+3)^2}G^{l+1}$$

$$\left(l+\tfrac{1}{2},\tfrac{1}{2}\right)_{l} = \,,, \,,, + F^0 - \frac{1}{(2l+3)}G^{l+1}$$

$$\left(l-\tfrac{1}{2},\tfrac{3}{2}\right)_{l+1} = -(l+1)\frac{b_1}{2} + \frac{b_2}{2} + F^0 + \frac{l-1}{5(2l+1)}F^2 - \frac{3(l-1)}{(2l+1)(4l^2-1)}G^{l-1} - \frac{9}{(2l+3)^2(2l+1)^2}G^{l+1}$$

$$\left(l-\tfrac{1}{2},\tfrac{3}{2}\right)_{l} = \,,, \,,, + F^0 - \frac{(l-1)(2l+5)}{5(4l^2-1)}F^2 - \frac{(l-1)(4l^2-13)}{(4l^2-1)^2}G^{l-1} - \frac{9}{(2l+3)(2l+1)^2}G^{l+1}$$

$$\left(l-\tfrac{1}{2},\tfrac{3}{2}\right)_{l-1} = \,,, \,,, + F^0 - \frac{(l+1)(2l-5)}{5(4l^2-1)}F^2 + \frac{8l^2-4l-13}{(4l^2-1)^2}G^{l-1} - \frac{9(l+1)}{(2l+3)(2l+1)^2}G^{l+1}$$

$$\left.\begin{aligned}
\left(l-\tfrac{1}{2},\ \tfrac{3}{2}\right)_{l-2} &= \quad ,, \quad ,, \quad + F^0 + \frac{l+1}{5(2l-1)} F^2 \\
&\quad - \frac{3}{(4l^2-1)(2l-1)} G^{l-1} - \frac{3(l+1)}{(2l+3)(2l+1)} G^{l+1} \\
\left(l-\tfrac{1}{2},\ \tfrac{1}{2}\right)_{l} &= -(l+1)\frac{b_1}{2} - b_2 + F^0 - \frac{1}{(2l-1)} G^{l-1} \\
\left(l-\tfrac{1}{2},\ \tfrac{1}{2}\right)_{l-1} &= \quad ,, \quad ,, \quad + F^0 + \frac{1}{(2l-1)^2} G^{l-1}
\end{aligned}\right\} \quad \ldots \quad (14) \ (contd.)$$

From (14), (8) and (10) it is easily noted that the sum of the spin-orbit and electrostatic energies for terms of the same J value are same in both LS and jj coupling. Thus if we denote the spin-orbit energy by Γ and the electrostatic energy by δ, then we can say that Γ-sum and δ-sum for all the terms of same J are independent of coupling. This, as will be presently shewn, is a special case of a more general sum rule valid for all configurations.

SUM RULES FOR THE MULTIPLETS

Let us now consider the case of N electrons. The antisymmetric wave functions can be written in the determinant form,

$$\chi_{n_1 l_1 m_{l_1} m_{s_1};\ n_2 l_2 m_{l_2} m_{s_2};\ \ldots\ldots} = \frac{1}{\sqrt{N!}} \begin{Vmatrix} \chi^{(1)}_{n_1} & \chi^{(2)}_{n_1} & \cdots & \chi^{(N)}_{n_1} \\ \chi^{(1)}_{n_2} & \chi^{(2)}_{n_2} & \cdots & \chi^{(N)}_{n_2} \\ \cdots & \cdots & \cdots & \cdots \\ \cdots & \cdots & \cdots & \cdots \\ \chi^{(1)}_{n_N} & \chi^{(2)}_{n_N} & \cdots & \chi^{(N)}_{n_N} \end{Vmatrix} \quad \ldots \quad (15)$$

where n_1, n_2 etc in the determinant (15) stand for the complete set of quantum numbers $n_1 l_1 m_{l_1} m_{s_1}$ etc. Since the system is degenerate with respect to $m_{l_1}, m_{s_1}; m_{l_2} m_{s_2}$; ... etc., the general wave function can be written in the form,

$$\chi_{n_1 l_1;\ n_2 l_2;\ \ldots} = \sum_{m_{l_1} m_{s_1}; m_{l_2} m_{s_2}; \ldots} \alpha_{m_{l_1} m_{s_1}; m_{l_2} m_{s_2}; \ldots} \chi_{n_1 l_1 m_{l_1} m_{s_1};\ n_2 l_2 m_{l_2} m_{s_2}; \ldots} \quad (15.1)$$

There are as before three perturbing energies,

$$\begin{aligned}
&(1). \quad \text{electrostatic} \quad H_1 = \sum_{i>j=1}^{N} \frac{e^2}{ri}; \\
&(2). \quad \text{spin-orbit} \quad H_2 = \sum_{k=1}^{N} \frac{Ze^2}{2m_0^2 c^2} \frac{(L_k S_k)}{r^3} \qquad (15.2) \\
&(3). \quad \text{magnetic} \quad H_3 = \sum_{k=1}^{N} a(m_{l_k} + 2m_{s_k})
\end{aligned}$$

From the general theory of perturbation, we get corresponding to (4),

$$\int (H-\epsilon)\chi_{n_1 l_1;\, n_2 l_2;\, \cdots}\, \chi_{n_1 l_1 m_1 m_{s_1},\, n_2 l_2 m_2 m_{s_2};\, \cdots}\, d\tau = 0 \qquad (16)$$

Where $H = H_1 + H_2 + H_3$. As has already been pointed out in the begining, equation (16) gives a determinantal equation for each value of $M = \sum_k (m_{l_k} + m_{s_k})$. Though the general solution of any determinant is not possible, yet the sum of the roots of any equation of a particular M value can be obtained from the diagonal sum rule, if we know these diagonal terms of the determinant. It can be easily shown that the diagonal terms are given by,

$$\sum_{k\,\cdot\,l=1}^{N} E_{n_k n_l} + \sum_{k=1}^{N} b_k m_{l_k} m_{s_k} + \sum_{k=1}^{N} a(m_{l_k} + 2m_{l_k}) \qquad \cdots \quad (17)$$

where,

$$\left.\begin{aligned} E_{n_k n_l} = \int\int \chi^{*(i)}_{n_k}\, \chi^{(j)}_{n_l}\, \frac{e^2}{r_{ij}}\, \chi^{(i)}_{n_k}\, \chi^{(j)}_{n_l}\, d\tau \\ - \int\int \chi^{(i)}_{n_k}\, \chi^{*(j)}_{n_l}\, \frac{e^2}{r_{ij}}\, \chi^{(i)}_{n_l}\, \chi^{(j)}_{n_k}\, d\tau \end{aligned}\right\} \quad \cdots \quad (17.1)$$

and b_k and a have usual meaning. In (17), first is the electrostatic interaction term and the second and the third are the spin-orbit and magnetic terms respectively. To get the sum of the energies of all levels with a particular value of M, we have to sum the diagonal term given by (17) over all values of $(m_{l_1} m_{s_1};\ m_{l_2} m_{s_2};\ \cdots)$ consistent with the condition, $\sum_{k=1}^{N} (m_{l_k} + m_{s_k}) = M$. It is easily seen from the form of (17) that for any configuration, the total electrostatic, spin-orbit or magnetic contribution, in the sum of the energies of all states having a particular value of M, does not depend on the relative magnitudes of the three perturbing energies. This, in essence, contains the well known sum rules of the multiplet spectra. Let us suppose that the spin-orbit interaction energies of the different terms can be represented separately by a factor Γ. Then it is evident from what has been said before that the sum of the Γ values for all terms of same M will be independent of magnetic field strength and electrostatic interaction energy. Similar rules hold for electrostatic energy δ and magnetic energy agM (g is the well known Lande factor). Thus we obtain that δ-, Γ- and g-sums for all terms of same M value arising out of a configuration, are independent of coupling and field strength. Thus we get in addition to the well known Γ- and g-sum rules [Goudsmit (1928); Pauli (1923)], a new δ-sum rule, which is applicable to the electrostatic interaction energies.

It is well known that in the absence of a magnetic field, the different terms of a multiplet are degenerate with respect to M, *i.e.*, Γ and δ for such cases do not depend on M. For weak field the magnetic contribution to

energy is of the form agM where g, the Lande factor, is independent of M. Thus for weak field δ-, Γ- and g-sums depend only on the J values of the terms. If now S_M and S_{M-1} denote these sums for two M values, M and $M-1$, then evidently $S_{J=M}=S_M-S_{M-1}$ will give the δ-, Γ- and g-sums for those levels whose J values are same and equal to M. Since both S_M and S_{M-1} are independent of coupling (from the sum rules[1]), we get the result that in a weak magnetic field, the δ-, Γ- and g-sums for all terms of same J, arising out of a configuration are independent of coupling. This gives the well known weak field Γ-sum and g-sum rules. We notice that the rule is equally true for the δ-sum. For sl- and pl-configurations the rules can be easily verified from the formulæ already given.

COMPARISON WITH EXPERIMENTAL RESULTS

We shall now verify the δ-sum rule by taking the experimental results for a number of elements. We shall consider only the no field case. The sum rules here, give us a number of equations, each for the sum of the energies of all possible levels for a particular value of J, arising out of a given configuration. Each sum is given in terms of a number of parameters. If the number of these parameters be less than the number of equations obtained then we can eliminate these parameters and obtain a relation between the different sums. For np^3 configuration, the allowed terms are $^2D_{\frac{5}{2}}$, $^2D_{\frac{3}{2}}$, $^2P_{\frac{3}{2}}$, $^4P_{\frac{1}{2}}$ and $^4S_{\frac{3}{2}}$. The sum rules give,

$$\left.\begin{aligned} &^2D_{\frac{5}{2}}=3F_0-6F_2=\text{I}\\ &^2D_{\frac{3}{2}}+{}^2P_{\frac{3}{2}}+{}^4S_{\frac{3}{2}}=9F_0-21F_2=\text{II}\\ &^2P_{\frac{1}{2}}=3F_0=\text{III}\end{aligned}\right\} \quad \ldots \quad (18)$$

where $F_0=F^0$ and $F_2=\dfrac{F^2}{25}$.

Instead of calculating these sums directly from (17), we can also calculate them from the energy levels in the LS or jj coupling, in the cases where they are known. This is obviously possible, because the sums given in (18) are independent of coupling. Thus from (18) we get, eliminating the constants F_0 and F_2,

$$\sigma=\frac{\text{III}+2\text{II}}{7\text{I}}=1 \qquad (18.1)$$

Thus relation will evidently be valid in all coupling strength. In column three of the following table are given the experimental values of σ for a number of elements. All the data used in this paper are taken from Bacher and Goudsmit (1932).

From $_7NI$ to $_{85}BiI$ we have progressive departure from LS coupling. In spite of this departure, the experimental values of σ are, however, in agreement with the theoretical value 1 in all cases.

TABLE IV

element	Configuration	σ
Theoretical	np^3	1.00
7N *I*	$2p^3$	1.01
16S *II*	$3p^3$	.99
33As *I*	$4p^3$	1.00
51Sb *I*	$5p^3$	1.02
83Bi *I*	$6p^3$	.97

For np^2 configuration the allowed terms are $^1D_2$, $^3P_2$, $^3P_1$, $^3P_0$ and $^1S_0$. From the sum rules we get,

$$\left.\begin{aligned} {}^1D_2+{}^3P_2 &= 2F_0-4F_2+\frac{b}{2}=\mathrm{I} \\ {}^3P_1 &= F_0-5F_2-\frac{b}{2}=\mathrm{II} \\ {}^3P_0+{}^1S_0 &= 2F_0+5F_2-b=\mathrm{III} \end{aligned}\right\} \quad \ldots \quad (19)$$

Here we have three constants and three equations. Hence It is not possible to eliminate the constants. From (19) we get,

$$\frac{3}{2}b=\frac{1}{5}\left(5\mathrm{I}-6\mathrm{II}-2\mathrm{III}\right) \quad \ldots \quad (19.1)$$

This relation is valid in all coupling. In *LS* coupling and extreme *jj* coupling, we have the relation,

$$\frac{3}{2}b={}^3P_2-{}^3P_0 \quad \ldots \quad (19.2)$$

In Table V, we have given the values of $\frac{3}{2}b$ calculated fron (19.1) and (19.2) for various cases.

TABLE V

Element	Configuration	$\frac{3}{2}b$ from (19.1)	$\frac{3}{2}b$ from (19.2)
14Si *I*	$3p^2$	271.6	223.14
32Ge *I*	$4p^2$	1320.0	1499.9
50Sn *I*	$5p^2$	3146.0	3428.0
82Pb *I*	$6p^2$	10941	10648
83Bi *II*	$6p^2$	17302	17025

It is noticed from the table that the agreement between the two values is fairly good in all coupling. Thus taking (19.2) to be valid for all coupling we can eliminate the constants from (19) and get,

$$\sigma = \frac{^1S_0 - ^1D_2}{^3P_0 + ^1S_0 - 2^3P_1} = .6 \qquad \ldots \quad (20)$$

Experimental values of σ for a number of elements are given in Table VI.

TABLE VI

Element	Configuration	σ
Theoretical	np^2	.6
6C I	$2p^2$	.53
8O III	$2p^2$	.53
14Si I	$3p^2$	.50
32Ge I	$4p^2$	.60
50Sn I	$5p^2$	.62
82Pb I	$6p^2$	.58
83Bi II	$6p^2$	.58

From Table VI we note that the agreement is throughout fairly good. Since, however, (19.2) is strictly true in the LS coupling we should expect better agreement in this case. But Table VI shows that here disagreement is rather greater. This is possibly due to the perturbing effects of other configurations.

For d^2 and d^3 configurations, elimination of the constants is possible. But all the terms resulting from the configuration are known only for a very few cases. Hence no useful comparison with the experimental results can be made.

TABLE VII

Element	Configuration	Predicted value of $^3P_0 - ^1S_0$ in cm^{-1}
32Ge III	$4p^2$	5146
50Sn III	$5p^2$	6195
51Sb IV	$5p^2$	3221
52Te V	$5p^2$	2140

In some cases where one or two terms of the configuration is not identified or detected, the approximate position of this terms can be predicted from the sum rules. In many cases of P^2-configuration all the levels except $^1S_0$ are known. From (20) we can predict the position of this level. Table VII gives the pridicted value of $^1S_0$ for some elements. Instead of giving the actual term values, we have given the separation $^3P_0 - {}^1S_0$ in the table.

In conclusion we hope that the δ-sum rule, established in the present paper will prove of great help in the classification and identification of different spectra, specially those in the intermediate coupling.

ACKNOWLEDGMENTS

The author's thanks are due to Prof. K. C. Kar, D.Sc. of Presidency College, under whose guidance the work has beeen conducted. He would also thank the Goverment of West Bengal for the award of a research scholarship which enabled him to carry on the work.

PHYSICAL LABORATORY,
PRESIDENCY COLLEGE.

REFERENCES

Bacher and Goudsmit, 1932. Atomic Energy states (Mc Graw-Hill).
Condon and Shortley, 1935. Theory of Atomic spectra (Camb. Univ.)
Gaunt, 1929, *Trans, Roy Soc.* **A, 228,** 151.
Goudsmit, S., 1930, *Phys. Rev.*, **35**, 1325.
Goudsmit, S., 1928. *Phys. Rev.*, **31**, 946.
Houston, W. V., 1920, *Phys. Rev.*, **33**, 297.
Inglis, D. R., 1931 *Phys. Rev.*, **38**, 862.
Kar, K. C. and Sengupta, S., 1949, *Ind. Jour. Phys.*, **23**, 19.
Pauli, W., 1923, *Zeit. f. Phys.*, **16**, 155.
Racah, G., 1942, *Phys. Rev.*, **61**, 186.
Racah, G., 1942, *Phys. Rev.*, **62**, 438.
Sengupta, S., 1949, *Ind. Jour. Phys.*, **23**, 287.
Shortley and Freid 1938, *Phys. Rev.*, **54**, 739 .
Slater, J. C., 1929, *Phys. Rev.*, **34** 1293.